Imperial College of Science and Technology
University of London

SIMULATION OF THE HYPERBAR DIESEL ENGINE TURBOCHARGING SYSTEM

by

A. D. PILLEY

November 1982

This thesis forms part of the requirements
for the Doctor of Philosophy degree of
the University of London and the
Diploma of Imperial College

ABSTRACT

An existing non-linear digital simulation model of a turbocharged, direct injection, four stroke diesel engine has been developed to allow the performance of the Hyperbar turbocharging system to be predicted. The simulation employs the quasi-steady "filling and emptying" approach to describe the changes in thermodynamic state and gas flow into and out of the various control volumes, representing the engine cylinders, the inlet and exhaust manifolds, the Auxiliary Combustion Chamber (ACC) and the exhaust mixer.

Dynamic models have been developed for the engine and turbocharger, the governor, the by-pass valve and the ACC. This allows both the steady state and transient performance of the engine and turbocharging system to be solved from a set of coupled ordinary differential equations, in the form of an initial value problem. The governing equations are integrated numerically.

The model includes the effects of combustion in the engine cylinders and the ACC, based on the fuel burning rate approach. Burning rate data obtained from experimental tests were correlated to the principal controlling parameters, such as ignition delay, engine speed and trapped equivalence ratio for the engine cylinders. Heat transfer from the cylinder and exhaust gases was taken into consideration and a one-dimensional heat transfer model was used to calculate the cylinder wall temperatures.

A comparison between experimental test data for a 6 cylinder Hyperbar engine, measured by the manufacturer, and the simulation model showed a reasonable agreement. The model was formulated in such a way that the effect of changes in the main design parameters of the engine and turbocharging system could be investigated. The results of a detailed parametric study show the need to improve the control over vital components in the system, such as the by-pass valve position and the ACC fuelling regulator.

It is concluded that the simulation model can be a useful development tool, reducing the amount of engine testing required, especially for this (relatively) new system.

ACKNOWLEDGEMENTS

"An expert is a man who has made all the mistakes, which can be made, in a very narrow field." Niels Bohr.

I would like to express my gratitude to Dr. N. Watson for his guidance, patience and encouragement throughout this work, and for his many helpful suggestions.

I wish to especially thank Mr. S.A. Ali for his help and advice, particularly in computing matters. The many discussions that we have had regarding engine systems, experimental methods and simulation models, and his friendship have been invaluable.

Special thanks are also due to Dr. M. Marzouk, who wrote the original simulation program on which this work has been based, for his advice. I would also like to thank Dr. M. Kamal, Dr. N. Kyrtatos and Dr. B. Holness for many stimulating discussions.

Mr. C. Hall and Mr. R.D. Bloxham have also contributed many useful suggestions concerning the practical aspects of engine testing, and microprocessor system design respectively.

I would like to thank Ms. D. Day, the departmental secretary, and Ms. E. Archer, the departmental librarian, and her staff, for their advice and help.

It is not possible to undertake any work of this nature, without the encouragement and support of family and friends. I would especially like to thank my close friends for helping to keep me relatively sane, and my mother for her unfailing confidence in my ability. To her I dedicate this thesis.

LIST OF CONTENTS

NOTATION

A	area	m^2
B	bore	m
c	polytropic exponent of compression	-
c_d	coefficient of discharge	-
c_p	specific heat at constant pressure	kJ/kg.K
c_v	specific heat at constant volume	kJ/kg.K
C	isentropic gas velocity at the turbine exit	m/s
C	governor constant	-
C_m	mean piston velocity	m/s
CN	Cetane Number of the Fuel	-
CR	compression ratio	-
C_v	lower calorific value of the fuel	kJ/kg
D	diameter	m
E	energy	kW
f	fuel-air ratio	-
F	force	kN
F	fuel-air equivalence ratio	-
g	gravitational acceleration	m/s^2
G_r	Grashof Number	-
h	heat transfer coefficient	$kW/m^2.K$
h	specific stagnation enthalpy	kJ/kg
I	polar moment of inertia	$kg.m^2$
k	spring rate	kN/m
k	thermal conductivity	kW/m.K
K	propeller law constant	$kW.min^3$
l	length	m
l	connecting rod length	m
m	mass	kg
$\dot{m}$	mass flow rate	kg/s
M	non-dimensional fuel burnt	-

$\dot{M}$	non-dimensional fuel burning rate	-
N	speed	rpm
N_u	Nusselt Number	-
p	pressure	kN/m^2
P	power	kW
P_r	Prandtl Number	-
$\dot{Q}$	heat transfer rate	kW
r	crank radius	m
R	gas constant	kJ/kg.K
R	thermal resistance	K/kW
R_e	Reynolds Number	-
s	smoke	-
s	specific entropy	kJ/kg.K
S	stroke	m
t	time	s
T	temperature	K
u	specific internal energy	kJ/kg
U	turbine blade tip velocity	m/s
v	velocity	m/s
V	volume	m^3
w	rack limiter (aneroid) position	-
x	displacement	m
x	rack position	-
y	demand speed	-
α	time constant for the heat exchanger	s
α_1	time constant for the cylinder walls	s
β	mode of burning proportionality factor	-
β	coefficient of thermal expansion	K^{-1}
γ	specific heats ratio	-
δ	ignition delay	ms
Δ	nominal burning duration	°CA
ε	heat exchanger effectiveness	-
ε	error tolerance	-

η	isentropic efficiency/efficiency	-
Θ	crank angle	°CA
λ	damping coefficient	kN.s/m
μ	viscosity	kg/m.s
ρ	density	kg/m^3
τ	torque	kN.m
τ	normalised crank angle	-
Φ	by-pass valve inclination	degrees
$\oint$	integration over one engine cycle	-

The units are as stated above unless specified otherwise in the text.

Subscripts

a	air/ambient/actual
acc	auxiliary combustion chamber
b	boost
bp	by-pass
B	brake
c	control/compressor/coolant
cc	charge cooler/closed cycle
cl	clearance
cr	critical
cyl	cylinder
d	density/downstream/diffusion
D	damping
e	exhaust/effective/end of combustion
egr	exhaust gas recirculation
ex	experimental
E	engine
f	fuel/film
F	friction
g	geometric/gas
h	cylinder head
i	start of combustion
imh	inlet manifold heater
is	isentropic
I	indicated/inertia
l	liner
L	load
m	mean/mechanical/mean value during the ignition delay/metal
max	maximum
min	minimum
o	overall/oil/control variable/orifice
p	premixed/piston

pr	predicted
ref	reference
s	stoichiometric
sc	scavenge
ss	steady state
sw	swept
t	total/turbine
tc	turbocharger
u	upstream
v	valve/volumetric
w	water/wall

0	control/initial
1	compressor inlet/by-pass valve head
2	compressor outlet/by-pass valve stem
2'	charge cooler outlet/inlet manifold
3	by-pass valve damping piston/turbine inlet
4,5,6	control areas/exhaust positions

Abbreviations

abs	absolute
ABDC	After Bottom Dead Centre
ACC	Auxiliary Combustion Chamber
ADC	Analogue to Digital Converter
AFBR	Apparent Fuel Burning Rate
A/F	Air-Fuel
AHRR	Apparent Heat Release Rate
ALU	Arithmetic Logic Unit
ATD	Aneroid Timing Device
ATDC	After Top Dead Centre
BDC	Bottom Dead Centre
BMEP	Brake Mean Effective Pressure
BSAC	Brake Specific Air Consumption
BSFC	Brake Specific Fuel Consumption
BTDC	Before Top Dead Centre
CA	Crank Angle
CCMEP	Closed Cycle Mean Effective Pressure
CI	Compression Ignition
CPU	Central Processor Unit
DC	Direct Current
DCE	Differential Compound Engine
DI	Direct Injection
DIP	Dynamic Injection Point
EMS	Engine Management System
EPROM	Erasable Programmable Read Only Memory
EVC	Exhaust Valve Closing
EVO	Exhaust Valve Opening
FMEP	Friction Mean Effective Pressure
FIE	Fuel Injection Equipment
HP	High Pressure
IDI	Indirect Injection

IMEP	Indicated Mean Effective Pressure
ISAC	Indicated Specific Air Consumption
ISFC	Indicated Specific Fuel Consumption
IVC	Inlet Valve Closing
IVO	Inlet Valve Opening
LBMEP	Load Brake Mean Effective Pressure
LP	Low Pressure
LVDT	Linear Variable Displacement Transducer
MOC	Method of Characteristics
NEC	Nippon Electric Company
PMEP	Pumping Mean Effective Pressure
rpm	revolutions per minute
RAM	Random Access Memory
ROM	Read Only Memory
SI	Spark Ignition
T/C	Turbocharger
TDC	Top Dead Centre
TTL	Transistor Transistor Logic
UART	Universal Asynchronous Receiver Transmitter
UV	Ultra Violet

CHAPTER 1

INTRODUCTION

1.1 Supercharging Systems for Highly Rated Diesel Engines.

Over the past 30 years the commercial rating of medium speed four stroke diesel engines for marine and rail propulsion and electricity generation has risen very rapidly, due mainly to the development of "supercharging" systems. The ratings of smaller high speed automotive diesel engines has lagged behind that of the medium and slow speed engines because of the high cost of the supercharging system relative to the engine, and the problems involved in developing suitable high efficiency turbomachinery.

More recently the development of higher output high speed diesel engines has been accelerated by the effects of legislation regarding pollutant emissions and minimum power to weight ratio's for truck engines. The "energy crisis" of the early 1970's has increased the demand for more efficient use of our finite mineral resources and the development of "alternative" fuels. The diesel engine has proved to be a versatile power unit, principally because of its high thermal efficiency over a wide operating range, compared to other prime movers, and its ability to be adapted to run on a wide range of fuels. The demands for greater power, lower cost, size and weight and better fuel economy with lower emissions can be realised by continuing development of the current engine systems and the introduction of new concepts and materials. This inevitably leads to new problems, such as higher thermal and mechanical loadings, with corresponding effects on the life and reliability of the engine, and a deterioration in the engine response and cold starting behavior. Many of these problems are a direct consequence of the higher ratings, and the need to run automotive diesel engines over a wide speed range with a suitable torque curve has resulted in the more conservative power outputs for these engines.

The power output of a diesel engine may be raised by increasing either the speed or the torque. Increasing the engine speed is undesirable in many cases, because of the corresponding increases of the inertia stresses in the connecting rod, piston, valve train, etc., and the rapid increase in frictional losses with engine speed (104)*.

* Numbers in parentheses designate References at the end of the Thesis.

The time available for the combustion process is inversely proportional to the engine speed. Therefore, as the speed increases the mixing of the injected fuel with air in the cylinder must be faster or else combustion will occur late in the cycle, resulting in a deterioration in the thermal efficiency of the engine. The engine speed range will consequently be influenced by the combustion system adopted (direct injection (DI) or indirect injection (IDI)), and the efficiency of the mixing process between the fuel and the air (i.e. the swirl, squish, turbulence, injection pressure, number of injector holes, etc.).

The valve timing can only be optimised at one engine speed, and there will be a reduction in the pumping efficiency (volumetric efficiency) of the engine at other speeds. A large speed range may therefore lead to poor engine "breathing" at high speeds if the low speed performance is optimised (118). The combination of these factors make the alternative of increasing the engine torque the more desirable option in many cases.

The engine torque can be increased by raising either the swept volume or the Brake Mean Effective Pressure (BMEP). Increases in swept volume usually involve an increase in engine weight and bulk, while increases in BMEP are associated with greater thermal and/or mechanical loading.

For automotive applications the specific volume (bulk volume of the engine divided by the maximum power output), and specific weight (weight divided by the maximum power output) are often critical, and so the option of increasing the BMEP is usually preferred. Most manufacturers therefore offer a range of power outputs for a given engine design. For example, the Poyaud 520 series 6 cylinder engine (189) is rated at 145 kW naturally aspirated, 176 kW turbocharged and 241 kW turbocharged and intercooled, at the maximum engine speed of 2500 rpm. Further increases in engine power are possible by raising the swept volume (i.e. specifying 8 or 12 cylinder versions of the same engine), rather than increasing the BMEP.

In order to increase the engine BMEP significantly the mass of air trapped by the engine per cycle must be raised, which allows more fuel to be burnt, for the same overall air-fuel (A/F) ratio. Assuming that the swept volume of the engine is not changed, then a significant increase in the air mass flow rate through the engine can

be achieved by increasing the density of the air in the induction manifold. A compressor mounted in series with the engine can be used to raise the inlet manifold pressure. If the compressor takes its power from the engine crankshaft, the engine is said to be "supercharged", Fig. 1.1a. Obviously the energy required to drive the compressor reduces the overall engine power output. If very high compressor pressure ratio's are required, a point will eventually be reached where the compressor power required will be equal to the engine power output, and no work is available at the engine crankshaft. In this case the engine exhaust gas is usually used to drive a turbine which provides the external power, and the engine simply acts as a gas generator, Fig. 1.1b, as in the case of the Sulzer free piston engine (102).

Numerous different types of compressors that can be combined with an internal combustion engine, for example, reciprocating piston, rotary piston, intersecting axis, vane, screw, Roots, centrifugal and axial compressors (6). Usually either positive displacement or rotary compressors are preferred because of their ability to deliver high air flow rates, while being compact enough for practical applications. Centrifugal compressors have become highly developed for automotive applications (164), while multi-stage axial (or axial/radial combinations) are widely used for gas turbines.

Despite the disadvantages of mechanical supercharging many engines using this system have proved to be extremely successful, for example, the Rolls Royce Merlin aero engine developed in the 1940's (39,117). Currently there is much interest in the future of mechanical supercharging for small automotive engines (41,103), where the compressor power required is relatively low.

A more efficient method of driving the compressor is to connect it to a turbine, which can be driven by the exhaust gases from the engine. The engine is then said to be "turbocharged", Fig. 1.1c.

Any increase in the engine inlet manifold pressure produced by the supercharger compressor will be accompanied by an increase in the inlet air temperature, due to the compression process, and this reduces the charge density somewhat. A heat exchanger can be used between the compressor and the engine to increase the inlet air density still further by lowering the air temperature, and this will allow an increase in engine rating. Charge cooling can also be used to reduce the cycle temperatures, and hence the thermal loading of the engine and/or the turbocharging system and

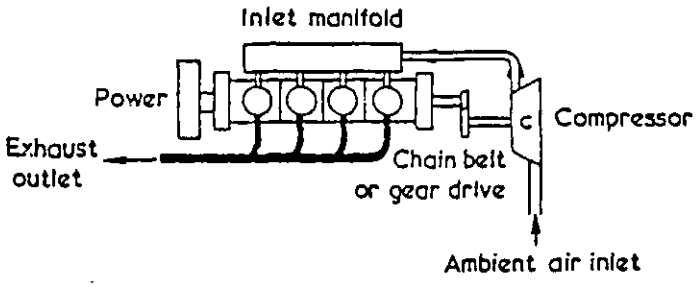

Fig. 1.1a Schematic of a Supercharged Engine.

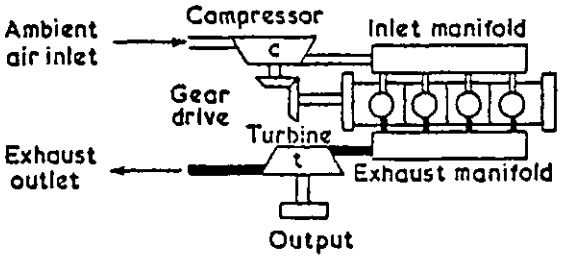

Fig. 1.1b Schematic of a Gas Generator Engine.

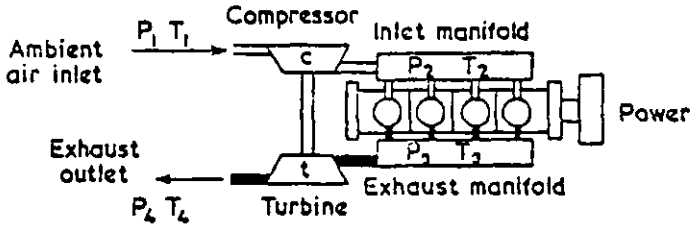

Fig. 1.1c Schematic of a Turbocharged Engine.

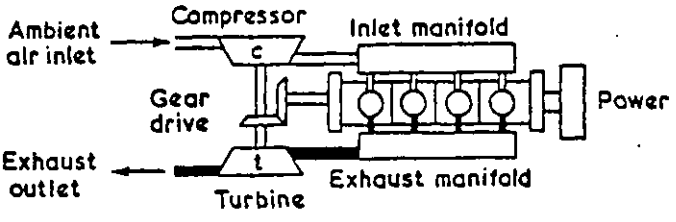

Fig. 1.1d Schematic of a Turbocompound Engine.

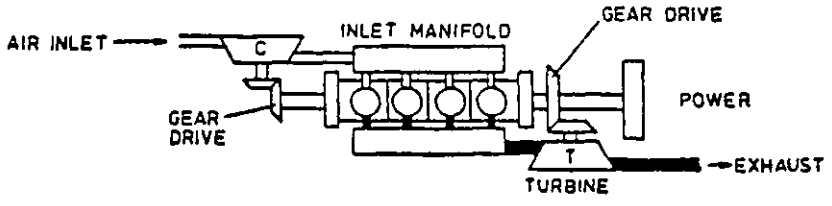

Fig. 1.1e An Alternative Turbocompound Engine Arrangement.

Fig. 1.1 Arrangements for Supercharging the Internal Combustion Engine.

emissions (53,105). However, for high air flow rates large coolers may be required, to avoid excessive pressure losses, which increases the bulk and weight of the engine. This is not usually a problem with large stationary engines, but the combination of the extra volume, weight and cost can be prohibitive in automotive applications.

If the compressor is connected in series with the engine, then the air flow rate, and hence the BMEP that can be achieved, will increase with the boost pressure. However, higher boost pressures result in an increase in the mechanical loading of the engine, because of the higher cylinder pressures involved. If the compressor pressure ratio, p_2/p_1, is increased significantly, it may be necessary to either retard the injection timing (116) or reduce the engine compression ratio, or both, to limit the peak cylinder pressure and the rate of pressure rise (which has a significant effect on the engine combustion noise). Both of these solutions will be accompanied by some penalty in Brake Specific Fuel Consumption (BSFC), due to the reduced cycle thermal efficiency. For high BMEP applications it is usually necessary to reduce the engine compression ratio according to the increase in boost pressure.

If the compression ratio is maintained at a level high enough to ensure good starting behavior, then the injection system can be designed to provide high heat release rates late in the engine cycle, thus avoiding excessively high peak cylinder pressures. However, this will result in a reduction in the thermal efficiency of the engine and an increase in the exhaust energy level. The fuel economy can be improved by using additional exhaust energy recovery systems, such as turbocompounding, Fig. 1.1d. In this case the excess turbine energy is fed to the engine crankshaft via a reduction gearbox. Conversely at low speeds and loads, when the exhaust energy level is low, energy can be transferred from the engine to the turbocharger, raising the boost pressure and therefore the engine power output, for a given A/F ratio. Alternatively the compressor and turbine can be separated, the turbine feeding all its power to the engine crankshaft and the compressor being driven directly by the engine, Fig. 1.1e. In this case the compressor and turbine are not required to run at the same speed, and the optimum gear ratio's for each component can be selected.

Reducing the engine compression ratio can lead to problems during cold starting or when running at light loads, when the boost pressure is very low for turbocharged engines. Poor ignition and retarded combustion result from excessive ignition delay, caused by the low cylinder pressures and temperatures. One solution to this problem is

to have a variable compression ratio, that will automatically change to limit the maximum cylinder pressure, and hence the mechanical loading of the engine. For example, a two piece piston can be used to vary the combustion chamber volume as a function of the peak cylinder pressure, see Fig. 1.2a, from (9). During cold starting and at light loads, the compression ratio can be as high as 22:1. As the load increases the compression ratio reduces to maintain a constant peak cylinder pressure. Once the minimum compression ratio is reached, which is of the order of 10:1, the maximum cylinder pressure will again rise with increasing load, Fig. 1.2b. However, such systems involve variations in combustion chamber geometry which may adversely affect the engine performance. A great deal of work has been done to improve the reliability of variable compression ratio systems (9,50,142,163), but the complexity and economics of such designs usually discourage their use in automotive applications (i.e. at moderate BMEP's).

A simpler solution to the problems of running at low loads is to heat the intake air and by-pass the charge air cooler, but this also involves additional complexity (85). Fig. 1.3a shows the relationship between the compression ratio, the ambient cold soak temperature and the compression temperature, from (68). The diagram also shows the fuel ignition temperature and the white smoke limit. Cold starting with a low compression ratio can be improved by heating the intake air by burning fuel in the intake manifold. Fig. 1.3b shows experimental results for cold starting a 10.8:1 compression ratio engine after cold soaking for 24 hours at 241 K (-25°F), from (68). Excellent cold starting could be achieved by proper control of the inlet manifold heater fuel flow rate. Fig. 1.3c shows the effectiveness of an inlet manifold heater in reducing unburnt hydrocarbons (white smoke).

The conventional turbocharged diesel engine is effectively a compound engine in which the work is divided between the engine itself, which handles the high pressure parts of the cycle, and the turbocharger which handles the low pressure phases. Because the turbocharger derives its power exclusively from the engine exhaust gases, its operating characteristics are linked to the engine load and speed.

The flow characteristics of the reciprocating engine and rotary turbocharger are such that there is often difficulty in achieving a satisfactory match between the two. If the turbocharger is matched at low engine speeds, it will allow an increase in low speed torque for a given engine A/F ratio (or smoke limit), and this will result in an

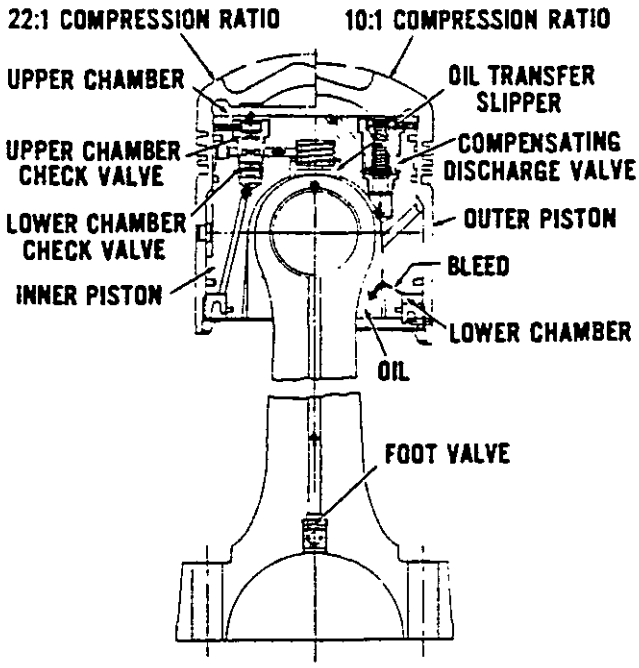

Fig. 1.2a The Essential Elements of a Variable Compression Ratio Piston.

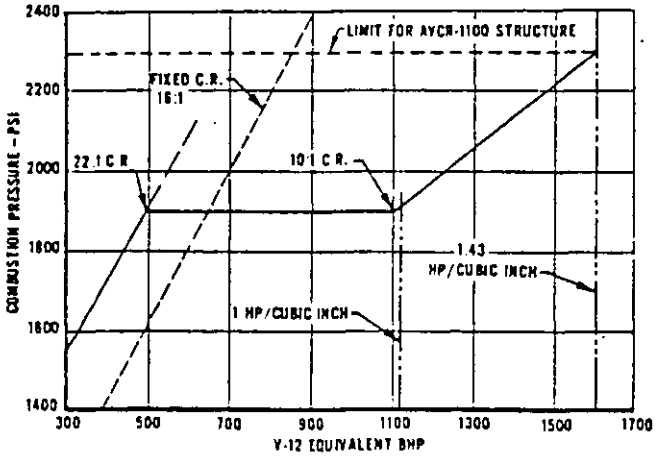

Fig. 1.2b Variation in Combustion Pressure and Compression Ratio with Engine Power.

Fig. 1.2 A Variable Compression Ratio Arrangement, from (9).

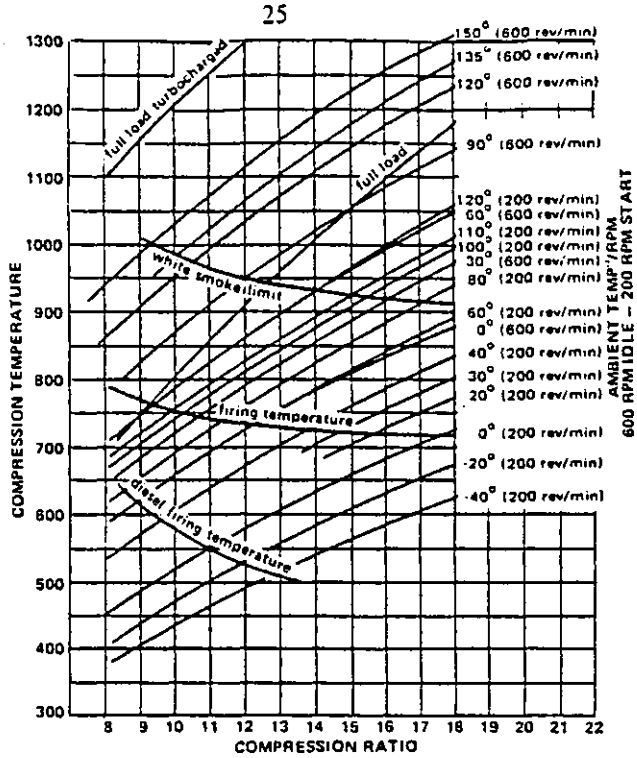

Fig. 1.3a Relationship Between Compression Ratio and Compression Temperature for Diesel Ignition, Starting and White Smoke at Various Ambient Conditions.

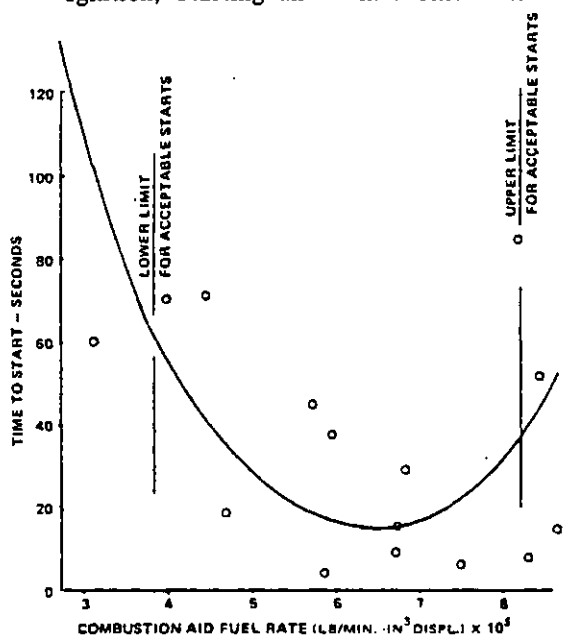

Fig. 1.3b Cold Start Characteristics of a Low Compression Ratio Engine at 247 K to 240 K With a Combustion Aid.

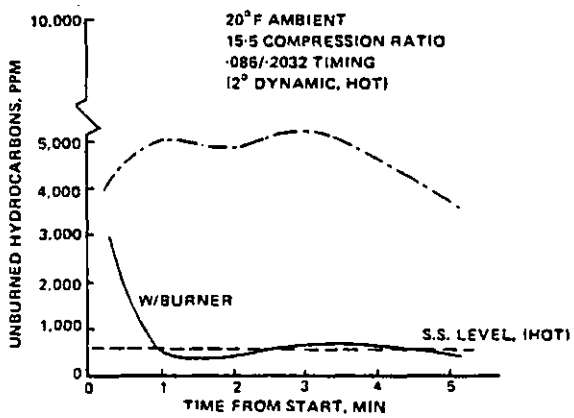

Fig. 1.3c Cold Start White Smoke Characteristics of a Diesel Engine With and Without an Inlet Air Heater.

Fig. 1.3 Effect of an Inlet Air Heater on the Cold Start Characteristics of a Low Compression Ratio Diesel Engine, from (68).

improvement in the transient response of the engine. However at higher engine speeds, the boost pressure and turbocharger speed may become excessive, which will lead to high peak cylinder pressures and mechanical loading. To a certain extent, these problems can be avoided by either restricting the speed range of the engine, or reducing the engine fuelling (and hence torque) at higher speeds (167). An alternative to restricting the maximum engine speed and/or torque is to use an exhaust wastegate, Fig. 1.4. This allows a proportion of the exhaust gas to by-pass the turbine, and so effectively controls the maximum boost pressure level (31), (this solution is usually preferred for spark ignition (SI) engine applications, where the engine speed range is relatively large and good response is essential).

If the turbocharger is matched at high engine speeds, the boost pressure at low speeds will be very low, and so the low speed torque of the engine must be reduced to avoid smoke problems. This reduction in low speed torque can cause a severe deterioration in the engine transient response and "drivability" in automotive applications. If the speed and/or load range of the engine is large the problems of achieving an acceptable match between the engine and turbocharger over the entire operating range will inevitably lead to compromises in the engine design, and possibly downrating. Many different types of turbocharging systems have been developed, such as the pulse system, constant pressure system and pulse converter systems (186), which attempt to improve the efficiency of the turbocharging systems for a given application (usually dependent on the engine rating).

Pulse turbocharging, Fig. 1.5a, is almost exclusively used on low and medium rated engines, and endevours to make use of the high gas pressure and temperature which exist in the cylinder when the exhaust valve opens. The exhaust system usually consists of a number of short pipes joining groups of one, two or preferably three cylinders to a turbine entry, so that the exhaust pulses from each cylinder do not interfere with the scavenging of the other cylinders in the group. The geometry of the exhaust system (pipe lengths, volumes and cross sectional areas) has a major influence on the efficiency of the turbocharging system. Rapid opening of the exhaust valves and a small pipe cross sectional area and volume are important requirements to minimise the throttling losses across the exhaust valve. Care must be taken not to reduce the pipe diameter below the optimum value, since the frictional losses will then exceed any benefits from the reduced pipe volume.

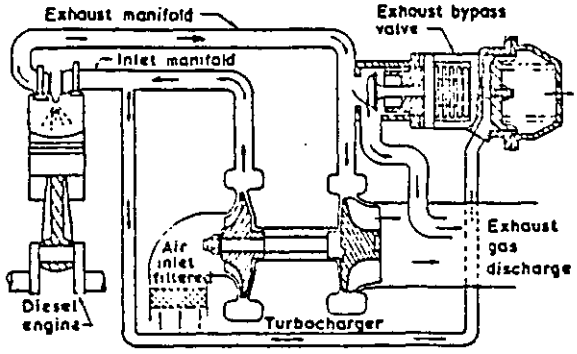

Fig. 1.4 A Turbocharged Spark Ignition Engine With an Exhaust Wastegate.

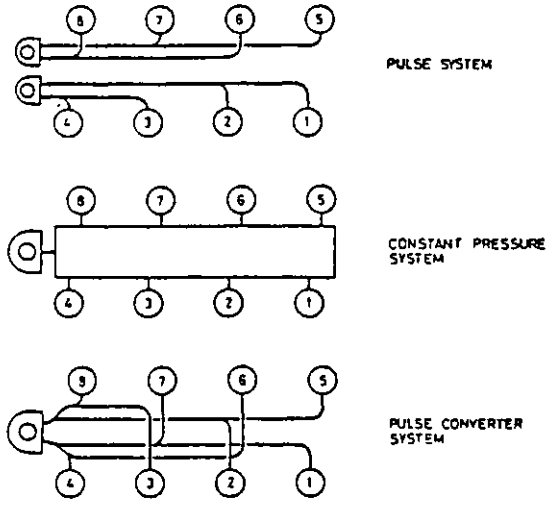

Fig. 1.5a Alternative Turbocharging Exhaust System Arrangements.

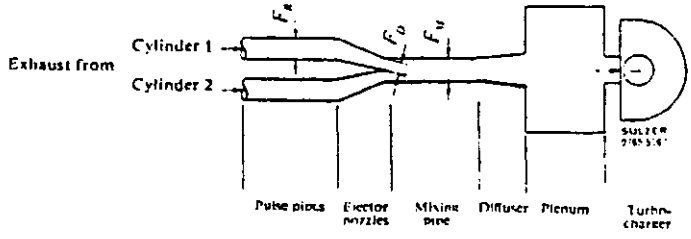

Fig. 1.5b Schematic of the Pulse Converter.

Because of the pulsating nature of the exhaust pressure, and the relatively constant turbine speed (under steady state conditions) the turbine will not operate at the optimum efficiency throughout the cycle. In addition, partial admission losses resulting from multiple entry turbines cause a further drop in turbine efficiency, due to windage and end of sector losses.

With the constant pressure system, Fig. 1.5a, all the cylinders are connected to a single large exhaust manifold. This damps out the pressure fluctuations and provides a steady pressure drop across the turbine, which can then be matched to operate at the optimum efficiency throughout the cycle. The pressure wave created during the blowdown period of each cylinder is reduced to such a level that the scavenging of the other cylinders will not be affected, and so the pulse energy is lost, to a large extent, by turbulence.

This system has the advantage of greatly simplifying the installation layout of the engine, and has been sucessfully applied to many engines, usually at high ratings, above 15 bar BMEP. However, at part load conditions the exhaust energy level will be low and so the boost pressure and scavenge pressure drop will reduce considerably. This results in an increase in the engine fuel consumption at low loads.

The pulse converter system, Fig. 1.5a, attempts to combine the advantages of both the constant pressure and pulse turbocharging systems. The cylinders are grouped together by narrow exhaust pipes as in the pulse system, but these pipes are then connected to a pulse converter junction and a single entry turbine, Fig. 1.5b. A plenum chamber and diffuser may be fitted after the pulse converter to provide a steady turbine inlet pressure, thus ensuring that the turbine operates at the optimum efficiency, as in the constant pressure system. This system relies on the pulse converter junction to prevent interference between the exhaust and scavenge periods of the various cylinders, while preserving the pulse energy available when the exhaust valve opens.

The combination of a conventional turbocharger and a tuned inlet system has been developed by Cser (33) and others (24,165), Fig. 1.6. The Helmholtz resonator inlet manifold system, is tuned to increase the inlet manifold pressure during the inlet valve periods at low engine speeds, where the boost level is low. This increases the trapped mass of air in the cylinders and allows an increase in engine fuelling, and hence torque, for a given A/F ratio. At higher speeds, there will be a reduction in the

volumetric efficiency as the pressure waves become out of phase with the inlet valve periods, but careful matching of the turbocharger will ensure that the boost pressure is high enough at high speeds to overcome this problem. This system only allows a relatively modest increase in low speed torque to be achieved, but has the advantage of requiring no additional moving parts.

The increase in engine performance that can be realised by supercharging is limited by the pressure ratio, efficiency and flow range that can be achieved using current turbomachinery. The search for higher engine power outputs has resulted in the connection of compressors in series to raise the boost pressure, and hence the engine BMEP. Two stage turbocharging, see Fig. 1.7, has been widely discussed as a method of increasing engine performance (70,93,119,141). However, the part load performance of a two stage turbocharged engine is normally inferior to that with single stage turbocharging, due to the relatively low overall efficiency of the combined turbocharging system at low loads (168,182). Experimental test results indicate that there is an improvement in the steady state engine efficiency at full load using two stage turbocharging (46). An advantage of this system is that conventional turbochargers can usually be used to produce high boost pressures without resorting to purpose built turbomachinery requiring exotic materials.

The Differential Compound Engine (DCE) has been extensively developed, notably by Wallace et. al. (149,150,156,159). In this system the engine drives the ring gear of a fully floating epicyclic gearbox. The planet carrier is geared to the output shaft which, in turn, receives a direct power input from the exhaust turbine connected by direct spur reduction gearing. The supercharging compressor is driven by the sunwheel member of the epicyclic gear train. This allows the compressor shaft to increase in speed as the output shaft slows down and the engine speed is held constant. The arrangement makes it possible for the engine to operate under optimum conditions for any given level of power demand, irrespective of the output shaft speed. This provides the basis for very high torque back up, which is the major advantage of the DCE compared to other high output turbocharging systems (161). Fig. 1.8 shows two alternative DCE systems, from (150).

The advantage of combining the engine and transmission systems are weighed against possible penalties in cost, noise, complication, fuel economy and reliability with this arrangement. The transient response of the DCE should be superior to that of

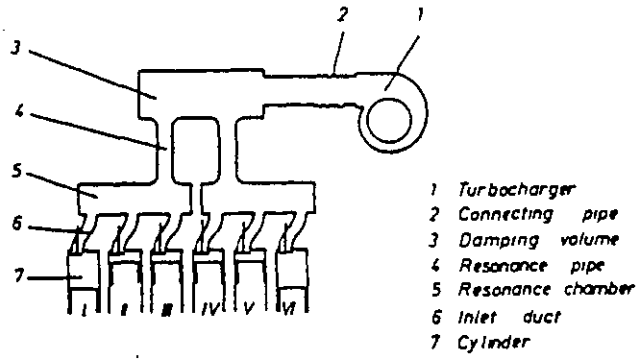

Fig. 1.6 Layout of a Helmholtz Resonator Tuned Induction System, from (33).

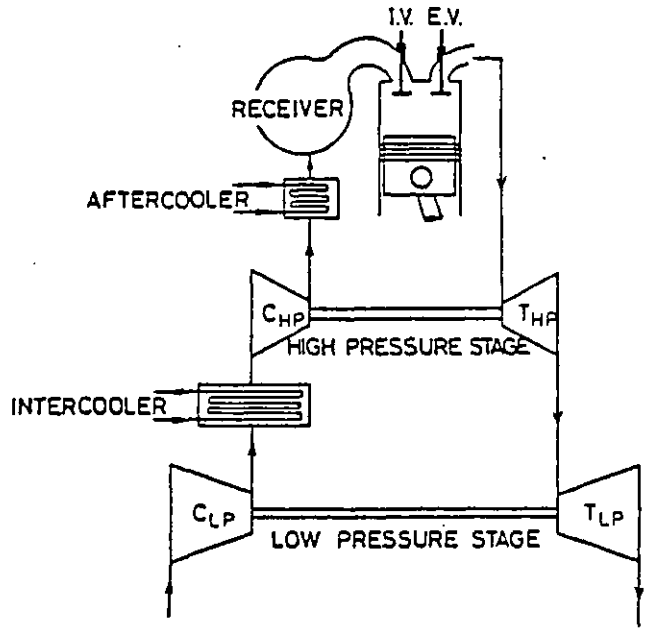

Fig. 1.7 Schematic of a Two Stage Turbocharging Arrangement.

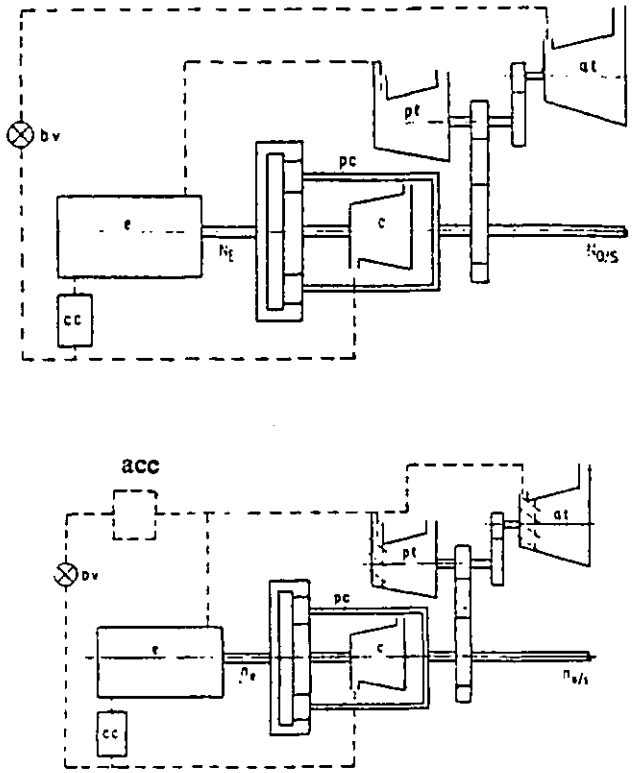

acc - auxiliary combustion chamber
at - auxiliary turbine
bv - by pass control valve
c - compressor
cc - charge cooler
e - engine
o/s - output shaft
pc - planet carrier
pt - power turbine

Fig. 1.8 Alternative Differential Compound Engine Systems, from (150).

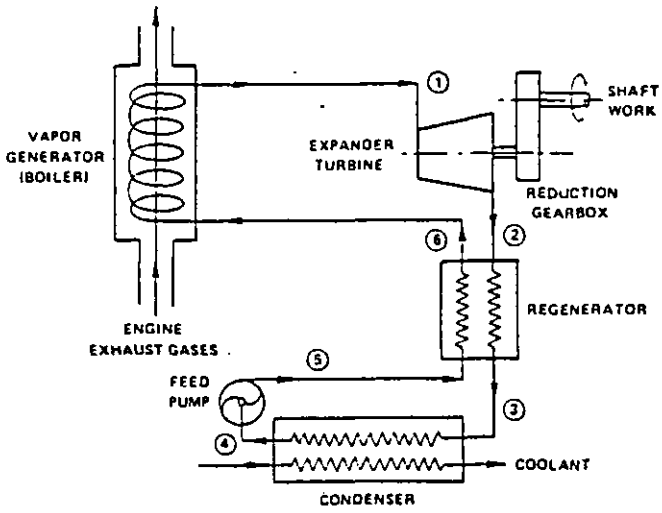

Fig. 1.9a Schematic of an Organic Rankine Bottoming Cycle.

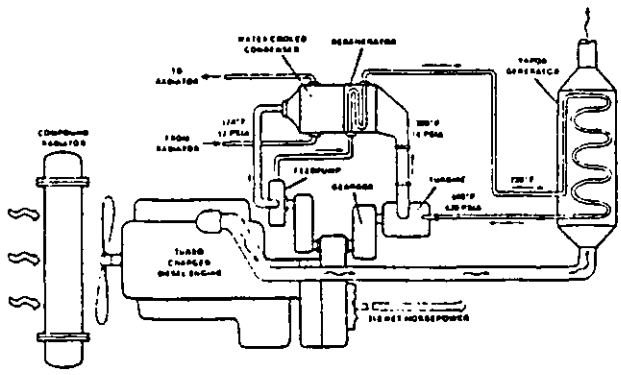

Fig. 1.9b A Diesel Organic Rankine Compound Engine for Long Haul Trucks.

Fig. 1.9 Layouts of Diesel Organic Rankine Cycles.

conventional turbocharged engines in most respects, due to the improved torque back up and flexibility of operation (157). While the potential for future development of this system is considerable (155), its complexity must be considered as a serious disadvantage.

An alternative method of recovering some of the exhaust gas energy available after the turbocharger turbine is to use a "Bottoming Cycle". Fig. 1.9a shows a schematic of an organic Rankine Bottoming system which can be used to recover as much as 20% of the base diesel engine power from the exhaust gas energy. This system is probably most cost effective for engines with high-duty load factors, e.g. marine diesel engines (which have a large, low temperature heat sink readily available). Fig. 1.9b shows a similar schematic for a diesel organic Rankine compound engine for long haul trucks, however for vehicle applications, the temperature drop available for the Rankine Bottoming Cycle is low, and this severly restricts its efficiency (82).

Logical developments of this philosophy results in the "Adiabatic Turbocompound engine with a Rankine Bottoming Cycle", suggested by Kamo and Bryzik (69), Fig. 1.10. Insulated combustion chamber and exhaust system components are used to reduce the heat energy lost to the coolant, while a second turbine is geared to the engine crankshaft to recover some of the additional exhaust gas energy that is produced, Fig. 1.10a. Some of the remaining exhaust energy can be recovered using a Rankine Bottoming Cycle, Fig. 1.10b, but the temperature difference between the exhaust gas and the heat sink will be relatively small, limiting the power that can be produced. Further developments are aimed at reducing the engine frictional losses by using a gas lubricated piston ring and liner combination, unlubricated ceramic roller bearings for the gudgeon pin and crankshaft, and solid lubricant coatings for the gears, valve guides and rocker arm assemblies. However the various practical considerations associated with the use of ceramics in the hostile environment presented by the internal combustion engine, pose a number of challenging problems (172). Components manufactured from partially stabilized Zirconia (PSZ) have the required high strength at high temperatures, good insulating properties, low coefficient of expansion and low cost. Alternative materials such as Silicon Carbide (SiC) and Silicon Nitride (Si_3N_4) have also been considered. Fig. 1.10c shows the proposed design of an engine using ceramic and composite materials.

The Brown-Boveri "Comprex" (34,49,123) is a mechanically driven supercharger which

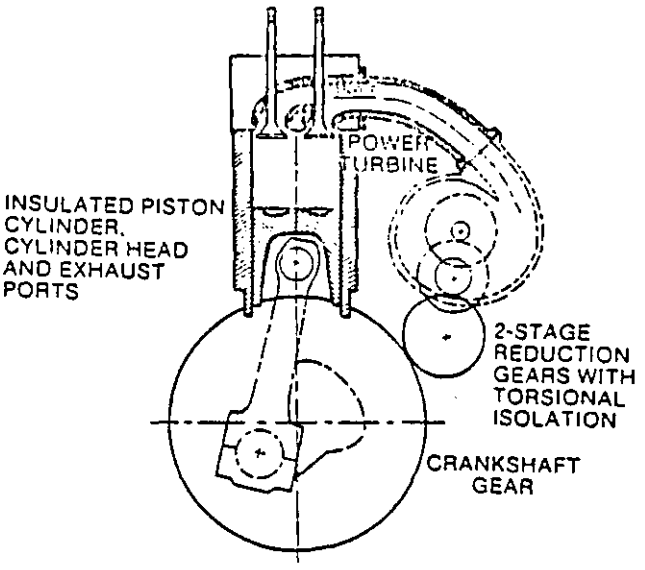

Fig. 1.10a Cummins Adiabatic Turbocompound Engine.

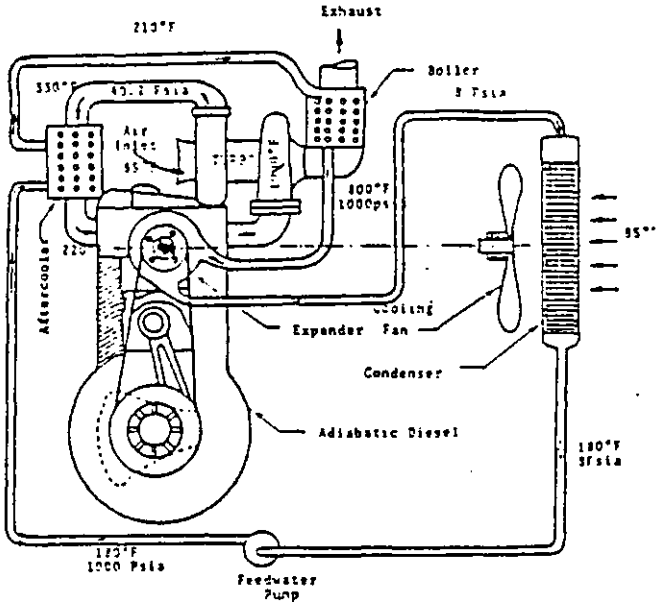

Fig. 1.10b Schematic of an Adiabatic Diesel Engine with a Rankine Bottoming Cycle.

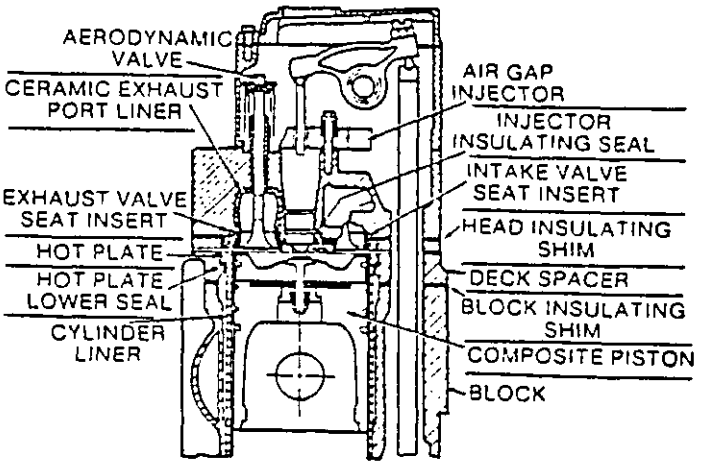

Fig. 1.10c Cross Section of the Cummins Insulated Diesel Engine.

Fig. 1.10 Cummins Total Energy Recovery System, from (69).

transfers energy directly from the exhaust gas to the inlet air, via pressure waves generated by the sudden opening of ports at the ends of pressure exchange cells. These cells are formed in the annular space of a cylindrical rotor, driven by the engine crankshaft, Fig. 1.11. The principal advantage of the "Comprex" system is its ability to produce greater boost than a turbocharger at low engine speeds (18,152). The transient response of a diesel engine using the "Comprex" supercharger is significantly better than that using a turbocharger due to the faster energy transfer between the exhaust gas and the inlet air (138). Careful rotor design has considerably reduced the noise levels of the "Comprex" supercharger to acceptable levels. The "Comprex" is at present limited to a pressure ratio of around 3:1, and so design effort is concentrating on small high speed passenger car applications (37,72).

Different types of variable geometry compressor and turbine arrangements have also been proposed. These devices attempt to modify the characteristics of the turbomachine as the engine operating conditions change, in order to optimise the overall efficiency of the system.

Attempts have been made to increase the flow range of centrifugal compressors by varying the inlet prewhirl either mechanically using movable guide vanes (160) or aerodynamically using recirculated compressor air flow (76). Movable vane diffusers have also been reported to improve the surge margin of the compressor (19,55). These devices will not improve the low speed boost if the turbine energy is low, but may allow the engine fuelling to be increased slightly without surging the compressor. Air injection into the compressor has also been used to improve the response of the turbocharger to rapid changes in engine speed and/or load (79,80). The degree of improvement in compressor performance using these methods is encouraging, but is usually insufficient for most automotive applications.

Increasing the available turbine energy by varying the effective turbine area, using movable guide vanes at the turbine inlet (19) has been widely developed. This allows a relatively large reduction in the effective turbine area, which results in a significant increase in boost pressure. Unfortunately there will be some loss in "off-design" efficiency, but this can be reduced by careful design (115). Other methods of varying the effective turbine area have been proposed (40,153,165), but none of these have reached the production stage at the time of writing.

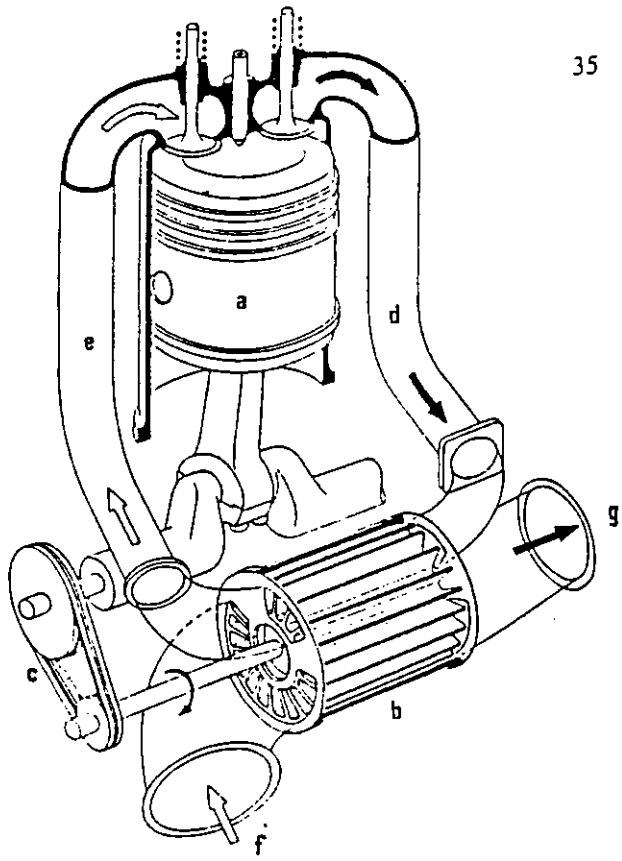

a ENGINE
b CELL WHEEL (ROTOR)
c BELT DRIVE
d HIGH PRESSURE GAS (G-HP)
e HIGH PRESSURE AIR (A-HP)
f LOW PRESSURE AIR (A-LP)
g LOW PRESSURE GAS (G-LP)

Fig. 1.11a Schematic of the Engine and Comprex Supercharger Arrangement.

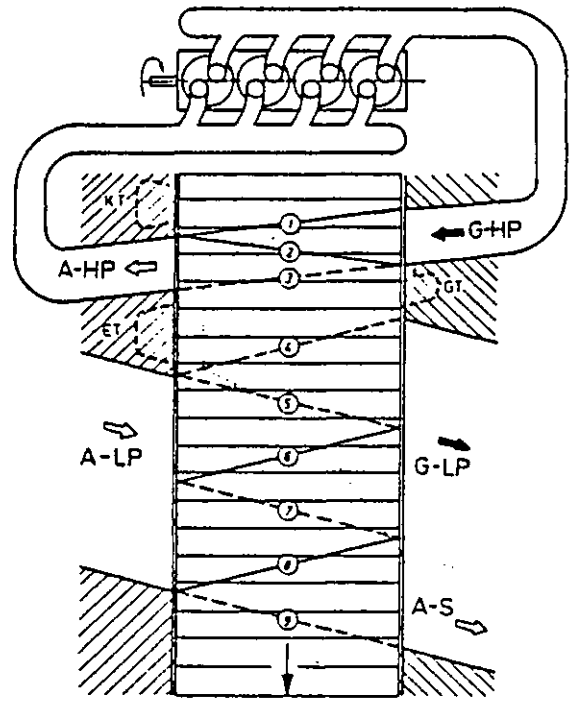

A - AIR G - GAS S....SCAVENGING
HP (LP).... HIGH (LOW) PRESSURE
KT GT ET ..... POCKETS

Fig. 1.11b Unrolled View of the Comprex Pressure Wave Process.

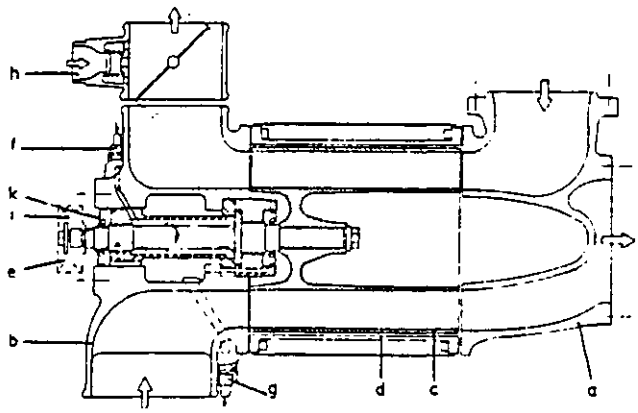

a GAS CASING
b AIR CASING
c ROTOR
d JACKET
e SHAFT
f OIL INLET
g OIL OUTLET
h COLD START VALVE
i PULLEY
k SHAFT SEAL

Fig. 1.11c Longitudinal Section of the Comprex Supercharger.

Fig. 1.11 The Brown Boveri Comprex Supercharger, from (34).

Various methods of increasing the energy available to the turbocharger system have also been proposed. The system described by Timoney (142) used a small Pelton wheel drive on the turbocharger shaft to accelerate the turbocharger when required, and this eliminated the need for a scavenge blower on the two stroke engine tested, Fig. 1.12. High pressure oil was used to drive the Pelton wheel, and so a separate oil pump and control system was required. A similar method of improving the turbocharger response has been proposed by Holzhausen et. al. (58), Fig. 1.13. In this case a separate compressor was driven by a small oil powered turbine, when extra air was required by the engine, for example during rapid accelerations or load applications.

The Hyperbar turbocharging system (97) has been developed to allow the work division between the engine and the turbocharger to be varied independently of the engine operating conditions, Fig. 1.14. There is no mechanical link between the engine and turbocharger, instead an Auxiliary Combustion Chamber (ACC) is located in the exhaust system before the turbine. This allows the turbine energy (and hence the boost pressure) to be varied independently of the engine speed and load. The fuel burnt in this ACC is mixed with air taken from the compressor outlet. The compressor operating conditions are further regulated by using a by-pass system that allows the proportion of the total compressor flow that passes through the engine to be controlled, by diverting some of the air directly to the turbine.

The Hyperbar system allows high engine torque to be developed at any engine speed, and ensures that the compressor is always operating in the high efficiency region of the map. The very high boost pressures that can be developed with this system, and the narrow compressor flow range required and high compressor efficiency that can be achieved using the by-pass, ensure that high BMEP's can be developed (in the range 20-25 bar) with single stage turbocharging.

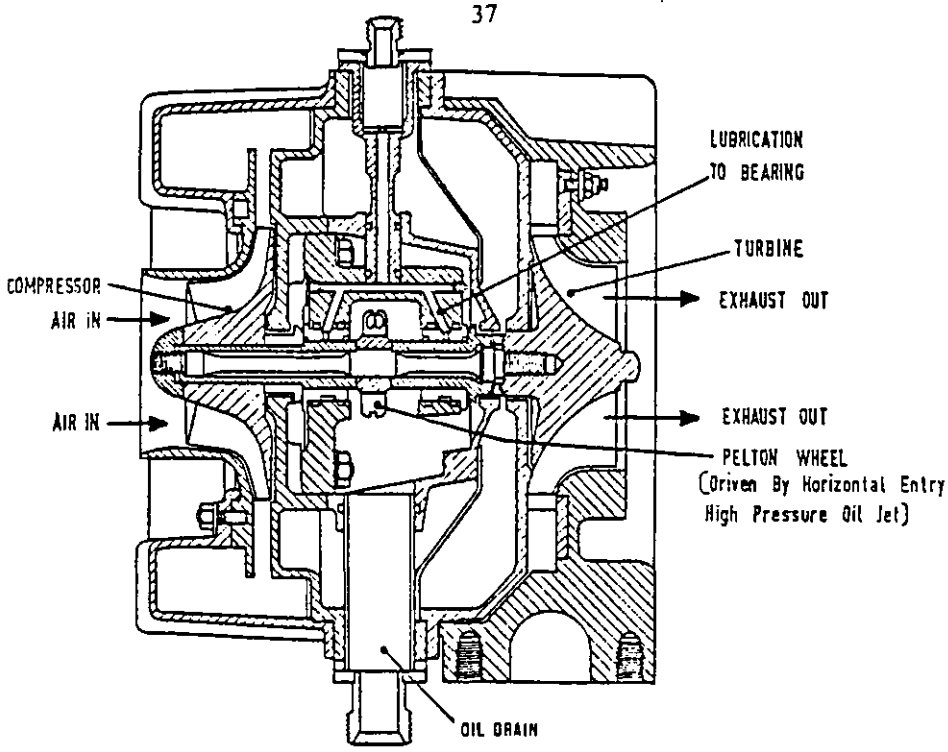

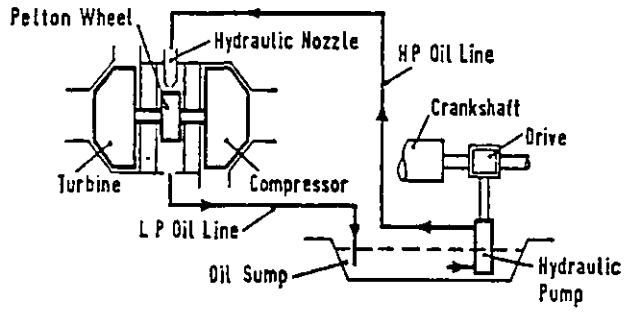

Fig. 1.12 Pelton Wheel Drive for a Turbocharger, from (142).

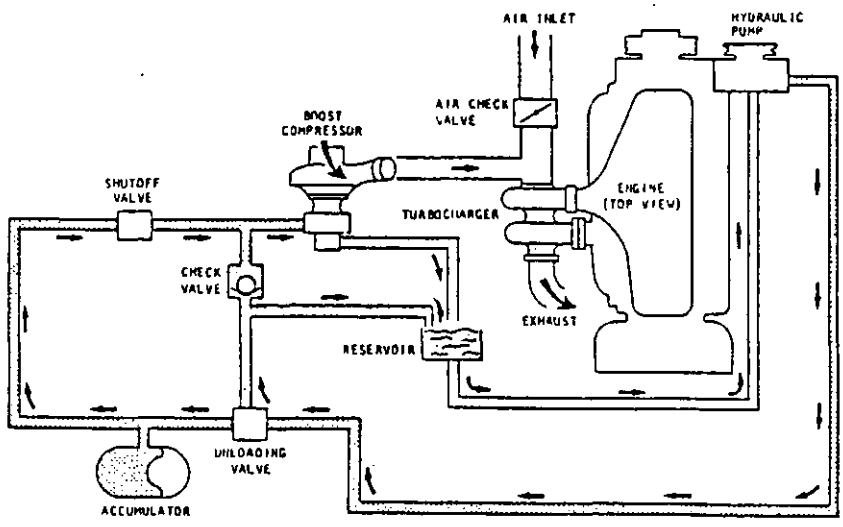

Fig. 1.13 Hydraulic Boost Compressor System, from (58).

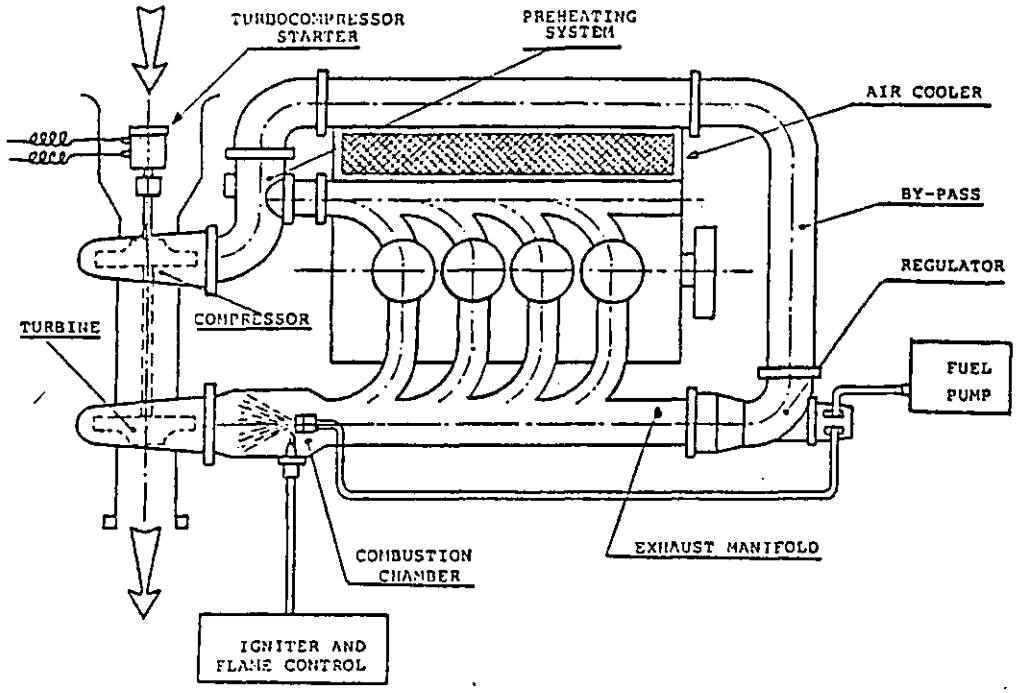

Fig. 1.14 The Hyperbar System, from (97).

1.2 Objectives of this Project.

The objectives of this work may be stated as follows :-

(1) To develop a mathematical simulation model for the Hyperbar turbocharging system operating with a four stroke, direct injection, compression ignition engine.

(2) The model is to be a development of an existing "filling and emptying" simulation program (89,166), and must be capable of predicting both the steady state and transient performance of the engine and turbocharging system.

(3) The mathematical model of the various systems unique to the Hyperbar system, for example, the by-pass valve and Auxiliary Combustion Chamber, should be based on the fundamental operating principles of the particular components, and should allow the effects of design changes on the performance of the component, and the system, to be assessed.

(4) The accuracy of the model in predicting the performance of an existing engine should be assessed, and the model should then be used to predict the effects of various design changes to the system on the steady state and transient performance of the engine.

(5) Based on the results from the simulation model to make suggestions for the future development of the system.

1.3 Outline of the Present Work.

The Hyperbar turbocharging system is at an early stage of its development. Relatively little has been published about the design and performance of the system. The present work has set out to develop a detailed mathematical model of Hyperbar type systems applied to conventional four stroke, direct injection, diesel engines. A comparison of the engine performance predicted by the model with steady state experimental test data allows the accuracy of the model to be assessed. Having developed a reliable model, it can then be used to investigate the importance of changes in design parameters of the system on the steady state and transient performance of the engine. The report then recommends possible avenues for future development of the system.

In Chapter 2 the development of the Hyperbar system up to the present time is outlined. Experimental test results presented by various authors are discussed, together with typical applications of the Hyperbar system. The requirement for efficient high pressure ratio turbochargers is stressed. Only one mathematical model of the Hyperbar system is known to the author, and this uses relatively simple models for the principal components in the system, and so cannot readily predict the effects of design changes. This model cannot accurately predict the transient response of an engine using the Hyperbar turbocharging system, due to the simplifications inherent in it.

The fundamental principles on which the Hyperbar turbocharging system operates are described in Chapter 3. The principal design parameters are discussed and their influence on the overall performance of the system is demonstrated. Control of the compressor operating line is an essential feature of the system, and methods of achieving this are described. Finally the potential of the system is discussed.

The mathematical simulation model used to predict the performance of the engine and turbocharging system is described in Chapter 4. The fundamental energy and mass continuity equations used to describe the behavior of the gases in the "filling and emptying" control volumes are given.

Individual component models for valve flows, heat transfer, engine frictional losses, volume changes, etc. are described. The combustion process is modelled using an

Apparent Fuel Burning Rate (AFBR) model based on extensive experimental test data recorded by the engine manufacturer, on a similar engine. The turbocharger characteristics have been estimated using what experimental test data was available. Models have also been developed for an automotive type two speed governor and an isochronous type governor, used in electricity generating applications.

Detailed models are developed for the by-pass valve and the Auxiliary Combustion Chamber, which are the components that control the operation of the Hyperbar engine.

A comparison of experimental and predicted engine performance over the speed and load range is given in Chapter 5. This shows the ability of the mathematical model to predict the overall effects of load and speed changes on the engine performance. Details of the results predicted using the model are also analysed.

The model is then used to predict the effect of changing various design parameters on the steady state engine performance. In Chapter 6 the effect of the exhaust system pressure losses, by-pass valve area ratio and control pressure, Auxiliary Combustion Chamber fuelling characteristics, minimum boost pressure level, compression ratio, and injection timing are studied. The part load engine performance at one engine speed, 1200 rpm, is analysed and the results used to decide how the system can best be used to improve the engine performance (low speed torque). Maximum torque curves are presented with and without the burner operating, and a method for optimising the burner fuelling is described. Various engine performance limiting parameters are considered when optimising the engine and burner fuellings, such as the peak cylinder pressure, engine A/F ratio, exhaust gas temperatures and smoke. Finally the overall engine efficiency characteristics are presented.

Having studied the steady state engine performance the model is then used to compare the transient response of the Hyperbar turbocharged engine with a two stage turbocharged version of the same engine, at the same rating. Chapter 7 compares the experimental and predicted response of the two stage turbocharged engine to verify the accuracy of the model. Propeller law accelerations and sudden load application tests are used to compare the response of the two engines. The effect of design changes such as turbocharger inertia, burner fuelling level, engine compression ratio and minimum boost pressure level, and ACC damping on the response of the Hyperbar

engine are demonstrated.

Suggestions concerning the future development of the Hyperbar turbocharging system, based on the results of this work, are discussed in Chapter 8. Electronic governing of the engine and turbocharging system using an on-board, microprocessor based, system is seen as the best way of ensuring that the Hyperbar engine remains competitive with other high output diesel engine systems. In particular, the need for optimising the total BSFC of the engine system is stressed. Methods of improving the accuracy of the mathematical model are also discussed.

Chapter 9 discusses the conclusions of this work and assesses the degree to which its objectives have been achieved.

CHAPTER 2

DEVELOPMENT OF THE HYPERBAR SYSTEM

2.1 Introduction.

The Hyperbar turbocharging system was originally developed in France for powering an AMX tank and has been designed and patented by Melchior and Andre-Talamon (95,96,98,99,100,101). The fundamental principles of the system have been described by Melchior (94,97), Kunberger (75) and others (192) and will be described in detail in Chapter 3. A more detailed description of the major components of the system (i.e. the by-pass valve and Auxiliary Combustion Chamber burner) has been given by Andre-Talamon (1,2) and will be discussed in Chapter 4.

Many elements of the Hyperbar system have been proposed previously. In 1939 Rateau (135) proposed a controlled air to exhaust by-pass, the advantages of which were discussed by Zinner (188) in 1965. In 1946-8 Nettel (107) suggested low compression ratio, combustion chambers for part load operation. However it is the development of high pressure ratio, high efficiency turbochargers over the last 10 years, and the requirement for high BMEP diesel engines, that have encouraged the development of this system.

2.2 Experimental Tests Using the Hyperbar Turbocharging System.

Melchior and Andre-Talamon (97) have reported results of applying the Hyperbar turbocharging system to the Poyaud 6L-520 engine (and a V8 version) and the SACM AGO-240.

The Poyaud 6L-520 engine (89) is normally rated at 6.73 bar BMEP naturally aspirated, 8.08 bar BMEP turbocharged and 11.11 bar BMEP turbocharged and aftercooled, at the maximum engine speed of 2500 rpm. Using the Hyperbar turbocharging system the output has been raised to 20.20 bar BMEP with single stage turbocharging, and 25.25 bar BMEP with two stage turbocharging, at the same

maximum engine speed.

For the single stage turbocharged Hyperbar system, using a Brown Boveri RR150 turbocharger, it was necessary to reduce the engine compression ratio to 9.18:1 (compared to 15.0:1 in the naturally aspirated form and 13.9:1 turbocharged and aftercooled). The two stage turbocharged version was equipped with a Brown Boveri RR180 turbocharger for the low pressure stage, and a RR150 for the high pressure stage. The compression ratio was reduced to 6.82:1 in the two stage form and, using an aftercooler and an intercooler the maximum overall compressor pressure ratio was 6.5:1, compared to 5:1 for the single stage version.

The increase in performance was achieved without increasing the exhaust manifold gas temperature above that of the standard engine (turbocharged and aftercooled), i.e. 873 K, or the maximum cylinder pressure above 140 bar.

For the 6L-520 Hyperbar engine, operation of the ACC was required over the entire speed range at low loads to maintain good ignition conditions. At low speeds the burner operation was required at low loads to maintain the minimum boost pressure level, and at high loads to achieve good torque back up. Because of the additional turbine energy supplied by the burner, the speed range of the turbocharger was reduced, (varying between the maximum speed at the rated point, and half speed at engine idling) which enabled an improvement in the engine transient response to rapid load changes to be achieved. In addition, the compressor was always operating in the high efficiency region of the map. The penalty for this improvement in performance was a 3.3% and 10.1% increase in the total BSFC at the maximum engine power for the single and two stage turbocharged engines respectively, when compared with the turbocharged aftercooled version. Details of the engine performance are discussed in Chapter 6, and shown in Figs. 6.27 and 6.28.

Further test results using the Poyaud 6 and 8 cylinder engines are given by LeMerer (83) and LeMerer and Tord (84). Fig. 2.1 shows typical arrangements for the Hyperbar turbocharging system on an in-line 6 cylinder engine and a V8 engine, from (83). Fig. 2.2 shows the engine performance for the Poyaud V8 520 S3 Hyperbar engine rated at 588 kW at 2500 rpm (20.2 bar BMEP), from (83). The diagram shows lines of constant BMEP ranging from 10 to 20 bar and lines of constant BSFC from 190 g/ch.hr (0.258 kg/kW.hr) to 165 g/ch.hr (0.224 kg/kW.hr). The

corresponding brake thermal efficiencies ranging from 38.3% to 33.26% are calculated using a calorific value for the fuel of 41912 kJ/kg. Fig. 2.3 shows the performance of the same engine rated at 882 kW at 2500 rpm (30.3 bar BMEP). Again values of BSFC ranging from 200 g/ch.hr (0.272 kg/kW.hr) to 168 g/ch.hr (0.229 kg/kW.hr) and the corresponding brake thermal efficiencies are shown.

Experimental tests have also been reported for a 6 cylinder in-line AGO 240 engine, using a two stage turbocharged Hyperbar system with intercooling and aftercooling (97). This engine is normally rated at 16.33 bar BMEP at 1350 rpm. By reducing the compression ratio from 13.1:1 to 7.0:1 the output of the Hyperbar version was raised to 28.85 bar BMEP at the same speed. There was an increase of 5.6% in engine BSFC, but no figures for the increase in total BSFC at maximum power were quoted. No increase in the maximum cylinder pressure limit was necessary with a compressor pressure ratio of 7.3:1.

The MTU MT40H672 engine (193) also uses the Hyperbar turbocharging system to increase its power output. Intended for use in high speed naval craft where the total weight and bulk of the engine system is paramount, the increased thermal efficiency of a diesel engine, when compared to an equivalent gas turbine, is a critical factor, particularly if a great deal of part load operation is required. The 40 cylinder I form engine has had its compression ratio reduced from 13:1 to 12:1, and the peak cylinder pressure was limited to 106 bar, the same as the conventionally turbocharged version. Four turbochargers were positioned on the top of the engine, each pair delivering the charge air through a common aftercooler to the manifolds of one 20 cylinder bank, so that each half of the engine was completely independent. Each pair of turbochargers had its own ACC and by-pass valve. For starting there was also provision for the charge air to by-pass the aftercooler.

A 20 cylinder Hyperbar engine has been tested rated at 19.3 bar BMEP at 1700 rpm. Following satisfactory tests a 40 cylinder version will be tested rated at 19.3 bar BMEP initially, and then 23.3 bar BMEP at 1700 rpm. In addition to increasing the specific output of the 40H672 engine the Hyperbar system is claimed to improve the engine acceleration, without exceeding the smoke limits, and also offers the possibility, when driving controllable pitch propellers, of increasing the torque developed at low speeds. Despite the reduction in thermal efficiency caused by the necessity of burning extra fuel in the ACC, the Hyperbar system is expected to offer a distinct increase in

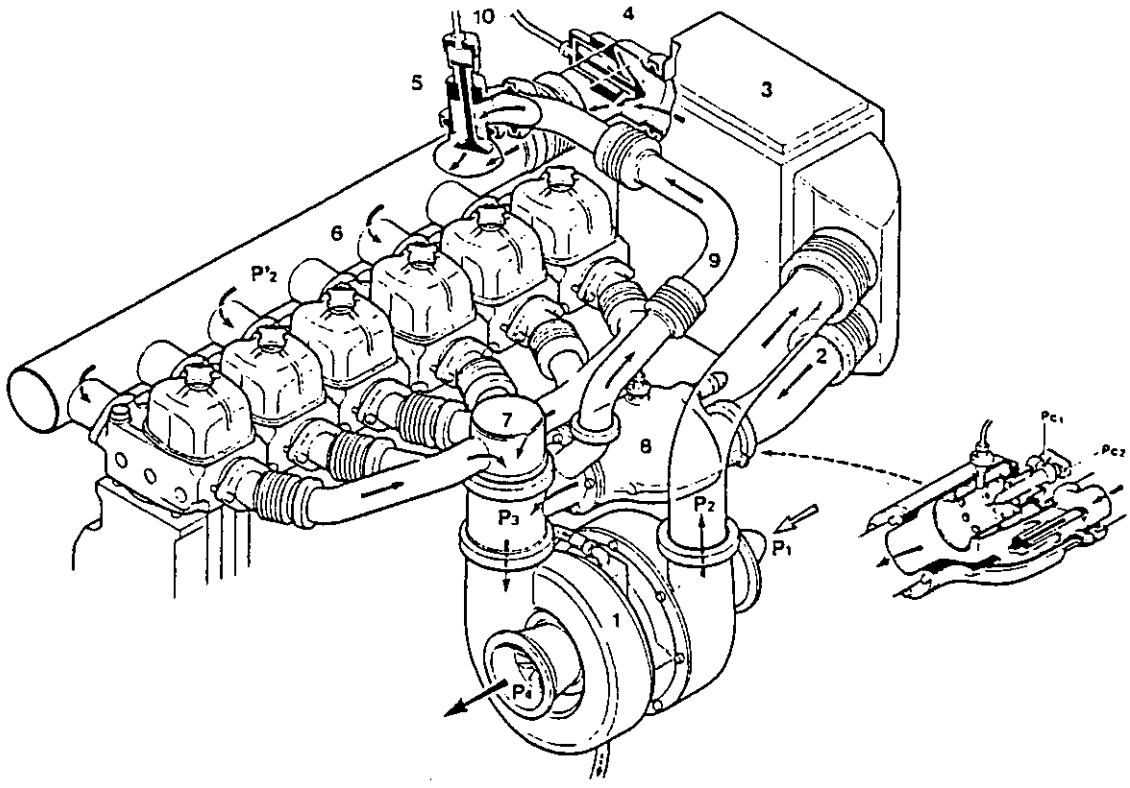

1. Turbocharger
2. Air Inlet to the Auxiliary Combustion Chamber
3. Charger Cooler
4. By-Pass Valve
5. Inlet Air Heater Valve
6. Inlet Manifold
7. Mixer
8. Auxiliary Combustion Chamber
9. Exhaust Recirculation Pipe
10. Control Valve Pressure Line

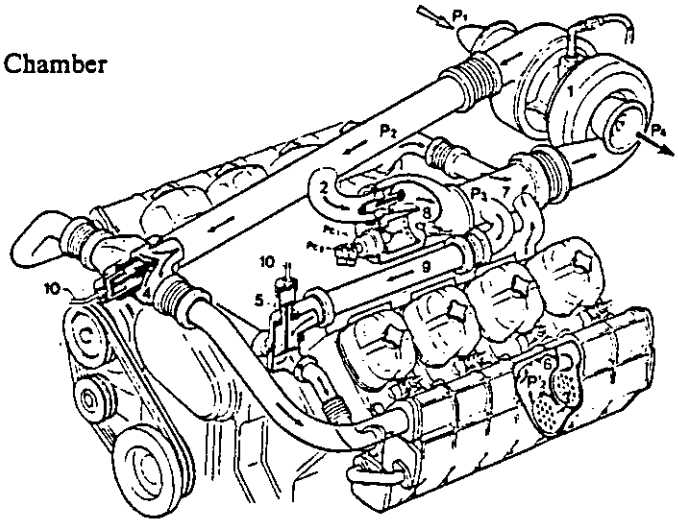

Fig. 2.1 Layout of Hyperbar Turbocharging Arrangements for a 6 Cylinder In-Line and a V-8 Engine, from (83).

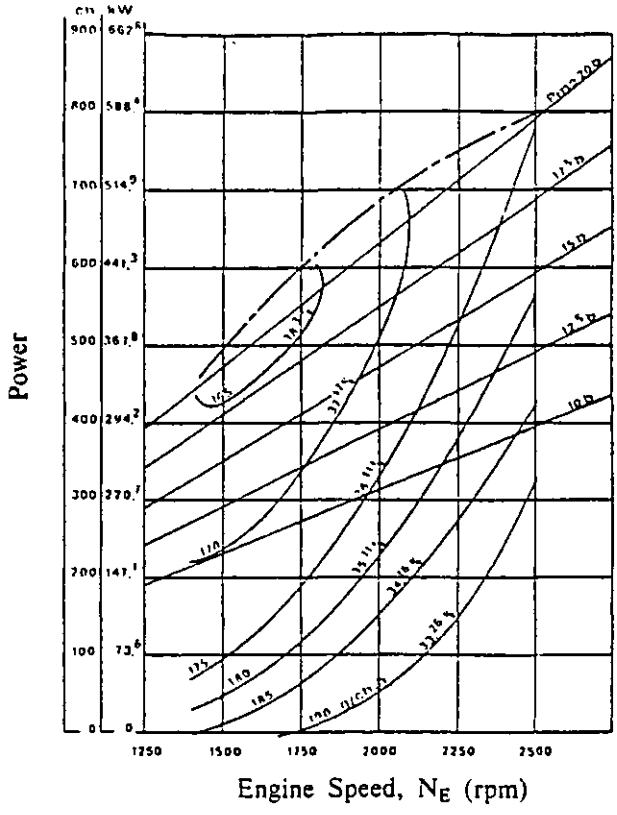

Fig. 2.2 Experimental Performance of the Poyaud V8 520 S3 Hyperbar Engine Rated at 20.2 bar BMEP at 2500 rpm, from (83).

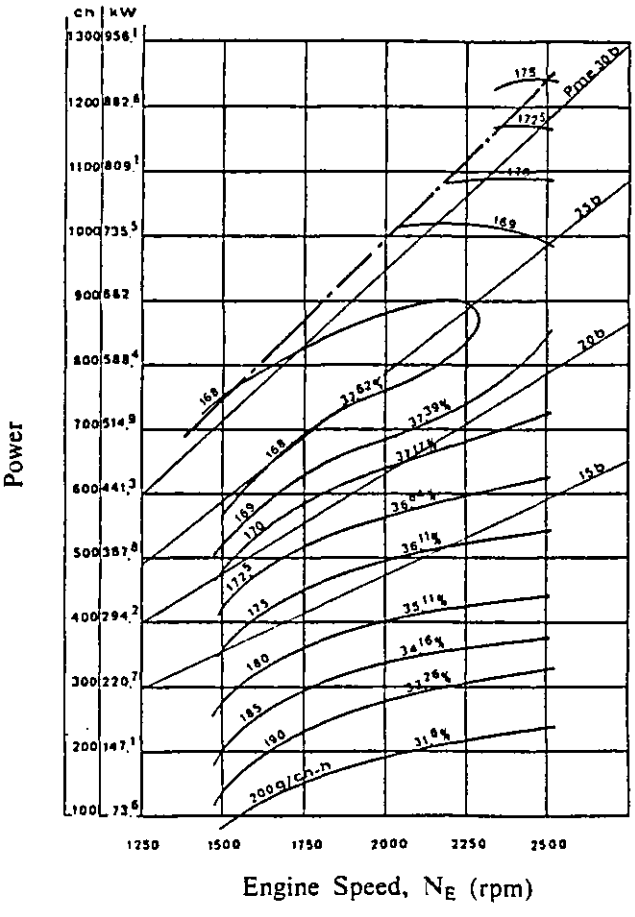

Fig. 2.3 Experimental Performance of the Poyaud V8 520 S3 Hyperbar Engine Rated at 30.3 bar BMEP at 2500 rpm, from (83).

overall efficiency compared to gas turbine installations of similar output.

The first firm to release a Hyperbar turbocharged engine for regular service was Société Surgerienne de Constructions Méchaniques (SSCM), now part of the SACM group. Over 8000 hours of test bed operation were accumulated on the Poyaud 520 V8 Hyperbar engine rated between 20.2 and 30.3 bar BMEP at 2500 rpm. This compares with the naturally aspirated rating for this engine of 5.1 bar BMEP and the turbocharged, aftercooled version of 10.1 bar BMEP, again at 2500 rpm.

Duflot (35) has described tests undertaken by the French Railways (SNCF) using the Poyaud 520 Hyperbar engine, rated at 20.2 bar BMEP at 2500 rpm, installed in a lightweight long-distance passenger train (RGP X2730). These trains were originally fitted with the SACM type MGO V12 ASH engine rated at 8.9 bar BMEP at 1500 rpm. A considerable weight saving was achieved by using the Hyperbar engine, which weighed 1350 kg, compared to 4600 kg for the MGO engine. The specific weight of the power unit was therefore reduced from 7.58 kg/kW to 2.29 kg/kW. The Hyperbar engine was 1.69 m long, compared to 2.26 m for the MGO engine, which allowed ample space for the inclusion of a speed reduction gear to suit the input speed of the Mekhydro hydro-mechanical transmission. The overall specific volume was reduced from $8.76.10^{-3}$ to $4.58.10^{-3}$ m^3/kW.

After a period of testing, the train powered by the Poyaud Hyperbar engine entered service in November 1977 between Paris and LeTouquet. The Hyperbar version of the X2730 required no special treatment and was found to behave like the other RGP trains. The starting sequence was automatic, taking 40-50 seconds from cold, and was unaffected by low ambient temperatures (exhaust gas from the ACC burner being used to heat the intake air when required). The Hyperbar engine should itself be well adapted to the rapid and frequent load changes encountered during operation, and the response was found to be better than the MGO powered unit. By September 1978, the X2730 had accumulated 96000 km, and 1350 hours service.

The service fuel consumption of the Hyperbar engine proved to be 10% higher than that of the MGO engine, whilst the specific fuel consumption at the rated point was 8.7% higher (0.238 kg/kW.hr compared to 0.219 kg/kW.hr). Lubricating oil consumption was found to be 0.42% of the fuel consumption.

Relatively small intake air silencers were used to attenuate the increased noise caused by the higher air flow rates, which was found to be excessively high during starting.

The higher specific output of the Hyperbar engine should enable either higher track speeds from trains of the same weight and capacity, or greater passenger capacity at the same speed. In both cases, the earning capacity of the train is increased, and the fuel consumption per passenger-km is reduced. There should also be some reduction in the unit capital cost of the same power.

2.3 Turbochargers.

Operation using the Hyperbar system is dependent upon the availability of high pressure ratio compressors and turbines. Early work reported by Melchior using the Poyaud 520 engine of 10.48 litres swept volume was carried out using a single stage Schwitzer modified Holset 5LF turbocharger, capable of pressure ratio's of up to 4.8:1 (189). The turbocharger was started up using a compressed air turbine acting on a bucket wheel.

Later tests were carried out using a Microturbo TCS14 turbocharger, which incorporated a declutchable electric starter motor and was capable of achieving boost pressures of up to 5 bar (191).

A Brown Boveri RR150 turbocharger, capable of pressure ratio's of up to 5:1 has been tested on the Poyaud engine (97), and a two stage turbocharged version of this engine, using the RR180 turbocharger for the low pressure (LP) stage and the RR150 for the high pressure (HP) stage, has also been tested. Fig. 2.4 shows a cross section of the RR turbocharger and typical pressure ratio-flow ranges for different size machines.

The Poyaud 520 V8 S3 engine described by Duflot (35), of swept volume 13.97 litres, used a larger Microturbo TCS16 turbocharger which can supply an air flow rate of up to 1.6 kg/s at a pressure ratio of 3.9:1.

The Microturbo TCS range of turbochargers employ an integral electric starter motor (190) which allows the turbocharger to be run as a small gas turbine independently of

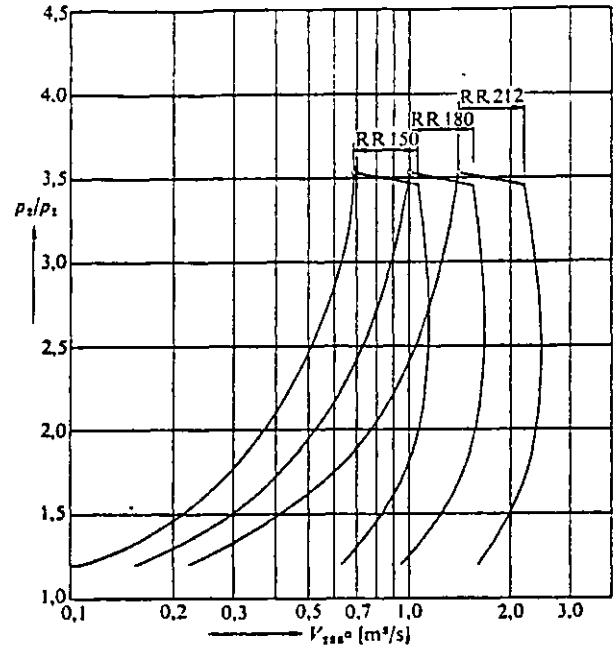

Fig. 2.4a Typical Pressure-Volume Range of the Type RR Turbochargers.

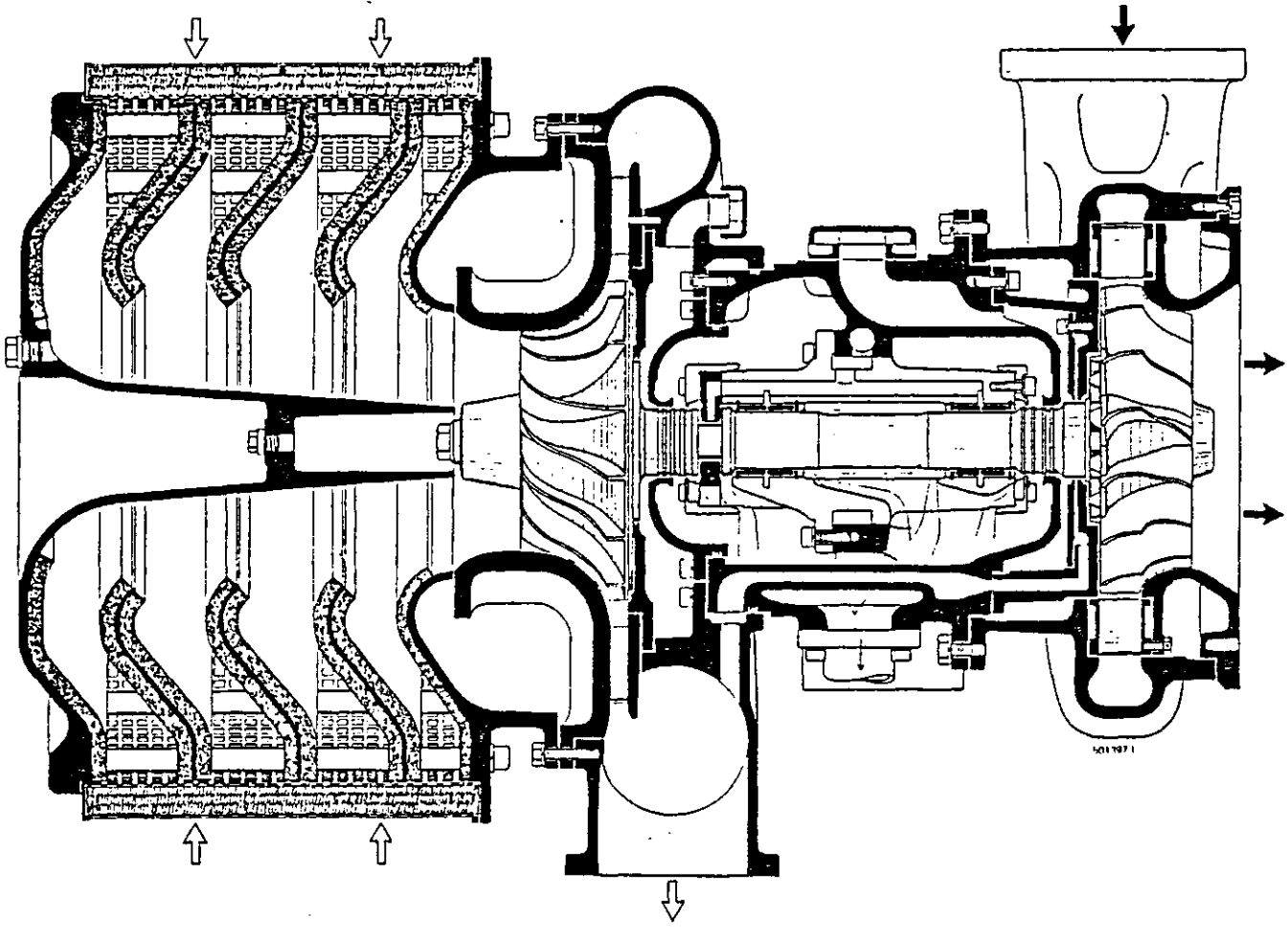

Fig. 2.4b Cross-Section Through an RR Turbocharger.

Fig. 2.4 The Brown Boveri RR Turbocharger.

the diesel engine. A larger turbocharger unit is being developed to suit Hyperbar applications by Turbomeca (194). The TM307 is capable of producing pressure ratio's of up to 7.9:1 using a two stage axial compressor followed by a single stage radial compressor. The single shaft turbocharger uses a two stage axial turbine and is capable of handling air flow rates of up to 2.5 kg/s. At the compressor end is a 5 kW starter/generator and a fuel pump used to feed the Hyperbar ACC, see Fig. 2.5.

2.4 Hyperbar System Modelling.

Wallace and Winkler (161) have compared three different turbocharging systems designed to achieve high power output, high torque back up, good economy and emissions characteristics, without exceeding conventional operating limits (cylinder pressure, exhaust temperature, turbocharger speed and smoke). Using the Poyaud 520 diesel engine (189) in the following configurations:-

(1) Two stage turbocharged.

(2) The Hyperbar system.

(3) The Differential Compound Engine.

Wallace and Winkler have developed a simulation model capable of predicting both steady state and transient engine performance, based on earlier work (177). Their model assumed that the closed cycle period can be divided into four distinct portions (compression, constant volume and constant pressure combustion, and expansion) while allowances were made for heat dissipation to the coolant. During the open cycle period allowances were made for valve timing, the engine pressure drop characteristics, pumping work and a simplified pressure pulse formation model was used in the exhaust system. The turbocharger compressor was represented by numerical arrays giving the compressor flow field in terms of the pressure ratio, dimensionless mass flow, dimensionless speed and isentropic efficiency. The turbine characteristics were calculated using a one-dimensional model for the stator and rotor, with allowances for passage, incidence and leaving losses. The various component models representing individual parts of the system were linked together by "flow" or "storage" components (which were used to represent the effects of mass and energy storage).

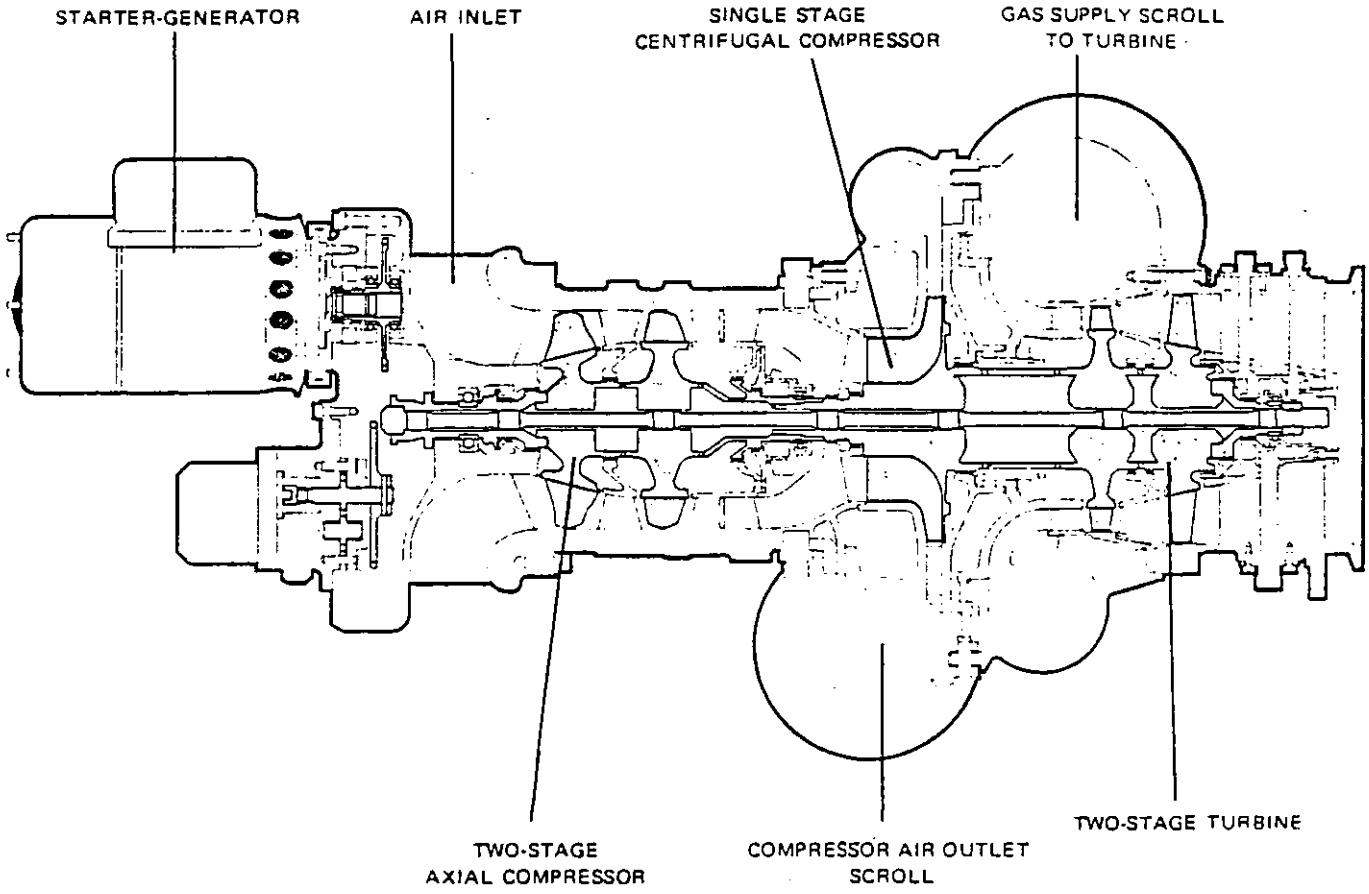

Fig. 2.5 The Turbomeca TM 307 Turbocharger.

In the case of the Hyperbar simulation, the program was matched to give a good agreement with experimental test data for the Poyaud 520 engine, published by Melchior and Andre-Talamon (97). The by-pass system flow area and fuel flow rate were varied according to the test condition. Fig. 2.6 shows the Hyperbar engine performance predicted over the load and speed range of the engine, showing lines of constant brake thermal efficiency and the calculated thermal efficiencies at each test condition.

The engine performance was predicted at engine speeds of 2500, 2000, 1500 and 1000 rpm and loads of 21, 15, 10 and 5 bar BMEP. At each test condition the by-pass flow area and ACC fuelling rate were varied to maintain the engine A/F ratio close to the design point value of 31:1. Fig. 2.6 also indicates the range of engine operation over which the burner is required. Wallace and Winkler found that the speed range over which burner assistance was required to maintain the air flow rate (or minimum boost pressure level) increased as the load reduced, so that at 5 bar BMEP some burner assistance was required over the entire speed range.

At the design point 2500 rpm/21.0 bar BMEP a reasonable agreement between experimental and predicted engine performance was achieved, but lack of sufficiently detailed models of the by-pass and burner systems led to significant errors in the by-pass flow rate (-72.2%), total compressor flow rate (-13.5%), burner fuelling rate (+40.0%), mean exhaust manifold gas temperature (+22.7%) and turbine inlet temperature (+15.5%).

They concluded that due to the need to employ by-pass system burning over a wide range of conditions at both high and low BMEP's the thermal efficiency falls off rapidly with decreasing speed at high BMEP's, and with both speed and load at low BMEP's. The best efficiency predicted for the system was slightly in excess of 34%, which occured in the speed range between 1500 and 2500 rpm and at loads of between 15 and 20 bar BMEP, where the minimum burner assistance was required.

A comparison of the torque and efficiency characteristics of the Hyperbar engine with the two stage turbocharged and Differential Compound systems, Fig. 2.7, showed that the Hyperbar system was capable of producing the maximum BMEP over its entire operating speed range. The torque for the two stage turbocharged version was limited

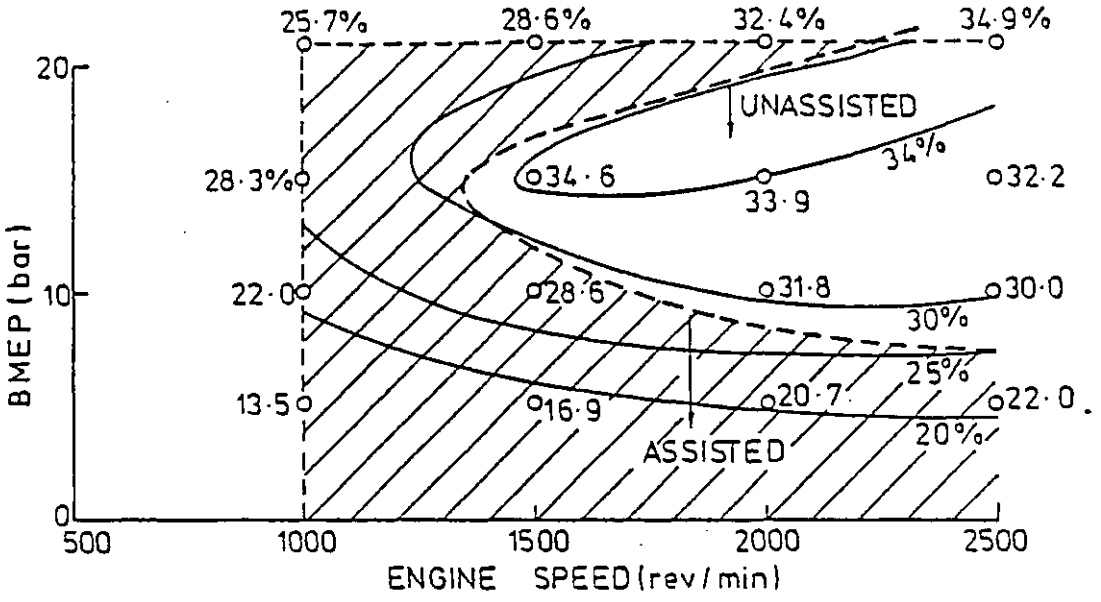

Fig. 2.6 The Predicted Hyperbar System Performance, from (161).

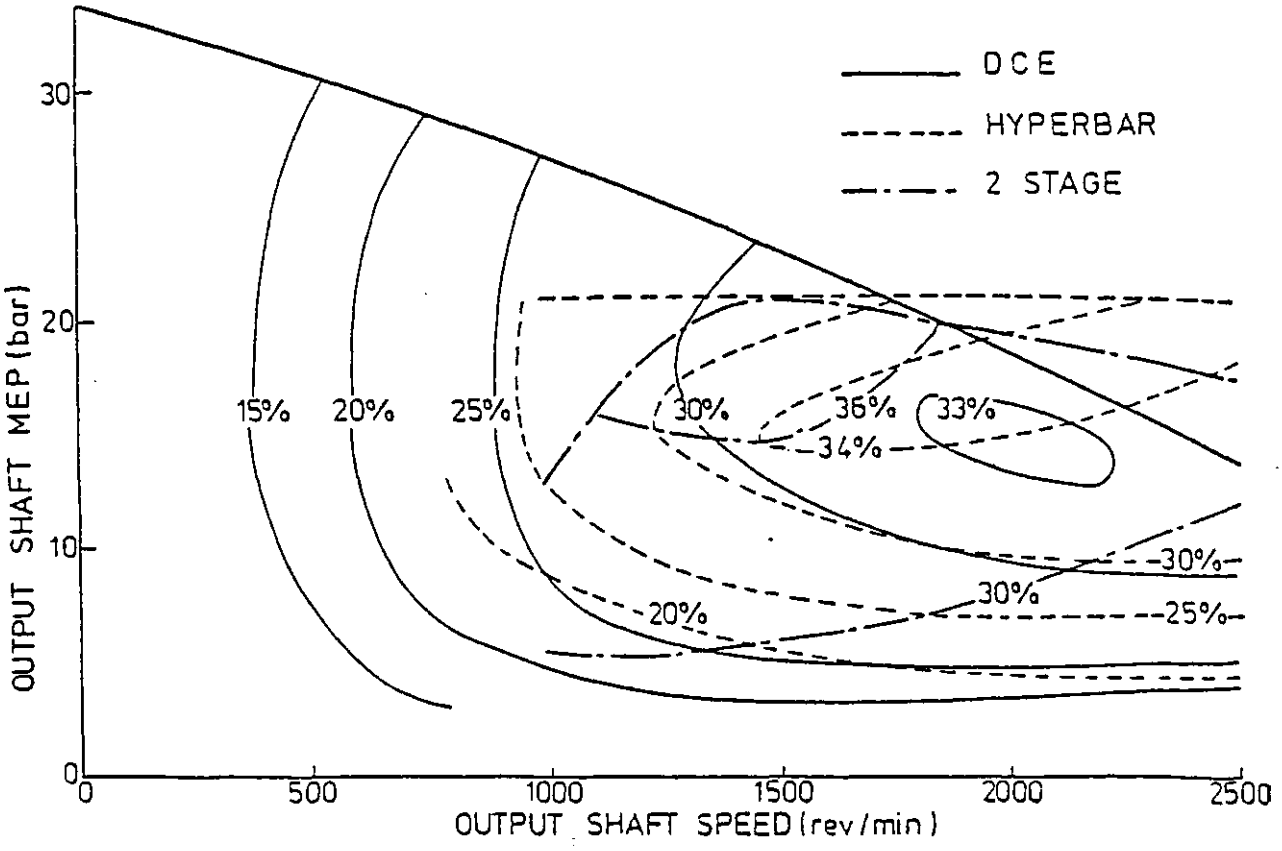

Fig. 2.7 Comparative Performance Maps for the Two Stage Turbocharged, Hyperbar and Differential Compound Engines, from (161).

by smoke at low speeds (where the air flow was limited) and by peak cylinder pressure at high speeds (due to the higher geometric compression ratio). The DCE, by contrast, produced less torque at its maximum output shaft speed than either of the other engines, but had a continuously rising torque down to its stall condition.

The two stage turbocharged version, however, was clearly the most efficient power unit, with peak thermal efficiencies of the order of 37.6% at maximum torque, and greater than 30% over the majority the speed range at loads above 5 bar BMEP, (the efficiency reducing with increasing engine speed at constant load). The DCE produced a peak efficiency of 33.4% at 2000 rpm/15 bar BMEP and was, in general, more efficient than the Hyperbar engine except when the burner fuelling was at the minimum level.

It would appear that the Hyperbar model developed by Wallace and Winkler was not sufficiently detailed to be able to simulate design changes to either the by-pass or burner systems (except by specifying different by-pass valve flow areas and ACC fuelling rates), and was not capable of predicting the transient response of the Hyperbar system, because of the need to specify the by-pass area and ACC fuelling at each test condition. In addition the models rely on a great deal of empirical information, for example, in the combustion, scavenging, exhaust system pulses and gas exchange models, which limits its generality, and therefore its usefulness as a design tool.

At the time of writing, however, the model described by Wallace and Winkler is the only attempt to simulate the Hyperbar system that is known to the author.

CHAPTER 3

FUNDAMENTAL PRINCIPLES OF THE HYPERBAR SYSTEM

3.1 Introduction.

In this chapter, the fundamental thermodynamic relationships that govern the steady state operation of the turbocharger in a turbocharged, charge cooled, compression ignition (CI) engine are described.

The basic principles that allow the Hyperbar system to control the turbocharger operating point throughout the speed and load range of the engine are also outlined.

The operation of the by-pass valve and Auxiliary Combustion Chamber (ACC), together with their control systems and operating characteristics are introduced.

The ways in which the Hyperbar turbocharging system can be used to improve the performance of conventional diesel engines, without increasing the thermal or mechanical loading of the engine, and its potential advantages and disadvantages are also described.

3.2 Controlling Parameters for the Turbocharger.

Fig. 3.1 shows diagramatically the basic configuration of a turbocharged, charge cooled, diesel engine. In order to simplify the analysis, the following assumptions have been made:-

(1) The turbocharger is operating under steady state conditions, i.e. the compressor mass flow rate, $\dot{m}_c$, the turbine mass flow rate, $\dot{m}_t$, and the turbocharger speed, N_{tc}, are constant.

(2) The compressor inlet pressure, p_1, inlet temperature, T_1, and the turbine outlet pressure, p_4, are fixed.

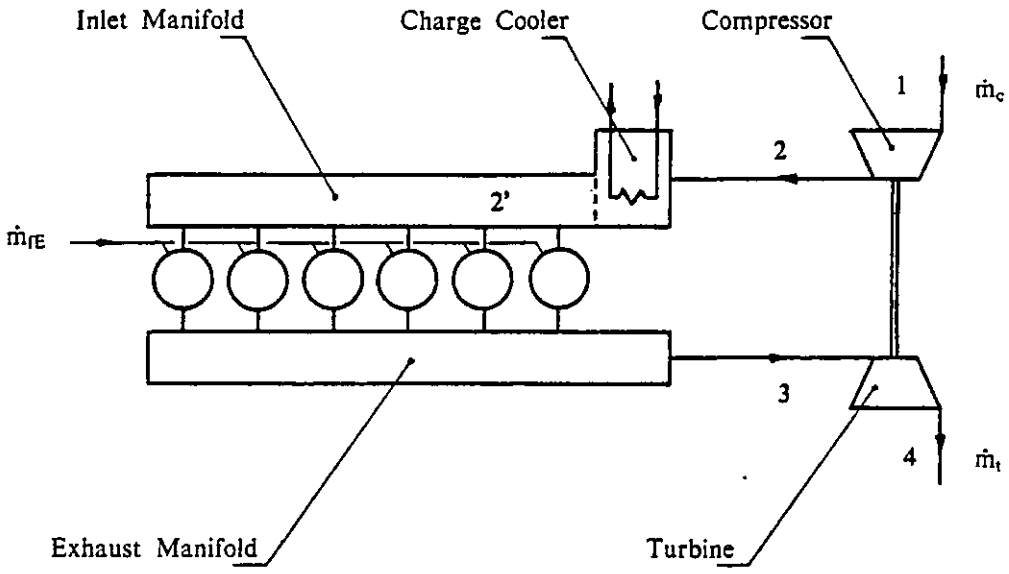

Fig. 3.1 Schematic of a Turbocharged Diesel Engine.

(3) The gas properties for air (R_a, c_{pa}, γ_a, μ_a) and for the exhaust gases (R_e, c_{pe}, γ_e, μ_e) are constant.

(4) Reynolds Number ($(p.N_{tc}.D^2)/(R.T.\mu)$) effects are small, and can be neglected.

(5) The gas pressures and temperatures at the compressor outlet, p_2 and T_2, and the turbine inlet, p_3 and T_3, are steady.

Using these assumptions, dimensional analysis gives the following relationships:-

$$f_1\left(\frac{\dot{m}_c.\sqrt{T_1}}{p_1}, \frac{p_2}{p_1}, \frac{N_{tc}}{\sqrt{T_1}}\right) = 0 \qquad (3.1)$$

$$f_2\left(\eta_c, \frac{p_2}{p_1}, \frac{N_{tc}}{\sqrt{T_1}}\right) = 0 \qquad (3.2)$$

$$f_3\left(\frac{\dot{m}_t.\sqrt{T_3}}{p_3}, \frac{p_3}{p_4}, \frac{N_{tc}}{\sqrt{T_3}}\right) = 0 \qquad (3.3)$$

$$f_4\left(\eta_t, \frac{p_3}{p_4}, \frac{N_{tc}}{\sqrt{T_3}}\right) = 0 \qquad (3.4)$$

Equations (3.1) and (3.2) define the relationship between the compressor mass flow parameter, $\dot{m}_c.\sqrt{T_1}/p_1$, the isentropic efficiency, η_c, the pressure ratio, p_2/p_1, and the speed parameter, $N_{tc}/\sqrt{T_1}$. Equations (3.3) and (3.4) define similar relationships for the turbine. The isentropic efficiency of the turbine, η_t, can also be expressed in terms of the blade speed ratio, U/C, and therefore eqn. (3.4) may appear as:-

$$f_5\left(\eta_t, \frac{U}{C}, \frac{N_{tc}}{\sqrt{T_3}}\right) = 0 \qquad (3.5)$$

The power supplied by the turbine under steady state operating conditions, P_t, must be equal to the power required by the compressor, P_c, plus the frictional losses, P_F. The turbocharger energy balance can therefore be expressed as:-

$$\frac{T_3}{T_1} = \frac{\left(\frac{\dot{m}_c}{\dot{m}_t}\right)\left(\frac{c_{pa}}{c_{pe}}\right)\left(\frac{1}{\eta_c\eta_t\eta_m}\right)\left[\left(\frac{p_2}{p_1}\right)^{(\gamma a-1)/\gamma a} - 1\right]}{\left[1 - \left(\frac{p_3}{p_4}\right)^{(1-\gamma e)/\gamma e}\right]} \qquad (3.6)$$

The turbocharger operation is therefore determined by 5 equations, eqns. (3.1), (3.2), (3.3), (3.4) or (3.5), and (3.6) in 7 parameters:-

$$\frac{\dot{m}_c \cdot \sqrt{T_1}}{p_1} \; , \; \frac{p_2}{p_1} \; , \; \frac{N_{tc}}{\sqrt{T_1}} \; , \; \eta_c \; , \; (\eta_t \cdot \eta_m) \; , \; \frac{T_3}{T_1} \; , \; \frac{p_3}{p_1} \qquad (3.7)$$

(assuming that $\dot{m}_t/\dot{m}_c$ is fixed, i.e. that the overall A/F ratio is constant). This leaves two independent parameters which must be defined in order to solve these equations.

Fig. 3.2 shows a typical match between a conventional automotive turbocharged (non-aftercooled) diesel engine and the turbocharger compressor, taken from data presented by Marzouk (89). The Leyland 520 series automotive diesel engine (134) was rated at 9.02 bar BMEP at 2500 rpm. Fig. 3.2 shows lines of constant engine speed and the maximum torque curve measured for this engine.

The ratio of the maximum to minimum engine mass flow rate, in this example, is 3.7:1, but may be much higher, depending upon the level of supercharging, and whether or not the engine is charge cooled. The flow range of the centrifugal compressor decreases as the pressure ratio increases, and is limited by the surge line and the maximum allowable turbocharger speed or choking of the compressor. For this compressor, the ratio of maximum to minimum flow decreases from 5.5:1 at a pressure ratio of 1.4, to 2.0:1 at $p_2/p_1 = 2.0$. These ratio's are further reduced if a safe surge margin (the distance between the engine operating line and the surge line) is required.

This makes it difficult to match the engine and compressor flow characteristics. In particular, Fig. 3.2 shows how the low speed boost pressure (and therefore torque for a given A/F ratio) is limited by the compressor surge line, while at high engine speeds the compressor is forced to operate in regions of decreasing efficiency, or is limited by the turbocharger speed. It is also evident that very little boost pressure is produced at the lowest engine speed, 1000 rpm, and the compressor pressure ratio may even become less than 1.0 at very low loads.

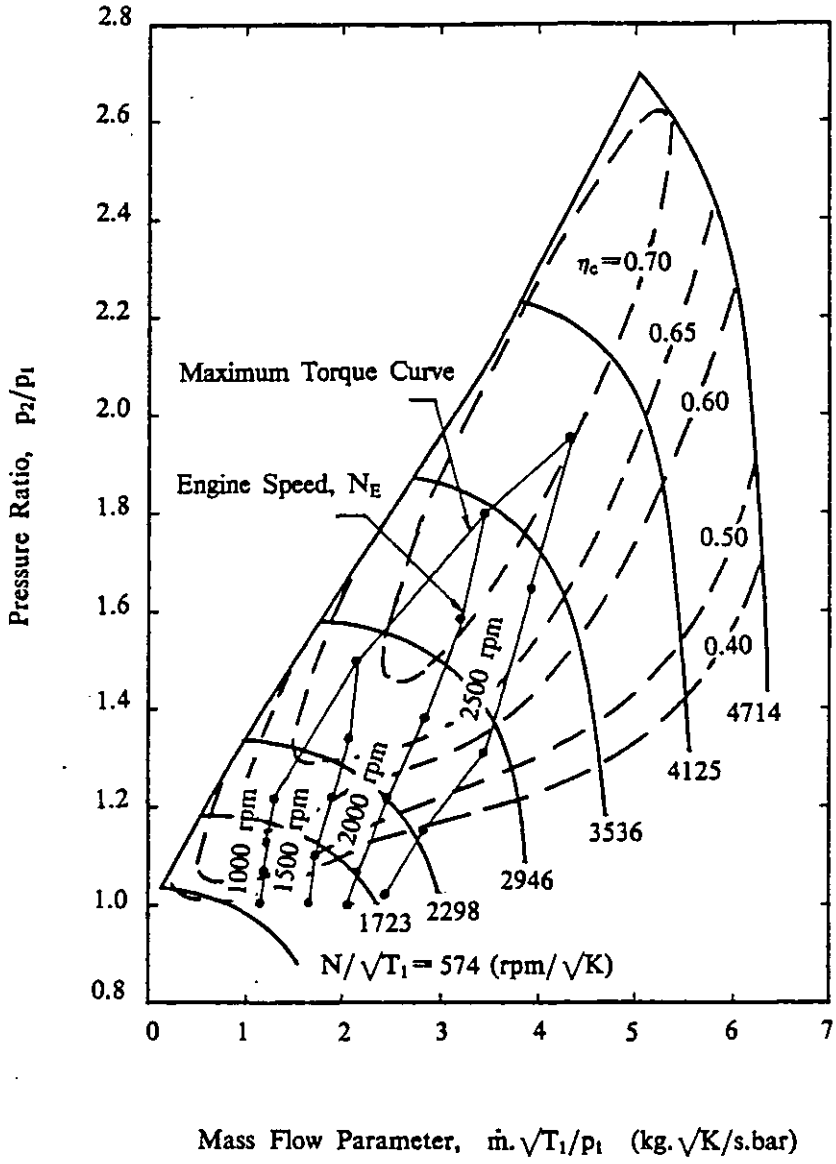

Fig. 3.2 A Typical Compressor Match for an Automotive Turbocharged Diesel Engine, from Marzouk (89).

3.3 The Hyperbar System.

The Hyperbar system attempts to derive an additional relationship between the 7 parameters that control the operation of the turbocharger, eqn. (3.7). In this way a unique solution to the operating point of the turbocharger can be found by defining one independent parameter. This allows, for example, the compressor operating point to be defined as a function of the pressure ratio, p_2/p_1, only, rather than the pressure ratio and speed parameter, $N_{tc}/\sqrt{T_1}$, or the flow parameter, $\dot{m}_c.\sqrt{T_1}/p_1$, in conventional turbocharging configurations.

Once a unique operating line for the system is defined, the engine and turbocharger system design can be optimised so that, for example, the compressor is always operating at peak efficiency for a given engine speed and load.

A practical relationship between one or more of the 7 parameters given in eqn. (3.7) is therefore required. One possible solution is to fix one of the parameters, however, a suitable method of operating the engine with, for example, the compressor pressure ratio held constant may not be practical.

The simplest of these parameters to control are the compressor and turbine pressure ratio's, therefore a relationship may be derived of the form:-

$$f_6\left(\frac{p_2}{p_1}, \frac{p_3}{p_1}\right) = 0 \qquad (3.8)$$

3.3.1 Gas Turbine Operating Line.

The simplest form of relationship for eqn. (3.8) is:-

$$\frac{p_2}{p_1} = \frac{p_3}{p_1} \qquad (3.9)$$

In this case the compressor pressure ratio, p_2/p_1, and turbine expansion ratio, p_3/p_4, are equal (for $p_1 = p_4$). This can be achieved by connecting a duct between the

compressor outlet and turbine inlet, which maintains the pressures equal ($p_2=p_3$), Fig. 3.3.

The turbocharger then behaves somewhat like a gas turbine, with the engine acting as the combustor, and the operating region on the compressor map shown in Fig. 3.2 is reduced to a unique line. This can then be arranged to lie in the area of optimum compressor efficiency, i.e. close to the surge line.

This solution, eqn. (3.9), causes a number of problems, however, because there will always be a pressure loss across the charge cooler (which acts as a flow restriction), and therefore the engine inlet pressure, $p_{2'}$, will always be lower than the exhaust pressure, p_3. The negative scavenge pressure drop has a number of adverse effects on the engine performance, namely:-

(1) Poor scavenging of the residual products of combustion during the valve overlap period.

(2) Higher cylinder metal temperatures (thermal loading), due to insufficient cooling scavenge flow through the cylinder during valve overlap.

(3) Higher pumping work, due to the exhaust manifold pressure always being greater than the inlet manifold pressure.

(4) Uncontrolled recirculation of the exhaust gases.

3.3.2 Throttled By-Pass Duct.

An alternative solution to that proposed in section 3.3.1 is to throttle a by-pass duct connecting the compressor outlet to the turbine inlet. This ensures that the compressor delivery pressure, p_2, is always higher than the turbine inlet pressure, p_3. If the pressure drop across the duct is kept sufficiently large, then a positive scavenge pressure drop across the engine can be maintained, irrespective of the charge cooler pressure loss.

In the Hyperbar system, the by-pass duct is throttled by means of a pneumatically

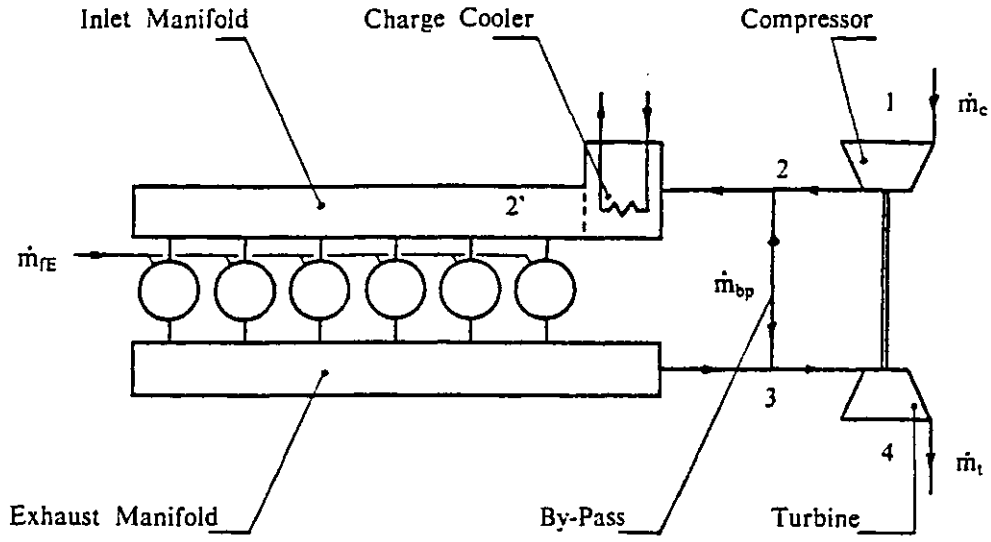

Fig. 3.3 Schematic of a Turbocharged Diesel Engine with a By-Pass.

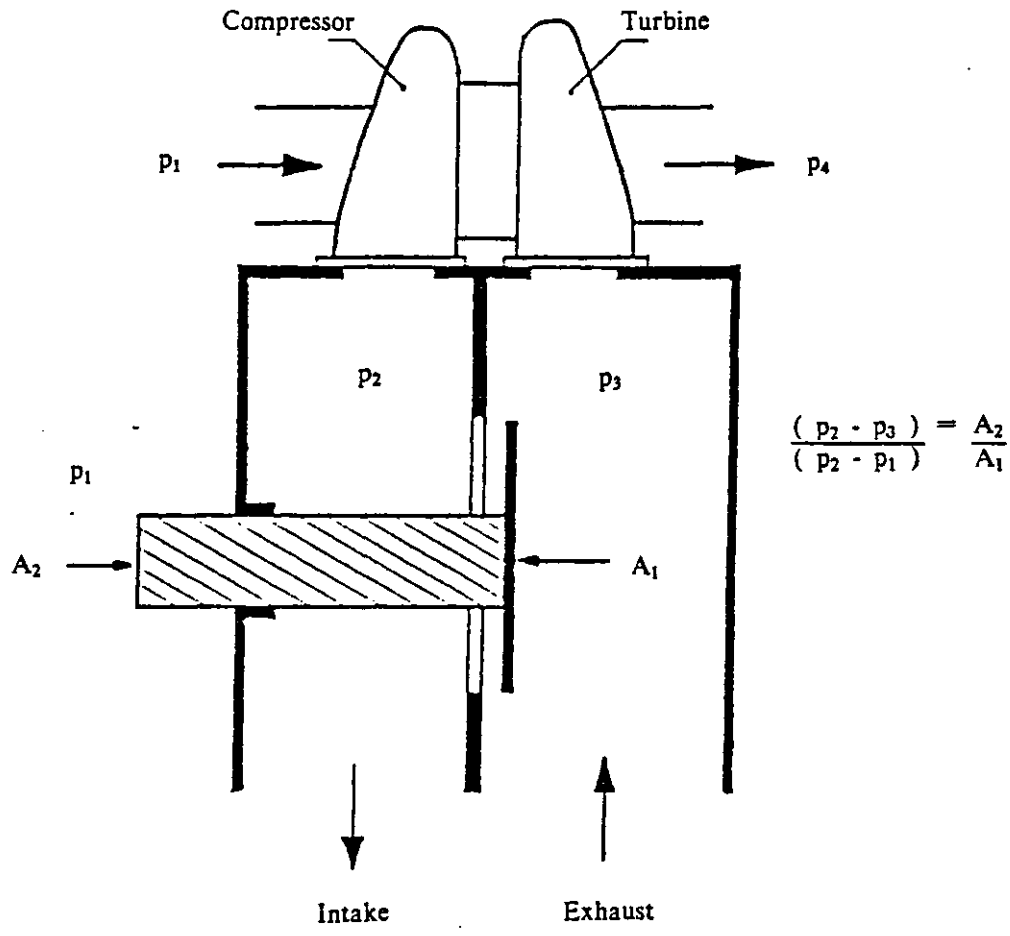

Fig. 3.4 The By-Pass Valve, from (2).

controlled valve, Fig. 3.4. The geometry of the valve is designed so that the relationship between the compressor delivery pressure and the turbine inlet pressure is:-

$$\frac{(p_2 - p_3)}{(p_2 - p_1)} = \frac{A_2}{A_1} \tag{3.10}$$

where A_2/A_1 is the valve head to stem area ratio, shown in Fig. 3.4. It can be seen that eqn. (3.10) reduces to eqn. (3.9) as the area ratio becomes smaller (i.e. the valve flow area increases).

3.3.3 Control of the Scavenge Pressure Drop.

It has been shown in section 3.3.1 that a positive scavenge pressure drop between the compressor outlet and the turbine inlet is desirable. What must now be determined is:-

(1) the magnitude of the pressure drop, (p_2-p_3),

(2) the relationship between the pressure drop and other controlling parameters.

For the simple valve arrangement shown in Fig. 3.4 the pressure drop is proportional to the guage boost pressure, eqn. (3.10).

By assuming an overall fuel-air ratio of 0.03, and hence the ratio between the compressor and turbine mass flow rates, $\dot{m}_t/\dot{m}_c$, the turbocharger energy balance equation, eqn. (3.6), can be used to calculate the turbine inlet temperature, T_3, required to achieve a given compressor pressure ratio, p_2/p_1, and engine pressure drop, (p_2-p_3), Fig.3.5.

It is evident that the turbine inlet temperature required for match increases as the overall turbocharger efficiency, η_{tc}, reduces, where:-

$$\eta_{tc} = \eta_c.\eta_t.\eta_m \tag{3.11}$$

If the by-pass valve area ratio, A_2/A_1, is held constant, then the importance of achieving a high overall turbocharger efficiency can be seen in Fig. 3.5. For example,

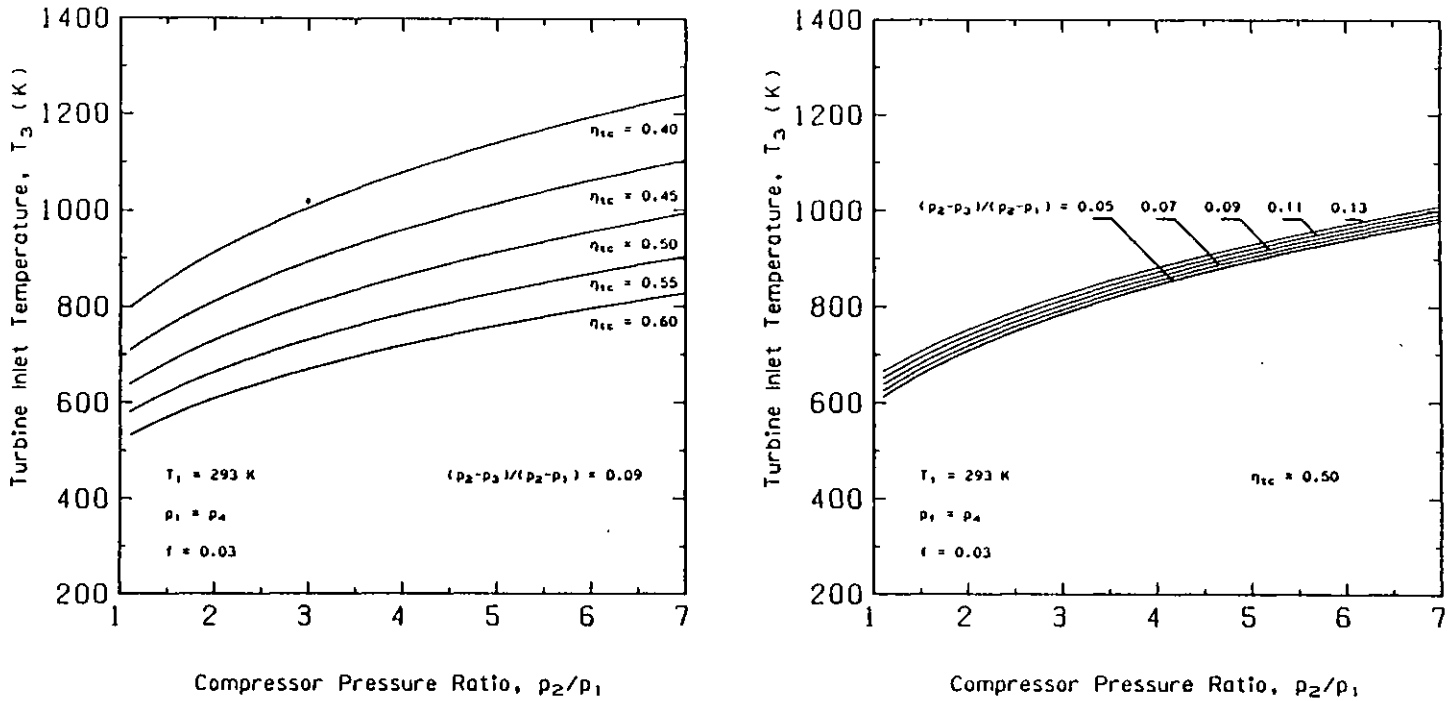

Fig. 3.5 Turbocharger Energy Balance.

for a turbine inlet temperature limit, T_3, of 1000 K, an increase in η_{tc} from 0.40 to 0.45 enables an increase in compressor pressure ratio from 2.9:1 to 4.7:1 to be achieved.

Fig. 3.5 also shows the influence of the by-pass valve area ratio, A_2/A_1. It can be seen that, for a given turbine inlet temperature limit, the compressor pressure ratio that can be achieved reduces as the valve area ratio increases. Alternatively the turbine inlet temperature limit must be increased to achieve a higher compressor pressure ratio with a fixed valve area ratio.

The potential benefits to the engine performance of a higher scavenge pressure drop (proportional to the valve area ratio, A_2/A_1) have already been discussed.

3.3.4 Control of the Compressor Operating Line.

Once the geometry of the by-pass valve system is decided, the operating characteristics of the engine and turbocharger are defined. Equation (3.10) together with eqns. (3.1), (3.2), (3.3), (3.4), and (3.6) define 6 equations in 7 parameters, eqn. (3.7), which leaves 1 unknown, i.e. the controlling parameter.

The engine power output is determined by the amount of fuel that can be burnt in the cylinders, which is, in general, determined by the engine air flow rate (for a given A/F ratio), i.e. the speed, N_E, and compressor pressure ratio, p_2/p_1. The compressor pressure ratio is therefore a logical controlling parameter for determining the turbocharger operating point.

Having decided the engine speed, A/F ratio and power required, the compressor pressure ratio is known (changes in torque can also be achieved by varying the injection timing, valve timing, engine A/F ratio, etc.). All the parameters in eqn. (3.7) are then known. The engine air mass flow rate is a function of the compressor pressure ratio and engine speed, and the compressor mass flow rate is determined from eqns. (3.1), (3.2), (3.3), (3.4), (3.6) and (3.10). The difference between these two flows goes through the by-pass system.

Fig. 3.6 shows the engine operating lines plotted on the compressor map for the

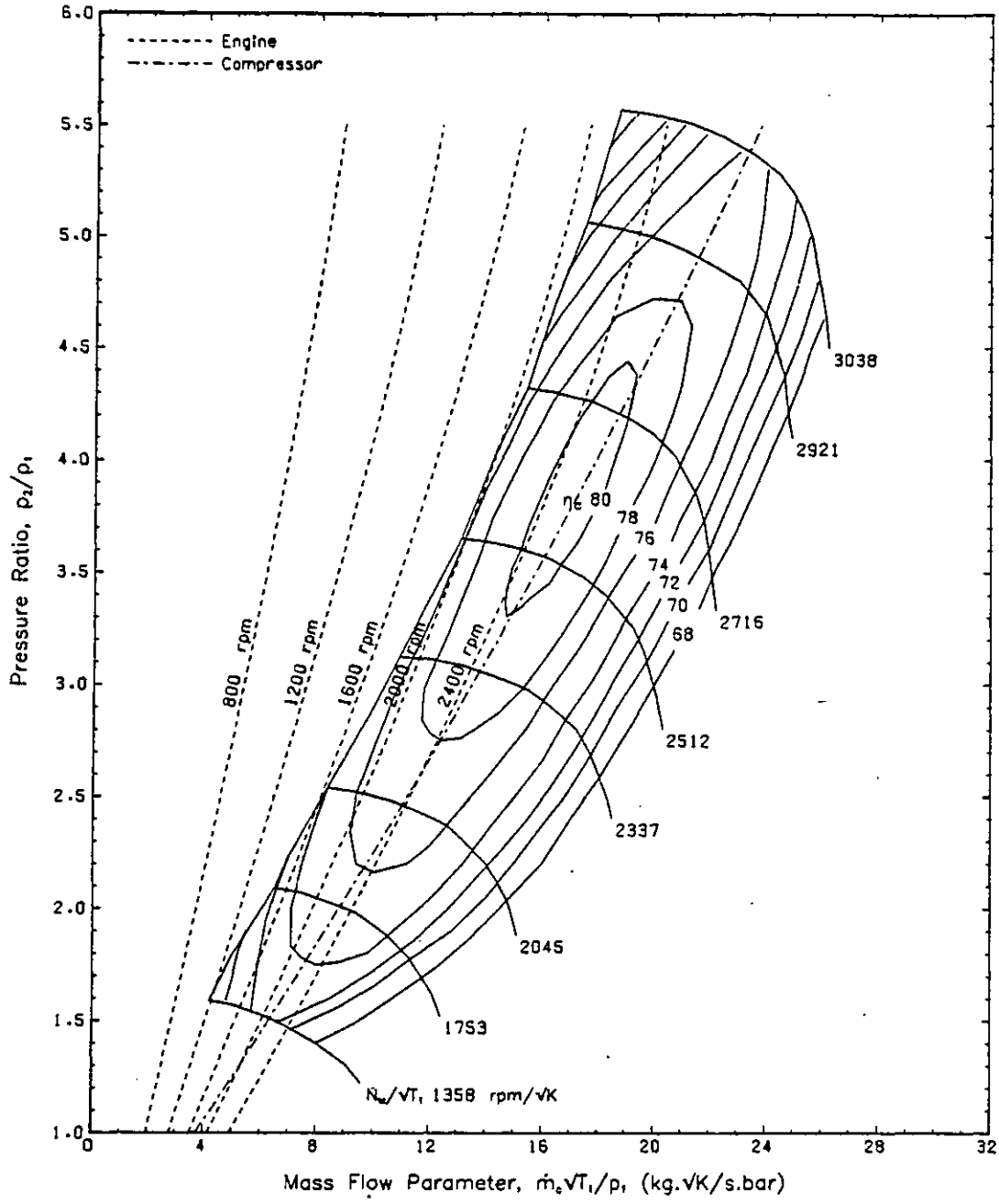

Fig. 3.6 The Engine Operating Lines and Optimum Compressor Operating Line.

Hyperbar engine. The engine air flow rate increases with engine speed and compressor pressure ratio, the gradient of the constant speed lines becoming steeper as the boost pressure increases. Also shown on Fig. 3.6 is the optimum compressor operating line giving the peak compressor efficiency as a function of the pressure ratio only. For the Hyperbar system the difference between the compressor and engine air flow rates must be handled by the by-pass system. The by-pass system mass flow rate must therefore reduce as the engine speed (and power) increases, at a given p_2/p_1, but increase as the compressor pressure ratio increases (engine power increases) for a given engine speed, in order to maintain the compressor operating at optimum efficiency. The valve must therefore operate over the entire engine speed and load range to control the total compressor flow.

Due to the difference in gradients between the engine and compressor operating lines it can be seen that the engine air flow exceeds the optimum compressor air flow at pressure ratio's below 2.6 at the highest engine speed, 2400 rpm, and at pressure ratio's below 1.2 at 2000 rpm. In this case the by-pass system will be unable to control the compressor flow and as a certain amount of air is required to ensure good combustion in the Auxiliary Combustion Chamber (see section 3.3.5), particularly at low boost pressures, the actual compressor operating line will be to the right of the optimum line, leading to a reduction in the compressor efficiency. However, a larger compressor frame size will allow more efficient compressor operation to be achieved.

Varying the by-pass valve area ratio, A_2/A_1, will change the steady state pressure drop between the inlet and exhaust systems, eqn. (3.10). Increasing A_2/A_1 results in an increase in the pressure drop (p_2-p_3) for a given compressor pressure ratio. Assuming that the engine mass flow rate does not change significantly, the reduction in p_3 occurs because of a reduction in the by-pass flow, i.e. the valve effective flow area reduces. The reduced by-pass flow results in a drop in the total compressor flow, and so the operating point moves closer to the surge line. In this way the by-pass valve area ratio, A_2/A_1, can be chosen to match the operating line to the compressor map.

However, because of the efficiency characteristics of most axial and centrifugal compressors, additional control of the compressor operating line may be required to ensure that it is always working in the most efficient part of the map. A simple method of varying the by-pass valve control equation has been proposed by Andre-

Talamon (2). In this case the control pressure, p_0, on the by-pass valve stem is varied according to the compressor pressure ratio, p_2/p_1. The steady state valve equation then becomes:-

$$\frac{(p_2 - p_3)}{(p_2 - p_0)} = \frac{A_2}{A_1} \tag{3.12}$$

Equation (3.12) reduces to eqn. (3.10) when the control presure, p_0, is vented to the atmosphere, p_1. Figs. 3.7 and 3.8 show a mechanism for varying p_0, and the various values used to match the compressor operating line to the map in a certain application. In this case the compressor is always operating at maximum efficiency and close to the surge line.

Fig. 3.9 shows the effect of the boost pressure, p_2, on the pressure drop across the engine, (p_2-p_3), for different control pressures, p_0. Increasing the control pressure reduces the by-pass valve pressure drop for a given boost pressure, p_2. This has a similar effect to reducing the by-pass valve area ratio, A_2/A_1, also shown in Fig. 3.9. In this way the compressor operating line can be varied while the engine is running, provided that an adequate control system for varying p_0 can be devised.

Further details of the by-pass valve operation are given in section 4.8.

3.3.5 The Hyperbar Auxiliary Combustion Chamber.

The Hyperbar system uses an Auxiliary Combustion Chamber (ACC) in parallel with the by-pass valve in the engine exhaust system, Fig. 3.10. Air from the compressor outlet is used to burn extra fuel in the exhaust system for three main reasons:-

(1) Due to the low engine compression ratio, self ignition of the fuel cannot be achieved when cold starting, or when the engine is operating at low speeds and loads, (or else the ignition delay is unacceptably long). Under these conditions the exhaust gas energy is insufficient to maintain the boost pressure, and temperature, necessary for self ignition. Extra energy is then required to drive the turbine to increase the boost pressure, and this is supplied by the ACC.

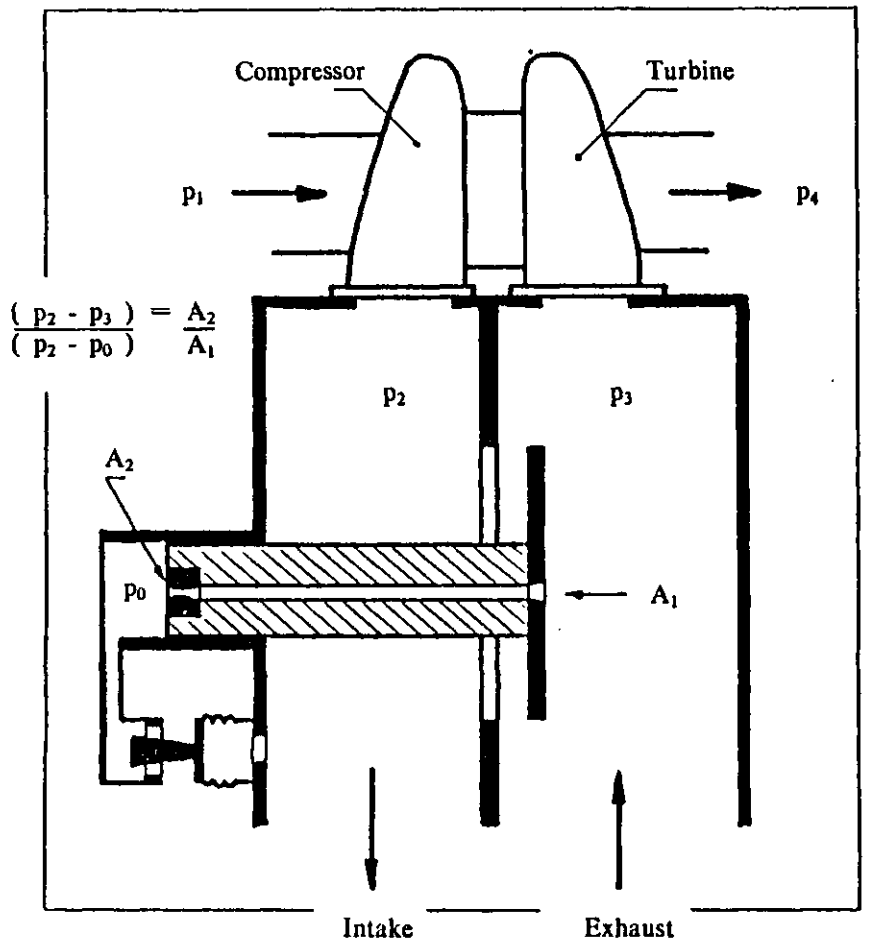

Fig. 3.7 Varying the By-Pass Valve Characteristics by Changing the Control Pressure, from (2).

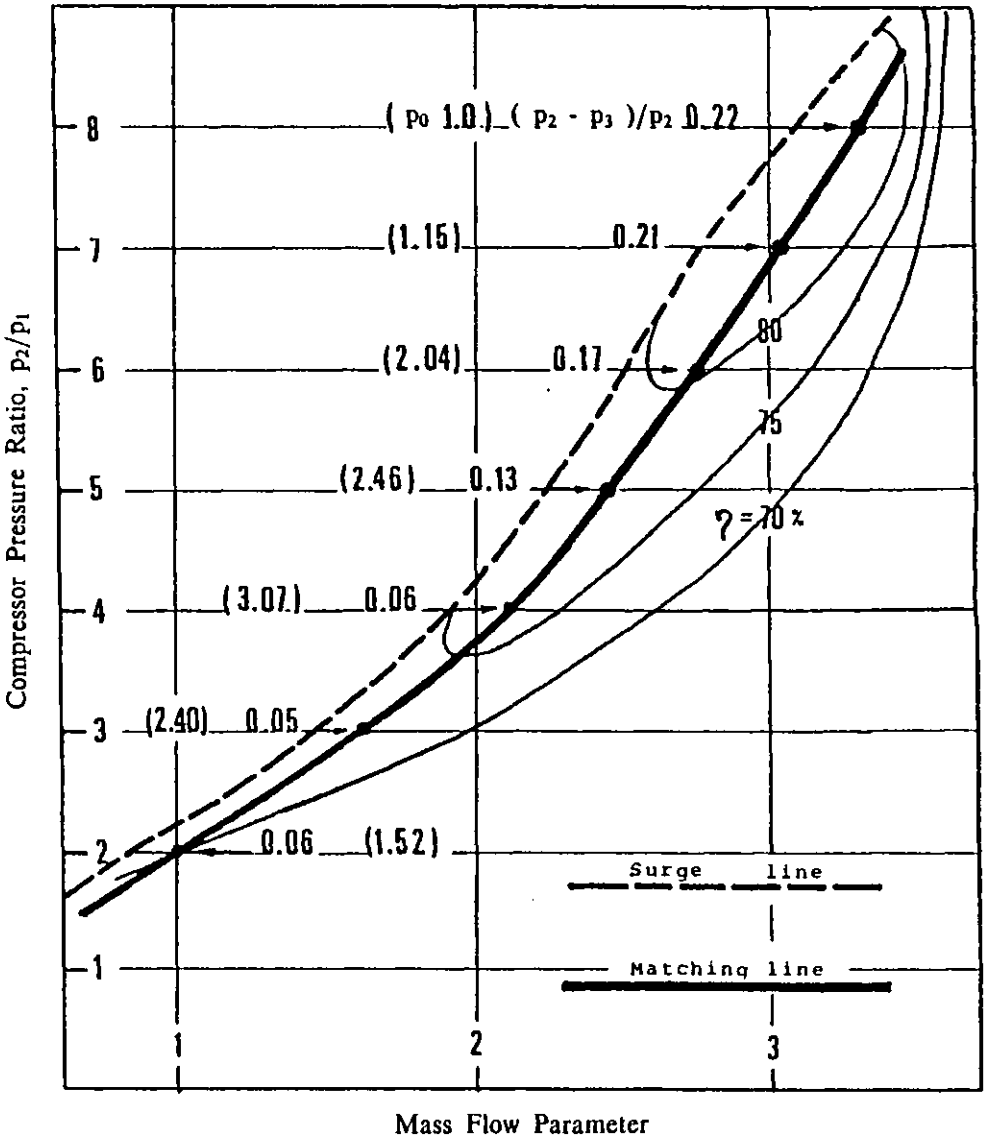

Fig. 3.8 Matching the Compressor Operating Line by Varying the By-Pass Valve Control Pressure, from (2).

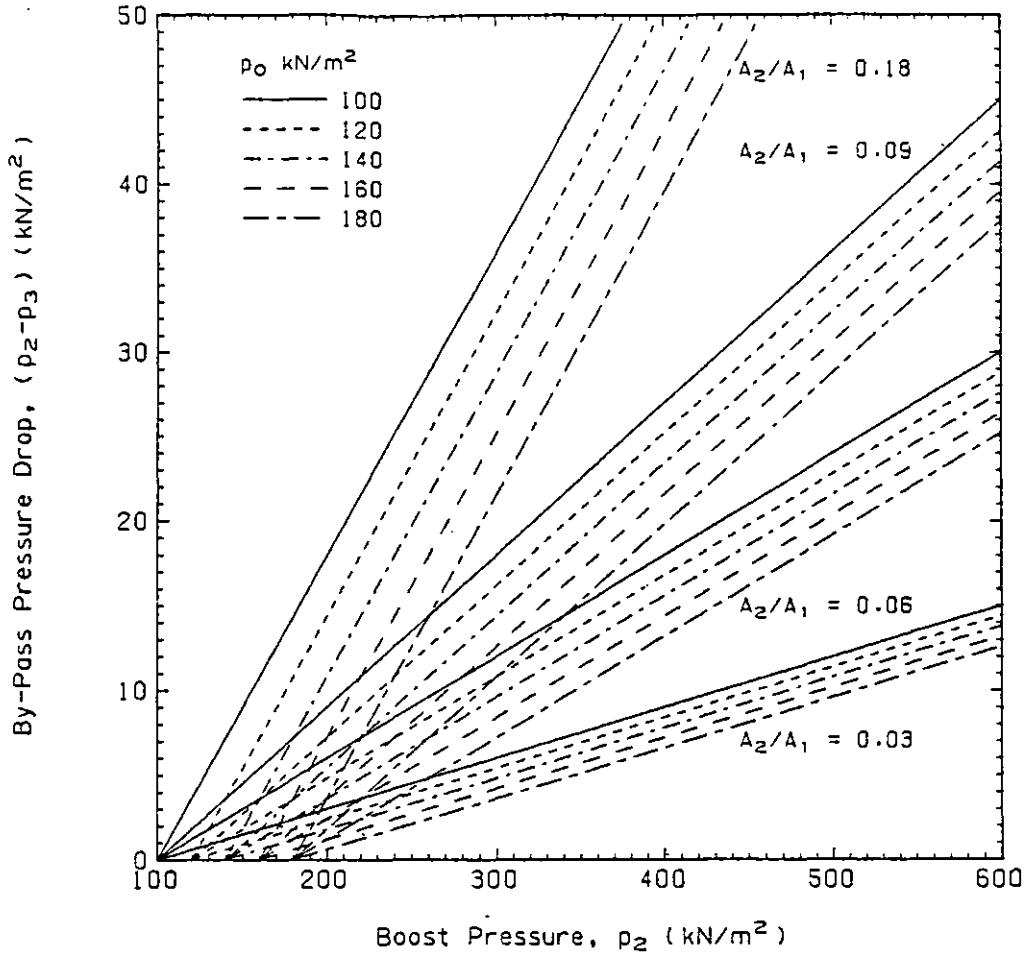

Fig. 3.9 Control of the Engine Pressure Drop by Varying the By-Pass Valve Area Ratio A_2/A_1 and the Valve Control Pressure p_0.

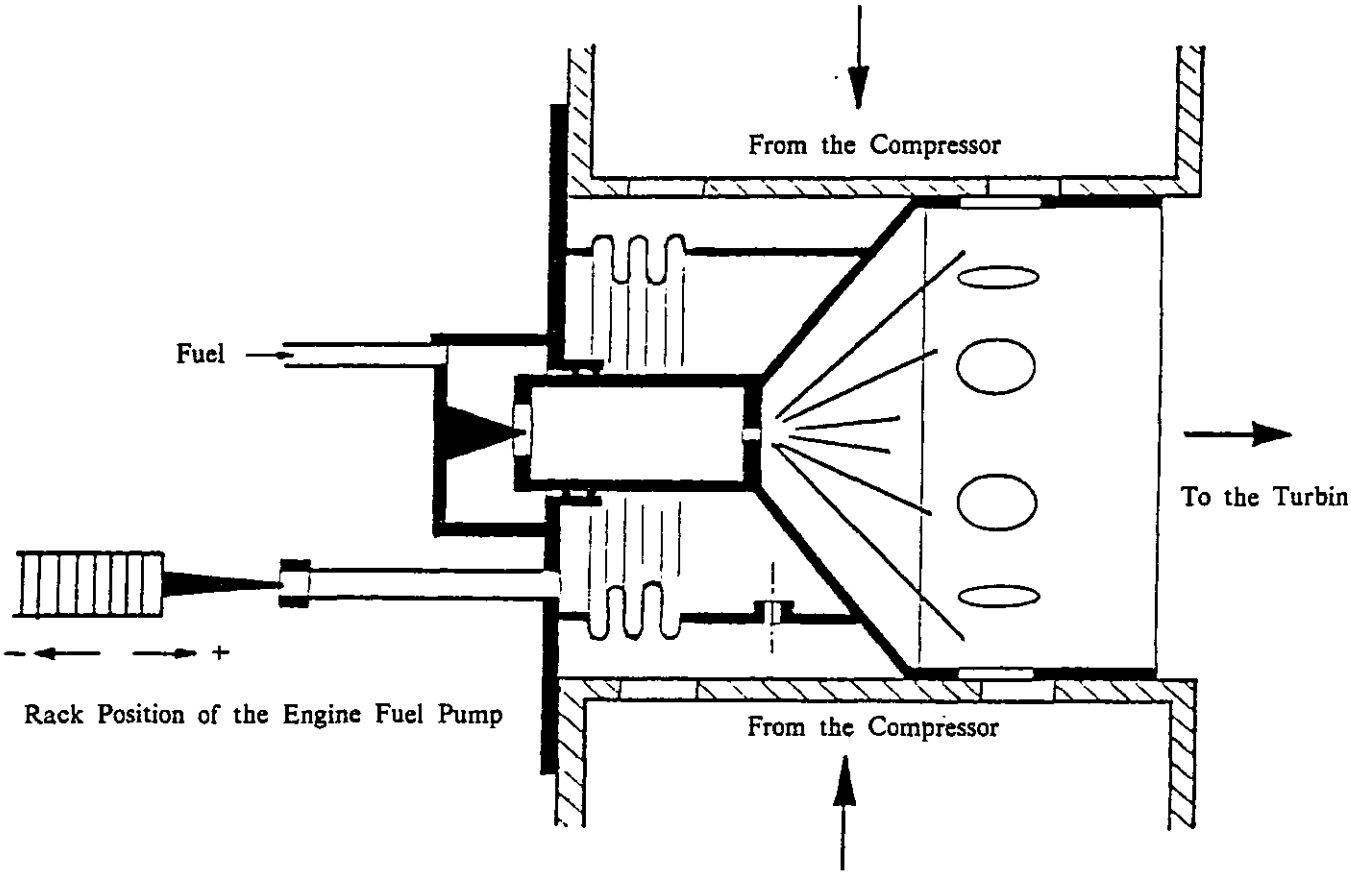

Fig. 3.10 Regulation of the Hyperbar Burner, from (2).

(2) The ACC provides extra energy to the turbine when engine acceleration or high torque is required. This enables the engine to operate at very high BMEP's at any speed.

(3) By using a starter motor on the turbocharger (or a compressed air supply), opening the by-pass valve and burning fuel in the ACC, the turbocharger can be operated as a gas turbine, independently of the engine. When stable operating conditions are achieved the engine can then be started. This overcomes the problems normally associated with the starting of low compression ratio diesel engines.

The energy supplied to the turbine from the ACC is therefore used to supplement the exhaust gas energy from the engine at low speeds and loads, or when an increase in turbine power is required. The ACC has its own control system that regulates the fuel flow rate according to pneumatic and/or hydraulic control pressures within the ACC. Air from the compressor outlet is supplied to the burner to atomise, distribute and burn the fuel.

The gas pressure in the ACC is the main control parameter that governs the position of the movable inner section of the burner, which in turn controls the air and fuel flow rates. This chamber gas pressure is regulated by air from the by-pass valve, which mixes with the contents of the combustion chamber before entering the exhaust mixer. The exhaust mixer joins the gas flow paths from the engine exhaust system and the by-pass system before they enter the turbine.

Making the same simplifying assumptions as described in section 3.2, the temperature rise across the ACC can be expressed as:-

$$T_{acc}-T_2 = \frac{C_v}{c_{pm}\cdot A/F_{oacc}} \qquad (3.13)$$

where,

T_{acc} = ACC gas outlet temperature (K)

T_2 = compressor outlet temperature (K)

C_v = lower calorific value of the fuel (kJ/kg)

c_{pm} = mean specific heat at constant pressure for air and exhaust gas (kJ/kg.K)

A/F_{oacc} = overall by-pass A/F ratio

The turbine inlet temperature, T_3, will depend upon the by-pass and exhaust gas temperatures, and the proportions of each that enter the turbine. This can be approximated by:-

$$T_3 = T_{acc}\left(\frac{\dot{m}_{bp} + \dot{m}_{acc}}{\dot{m}_t}\right) + T_5\left[1 - \left(\frac{\dot{m}_{bp} + \dot{m}_{acc}}{\dot{m}_t}\right)\right] \qquad (3.14)$$

where,

T_5 = engine exhaust gas temperature (K)

$(\dot{m}_{bp}+\dot{m}_{acc})/\dot{m}_t$ = by-pass flow to turbine flow ratio

Equations (3.6), (3.13) and (3.14) can be used to find the amount of fuel required to be burnt in the ACC to achieve a given operating condition. Further details of the ACC operation are given in section 4.9.

A method of increasing the overall efficiency of the Hyperbar system has been proposed by Lawton (78). The arrangement is shown diagramatically in Fig. 3.11. In principle the layout is similar to that of a gas turbine regenerator, using the exhaust gas energy after the turbine to pre-heat the by-pass air before it enters the ACC. This results in less fuel being required by the burner, for a given turbine inlet temperature, and hence a reduction in the overall BSFC.

There are, however, a number of practical problems that will limit the use of this regenerator system to stationary engine applications. The most important of these is the requirement for a compact power plant for automotive use. Most of the fundamental problems involved in using a regenerator in this type of application have been solved in automobile gas turbine designs, an example of which is given by Penny (112). There will also be a pressure loss across the heat exchanger which will effect the by-pass system performance.

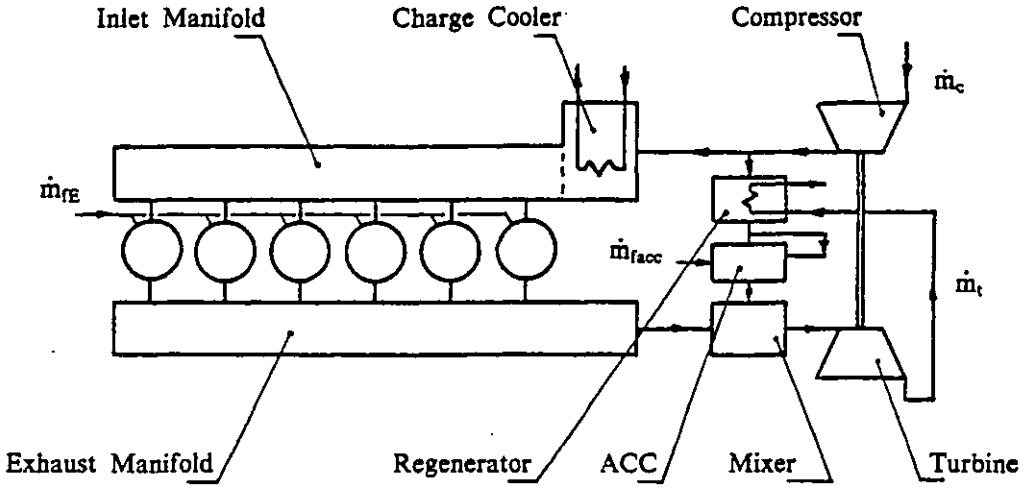

Fig. 3.11 Schematic of the Hyperbar Engine with a Regenerator.

The benefit of a regenerator to the power plant overall thermodynamic efficiency will probably be most noticable at low engine speeds, where the ACC fuelling becomes a significant proportion of the total.

3.3.6 Potential of the Hyperbar System.

The potential advantages of the Hyperbar system are:-

(1) High pressure ratio turbocharging can be achieved with high compressor efficiencies.

(2) Compressor matching, without the problems of surging, is greatly simplified, due to the compressor operating line being independent of the engine speed.

(3) The system allows increases of engine power to be achieved without necessarily increasing the thermal and mechanical loading of the engine, or excessive bulk.

(4) High torque can be achieved at any engine speed by using the ACC burner.

(5) High overall and engine A/F ratio's leads to a reduction in smoke, and possibly NO_x, due to lower combustion temperatures.

(6) The turbocharger speed varies between the maximum speed at the rated point and about half speed at engine idling, and the compressor is always working in the high efficiency region of the map. This should lead to an improvement in the transient response of the turbocharger (depending upon its size).

(7) Ease of starting and low load operation, due to the ACC controlling the minimum boost pressure.

The principal disadvantages of the system are:-

(1) Increased fuel consumption, especially when operating at low loads and low engine speeds, due to the extra fuelling required by the burner to maintain sufficient boost for ignition in the cylinder.

(2) Reduced engine thermal efficiency due to the lower compression (expansion) ratio.

(3) Increased charge cooler heat rejection (and consequently cooler size) because of the higher engine A/F ratio's.

(4) Increased complexity compared to conventional turbocharging systems. Control systems are required for the by-pass valve and the ACC burner.

CHAPTER 4

MATHEMATICAL MODEL OF THE HYPERBAR SYSTEM

4.1 Fundamental Principles.

The engine thermodynamics and fluid dynamics are treated on a quasi-steady basis employing the "filling and emptying" concept, commonly applied in constant speed engine simulation programs (12,22,65,91,137,173). The engine is considered as a series of control volumes, interconnected via orifices of varying geometry (simulating valves and ports) and coupled by heat, mass and/or work transfer, see Fig. 4.1. Therefore the problem of determining the time varying conditions of the gas in each control volume is transformed into a case of simultaneous charging and discharging, governed by the instantaneous values of the controlling parameters.

Some simplifying assumptions are made in the model. For example, thermodynamic equilibrium and ideal gas behavior are assumed at all times. It is also assumed that the control volumes contain a homogeneous mixture of air and combustion products, although the ratio may vary from zero to infinity. Property gradients and phenomena such as pressure waves, non-equilibrium compositions, fuel vapourisation before combustion, etc. are neglected. The simulation does account for unsteady flow in the exhaust pipes of pulse turbocharged engines, although spacial variations are ignored.

The energy equation for an open thermodynamic system can be written as:-

$$\frac{d(m.u)}{dt} = -p.\dot{V} + \sum_i \dot{Q}_i + \sum_j \dot{m}_j.h_j \qquad (4.1)$$

where,

h_j = total (stagnation) specific enthalpy of the mass entering or leaving the system through the flow surface j (kJ/kg)

m = mass in the system (kg)

$\dot{m}_j$ = rate of mass flow through surface j (kg/s)

p = total (stagnation) pressure in the system (kN/m^2)

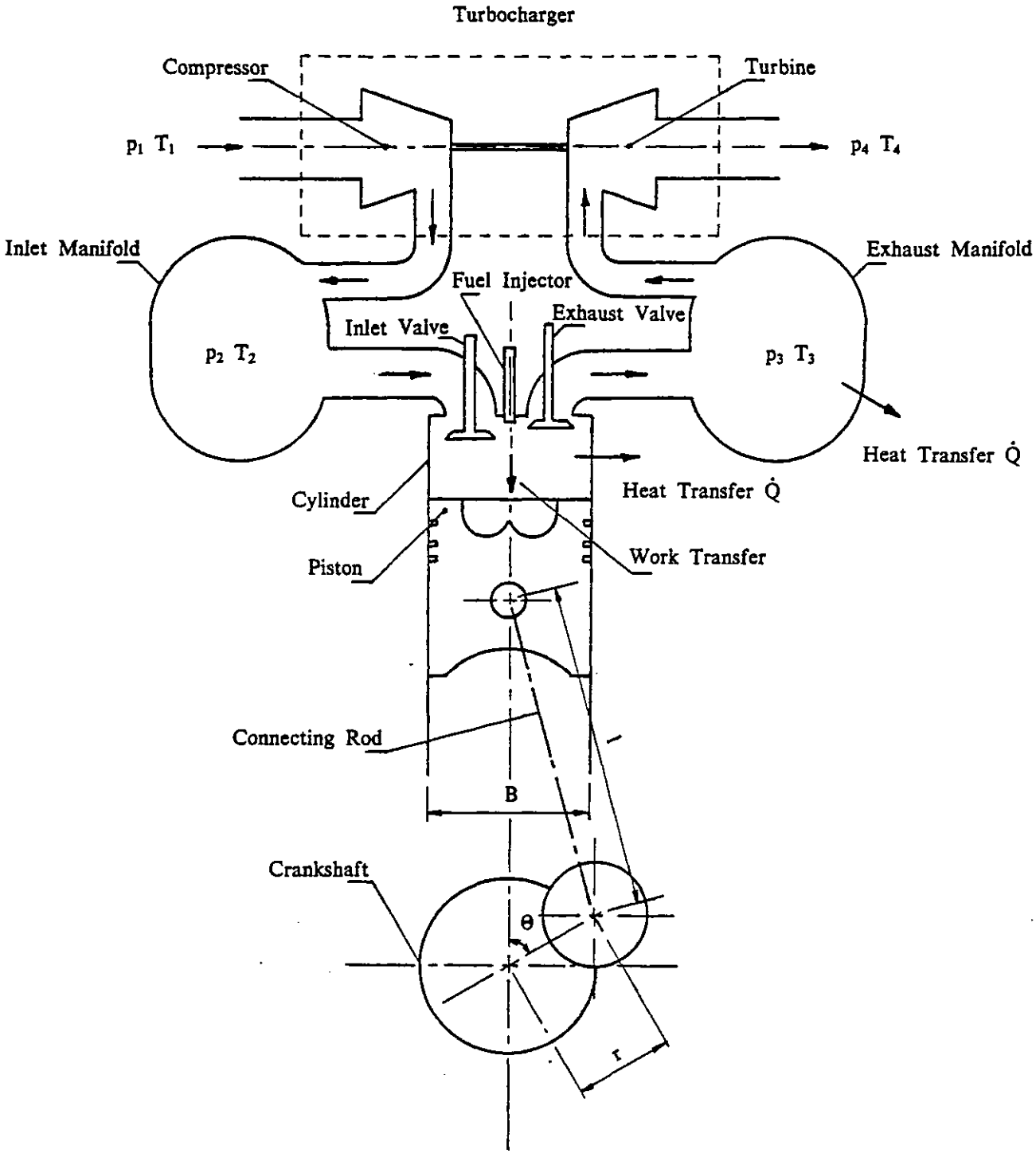

Fig. 4.1 Thermodynamic Model of a Turbocharged Diesel Engine.

$\dot{Q}_i$ = rate of heat transfer through surface i (kW)

t = time (s)

u = specific internal energy of the medium (kJ/kg)

$\dot{V}$ = rate of change of volume of the system (m^3/s)

The mass continuity equation is:-

$$\dot{m} = \sum_j \dot{m}_j \tag{4.2}$$

The fuel-air equivalence ratio, F, is defined as:-

$$F = \frac{f}{f_s} \tag{4.3}$$

where,

f = fuel-air ratio

f_s = stoichiometric fuel-air ratio

F = equivalence ratio

The thermodynamic property relationships are of the form:-

$$u = u\,(T, p, F) \tag{4.4}$$

$$R = R\,(T, p, F) \tag{4.5}$$

where,

R = gas constant for the mixture (kJ/kg.K)

T = total (stagnation) temperature in the system (K)

The ideal gas equation of state is:-

$$p = \frac{m.R.T}{V} \tag{4.6}$$

where,

V = volume of the system (m^3)

Equations (4.1) to (4.6) can be rearranged to give the rate of change of temperature

in the system, T, in terms of the other parameters, from (22):-

$$\dot{T} = \frac{\Phi_1 - \frac{p.\delta u}{\Phi_3 \delta p}\left[\frac{\dot{m}}{m} + \frac{\dot{F}\delta R}{R\delta F} - \frac{\dot{V}}{V}\right] - \frac{\dot{F}\delta u}{\delta F}}{\frac{\delta u}{\delta T} + \frac{\delta u.p.\Phi_2}{\delta p.T.\Phi_3}} \tag{4.7}$$

where,

$$\Phi_1 = \frac{-R.T.\dot{V}}{V} + \frac{1}{m}\left[\sum_i \dot{Q}_i + \sum_j \dot{m}_j.h_j - u.\dot{m}\right] \tag{4.8}$$

$$\Phi_2 = 1 + \frac{T.\delta R}{R\,\delta T} \tag{4.9}$$

$$\Phi_3 = 1 - \frac{p.\delta R}{R.\delta p} \tag{4.10}$$

From the definition of equivalence ratio, eqn. (4.3), the mass of burned fuel, m_f, present in a mixture of combustion products of mass, m, is:-

$$m_f = \frac{m.f_s.F}{(1 + f_s.F)} \tag{4.11}$$

Applying the principle of mass conservation to the fuel species, and substituting eqn. (4.3) into eqn. (4.11) yields:-

$$\dot{F} = \frac{(1 + f_s.F).[(1 + f_s.F).(\Phi_4 + \dot{m}_f) - f_s.F.\dot{m}]}{f_s.m} \tag{4.12}$$

from j entries, with suffix u denoting the upstream conditions, and:-

$$\Phi_4 = \sum_j \left[\frac{(\dot{m}_j.f_s.F_{j,u})}{(1 + f_s.F_{j,u})}\right] \tag{4.13}$$

where,

$\dot{m}_f$ = fuel burning rate in the control volume (kg/s)

Φ_4 = fuel mass flow rate entering and/or leaving the control volume via the orifices or ports (kg/s).

4.1.1 Determination of Instantaneous Mass Flow Rates.

The mass flow rate through the system boundaries is treated as quasi-steady, one-dimensional, compressible, adiabatic, frictionless and therefore isentropic if subsonic. Ignoring the effects of gas inertia and pressure waves the steady flow energy equation can be solved for the mass flow rate of an ideal gas through a flow restriction, which can be written as:-

$$\dot{m} = A_g.c_d.p_u.\left[\frac{2}{R_u.T_u}\left(\frac{\gamma}{\gamma-1}\right)\left\{\left(\frac{p_d}{p_u}\right)^{2/\gamma} - \left(\frac{p_d}{p_u}\right)^{(\gamma+1)/\gamma}\right\}\right]^{0.5} \qquad (4.14)$$

where,

A_g = geometric flow area (m^2)
c_d = coefficient of discharge
p_d = downstream pressure (N/m^2)
p_u = upstream stagnation pressure (N/m^2)
R_u = upstream gas constant (J/kg.K)
T_u = upstream stagnation temperature (K)
γ = specific heat ratio at the upstream conditions.

The critical pressure ratio is defined as:-

$$\left(\frac{p_d}{p_u}\right)_{cr} = \left(\frac{2}{\gamma+1}\right)^{\gamma/(\gamma-1)} \qquad (4.15)$$

If the pressure ratio, p_d/p_u, is less than the critical pressure ratio, then the mass flow rate is given by:-

$$\dot{m} = A_g.c_d.p_u\left[\frac{\gamma}{R_u.T_u}\left(\frac{2}{\gamma+1}\right)^{(\gamma+1)/(\gamma-1)}\right]^{0.5} \qquad (4.16)$$

The coefficient of discharge, c_d, can be determined by steady flow measurements as a function of the instantaneous geometric area and the pressure ratio, p_d/p_u.

Equations (4.14) to (4.16) are used to determine the instantaneous mass flow rates through the orifices in the system (including the inlet and exhaust valves). The

calculation of the coefficient of discharge for the valves is discussed in section 4.1.2. The flow geometry for the components of the Hyperbar system are discussed in sections 4.7 and 4.8, and the boundary conditions for the turbocharger compressor and turbine are discussed in sections 4.2.1 and 4.2.2 respectively.

4.1.2 Valve Effective Areas.

The instantaneous mass flow rates through the inlet and exhaust valves are calculated according to eqns. (4.14), (4.15) and (4.16). The valve effective areas are defined as:-

$$A_e = A_g.c_d \tag{4.17}$$

where,

A_e = valve effective area (m^2)

A_g = geometric valve area (m^2)

The volumetric flow rate through the twin inlet and exhaust valves was measured by the engine manufacturer on the cylinder head with the liner attached. The pressure drop across the valves was held constant, and the flow rate was measured at a number of valve lifts. This data was then used to calculate the valve effective areas as a function of valve lift. No data was available to determine the effect of valve pressure ratio on the effective flow areas.

The steady flow energy equation for the valves (for pressure ratio's above the critical pressure ratio, eqn. (4.15)) is given by eqn. (4.14), which can be solved to give the effective area, A_e, from the measured pressure ratio, p_d/p_u, the mass flow rate, $\dot{m}$, and the upstream conditions, p_u, T_u, R_u, γ_u and ρ_u.

The valve lift was obtained from the camshaft lift, rocker ratio and tappet clearance, which enabled the geometric valve areas to be calculated, and the coefficient of discharge was found using eqn. (4.17).

4.1.3 Determination of the Instantaneous Heat Transfer Rates.

The rate of heat transfer between the gas and the gas exposed surface i can be expressed as:-

$$\dot{Q}_i = h_i.A_i.(T_g - T_i) \tag{4.18}$$

where,

A_i = instantaneous heat transfer area of the surface i exposed to the gas (m^2)

h_i = instantaneous heat transfer coefficient for surface i ($kW/m^2.K$)

T_g = instantaneous bulk gas stagnation temperature (K)

T_i = average temperature of surface i (K)

The calculation of the instantaneous heat transfer coefficients is discussed in section 4.4.2. The cylinder wall temperatures are updated every cycle, by using a simple one-dimensional heat transfer model, described in section 4.4.1. The heat transfer from the exhaust system is discussed in section 4.4.4.

4.1.4 Determination of the Cylinder Volume and Rate of Change of Volume.

The instantaneous cylinder volume and rate of change of volume can be calculated from the engine geometry, see Fig. 4.1,

$$V = \frac{\pi.B^2}{4}.[r.(1 - \cos\Theta) + l.(1 - (1 - (r/l)^2.\sin^2\Theta)^{0.5})] \tag{4.19}$$

$$V = \frac{\pi.B^2}{4}.\frac{d\Theta}{dt}.\left[r.\sin\Theta + \frac{r^2.\sin\Theta.\cos\Theta}{l.(1 - (r/l)^2.\sin^2\Theta)^{0.5}} \right] \tag{4.20}$$

where,

B = cylinder bore (m)

l = connecting rod length (m)

N_E = engine speed (rpm)

r = crank radius (m)

Θ = crank angle

and,

$$\frac{d\Theta}{dt} = \frac{N_E.2.\pi}{60} \tag{4.21}$$

The intake and exhaust system volumes do not vary with time (i.e. there is no charge cooler by-pass system).

4.1.5 Engine Dynamics.

During transient operation, the engine speed will vary according to the torque developed by the engine and that absorbed by the loading system (which may be a dynamometer, or a vehicle, or some other type of load). A simple dynamic system has been used to calculate the instantaneous engine acceleration:-

$$\ddot{\Theta}_E = \frac{(\tau_E - \tau_F - \tau_L).1000}{(I_E + I_L)} \tag{4.22}$$

where,

I = rotating inertia ($kg.m^2$)

$\ddot{\Theta}$ = angular acceleration of the engine and load (s^{-2})

τ = torque (kN.m)

and the subscripts E, F and L denote engine, friction and load respectively.

The load torque, τ_L, is assumed to include windage and other types of friction torques generated by the loading system. The power transmission shaft is assumed to be sufficiently rigid so that any shaft twist between the engine and the load can be neglected.

4.2 The Turbocharging System Characteristics.

4.2.1 The Compressor

Dimensional analysis, see section 3.2, suggests that the compressor characteristics can be represented by the following pseudo non-dimensional variables:-

$$f_1\left(\frac{\dot{m}_c.\sqrt{T_1}}{p_1}, \frac{p_2}{p_1}, \frac{N_{tc}}{\sqrt{T_1}}\right) = 0 \qquad (3.1)$$

$$f_2\left(\eta_c, \frac{p_2}{p_1}, \frac{N_{tc}}{\sqrt{T_1}}\right) = 0 \qquad (3.2)$$

where,

$\dot{m}_c$ = compressor mass flow rate (kg/s)
N_{tc} = turbocharger speed (rpm)
p_1 = stagnation compressor inlet pressure (kN/m^2)
p_2 = stagnation compressor outlet pressure (kN/m^2)
T_1 = stagnation compressor inlet temperature (K)
η_c = total to total compressor isentropic efficiency.

Engine tests have been carried out by the manufacturer, using a high pressure ratio single stage centrifugal compressor. Flow adjustments being made by varying the diffuser ring, if required.

In the simulation program the compressor is treated on a quasi-steady basis, the instantaneous values of compressor mass flow rate and efficiency being determined according to the pressure ratio and turbocharger speed parameter. The instantaneous compressor torque required can be calculated from:-

$$\tau_c = \frac{P_c.60}{N_{tc}.2\pi} \qquad (4.23)$$

where,

P_c = compressor power (kW)
τ_c = compressor torque (kN.m)

A compressor map has been constructed, based on the limited amount of test data supplied by the engine and turbocharger manufacturers. Fig. 4.2 shows the normal compressor operating range, and the effective surge limit for steady state operation.

Very little is known of the instantaneous operating conditions inside a centrifugal compressor during transients. Yano (184), using the Method of Characteristics (MOC) showed that the steady flow compressor characteristics could be used to predict the pressure fluctuations in the inlet system, but deviations of up to 5% between measured and calculated mass flow rates were observed.

In addition to a displacement of the surge line, Jenny (67) showed that there is a drop in compressor efficiency under non-steady flow conditions. Benson and Whitfield (15,16) studied compressors with vaneless diffusers and found that both the onset of surge and the steady flow characteristics of radial compressors were affected by the diffuser design. They concluded that the characteristics of the compressor/pipe system were modified under non-steady flow conditions, the operating range of the compressor being reduced (i.e. the surge line occurs at higher mass flow rates). The displacement of the surge line was found to be dependent upon the amplitude and frequency of the pulses in the inlet system.

Benson (11) has also investigated the pressure wave forms in the intake system of a highly supercharged four stroke engine using the MOC. He concluded that the pressure wave form in the intake system is dependent upon the shape of the pressure ratio, mass flow, speed characteristics of the compressor. In addition the pressure wave amplitude may be sufficiently large at the compressor delivery, and of such frequency, to reduce the operating region under non-steady flow, leading to the possibility of surge.

In Hyperbar applications, a wide compressor flow range is not a primary requirement, but high efficiencies are essential. However during transients, the system will not behave in the same way as it does under steady state conditions, and the compressor surge margin may become a limiting factor. The instantaneous compressor and engine operating points are discussed in more detail in sections 5.3 and 5.4.

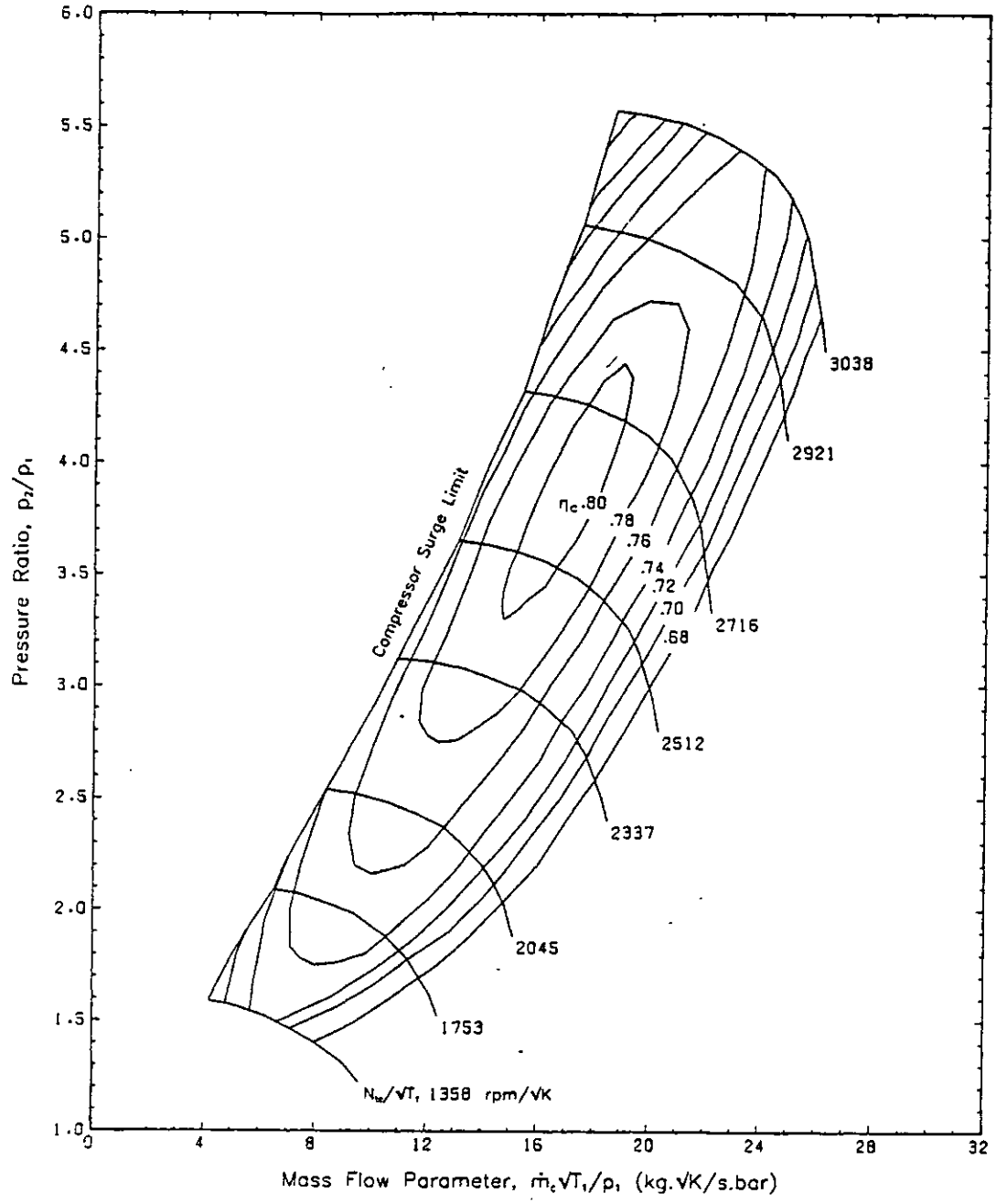

Fig. 4.2 The Compressor Characteristic.

4.2.2 The Turbine.

Dimensional analysis, see section 3.2, suggests that the turbine characteristics can be represented by the following pseudo non-dimensional variables:-

$$f_3\left(\frac{\dot{m}_t.\sqrt{T_3}}{p_3}, \frac{p_3}{p_4}, \frac{N_{tc}}{\sqrt{T_3}}\right) = 0 \qquad (3.3)$$

$$f_4\left(\eta_t, \frac{p_3}{p_4}, \frac{N_{tc}}{\sqrt{T_3}}\right) = 0 \qquad (3.4)$$

where,

$\dot{m}_t$ = turbine mass flow rate (kg/s)
p_3 = stagnation turbine inlet pressure (kN/m^2)
p_4 = static turbine outlet pressure (kN/m^2)
T_3 = stagnation turbine inlet temperature (K)
η_t = total to static turbine isentropic efficiency

The Hyperbar engine considered uses a single entry radial flow turbine, flow adjustments being made by changing the nozzle guide ring, if required. The turbine operating parameters are treated on a quasi-steady basis (13,151,154,158), the instantaneous mass flow rate and efficiency being calculated from the total to static expansion ratio, and the blade speed ratio and speed parameter respectively. Exhaust diffusers are not usually used on turbochargers, and the exit gas velocity can be quite significant, therefore the total to static efficiency is usually specified.

The turbine flow characteristics, eqn. (3.3) are represented by a single "self sustaining swallowing capacity curve", the effect of the speed parameter, $N_{tc}/\sqrt{T_3}$, being neglected. The engine has been tested with a number of different turbine nozzle guide rings. The swallowing capacity curve used in this work is shown in Fig. 4.3, which demonstrates the high expansion ratio's required for the Hyperbar system. It is important to remember that the instantaneous expansion ratio versus mass flow parameter curve can deviate significantly from the mean values measured on the test bed, and this may lead to errors in predicting the turbine flow. However, due to the difficulties involved in measuring the instantaneous turbine flow, or gas velocity, the

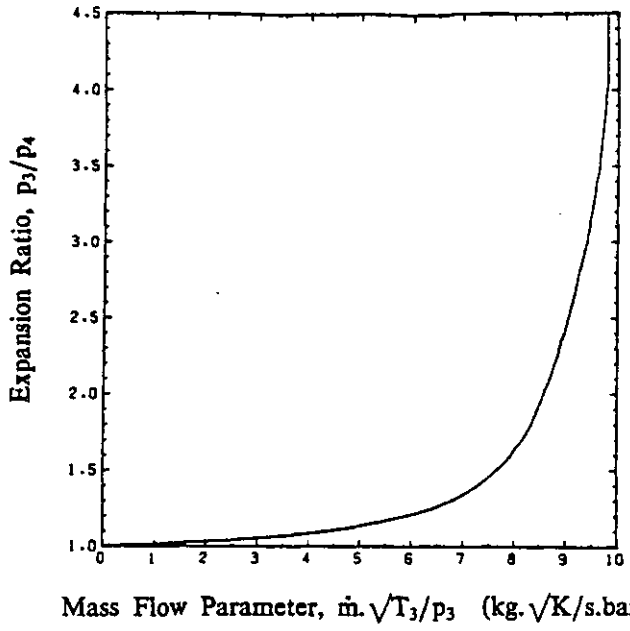

Fig. 4.3 Turbine Swallowing Capacity Characteristic.

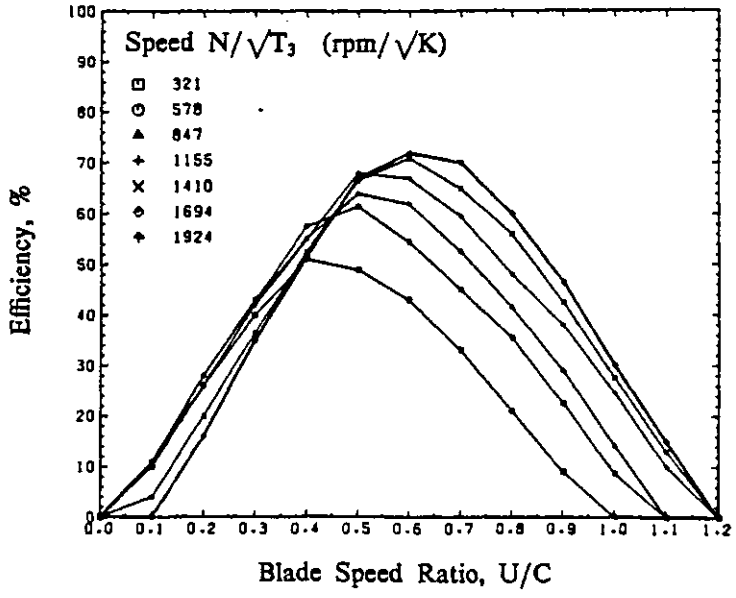

Fig. 4.4 Turbine Efficiency Characteristics.

data shown in Fig. 4.3 has been used without modification.

No data was available for the turbine efficiency over the operating range, partly due to the difficulties involved in measuring turbine efficiency accurately (166). Turbine data for another radial flow turbine (8) was used and the efficiencies were scaled to give a good agreement with the values calculated from a turbocharger energy balance for the Hyperbar engine. The turbine data was available in the form given in eqn. (3.5), where the blade tip speed, U, is given by:-

$$U = \frac{\pi . D_t . N_{tc}}{60} \tag{4.24}$$

where,

D_t = turbine diameter (m)

U = blade tip speed (m/s)

and the isentropic gas velocity at the exit from the turbine, C, is given by:-

$$C = [\ 2.(\ h_3 - h_{4'}\ )\ ]^{0.5} \tag{4.25}$$

where,

C = isentropic gas velocity (m/s)

h_3 = specific stagnation enthalpy at the turbine inlet (J/kg)

$h_{4'}$ = specific static isentropic enthalpy at the turbine outlet (J/kg)

Taking a mean value for the specific heat of exhaust gas, c_{pe}, at the inlet and exit conditions and using eqns.(4.24) and (4.25) it can be seen that eqns. (3.4) and (3.5) are equivalent, i.e.:-

$$\frac{U}{C} = \left[\frac{N_{tc}}{\sqrt{T_3}}\right] \frac{\pi . D_t}{60.[\ 2.c_{pe}.(1-(p_4/p_3)^{(\gamma e-1)/\gamma e}\ )]^{0.5}} \tag{4.26}$$

where,

c_{pe} = mean specific heat of the exhaust gas at constant pressure (J/kg.K)

γ_e = exhaust gas specific heats ratio.

The assumed turbine efficiency characteristics are shown in Fig. 4.4, demonstrating the

effect of both the blade speed ratio, U/C, and the turbine speed parameter, $N_{tc}/\sqrt{T_3}$.

The instantaneous turbine torque is given by:-

$$\tau_t = \frac{P_t.60}{N_{tc}.2.\pi} \tag{4.27}$$

where,

P_t = turbine power (kW)

τ_t = turbine torque (kN.m)

It is important to note that the turbine efficiencies shown in Fig. 4.4 are based on the total to static expansion ratio and include windage and bearing losses.

4.2.3 The Turbocharger Dynamics.

Applying the angular momentum equation to the turbocharger, the rate of change of turbocharger speed can be calculated at each step (assuming no twist in the shaft) from:-

$$\ddot{\Theta}_{tc} = \frac{(\tau_t - \tau_c).1000}{I_{tc}} \tag{4.28}$$

where,

I_{tc} = total polar moment of inertia of the turbocharger (kg.m^2)

$\ddot{\Theta}_{tc}$ = angular acceleration of the turbocharger (s^{-2}).

4.2.4 The Charge Air Cooler.

Because of the low engine compression ratio and the necessity of ensuring good self ignition conditions in the engine cylinder, the charge air cooler may be by-passed in the Hyperbar system, and the charge air heated by a small burner in the inlet manifold or exhaust gas recirculation. However, at high engine loads, and consequently high compressor outlet temperatures, a charge cooler is required to maintain the desired engine air flow (by increasing the air density) and to reduce the cycle temperatures, and hence the thermal loading of the engine.

The charge cooler model must be capable of predicting:-

(1) The cooler outlet air temperature.

(2) The pressure loss through the cooler.

(3) The transient response of the cooler under rapidly changing inlet air conditions.

While very detailed models for the charge cooler have been developed for use in engine simulation programs, e.g. Baazaari (8), the computer time required for the cooler calculations becomes disproportionately large, and this approach cannot be justified except for cooler design studies. Consequently simplified models, based on observation, and a limited amount of test data, have been developed.

Much of the experimental test data for this engine has been measured using a constant inlet manifold air temperature of 343 K (70°C), which was controlled by regulating the charge cooler water supply. Consequently no data was available regarding the effectiveness of the charge cooler. Measurements of the compressor outlet and inlet manifold pressures under steady state conditions were available, however, and these were used to estimate the charge cooler pressure loss. No transient response data was available for the cooler and consequently some simplifying assumptions about the response of the heat exchanger have been made. The models used to predict the charge cooler performance are described in the following sections.

4.2.4.1 The Charge Cooler Effectiveness.

Under steady state conditions, the charge cooler air outlet temperature, $T_{2'}$, can be defined in terms of the inlet air temperature, T_2, the coolant inlet temperature, T_{ic}, and the charge cooler effectiveness, ε, which can be defined, for a perfect gas, as:-

$$\varepsilon = \frac{T_2 - T_{2'}}{T_2 - T_{ic}} \tag{4.29}$$

where,

T_2 = cooler stagnation inlet air temperature (K)

$T_{2'}$ = cooler stagnation outlet air temperature (K)

T_{ic} = coolant inlet temperature (K)

Using a detailed finite difference model of an air to water cross flow heat exchanger, Baazaari (8) studied the effects of various parameters on the cooler performance. He found that the cooler effectiveness:-

(1) reduces as the air mass flow rate through it increases,

(2) increases as the inlet air temperature increases,

(3) increases as the coolant inlet temperature increases.

He also found that the cooling water mass flow rate had little influence on the effectiveness at low air mass flow rates, but at high air flow rates increasing the water flow can significantly improve the heat exchanger effectiveness.

Experimental test data, measured by the engine manufacturer, was available for a single stage turbocharged aftercooled version of this engine, over a wide load and speed range. Unfortunately insufficient data was available to correlate the charge cooler effectiveness with the air mass flow rate, air inlet temperature, coolant inlet temperature and coolant mass flow rate, and so a simpler correlation has been developed, which gives the charge cooler effectiveness as a function of the air mass

flow rate only:-

$$\varepsilon = 0.905 - 0.171.\dot{m}_E - 0.058.\dot{m}_E^2 \qquad (4.30)$$

where,

$\dot{m}_E$ = engine mass flow rate (kg/s)

This correlation is compared with the test data in Fig. 4.5a. There is some scatter in the test data, especially at low engine speeds, where the temperature drop is small and measurement errors become more significant.

Equation. (4.30) has been used throughout this work for the Hyperbar engine, with the coolant inlet temperature, T_{ic}, maintained at 298 K (25°C), except for the cases where the cooler outlet temperature was fixed, in the comparison of the experimental and predicted engine performance, see Chapter 5.

It is important to note that the Hyperbar engine is designed to run at much higher engine A/F ratio's than conventionally turbocharged engines, and consequently at a given rating, the engine air flow will be higher, and the cooler effectiveness lower, unless the cooler is rematched for this engine. The heat transfer rate from the charge cooler has been shown to be significantly higher than for conventional turbocharging systems, because of the higher air flow rates and boost pressures (97).

4.2.4.2 The Charge Cooler Pressure Loss.

The pressure drop across the charge cooler can be related to the dynamic head of the air entering the cooler (89). In this case the relationship will be of the form:-

$$\Delta p = 0.5.C.\rho_2.u_2^2.10^{-3} \qquad (4.31)$$

where,

C = empirical constant for the cooler

Δp = pressure drop across the cooler (kN/m^2)

u_2 = air velocity at entry to the cooler (m/s)

ρ_2 = air density at entry to the cooler (kg/m^3)

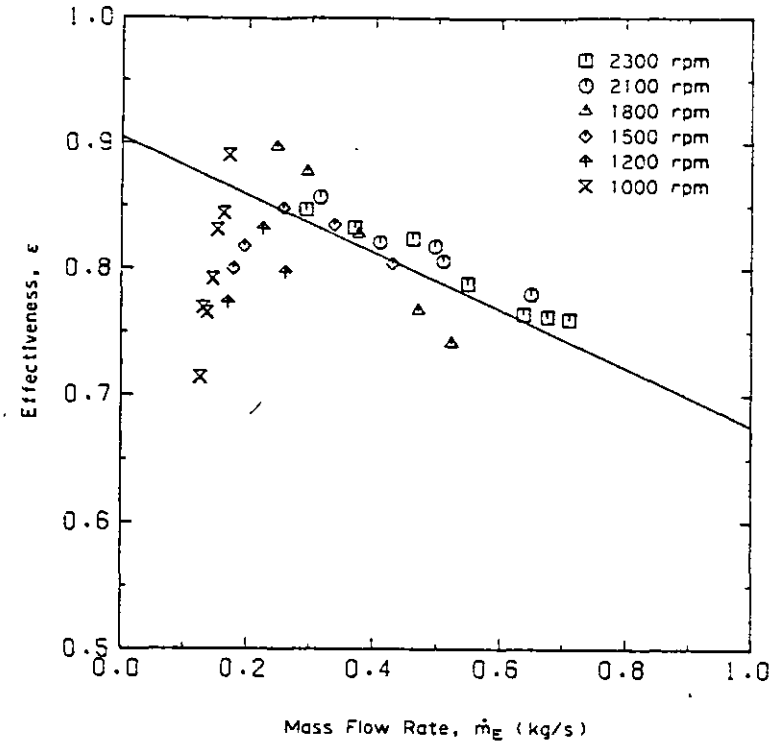

Fig. 4.5a The Charge Cooler Effectiveness ε.

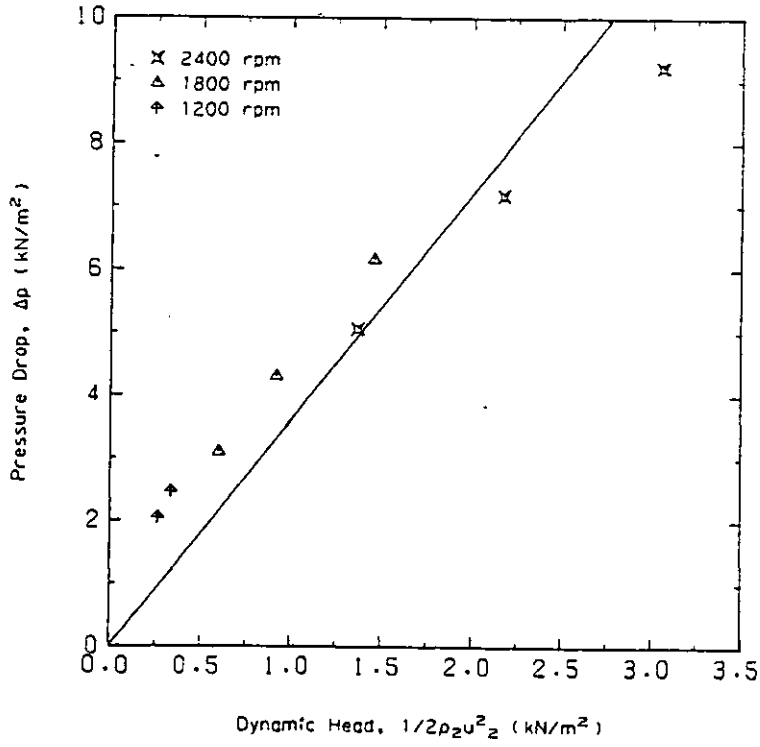

Fig. 4.5b The Charge Cooler Pressure Drop Δp.

Equation (4.31) can be written in terms of the mass flow rate entering the cooler, m_E, and the cooler inlet pressure and temperature:-

$$\Delta p = 0.5.C.\left(\frac{R_2.T_2}{p_2}\right).\left(\frac{\dot{m}_E}{A_{cc}}\right)^2.10^{-3} \qquad (4.32)$$

where,

A_{cc} = cross sectional area at entry to the cooler (m^2)

p_2 = air pressure at entry to the cooler (kN/m^2)

R_2 = gas constant for the air entering the cooler (kJ/kg.K)

T_2 = air temperature at entry to the cooler (K)

Thus it can be seen that the pressure drop will increase with higher air mass flow rates and inlet temperatures, and decrease with higher inlet pressures.

Fig. 4.5b shows the limited amount of test data that was available for the Hyperbar engine charge cooler pressure drop, at three engine speeds. Taking measured values of the cooler inlet conditions, p_2 and T_2, the estimated engine mass flow rate, $\dot{m}_E$, and the geometric cooler inlet area, the best fit to the test data was obtained by using, C=3.60 in eqn. (4.32).

4.2.4.3 The Charge Cooler Transient Response.

Baazaari (8) has calculated the response of the charge cooler air outlet temperature to a step change in the air inlet temperature (the air mass flow rate, coolant flow rate and inlet temperature, etc., being held constant). The response of the cooler air outlet temperature was found to be primarily a function of the air mass flow rate and the size of the cooler (i.e. as soon as the heat exchanger was filled with air at the new temperature the main part of the response was completed). The rest of the outlet air temperature response takes place more slowly, due to the thermal capacity of the heat exchanger walls, which therefore have a relatively minor influence on the air outlet temperature.

The charge cooler effectiveness, calculated from steady state test data, eqn. (4.30)

cannot therefore, be used to predict the instantaneous charge cooler air outlet temperature under conditions of changing engine speed and/or load.

A simple empirical model has been used to calculate the charge cooler air outlet temperature, which changes to the new steady state value in an exponential manner, i.e.:-

$$T_{2',n+1} = T_{2',n} + (T_{2'ss,n+1} - T_{2',n}).(1 - e^{-\Delta t/\alpha}) \quad (4.33)$$

where,

Δt = calculation time step between n and n+1 (s)

n = step number

α = time constant for the cooler (s)

and the subscript, ss, indicates the conditions that would be achieved during steady state operation. $T_{2'ss,n+1}$ is therefore calculated using eqns. (4.29) and (4.30).

The "time constant", α, represents the filling time for the charge cooler and the thermal capacity of its walls. The filling time is a function of the air mass flow rate entering the cooler and its volume, while the thermal capacity of the cooler depends upon the wall thickness, material, geometry, etc. Neglecting the thermal capacity effects, the "time constant" can be approximated by:-

$$\alpha = \frac{V_{cc}.p_2}{\dot{m}_E.R_2.T_2} \quad (4.34)$$

where,

V_{cc} = charge cooler air side volume (m^3)

Clearly the "time constant", α, will vary according to the engine operating conditions. Fig. 4.5c shows the air outlet temperature predicted using eqn. (4.33) as a function of the "time constant" for a steady state change in the outlet temperature ($T_{2'ss,n+1}$-$T_{2',n}$) of 50°C.

As no response data was available for the actual charge cooler used on the Hyperbar engine, a suitable value for the "time constant" has been estimated. Comparing the

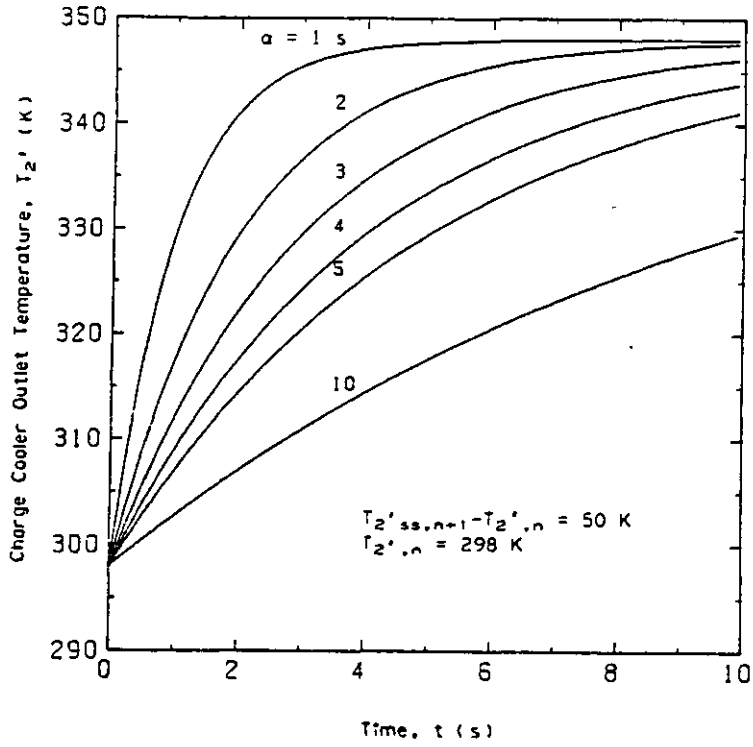

Fig. 4.5c Transient Response of the Charge Cooler.

response curves predicted using eqn. (4.33) with the data presented in (8), for an 8.2 litre two stage turbocharged intercooled and aftercooled engine, shows that typical values for α are in the range 1.4 to 3.1 seconds. The Hyperbar engine has a large charge cooler volume (1.27 times the engine swept volume), and typical values of the volumetric engine flow rate vary from 0.12 m^3/s at 800 rpm/17.74 bar BMEP to 0.37 m^3/s at 2400 rpm/17.09 bar BMEP.

The value used for the charge cooler "time constant" throughout this work was:-

$$\alpha = 4.0 \quad s \tag{4.35}$$

although lower values of α would probably have been more realistic, due to the high engine A/F ratio's which reduce the "filling time".

4.3 The Combustion Process.

4.3.1 Introduction.

A simplified model is required to reproduce the effects of combustion in a direct injection diesel engine. The model must be capable of predicting the engine performance parameters required by the designer (IMEP, maximum cylinder pressure, etc.) accurately over the entire operating range of the engine, and must respond sensibly to changes in operating conditions, such as the ambient pressure and temperature. In addition a model is required that will allow the effects of combustion to be predicted when the engine speed and/or load is changing during transient operation.

Consequently an empirical model has been developed, based on a limited amount of engine test data, and experience gained with other engines with similar combustion systems. Component models are required for:-

(1) The injection delay.

(2) The ignition delay.

(3) The combustion process.

(4) The gas properties.

Only experimental versions of the Hyperbar engine had been built at the start of this project, and consequently very little test data was available. The correlations for the injection delay, ignition delay and combustion processes have therefore been developed using data from a conventional single stage turbocharged and aftercooled version of the same basic engine. The models have been used for the Hyperbar engine without modification, despite the changes in engine compression ratio and fuel injection equipment, which will inevitably effect the combustion process.

4.3.2 Injection Timing.

The fuel pump starts to deliver fuel into the injector feed lines at a certain crank angle, known as the static injection timing. The resulting pressure pulse travels along the pipe until it opens the injector needle and fuel injection into the cylinder commences. The injection delay can therefore be defined as the period between the start of pumping and the start of injection. The start of pumping can be varied on some fuel pumps, but was fixed in this particular application.

The velocity of the pressure pulses travelling along the injector feed lines is a function of the fuel bulk modulus of elasticity, which is primarily a function of the fuel temperature, which remains approximately constant. Therefore the injection delay is primarily a function of the length of the feed lines. The dynamic injection timing is the point at which the injector needle starts to open and fuel injection begins. Fig. 4.6 shows the dynamic injection timing for this engine as a function of load and speed, for a static injection timing of 22°CA BTDC. There is no aneroid (boost controlled) timing device (ATD) on this fuel pump.

The increase in injection delay, in terms of crank angle, with engine speed is clearly shown. Fig. 4.6 also shows the injection delay time as a function of load and speed, demonstrating the reduction in injection delay with increased load, but no clear dependence on engine speed.

No strong correlation could be found between the injection delay and the speed and/or load, although such correlations have been developed by other workers (8). Consequently a simple time delay has been used to calculate the dynamic injection timing:-

$$\delta_{inj} = 0.6 \quad \text{ms} \tag{4.36}$$

This value of injection delay is biased towards the experimental values measured at the higher loads, because the effect of errors in injection timing on IMEP and maximum cylinder pressure are generally more critical at high engine power outputs.

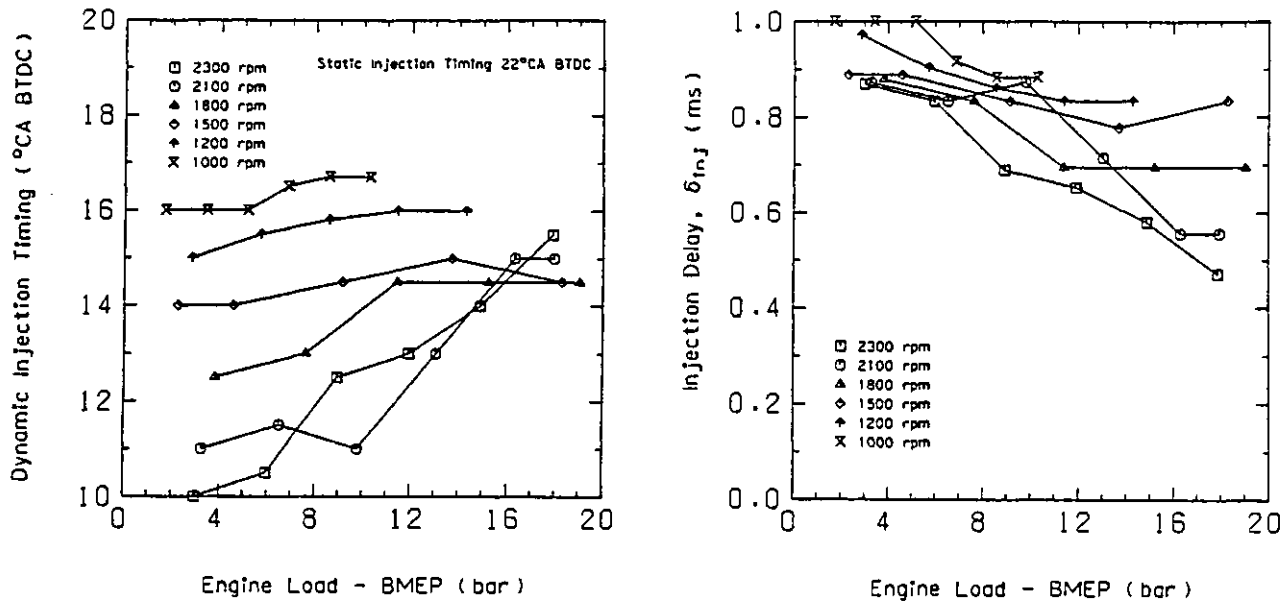

Fig. 4.6 Experimental Dynamic Injection Timing as a Function of Load and Speed.

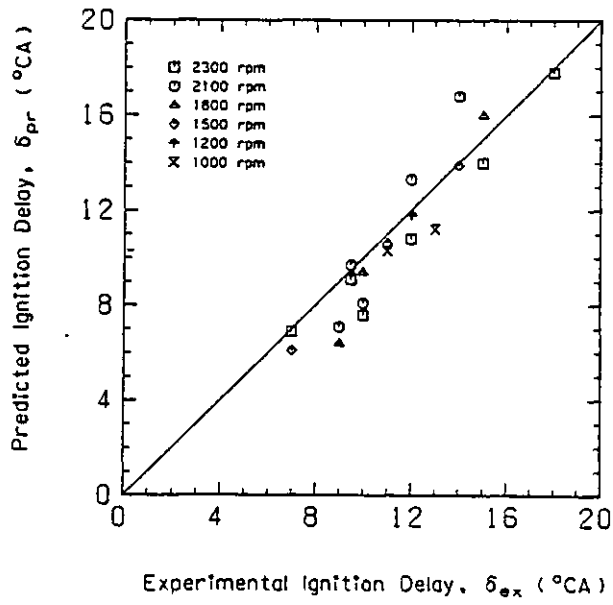

Fig. 4.7 Comparison of Experimental and Predicted Ignition Delay.

The experimentally measured dynamic injection timing was used at each operating condition during the development of the combustion model, to eliminate any errors in dynamic timing caused by using a correlation of the form given in eqn. (4.36). This also enabled the ignition delay to be calculated from the correct dynamic injection point.

Later tests were carried out with the static injection timing retarded to 20°CA BTDC to give the same dynamic timings over the speed range as that of the two stage turbocharged version of this engine, and to enable very high BMEPs to be developed without excessively high peak cylinder pressures. For these and all subsequent tests eqn. (4.36) has been used without modification.

4.3.3 Ignition Delay.

Combustion in a diesel engine cylinder is normally considered to commence at the dynamic injection point, and to comprise of an ignition delay followed by a period of heat release. The length of the ignition delay is of considerable importance since it affects the development of the processes following ignition and hence the rate of pressure rise, IMEP, etc.

The duration of the ignition delay is influenced by the physical and chemical properties of the fuel, the temperature and pressure of the compressed air, the degree of fuel atomisation, the nature and degree of swirl, the cylinder wall temperatures, the injection pressure and rate, the number of injector holes and their size and orientation, etc.

The delay period can be subdivided into physical and chemical parts, the former representing the time between the start of injection and the preflame reactions. The physical processes involved are, spray disintegration and droplet formation, air entrainment, heating of the liquid fuel and evaporation, mass transfer away from the droplet surface and combustible mixture formation. The chemical delay is due to the decomposition of the heavy hydrocarbons into lighter compounds, the formation of intermediate compounds and autoignition reactions. There is no distinct line between the time taken for the physical and chemical processes involved, as they overlap due to the highly heterogeneous state of the fuel-air mixture, and the fact that injection

takes a finite time.

The chemical processes start at a very slow rate directly after the fuel vapour comes into contact with the air, and consequently the chemical delay period reduces rapidly with increasing temperature and slightly with increasing pressure. However, during the early stages of combustion the mass of fuel vapour which undergoes chemical reaction is small compared to the masses necessary to cause a detectable pressure or temperature rise due to combustion. The early stages of the preignition process may therefore be considered to be dominated by the physical processes. The physical delay can be reduced by employing high injection pressures, and high turbulence in addition to high gas temperatures, but this will also be accompanied by an increase in the amount of combustible "premixed" fuel-air mixture.

Immediately after the begining of injection the gas temperature is usually relatively low and the burning rate is slow. Heat is transferred from the compressed air to the incoming fuel as it evaporates, which causes an apparent negative rate of heat release (see section 4.3.4). As the temperature rises, the burning rate increases, accelerating the temperature rise until the cylinder pressure increases above that due to the compression process alone. The ignition point can therefore be considered as the point at which the rate of heat release becomes positive.

4.3.3.1 Empirical Correlations for the Ignition Delay.

The ignition delay is considered as the time interval between the dynamic injection point (defined as the point at which the injector needle starts to lift), and the ignition point (defined as the start of positive heat release due to combustion). Other definitions of ignition delay are unsuitable for use in a simulation program, since they rely upon either changes of the shape of the cylinder pressure diagram, flame visibility or reaction temperature.

Many researchers have developed empirical correlations between the ignition delay period, δ, and the mean gas pressure, p_m, and temperature, T_m, during the delay. Many of the correlations have the general form:-

$$\delta = a_1.\exp(a_2/T_m).p_m^{a3} \qquad (4.37)$$

where,

p_m = mean gas pressure during the ignition delay (bar)

T_m = mean gas temperature during the ignition delay (K)

δ = ignition delay (ms)

The values for the empirical constants, a_1, a_2 and a_3, obtained by various researchers are given in Table 4.1.

	a_1	a_2	a_3
Baazaari (8)	3.454	2100.8	-1.0218
Marzouk (89)	3.52	2100.8	-1.0218
Schmidt (122)	0.0646	6330	-1.08
Wolfer (179)	0.429	4650	-1.19
Zimmerman (187)	0.392	4650	-1.05

Table 4.1 Empirical Constants for the Ignition Delay Correlation, eqn. (4.37).

Sitkei (130) has attempted to separate the physical and chemical parts of the ignition delay. His correlation, eqn. (4.38), is suitable for quiescent type, medium speed engines:-

$$\delta = 0.5 + 0.1332.\exp(3928/T_m).p_m^{-0.7} + 4.6345.\exp(3928/T_m).p_m^{-1.8} \quad (4.38)$$

The above correlations are applicable for a "typical" diesel fuel (with a Cetane No. of approximately 52). Other researchers have included the influence of the fuel quality, represented by the Cetane No.

Shipinski et. al. (127) give:-

$$\delta = .0.00965.(40/CN)^{0.69}.p_m^{-0.386}.\exp(4644.4/T_m) \quad (4.39)$$

where,

CN = Cetane No.

Hardenberg and Hase (54) also considered the effect of engine speed and mean piston velocity on the ignition delay period:-

$$\delta = \frac{(60+36.7.C_m).\exp\left[\frac{74430}{(CN+25).T_{im}.CR^{c-1}} - \frac{36}{(CN+25)} + \left(\frac{21.2}{p_{im}.CR^c-12.4}\right)^{0.63}\right]}{N_E} \quad (4.40)$$

where,

c = polytropic exponent of compression (typically 1.37)

C_m = mean piston velocity (m/s)

CR = compression ratio

N_E = engine speed (rpm)

p_{im} = mean pressure in the inlet manifold (bar)

T_{im} = mean temperature in the inlet manifold (K)

The terms $p_{im}.CR^c$ and $T_{im}.CR^{c-1}$ replace the mean gas pressure and temperature during the ignition delay, p_m and T_m, in the correlations based on eqn. (4.37).

The dynamic injection timing at each engine test condition was taken from the experimental injector needle lift diagram, and the ignition point was taken as the point at which the cylinder pressure diagram deviated from the compression curve. The various ignition delay correlations discussed were then used to predict the ignition point using the experimental dynamic injection timings at each operating condition, and the gas pressure and temperature predicted by the simulation program. The best agreement with the test data was obtained using the correlation developed by Baazaari (8):-

$$\delta = 3.454.\exp(2100.8/T_m).p_m^{-1.0218} \quad (4.41)$$

The experimental and predicted ignition delays are compared in Fig. 4.7. It should be noted that the definition of the ignition delay is different for the experimental and predicted data, the former using the time delay from the start of injector needle lift

to the start of cylinder pressure rise due to combustion, and the latter using the time delay up to the start of positive heat release. This correlation does, however, predict the ignition delay with reasonable accuracy over the load and speed range of the test data.

4.3.4 Combustion Models.

There are many models currently under development to simulate the combustion processes and pollutant formation in a diesel engine. A diesel combustion simulation requires models of compressible, viscous air motion, fuel spray penetration, droplet break-up and evaporation, air entrainment, chemical kinetics, turbulent diffusion, etc. To cater for the spacial and temporal variations in composition and burning rate, the model should be three-dimensional and unsteady. Results published by Hiroyasu (56,57), Shahed et. al. (30,125,126) and others are encouraging, but current predictions are qualitative rather than quantitive and require extensive experimental test data for their development. A multi-zone diesel combustion model is being developed for use in, or with, the transient response simulation program, and this is capable of predicting realistic heat release diagrams, see Meguerdichian et. al. (92). At the present stage of development, however, it is inappropriate to adopt anything more than an empirical model in a transient simulation program.

A relatively successful approach to the problem of combustion modelling within an engine cycle simulation has been to represent the overall thermal effects of the combustion process by an apparent heat release rate (AHRR) or apparent fuel burning rate (AFBR). While this approach cannot replace fundamental combustion research, because it tells us nothing about the details of the processes involved, it does represent the overall effects of combustion, enabling predictions to be made of the engine performance parameters required by the designer.

4.3.5 Analytical Expressions for the Fuel Burning Rate.

Analytical functions describing the pattern of the AFBR have been reported, the most common being a triangular shape (86), or the Wiebe function (175) because of their simplicity. The influence of the shape of the analytical AFBR function on the cylinder pressure diagram has been studied by Lyn (86).

Lyn (87) has also proposed a graphical method for obtaining the AFBR, which subdivides the injection rate diagram into elements of equal duration. Fuel elements were assumed to enter the combustion chamber and mix with the air successively, each becoming ready for burning according to a specified (triangular) pattern. Fuel mixing during the ignition delay period was added to the total rate of mixture preparation diagram, this leading to the high initial burning rate. The high degree of empiricism involved greatly limits the applicability of this method.

Austin and Lyn (7) used a modified model based upon the burning of single droplets in free air to take account of the decrease in burning rate later in the combustion period. The burning time for each element injected was allowed to increase progressively.

Nagao et. al. (106) used the same incremental injection approach, and assumed that each element burned completely within 1°CA following its injection delay period. The vapourisation rate and ignition delay were computed for each element using single droplet theory and Wolfer's formula (179) respectively.

A modified spray droplet burning model based on single droplet theory was presented by Shipinski et. al. (127), in which the Sauter mean diameter and droplet size distribution were calculated according to proposals by Knight (71) and Tanasawa (139). Ignition delay for each element was determined by a Wolfer type formula.

A simple empirical model linking the cumulative fuel injected and the burning histories was described by Whitehouse et. al. (174). The rate of mixture preparation was related to the surface area of the fuel droplets and the partial pressure of the oxygen. An Arrhenius type expression was used to describe the heat release pattern

during the initial premixed combustion phase (starting at the injection point).

4.3.6 Apparent Fuel Burning Rate.

A simplified single zone combustion model has been widely applied to engine cycle simulations (73,89,128,181). This approach considers the cylinder contents to be a homogeneous mixture of ideal gases which are always in thermodynamic equilibrium, free of temperature and property gradients, pressure waves, etc. Combustion is modelled as a uniformally distributed heat source, which emits instantaneously burning fuel at a rate equivalent to a specified time varying pattern, known as the apparent fuel burning rate (AFBR).

The relationship between the fuel burning rate and the resultant heat release rate is based on the assumption that thermodynamic and chemical equilibrium exist at all times. All the fuel injected is considered to react (not necessarily completely) irrespective of the equivalence ratio. For lean mixtures ($F<1$) and in the absence of dissociation effects, the two rates are directly proportional. This linear relationship is considered to apply until either dissociation starts or the charge equivalence ratio exceeds unity. Beyond the stoichiometric equivalence ratio any increase in the amount of reacting fuel leads to a reduction in the specific cumulative heat release. Dissociation affects the above relationships in regions of high temperature, low pressure and when the equivalence ratio is close to unity. Thus formulation of a correlation based upon the AFBR rather than the AHRR greatly simplifies the handling of rich fuel-air mixtures.

Apparent fuel burning rate diagrams may be derived from experimental cylinder pressure diagrams using the assumptions described in section 4.1. The proceedure is to conduct an instantaneous energy balance of the cylinder contents during the closed cycle period. This, in effect, is the reverse of the normal cycle calculation, when combustion rate is an input parameter and the resultant cylinder pressure diagram is calculated.

Probably the first attempt to calculate the AFBR was by Schweitzer (124) which resulted in burning curves that could only be used for comparative purposes, due to the crude simplifications necessarily employed at the time. With the introduction of

detailed mathematical simulations of engine cycles, and computer based data logging of engine performance parameters, methods of obtaining more accurate AFBR diagrams have been developed. Probably the best known method for determining the AFBR from cylinder pressure data is described by Krieger and Borman (73), and this is outlined in section 4.3.7.

4.3.7 Calculation of the Apparent Fuel Burning Rate.

Using the energy eqn. (4.1), the thermodynamic property relationships, eqns. (4.4) and (4.5), the ideal gas equation of state, eqn. (4.6), and the definition of equivalence ratio, eqn. (4.3), for the closed cycle period the AFBR can be calculated.

The equivalence ratio at any instant during the closed cycle is given by:-

$$F = \frac{(m_{fo} + m_f)}{m_{ao}.f_s} \tag{4.42}$$

where,

m_{ao} = initial mass of air trapped in the cylinder (kg)

m_f = fuel mass added during combustion (kg)

m_{fo} = initial mass of fuel trapped in the cylinder (kg)

and,

$$m_{ao} = \frac{m_o}{(1 + f_o)} \tag{4.43}$$

where,

f_o = initial fuel-air ratio in the cylinder $[f_o = m_{fo}/m_{ao}]$

m_o = initial mass in the cylinder (kg) $[m_o = p_o.V_o/(R_o.T_o)]$

where p_o, T_o, R_o and V_o are the cylinder gas pressure, temperature, gas constant and volume at the start of the calculation, typically at inlet valve closure (IVC), and:-

$$m_{fo} = \frac{m_o.f_o}{(1 + f_o)} \tag{4.44}$$

Using eqns. (4.42), (4.43) and (4.44) the instantaneous equivalence ratio is given by:-

$$F = F_o + \left(\frac{m}{m_o} - 1\right)\left(\frac{1 + f_o}{f_s}\right) \tag{4.45}$$

where,

m = instantaneous cylinder mass (kg)

Differentiating eqn. (4.45) with respect to time gives:-

$$\dot{F} = \left(\frac{1 + f_o}{f_s}\right)\frac{\dot{m}}{m_o} \tag{4.46}$$

The rate of change of cylinder mass during the closed cycle combustion period is equivalent to the AFBR, which can be expressed, from (73), as:-

$$\dot{m} = \frac{\frac{-m.R.T.\dot{V}}{V} - m.\frac{\delta u}{\delta p}.\dot{p} + \Sigma\dot{Q}_i - m.\Phi_5.\Phi_6}{u - h_f + \Phi_7.\frac{\delta u}{\delta F} - \Phi_6\left(1 + \frac{\Phi_7.\delta R}{R.\delta F}\right)} \tag{4.47}$$

where,

$$\Phi_5 = \frac{\dot{p}}{p} + \frac{\dot{V}}{V} - \frac{\dot{p}.\delta R}{R.\delta p} \tag{4.48}$$

$$\Phi_6 = \frac{T.\delta u/\delta T}{\left[1 + \frac{T.\delta R}{R.\delta T}\right]} \tag{4.49}$$

$$\Phi_7 = \left(\frac{1 + f_o}{m_o.f_s}\right).m \tag{4.50}$$

and,

h_f = total (stagnation) specific enthalpy of the fuel (kJ/kg)

Therefore to calculate the AFBR requires only measured values of cylinder pressure, p, and its first derivative, $\dot{p}$, all the other terms in eqn. (4.47) can be calculated. Reasonable estimates of the cylinder fuel-air ratio, f_o, and temperature, T_o, must be made at the start of the calculation, (typically at IVC) to enable the initial cylinder mass, m_o, and equivalence ratio, F_o, to be estimated. The resulting AFBR and its sensitivity to errors in pressure measurements, phase angle, initial conditions, etc., have been described in detail by Marzouk and Watson (90), who concluded that very

accurate cylinder pressure data is required in order to obtain reasonable AFBR diagrams.

This analysis does not take account of the fact that the cylinder mass actually changes only during the relatively short injection period (assuming no blow-by past the piston rings), and the reduction in gas temperature due to fuel evaporation after injection will result in negative AFBR's. Clearly the cylinder pressure data for this engine, obtained from photographs of oscilloscope traces, cannot be used to perform this type of AFBR analysis. The accuracy with which cylinder pressure measurements can be read from the photographs is doubtful, and the trace shows only one individual cycle (in some cases subsequent cycles can be overlaid) which may not be statistically representative of the engine performance at the test conditions (77), although cyclic variations in diesel engines are less severe than in spark ignition engines. In addition the AFBR is strongly dependent on the rate of change of cylinder pressure, which is difficult to read accurately from oscilloscope diagrams. Consequently an alternative proceedure for obtaining the AFBR has been developed.

4.3.7.1 Direct Calculation of the Apparent Fuel Burning Rates.

This method for deriving the AFBR, from limited experimental data, has been developed by the author, from an idea suggested by Marzouk. The method assumes that the AFBR will conform to a given pattern, as defined by a set of algebraic expressions. The shape of the AFBR can then be varied for different operating conditions by varying the "shape factors" in these expressions to match the experimental and predicted cylinder pressure diagrams. The optimum "shape factors" obtained, at different operating conditions over the speed and load range of the engine, can then be correlated to the dominant engine controlling parameters, such as engine speed, trapped equivalence ratio, ignition delay, etc.

The actual functions used to describe the AFBR have been taken from earlier work by Marzouk (89), and have been shown to be flexible enough to describe the AFBR over a wide range of engine operating conditions.

4.3.7.2 Analytical Representation of the AFBR.

The combustion process is assumed to start at the dynamic injection point and to comprise of two distinct phases, ignition delay and heat release. Ignition delay is related to conditions in the cylinder after the start of injection, see section 4.3.3.1. The heat release phase is considered to consist of two distinct modes of burning, "premixed" and "diffusion". These two mechanisms are assumed to begin at the ignition point and to proceed concurrently for a small proportion of the heat release period, until the amount of fuel-air mixture prepared prior to ignition is exhausted. Burning then proceeds by "diffusion" burning alone.

Analytically, the instantaneous rate of burning may be expressed as the sum of these two components:-

$$\dot{m}_t = \dot{m}_p + \dot{m}_d \qquad (4.51)$$

where $\dot{m}$ is the fuel burning rate and the subscripts t, p and d denote total, premixed and diffusion respectively. The use of a two part burning rate expression ensures that the shape of the AFBR can faithfully reproduce the measured AFBR diagrams, particularly on high speed DI engines. A single expression, such as a Wiebe function has been applied to quiescent type, direct injection, medium speed engine combustion chambers by Woschni et. al. (181) with some success, but cannot reproduce the "premixed" burning mode commonly observed.

In order to quantify the proportion of the fuel burnt by either mechanism, a "mode of burning factor", β, is introduced. This expresses the cumulative fuel burnt by "premixed" burning as a function of the total fuel injected:-

$$\beta = \frac{m_p}{m_t} \qquad (4.52)$$

where,

$$m_t = m_p + m_d \qquad (4.53)$$

Non-dimensionalising eqn. (4.51) using the nominal burning duration, Δ, and the total quantity of fuel injected, m_t, gives:-

$$\dot{M}_t(\tau) = \beta.\dot{M}_p(\tau) + (1 - \beta).\dot{M}_d(\tau) \tag{4.54}$$

$$\dot{M}_k(\tau) = \frac{\dot{m}_k(\tau).\Delta}{m_k} \tag{4.55}$$

for k=d, p or t, and,

$$\tau = \frac{\Theta - \Theta_i}{\Theta_e - \Theta_i} = \frac{\Theta - \Theta_i}{\Delta} \tag{4.56}$$

where,

Θ = instantaneous crank angle

Θ_i = crank angle at the start of combustion

Θ_e = crank angle at the nominal end of combustion

Equation (4.54) gives the rate of burning as the sum of two dimensionless distributions weighted by the factor β. This weighting factor is considered to be controlled by the length of the ignition delay period and the trapped overall equivalence ratio (i.e. the amount of fuel injected in the delay period).

The shapes of the component burning rate distributions were selected by Marzouk (89) after consideration of the experimental burning rate data. The best representation of the experimental data was achieved using the following functions:-

$$M_p(\tau) = 1 - (1 - \tau^{cp1})^{cp2} \tag{4.57}$$

or,

$$\dot{M}_p(\tau) = c_{p1}.c_{p2}.\tau^{cp1-1}.(1 - \tau^{cp1})^{cp2-1} \tag{4.58}$$

and,

$$M_d(\tau) = 1 - \exp(- c_{d1}.\tau^{cd2}) \tag{4.59}$$

or,

$$\dot{M}_d(\tau) = c_{d1}.c_{d2}.\tau^{cd2-1}.\exp(- c_{d1}.\tau^{cd2}) \tag{4.60}$$

where c_{p1}, c_{p2}, c_{d1} and c_{d2} are the "shape factors". Note that the expression for the "diffusion" burning rate, eqns. (4.59) and (4.60), is a Wiebe function (175). The Wiebe function has also been used for the "premixed" rate equation (8), but less satisfactory results were obtained.

4.3.7.3 Effect of the "Shape Factors" on the Apparent Fuel Burning Rate.

The form and duration of the "premixed" burning portion of the AFBR is controlled by the "shape factors" c_{p1} and c_{p2}. The proportion of the total fuel that burns in this way is determined by the "mode of burning factor", β. Because eqns. (4.57) and (4.58) are non-dimensional the nominal combustion duration, Δ, will also affect the shape of the actual "premixed" burning rate.

Figs. 4.8 and 4.9 show the effect of varying c_{p1} and c_{p2} on the "premixed" burning rate diagram for $\beta=1$ (total "premixed" burning) and a nominal burning duration, Δ, of 125°CA. Fig. 4.8a shows the effect of increasing c_{p1} from 2.5 to 4.5 on the "premixed" burning diagram. The timing and magnitude of the peak and the "premixed" burning duration are controlled by c_{p1}. Fig. 4.8b shows the influence of c_{p1} on the "premixed" burning duration (defined as the period when $\dot{M}_p/\Delta > 4.10^{-5}$ °CA^{-1}), and the maximum burning rate, and its position with the "shape factor" $c_{p2}=5000$ and the total burning duration $\Delta=125$°CA. It can be seen that for values of c_{p1} below 1.25 the effective "premixed" burning duration is less than 1°CA. The cycle simulation program is usually run with a calculation step size of 1°CA, this being a compromise between accuracy and the computer time required. Therefore if c_{p1} is less than 1.25, depending upon the crank angle at which ignition occurs, the "premixed" burning rate at the calculation step could be zero, or any value up to the maximum $\dot{M}_p/\Delta$ (which is, for example, 14.66°CA^{-1} with $c_{p1}=1.1$). Consequently only values of c_{p1} greater than 2.0 were considered, giving an effective "premixed" duration of 6°CA or greater, and a maximum $\dot{M}_p/\Delta$ of 0.49°CA^{-1} or less.

Fig. 4.9 shows the effect of increasing c_{p2} in the range 1000 to 9000 on the "premixed" burning diagram. Large values of c_{p2} in eqn. (4.58) produce a burning rate curve with a steep rise and fall, characteristic of experimental "premixed" burning curves. Values of c_{p2} larger than 5000 do not produce any significant change in the shape of the "premixed" burning curve. The "premixed" burning can be eliminated

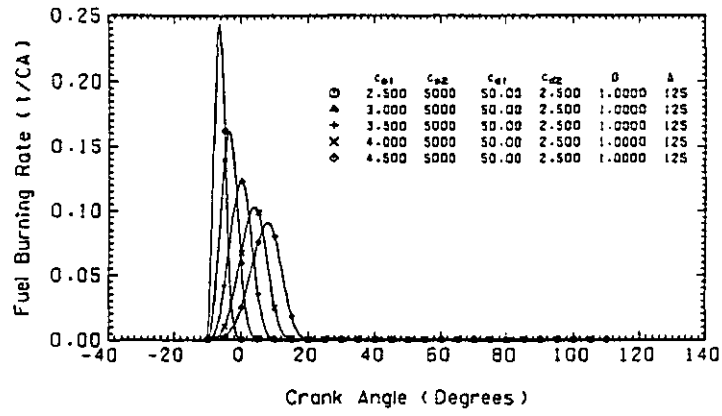

Fig. 4.8a Effect of the "Shape Factor" c_{p1} on the AFBR.

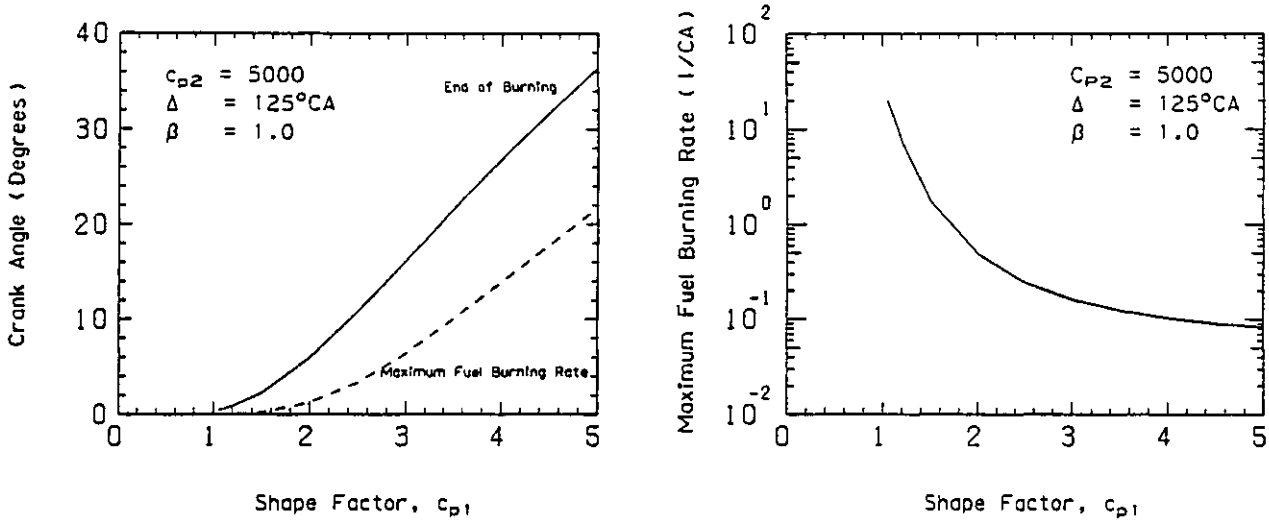

Fig. 4.8b Effect of the "Shape Factor" c_{p1} on the "Premixed" Burning Diagram.

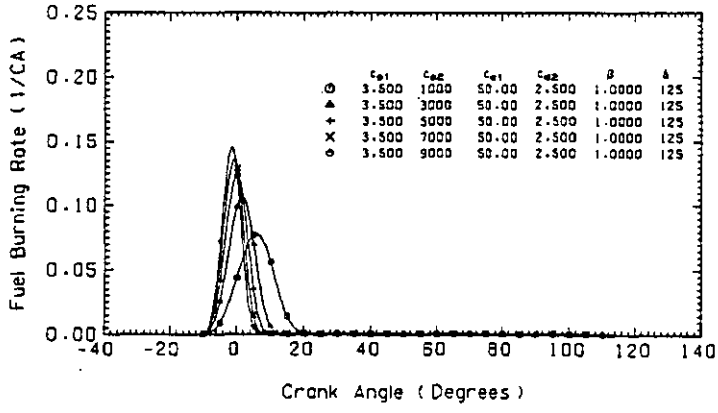

Fig. 4.9 Effect of the "Shape Factor" c_{p2} on the AFBR.

altogether by reducing β to zero.

Variation of c_{d1} and c_{d2} controls the shape of the "diffusion" burning part of the AFBR. As for the "premixed" case, the values of β and Δ will also influence the actual "diffusion" burning rate. Figs. 4.10 and 4.11 show the effect of c_{d1} and c_{d2} on the AFBR. The "shape factor" c_{d1} alters the rate of "diffusion" burning and therefore its duration, whilst c_{d2} has a stronger influence on the timing of the peak "diffusion" burning rate. However c_{d1} and c_{d2} interact more strongly than c_{p1} and c_{p2}, both terms effecting the actual combustion duration. Note that the scale on the AFBR axis is different from that in Figs. 4.8 and 4.9.

The parameter c_{d1} can be considered as a "combustion efficiency" term, since selection of an appropriate value ensures that the exponential burning rate term integrates to 100% fuel burnt by the end of combustion. With $c_{d1}=6.9$ in eqn. (4.59), 99.9% of the fuel in the "diffusion" burning mode burns by the end of combustion ($\tau=1$). Fig. 4.12 shows the influence of very low values of c_{d1} on the cumulative fuel burnt for typical values of c_{p1}, c_{p2}, c_{d2}, β and Δ. The influence of c_{d1} on the "combustion efficiency" will also depend upon the proportions of "premixed" and "diffusion" burning, ($\beta=0.5$ in Fig. 4.12).

Fig. 4.13 shows the effect of the "mode of burning factor", β, on the AFBR for variations between 0 and 100% "premixed" combustion. The area enclosed by the AFBR diagram is identical for each value of β (because c_{d1} is relatively large), and so a greater proportion of "premixed" burning causes a rapid increase in the initial burning rate, due to the relatively short duration, 21°CA, of the "premixed" burning part ($c_{p1}=3.5$).

Fig. 4.14 shows the influence of the nominal burning duration, Δ, on the shape of the AFBR for fixed values of c_{p1}, c_{p2}, c_{d1}, c_{d2} and β. It can be seen from these diagrams that the actual burning duration is always significantly shorter than the nominal duration, depending on the "shape factors" used, and so a constant value of Δ can be specified without any loss of generality.

This formulation of the combustion correlation provides a high degree of flexibility. Burning rate curves varying between the two extremes of 0 and 100% "premixed" burning can be represented by simply altering the value of β. Furthermore changes in

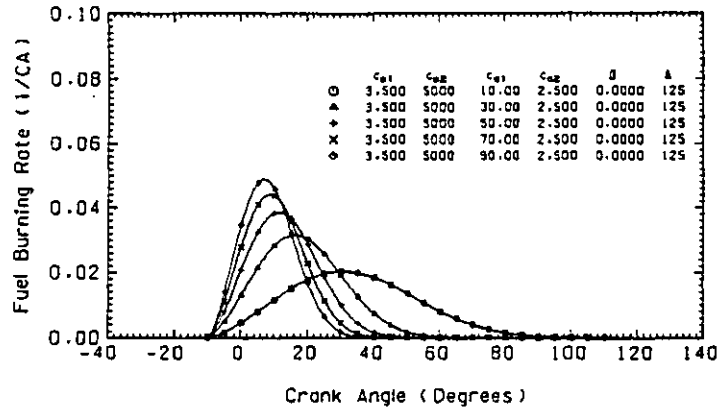

Fig. 4.10 Effect of the "Shape Factor" c_{d1} on the AFBR.

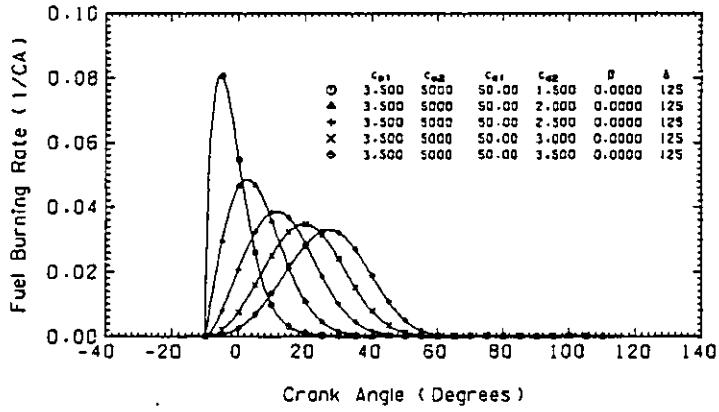

Fig. 4.11 Effect of the "Shape Factor" c_{d2} on the AFBR.

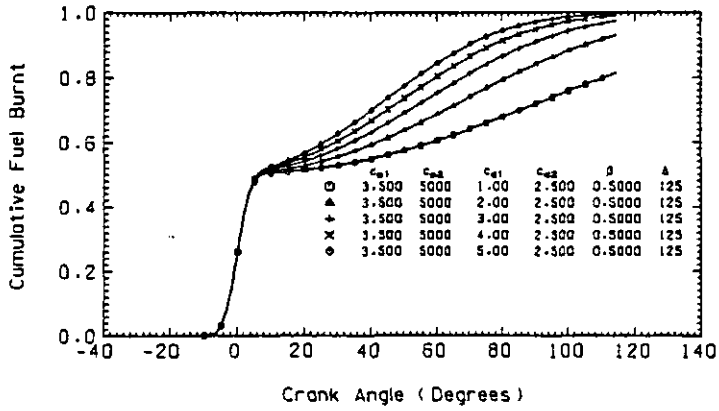

Fig. 4.12 Effect of Low Values of the "Shape Factor" c_{d1} on the Cumulative Fuel Burnt.

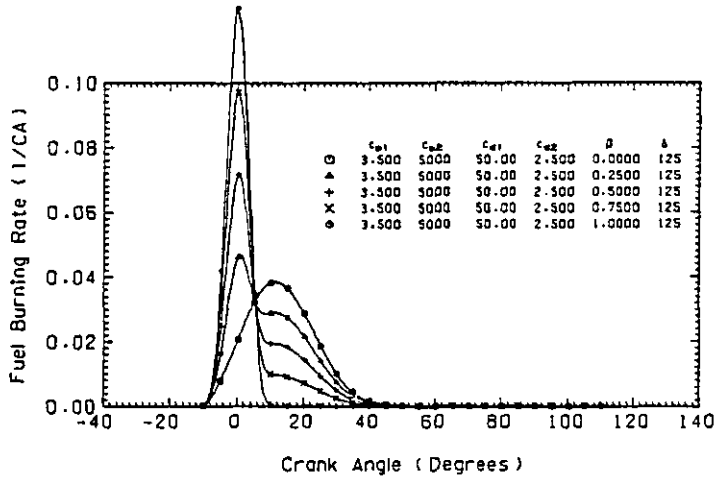

Fig. 4.13 Effect of the "Mode of Burning Factor" β on the AFBR.

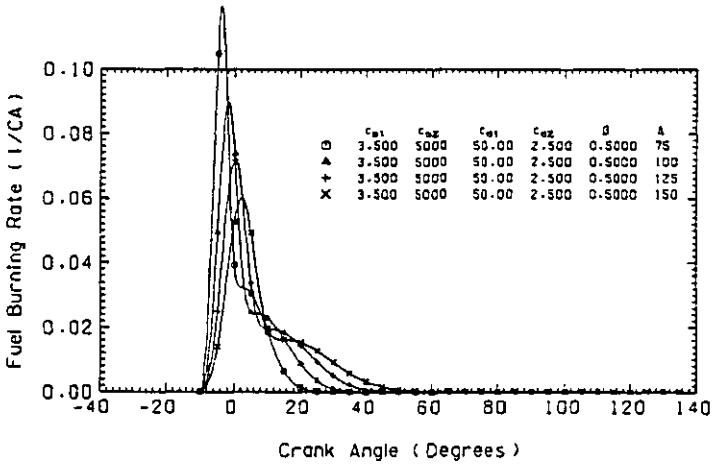

Fig. 4.14 Effect of the Nominal Combustion Duration Δ on the AFBR.

the burning rate with engine operating conditions can be described by correlating the "shape factors" c_{p1}, c_{p2}, c_{d1}, c_{d2} and β, as well as Δ, with engine operating conditions.

4.3.7.4 Calculation of the AFBR "Shape Factors".

Having defined the basic analytical framework for the AFBR, it was then necessary to find the "shape factors" c_{p1}, c_{p2}, c_{d1}, c_{d2}, β and Δ at a number of engine speeds and loads, and then to correlate these to the operating conditions.

The simulation program has been adapted to calculate the "best values" of the "shape factors", so that the predicted cylinder pressure diagram agrees as closely as possible with the experimental data available. Cylinder pressure data from the oscilloscope traces was digitized and scaled at 5°CA intervals over the closed cycle period at 21 steady state test conditions covering a speed range of 1000 to 2300 rpm, and a load range of 2.98 bar to 19.03 bar BMEP. Unfortunately, the majority of the data was at relatively high loads and speeds, and consequently and subsequent correlation will be biased to these conditions.

The simulation program was first run steady state for a number of engine cycles with a fixed boost conditions (taken from the test measurements), using the combustion correlation developed by Marzouk (89) for a high speed DI diesel engine. This allowed the program to calculate reasonable values of the wall temperatures and trapped conditions before the AFBR analysis commenced. Once the engine performance had stabilized, the calculated compression stroke was compared with the test data.

The mean pressure and crank angle compression stroke error may be defined between IVC and the dynamic injection point (DIP) as:-

$$\bar{p} = \left[\sum_{i=1}^{n} \frac{(p_{pri} - p_{exi})_{\theta i}^2}{n} \right]^{0.5} \tag{4.61}$$

and,

$$\bar{\theta} = \left[\sum_{i=1}^{n} \frac{(\theta_{pri} - \theta_{exi})_{pi}^2}{n} \right]^{0.5} \tag{4.62}$$

where n is the number of experimental points between IVC and DIP, p refers to the cylinder pressure and Θ to crank angle, and the subscripts pr and ex refer to predicted and experimental values respectively.

The cylinder pressure predicted during the compression stroke will not be affected by the combustion "shape factors" used in the subsequent closed cycle analysis. If the error in either the pressure or the crank angle was greater than a specified tolerance, the computation was temporarily aborted. For example, if the calculated pressure is significantly below the experimental value at the ignition point, then the combustion model will overestimate the initial AFBR in order to achieve a good cylinder pressure match over the entire combustion period. This results in an unrealistically high proportion of "premixed" burning, and a very rapid rate of pressure rise. If the cylinder pressure data is taken from an oscilloscope trace then there may be systematic errors in both the pressure and crank angle datums. The program can therefore shift the experimental data within the expected tolerance, in order to minimise the mean pressure and angle errors, $\overline{p}$ and $\overline{\Theta}$. As in other types of heat release analysis, described in section 4.3.7, the results are very sensitive to errors in the phase angle of the test data. For example, at the rated engine power at 2300 rpm, an angle error of -1°CA in the experimental test data causes a reduction in the predicted BMEP from 17.83 to 16.63 bar (the measured load was 17.88 bar BMEP).

The program then calculates the closed cycle of cylinder number 1 only, this being the cylinder for which the test data was recorded. A non-linear curve fitting technique, based on an algorithm developed by Powell (114), was used to vary the "shape factors" c_{p1}, c_{p2}, c_{d1}, c_{d2}, β and Δ and so produce a predicted closed cycle cylinder pressure diagram, using the measured engine fuelling. This diagram was then compared with the test data and the "shape factors" modified until the best least squares agreement was obtained.

For these tests the nominal burning duration, Δ, was fixed at the value used by Marzouk (89), so that the final correlation could be compared with his results. The nominal burning duration must be long enough to cover all the burning durations expected, but the actual end of combustion will effectively be decided by the "shape factors" c_{d1}, c_{d2} and β. The dynamic injection timing at each operating condition was taken as the start of injector needle lift from the experimental test data, and the

ignition delay calculated, based on the predicted cylinder gas temperature and pressure, see section 4.3.3.1. This enabled a check of the ignition delay correlation to be made, because if the delay is predicted inaccurately then the rest of the pressure diagram will be in error, or else the shape of the AFBR will be inappropriate.

The program was then run for a number of cycles for the complete engine (again with a fixed boost pressure and temperature to eliminate errors in predicting the turbocharger performance) using the best "shape factors", to obtain the overall performance parameters such as BMEP, BSFC, air flow rate, etc.

This calculation proceedure has been compared with the method described in section 4.3.7 for another high speed DI engine, the Perkins TV8 510, for which detailed experimental cylinder measurements were made by the author. The results show that this method can produce reasonably accurate AFBR diagrams, depending upon the quality of the original cylinder pressure data, and are discussed in detail by Watson et. al. (169).

Fig. 4.15 shows the predicted cylinder pressure diagrams over the load and speed range of the engine together with the experimental test data points at 5°CA intervals during the closed cycle period. Fig. 4.16 shows the resulting AFBR diagrams.

At 1000 rpm the combustion duration can be seen to increase with load, but the "premixed" burning peak should reduce as the load increases and the ignition delay reduces (compare the AFBR's at 1000 rpm with the results at 1200 rpm and 1500 rpm). At 1500 rpm/9.14 bar BMEP, the combustion duration should be between that predicted at 4.57 bar and 18.50 bar. At the higher speeds, 2100 rpm and 2300 rpm, it is possible to examine the effect of load on the AFBR in more detail. These diagrams show the reduction in the initial "premixed" peak and the increasing dominance of the "diffusion" burning mode as the load increases. The AFBR at 2300 rpm/2.98 bar BMEP appears to have an excessively long combustion duration and low "premixed" burning peak, this is probably due to errors in the cylinder pressure data, the simulation program requiring a good deal of late burning in order to raise the predicted pressure diagram to the experimental level. The AFBR's predicted at 2300 rpm/14.89 bar BMEP and 2300 rpm/17.88 bar BMEP are not consistent with the observations made at other speeds (or for other engines). The ignition delay, and hence the proportion of "premixed" burning should be larger at the lower load level.

1000 rpm/3.43 bar BMEP

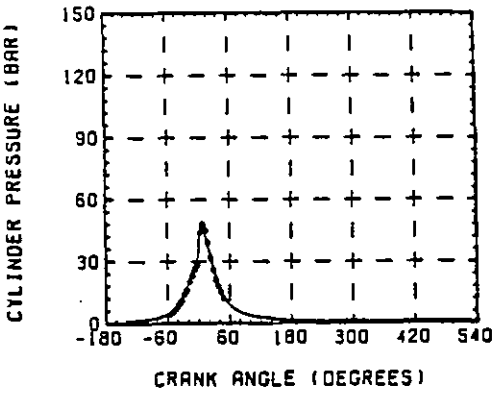

1000 rpm/6.85 bar BMEP

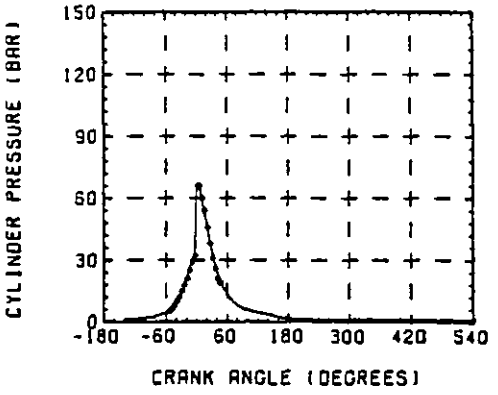

1200 rpm/5.71 bar BMEP

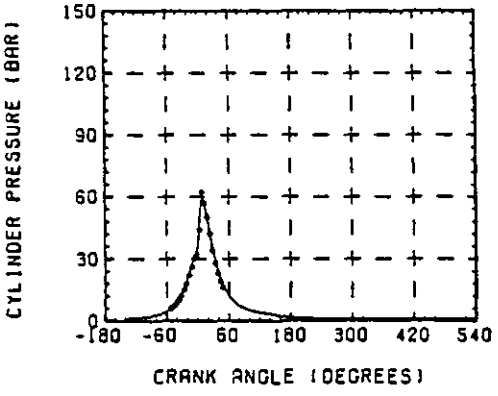

1200 rpm/11.42 bar BMEP

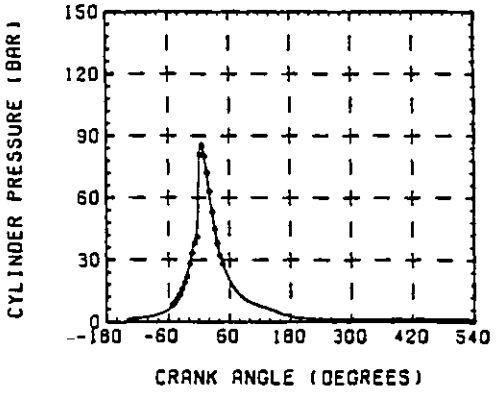

1500 rpm/4.57 bar BMEP

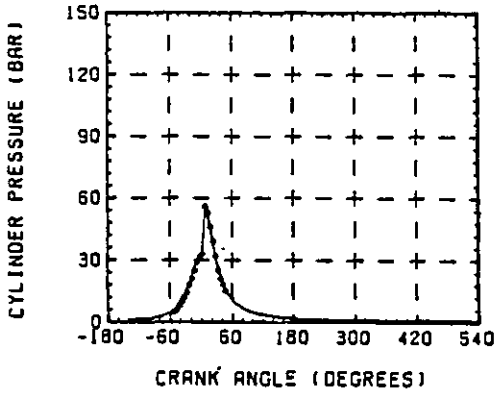

1500 rpm/9.14 bar BMEP

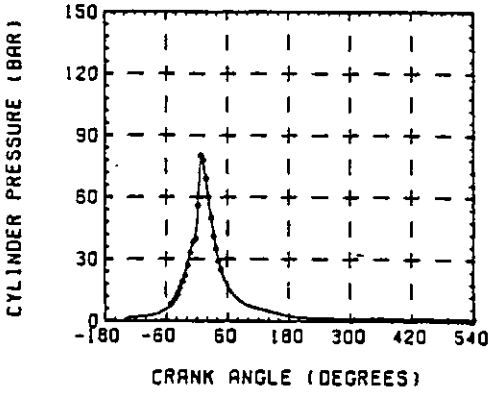

1500 rpm/18.50 bar BMEP

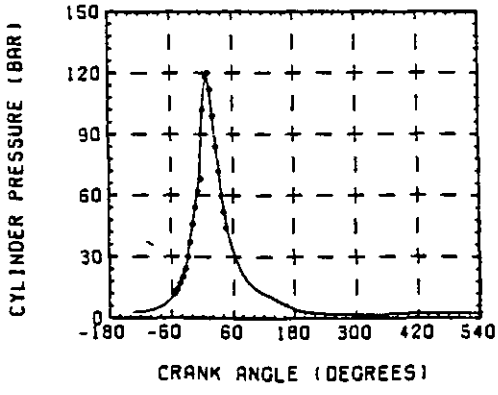

Fig. 4.15a Comparison of Experimental and Predicted Cylinder Pressure Data.

1800 rpm/3.81 bar BMEP

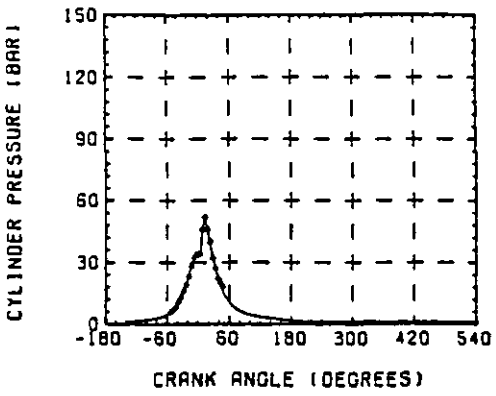

1800 rpm/11.42 bar BMEP

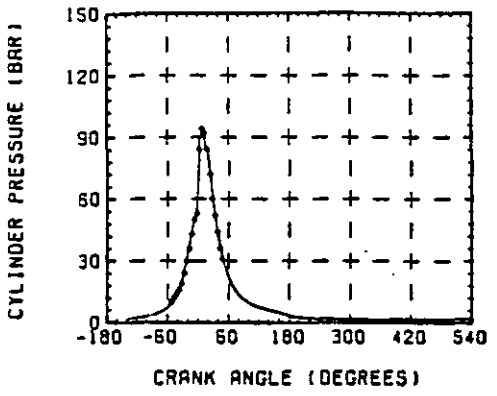

1800 rpm/19.03 bar BMEP

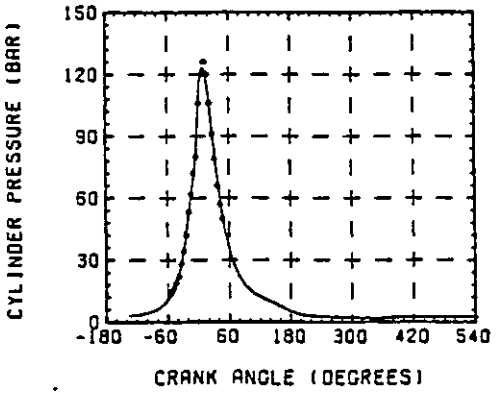

2100 rpm/3.26 bar BMEP

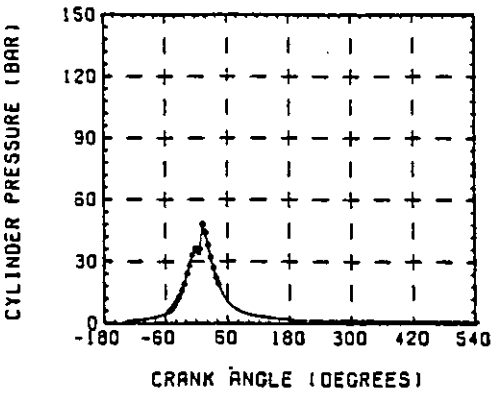

2100 rpm/6.52 bar BMEP

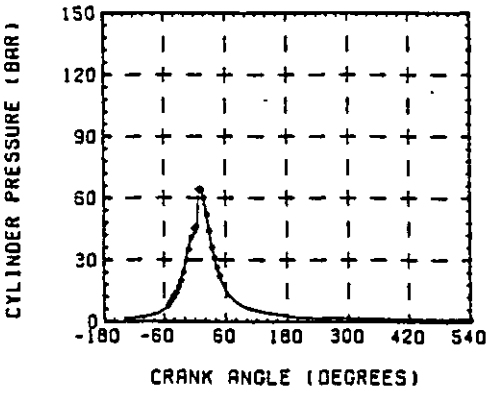

2100 rpm/9.79 bar BMEP

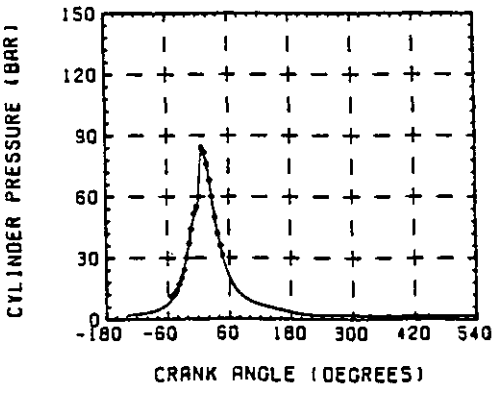

2100 rpm/13.05 bar BMEP

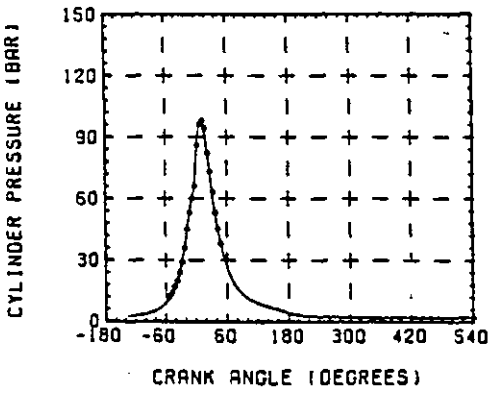

Fig. 4.15b Comparison of Experimental and Predicted Cylinder Pressure Data.

2100 rpm/16.31 bar BMEP

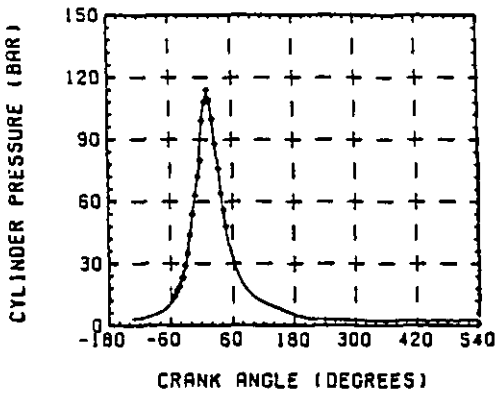

2300 rpm/2.98 bar BMEP

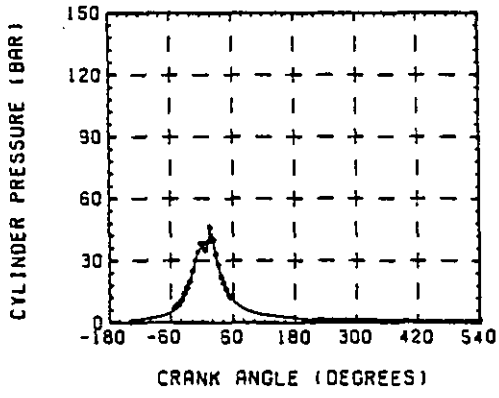

2300 rpm/5.96 bar BMEP

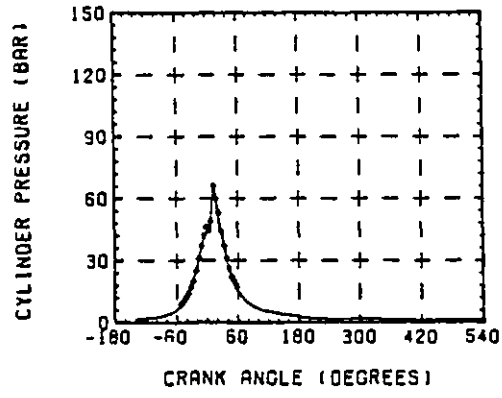

2300 rpm/8.94 bar BMEP

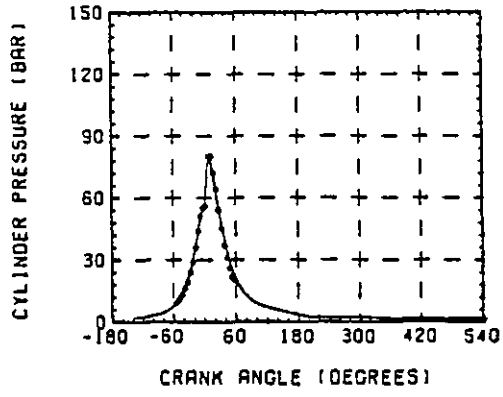

2300 rpm/11.91 bar BMEP

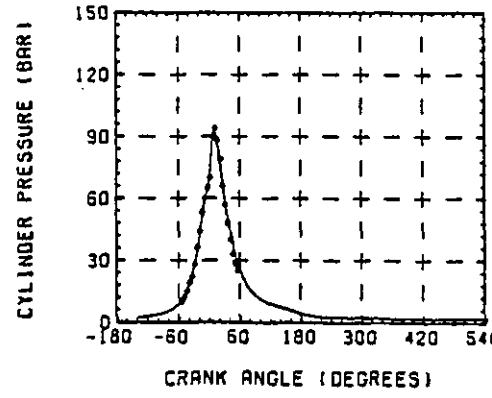

2300 rpm/14.89 bar BMEP

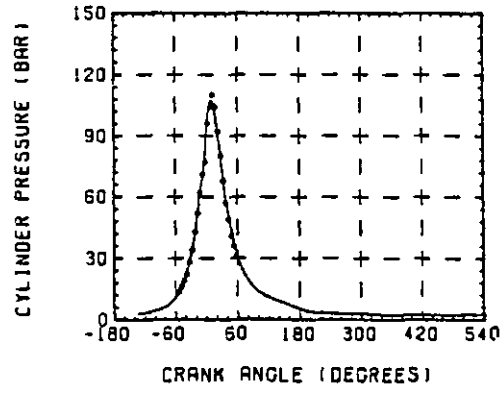

2300 rpm/17.88 bar BMEP

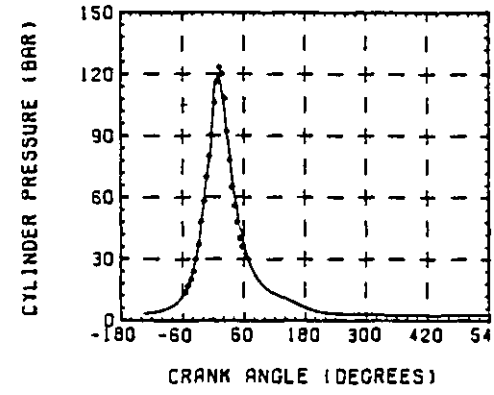

Fig. 4.15c Comparison of Experimental and Predicted Cylinder Pressure Data.

1000 rpm/3.43 bar BMEP

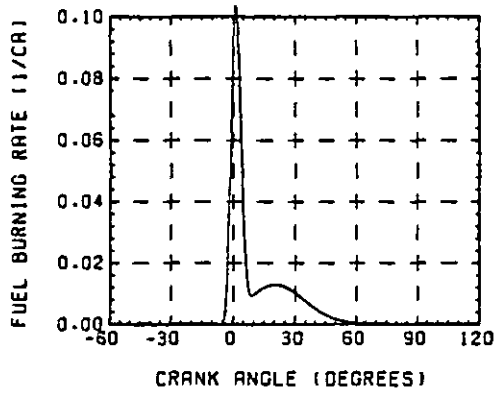

1000 rpm/6.85 bar BMEP

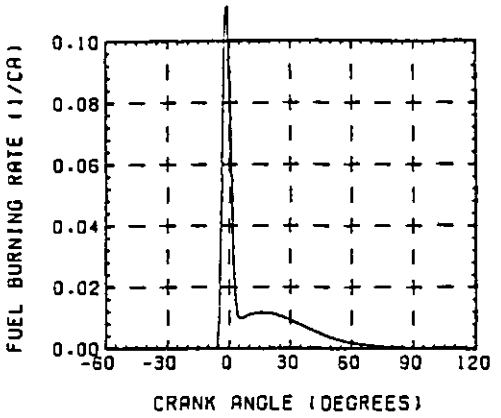

1200 rpm/5.71 bar BMEP

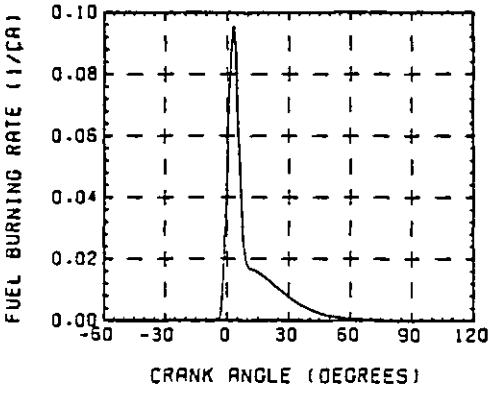

1200 rpm/11.42 bar BMEP

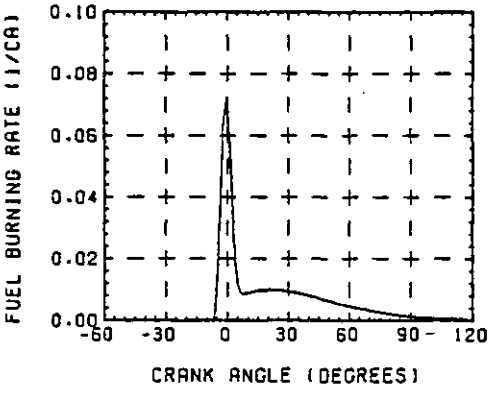

1500 rpm/4.57 bar BMEP

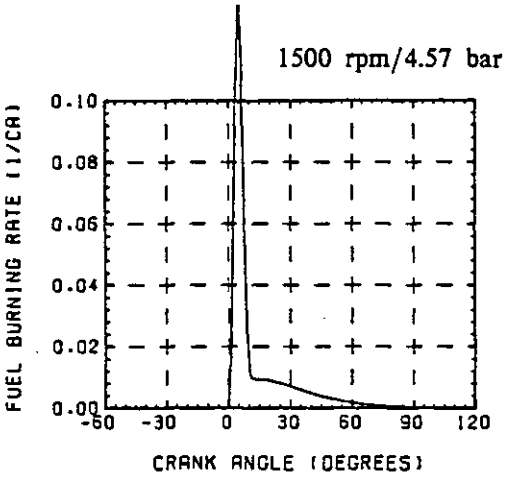

1500 rpm/9.14 bar BMEP

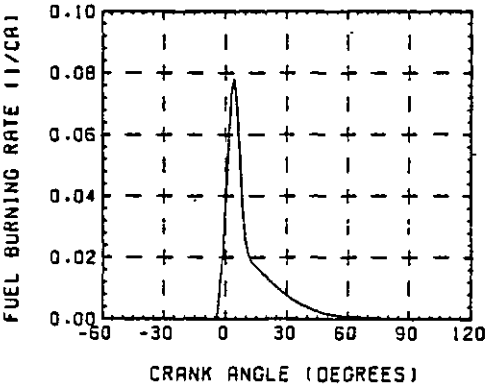

1500 rpm/18.50 bar BMEP

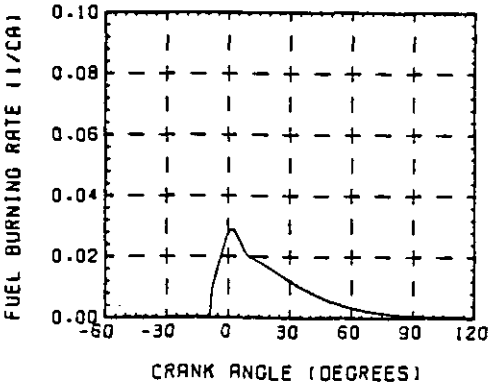

Fig. 4.16a Predicted Apparent Fuel Burning Rates.

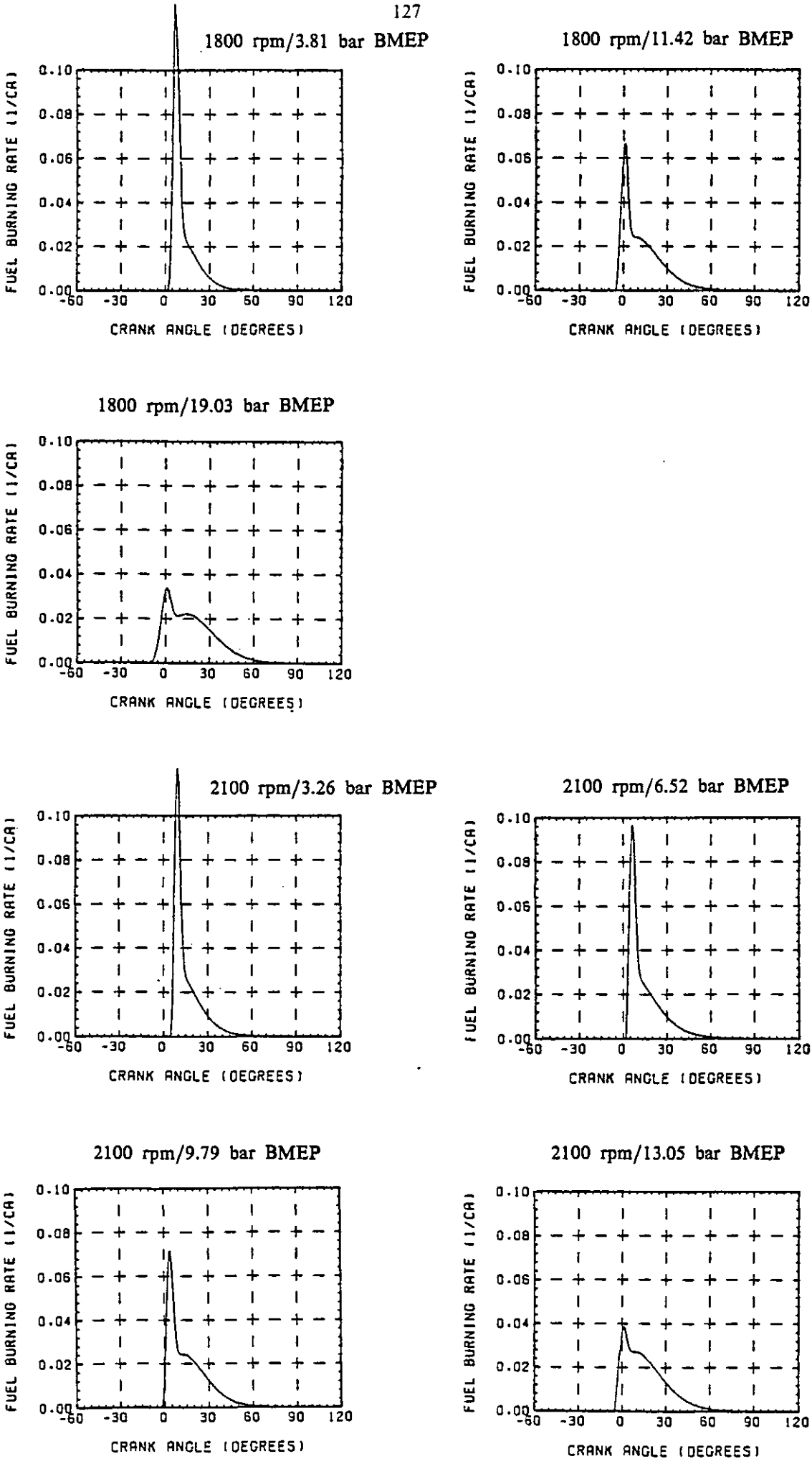

Fig. 4.16b Predicted Apparent Fuel Burning Rates.

2100 rpm/16.31 bar BMEP

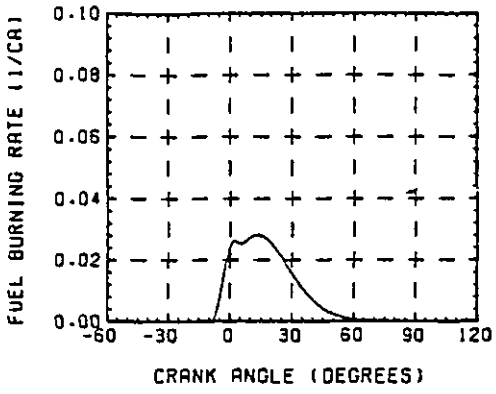

2300 rpm/2.98 bar BMEP

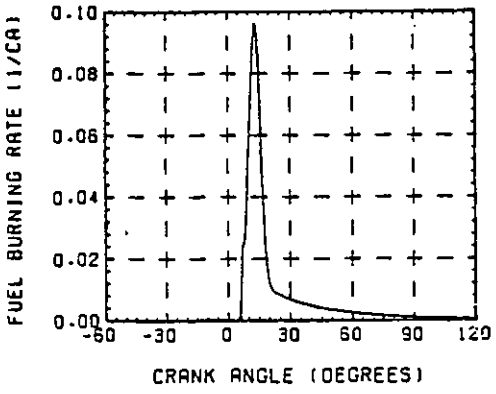

2300 rpm/5.96 bar BMEP

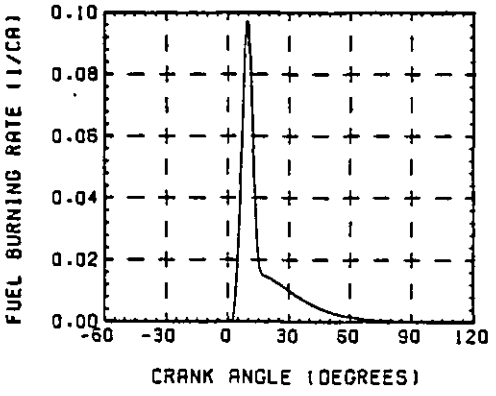

2300 rpm/8.94 bar BMEP

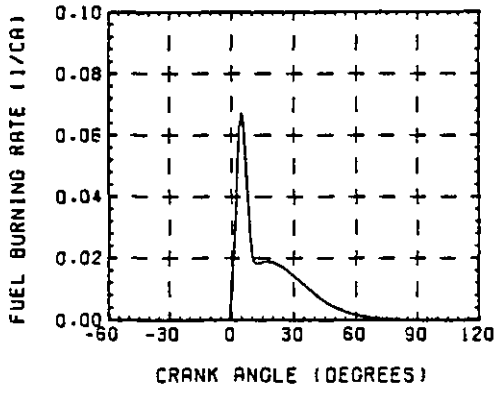

2300 rpm/11.91 bar BMEP

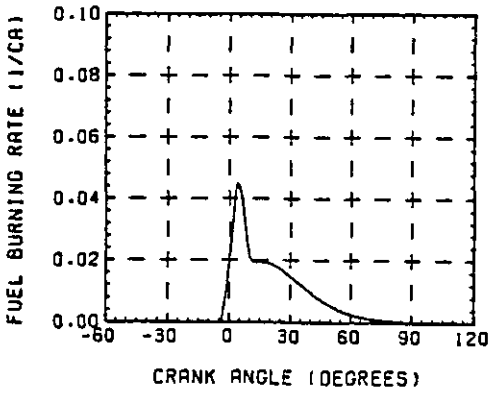

2300 rpm/14.89 bar BMEP

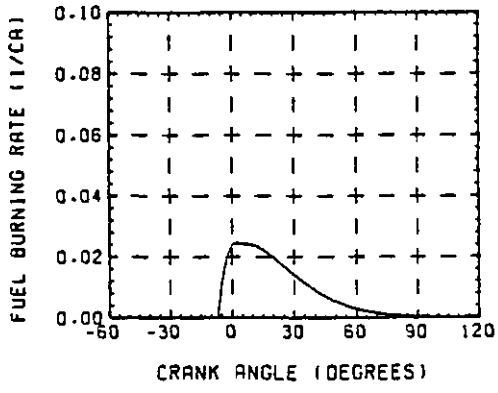

2300 rpm/17.88 bar BMEP

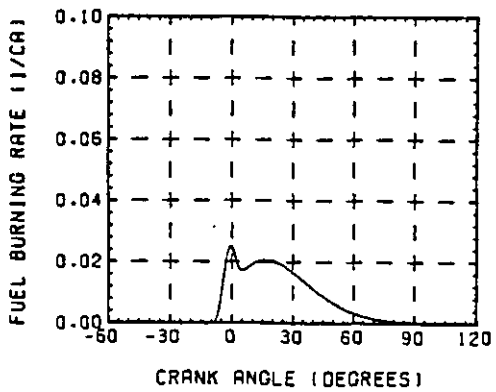

Fig. 4.16c Predicted Apparent Fuel Burning Rates.

The inconsistencies in the predicted AFBR's for this engine are attributed to the poor quality of the original test data (which was not recorded for this purpose) and this inevitably results in some scatter in the "shape factors" derived. It is therefore essential to correlate the "shape factors" to their logical controlling parameters, for example; combustion duration should increase with load, or trapped equivalence ratio.

4.3.7.5 Correlation of the "Shape Factors" with Engine Operating Conditions.

Experiment showed that the representation of the initial "premixed" burning peak improved with high values of c_{p2}, the program predicting values ranging from 2861 to 9196. It can be seen from Fig. 4.9 that the shape of the "premixed" burning rate is little affected by variations in c_{p2} over this range. Consequently it was decided to fix the value of c_{p2} at 5000 (this being the value used by Marzouk (89)). The large value of c_{p2} in eqn. (4.58) means that $\dot{M}_p$ will tend to zero at relatively small values of τ, and that $(c_{p2}-1)^{c_{p2}}$.

Because this engine is turbocharged and charge cooled, the inlet manifold temperature does not vary greatly over the speed and load range, compared to a non charge cooled engine. Consequently the range of ignition delays encountered in the test data is relatively limited (varying between 2.17 ms at 1000 rpm/3.43 bar BMEP and 0.51 ms at 2300 rpm/17.88 bar BMEP). The "shape factor" c_{p1} is used to correlate the duration and peak of the "premixed" burning period to the predicted ignition delay duration. No positive correlation for c_{p1} as a function of ignition delay could be established from the limited test data available, and so the correlation developed by Marzouk (89) was used without modification. Fig. 4.17 shows the scatter of the data for this engine when compared with eqn. (4.63). This correlation indicates that the position of the "premixed" burning peak retards in relation to the ignition point with increasing ignition delay (in time) and/or engine speed. This implies that the resultant increase in the amount of combustible mixture prepared during ignition delay lengthens the duration of the "premixed" burning. Alternatively a constant value for c_{p1} could have been used ($c_{p1}=3.0$) and the "premixed" burning rate controlled entirely by the "mode of burning factor", β.

Fig. 4.17 also shows that the "diffusion" burning coefficient, c_{d1}, decreases with

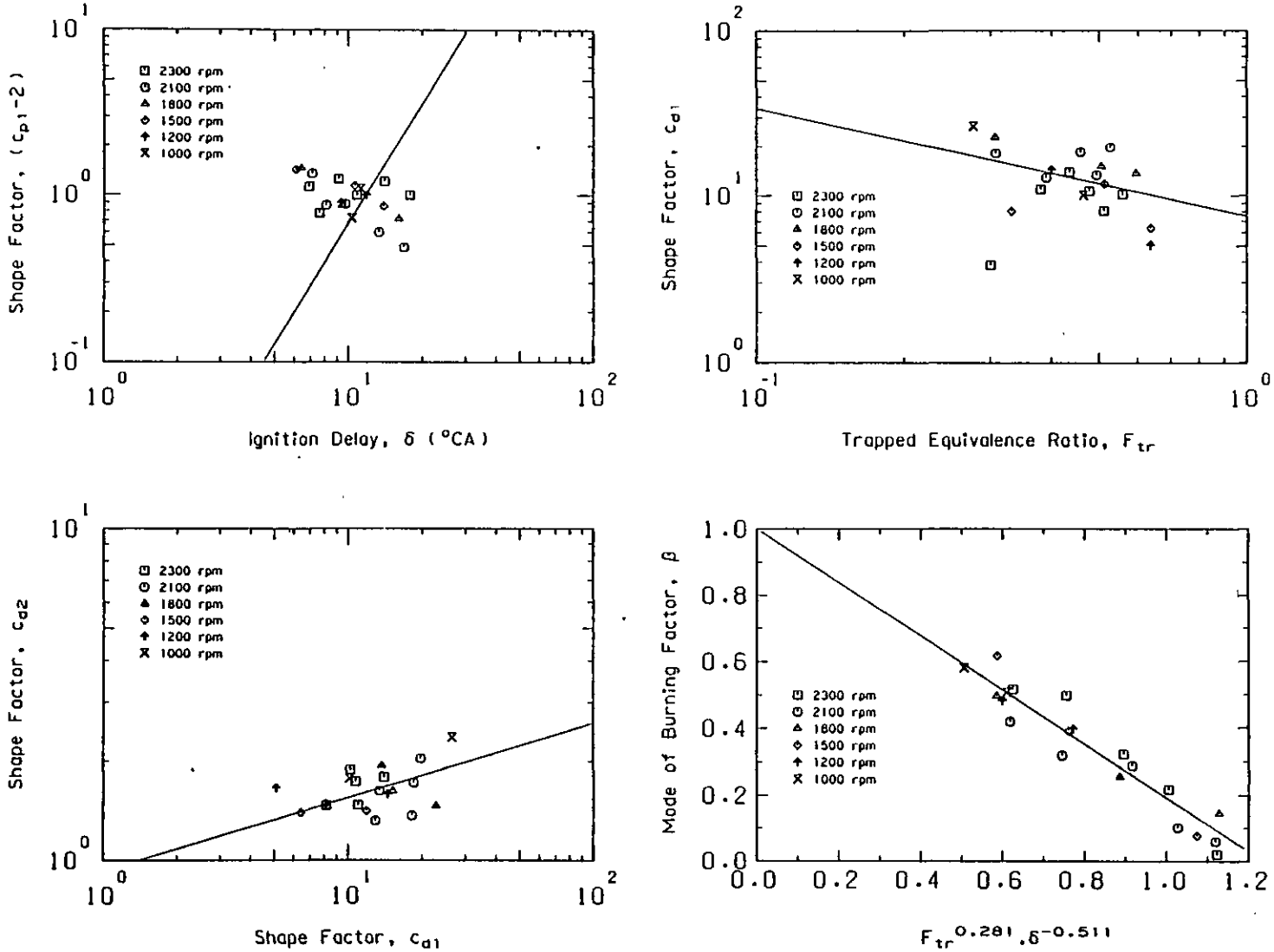

Fig. 4.17 Correlation of the AFBR "Shape Factors".

increasing trapped equivalence ratio. This can be seen as a means of relating the effective duration of combustion to the trapped equivalence ratio, F_{tr}, richer fuel-air mixtures resulting in longer burning durations. Unfortunately no data was available at very low loads, low F_{tr}, limiting the value of this correlation.

Cross plotting the resulting values of the coefficients of the "diffusion" burning distribution, c_{d1} and c_{d2}, showed a clear dependence, Fig. 4.17. Therefore c_{d2} was related to the trapped equivalence ratio only.

As expected, the "mode of burning factor", β, controlling the proportion of the total fuel that burns in the "premixed" mode, exhibited a strong dependence on ignition delay and trapped equivalence ratio, Fig. 4.17.

The final correlation developed for this engine was therefore:-

$$c_{p1} = 2.0 + 1.25.10^{-8}.(\delta.N_E)^{2.400} \quad (4.63)$$

$$c_{p2} = 5000 \quad (4.64)$$

$$c_{d1} = 7.537.F_{tr}^{-0.654} \quad (4.65)$$

$$c_{d2} = 0.929.c_{d1}^{0.224} \quad (4.66)$$

$$\beta = 1.0 - 0.808.F_{tr}^{0.281}.\delta^{-0.511} \quad (4.67)$$

$$\Delta = 125°CA \quad (4.68)$$

where,

F = fuel-air equivalence ratio
N_E = engine speed (rpm)
β = "mode of burning factor"
δ = ignition delay (ms)
Δ = nominal combustion duration (°CA)

and c_1 and c_2 are the "shape factors" and the subscripts p and d refer to "premixed" and "diffusion" respectively, and tr refers to the trapped conditions (after completion

of combustion).

The optimum correlations for c_{d1}, c_{d2} and β for this engine, ENGINE 3, are compared with correlations developed from accurate cylinder pressure measurements for the Leyland 500 engine (89) and for the Perkins TV8 510 turbocharged and intercooled engine in Fig. 4.18. Relative to the other two engines ENGINE 3 requires a lower value of c_{d1}, implying that more diffusion burning occurs later in the cycle, a longer combustion duration and lower "combustion efficiency". The correlation for ENGINE 3 also requires lower values of c_{d2} over the load range, which somewhat compensates for the lower values of c_{d1} by increasing the initial "diffusion" burning peak. ENGINE 3 also requires a larger proportion of premixed burning for a given trapped equivalence ratio and injection delay, especially at high loads, implying a higher injection rate.

4.3.8 Gas Properties.

The application of Powell's concept (113) of absolute enthalpy and internal energy simplifies the analysis and computation of "1st law" processes, including those which involve mixing and combustion. Assuming that thermodynamic equilibrium exists, the absolute enthalpy is the sum of the sensible heat and the heat of formation, and can be defined as:-

$$h_T = h_o + \Delta h_T \tag{4.69}$$

where,

h_o = heat of formation at T=0 K from the elements in their standard reference states at 0 K (kJ/kg)

h_T = absolute enthalpy (kJ/kg)

Δh_T = sensible heat at T K above that at 0 K (kJ/kg)

Consequently, the enthalpies of various systems, which are at different thermodynamic states and compositions, become similar and compatible properties.

For simplicity, computational convenience and economy, mathematical expressions were fitted to tabulated values of internal energy, u, and gas constant, R, and their partial

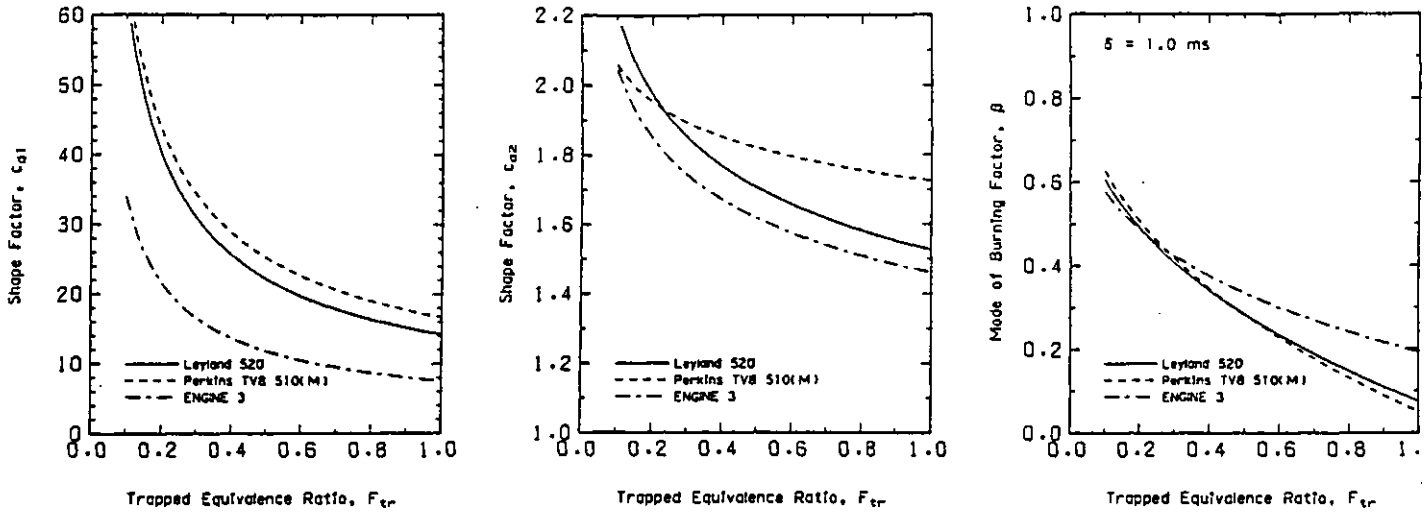

Fig. 4.18 Comparison of "Shape Factor" Correlations for Three Direct Injection Diesel Engines.

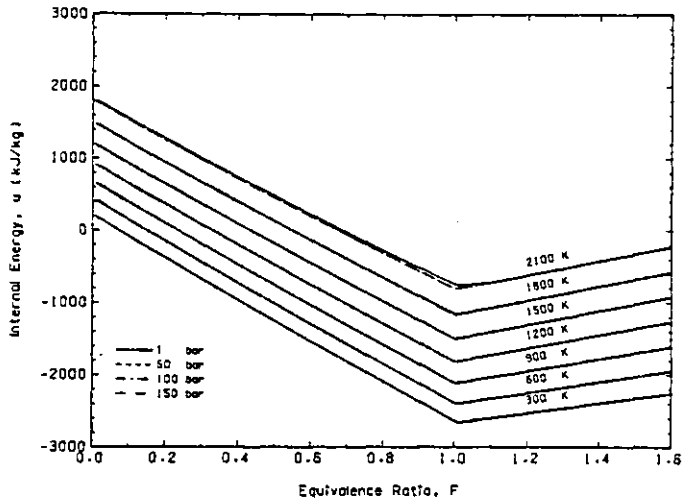

Fig. 4.19 Internal Energy as a Function of Pressure, Temperature and Equivalence Ratio.

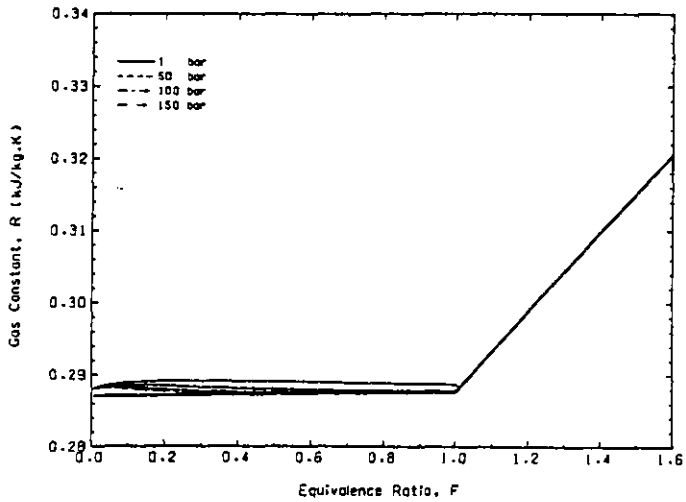

Fig. 4.20 Gas Constant as a Function of Pressure, Temperature and Equivalence Ratio.

derivatives with respect to temperature, pressure and equivalence ratio, for the combustion products of air and diesel fuel.

The carbon/hydrogen ratio for diesel fuels varies from $C_{12}H_{26}$, for light diesel oils, to $C_{14}H_{30}$ for a heavy diesel oil (140). The equilibrium thermodynamic properties of the products of combustion of air and diesel fuel (assumed to be C_nH_{2n}) were expressed analytically in the form of shown in eqns. (4.4) and (4.5).

The required formulae for lean fuel-air mixtures ($F \leq 1$) were taken from Krieger and Borman (73), who curve fitted data calculated by Newhall and Starkman (108). For properties of rich mixture products ($1 < F < 1.6$), other formulae were fitted to data published by the General Electric Company (45). These equations are given in full by Marzouk (89).

Fig. 4.19 shows the internal energy, u, as a function of pressure, temperature and equivalence ratio, over a range of values usually encountered in diesel engines. The appearance of negative internal energies is a characteristic feature when using the absolute zero internal energy reference state. By definition elements at 0 K have zero energy content (the main combustion products CO_2 and H_2O have large negative heats of formation), while on the other hand the sensible heat of an equilibrium mixture is always positive. Consequently the resulting absolute internal energy may be positive or negative.

The specific internal energy for undissociated products (below temperatures of approximately 1450 K) is a linear function of equivalence ratio. Dissociation tends to effect the internal energy at higher temperatures and to cause some deviation from straight lines near the stoichiometric equivalence ratio ($F = 1$). In general, the effects of dissociation are largest at low pressures, high temperatures and equivalence ratio's close to unity.

As the equivalence ratio is increased from pure air ($F = 0$) the amounts of CO_2 and H_2O, with their large negative heats of formation, increase. At the stoichiometric equivalence ratio, there is no more free oxygen available and so any increase in the equivalence ratio causes a replacement of CO_2 and H_2O with other products which have lower heats of formation, for example CO. The derivative $\delta u/\delta F$ therefore changes sign from negative (for lean mixtures) to positive (for rich mixtures) at, or

close to, F=1.

Fig. 4.20 shows the effects of pressure, temperature and equivalence ratio on the gas constant, R. For equivalence ratio's lean of stoichiometric (F<1) the pressure, temperature and equivalence ratio do not greatly effect the gas constant. There is a discontinuity in $\delta R/\delta F$ at F=1, caused by the reduced molecular weight of the products with increased fuel/air ratio due to the increasing proportions of H, H_2, H_2O and CO formed, and this causes an increase in the gas constant, R, for rich mixtures. Dissociation does not effect the gas constant for rich mixtures at temperatures below approximately 2100 K.

4.4 The Heat Transfer Model.

4.4.1 Heat Transfer in the Engine Cylinder.

Heat transfer between the gases and the cylinder walls is important for two reasons:-

(1) Its effect on the thermodynamic cycle and its efficiency.

(2) Its effect on the resulting metal temperatures and the thermal loading of the components.

In the mathematical simulation model the cylinder surface is divided into three heat transfer areas, the head, the piston and the liner. The heat transfer to the head includes the valves, which are considered to be always closed for this particular model.

The model is based on the following assumptions:-

(1) Each heat transfer surface is at a uniform temperature, i.e. surface temperature variations across a particular area are neglected.

(2) The heat transfer surface temperatures are constant with time during a particular engine cycle, i.e. cyclic surface temperature variations are not considered.

(3) Possible surface deposits on either side of the wall are neglected.

(4) The instantaneous heat transfer coefficient for each gas exposed surface is uniform.

(5) Heat transfer by conduction through the cylinder walls is treated on a one-dimensional basis.

(6) The coolant temperature and coolant side heat transfer coefficient are uniform for each heat transfer surface.

The heat transfer process between the working gas and the coolant consists of three parts:-

(1) Heat transfer from the gas to the wall.

(2) Heat transfer by conduction through the wall.

(3) Heat transfer from the wall to the coolant.

The one-dimensional, steady state heat transfer model used in this analysis, follows the earlier work of Streit and Borman (137) and is briefly described below.

The heat transfer rate from the gas to the coolant may be expressed as:-

$$\dot{Q} = \frac{T_{eg} - T_c}{R_{eg} + R_w + R_c} \tag{4.70}$$

where,

$\dot{Q}$ = heat transfer rate (kW)

R = thermal resistance (K/kW)

T = stagnation temperature (K)

and the subscripts c, e, g and w represent coolant, effective, gas and wall respectively.

The thermal resistances on the gas and coolant sides of the wall can be expressed as:-

$$R_y = \frac{1}{h_y.A_y} \tag{4.71}$$

where,

A = heat transfer area (m^2)

h = heat transfer coefficient ($kW/m^2.K$)

and y=eg for the gas side and y=c for the coolant side.

The thermal resistance for the wall is given by:-

$$R_w = \frac{x_w}{k_w.A_w} \tag{4.72}$$

where,

k = thermal conductivity of the wall (kW/m.K)

x = wall thickness (m)

Since the gas temperature, the gas side heat transfer coefficient and, in the case of the liner, the heat transfer area, change continuously during an engine cycle, the corresponding effective quantities have been used.

The effective liner area is:-

$$A_{eg} = \frac{\oint A_g(t).dt}{\oint dt} \tag{4.73}$$

The effective time averaged heat transfer coefficient is given by:-

$$h_{eg} = \frac{\oint A_g(t).h_g(t).dt}{\oint A_g(t).dt} \tag{4.74}$$

and the expression for the effective gas temperature is:-

$$T_{eg} = \frac{\oint T_g(t).A_g(t).h_g(t).dt}{\oint A_g(t).h_g(t).dt} \tag{4.75}$$

where,

t = time (s)

$\oint$ = cyclic integral over one engine cycle.

The heat transfer resistance network for the cylinder liner, piston and head is shown in Fig. 4.21. Note that it is assumed that no heat transfer takes place between the liner and the head (i.e. the thermal resistance of the gasket is infinite). The one-dimensional treatment constitutes a considerable simplification for surfaces with large temperature variations or complicated geometries, such as the piston crown. Thus the computed surface temperatures represent some average temperature which are indicative of the particular surface level only, and therefore cannot be used for

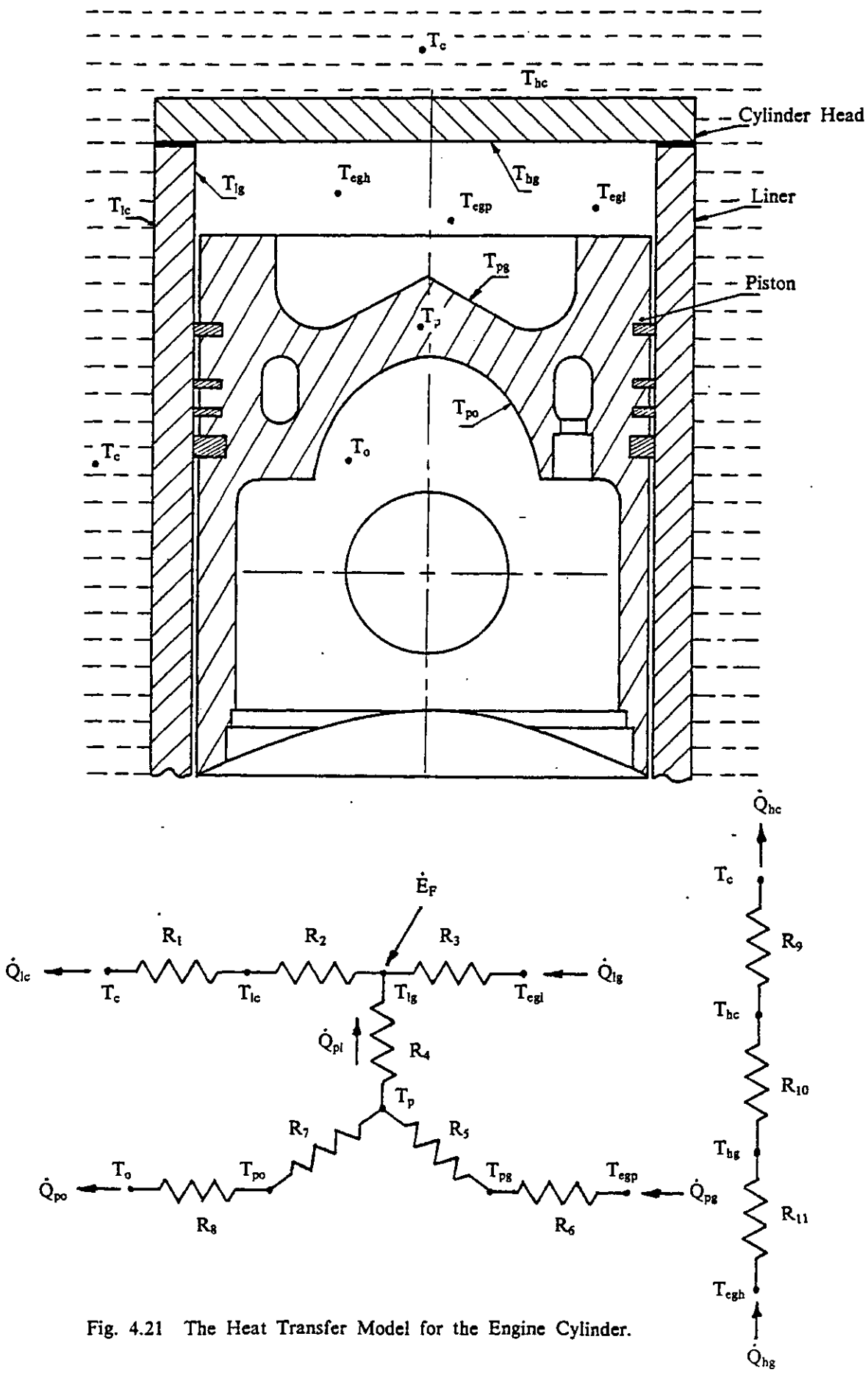

Fig. 4.21 The Heat Transfer Model for the Engine Cylinder.

thermal stress calculations.

The heat transfer model can be represented analytically by an analogous thermal circuit for the piston, liner and cylinder head, Fig. 4.21. The heat transfer conditions at the liner surface are complex since the heat flux received by the liner consists of three parts:-

(1) from the cylinder gas,

(2) from the piston, via the piston rings and skirt, and

(3) due to friction between the piston and the liner.

In fact these quantities not only vary with time, but also along the cylinder axis, due to changes in liner temperature, varying contact pressure between the piston rings and the liner, and the fluctuating piston velocity.

The resistance network given in Fig. 4.21 can be solved for the metal temperatures on the gas and coolant sides.

The gas side wall temperatures are:-

$$T_{hg} = \frac{T_{egh}.(R_9 + R_{10}) + T_c.R_{11}}{R_9 + R_{10} + R_{11}} \tag{4.76}$$

$$T_{lg} = R_4.\left[\frac{T_p - T_{egp}}{R_5+R_6} + \frac{T_p - T_o}{R_7+R_8}\right] + T_p \tag{4.77}$$

$$T_{pg} = \frac{R_5.T_{egp} + R_6.T_p}{R_5 + R_6} \tag{4.78}$$

where,

$$T_p = \frac{E_F + \frac{T_{egl}}{R_3} + \frac{T_c}{R_1+R_2} + \left[1 + \frac{R_4}{R_3} + \frac{R_4}{R_1+R_2}\right]\left[\frac{T_{egp}}{R_5+R_6} + \frac{T_o}{R_7+R_8}\right]}{\frac{1}{R_3} + \frac{1}{R_1+R_2} + \left[1 + \frac{R_4}{R_3} + \frac{R_4}{R_1+R_2}\right]\left[\frac{1}{R_5+R_6} + \frac{1}{R_7+R_8}\right]} \tag{4.79}$$

and the coolant side wall temperatures are:-

$$T_{hc} = \frac{T_c.(R_{10} + R_{11}) + T_{egh}.R_9}{R_9 + R_{10} + R_{11}} \quad (4.80)$$

$$T_{lc} = \frac{T_{lg}.R_1 + T_c.R_2}{R_1 + R_2} \quad (4.81)$$

$$T_{po} = \frac{T_o.R_7 + T_p.R_8}{R_7 + R_8} \quad (4.82)$$

where,

E_F = heat input due to friction between the piston rings and the liner (kW)

and the subscripts F, l, o and p refer to friction, liner, oil and piston respectively.

The energy input due to friction, E_F, is added at the piston-liner interface. In the absence of experimental data for the piston-liner friction, the total heat input due to friction was taken to be 25% of the total mechanical losses.

The coolant temperature, T_c, was taken to be 361 K (88°C) and the oil temperature, T_o, was 343 K (70°C) throughout this work.

4.4.2 Determination of the Thermal Resistances.

In order to calculate the steady state wall temperatures at the end of the engine cycle, the thermal resistances R_1 to R_{11} must be established. These were calculated as follows.

4.4.2.1 Wall Thermal Resistances.

The general form for the wall thermal resistances for the "dry" liner, R_2, the piston, R_4, R_5, R_7, and the cylinder head, R_{10}, is given by eqn. (4.72). It is therefore necessary to establish the wall thickness, x, (or the effective thickness if the geometry is complex, as in the case of the piston thermal resistances, R_4, R_5 and R_7), the thermal conductivity, k, and the cross sectional area, A. The effective wall thicknesses and heat transfer areas were estimated from the engine geometry.

The thermal conductivity for the cast iron cylinder head and liner is in the range 0.023 to 0.057 kW/m.K, and for the alluminium alloy piston, in the range 0.092 to 0.173 kW/m.K. Surface deposits on the gas side (e.g. carbon) and the water side (e.g. scale) can greatly reduce the local heat transfer rates. Wu (183) has shown that even a thin scale deposit (0.5mm) can cause a significant increase in wall temperatures because of its low thermal conductivity (of the order of 0.0023 kW/m.K).

Consequently the thermal conductivity of the cylinder head and liner material was estimated to be:-

$$k_{h,l} = 0.040 \quad kW/m.K \tag{4.83}$$

and the thermal conductivity of the piston was:-

$$k_p = 0.132 \quad kW/m.K \tag{4.84}$$

these being the mean values of the ranges quoted above.

4.4.2.2 Coolant Side Thermal Resistances.

The general form of the metal-coolant thermal resistances for the liner, R_1, the cylinder head, R_9, and the piston, R_8, is given by eqn. (4.71). The heat transfer cross sectional area can be established from the engine geometry, however, a considerable gap in knowledge exists regarding the heat transfer coefficient at the metal-coolant interface of the water cooled "dry" liner and cylinder head used on this engine. Heat transfer can be by natural convection, forced convection and/or nucleate boiling, between the cylinder head and liner and the cooling water. "As of cast" surfaces of cast iron often have a thermal barrier which leads to much higher temperature differences between the wall and the coolant than expected. Studies of the heat transfer from the wall to the water have shown that the heat transfer formulae for forced convection in pipes, eqn. (4.85) is not appropriate due to the predominant influence of free convection and/or nucleate boiling.

$$N_u = C_1.R_e^a.P_r^b \tag{4.85}$$

where,

N_u = Nusselt No. ($N_u = hl/k$)

P_r = Prandtl No. ($P_r = \mu c_p/k$)

R_e = Reynolds No. ($R_e = \rho ul/\mu$)

and,

c_p = specific heat at constant pressure (kJ/kg.K)

l = reference length (m)

u = velocity (m/s)

μ = dynamic viscosity (kg/m.s)

ρ = density (kg/m^3)

and a, b and C_1 are empirical constants.

The following correlation has therefore been used for the coolant side heat transfer coefficients in R_1 and R_9, from Streit and Borman (137):-

$$h = 0.127.[\ \dot{Q}/A\ ]^{0.644} \quad kW/m^2.K \qquad (4.86)$$

The heat transfer coefficient between the piston and the cooling oil, in R_8, is very difficult to measure on a running engine. Furthermore, the varying inertia forces due to the piston motion may, with some designs of piston cooling chamber, superimpose an additional velocity component which can alter the heat transfer conditions considerably. The pistons for the Hyperbar engine are oil cooled using high pressure oil jets directed at the underside of the piston, and have cooling galleries beneath the piston crowns.

Data is available for "cocktail shaker" type pistons with cooling passages in the piston, Bush and London (27) quote heat transfer coefficients in the range 0.57 to 1.14 $kW/m^2.K$. French (43) gives experimental values for a large, slow running engine in the range 1.15 to 1.70 $kW/m^2.K$, and for extreme running conditions 2.49 $kW/m^2.K$. The empirical values quoted by Pachernegg (111) are in the range of 0.011 to 0.079 $kW/m^2.K$, for convection to crankcase air with no additional means of increasing turbulence, 0.113 to 0.568 $kW/m^2.K$ for oil jets providing a turbulent mixture of oil droplets and air, and 0.227 to 1.136 $kW/m^2.K$ for cooling oil by splash or full flow (e.g. in a "cocktail shaker" type piston).

A constant value for the heat transfer coefficient between the piston and the oil has been used in the calculation of R_8, from (111) for turbulent oil cooling jets:-

$$h_{co} = 1.136 \quad kW/m^2.K \tag{4.87}$$

4.4.2.3 Gas Side Thermal Resistances.

The thermal resistances between the cylinder gas and the walls have the general form of eqn. (4.71). The heat transfer areas required for the piston, R_6, liner, R_3, and the cylinder head, R_{11}, can be calculated from the engine geometry, the liner effective area being calculated from eqn. (4.73). It therefore remains to find the heat transfer coefficient between the cylinder gas and the walls.

Numerous empirical correlations for the instantaneous heat transfer coefficient between the cylinder gases and the walls have been reported, one of the simplest and most widely used being that of Eichelberg (36). Dimensional analysis suggests that the heat transfer coefficient for forced convection can be expressed in the form of a Nusselt, Reynolds, Prandtl relationship given in eqn. (4.85).

The Prandtl No. is usually assumed to be constant (for example, P_r is approximately 0.7 for air under motored conditions) and therefore eqn. (4.85) can be reduced to:-

$$N_u = C_2.R_e^a \tag{4.88}$$

where,

$$C_2 = C_1.P_r^b \tag{4.89}$$

Equation (4.88) can be solved for the heat transfer coefficient, h,

$$h = C_2.\frac{k.}{l}\left(\frac{\rho.u.l}{\mu}\right)^a \tag{4.90}$$

Substituting for the density, ρ, from the equation of state:-

$$\rho = \frac{p}{R.T} \tag{4.91}$$

and assuming that the gas constant, R, is approximately constant over the pressure, temperature and equivalence ratio range under consideration, eqn. (4.90) becomes:-

$$h = C_3.k.p^a.u^a.l^{a-1}.T^{-a}.\mu^{-a} \tag{4.92}$$

where,

$$C_3 = C_2.R^{-a} \tag{4.93}$$

It can also be assumed that the thermal conductivity, k, and viscosity, μ, of the gas will only vary significantly with temperature, i.e.

$$k = k(T) = C_4.T^c \tag{4.94}$$

$$\mu = \mu(T) = C_5.T^d \tag{4.95}$$

Substituting from eqns. (4.94) and (4.95) into eqn. (4.92) gives:-

$$h = C_6.p^a.u^a.T^{c-a(1+d)}.l^{a-1} \tag{4.96}$$

where,

$$C_6 = C_3.C_4.C_5^{-a} \tag{4.97}$$

Equation (4.96) forms the basis of many of the empirical correlations for the cylinder gas heat transfer coefficient, h, based on turbulent forced convection. The mean piston velocity, C_m, is usually used for the velocity term, u, in eqn. (4.96), the cylinder diameter, B, for the length term, l, and the bulk mean gas temperature and pressure are used.

After discussing many empirical correlations for the cylinder gas side heat transfer coefficient, Annand (3) concluded that the majority of the earlier correlations were dimensionally incorrect. He produced a correlation based on eqn. (4.96), but also included a radiation term of the form:-

$$h_r = C_7.\frac{(T^4 - T_w^4)}{(T - T_w)} \tag{4.98}$$

which was only used during the combustion and expansion processes. Unfortunately due to the large degree of scatter in the data he used, a wide range of values for the constant, C_6, was obtained, ranging from 0.35 to 0.80, the value rising with increasing intensity of charge motion. The exponent in the Reynolds No. term, a, was 0.7.

Sitkei et. al. (131) have also used eqn. (4.96) as the basis for their correlation, as have LeFeuvre et. al. (81), Zapf (185) and others.

Woschni's (180) heat transfer correlation has been used to predict the gas side heat transfer coefficient throughout this work. Based on eqn. (4.96), Woschni derived the following coefficients, from extensive experimental tests.

The representative velocity, u, was calculated from:-

$$u = C_8.C_m \tag{4.99}$$

where,

C_m = mean piston velocity (m/s)

The representative length, l, was taken as the cylinder diameter, B, and the following constants were found by correlating the experimental data:-

$$a = 0.80 \ , \ c = 0.75 \ , \ d = 0.60 \tag{4.100}$$

During the scavenge period, the best value for the constant, C_8, was found to be:-

$$C_{8sc} = 6.18 \tag{4.101}$$

and during the compression and expansion periods (the closed cycle) C_8 is given by:-

$$C_{8cc} = 2.28 \tag{4.102}$$

Woschni considered an additional gas velocity caused by the combustion process to be superimposed on that caused by the piston motion. Therefore, during combustion:-

$$u = C_{8cc}.C_m + u_c \tag{4.103}$$

where,

$$u_c = \frac{C_9.V_s.T_1.(p - p_o)}{p_1.V_1} \quad (4.104)$$

and,

p = bulk cylinder gas pressure (kN/m^2)

p_o = corresponding pressure with no combustion (motored) (kN/m^2)

p_1 = cylinder pressure at the reference conditions (e.g. at IVC) (kN/m^2)

T_1 = cylinder temperature at the reference conditions (K)

u_c = combustion induced velocity (m/s)

V_1 = cylinder volume at the reference conditions (m^3)

V_s = maximum cylinder volume, including the clearance volume (m^3)

and the best values obtained for the empirical constants C_6 and C_9 were:-

$$C_6 = 3.264.10^{-3} \quad (4.105)$$

and,

$$C_9 = 3.24.10^{-3} \quad m/s.K \quad (4.106)$$

Woschni did not consider that a separate radiation term was required, this being taken into account via the combustion induced velocity term, u_c.

Woschni's work represents a comprehensive study of the gas side heat transfer coefficient for internal combustion engine applications, in a form convenient for mathematical simulation applications, and has been used throughout this work without modification.

4.4.3 Transient Wall Temperatures.

Due to the thermal capacity of the cylinder walls a step change in the effective gas temperature does not result in an instantaneous response in the metal temperature. The time lag experienced is usually of a greater order of magnitude than the response of the engine to rapid changes in load and/or speed. A simplified method has been employed, based on expressions developed by Sitkei (129), to calculate the actual changes in wall temperature during transient operating conditions.

The steady state heat transfer model, described in the previous sections, was applied at the end of every engine cycle to calculate the wall temperatures for the case of zero thermal capacity. The actual wall temperature was then allowed to follow an exponential form, given by:-

$$T_{w,n+1} = T_{w,n} + [\, T_{w,n+1,c=0} - T_{w,n} \,].(1 - e^{-\Delta t/\alpha 1}) \qquad (4.107)$$

where,

T_w = actual wall temperature (K)

$T_{w,c=0}$ = wall temperature for the case of zero thermal capacity (K)

n = cycle number

Δt = cycle duration (s)

α_1 = time constant (s)

The "time constant", α_1, was estimated to be 150 seconds, based on work published by Marzouk (89), although there was no experimental justification for using this value.

Fig. 4.22 shows the effect of changing the "time constant" on the response of the wall temperature, T_w, during a rapid load application. The initial value of the wall temperature at 1560 rpm/0 bar BMEP was predicted to be 400 K under steady state conditions. After a load application of 24.19 bar BMEP, the final steady state wall temperature predicted is 550 K, representing a temperature change ($T_{w,n+1,c=0}$ - $T_{w,n}$) of 150 K in eqn. (4.107). It is evident from Fig. 4.22 that the actual change in the wall temperature is negligible during the time period of a typical transient, this load application test takes approximately 5 seconds to achieve the final steady state

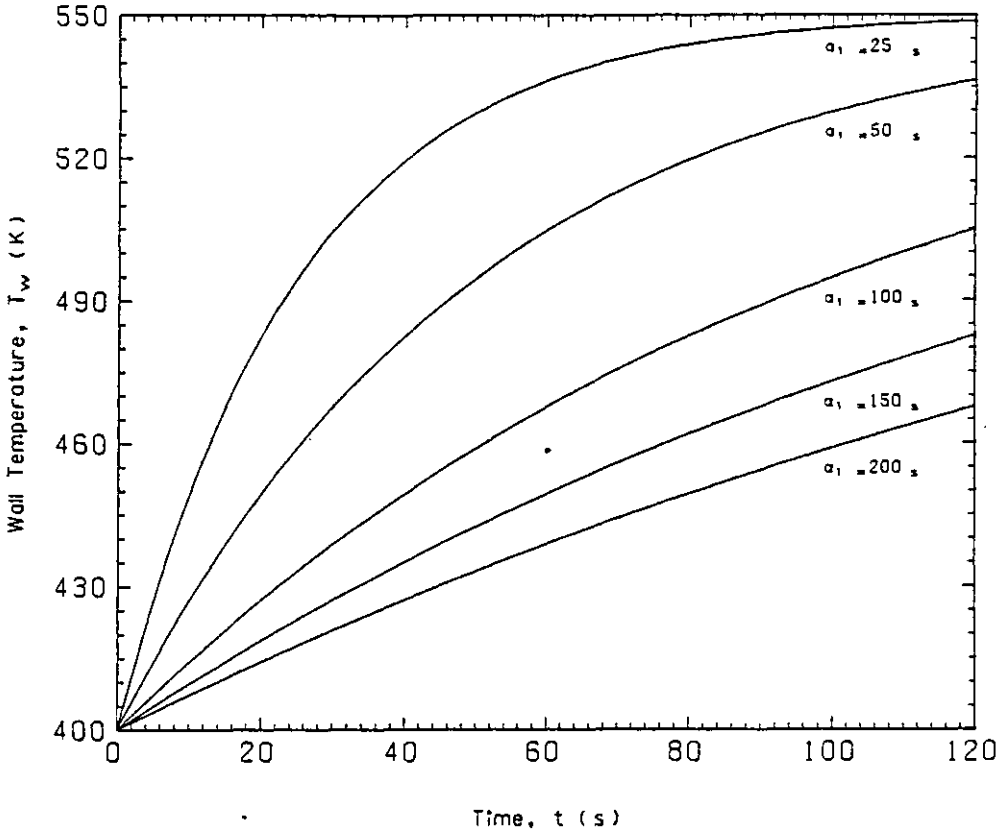

Fig. 4.22 Effect of the Cylinder Wall Time Constant α_1 on the Wall Temperature Response.

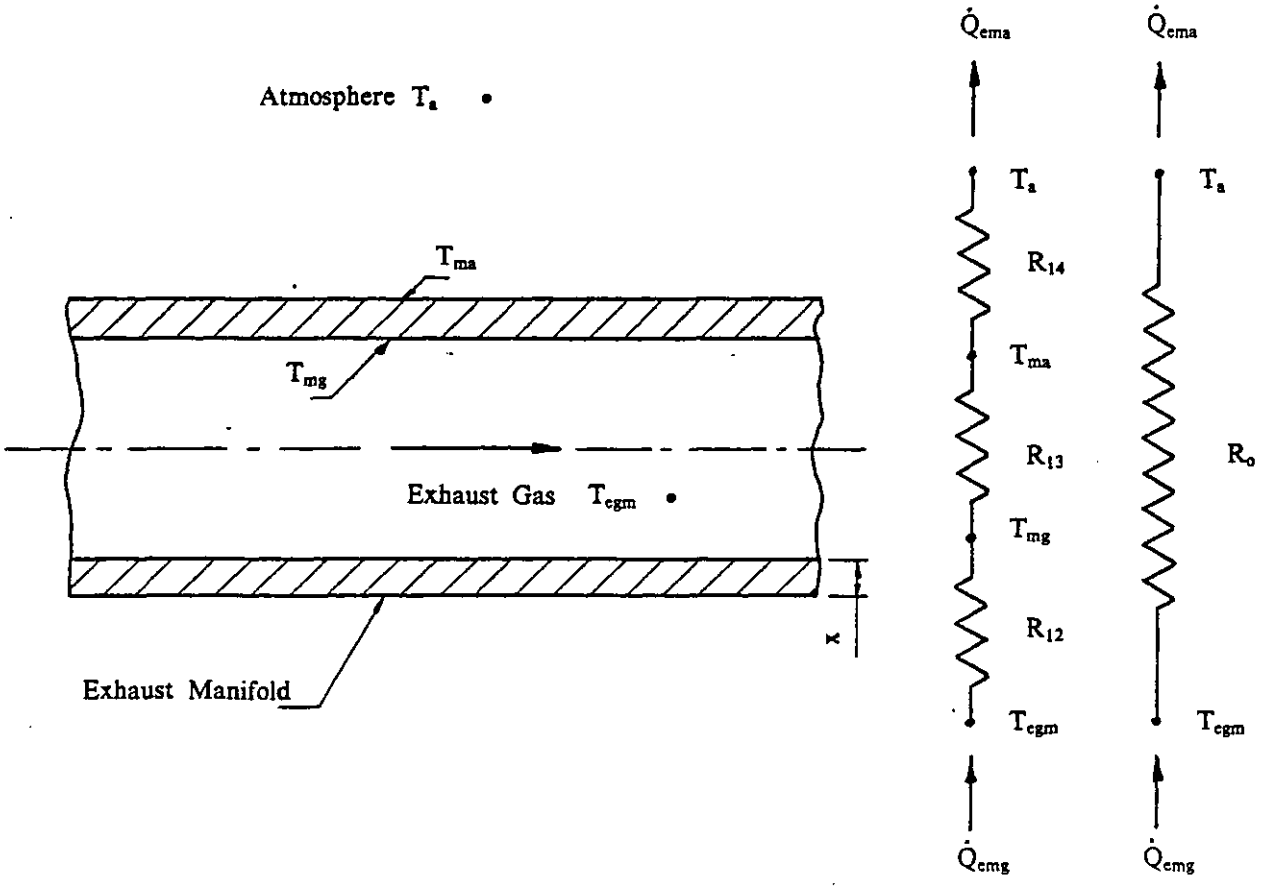

Fig. 4.23 The Heat Transfer Model for the Exhaust System.

engine speed, by which time the actual wall temperature ($T_{w,n+1}$-$T_{w,n}$) has increased by only 5 K, for α_1=150 s. Lower values of α_1 will result in a faster response of the wall temperature with less heat transfer from the cylinder gases during the transient. However, a more rapid increase in the wall temperatures will also result in a reduction in the volumetric efficiency of the engine, due to the heating of the charge air during the intake stroke.

A similar response lag in the turbine inlet conditions can be observed during transients. In this case there is a relatively rapid change in the turbocharger speed as the engine load and/or speed changes, followed by a gradual change in the turbocharger speed as the exhaust manifold temperature stabilizes. The heat transfer from the exhaust system will be discussed in section 4.4.4.

4.4.4 Exhaust Manifold System Heat Transfer.

The exhaust system for turbocharged diesel engines generally consists of cast or fabricated pipe arrangements connecting the engine cylinders to the tubine housing. The Hyperbar engine exhaust system is complicated by the by-pass, burner and mixer systems, which transfer energy to the atmosphere and to each other by heat transfer.

A simplified one-dimensional model for the heat transfer from a straight pipe to the atmosphere, together with the analogous thermal resistance network, is shown diagramatically in Fig. 4.23. The thermal resistances between the exhaust gas and the manifold, R_{12}, and between the manifold and the atmosphere, R_{14}, are of the form given in eqn. (4.71). The wall thermal resistance, R_{13}, has the general form of eqn. (4.72), for large diameter pipes.

The geometry of a simple pipe system enables the wall thickness, x, and the heat transfer area, A, to be calculated. The thermal conductivity of the manifold depends upon the material and method of construction used, typical values for cast iron are given in section 4.4.2.1. The problem is to evaluate the heat transfer coefficients on the air side, h_{ma}, and the exhaust gas side, h_{mg}, of the manifold.

A Nusselt, Reynolds, Prandtl relationship, similar to that described in section 4.4.2.3 can be used to estimate the gas side heat transfer coefficient, h_{mg}. Most empirical

correlations for the heat transfer coefficient for forced turbulent convection in straight pipes are of the form:-

$$N_u = N_1.P_r^{n1} + N_2.P_r^{n2}.R_e^{n3} \quad (4.108)$$

where, N_1, N_2, n1, n2 and n3 are empirical constants.

By assuming that the Prandtl No. is constant, eqn. (4.108) reduces to:-

$$h = \frac{k}{D}(N_3 + N_4.R_e^{n3}) \quad (4.109)$$

where,

$$N_3 = N_1.P_r^{n1} \quad (4.110)$$

$$N_4 = N_2.P_r^{n2} \quad (4.111)$$

and,

D = pipe diameter (m)

For the case where the instantaneous mass flow rate falls to zero (as can occur in a pulse turbocharged engine exhaust manifold), then $R_e=0$ and eqn. (4.109) becomes:-

$$h = \frac{N_3.k}{D} \quad (4.112)$$

Usually the Reynolds No. term is large compared to the free convection term, for high gas velocities, and eqn. (4.109) can be reduced to:-

$$h = \frac{N_4.k.R_e^{n3}}{D} \quad (4.113)$$

Data for turbulent forced convection in pipes (63) suggests that appropriate values for the constants in eqn. (4.108) are:-

$$N_1 = 0 \ , \ N_2 = 0.023 \ , \ n1 = 0 \ , \ n2 = 0.3 \ , \ n3 = 0.8 \quad (4.114)$$

The physical quantities are all determined at the arithmetic mean temperature of the

fluid at the entrance and exit of the pipe, and h is based on the difference between the surface and the bulk gas temperatures.

Empirical correlations for the heat transfer coefficient on the air side are of the form (63):-

$$N_u = N_5.(G_r.P_r)^{n4} \quad (4.115)$$

where,

G_r = Grashof No.

$$G_r = \frac{D^3.\rho_f^2.\beta.g.\Delta T}{\mu_f^2} \quad (4.116)$$

and,

$$P_r = \frac{\mu_f.c_p}{k_f} \quad (4.117)$$

where,

g = gravitational acceleration (m/s^2)

β = coefficient of thermal expansion (K^{-1})

ΔT = temperature difference between the wall and the fluid (K)

The subscript f indicates that the physical property is evaluated at the film temperature, as defined by:-

$$T_f = \frac{T_{ma} + T_a}{2} \quad (4.118)$$

where,

T_a = ambient temperature (K)

T_{ma} = manifold air side temperature (K)

The values of the constants N_5 and n4 in eqn. (4.115) depend upon the product ($G_r.P_r$), typical values being:-

$$N_5 = 0.525 \ , \ n4 = 0.25 \quad (4.119)$$

for $(G_r.P_r) \geq 10000$

In general the value of the exponent, n4, will increase as the product $(G_r.P_r)$ increases.

The majority of the heat transfer data available in the literature is for fully developed flow in straight pipes, and is not suitable for heat transfer calculations in the exhaust system, where the boundary layer inside the pipe does not stabilize, due to the pulsating nature of the flow. Consequently a much simpler overall thermal resistance for the gas side, wall and the air side has been adopted, see Fig. 4.23.

The overall heat transfer rate from the exhaust gas has been calculated from:-

$$\dot{Q} = \frac{T_{egm} - T_a}{R_{12}+R_{13}+R_{14}} = \frac{T_{egm} - T_a}{R_o} \qquad (4.120)$$

where,

$$R_o = \frac{1}{h_o.A} \qquad (4.121)$$

where,

A = heat transfer area (m^2)

h_o = overall heat transfer coefficient ($kW/m^2.K$)

R_o = overall thermal resistance (K/kW)

Janota (64) measured the heat transfer from 5 "compact" exhaust manifold arrangements under steady flow conditions, with varying mass flow rates and inlet gas temperatures, to evaluate the overall heat transfer coefficient, h_o. He concluded that a constant value for h_o of 0.0227 $kW/m^2.K$ could be used for all the manifolds tested, with little error. However, neglecting the heat transfer from the exhaust system was found to lead to considerable errors in the calculated exhaust mass flow rate and available turbine energy, particularly for large exhaust manifolds (up to 3.9% for the largest manifold tested).

The overall heat transfer coefficient, h_o, used for the exhaust system of the Hyperbar engine was taken from the work of Marzouk (89):-

$$h_o = 0.0142 \quad kW/m^2.K \tag{4.122}$$

The actual heat transfer areas used in the exhaust system are discussed in section 4.8. The thermal inertia of the exhaust system has been ignored, due to the lack of suitable data required to develop a more detailed model. However, this can easily be incorporated in the simulation at a later date if required.

4.5 Engine Frictional Losses.

The simulation model predicts an indicated cylinder pressure diagram, which is then integrated to give the indicated mean effective pressure (IMEP), and from this the indicated power (P_I) can be found:-

$$IMEP = \frac{\int_{\theta_1}^{\theta_4} p.dV}{V_{sw}} \tag{4.123}$$

$$P_I = \frac{IMEP.V_{sw}.N_E}{60.y} \tag{4.124}$$

where,

IMEP = indicated mean effective pressure (kN/m^2)
N_E = engine speed (rpm)
p = instantaneous cylinder pressure (kN/m^2)
P_I = indicated power (kW)
V_{sw} = swept volume (m^3)
dV = change in cylinder volume (m^3)

and,

Θ_1 = BDC before the exhaust stroke
Θ_4 = BDC after the expansion stroke
y = number of revolutions per cycle (y=2 for a four stroke engine)

Subtracting the frictional losses, expressed in terms of the friction mean effective pressure (FMEP) or friction power (P_F) enables the brake mean effective pressure (BMEP) and the brake power (P_B) to be calculated:-

$$BMEP = IMEP - FMEP \tag{4.125}$$

$$P_B = P_I - P_F \tag{4.126}$$

where,

BMEP = brake mean effective pressure (kN/m^2)
FMEP = friction mean effective pressure (kN/m^2)

P_B = brake power (kW)

P_F = friction power (kW)

One method of determining the frictional losses is to measure the cylinder pressure diagram, and hence calculate the IMEP, and to measure the brake power output, or the BMEP, and then to calculate the FMEP from eqn. (4.125). This method does, however, require very accurate cylinder pressure data, and is discussed in detail by Brown (26).

Fig. 4.24 shows the hot motoring FMEP for a conventional single stage turbocharged version of the Hyperbar engine, measured by the manufacturer. The frictional losses clearly increase with engine speed, under motored conditions, but experimental evidence suggests that the engine load will also affect the FMEP.

The hot motoring FMEP is found by simply measuring the power required to motor the engine at a given speed, (with the oil and water heated externally to simulate the normal operating conditions) and so includes the pumping work done by the piston during the intake and exhaust strokes.

Using the definitions proposed by Lancaster et. al. (77) the pumping mean effective pressure (PMEP) can be defined as:-

$$PMEP = \frac{\int_{\theta 1}^{\theta 2} p.dV}{V_{sw}} \qquad (4.127)$$

where,

PMEP = pumping mean effective pressure (kN/m^2)

Θ_2 = BDC after the intake stroke.

The PMEP is the effective pressure on the piston during the exhaust and intake processes. The closed cycle mean effective pressure (CCMEP) is defined as the mean pressure on the piston during the compression and expansion strokes, i.e.

$$CCMEP = \frac{\int_{\theta 3}^{\theta 4} p.dV}{V_{sw}} \qquad (4.128)$$

where,

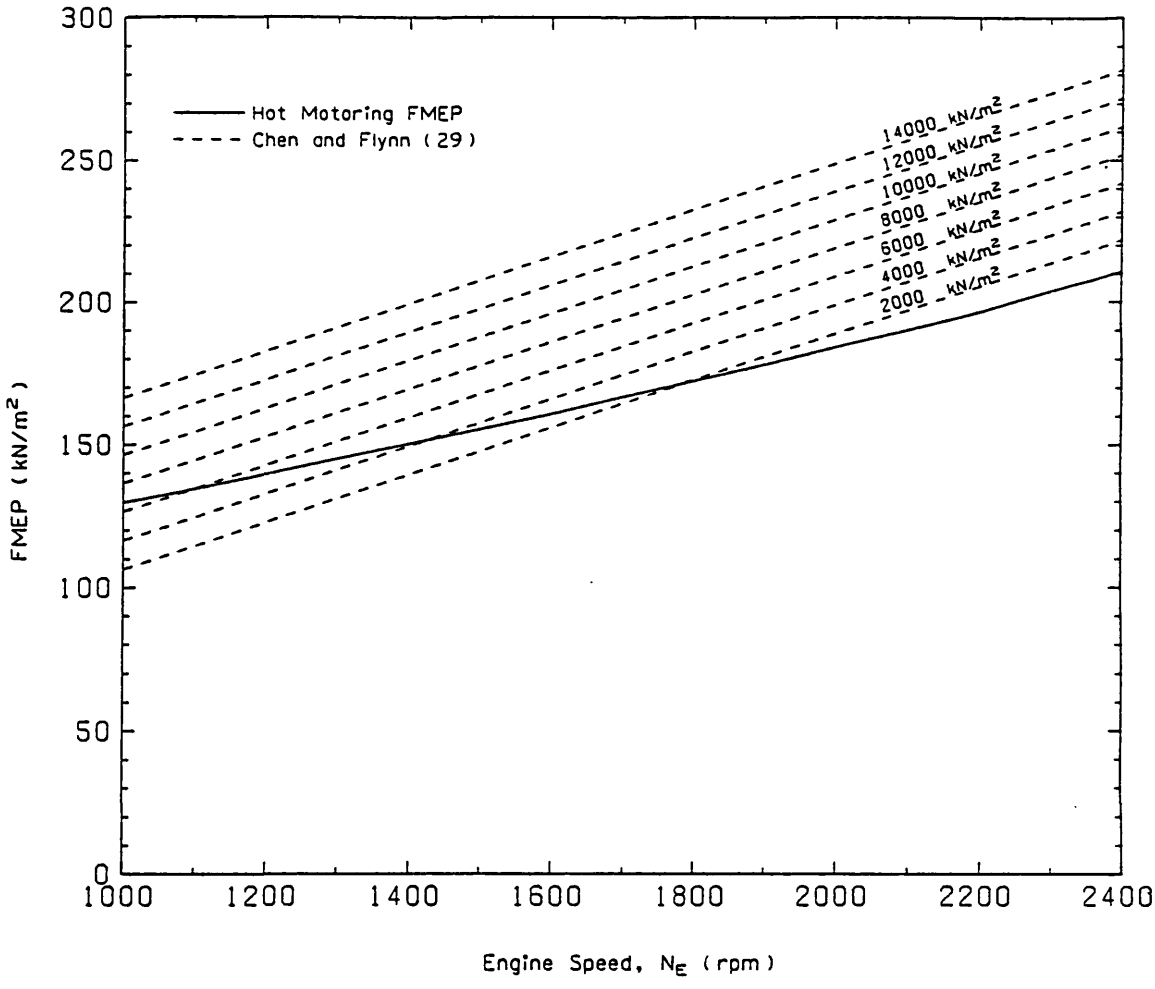

Fig. 4.24 Comparison of Experimental and Predicted Engine Frictional Losses.

CCMEP = closed cycle mean effective pressure (kN/m^2)

Θ_3 = BDC before the compression stroke.

and,

$$IMEP = PMEP + CCMEP \tag{4.129}$$

Under motored conditions, both the CCMEP and the PMEP are negative. Fig. 4.25 shows cylinder pressure data measured by the author under motoring conditions on a turbocharged Perkins V8 engine, and shows the increasing importance of the pumping losses as the engine speed increases. The hot motoring FMEP therefore overestimates the frictional losses, by including the pumping losses and the error increases as the engine speed rises. Note that the engine was motored for one cylinder only, by removing the fuel injector. The boost pressure therefore varied slightly with engine speed.

Any error in the predicted FMEP will become more important as the engine load (BMEP) reduces to zero, where small errors in FMEP can cause large discrepancies in the BSFC predicted.

Bishop (21) attempted to separate the friction losses due to each individual component in the engine (e.g. the piston rings, the bearings, the water and oil pumps, etc.) and produced a series of empirical correlations (for spark ignition engines). Millington and Hartles (104) have correlated the results of numerous motoring tests, for naturally aspirated diesel engines, which suggest that the total motoring losses comprises of a component invariant with speed, a component varying linearly with speed and a pumping loss term varying as the square of the engine speed.

Chen and Flynn (29) have developed a correlation for a fired engine, based on results obtained from a single cylinder research engine. They correlated the frictional losses to the engine speed and the pressure load on the piston rings, bearings, etc. represented by the maximum cylinder pressure:-

$$FMEP = 13.79 + 0.005.p_{max} + 16.287.C_m \tag{4.130}$$

where,

C_m = mean piston velocity (m/s)

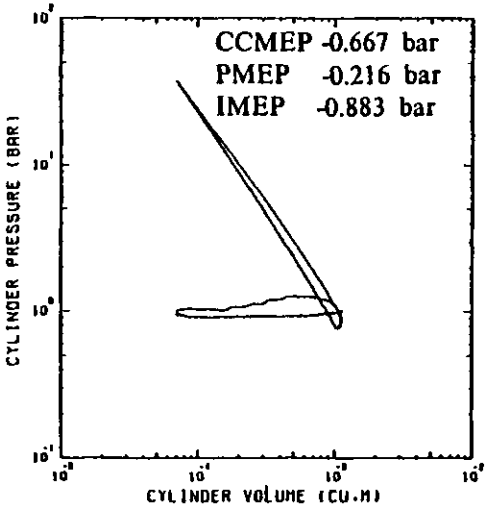

Engine Speed 1000 rpm

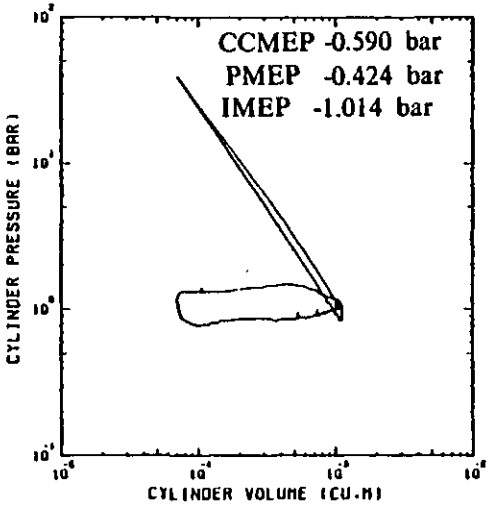

Engine Speed 1400 rpm

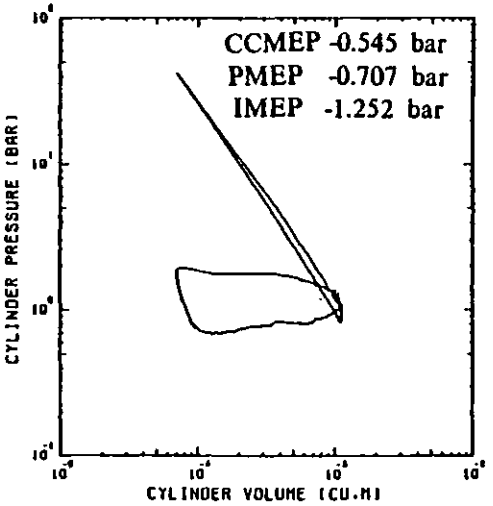

Engine Speed 1800 rpm

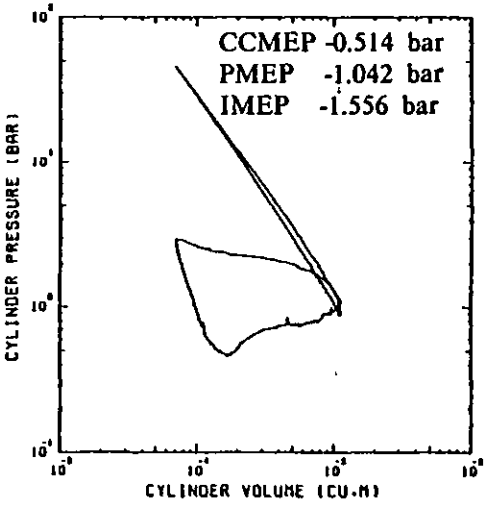

Engine Speed 2200 rpm

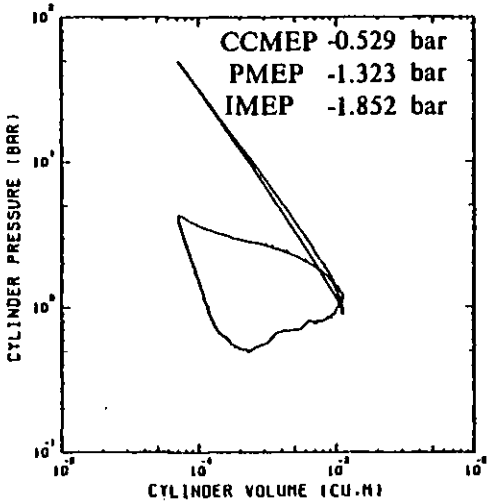

Engine Speed 2600 rpm

Fig. 4.25 Experimental Motored Cylinder Pressure Diagrams for the Perkins TV8 510 (M) Engine.

p_{max} = maximum cylinder pressure (kN/m^2)

The FMEP predicted using Chen and Flynn's correlation, for a range of engine speeds and maximum cylinder pressures is also shown in Fig. 4.24. The maximum cylinder pressures under hot motoring conditions will be of the order of 3000 kN/m^2 (with this geometric compression ratio of 12:1), which suggests that the Chen and Flynn correlation overpredicts the FMEP at high speeds and underpredicts it at low speeds. However, the detailed test data required to develop a new correlation of this form, for this particular engine, was not available and so eqn. (4.130) has been used without modification.

4.6 The Governor and Fuel Pump.

4.6.1 Introduction.

The governor is essentially a speed sensitive device which automatically controls or limits the engine speed by varying the fuel flow rate. The governor has two separate functions, firstly to measure the engine speed and find the error between the actual and desired speeds, and secondly to move the fuel pump rack so as to reduce this error. In many mechanical governors the same device is used to perform both functions (the flyweights), but where the force required to move the fuel pump rack is large, the speed error signal is usually amplified by means of a mechanical, pneumatic or hydraulic amplifier (171). More recently, electronic governors (85,133) have been developed because of their ability to analyse many different, and sometimes contradictory, input signals before deciding on the optimum engine fuelling. Governors with load sensing have been widely used, especially for electricity generating applications where a constant frequency is required during large and rapid load changes (170).

Two entirely different types of governor have been used in this work, because of the varying governing requirements for different applications. A mechanical all speed governor with a very limited speed range has been used to simulate the engine in a power generating type of application, where very close control of the engine speed is required. This is described in section 4.6.2. An electronic two speed governor is described in section 4.6.4, and this has been used to simulate vehicle type applications, where the governor only controls the engine fuelling at the maximum engine speed and during idling. Throughout the rest of the speed range the engine speed is controlled by the drivers demand. This system has been described in some detail because of its importance in the development of a comprehensive engine management system for the Hyperbar engine. Such a control system is desirable if the Hyperbar system is to be optimised, and leads to the analysis of an overall control system, described in Chapter 8.

The mathematical models used to represent the fuel pump and boost controlled rack limiter (aneroid), are described in sections 4.6.6 and 4.6.7 respectively.

4.6.2 Mechanical All Speed Governor.

Fig. 4.26 shows the general arrangement of a mechanical all speed governor. Speed sensing is performed by a pair of flyweights {1} located on opposite sides of a shaft {2} which is positively driven by the engine. The rotating weights produce a centrifugal force which opposes that of a spring {3}, which is itself compressed by a demand speed lever {4}. The fuel pump rack {5} position is controlled by the position of the speeder rod {2}. A simple boost pressure controlled rack limiting device (aneroid) {6} is also used to limit the movement of the fuel pump rack (and consequently the maximum engine fuelling) when the boost pressure is low. The rack is free to move between the minimum fuelling stop {7} and the maximum fuelling stop {8}, unless the aneroid limits its travel. The flyweights can pivot about point A, and the connecting arm {9} about the fixed pivot B. The ratio of the connecting arm lengths, d/c, enables the movement of the speeder shaft to be either amplified or attenuated, depending on the particular design.

This governor will control the engine fuelling over the entire speed range. However, if additional springs {10} are used to oppose the centrifugal force generated by the flyweights, once they reach a given position, then the movement of the speeder rod, Z, will be dependent on the demand speed, Y+y, only. In this case the governor acts like a two speed controller, with the flyweights only changing the rack position at very high and very low engine speeds. These springs {10} have not been included in this analysis.

By making the following assumptions, the equation of motion for the mechanical system shown in Fig. 4.26 can be derived:-

(1) Coulomb friction, which exerts a constant force opposing motion, is negligible.

(2) Stiction, which exerts a force opposing motion only so long as the system is at rest, is negligible.

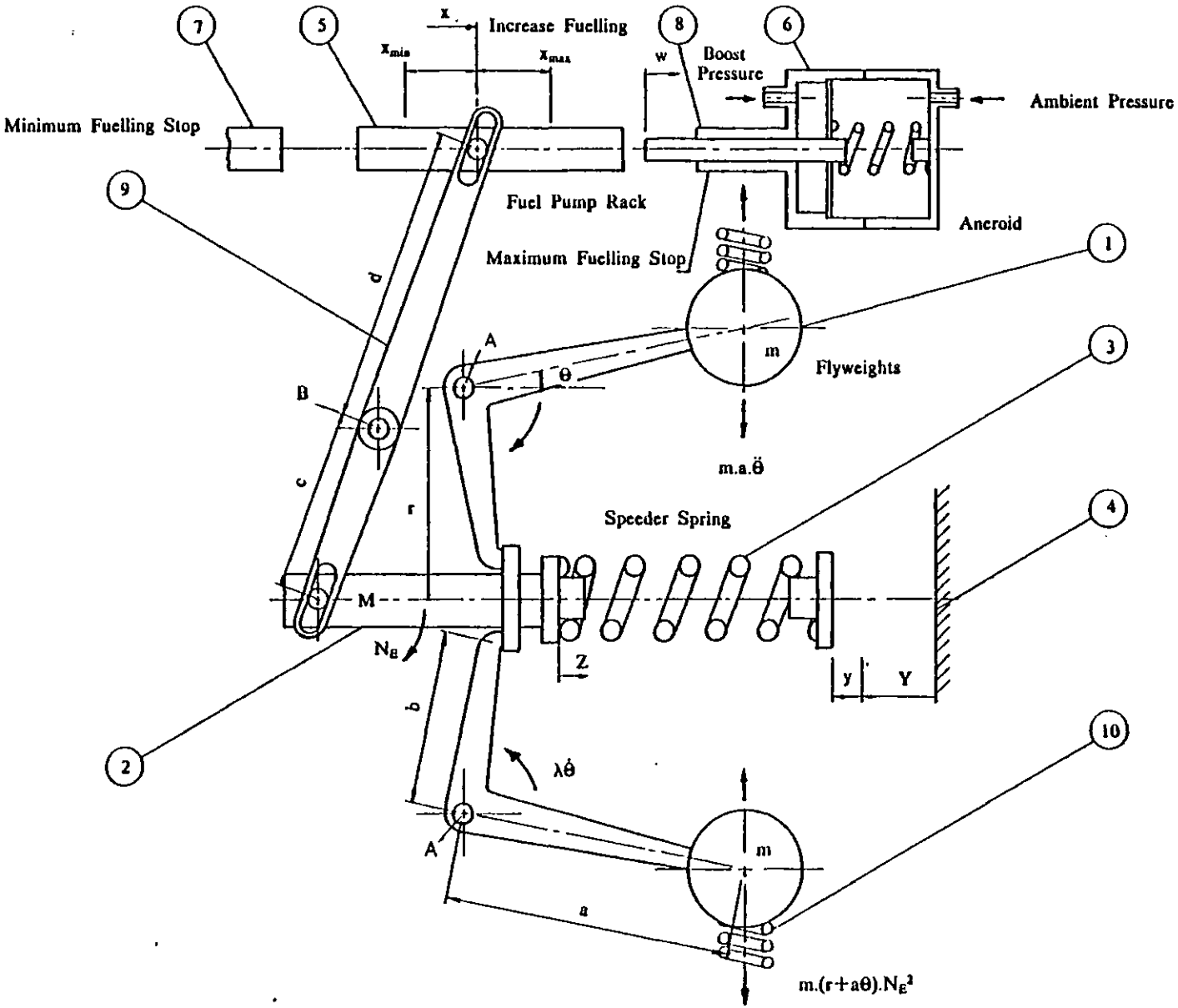

Fig. 4.26 Schematic of the Mechanical All Speed Governor.

(3) Friction is assumed to be viscous in nature.

(4) All movements are assumed to be small.

(5) Higher order products of small quantities are neglected.

(6) The mass of the flyweights are represented by an equivalent mass, m, concentrated at the centre of each ball.

(7) The mass of the speeder rod, and any parts attached to it, are represented by an equivalent mass, M.

(8) Any viscous friction in the system is replaced by an equivalent torque, $\lambda\dot{\Theta}$, at each pivot A.

(9) The top of the governor spring {3} has a fixed position, representing the compression of Y on the spring, and moves away from this position by small amounts, y.

(10) Any inertia and damping in the aneroid system is neglected, i.e. the rack limiter responds instantaneously to changes in boost pressure.

(11) The governor spring stiffness varies linearly with the governor setting, y.

The following equations describe the characteristics of the mechanical governor, from (42):-

$$\frac{\ddot{x}}{C_8} + C_1 .\dot{x} + \left(C_4 + C_5.y - C_6\left(\frac{N_E}{N_m}\right)^2\right).x = C_7\left[\left(\frac{N_E}{N_m}\right)^2 - \left(\frac{N_{ref}}{N_m}\right)^2\right] - (C_2 + C_3.y).y \qquad (4.131)$$

where,

$$C_1 = \frac{\lambda.d}{b.m_m.y_m.N_m^2.c} \qquad (4.132)$$

$$C_2 = \frac{0.5.b.k_t}{x_m.m_m.N_m^2} \qquad (4.133)$$

$$C_3 = \frac{0.5.b.k_2.y_m}{m_m.N_m^2.x_m} \quad (4.134)$$

$$C_4 = \frac{0.5.b.k_1.d}{y_m.m_m.N_m^2.c} \quad (4.135)$$

$$C_5 = \frac{0.5.b.k_2.d}{m_m.N_m^2.c} \quad (4.136)$$

$$C_6 = \frac{m.a^2.d}{m_m.y_m.b.c} \quad (4.137)$$

$$C_7 = \frac{m.a.r}{m_m.x_m.y_m} \quad (4.138)$$

$$C_8 = \frac{y_m.m_m.N_m^2.c}{(\ 0.5.b.M + m.a^2/b\ ).d} \quad (4.139)$$

and

x = rack position

y = governor setting (demand speed)

N_E = engine speed (rad/s)

λ = damping coefficient ($kg.m^2/s$)

m = mass of flyweights (kg)

M = mass of speeder rod (kg)

k_1 = constant speeder spring rate (N/m)

k_2 = variable speeder spring rate (N/m^2)

and a, b, c, d and r are dimensions of the system (m).

The subscripts, ref, represents the reference value, and m represents a constant value used to non-dimensionalise the terms in equations (4.131) to (4.139). The terms C_1 and C_8 are not non-dimensional, having units (s) and (s^{-2}) respectively, representing the normalised fuel pump rack inverse velocity and acceleration.

The boost controlled rack limiter position is given by:-

$$w = C_9 + C_{10}.(\ p_b - p_a\ ) \quad (4.140)$$

where,

w = rack limiter position

p_a = ambient pressure (kN/m^2)

p_b = boost pressure (kN/m^2)

and C_9 and C_{10} are constants.

For steady state operation, the rack position can be found by solving eqn. (4.131) with ($\dot{x}=\ddot{x}=0$), i.e.:-

$$x = \frac{C_7.\left[\left(\frac{N_E}{N_m}\right)^2 - \left(\frac{N_{ref}}{N_m}\right)^2\right] - (C_2 + C_3.y).y}{C_4 + C_5.y - C_6.\left(\frac{N_E}{N_m}\right)^2} \qquad (4.141)$$

The limits for the rack position, x, are:-

$$x_{min} \leq x \leq x_{max} \qquad (4.142)$$

where, x_{max} is either the maximum fuelling stop or the boost controlled rack limiter position, and x_{min} is the minimum rack limit.

Fig. 4.27 shows the steady state characteristics, from eqn. (4.141), of an all speed automotive governor measured experimentally by Marzouk (89), with no aneroid. This governor has been adapted to suit the particular requirements of a generating set application by varying some of the terms in eqns. (4.132) to (4.140).

4.6.3 Generating Set Governor Requirements.

The governing requirements for generating sets driven by turbocharged diesel engines, according to the British Standards Institution, are described in (25). In this particular application, the following requirements have been specified:-

(1) The steady state engine speed at 100% load is 1500 rpm.

(2) The governor speed droop from no load to 100% load is 4% of the full load speed, i.e. at no load the engine speed is 1560 rpm.

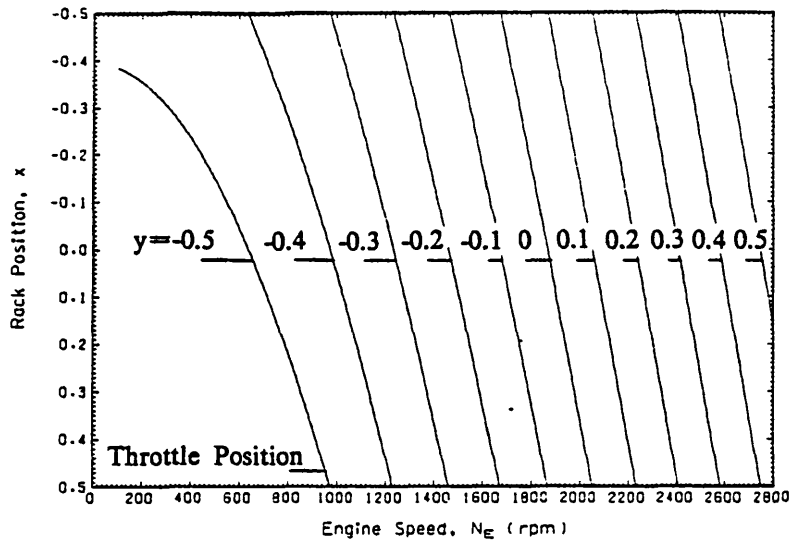

Fig. 4.27 All Speed Automotive Governor Characteristics.

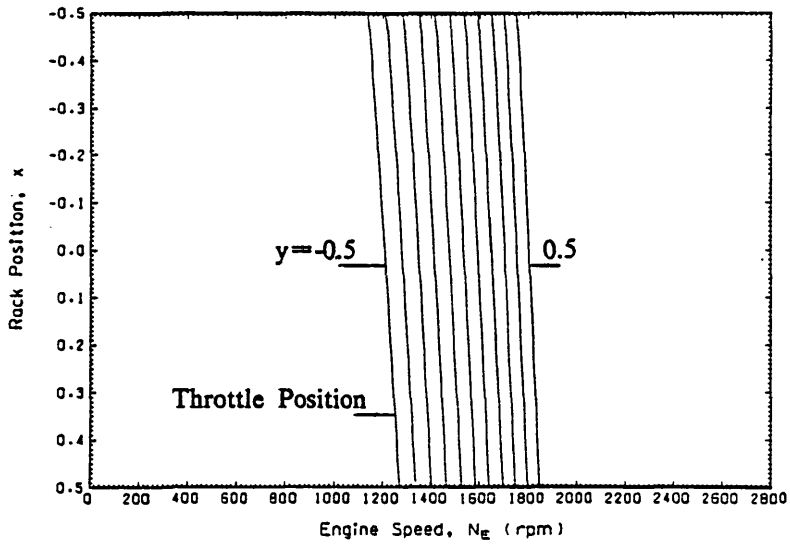

Fig. 4.28 Governor Characteristics for Electricity Generating Applications.

(3) The governor should hold the steady state engine speed to within 0.4% of the demand speed at all engine speeds, i.e. ± 6 rpm at 1500 rpm.

(4) The temporary speed change during load changes should be no more than 10% of the rated speed, i.e. 150 rpm. The magnitude of the rapidly applied load being, in general, a function of the engine rating (25).

(5) At no load, the engine speed must be capable of adjustment from 2.5% above to 2.5% plus the steady state speed droop at 100% load, below the normal no load speed, i.e. between 1461 and 1599 rpm.

(6) The engine should be capable of reaching its final steady state speed after a rapid 70% load application within 4 seconds.

(7) The fuel pump should permit 10% overfuelling during transients to allow the engine to recover from load applications of up to 100%.

The mechanical governor characteristics described in section 4.6.2 were modified to suit these requirements, by making the following assumptions:-

(1) The speeder spring rate is linear, i.e.

$$k_2 = C_3 = C_5 = 0 \qquad (4.143)$$

(2) The reference engine speed is 160.2 rad/s,

$$N_{ref} = 1530 \text{ rpm} \qquad (4.144)$$

(3) The speed droop of the governor is altered by modifying the constant, C_7, in eqn. (4.131). The radius of the flyweight pivot from the centreline of the speeder shaft, r, only occurs in the term, C_7, which can therefore be modified independently of the other parameters, see eqns. (4.132) to (4.139).

Using the rack position and the engine speed at no load (x_1 and N_1) and at 100% load (x_2 and N_2), eqn. (4.141) can be solved for the parameter C_7.

$$C_7 = \frac{x_2 \cdot \left[C_4 - C_6 \cdot \left(\frac{N_2}{N_m}\right)^2 \right] - x_1 \left[C_4 - C_6 \cdot \left(\frac{N_1}{N_m}\right)^2 \right]}{\left(\frac{N_2}{N_m}\right)^2 - \left(\frac{N_1}{N_m}\right)^2} \qquad (4.145)$$

The steady state governor characteristics are shown in Fig. 4.28, which demonstrates the limited speed range of this type of governor, and the large increase in rack position (engine fuelling) that will result from a relatively small change in engine speed, satisfying requirements (1), (2), (5) and (7). Whether or not the engine-governor system will respond rapidly enough to satisfy the response requirements (3), (4) and (6) can only be found by testing the complete system, see Chapter 7.

The final values of the constants used to define the governor characteristics in eqn. (4.131) were:-

$$C_1 = 135.0 \quad s$$

$$C_2 = 13975.1$$

$$C_3 = 0.0$$

$$C_4 = 2305.74$$

$$C_5 = 0.0 \qquad (4.146)$$

$$C_6 = -879.64$$

$$C_7 = 53031.34$$

$$C_8 = 0.60 \quad s^{-2}$$

$$N_{ref} = 1530 \text{ rpm}$$

$$N_m = 2600 \text{ rpm}$$

Note that C_7 has been altered for different builds of engine, with different fuel pump characteristics.

4.6.4 Electronic Two Speed Governor.

The Hyperbar turbocharged engine has also been modelled using a sophisticated electronic two speed governor, similar to that described by Leonard (85). This governor is suitable for automotive applications, the maximum engine speed and the idling speed being controlled by the governor. In the mid speed range, between 1100 and 2400 rpm, the rack position is controlled directly by the drivers demand (i.e. the pedal position).

For an in-line fuel pump the rack position is the main parameter that has to be determined by the governing system. As a high engine acceleration and deceleration rate is required, rapid governor response is necessary. In order to provide the necessary slew rate and positional accuracy, a closed loop control system is required to determine the rack position. To ensure shut down in the event of an electrical failure the rack can be biased towards the zero fuelling position by a spring, and then moved in the "open" direction by an actuator, under closed loop control from a position transducer. Transducers are also required to measure the engine speed and the demand speed (pedal position).

The control arrangement used by Leonard (85) provides two speed governing with "long range idle", and the steady state characteristics are shown in Fig. 4.29. In addition, excess fuel may be required at low engine speeds as a starting aid. Fig. 4.30 shows a block diagram of the governor control system which consists of two basic loops, the rack position actuator drive loop, and the speed loop. The rack position demand is generally determined by a signal derived from either the pedal position or the engine speed on a "lowest wins" basis, unless the speed falls into the idle region, in which case the throttle signal is modified to give the desired idling characteristic.

The maximum value of the pedal demand signal is modified as a function of significant engine parameters, so as to maximise the available power without damage to the engine or production of excessive smoke. A boost pressure signal, derived from a pressure transducer, can be used to limit the rack position if required. In order to avoid excessive exhaust gas temperatures, thermocouples in the exhaust manifold(s) can be used to provide signals so that the maximum fuelling can be reduced if the

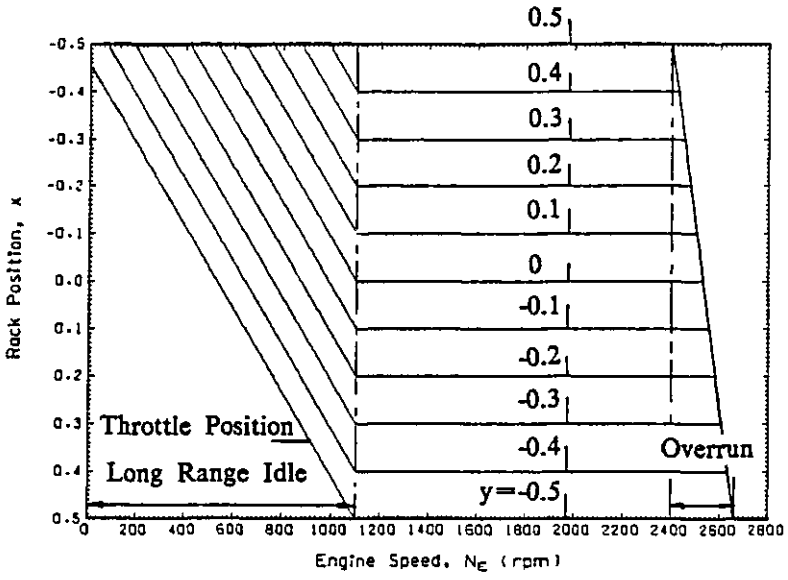

Fig. 4.29 Two Speed Governor Characteristics.

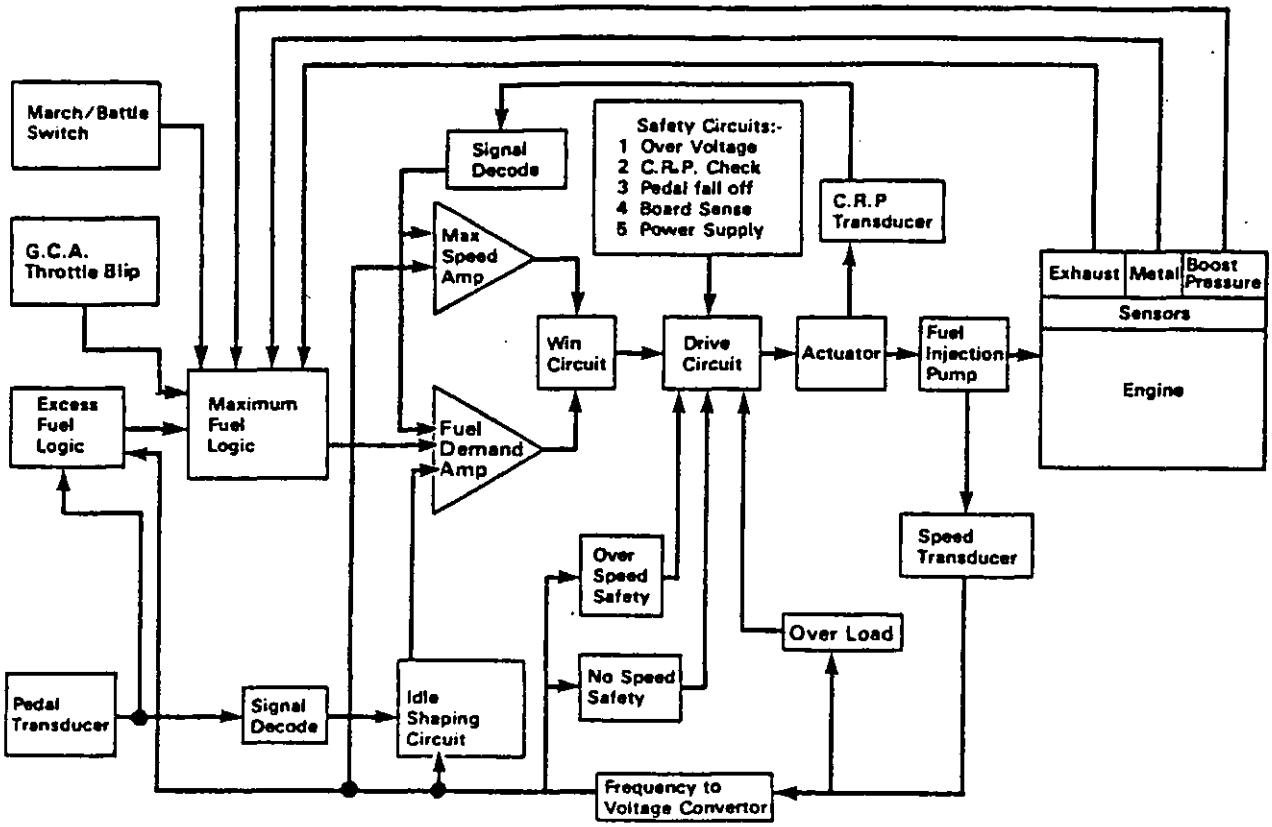

Fig. 4.30 Block Diagram of the CAV Electronic Governor, from (85).

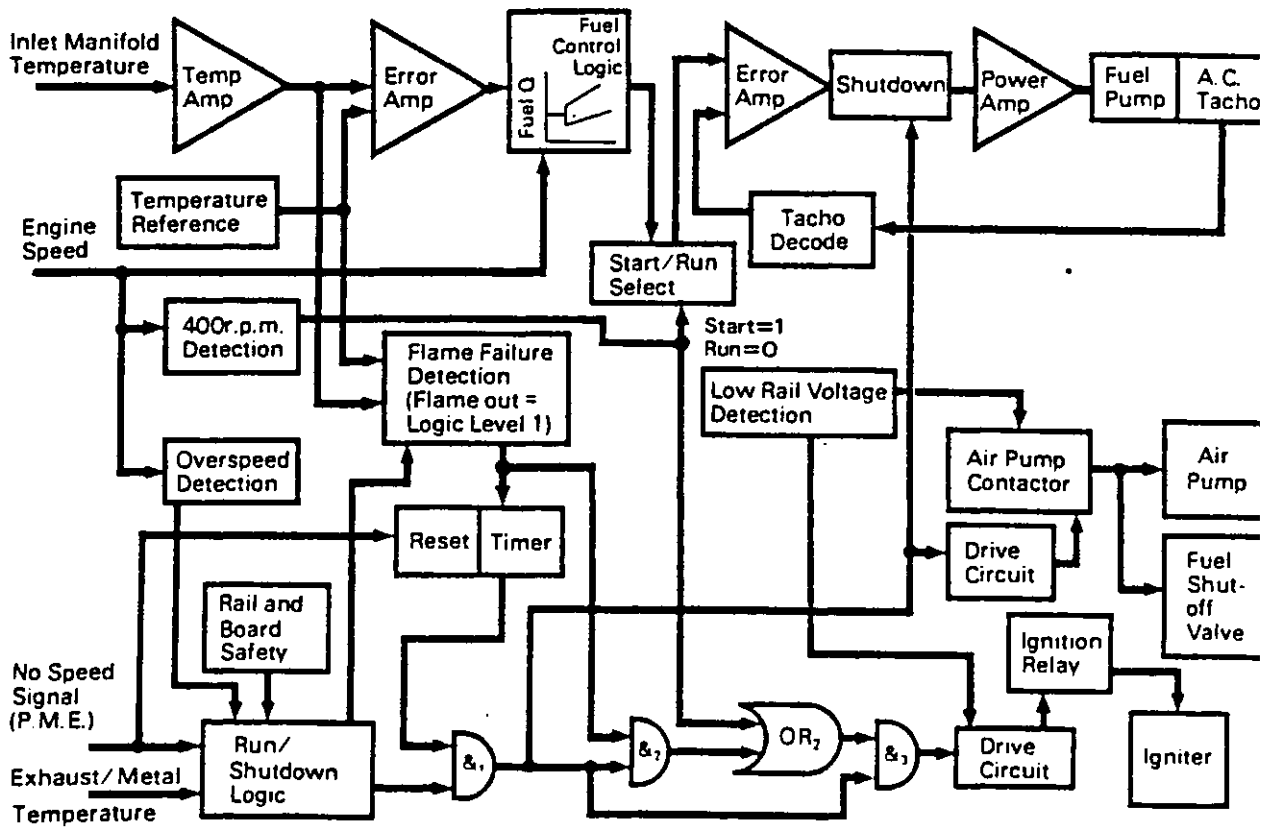

Fig. 4.31 Block Diagram of the Inlet Manifold Heater, from (85).

exhaust temperature exceeds a predetermined level. The maximum fuelling can also be reduced if the engine metal temperatures, measured by thermistors, exceed a preset value. In the idle speed region and when the boost pressure is low, a correction can be applied which effectively counteracts the reduction in fuel pump volumetric efficiency and engine efficiency with speed to minimise the possibility of stalling. Other modifications to the maximum fuelling schedule to provide "torque back up", etc. can also be considered.

For an engine designed to operate with high boost pressures, and therefore employing a low compression ratio, assistance in the form of inlet manifold heating is often required for cold starting, and to ensure good combustion without emission of unburnt hydrocarbons (white smoke) during light load running. The inlet manifold heater burns a relatively small amount of fuel in the manifold. The amount of fuel required varies with engine speed as well as the external air temperature, and provision must be made for turning the heater system on and off according to the engine demand.

Atomisation of the heater fuel spray is ensured by swirling air supplied by a vane pump, and it is ignited by a high energy spark ignition system. During starting the fuel delivery is constant, but once a predetermined speed is reached, just below idling, the control system can be arranged to hold the inlet manifold temperature, sensed by a thermocouple, at a constant value. A block diagram of this system is given in Fig. 4.31.

An alternative system using exhaust gas recirculation can be used to heat the inlet air, but this cannot usually be used during starting.

4.6.5 Modelling the Two Speed Governor.

The steady state governor characteristics which define the rack position, x, as a function of the engine speed, N_E, and the throttle position, y, can be seen in Fig. 4.29. The dynamics of the electronic governor were not known, however, and so a number of simplifying assumptions have been made.

The equation of motion for the two speed governor was assumed to be of the same form as that described in section 4.6.2 for the mechanical all speed governor, and the

similarities between the two have already been described, i.e.:-

$$\ddot{x} = \ddot{x} (x , \dot{x} , y , N_E) \qquad (4.147)$$

During steady state operation, this equation can be reduced to:-

$$x = x (y , N_E) \qquad (4.148)$$

A relationship defining eqn. (4.148) has been derived from the known steady state characteristics of the governor, Fig. 4.29. The inertia and damping terms were then required for eqn. (4.147).

The damping force, F_D, was assumed to be proportional to the velocity of the rack, i.e.

$$F_D = k_3.\dot{x} \qquad (4.149)$$

and the inertia force, F_I, was assumed to be proportional to the "effective mass" of the system, i.e.

$$F_I = k_4.\ddot{x} \qquad (4.150)$$

where,

k_3 = damping coefficient (N.s/m)

k_4 = inertia coefficient (kg)

Suitable values for k_3 and k_4 were found so that the critical damping ratio of the governor was 1.0 and the natural frequency was 100 radians/s. This ensures fast stable response of the governor, in excess of that achievable using conventional mechanical governors.

4.6.6 The Fuel Pump.

The steady state characteristics of the multi-element "in-line" fuel injection pump were represented by polynomial curve fits, giving fuel injected per cycle per cylinder, m_{fE}, as a function of the engine speed, N_E, and the rack position, x.

$$m_{fE} = [(w_1 + w_2.N_E + w_3.N_E^2) (w_4 + w_5.N_E + w_6.N_E^2).(x_{ref} - x) (w_7 + w_8.N_E + w_9.N_E^2).(x_{ref} - x)^2].w_{10} \quad (4.151)$$

where,

m_{fE} = fuel/cycle/cylinder (kg)
N_E = engine speed (rpm)
x = non-dimensional rack position
x_{ref} = reference rack position (x_{ref}=0.5)

and w_1 to w_{10} are empirical constants.

Experimental test data, measured on a Leyland 520 series engine with a Simms in-line fuel pump and four hole injectors (89), was used to give the general fuel pump characteristics (w_4 to w_9) as insufficient data was available for the Hyperbar engine. The shape of the maximum fuelling curve, (x=-0.5) was modified by varying the constants w_1, w_2 and w_3. The scaling factor w_{10}, was then used to vary the actual pump delivery according to the rating of the engine.

Typical fuel pump characteristics are shown in Fig. 4.32, which shows the fuelling non-dimensionalised over the fuelling at the maximum rack position at 2400 rpm. There is an increase in the fuel pump delivery of 7.0% at 1535 rpm and 5.1% at 1000 rpm, compared to that at the maximum speed.

The steady state fuel pump delivery characteristics are assumed to be applicable during transients, and it is assumed that the engine speed and rack position will not alter significantly during the injection period. The amount of fuel injected per cycle per cylinder is therefore evaluated at the static injection point during transients. The

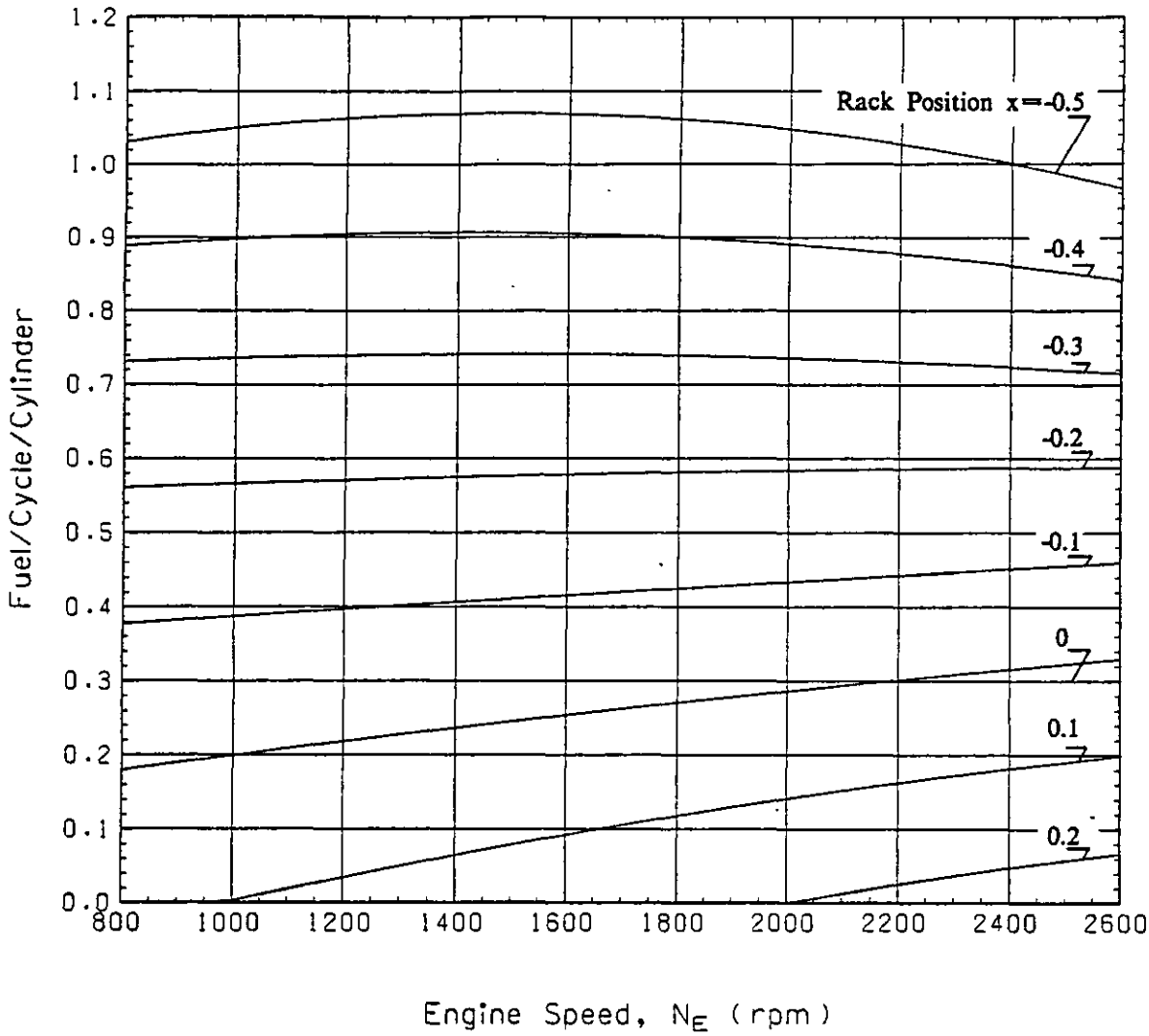

Fig. 4.32 Fuel Pump Characteristics.

models for the static and dynamic injection timings are described in section 4.3.2.

4.6.7 The Boost Controlled Rack Limiter.

For conventional highly rated turbocharged diesel engines some form of aneroid is usually required. This device restricts the limit of the rack travel according to the boost pressure (usually measured in the induction manifold), see Fig. 4.26. There are two main reasons for this:-

(1) If high fuelling rates are used at low engine speeds, under steady state conditions, to increase the low speed torque, the compressor may surge (or the surge margin will be greatly reduced), because the pressure ratio is high compared to the air flow rate through the compressor. Therefore the shape of the maximum torque curve may be dictated by the compressor match, at low engine speeds.

(2) At low speeds the turbine available energy is low. If the fuelling is increased rapidly to increase the engine BMEP, then the engine power may be limited by the black smoke emitted. Therefore the aneroid rack limiter controls the boost pressure/fuelling ratio, which is a simple method of controlling the A/F ratio. During transient operation, the response of the air supply is usually slower than that of the fuel system to rapid changes in load and/or speed, due to the inertia of the turbocharger and the compressibility of the exhaust gas link to the engine. In this case the instantaneous A/F ratio might become excessively rich if the fuel pump delivery is not limited in some way.

For the Hyperbar application the first of these problems should not occur. The compressor mass flow rate is a unique function of the pressure ratio, because of the action of the by-pass valve. This allows very high BMEP's to be achieved at low engine speeds. How the system reacts during transients remains to be established, see Chapter 7.

The aneroid rack limiter may still be required, however, to solve the problems of excessive black smoke following rapid increases in fuelling at low engine speeds. The

smoke produced is largely a function of the engine A/F ratio, which in the Hyperbar system is usually high relative to conventional turbocharging systems. When high loads at low speeds are required, the ACC burner can be used to increase the boost pressure.

No aneroid rack limiting device was therefore used for the Hyperbar engine model. The mathematical representation of the aneroid characteristics, eqn. (4.140), used for the later two stage turbocharged engine tests, see Chapter 7, is described in section 4.6.2.

4.7 The By-Pass Valve Model.

4.7.1 Description of the By-Pass Valve Arrangement.

The by-pass valve arrangement is shown diagramatically in Fig. 4.33. It consists of two main components, the valve {1} and the casing {2}. The valve is supported by a valve guide {3} in the casing. Air at compressor delivery conditions enters the chamber at the back of the valve head through circumferential ports {7}. If the boost pressure, p_2, is significantly higher than the exhaust back pressure, p_3, the valve will start to open, causing the boost air to flow to the exhaust side of the valve. This will continue until the exhaust back pressure has risen sufficiently to maintain the valve in an equilibrium position.

As the valve opens, air enters the chamber created behind the damping piston {6} through a fixed area jet {5}, and is expelled from the damping chamber through the orifice {4}. Varying the size of the fixed area jet enables the pressure in the chamber behind the damping piston {6} to be controlled, and therefore the degree of valve damping to be varied.

4.7.2 By-Pass Valve Dynamics.

Fig. 4.34 shows the free body diagram for the by-pass valve with the appropriate dimensions, pressures and forces. The valve damping force is assumed to be due to viscous friction. Experimental tests have shown that the valve is continuously moving, and the damping coefficient, λ, is assumed to include the effects of the lubricating oil film, seals, etc. The damping force term, $\lambda\dot{x}$, is entirely separate from the damping caused by the damping chamber, which depends upon the relative pressures, p_a and p_b.

The equation of motion for the by-pass valve can be written as:-

$$m.\ddot{x} = [p_2.(A_1 - A_2) - p_3.A_1 + p_b.A_3 - p_a.(A_3 - A_2) - \lambda.\dot{x}].1000 + m.g.\sin\Phi \quad (4.152)$$

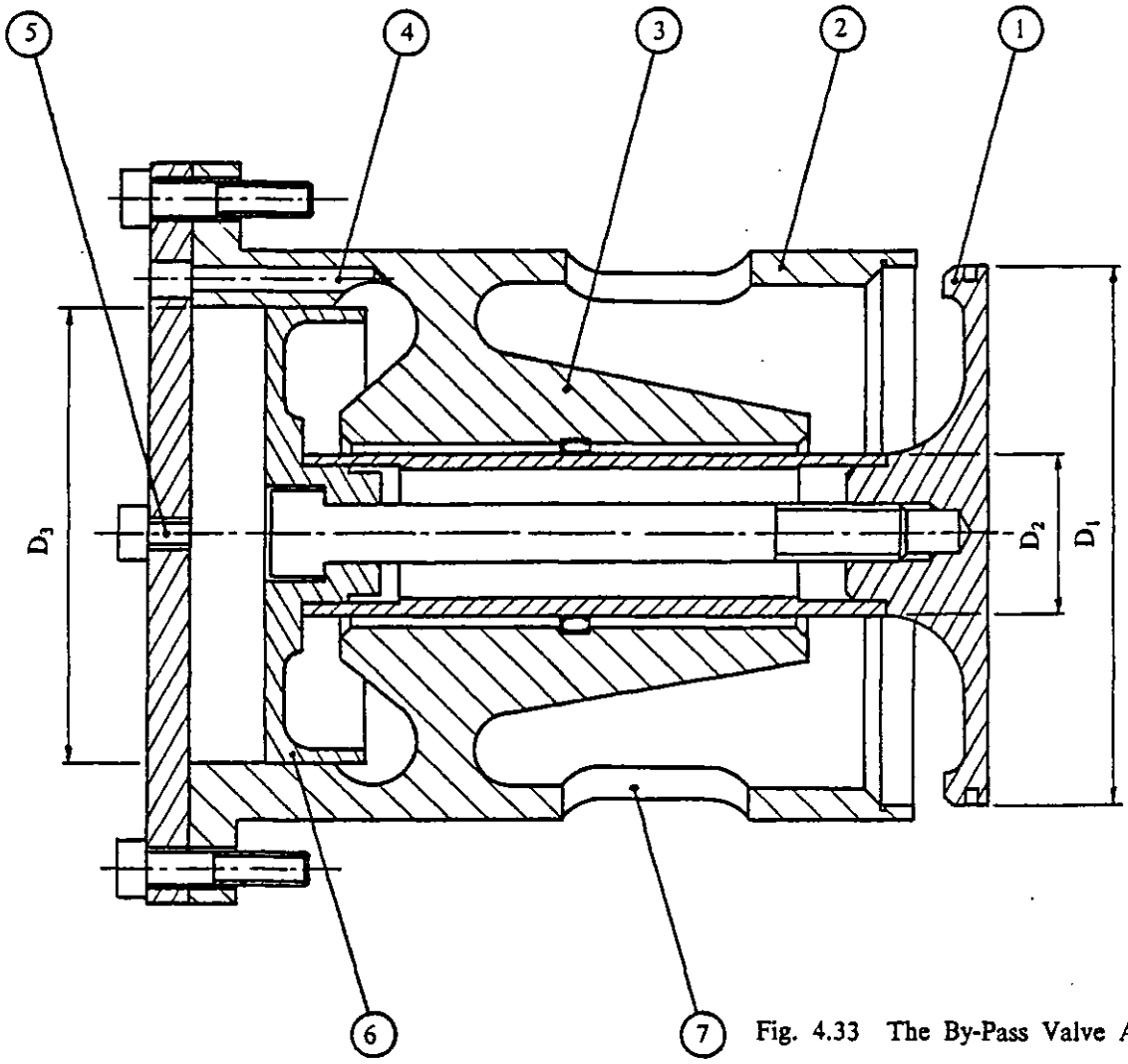

Fig. 4.33 The By-Pass Valve Arrangement.

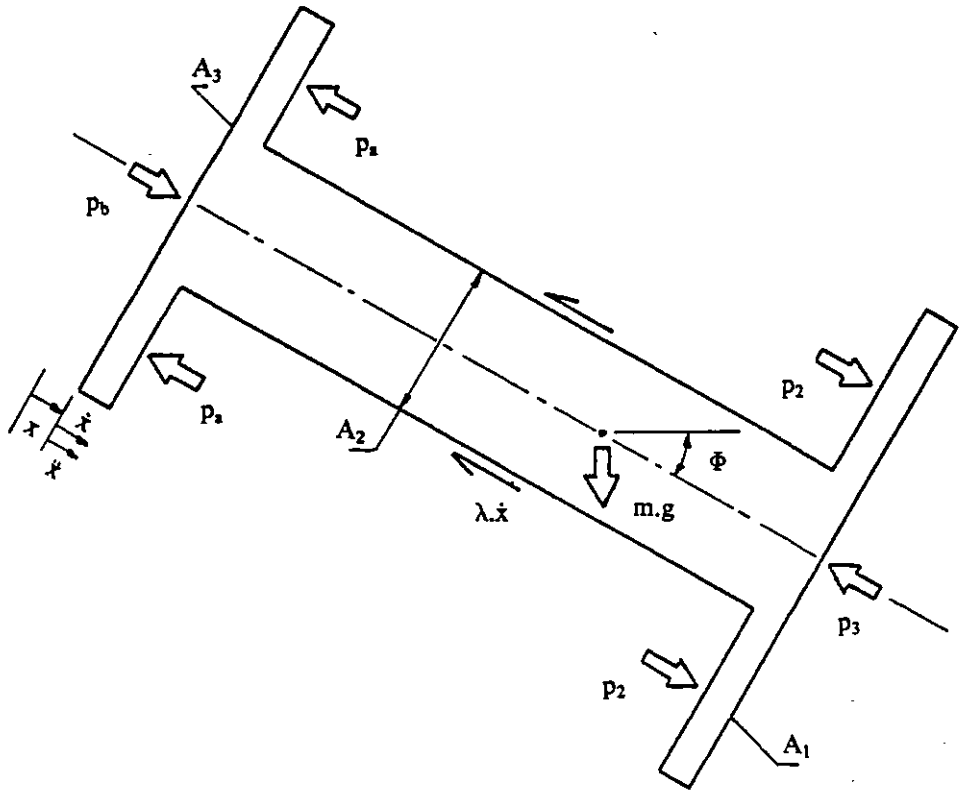

Fig. 4.34 The By-Pass Valve Forces.

where,

g = gravitational acceleration (m/s^2)

m = mass of the valve (kg)

p_a = damping chamber pressure (kN/m^2)

p_b = damping chamber pressure (kN/m^2)

p_2 = compressor delivery pressure (kN/m^2)

p_3 = exhaust back pressure (kN/m^2)

x = valve position (m)

$\dot{x}$ = valve velocity (m/s)

$\ddot{x}$ = valve acceleration (m/s^2)

λ = viscous damping coefficient (kN.s/m)

Φ = angle of inclination of valve axis (degrees)

The valve motion is thus controlled by the inertia, pressure, damping and gravity forces.

The damping chamber pressures, p_a and p_b, are dependent upon the valve position, velocity and acceleration, the damper geometry, the orifice and jet sizes and the ambient conditions. Both p_a and p_b can be calculated from the flow into and out of the respective damping chambers (the geometry of which are known). However, as an initial simplification, it is assumed that the valve moves relatively slowly and that the orifice sizes are large enough so that:-

$$p_a = p_b = p_1 \tag{4.153}$$

where,

p_1 = ambient pressure (kN/m^2)

Substituting from eqn. (4.153) into eqn. (4.152) and simplifying gives:-

$$\ddot{x} = [\, p_2.(A_1 - A_2) - p_3.A_1 + p_1.A_2 - \lambda.\dot{x} \,].1000/m + g.\sin\Phi \tag{4.154}$$

Under steady state conditions, when the valve velocity, $\dot{x}$, and acceleration, $\ddot{x}$, are zero, eqn. (4.154) becomes:-

$$\frac{(p_2 - p_3)}{(p_2 - p_1)} = \frac{A_2}{A_1} - \frac{m.g.\sin\Phi}{A_1.(p_2-p_1).1000} \qquad (4.155)$$

The steady state pressure drop across the by-pass valve, (p_2-p_3), is therefore a function of the guage boost pressure, (p_2-p_1), the valve area ratio, A_2/A_1, and the valve mass, m, geometry, A_1, and inclination, Φ.

4.7.3 By-Pass Valve Inclination.

In this particular application, the by-pass valve is mounted with its axis horizontal, and so $\Phi=0$, in eqn. (4.154), which then becomes:-

$$\ddot{x} = [\,(p_2 - p_3).A_1 - (p_2 - p_1).A_2 - \lambda.\dot{x}\,].1000/m \qquad (4.156)$$

and the steady state form of eqn. (4.156) can be written as:-

$$\frac{(p_2 - p_3)}{(p_2 - p_1)} = \frac{A_2}{A_1} \qquad (4.157)$$

However, if the valve were mounted with its axis vertical, so that it is fully open in the static position, $\Phi=90°$, eqn. (4.155) becomes:-

$$\frac{(p_2 - p_3)}{(p_2 - p_1)} = \frac{A_2}{A_1} - \frac{m.g}{A_1.(p_2-p_1).1000} \qquad (4.158)$$

The valve pressure drop, (p_2-p_3), is reduced, and so the by-pass flow increases, moving the compressor operating point away from the surge line, because of the increase in the compressor flow rate. The reduction in the valve pressure drop will depend upon the valve material and geometry, i.e. m and A_1, and the guage boost pressure, (p_2-p_1). Increasing the boost pressure will reduce the influence of the valve inclination, Φ.

Similarly, if the valve is inclined so that its axis is vertical and is fully closed in the static position, $\Phi=270°$, eqn. (4.155) becomes:-

$$\frac{(p_2 - p_3)}{(p_2 - p_1)} = \frac{A_2}{A_1} + \frac{m.g}{A_1.(p_2-p_1).1000} \qquad (4.159)$$

and the valve pressure drop increases, requiring less by-pass flow and moving the compressor operating line closer to surge. Therefore, the valve inclination, Φ, gives some control over the scavenge pressure drop and the compressor operating line, but the effect is limited by the necessity of using a fixed angle, Φ, for the valve in a particular application.

4.7.4 Experimental Measurements of the By-Pass Valve Motion.

A number of experimental tests were performed by the engine manufacturer to investigate the transient motion of the by-pass valve at constant engine speeds and loads. Measurements were made of the instantaneous values of:-

(1) By-pass valve displacement, x.

(2) Boost pressure, (p_2-p_1).

(3) Exhaust back pressure, (p_3-p_1).

The influence of valve damping was also investigated, by varying the size of the fixed area jet [5], see Fig. 4.33. The boost pressure was measured in the compressor delivery duct before the charge cooler, and the exhaust pressure transducer was mounted in the exhaust manifold, immediately before the burner box, see Fig. 4.35.

This test data was then used to investigate the influence of various key parameters on the by-pass valve motion, and to determine a realistic value for the valve damping coefficient, λ.

The measured boost pressure was assumed to be the valve upstream pressure, p_2, and the exhaust pressure to be the downstream pressure, p_3. The errors involved in making these assumptions are discussed in the following sections.

Using eqn. (4.156) for the valve with its axis mounted horizontally, the valve geometric areas, A_1, A_2 and A_3, and the valve mass, m, were measured, and the instantaneous upstream and downstream pressures, p_2 and p_3 respectively, were taken from the test data.

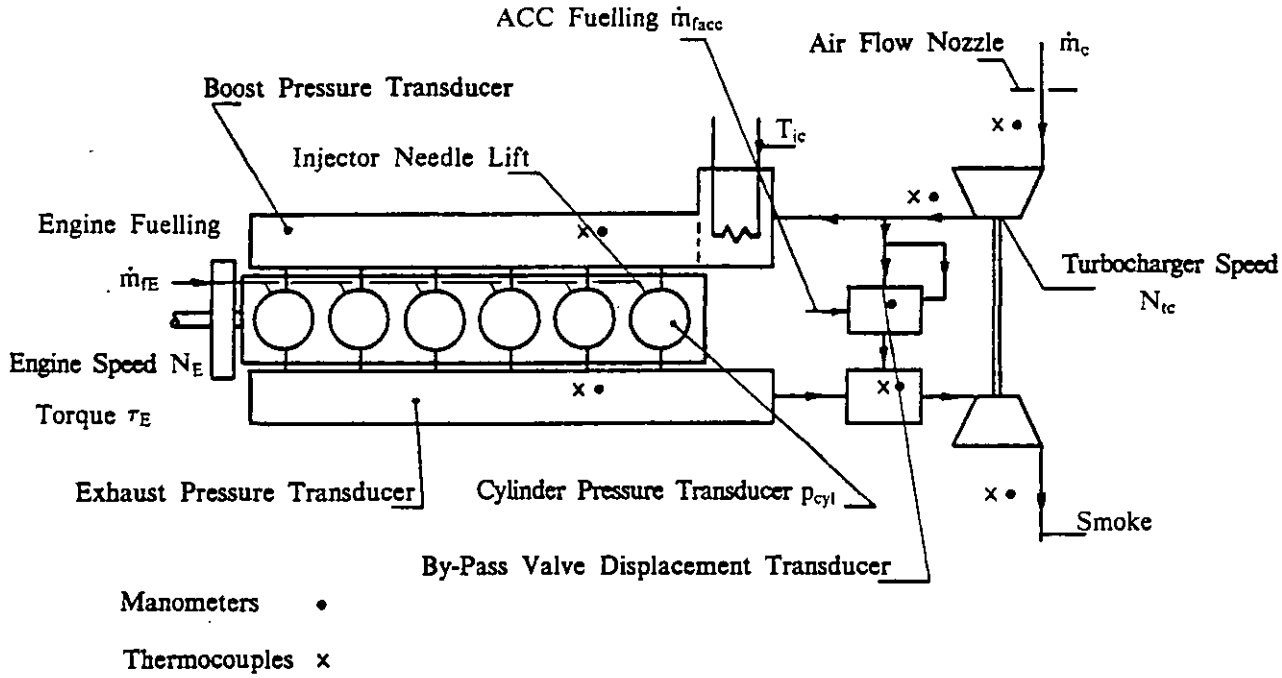

Fig. 4.35 Schematic of the Hyperbar Engine Instrumentation.

Equation (4.156) was then integrated numerically, once to give the instantaneous valve velocity, $\dot{x}$, and twice to give the instantaneous displacement, x, (the initial position and velocity being taken from the experimental data). The predicted valve motion was then compared with the measured valve motion by assuming a value of λ.

The total geometric flow area of the circumferential ports [7], see Fig. 4.33, is 1.3 times that of the geometric valve flow area at maximum valve lift, and therefore the restriction of the circumferential ports should not seriously affect the by-pass valve flow and has been neglected. The instantaneous valve geometric flow area was therefore calculated from:-

$$A_{vg} = \pi.D_1.x \tag{4.160}$$

where,

A_{vg} = valve geometric flow area (m^2)

D_1 = valve head diameter (m)

and,

$$A_1 = \frac{\pi.D_1^2}{4} \tag{4.161}$$

The instantaneous isentropic valve mass flow rate can be calculated, for subsonic flow, from:-

$$\dot{m}_{vis} = \frac{A_{vg}.p_2.}{\sqrt{T_2}}\left[\frac{2.}{R.}\left(\frac{\gamma.}{\gamma-1}\right)\left\{\left(\frac{p_3}{p_2}\right)^{2/\gamma} - \left(\frac{p_3}{p_2}\right)^{(\gamma+1)/\gamma}\right\}\right]^{0.5} \tag{4.162}$$

where,

$\dot{m}_{vis}$ = isentropic valve mass flow rate (kg/s)

R = gas constant for air (J/kg)

γ = specific heats ratio for air.

The upstream pressure, p_2, and temperature, T_2, are assumed to be constant throughout the cycle, and were taken from the experimental test measurements.

Integrating the instantaneous isentropic mass flow rate, $\dot{m}_{vis}$, over an engine cycle and then comparing this with the actual by-pass valve flow rate enables a mean value of the valve coefficient of discharge to be estimated, using:-

$$c_{dv} = \frac{\dot{m}_{va}}{\dot{m}_{vis}} \tag{4.163}$$

where,

c_{dv} = mean by-pass valve coefficient of discharge

$\dot{m}_{va}$ = actual by-pass valve mass flow rate (kg/s)

In practice, it is extremely difficult to measure the actual by-pass valve mass flow rate, $\dot{m}_{va}$, on an engine. The total by-pass flow can be estimated (including the ACC air flow) by subtracting the engine mass flow rate (calculated from the engine speed, boost pressure and temperature, and estimated volumetric efficiency) from the measured total compressor flow rate. The ACC air flow rate can be calculated if the ACC position, and hence the port areas, are known, but a coefficient of discharge for the ACC ports must also be estimated, see section 4.8.

A parametric study of the important parameters affecting the by-pass valve was therefore carried out.

4.7.5 Parametric Study of the By-Pass Valve Motion.

4.7.5.1 Introduction.

The object of this exercise was to find the value of the valve damping coefficient, λ, which gave the best agreement between the experimental and predicted valve motion. Other factors that influence the by-pass valve motion have also been investigated.

4.7.5.2 Exhaust Back Pressure Phase Angle.

The exhaust pressure transducer is positioned immediately before the burner box in the exhaust manifold, and so does not give a true indication of the instantaneous back pressure on the by-pass valve, p_3, in terms of:-

(1) The true absolute pressure, i.e. the shape and amplitude of the pressure pulses, or

(2) the phasing of the exhaust pulses.

Assuming that the pressure pulses travel at the speed of sound relative to the mean exhaust gas velocity (which is relatively small, and is therefore ignored) and that the mean exhaust manifold gas temperature at the test condition, described in section 4.7.5.5, is 925 K (652°C), at an engine speed of 1800 rpm, the velocity of the pressure waves (travelling at the speed of sound) is approximately 595 m/s. At this engine speed the pressure waves will travel 0.055m/°CA.

So, for example, if the position of the by-pass valve is 0.55m from the position of the transducer, then the pressure pulses at the valve will lag the pulses measured by the transducer by approximately 10°CA, (assuming that there is no phase lag in the measuring system).

As the pressure waves travel along the ducting their shape and amplitude change as well as their phase, and there may also be pressure wave reflections from various parts of the exhaust system which will alter their shape. The following analysis is very much simplified and is intended only to give an indication of the magnitude and importance of the phase angle errors.

4.7.5.3 Boost Pressure and Mean Exhaust Back Pressure.

In actual operation, as the boost pressure, p_2, increases the valve opens and the flow through the by-pass increases. This tends to increase the exhaust system pressure, p_3, until a new equilibrium position is reached. The model used for testing the by-pass valve dynamics has no such feedback. In this case the boost conditions and the mean exhaust pressure are maintained at the measured test values. Errors in the measured boost pressure, p_2, and exhaust pressure, p_3, levels will result in errors in the prediction of the by-pass valve motion and the instantaneous mass flow rate.

The mean boost pressure and exhaust pressure levels measured were therefore shifted to show the sensitivity of the valve dynamics to errors in these values.

4.7.5.4 Initial Conditions.

The calculation was started off by using the initial by-pass valve position, velocity and acceleration from the experimental test data. The measured by-pass valve position diagram was differentiated numerically, once to give the initial velocity, and again to give the initial valve acceleration.

4.7.5.5 Engine Test Conditions.

The effect of various parameters on the by-pass valve position was investigated using the test data measured at 1800 rpm/19.0 bar BMEP. The damping jet was removed and so the valve damping is due to the friction between the valve and the valve guide only, see section 4.7.2.

At this engine operating condition, the following mean pressures were measured using manometers:-

Ambient pressure, p_1	$= 100.5$ kN/m^2
Boost pressure, p_2	$= 359.8$ kN/m^2

Exhaust manifold pressure	= 340.7 kN/m^2
ACC gas pressure	= 335.5 kN/m^2
Mixer pressure	= 336.9 kN/m^2

By assuming that the mean valve back pressure, p_3, is equal the the mean ACC pressure, the effective valve area ratio can be calculated, and compared to the geometric area ratio. Substituting the above values in eqn. (4.157) gives:-

$$\frac{(p_2 - p_3)}{(p_2 - p_1)} = 0.0937$$

The actual geometric valve area ratio, A_2/A_1, is 0.09, and so either there must be some error in the assumed values of p_2 and/or p_3, or else the valve cannot accurately maintain the steady state pressure ratio given by eqn. (4.157) at this operating condition.

In order to calculate the isentropic mass flow rate through the by-pass valve over the engine cycle, the upstream air temperature is required in eqn. (4.162). This was taken from the measured thermocouple reading at the compressor outlet.

Boost temperature, T_2 = 468 K (195°C)

4.7.5.6 Effect of the By-Pass Valve Mass.

The influence of the valve mass, m, on the predicted valve motion has been investigated to show the sensitivity of the predicted results to errors in valve mass. The valve axis was mounted horizontally for this and all the subsequent tests.

Fig. 4.36 shows the effect of varying the valve mass from 0.1 kg to 5 kg. The boost conditions and the mean exhaust back pressure are given in section 4.7.5.5. The exhaust pressure phase lag was set to 0°CA and the valve damping coefficient to 0.5 kN.s/m.

Increasing the mass of the by-pass valve:-

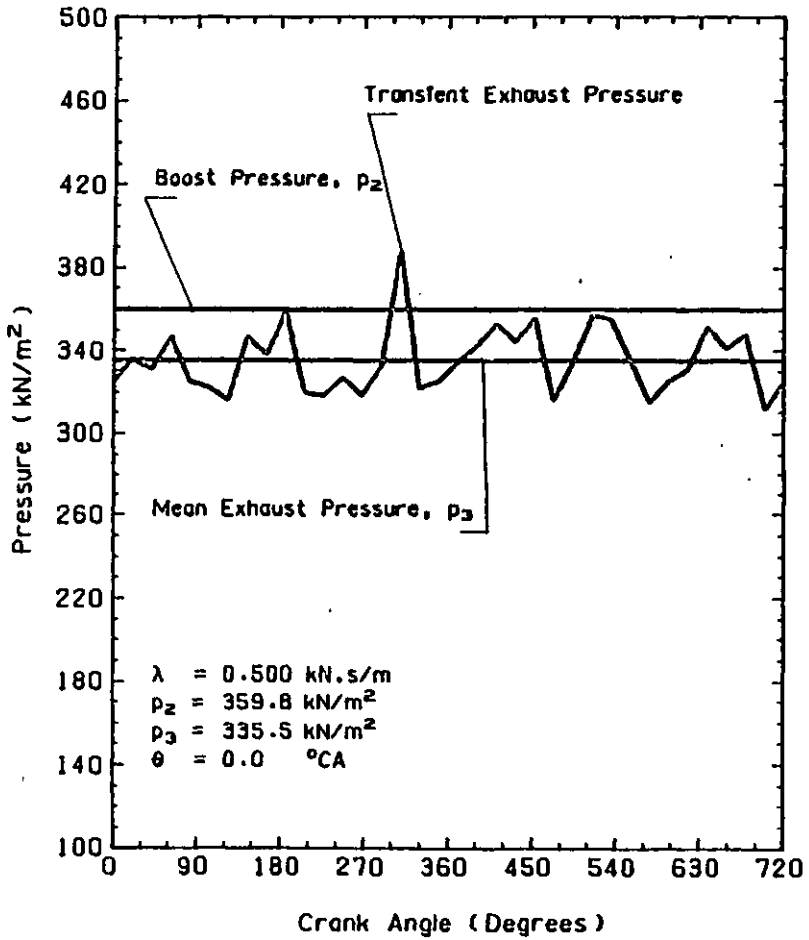

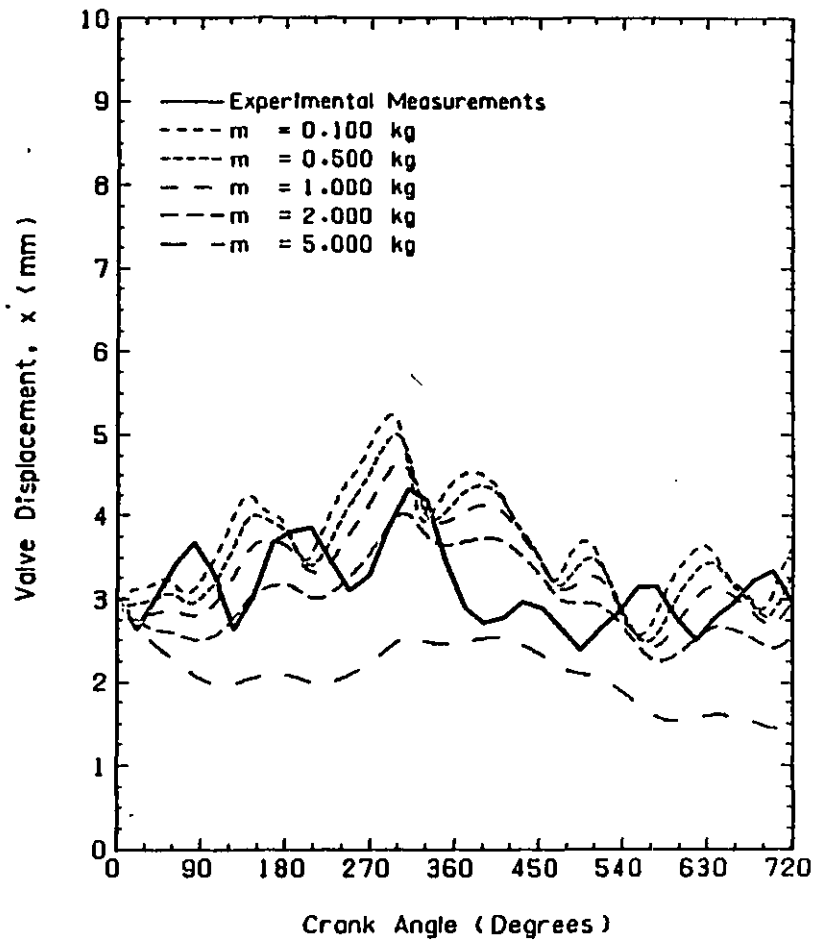

Fig. 4.36 Effect of the By-Pass Valve Mass m on the Predicted Valve Motion.

(1) reduces the amplitude of the fluctuations in valve position during the cycle,

(2) reduces the mean displacement of the valve, and

(3) reduces the valve effective flow area, and therefore the valve mass flow rate.

Increasing the valve mass above 2 kg, leads to practically no fluctuation in the valve position during the cycle. In the extreme case, with m=5 kg, the pressure ratio across the valve is barely sufficient to keep it open. Once it starts to close the inertia force dominates, and there is a drastic reduction in the valve flow. Therefore 2 kg would appear to be a reasonable upper limit for the valve mass.

Over the range of valve masses 0.1 to 2 kg the shape of the predicted valve position diagram is hardly affected by variations in mass. The phasing of the pulses in the valve position is primarily dictated by the exhaust pressure diagram. There is a definite phase angle error between the experimental and predicted valve motion in these diagrams, although both show 6 distinct pulses caused by the exhaust pressure pulses from the 6 engine cylinders.

For comparison, the valve mass measured by the engine manufacturer was 1.0 kg.

4.7.5.7 Effect of the By-Pass Valve Damping.

Fig. 4.37 shows the effect of varying the by-pass valve damping coefficient, λ, over the range 0.2 to 5.0 kN.s/m. The mass of the by-pass valve was 1.0 kg and the boost conditions and exhaust pressure were identical to those used in the previous section.

Obviously the extreme cases of λ=0.2 kN.s/m (underdamped) and λ=5.0 kN.s/m (overdamped) define the practical limits for this parameter.

Increasing the valve damping coefficient:-

(1) reduces the amplitude of the fluctuations in valve motion,

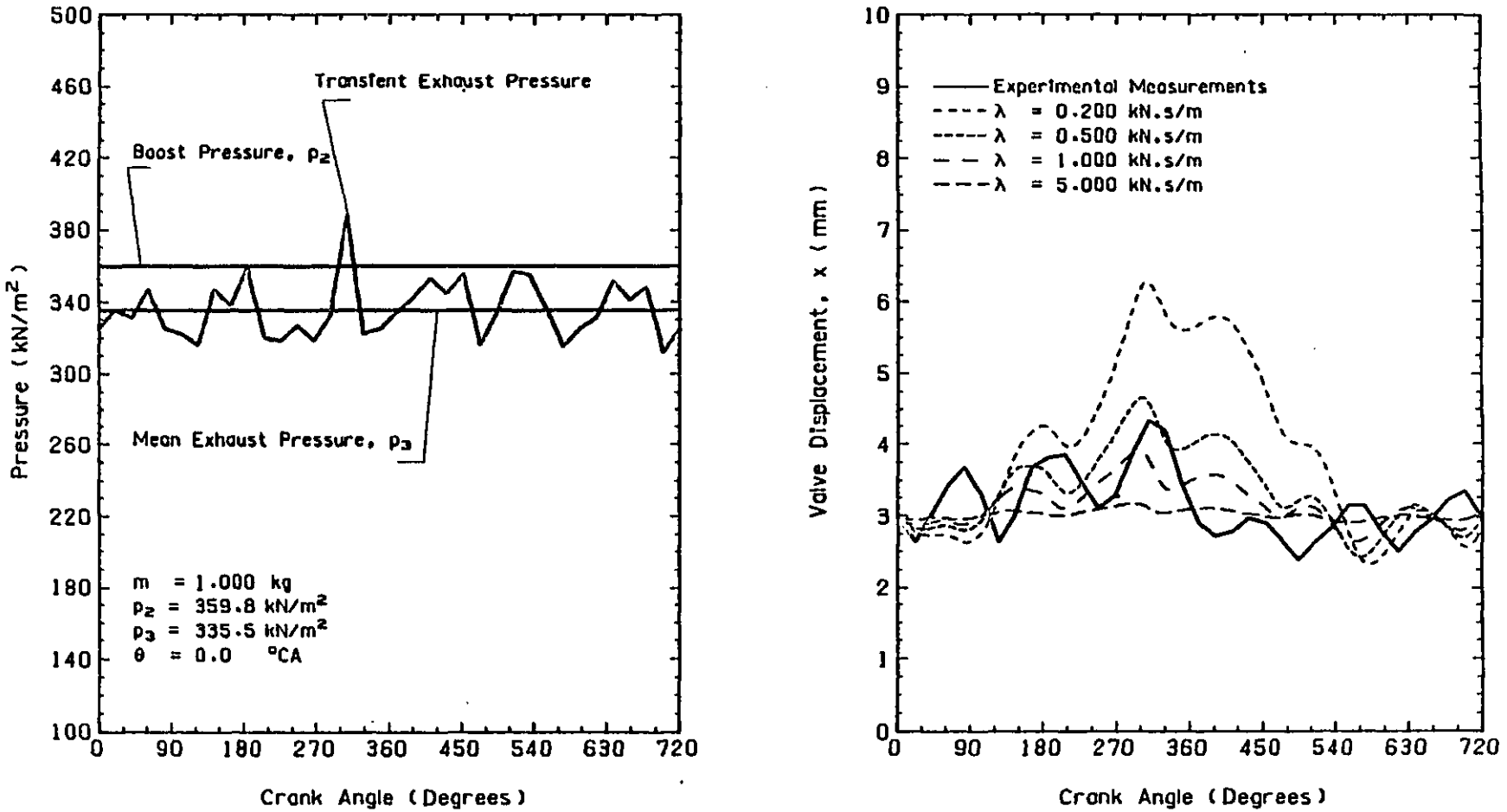

Fig. 4.37 Effect of the Damping Coefficient λ on the Predicted Valve Motion.

(2) reduces the mean valve displacement, and hence the flow area, although this effect is very small once the damping is increased above 2.0 kN.s/m, and

(3) reduces the valve mass flow rate, as the area reduces.

Judging by the amplitude of the fluctuations in the experimental valve motion, a reasonable value for λ, with this valve mass, is in the range 0.5 to 1.5 kN.s/m. Increasing the valve damping coefficient, λ, does not effect the predicted displacement diagrams enough to correct the phase angle error, over a reasonable range of values of λ. The peaks of the predicted valve displacement diagram occur before those measured experimentally, which implies that the exhaust pulses at the valve may occur later than those measured at the transducer.

4.7.5.8 Effect of the Exhaust Back Pressure Phase Angle.

Fig. 4.38 shows the effect of exhaust pressure phase angle shifts of 0, 10, 20 and 30°CA on the predicted valve motion. The mean exhaust pressure was held constant at 335.5 kN/m^2, the valve mass was 1.0 kg and the damping coefficient was 0.5 kN.s/m. It was assumed that the exhaust pressure at the valve lags that measured in the manifold, and these angle shifts cover an effective distance between the valve and the transducer of between 0 and 1.65 m (see section 4.7.5.2).

As the exhaust phase angle shift increases:-

(1) the phasing of the by-pass valve displacement diagram is shifted, so that the peaks and troughs occur at a later point in the engine cycle. The phasing of the major, third, peak is almost correct with a 10 to 20°CA phase shift in the exhaust pressure diagram,

(2) the mean by-pass valve position is increased, and so the flow through the valve is increased. This will obviously depend upon the degree to which the exhaust pressure diagram is shifted.

A phase angle shift of approximately 15°CA appears to give the best correlation between the experimental and predicted by-pass valve motion, although the mean

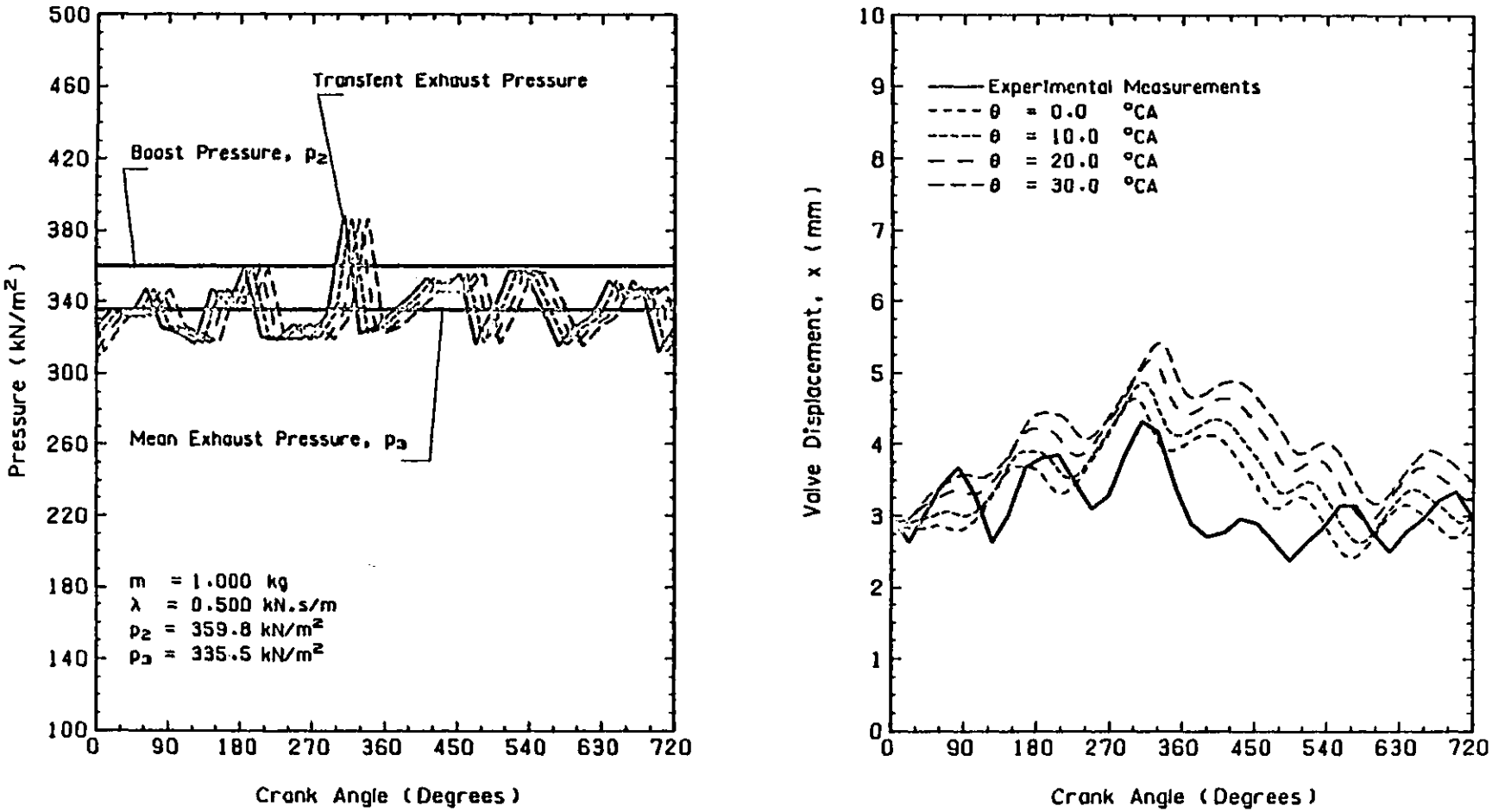

Fig. 4.38 Effect of the Exhaust Pressure Phase Angle Θ on the Predicted Valve Motion.

displacement is predicted too high. This corresponds to a distance of 0.83 m between the valve and the pressure transducer. No data was available concerning the detailed geometry of the system to confirm this conclusion.

4.7.5.9 Effect of the Mean Exhaust Back Pressure.

Fig. 4.39 shows the effect of shifting the exhaust pressure diagram so that the mean back pressure was 330, 335 and 340 kN/m^2. The phase angle shift was maintained at 0°CA, the valve mass was 1.0 kg and the damping coefficient was 0.5 kN.s/m. Fig. 4.39 shows the shifted mean and transient exhaust pressure diagrams, compared to the measured mean back pressure of 335.5 kN/m^2.

It can be seen that:-

(1) The mean back pressure has a dramatic effect on the predicted valve motion, as can be seen by comparing the extreme cases of p_3=330 kN/m^2 and 340 kN/m^2. Increasing the exhaust back pressure forces the valve to close due to the dynamics of the system. The mean exhaust pressure level is therefore a very important parameter if this method of analysis is to be used to find the damping coefficient, λ.

(2) For a realistic prediction of the valve motion, with p_2=359.8 kN/m^2, the mean exhaust back pressure, p_3, must be in the range 335.0 to 336.5 kN/m^2.

(3) The by-pass valve flow rate decreases with increases in the exhaust back pressure, because of the reduced valve flow area as the valve closes and the reduced pressure drop across the valve.

An error of $\pm$2% in the mean back pressure is enough to completely close or open the valve, and so this parameter is very important in the analysis of the valve motion. However, in the actual by-pass valve arrangement the valve flow will effect the exhaust back pressure, and so the valve is self regulating.

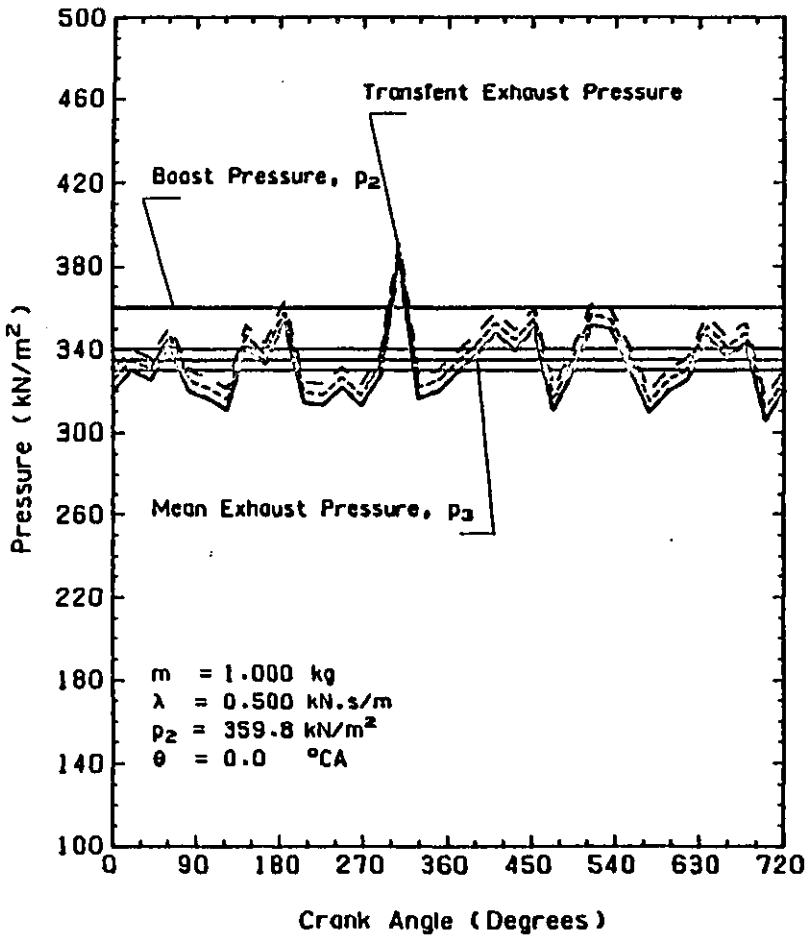

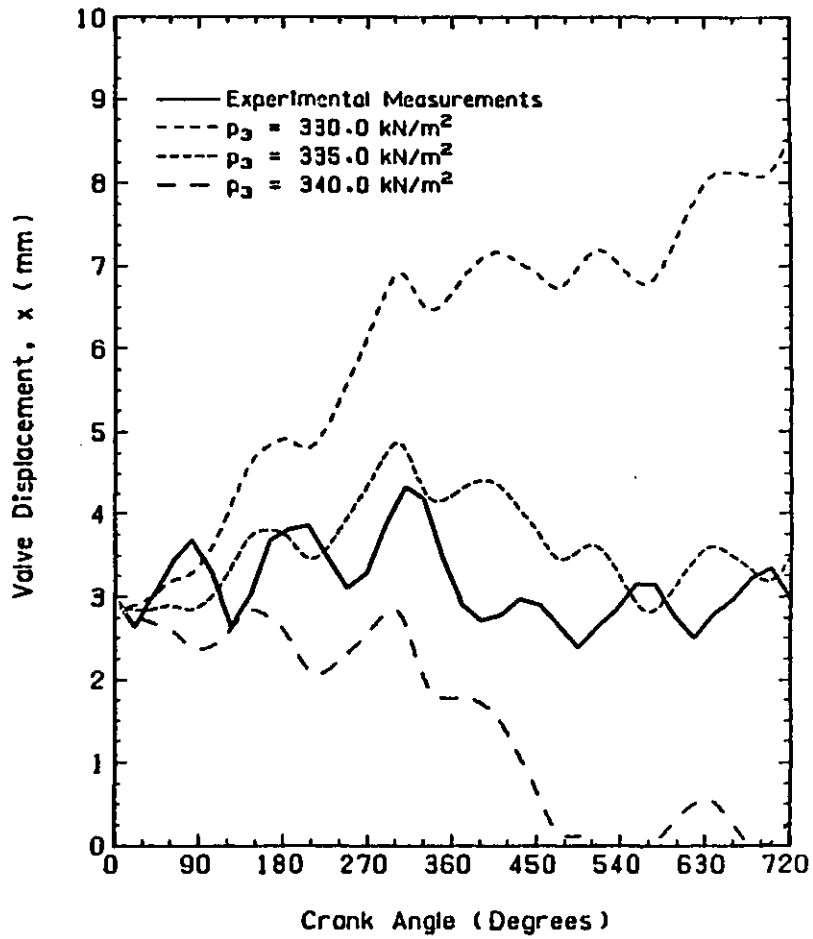

Fig. 4.39 Effect of the Mean Exhaust Back Pressure p_3 on the Predicted Valve Motion.

4.7.5.10 Effect of the Boost Pressure Level.

The motion of the by-pass valve has been shown to be very sensitive to the mean exhaust pressure level, and to the magnitude of the exhaust pressure fluctuations. The boost pressure, p_2, will have a similar influence on the valve dynamics.

Fig. 4.40 shows the effect of varying the boost pressure over the range 355 kN/m^2 to 365 kN/m^2. The valve mass, m, was 1.0 kg, the damping coefficient, λ, was 0.5 kN.s/m and the exhaust phase angle was 0°CA. The mean exhaust pressure level was maintained at the measured value of 335.5 kN/m^2.

Increasing the boost pressure level increases the valve displacement, flow area, pressure ratio and therefore the mass flow rate. Reducing the boost pressure can cause the valve to close completely. The experimentally measured boost pressure of 359.8 kN/m^2 can be seen to be close to the optimum value, but it is, in fact, the relative pressure difference between the boost and exhaust pressures that controls the motion of the by-pass valve in this model, (in contrast to the actual valve arrangement, where the by-pass valve motion and the relative boost and exhaust pressures are dependent upon each other). Small errors in either of these parameters will significantly alter the valve dynamics and the predicted by-pass mass flow rate.

4.7.5.11 Effect of Parametric Variations on the By-Pass Flow Rate.

The effect of the following parameters on the by-pass valve motion has been discussed in the previous sections:-

(1) By-pass valve mass, m.

(2) Damping coefficient, λ.

(3) Exhaust back pressure phase angle, Θ.

(4) Mean exhaust back pressure, p_3.

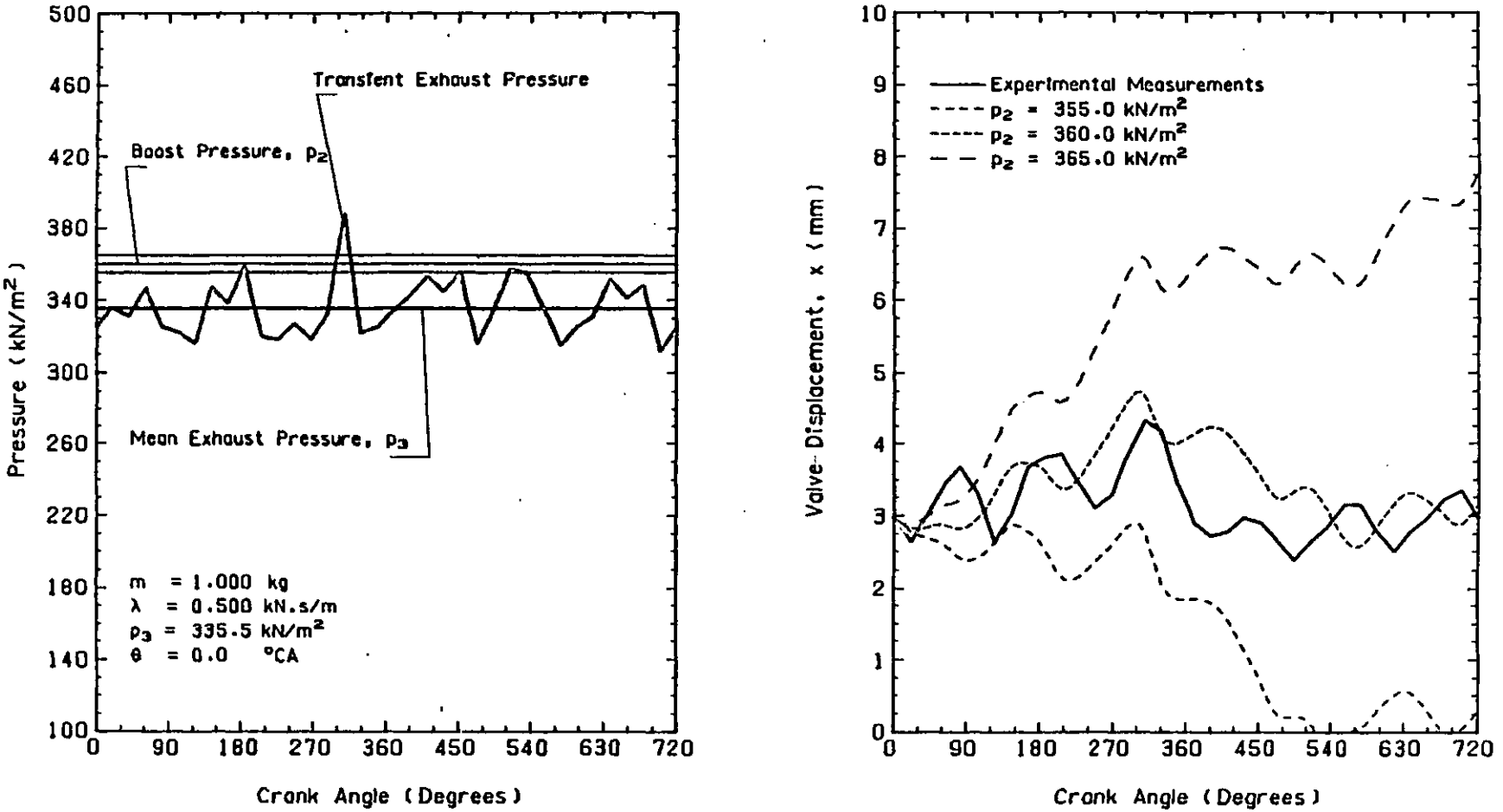

Fig. 4.40 Effect of the Boost Pressure p_2 on the Predicted Valve Motion.

(5) Mean boost pressure, p_2.

The isentropic by-pass valve mass flow rate was calculated in each case using eqns. (4.160) and (4.162). The total by-pass mass flow rate at this test condition can be estimated by measuring the compressor flow rate and subtracting the estimated engine flow rate, see section 4.7.4. This total by-pass flow includes the air flow through the ACC. The geometric by-pass valve area can be found by integrating the measured displacement diagram and using eqn. (4.160). At this engine speed and load the ACC is in the minimum fuelling position, and the geometric ACC flow area can be calculated, see section 4.8. By assuming that the pressure ratio and coefficient of discharge are similar for the by-pass valve and the ACC, (the former assumption is quite reasonable, but the later may cause serious errors) the proportion of the total by-pass flow that goes through the valve was calculated to be 89%. Therefore the experimental by-pass valve flow could be estimated.

Fig. 4.41 shows the effect of the parameters listed above on the mean by-pass valve coefficient of discharge, calculated using eqn. (4.163). The boost pressure, p_2, and the mean exhaust pressure, p_3, have the greatest influence on the isentropic by-pass flow rate. The valve isentropic flow decreases in proportion to the increase in valve mass, but increases rapidly as the damping coefficient is reduced below 1.0 kN.s/m. Increasing the damping coefficient above 1.0 kN.s/m has little effect on the valve motion and the by-pass air flow rate. Increasing the phase angle shift of the exhaust pressure diagram increases the by-pass valve flow, but this effect is strongly dependent on the relationship between the exhaust pressure fluctuations and the mean boost pressure level.

However, in practice, the coefficient of discharge of the by-pass valve has little effect on the engine performance (unless the valve is fully open), because the valve position is controlled by the relative boost and exhaust pressures, which are, in turn, regulated by the valve flow. If the valve coefficient of discharge is estimated too low, then the valve will open further to increase the by-pass flow rate. The by-pass valve position and the coefficient of discharge are therefore directly related. Both the valve effective flow area and the valve displacement are therefore plotted in Chapters 5, 6 and 7.

Using the optimum values of valve damping, mean exhaust pressure, exhaust phase

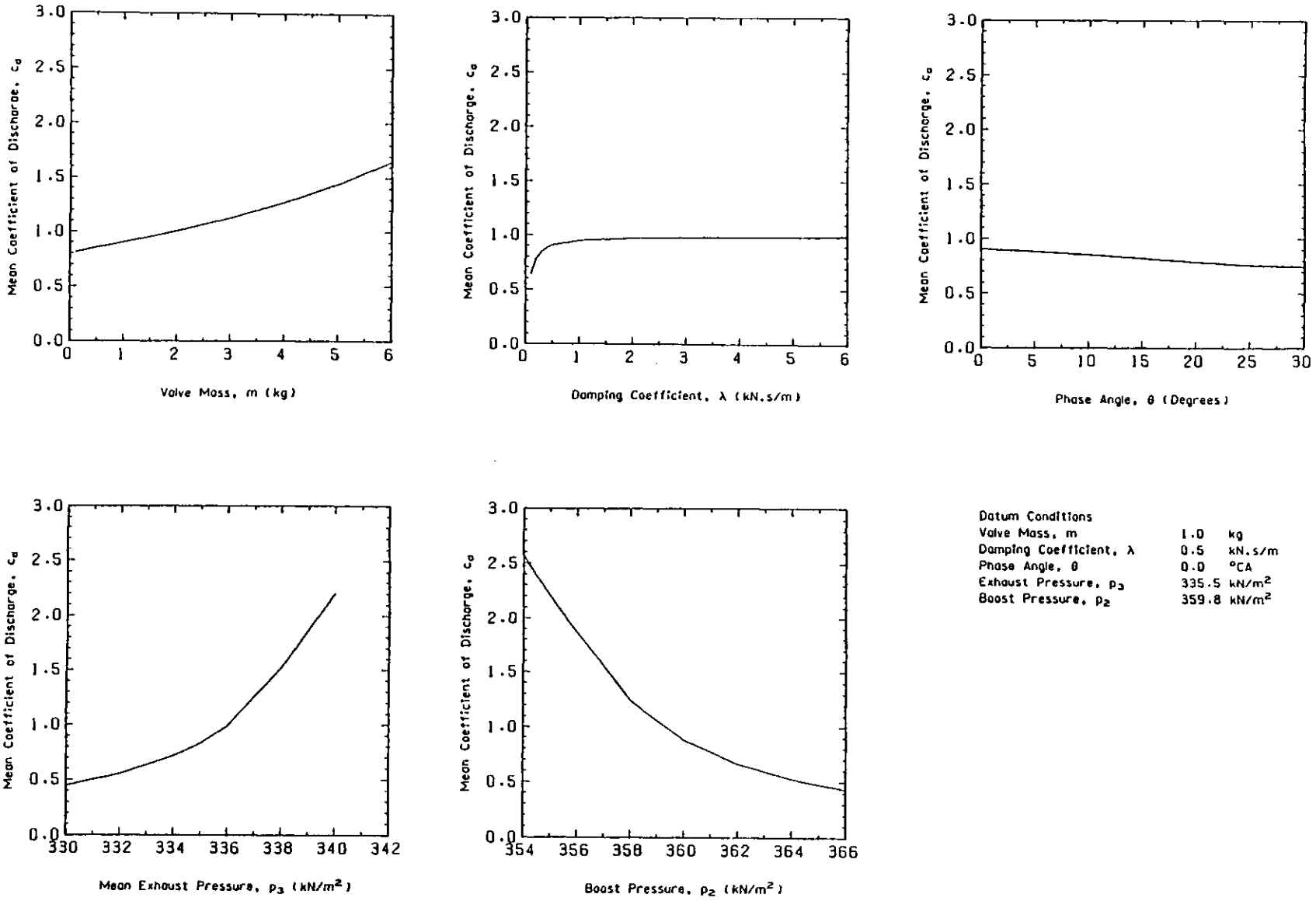

Fig. 4.41 Parametric Study of the Effect of Various Parameters on the Mean By-Pass Valve Coefficient of Discharge c_d.

angle shift, the by-pass valve coefficient of discharge, c_d, was estimated to be 0.89.

4.7.5.12 Optimisation of the By-Pass Valve Mass and Damping.

From the parametric study of the various parameters that effect the by-pass valve motion, the best agreement between the experimental and predicted valve displacement over the cycle was obtained with:-

By-pass valve mass, m	1.0 kg
Damping coefficient, λ	0.5 kN.s/m
Exhaust phase angle shift, Θ	15°CA
Mean boost pressure, p_2	359.8 kN/m^2
Mean exhaust pressure, p_3	336.0 kN/m^2

The experimental and predicted by-pass valve motion is shown in Fig. 4.42, together with the experimental and shifted exhaust pressure diagrams. It can be seen that the predicted second and third peaks in the valve displacement diagram have the correct phase but the magnitude of the valve displacement is too large. The first peak is almost entirely missing, which implies that the exhaust pressure trace should dip over the first 90°CA or so, to force the valve to open. The fourth peak is predicted to be much higher than the experimental motion shows, and the predicted peak occurs slightly before the experimental one. This implies that the exhaust pressure should not fall so much after the high third peak, at 300°CA, and should rise more gradually to the fourth peak. After the fourth peak in the valve motion the predicted valve displacement becomes less accurate. The predicted fifth and sixth displacement peaks occur before the measurements, which implies errors in the phase angle and magnitude of the exhaust pressure diagram, assuming the boost pressure level to be correct.

A closer examination of the experimental test data showed that consecutive engine cycles did not have identical valve displacement diagrams, despite the fact that the exhaust pressure diagrams for consecutive cycles were virtually identical. This implies that some other influence, apart from the boost and exhaust pressures, affects the valve motion and/or the measured valve displacement diagram does not faithfully represent the actual valve motion. It is possible that the assumption that the frictional forces are entirely viscous (i.e. proportional to the valve velocity) and that $p_a = p_b = p_1$,

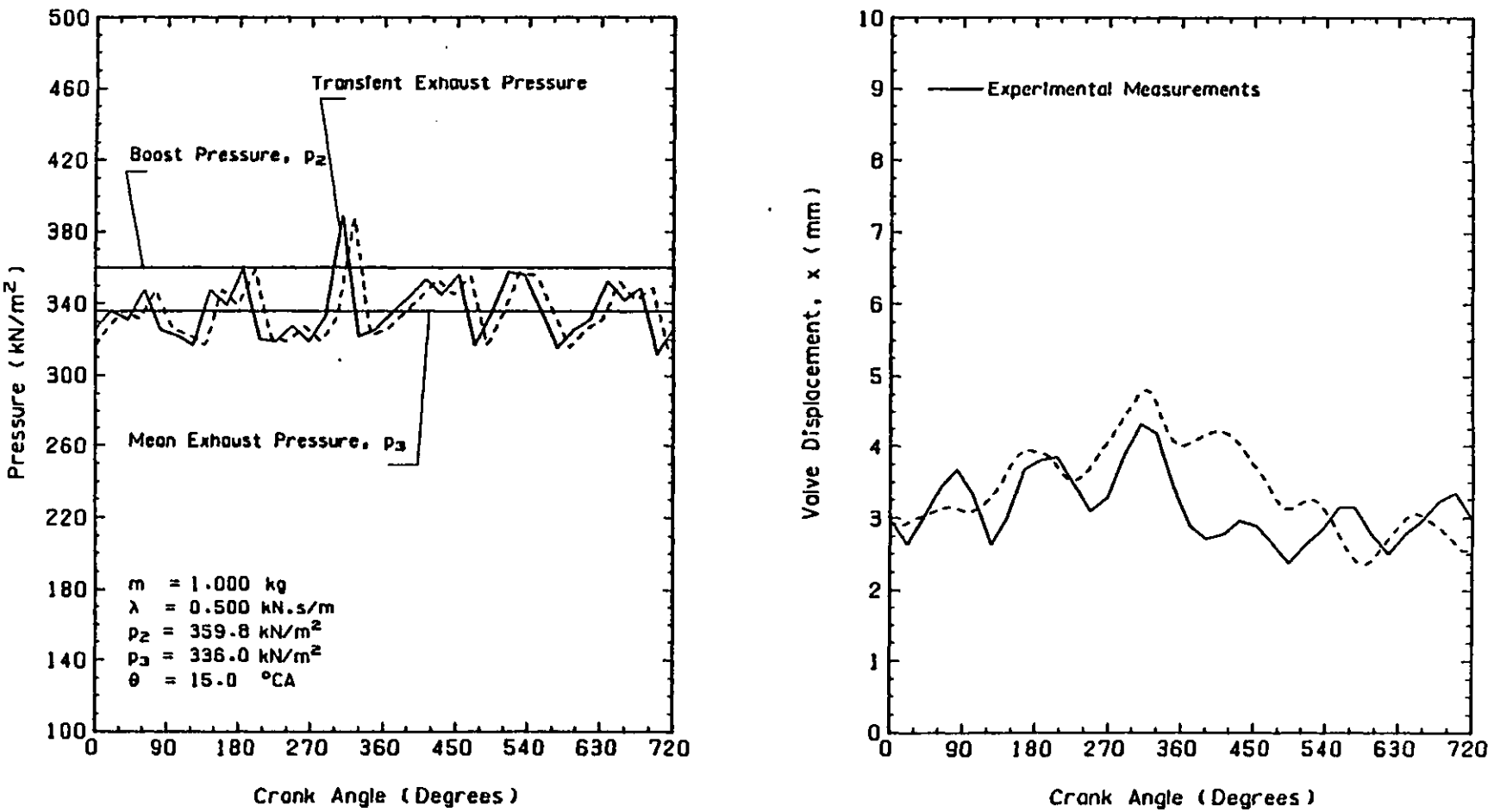

Fig. 4.42 The Optimum By-Pass Valve Damping and Exhaust Pressure.

see section 4.7.2, could be partly responsible for the errors.

However, considering the limitations of the data available, the predicted valve motion is considered to be representative of the motion of the actual by-pass valve.

4.7.5.13 Summary of the By-Pass Valve Characteristics.

A comparison between the valve motion predicted by the simple model, and that measured experimentally has shown the influence of the two main by-pass valve dynamic parameters, the valve mass and the damping, on the valve operation. The influence of the experimentally measured boost and exhaust pressures has also been established, together with the influence of the exhaust pressure phase angle. An analysis of the flow through the valve has also been carried out, to enable an estimate of the valve coefficient of discharge to be made.

Unfortunately this analysis has only been carried out at one test condition, 1800 rpm/19.0 bar BMEP, and the effect of the by-pass damping chamber jet has not been investigated, this analysis being for the minimum valve damping. A more thorough analysis would cover the effect of the engine speed and load and the jet size on the by-pass valve motion.

The range of practical values for the valve damping coefficient, λ, with "no jet" is $0.5 \leq \lambda \leq 1.5$ kN.s/m, see section 4.7.5.7, and the final estimate used for all the subsequent tests was:-

$$\lambda = 0.5 \quad \text{kN.s/m} \tag{4.164}$$

The value used for the valve coefficient of discharge, c_d, will not effect the engine performance unless the valve is fully open, but will affect the prediction of the valve displacement. The coefficient of discharge was therefore assumed to be independent of the valve displacement and pressure ratio. The value used in the following tests was:-

$$c_d = 0.65 \tag{4.165}$$

4.8 The Auxiliary Combustion Chamber and Exhaust System Models.

4.8.1 Introduction.

The function of the Auxiliary Combustion Chamber (ACC) has been outlined in section 3.3.5. Fig. 4.43 shows diagramatically the ACC arrangement in relation to the other components of the Hyperbar system, namely:-

(1) The exhaust manifold.

(2) The diluting chamber.

(3) The mixer.

(4) The by-pass valve.

(5) The turbine.

The majority of the by-pass air flow goes through the by-pass valve, and into the diluting chamber to mix with the combustion products from the ACC burner. Therefore the by-pass valve controls the pressures in the diluting chamber and the ACC. The mixture of by-pass valve air and the combustion products from the burner in the diluting chamber then enter the mixer, where they join together with the exhaust manifold gases before entering the turbine.

The by-pass valve position and mass flow rate will vary according to the engine operating conditions, the valve area reducing as the engine speed increases. At this stage of development, the burner must be operated continuously to ensure a stable and reliable flame in the ACC. Consequently a separate air supply to the burner, independent of the by-pass valve air flow, is required at all times. Air from downstream of the turbocharger compressor is therefore used to supply the burner with the air required for complete combustion of the injected fuel.

Diesel fuel is burnt continuously in the ACC, which is designed to allow large

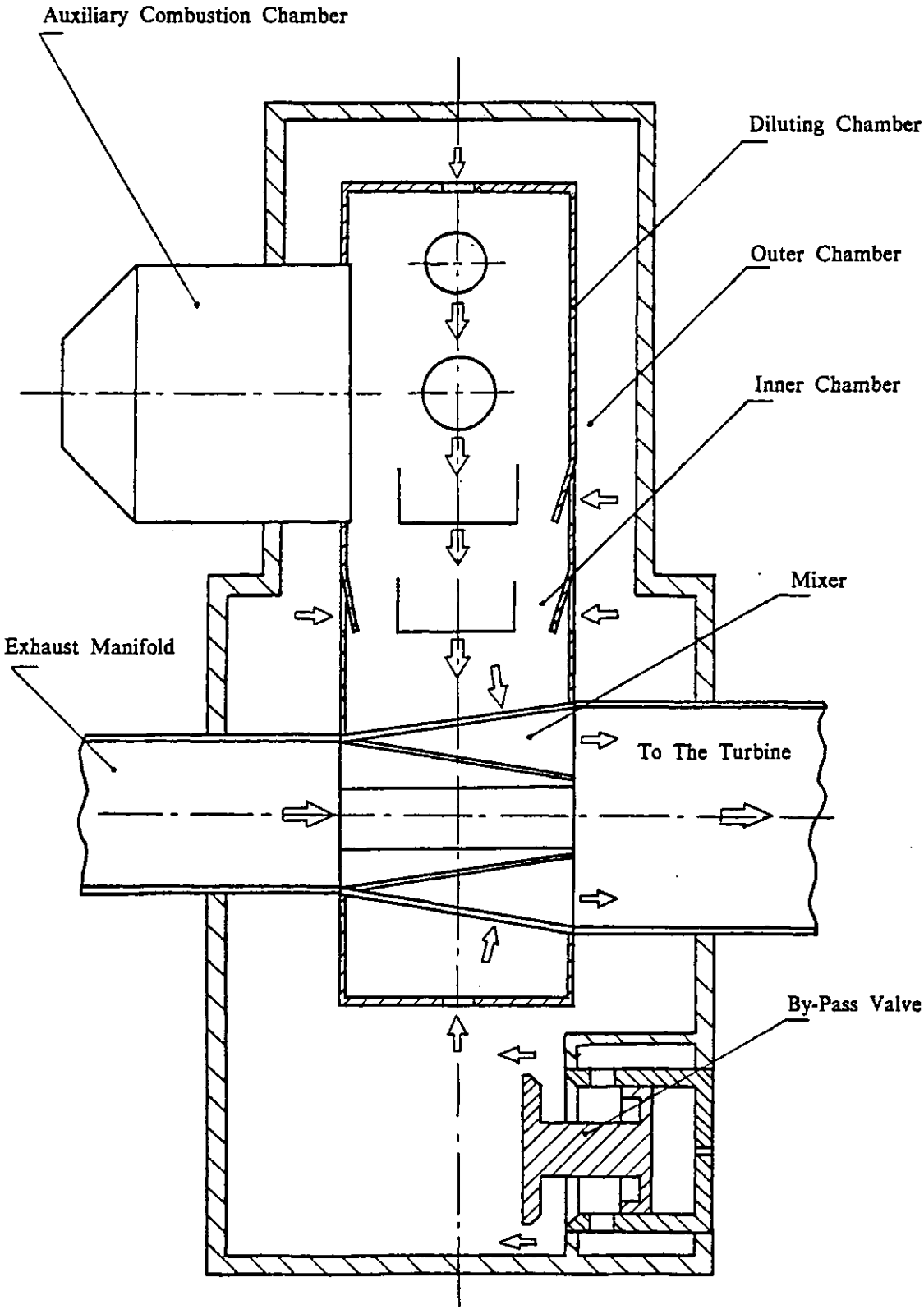

Fig. 4.43 Hyperbar Exhaust System Layout.

variations in the burner fuel flow rate (the ratio of the maximum to minimum fuel flow rate being as high as 60 (98)). A single mechanical fuel spraying system cannot ensure adequate atomisation and distribution of the injected fuel in the combustion chamber over such a wide range of fuel flow rates. Therefore a mixture of mechanical and pneumatic spraying is employed in this design. The mechanical fuel injection system is described in section 4.8.2, together with the control system used to vary the injection rate. Section 4.8.7 describes the pneumatic fuel injection system in detail. The actual ACC fuelling characteristics are dealt with in section 4.8.6.

A dynamic model for the ACC has been developed, similar to that described for the by-pass valve. The ACC position, and therefore the port air flow areas and fuelling rate, are calculated at each step throughout the engine cycle, (typically every 1°CA). The dynamic model is described in section 4.8.3, and the evaluation of the parameters required for the calculation, i.e. the chamber mass and damping coefficient, are dealt with in sections 4.8.4 and 4.8.5 respectively. The design and operational principles of the Hyperbar combustion chamber are discussed in greater detail in several patents (95,96,99,100,101) and by Andre-Talamon (2).

This section also includes a description of the exhaust manifold and mixer geometry, and a review of the Hyperbar models developed.

4.8.2 ACC Fuel Injection and Control Systems.

Diesel fuel is used in the ACC for two primary functions:-

(1) High pressure fuel is burnt in the combustion chamber to provide additional turbine energy.

(2) Low pressure fuel is used to control the position of the burner, and therefore the air and fuel flow rates.

Fig. 4.44 shows the fuel injection and control systems in detail. High pressure fuel (typically at 15 bar) enters the rear of the ACC {14} and passes along the centre of the needle valve {13}, which controls the flow area of a calibrated orifice {8}, according to the position of the movable centre section of the ACC. Provided that the fuel

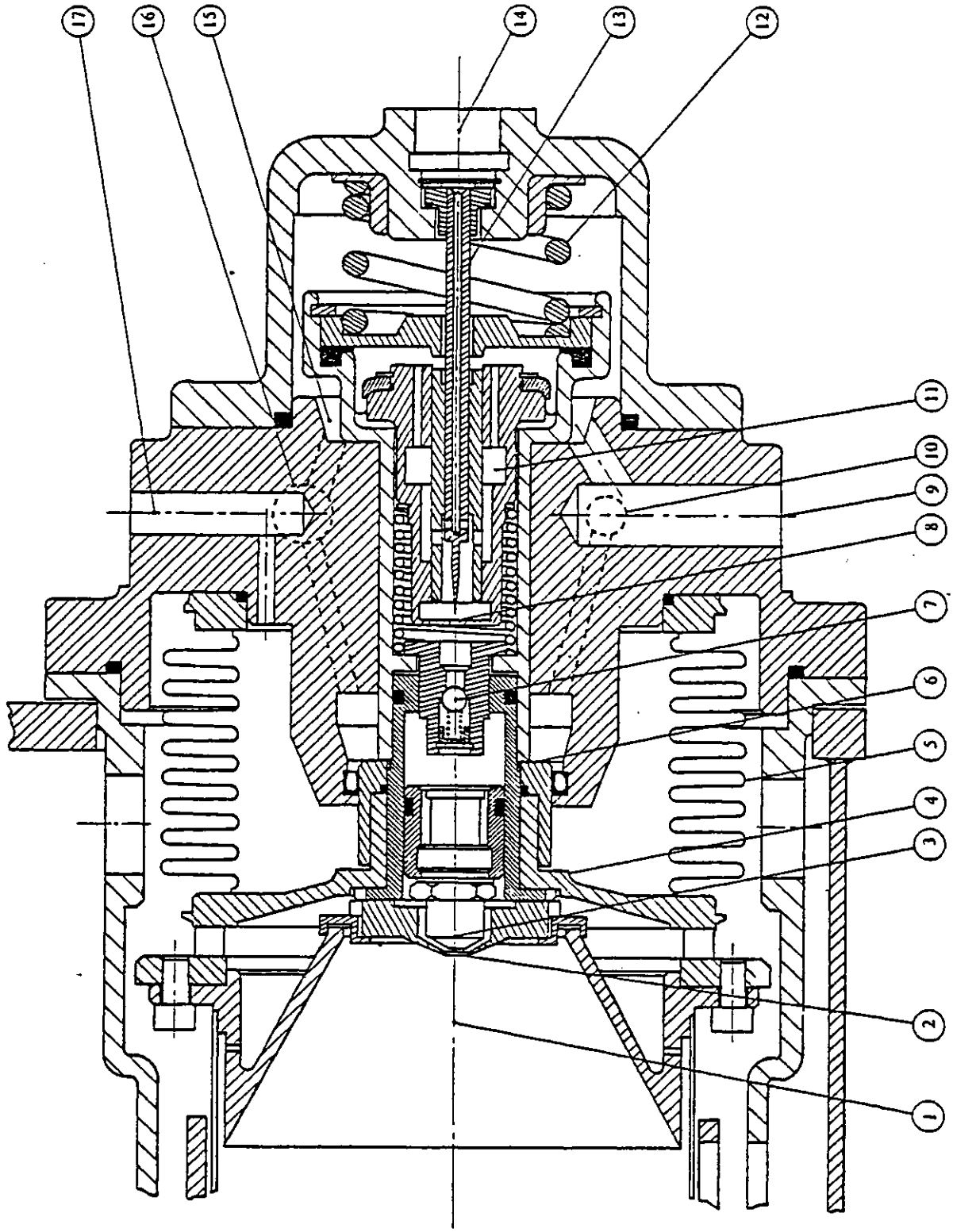

Fig. 4.44 The Auxiliary Combustion Chamber.

pressure is high enough to displace the spring loaded ball valve {7} the fuel then passes into the injector {3}, where it is either mechanically atomised, or distributed by high velocity air jets around the injector nozzle {2}, or a mixture of the two, depending on the fuel flow rate. Excess fuel is recirculated to the external pump via passages in the ACC body {11}.

Increasing the exhaust gas pressure in the ACC {1} causes the central section of the burner, supported by flexible bellows {5}, to move and the needle valve {13} to reduce the size of the regulating orifice {8}, which reduces the fuel pressure upstream of the ball valve {7}, and the fuel mass flow rate. The fuel injection rate will therefore depend on the ACC position, the fuel pressure, the geometry of the needle valve and the regulating orifices, and injector, and the spring force on the non-return ball valve. The geometry of the needle valve, shown in the maximum fuelling position, suggests that small displacements of the ACC will have little effect on the fuel flow rate, and similarly at large ACC displacements, the minimum fuel flow rate will be determined by the regulating orifice {8} and the needle stem diameters only. The way in which the fuel flow rate varies with ACC displacement is therefore controlled by the regulating orifice and needle valve profiles.

In the original patent (98), variations in burner fuel flow rate of 60 to 1 are claimed. The fuel flow rate is essentially proportional to the square root of the pressure drop across the injector orifice, and therefore a mechanical spraying device would require fuel pressures varying in the range 3600 to 1. In addition, the size of the injector orifice required to ensure atomisation of the fuel at the lowest flow rates will be so small that there is a distinct possibility of the injector becoming blocked, unless the fuel is carefully filtered. For example, fuel flow rates varying from 2 litres/hr. to 120 litres/hr., require fuel pressures (relative to the ACC gas pressure) ranging from 0.8 bar to 2880 bar, and an injector orifice diameter of 0.25 mm.

Therefore the injector orifice size is matched at the highest fuel flow rate required from the ACC, with a reasonable fuel pressure (of the order of 20 bar). Mechanical atomisation of the fuel is achieved by varying the relative fuel pressure down to, say, 0.8 bar, which reduces the fuel flow rate by a factor of 5. For lower fuel flow rates a mixture of mechanical and pneumatic spraying is used, with pneumatic spraying only at the lowest fuel flow rates, see section 4.8.7.

A pneumatic switch was originally designed into the system (98) to cut off the fuel flow to the burner when the boost air pressure dropped below the ACC gas pressure. A temperature sensitive device was also used to switch off the fuel, in the event of the flame extinguishing in the ACC. These devices have not been considered in the following analysis, but, as will be seen in Chapter 7, are very important aspects of the design of the fuel system.

The controlling fuel at a lower pressure (typically at 11 bar) enters the ACC body via ports {10}, and acts on a circumferential area around the injector nozzle {6}, to force the ACC into the maximum fuelling position, shown in Fig. 4.44. The controlling fuel is circulated to the outlet port {9} via internal ports {16} in the main body of the ACC. This fuel enters the rear chamber of the ACC {15} and is used to damp the motion of the burner. The ACC damping is therefore primarily viscous in nature (when the central section is in motion), and depends upon the fuel control pressure and the geometry of the inside of the chamber {15}.

The position of the ACC is also regulated by the main control spring {12}, the preload and spring rate of which will determine the equilibrium position of the ACC for a given exhaust gas and fuel control pressures. The fuel control pressure was originally regulated by an internal spring loaded relief valve (not shown), but this was later replaced by a remote proportional solenoid valve arrangement, that allowed the fuel control pressure to be varied according to the operating requirements of the engine.

The ACC position can also be regulated pneumatically by varing the "air control pressure" inside the flexible bellows {5}. Air under pressure enters the bellows via the port {17}, and acts on a circumferential area around the central fuel injector {4} to move the burner towards the maximum fuelling position. This control pressure is regulated by a valve (not shown), the air supply normally being taken from the compressor outlet. Therefore the control pressure can be adjusted between ambient and the instantaneous boost pressure by simply varying the regulating valve area.

It is clear that the fuel control pressure and the air control pressure serve the same basic function, both acting to increase the burner fuelling as they are increased. However, the fuel control pressure will also affect the ACC damping, as explained above. Early tests performed by the engine manufacturer have shown that the burner can be adequately controlled by varying the fuel control pressure only, and the air

control pressure inside the bellows was simply vented to the atmosphere, via port {17}, for the majority of the experimental tests.

The burner is ignited by a high energy igniter plug (not shown), which is rigidly fixed to the outer casing of the burner, and allowed to slide in a groove machined into the movable central section.

4.8.3 Dynamics of the Auxiliary Combustion Chamber.

Fig. 4.45 shows diagramatically the forces acting on the ACC and the respective geometric areas. The equation of motion for the ACC can be written as:-

$$\ddot{x} = (p_{acc}.A_6 - p_f.A_4 - p_c.A_5 - F_o - k.x - \lambda.\dot{x}).1000/m \qquad (4.166)$$

where,

F_o = initial spring force (kN)
k = spring rate (kN/m)
m = mass of the moving parts (kg)
p_{acc} = ACC gas pressure (kN/m^2)
p_c = air control pressure (kN/m^2)
p_f = fuel control pressure (kN/m^2)
x = ACC position (m)
$\dot{x}$ = ACC velocity (m/s)
$\ddot{x}$ = ACC acceleration (m/s^2)

and A_4, A_5 and A_6 are the geometric areas of the ACC (m^2).

The ACC motion must be effectively damped, because small changes in ACC position, such as that caused by pulses in the exhaust manifold pressure, can cause large variations in the ACC fuelling. This damping is achieved by using the fuel in the injector body to oppose the motion of the ACC. Thus the damping may be considered to be viscous. However, as soon as the minimum boost pressure level is achieved the ACC stays in the minimum fuelling (idling) position. Any significant drop in the boost or exhaust pressure requires the ACC to be accelerated from rest, where stiction and Coulomb friction, (which is of the order of ten times that of viscous friction at low

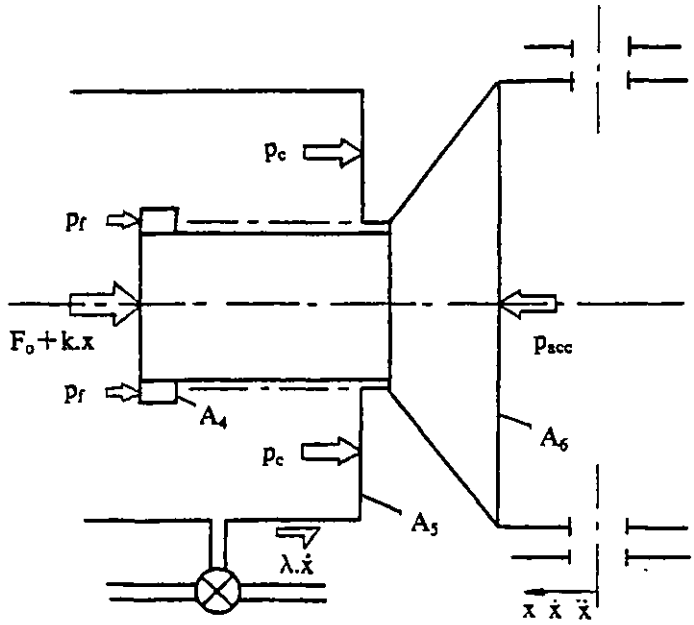

Fig. 4.45 Dynamics of the Auxiliary Combustion Chamber.

velocities) will dominate. Insufficient data was available about the transient characteristics of the ACC to develop a sufficiently detailed model including these effects, and this should be considered when the transient response of the Hyperbar system is discussed in Chapter 7.

The geometric areas, A_4, A_5 and A_6, were obtained from the manufacturer, and the initial spring force, F_o, and spring rate, k, have been calculated by measuring the force versus displacement characteristics of the assembled burner. The fuel control pressure, p_f, and the air control pressure, p_c, were set externally and are used to control the operation of the burner. The pressure in the ACC is largely determined by that in the diluting chamber, which is itself controlled by the by-pass valve, see Fig. 4.43. Therefore the ACC pressure, p_{acc}, is really a function of the boost pressure under steady state conditions, from eqn. (4.157), which can be written as:-

$$p_{acc} = p_2 - \frac{A_2}{A_1}.(p_2 - p_1) \qquad (4.167)$$

where,

A_2/A_1 = by-pass valve area ratio

p_1 = ambient pressure (kN/m^2)

p_2 = compressor outlet pressure (kN/m^2)

Equation (4.166) can be integrated numerically, once to obtain the instantaneous ACC velocity, and again to get the ACC position. However, it was first necessary to obtain the mass of the moving parts, m, and an estimate of the damping coefficient, λ, in order to solve eqn. (4.166).

4.8.4 Auxiliary Combustion Chamber Mass.

It was not convenient to dissasemble the ACC in order to measure the mass term in eqn. (4.166). The total mass of the moving parts of the ACC was therefore estimated by calculating the total volume of each individual moving component, and assuming that each part had the density of steel (7850 kg/m^3). A proportion, 1/3, of the main control spring and bellows (items {12} and {5} respectively in Fig. 4.44) was also considered to be moving. This method was also used to estimate the mass of the by-

pass valve, which was calculated to within 5% of the value measured by the manufacturer.

4.8.5 Auxiliary Combustion Chamber Damping Coefficient.

Little was known about the damping characteristics of the ACC, and it was not possible to instrument the ACC to determine the actual fluctuations in position during one engine cycle, and therefore calculate the damping. As stated in section 4.8.3 the damping was assumed to be viscous, and a further assumption was made, that the damping ratio (actual/critical) was 0.75.

The equation of motion for the ACC, eqn. (4.166) can be written as:-

$$\left[\frac{D^2}{\omega_o^2} + \frac{2.C.D}{\omega_o} + 1\right] x = f\,(\,p_{acc}\,,\,p_f\,,\,p_c\,,\,F_o\,,\,k\,,\,A_4\,,\,A_5\,,\,A_6\,) \quad (4.168)$$

where, $Dx=\dot{x}$, and $D^2x=\ddot{x}$.

The natural frequency of the system, ω_o, is given by:-

$$\omega_o = \sqrt{1000.k/m} \quad (4.169)$$

and the damping ratio, C, by:-

$$C = \frac{\lambda}{2\sqrt{k.m/1000}} \quad (4.170)$$

By substituting the measured spring rate, k, and the estimated mass of the moving parts in the system, m, into eqns. (4.169) and (4.170), the natural frequency, ω_o, and the damping coefficient, λ, can be obtained, assuming that C=0.75.

The damping coefficient, λ, used throughout these tests was calculated to be 0.50 kN.s/m. The natural frequency was found to be 17.8 cycles/s, which is far lower than the exhaust pulse frequency at the minimum engine operational speed of 800 rpm, which is 40 cycles/s.

4.8.6 Auxiliary Combustion Chamber Fuelling Characteristics.

Fig. 4.46 shows the ACC fuelling characteristics measured by the engine manufacturer, and gives the burner fuel flow rate as a function of the compressor delivery pressure, p_2. It is evident that the actual range of variation of ACC fuel flow rate is much smaller than that originally claimed by the designers (98), the ratio of the maximum to minimum fuelling being only 3.5. The problems resulting from this limited fuel flow range are discussed in detail in Chapter 6.

It has been shown in section 4.8.2 that it is the ACC displacement that actually determines the fuel flow rate and not the boost pressure directly. It was therefore necessary to find a relationship between the boost pressure, p_2, and the ACC displacement, x.

The steady state form of eqn. (4.166) can be written (with $\dot{x}=\ddot{x}=0$) as:-

$$x = \frac{p_{acc}.A_6 - p_f.A_4 - p_c.A_5 - F_o}{k} \qquad (4.171)$$

Under steady conditions the ACC pressure, p_{acc}, can be expressed by eqn. (4.167). Substituting this into eqn. (4.171) gives:-

$$x = \frac{[\ p_2 - A_2/A_1.(\ p_2 - p_1\ )\ ].A_6 - p_f.A_4 - p_c.A_5 - F_o}{k} \qquad (4.172)$$

Equation (4.172) gives a relationship between the boost pressure, p_2, and the ACC displacement, x, all the other parameters being considered constant.

The values of A_4, A_5, A_6, p_f, p_c, k and F_o are known and the by-pass valve area ratio, A_2/A_1 is 0.09, see section 4.7.5.5. For this analysis the ambient pressure, p_1, was taken to be 100 kN/m^2, and was equal to the air control pressure, p_c.

The fuelling characteristics, shown in Fig. 4.46, were curve fitted to give the burner fuelling as a function of the boost pressure, and then transformed, using eqn. (4.172), to give the fuelling as a function of the ACC displacement, Fig. 4.47. It can be seen

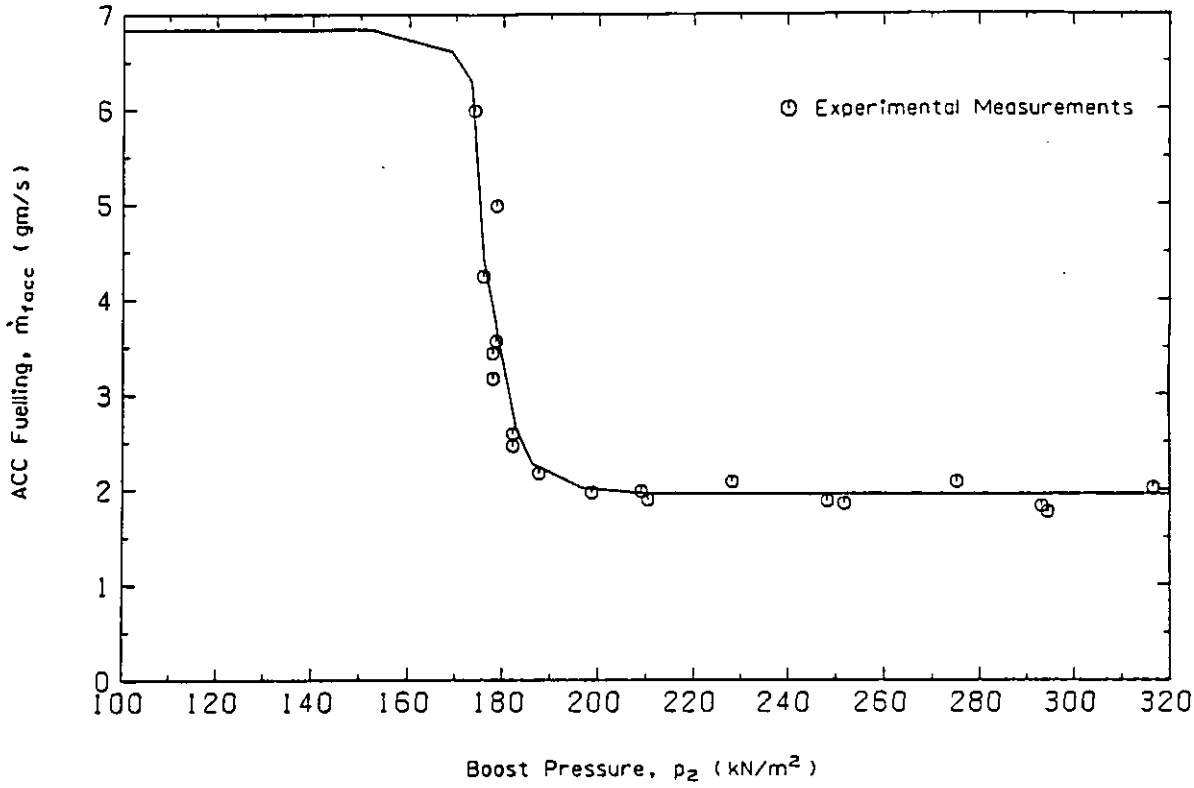

Fig. 4.46 Variation of the ACC Fuelling with Boost Pressure.

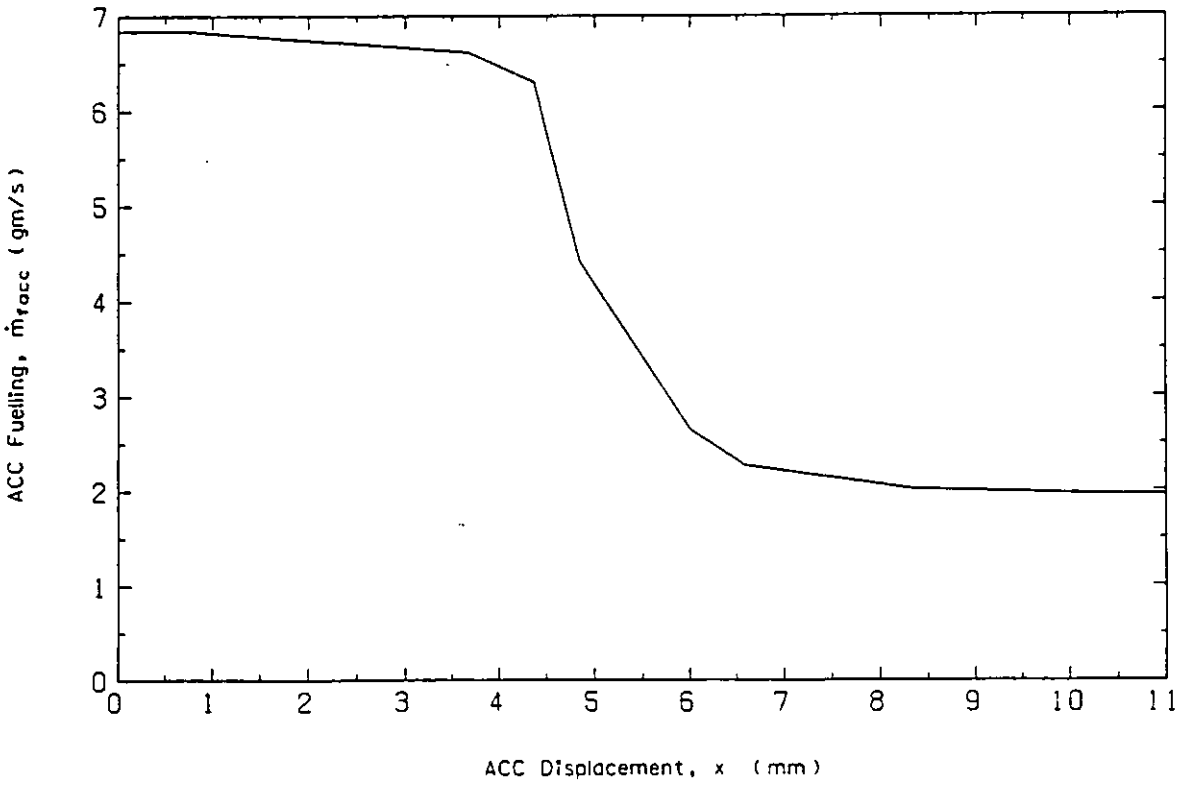

Fig. 4.47 Variation of the ACC Fuelling with Displacement.

that the burner fuelling varies considerably over the mid range of displacements, as explained in section 4.8.2. In this region effective damping of the ACC is essential, to prevent large fluctuations in ACC fuelling in response to small changes in the combustion chamber pressure.

4.8.7 Auxiliary Combustion Chamber Air Flow.

4.8.7.1 Geometric Flow Areas.

The ACC fuelling varies with its position from the idling (minimum) value to the maximum value over a relatively small range of displacements. Air is required in the ACC at all times, since the fuelling is never reduced to zero, and the air supply must respond rapidly to changes in the fuelling rate, (ideally the air flow should start to increase slightly before the fuel flow to ensure the air is present when an increase in the ACC demand is required).

Air at compressor delivery conditions is used in the burner, and this has three main functions:-

(1) To ensure atomisation and mixing of the fuel injected into the ACC at low fuel flow rates.

(2) To ensure that sufficient air is available in the ACC to burn the fuel completely.

(3) To cool the chamber walls and so minimise the distortion of the moving components.

The ACC air flow ports are shown in detail in Fig. 4.48. Air at compressor delivery conditions passes through the annular port {1} and then through 12 circumferential orifices {2}, spaced at 30° intervals around the back of the burner. The air is then free to travel through a number of parallel flow paths.

The primary air flow path is via the control valve {3}, which moves with the central section of the ACC and eventually shuts off the flow paths {3}–{4} and {3}–{7} when the

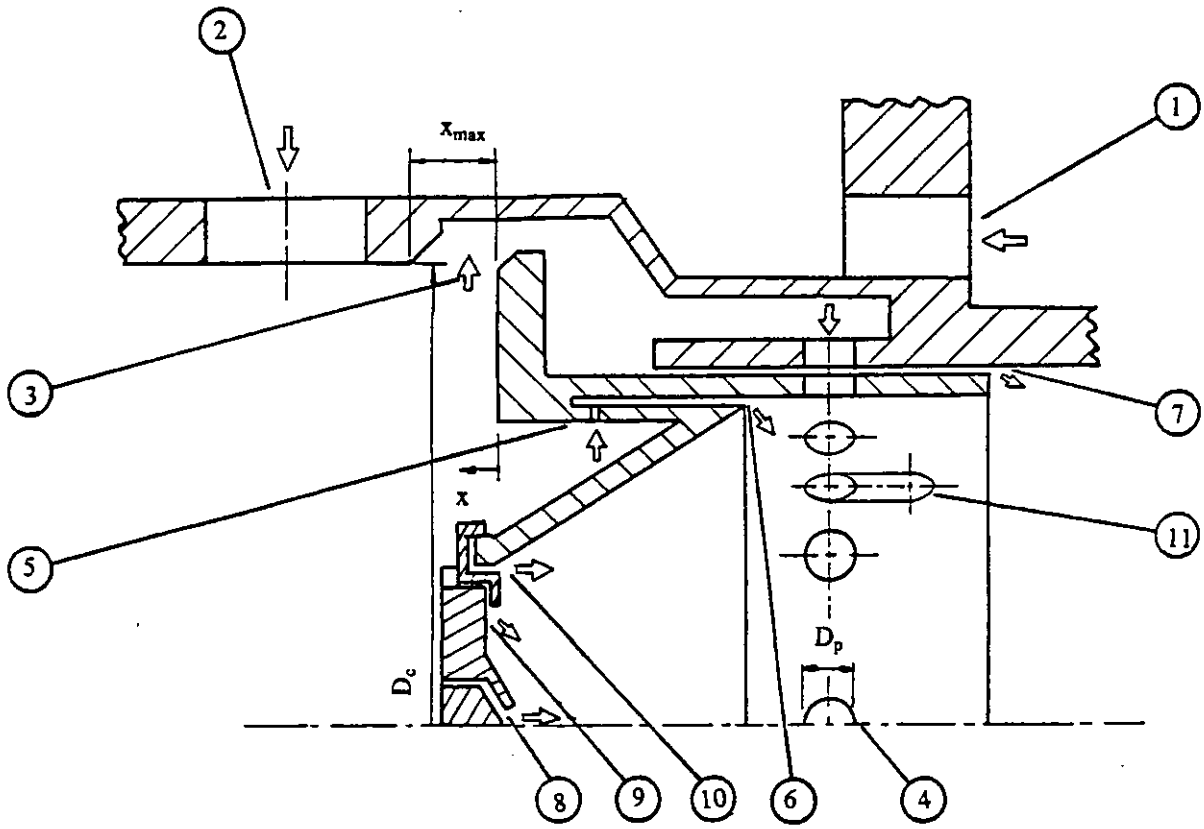

Fig. 4.48 Auxiliary Combustion Chamber Air Flow Paths.

burner is idling. The main body of the air passes from the control valve {3} through 12 circumferential ports around the ACC walls {4}. These ports line up with identical ports in the movable section of the burner, allowing the flow area to vary with the position of the central section. The ports are fully open in the maximum fuelling position, shown, and close as the burner fuelling reduces. There is a leakage flow path {7} which is the result of manufacturing tolerances, and is used for film cooling of the chamber walls, and to prevent the fuel spray from attaching to the chamber walls at high fuel velocities.

The remainder of the flow through the ACC is not regulated by the control valve {3} and is therefore only limited by the size of the ports {1} and {2}, (which are generously dimensioned), or the area of the individual flow path. In the original patent (98) this air was taken from downstream of the charge cooler, and was therefore at a lower temperature and a higher density (though lower pressure) compared to the majority of the ACC air flow. Only the arrangement used for the experimental tests has been considered, but further tests should certainly consider the differences between these configurations.

There are 48 small holes around the inner chamber walls {5} which allow air at high velocity to flow through the annulus {6} for film cooling of the combustion chamber walls, and to assist the air jets around the circumference of the chamber {7}. These jets form a layer of air parallel to the walls of the ACC when it is in the idling position.

Figs. 4.49 and 4.50 show details of the atomising and distribution jets {8}, {9} and {10}. The blower nozzle {8} consists of 6 machined slots oriented tangentially around the circumference of the injector nozzle. The air velocity and turbulence through these, and smaller jets perpendicular to the axis of the injector, must be high enough to pneunatically spray the fuel at low fuel flow rates. Greater flame stability is achieved by swirling the air flow around the injector, thus ensuring a suitable cone angle for the fuel spray (of between 60° and 90°), and more stable combustion. The number and cross sectional area of these nozzles (and nozzles {9}) are designed to ensure that the air-fuel ratio in the ACC remains close to stoichiometric at the lowest fuel fuel flow rates. In addition, there are 24 passages {9} arranged around the circumference of the injector, that direct air radially towards the fuel spray. The 12 jets {10} are arranged to direct air parallel to the axis of the chamber, but the jets are oriented to

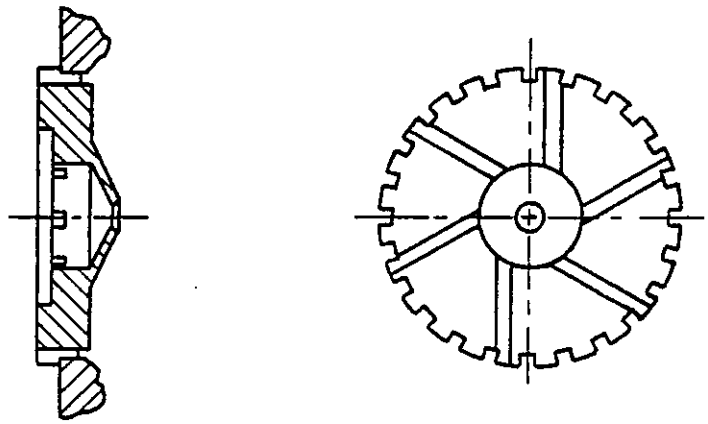

Fig. 4.49 Detail of the Atomising Jets {8} and {9}.

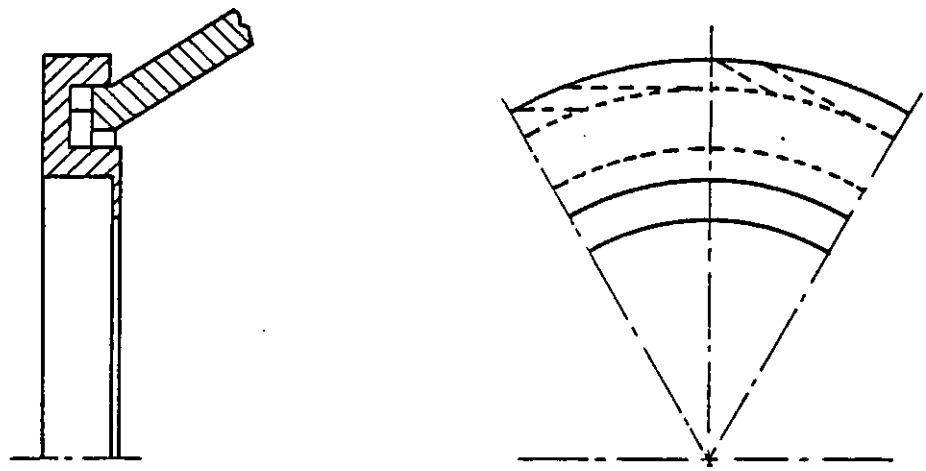

Fig. 4.50 Detail of the Cooling and Mixing Jets {10}.

form a rotating layer of air concentric with the injector nozzle, Fig. 4.50. This layer of air ensures cooling of the chamber walls and improves the mixing of the fuel spray and air, particularly during the transition from pnuematic to mechanical fuel spraying, as the fuelling rate increases.

The fuel igniter enters the ACC through the chamber walls and a slot in the movable portion of the ACC {11}, see Fig. 4.48, allows the chamber to move relative to the igniter plug. It is assumed that no air passes through the igniter plug hole {11}.

The geometric flow areas for each flow path {1}-{10} were calculated. As the chamber displacement, x, increases the main port area, A_p, reduces according to eqn. (4.173):-

$$A_p = \frac{n.D_p^2}{2}.[\ \cos^{-1}(x/D_p) - (x/D_p)\sqrt{1 - (x/D_p)^2}\ ] \qquad (4.173)$$

where,

A_p = geometric port area (m^2)
D_p = port diameter (m)
n = number of ports
x = ACC displacement (m)

for,

$$0 \leq x \leq D_p \qquad (4.174)$$

The variable flow area {3} is directly proportional to the ACC displacement, x,:-

$$A_c = \pi.D_c.(\ x_{max} - x\ ) \qquad (4.175)$$

where,

A_c = geometric port area {3} (m^2)
D_c = internal port diameter (m)
x_{max} = maximum ACC displacement (m)

4.8.7.2 Auxiliary Combustion Chamber Mass Flow Rate.

The air mass flow rate through the ACC ports was calculated from:-

$$\dot{m}_{aacc} = A_g.c_d.p_2\left[\frac{2}{R_2.T_2}\left(\frac{\gamma}{\gamma-1}\right)\left\{\left(\frac{p_{acc}}{p_2}\right)^{2/\gamma}-\left(\frac{p_{acc}}{p_2}\right)^{(\gamma+1)/\gamma}\right\}\right]^{0.5} \qquad (4.176)$$

where,

A_g = geometric flow area (m^2)
c_d = coefficient of discharge
$\dot{m}_{aacc}$ = ACC air mass flow rate (kg/s)
p_{acc} = ACC/diluting chamber pressure (N/m^2)
p_2 = compressor outlet pressure (N/m^2)
R_2 = gas constant for air (J/kg.K)
T_2 = compressor outlet temperature (K)
γ = specific heats ratio for air

The ACC/diluting chamber pressure is controlled by the by-pass valve, and the pressure ratio, p_{acc}/p_2, is subsonic for all practical cases.

No reverse flow from the ACC into the compressor delivery ducting has been considered, due to the complexity of the flow paths and the unlikeliness of such an occurance. No data was available to enable the coefficient of discharge, c_d, of the various ACC flow paths to be calculated, and so published data for flow in ports of similar geometry has been used.

4.8.7.3 Effective Flow Areas.

Experimental data for the coefficient of discharge, c_d, for radially directed ports, having no tendency to swirl, can be used for the 12 circumferential ports [4]. For a circular port, the value of c_d depends upon the fraction of the port that is uncovered, and the pressure ratio across it. Typically c_d will increase with fraction open and with pressure ratio, over the range 0.6 to 1.0 (based on the maximum geometric port area),

see Fig. 4.51.

A simple empirical relationship fitted to theoretical curves was given by Benson (10), based on measured values of c_d at small openings. However, in view of the uncertainty in calculating the ACC displacement accurately, and therefore the geometric port areas, this complication was not considered appropriate. A constant value of c_d of 0.65 has been assumed as a first approximation, this being the theoretical value appropriate to a free jet for small openings.

The coefficient of discharge, c_d, for all the port areas {1}-{10} was set to 0.65, although many of the ports are very small and the flow will be controlled by the boundary layers, consequently the coefficient of discharge will probably be much lower than this value.

Fig. 4.52 shows the calculated geometric and effective ACC port areas over the total range of ACC movement.

4.8.8 Combustion in the Auxiliary Combustion Chamber.

The ACC position, x, is calculated on a step-by-step basis, as described in section 4.8.2. The instantaneous fuelling rate is calculated by linear interpolation from the fuelling characteristics shown in Fig. 4.47, and the effective flow area is shown in Fig. 4.52. The mass flow rate through the ACC ports is calculated as described in section 4.8.7. This gives the instantaneous A/F ratio entering the ACC as:-

$$A/F_{acc} = \frac{\dot{m}_{aacc}}{\dot{m}_{facc}} \qquad (4.177)$$

where,

A/F_{acc} = instantaneous ACC air-fuel ratio

$\dot{m}_{facc}$ = instantaneous ACC fuel flow rate (kg/s)

and $\dot{m}_{aacc}$ is given by eqn. (4.176).

Equation (4.177) can be integrated over the cycle to obtain the overall ACC A/F

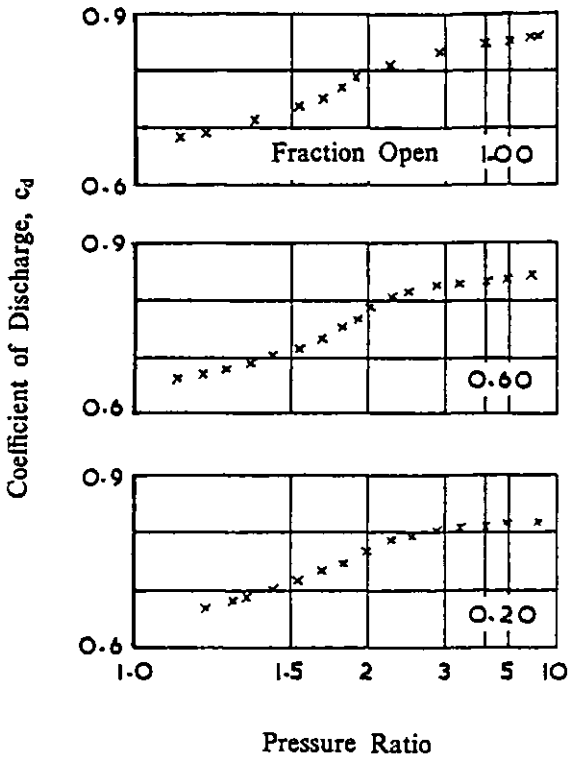

Fig. 4.51 Variation of the Port Coefficient of Discharge with Pressure Ratio and Fraction Open, from (10).

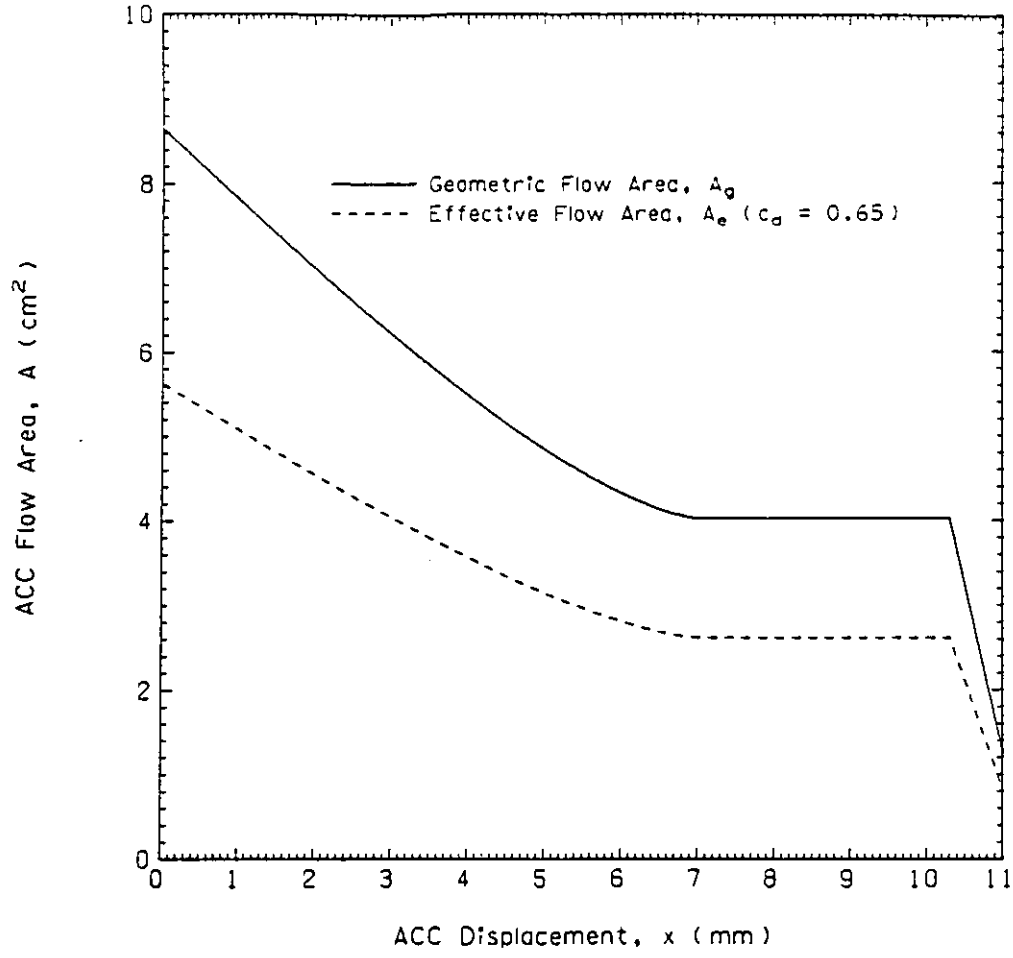

Fig. 4.52 Geometric and Effective ACC Air Flow Areas.

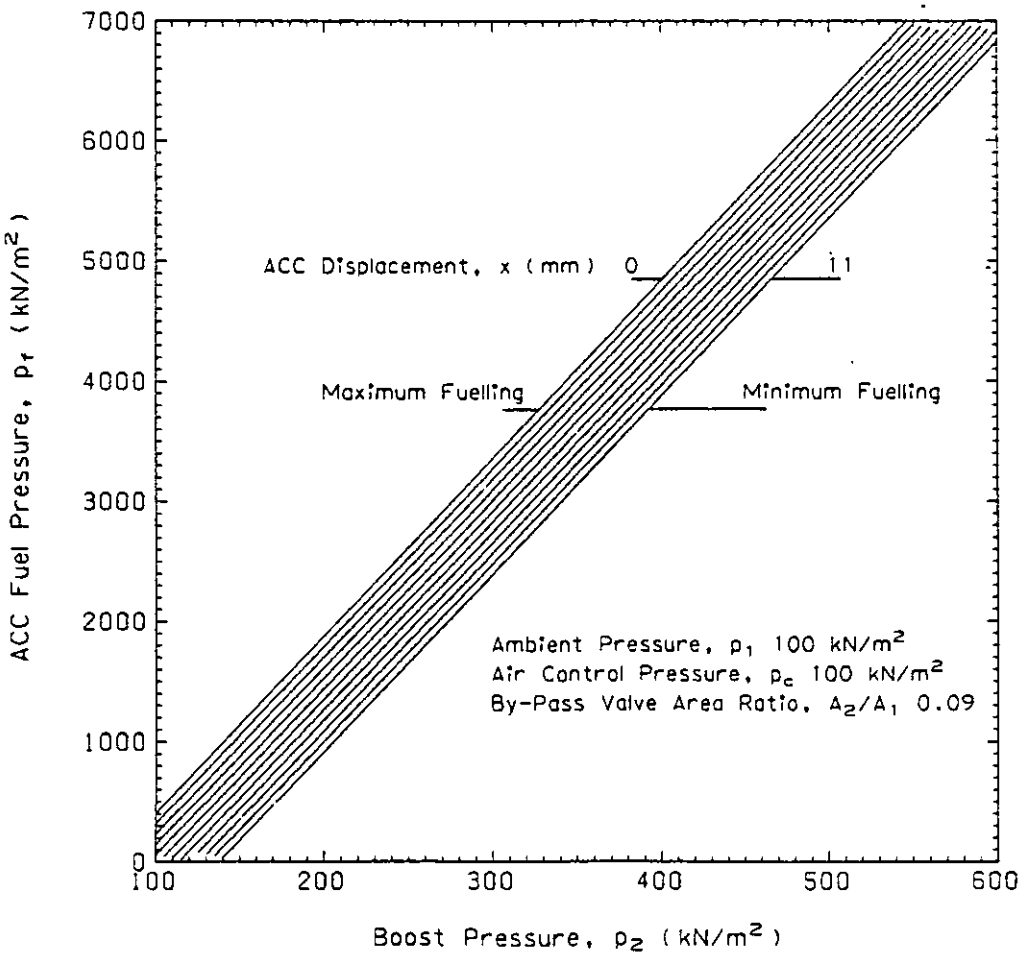

Fig. 4.53 Effect of the Boost Pressure p_2 and the ACC Fuel Pressure p_f on the ACC Displacement.

ratio. The heat released in the ACC due to the fuel burning is handled in the same way as that for the engine cylinder (see section 4.1).

However, as shown in Fig. 4.43, the ACC and the diluting chamber are considered as a single control volume, at a single instantaneous bulk mean pressure and temperature, and the by-pass valve flow also enters the ACC/diluting chamber and mixes with the ACC combustion products. So the overall A/F ratio in the ACC/diluting chamber control volume is actually much higher than that calculated by eqn. (4.177), and is given by:-

$$A/F_{oacc} = \frac{\dot{m}_{bp} + \dot{m}_{aacc}}{\dot{m}_{facc}} \tag{4.178}$$

where,

A/F_{oacc} = instantaneous overall ACC/diluting chamber air-fuel ratio

$\dot{m}_{bp}$ = instantaneous by-pass valve air flow rate (kg/s)

The calculation of the instantaneous by-pass valve air flow rate, $\dot{m}_{bp}$, is described in section 4.7.4.

4.8.9 Auxiliary Combustion Chamber Control Variables.

The steady state relationship governing the ACC position, and therefore the fuel flow rate and air flow areas is given by eqn. (4.172). The boost pressure, or the ACC gas pressure, range over which the ACC will operate to either increase or decrease the ACC fuelling (and so maintain the minimum boost pressure level), will be a function of the geometry of the combustion chamber, A_4, A_5 and A_6, the by-pass valve area ratio, A_2/A_1, the initial spring force, F_o, and the air and fuel control pressures, p_c and p_f. Fig. 4.53 shows the boost pressure range over which the ACC operates as a function of the ACC fuel control pressure, p_f, all the other terms in eqn. (4.172) remaining constant. The minimum boost level, p_2, can thus be easily regulated by varying the fuel control pressure. How well this minimum boost level is maintained at various engine loads and speeds will depend upon the way in which the ACC position, and hence fuelling, changes with the boost, or the ACC, pressure, see Fig. 4.46. Varying the ACC air control pressure, p_c, or the initial spring force, F_o, will have a

similar influence on the ACC steady state characteristics as varying the fuel control pressure, p_f, but will not affect the ACC damping to such an extent.

Fig. 4.54 shows the effect of varying the rate of the main control spring, k, see section 4.8.2. As the boost pressure increases for a given spring rate, the ACC displacement increases and the fuelling reduces to the minimum value. Increasing the spring rate, increases the range of boost pressures over which the ACC operates. Reducing the spring rate to zero, effectively means that the ACC acts as an "on-off" device, varying the ACC fuelling from minimum to maximum at a predetermined boost pressure level, which may cause stability problems in the control of the burner fuelling. Conversely, the higher the spring rate, the less sensitive the burner is to small fluctuations in the exhaust pressure.

4.8.10 Auxiliary Combustion Chamber Characteristics.

In this section, the characteristics of an ideal ACC are discussed. How well the actual arrangement agrees with the theoretical performance of the ideal ACC will be discussed in Chapter 6.

Consider the case where the compressor is operating at a constant pressure ratio, p_2/p_1, the exhaust manifold temperature, T_5, is constant (which implies that the engine A/F ratio is also constant), and the engine speed, N_E, is gradually reduced. The by-pass air flow rate increases, because the total compressor flow must remain constant (being a function of compressor pressure ratio only), and the engine flow reduces with the speed. The ACC fuelling rate is linked to the boost pressure only, and so the ACC fuelling will remain constant. The overall by-pass A/F ratio, eqn. (4.178) will therefore increase, and so the temperature rise across the ACC will reduce. Using a simplified steady flow analysis, the temperature rise across the ACC can be estimated from:-

$$(T_{acc} - T_2) = \frac{C_v}{c_p . A/F_{oacc}} \qquad (4.179)$$

where,

c_p = mean specific heat of the air and exhaust gas (kJ/kg.K)

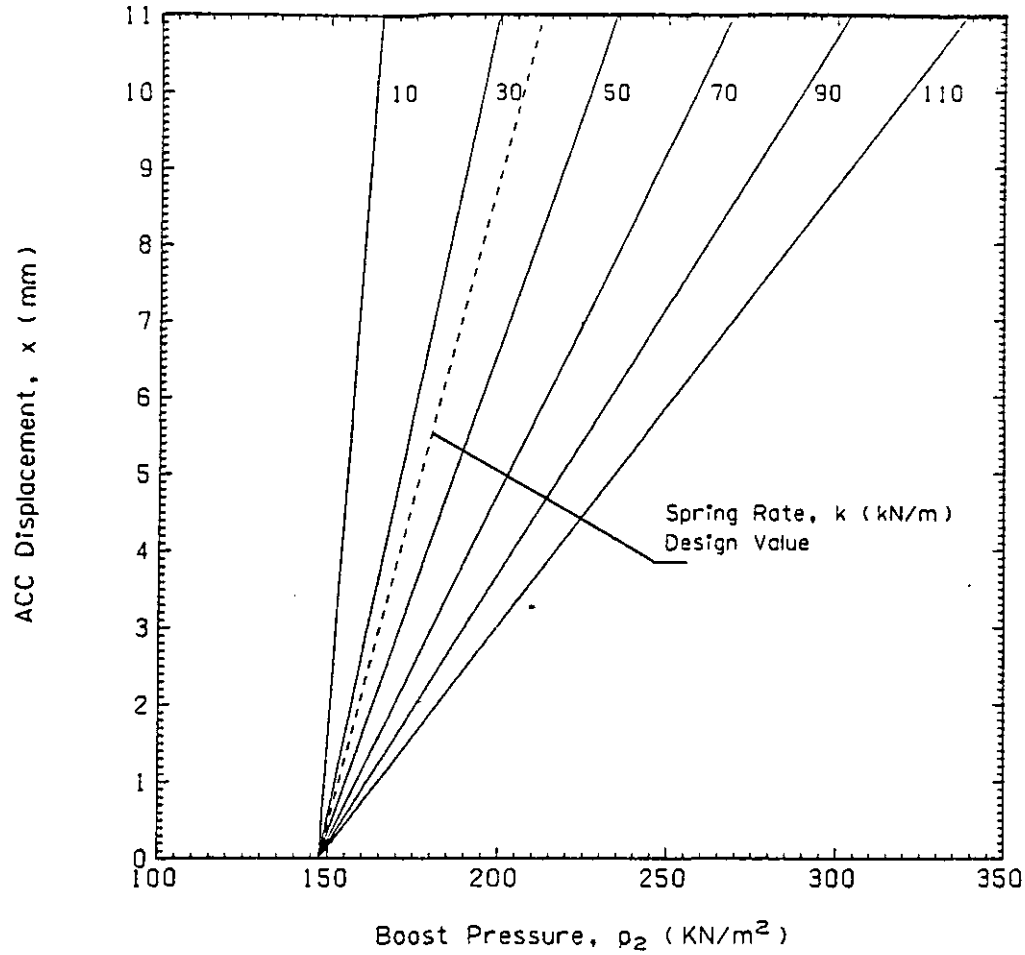

Fig. 4.54 Effect of the Spring Rate k on the ACC Displacement.

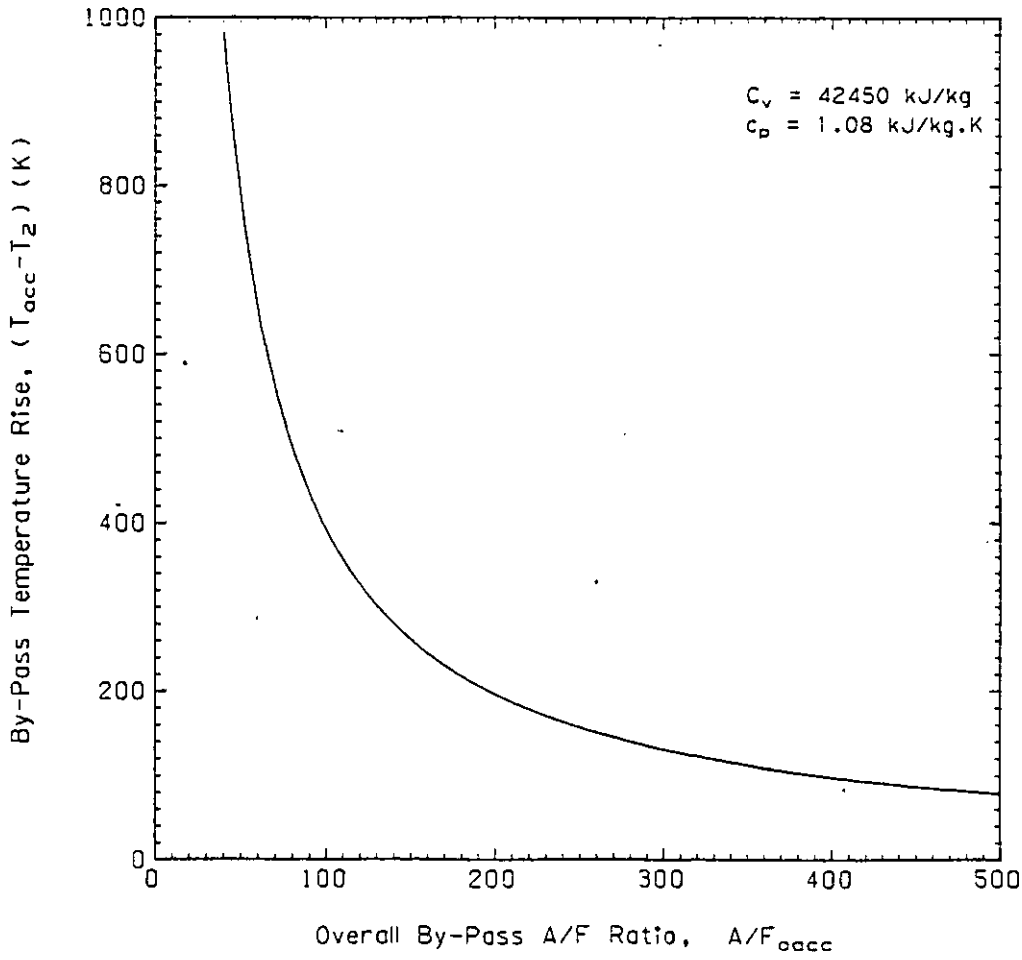

Fig. 4.55 The By-Pass System Temperature Rise as a Function of the Overall By-Pass A/F Ratio.

C_v = lower calorific value of the fuel (kJ/kg)

T_2 = compressor outlet temperature (K)

T_{acc} = ACC gas outlet temperature (K)

Fig. 4.55 shows the ACC temperature rise as a function of the overall by-pass A/F ratio, from eqn. (4.179). It can be seen that the temperature rise across the ACC initially reduces rapidly as the A/F ratio increases, and becomes asymptotic to the $(T_{acc}-T_2)=0$ axis as the fuel input tends to zero $(A/F_{oacc}=\infty)$. The ACC inlet temperature, T_2, will remain constant and so the outlet temperature, T_{acc}, will reduce as the engine speed falls at constant, p_2/p_1.

The turbine inlet temperature, T_3, has to be held constant in order to maintain the boost pressure level, see Fig. 3.5, and it has been assumed that the exhaust manifold gas temperature is constant. The ideal ACC gas temperature for a given exhaust manifold gas temperature and by-pass flow ratio can be estimated by assuming that a single value of c_p can be used for all the exhaust gases, and that the flow is steady:-

$$T_{acc} = \frac{T_3 - T_5.(1 - (\dot{m}_{bp} + \dot{m}_{aacc})/\dot{m}_t)}{(\dot{m}_{bp} + \dot{m}_{aacc})/\dot{m}_t} \qquad (4.180)$$

where,

T_3 = turbine inlet gas temperature (K)

T_5 = exhaust manifold gas temperature (K)

$\dot{m}_t$ = turbine mass flow rate (kg/s)

Fig. 4.56 shows the ACC outlet temperature required, T_{acc}, to maintain a constant turbine inlet temperature, T_3, of 900 K (627°C), for a range of exhaust manifold gas temperatures, T_5, and by-pass flow ratio's, calculated from eqn. (4.180). As the by-pass flow ratio increases, for constant ACC fuelling, the ACC gas temperature falls, and therefore if T_3 is to be maintained constant, T_{acc} must be higher than the turbine inlet temperature at high speeds. Then as the speed reduces and the by-pass flow ratio increases, T_3 can be maintained.

The variation of the overall ACC/diluting chamber A/F ratio, eqn. (4.178) is therefore the most significant parameter governing the ACC operation in the model. In practice the actual ACC A/F ratio eqn. (4.177) is also important to ensure complete

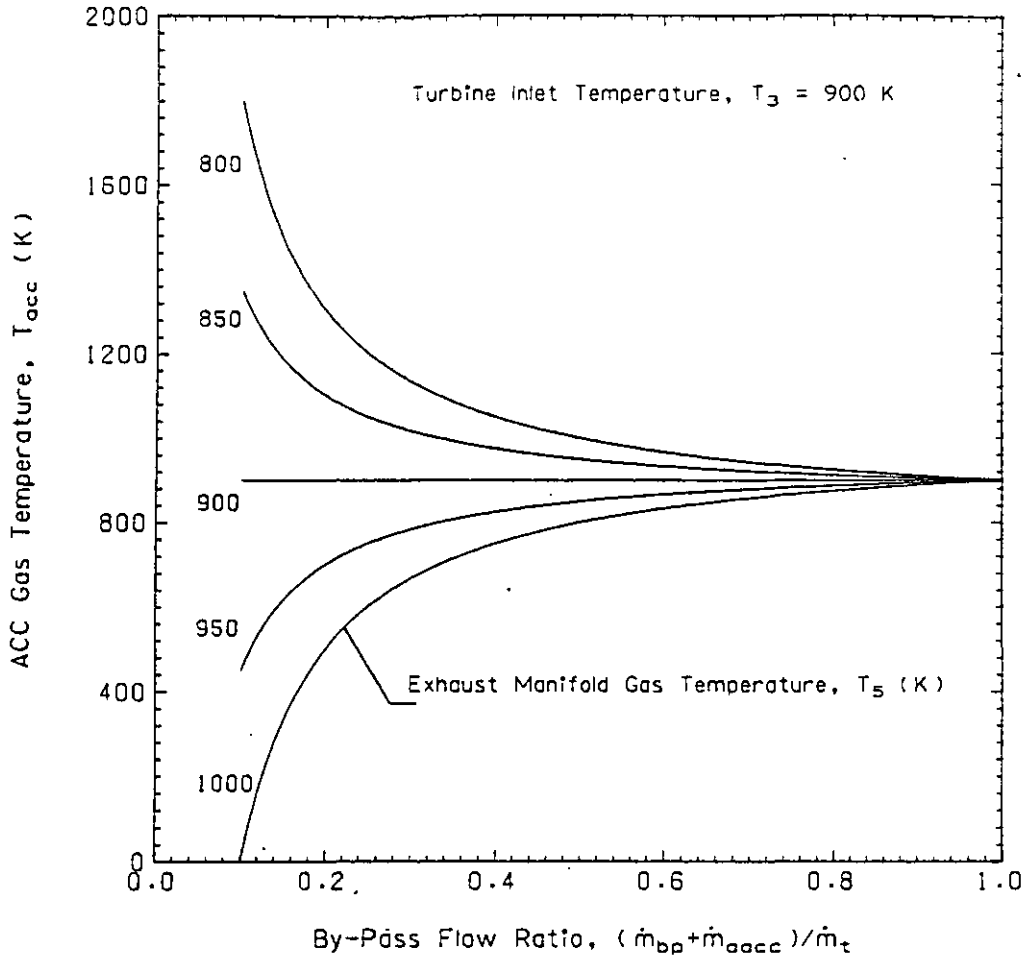

Fig. 4.56 The ACC Gas Temperature Required T_{acc} to Maintain the Turbine Inlet Temperature T_3 at 900 K.

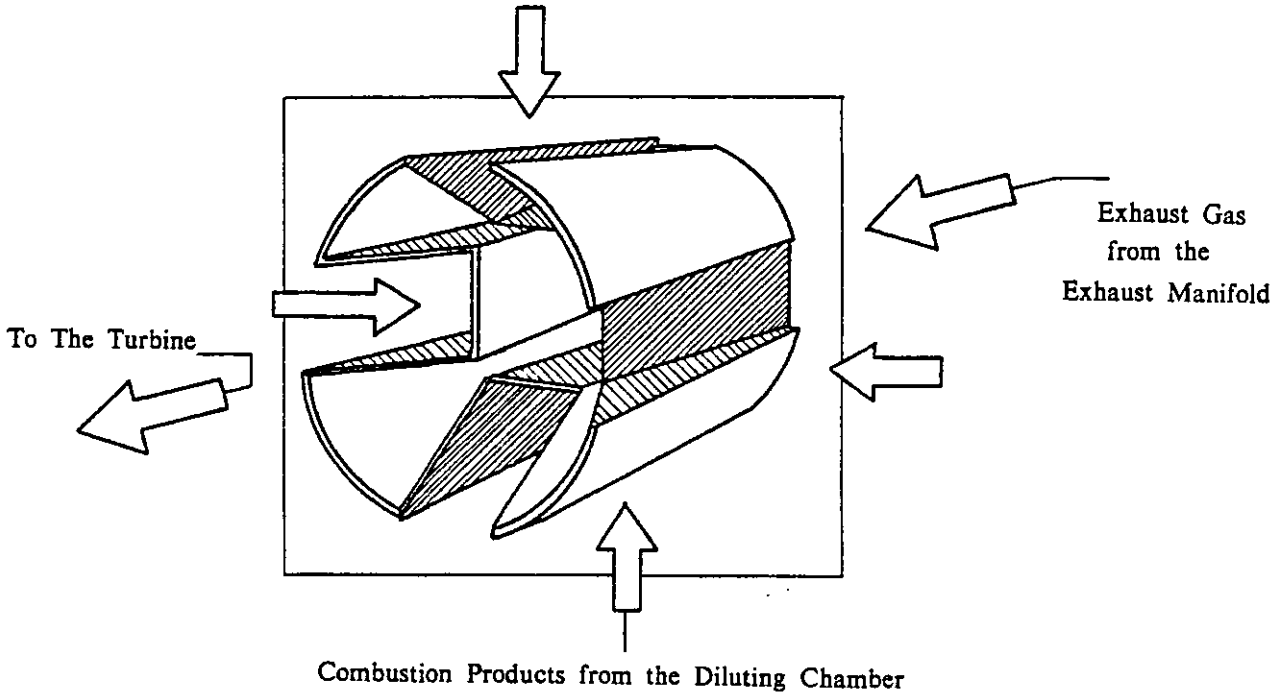

Fig. 4.57 The Exhaust Mixer.

combustion of the injected fuel.

4.8.11 ACC/Diluting Chamber Geometry.

The model considers the ACC and the diluting chamber as one control volume, which implies that the pressure drop across the interface between the inner and outer chambers can be neglected, see Fig. 4.43. However this control volume does not include the exhaust manifold and the mixer, which passes through the outer chamber. Heat transfer is assumed to take place between the ACC/diluting chamber and the atmosphere, using an overall heat transfer coefficient, similar to that used for the exhaust manifold, see section 4.4.4. No heat transfer is assumed to occur between the ACC/diluting chamber and the mixer, or the exhaust manifold. No experimental evidence was available to support these assumptions, and errors in estimating the heat transfer from the exhaust system will ultimately influence the turbine available energy, but these effects are expected to be minor.

4.8.12 The Exhaust Mixer.

The purpose of the mixer is to combine the by-pass and engine exhaust flows together before they enter the turbine. A "daisy" type mixer arrangement has been used, see Fig. 4.57, as this ensures good mixing with minimal pressure losses. The mixer is designed to minimise the interference of the pulsating exhaust manifold pressure on the ACC/diluting chamber pressure.

A separate control volume has been used in the model for the mixer, linking the exhaust manifold and the ACC/diluting chamber to the turbine. Complete and instantaneous mixing of the two flows entering the mixer is assumed, and flow in either direction between the mixer and the exhaust manifold, and the mixer and the ACC/diluting chamber, can occur. Because of the relatively high exhaust pressure levels, flow out of the mixer through the turbine can only occur in one direction (i.e. no reverse flow through the turbine is permitted).

The volume and heat transfer area of the "daisy" mixer, including the pipework connecting the mixer to the turbine inlet, was calculated. From Fig. 4.43 it can be

seen that some heat transfer between the mixer and the air in the ACC/diluting chamber will take place, but this has been neglected. The only heat transfer considered is between the mixer and the surrounding atmosphere, which was calculated in the same way as for the exhaust manifold, see section 4.4.4, based on an overall heat transfer coefficient and the bulk mean exhaust gas temperature.

Early tests showed some numerical instability in the pressure calculated in the mixer. This was due to the relative volumes and flow rates of the interconnected manifolds (the exhaust manifold, ACC/diluting chamber and the mixer being continuously connected by orifices). The ACC/diluting chamber volume is 69.4% of the exhaust manifold volume, while the mixer volume is only 21.7% of the exhaust manifold volume. The instability occurs because large mass flow rates out of the exhaust manifold and/or the ACC/diluting chamber will cause a significant increase in the mixer pressure, while not affecting the pressures in the larger volumes to the same degree. This causes a reversal of the pressure ratio between the exhaust manifold and the mixer, or the ACC/diluting chamber and the mixer, and therefore a sudden flow reversal on the next calculation step. This results in high frequency oscillation in the mixer pressure and a significant increase in the computer time for a cycle calculation, due to the difficulty in achieving convergence at each step, see section 4.9.

The mixer volume and heat transfer area were therefore arbitrarily doubled, and this solved the instability problem and reduced the computing time for a cycle by one third. While this is only a temporary solution to the problem, it is simple and effective, and does not cause any significant errors in the calculation of the various manifold pressures and flows under steady state conditions (but may affect the transient response of the system). A better solution would be to take into account the inertia of the gas in the manifolds, but this would involve using the "Method of Characteristics" or a similar type of solution procedure, which is both expensive and time consuming, especially if transient operation is to be considered, and is beyond the scope of this work.

4.8.13 Summary of the Hyperbar Models.

In addition to the control volumes normally associated with the model of a turbocharged diesel engine, two additional control volumes have been included:-

(1) The ACC/diluting chamber.

(2) The exhaust mixer.

Dynamic models of the by-pass valve (see section 4.7) and the ACC have also been developed. Fig. 4.58 shows the layout of the engine model with the Hyperbar components, and the possible flow directions indicated. The following additional assumptions have been made:-

(1) The instantaneous compressor flow is assumed to be equal to the sum of the by-pass flow and the flow into the induction manifold, ($\dot{m}_1 = \dot{m}_2 + \dot{m}_3$).

(2) If the by-pass flow exceeds the instantaneous compressor flow ($\dot{m}_2 > \dot{m}_1$) then reverse flow from the induction manifold through the by-pass is assumed to take place, ($\dot{m}_3 < 0$).

(3) There is no reverse flow through the by-pass valve or ACC ports ($\dot{m}_2 \geq 0$) i.e. there is no flow from the ACC into the induction manifold. This avoids any recirculation of products of combustion through the engine.

(4) The compressor operating point is calculated at each step according to the instantaneous pressure ratio and turbocharger speed parameter.

(5) The instantaneous turbine mass flow rate is calculated at each step according to the instantaneous inlet conditions and the expansion ratio. The efficiency is calculated from the speed parameter and the blade speed ratio.

(6) Flow can occur in both directions between the ACC and the exhaust mixer, and similarly between the exhaust manifold and the mixer.

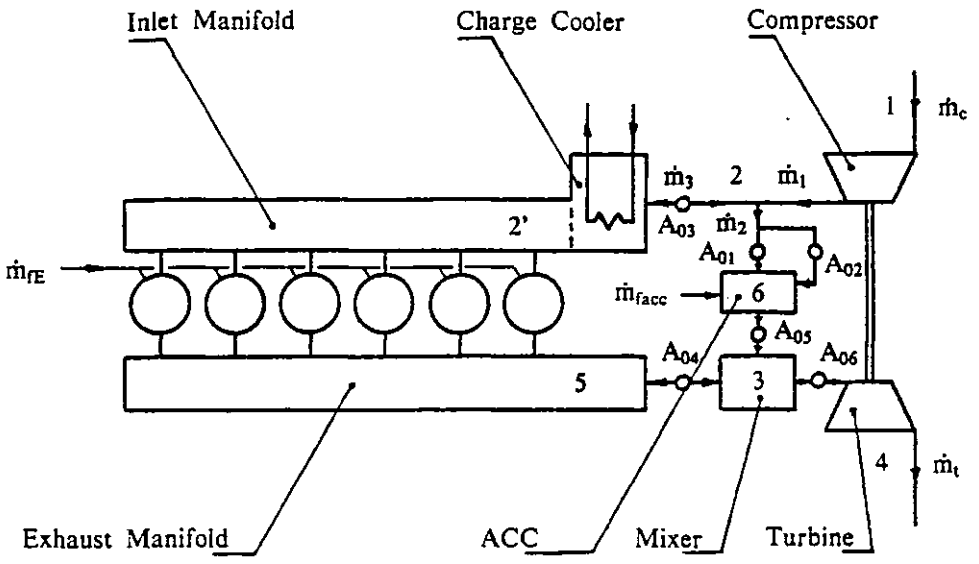

Fig. 4.58 Schematic of the Hyperbar Engine Arrangement.

(7) There is no exhaust gas recirculation system or charge cooler by-pass.

(8) There is no inlet manifold heater.

4.9 Numerical Methods.

The governing equations for the thermodynamic systems form a set of coupled ordinary differential equations of the form:-

$$\frac{dZ_i(t)}{dt} = f_i(Z_1 , Z_2 , \ldots , Z_m , t) \qquad (4.181)$$

for $i = 1, 2, \ldots , m$

where each of the variables, Z_i, is a function of the independent variable, t, and the initial conditions are:-

$$Z_i(t_0) = Z_0 \qquad (4.182)$$

These equations must be solved simultaneously to describe the thermodynamic cycle of these systems. Annand (4) compared various numerical techniques for simulation programs and concluded that a fourth order Runge-Kutta method was two-to-three times slower than an equivalent iterative (predictor-corrector) method. In addition the iterative method was stable over the whole engine cycle, while the Runge-Kutta method displayed instabilities at the begining of the gas exchange period.

Following Borman (22), Streit (136) and others, a modified 2nd order Euler method was used to solve the governing differential equations. The Euler formula was used to "predict" the first approximation to the conditions at time $t+\Delta t$,

$$Z_i^*(t+\Delta t) = Z_i(t) + \Delta t.f_i(Z_1(t) , Z_2(t) , \ldots , t) \qquad (4.183)$$

A corrector formula was then used to compute a better approximation at time $t+\Delta t$,

$$Z_i(t+\Delta t) = Z_i(t) + 0.5.\Delta t.[f_i(Z_1(t) , Z_2(t) , \ldots , t) + f_i(Z_1^*(t+\Delta t) , Z_2^*(t+\Delta t) , \ldots , t+\Delta t)] \qquad (4.184)$$

The difference between the predictor, Z_i^*, and the corrector, Z_i, at time $t+\Delta t$ was

used as a measure of the accuracy of the solution. If the absolute value of the difference $(Z_i - Z_i^*)$ was not within a specified tolerance, ε, the predicted value was updated according to eqn. (4.185) and the corrector recalculated.

$$Z_i^*(t+\Delta t) = Z_i^*(t+\Delta t) + C.[\ Z_i(t+\Delta t) - Z_i^*(t+\Delta t)\ ] \qquad (4.185)$$

where $0 \leq C \leq 1$.

If the solution did not converge to the specified tolerance, ε, after a preset number of iterations of the corrector, the calculation was continued as if convergence had been achieved, and error messages were printed. The calculation step size was fixed during run time, and therefore if no convergence was achieved the step size was reduced. For the majority of the runs described in the following chapters a step size of 1°CA has been used.

The predictor-corrector method was used to integrate eqns. (4.2), (4.7) and (4.12) for the engine thermodynamics, and a similar method was used to integrate the dynamic equations for the governor rack position, eqn. (4.131), the by-pass valve position, eqn. (4.154) and the ACC position, eqn. (4.166).

The dynamic equations for the engine, eqn. (4.22), and the turbocharger, eqn. (4.28) were integrated using a fourth order Adams (Adams-Bashforth) open type formula (28) of the form:-

$$Y_i(t+\Delta t) = Y_i(t) + \frac{\Delta t.}{24}[\ 55.\dot{Y}_i(t) - 59.\dot{Y}_i(t-\Delta t) + 37.\dot{Y}_i(t-2.\Delta t) - 9.\dot{Y}_i(t-3.\Delta t)\ ] \qquad (4.186)$$

where,

Y_i = engine or turbocharger speed (radians/s)

$\dot{Y}_i$ = rate of change of engine or turbocharger speed (radians/s^2).

CHAPTER 5

COMPARISON OF EXPERIMENTAL AND PREDICTED STEADY STATE ENGINE PERFORMANCE

5.1 Introduction.

Only a limited amount of test data was available for a prototype 6 cylinder Hyperbar engine. In the following sections the engine performance predicted using the simulation program is compared with this data, and the interactions between the various engine and turbocharger systems is discussed. Having established the accuracy with which the model can predict the important engine operating parameters, it can then be used to study the effects of design changes to the engine and Hyperbar system on the overall engine performance. This will be discussed in Chapter 6.

No transient test data was available to verify the accuracy of the fuel pump and governor models, or to demonstrate the ability of the program to predict the engine response to changes in load and/or demand speed. However, the predicted transient performance of the Hyperbar engine is compared to that of a two stage turbocharged, aftercooled version of the same engine (at the same rating) to demonstrate the potential of the system, see Chapter 7.

5.2 Overall Engine Performance Prediction.

The simulation program must be capable of predicting the overall engine performance parameters, to an acceptable accuracy over the load and speed range of the engine. It must also react sensibly to changes in the engine and/or turbocharging system specification.

Test data was available at three engine speeds 1200, 1800 and 2400 rpm, and loads ranging from 3.80 to 18.98 bar BMEP. The "nominal" values quoted in the following sections correspond to the measured engine performance, and the percentage errors are calculated as the (predicted value - experimental value) /(experimental value) x 100%.

Figs. 5.1, 5.2 and 5.3 compare the experimental and predicted engine performance at these three engine speeds. The engine speed and fuelling were taken as the independent parameters for the simulation, whereas speed and load (BMEP) are usually considered as the independent variables in experimental tests. The engine BMEP could have been used for the abscissa in Figs. 5.1, 5.2 and 5.3, but this would have lead to errors in both the horizontal and vertical directions (if the measured fuelling was used) or else required a number of runs at various fuellings to predict the correct BMEP, thus complicating the analysis.

The variables compared in Figs. 5.1, 5.2 and 5.3 include the engine and total Brake Specific Fuel Consumption, BSFC, the Brake Mean Effective Pressure, BMEP, the compressor pressure ratio, p_2/p_1, the engine and total air-fuel ratio's, A/F, the maximum cylinder pressure, p_{max}, the turbocharger speed, N_{tc}, the by-pass valve pressure ratio, $(p_2-p_3)/(p_2-p_1)$, the ratio of the total by-pass flow (valve and ACC) to the compressor flow, $\dot{m}_{bp}/\dot{m}_c$, the ratio of the ACC fuelling to the total fuelling, $\dot{m}_{facc}/\dot{m}_{ft}$, the mass flow rates through the compressor, $\dot{m}_c$, engine, $\dot{m}_E$, and by-pass system, $\dot{m}_{bp}$, the compressor outlet and turbine inlet pressures, p_2 and p_3 respectively, and the exhaust manifold and turbine inlet temperatures, T_5 and T_3 respectively.

It can be seen that the overall agreement between the experimental and predicted results is acceptable, over the wide range of loads and speeds considered. The simulation program faithfully reflects the effects of changing the speed and load on the important engine and turbocharging system parameters. The deviations in the predicted results, expressed as a percentage of the measured values, will generally decrease as the engine load is increased, due to the increase in magnitude of the parameters, and the fixed resolution at which they can be measured. This implies an increasing degree of accuracy of the test data with load. The engine frictional losses are a good example of this, any errors in predicting the FMEP becoming increasingly important as the load is reduced, and the FMEP becomes a greater proportion of the IMEP.

The static injection timing was maintained constant at 22°CA BTDC for all these tests, and the dynamic timing was calculated according to eqn. (4.36), and was therefore independent of load. The AFBR correlation developed in section 4.3.7 was used without modification, despite the fact that this engine has a lower compression ratio and different fuel injection system and piston design.

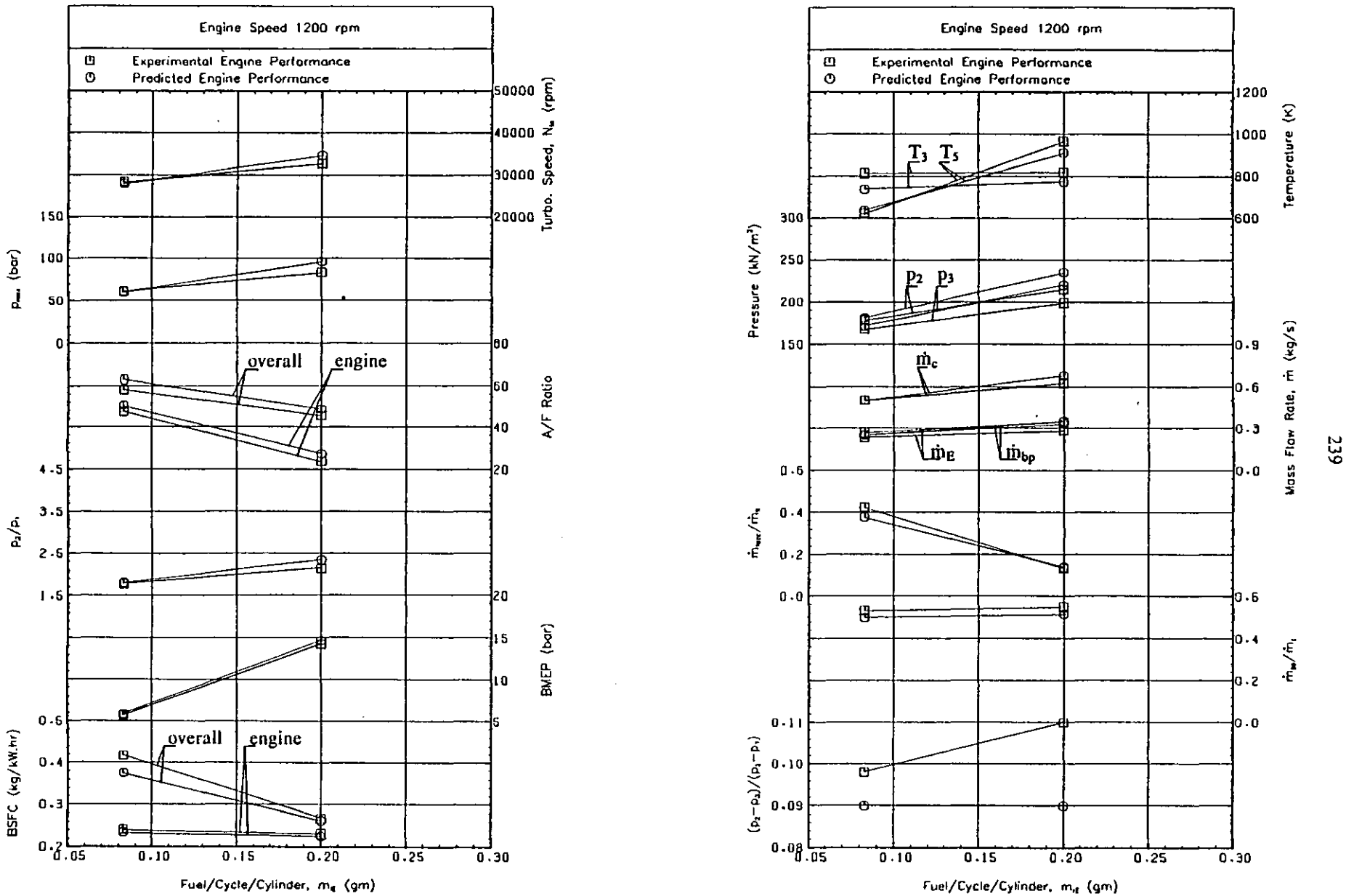

Fig. 5.1 Comparison of Experimental and Predicted Engine Performance at 1200 rpm.

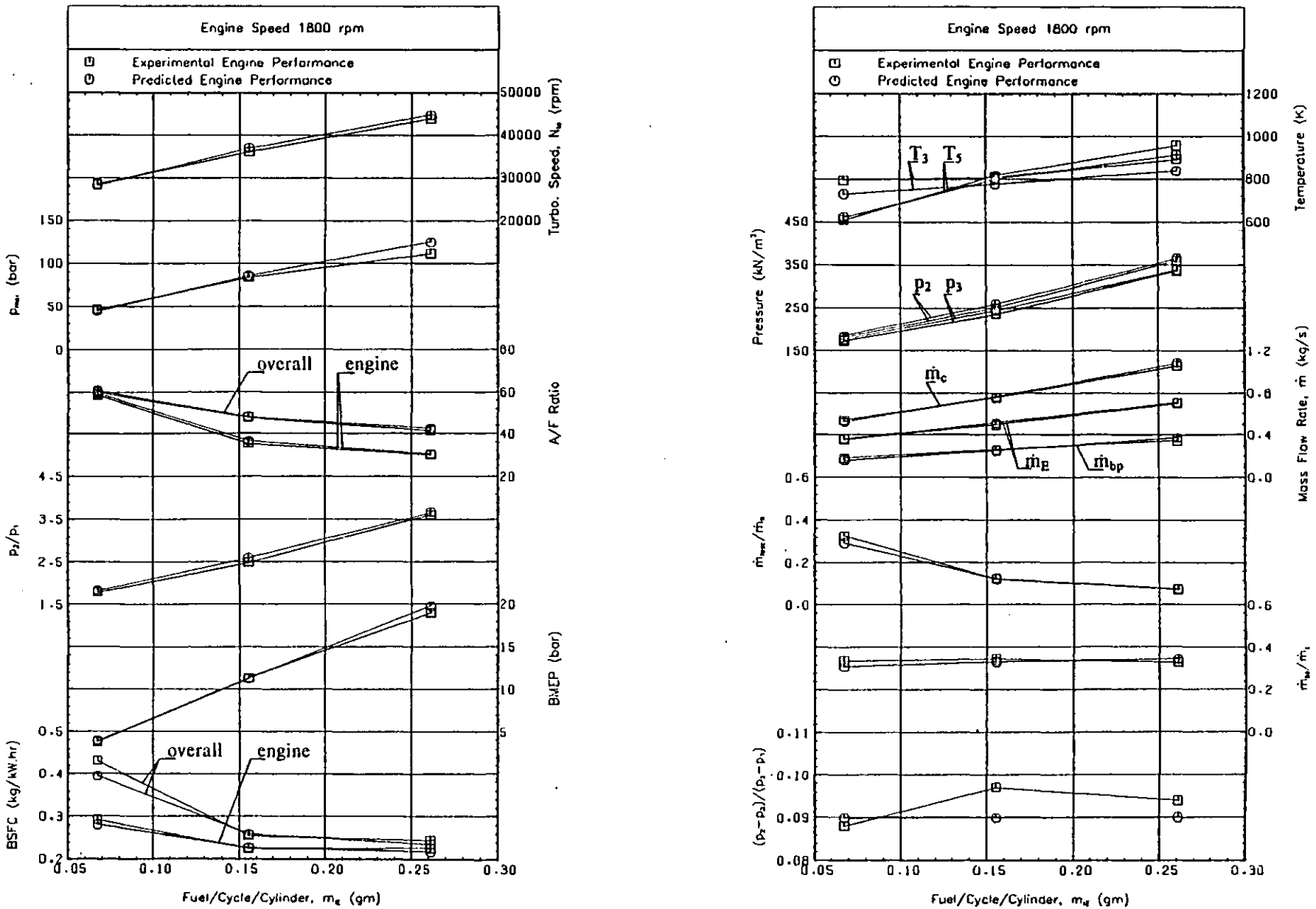

Fig. 5.2 Comparison of Experimental and Predicted Engine Performance at 1800 rpm.

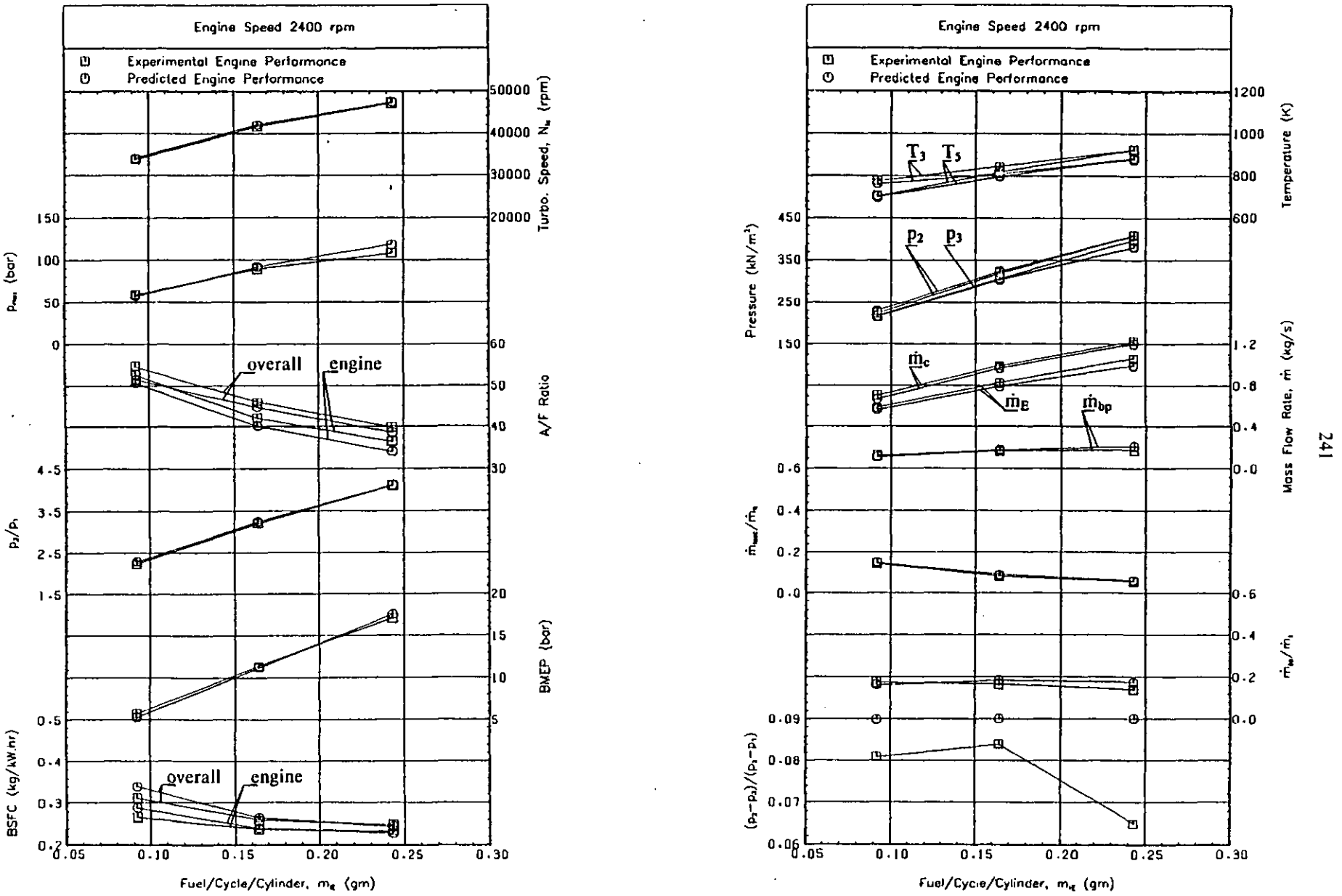

Fig. 5.3 Comparison of Experimental and Predicted Engine Performance at 2400 rpm.

The measured and predicted BMEP's agree well over the load and speed range, the maximum deviation being -7.5% at 2400 rpm/5.70 bar BMEP (nominal). Generally the BMEP is predicted to within 3% of the test data and the error at the rated power is +2.6%. Possible causes for these errors are due to inaccuracies in predicting the frictional losses, errors in the dynamic injection timing, and subsequent heat release rate, or errors in the predicted manifold pressures and consequently the piston pumping work.

As identical fuellings have been used for the experimental and predicted engine performance, errors in the predicted engine BSFC are inversely proportional to the errors in BMEP.

The maximum cylinder pressure is predicted lower than the test values at the lowest loads at each speed, by -1.5% at 1200 rpm, -4.2% at 1800 rpm and -3.6% at 2400 rpm, but the predicted maximum cylinder pressure increases faster with load and exceeds the measured data by +15.7% at 1200 rpm, +12.2% at 1800 rpm and +9.4% at 2400 rpm at the highest loads at each of these speeds. This implies that there is some error in the predicted AFBR, and subsequent heat release rate, although no accurate cylinder pressure diagrams were available to enable a more detailed comparison of the combustion effects to be carried out. Errors in the predicted cylinder pressure diagram will lead to errors in the IMEP (and consequently the BMEP) and also in the FMEP (which is related to the peak cylinder pressure). A possible reason for the large error in peak cylinder pressure at high loads is errors in the dynamic injection timing (see section 4.3.2) which become increasingly important as the load increases. For example, at the rated engine power, advancing the dynamic timing from 13.3°CA BTDC to 15.6°CA BTDC increases the maximum cylinder pressure from 118.1 bar to 124.0 bar, and the error increases from +9.4% to +14.8%. There will obviously be errors introduced due to the fact that the AFBR has been developed for an engine with a different fuel injection system, (the injection pressure and rate of injection having a significant effect on the subsequent combustion process), and the AFBR is being extrapolated to higher loads than that used in the original correlations, see section 4.3.7.

The predicted boost pressure is very important, because it effects the engine air flow and the cylinder pressure and the subsequent combustion processes, via the ignition

delay, trapped mass and trapped equivalence ratio. The experimental and predicted compressor pressure ratio's are shown in Figs. 5.1, 5.2 and 5.3. In order to correctly predict the boost pressure, (or compressor pressure ratio since the measured ambient, or compressor inlet, conditions were used in the simulation program) reliable compressor and turbine characteristics must be used (see section 4.2.1 and 4.2.2) and the turbocharger speed and exhaust energy must be calculated accurately. At low loads the ACC burner will control the minimum boost level, by varying the ACC fuelling rate. This happens at 1200 rpm/5.70 bar BMEP and 1800 rpm /3.80 bar BMEP (nominal) while at higher loads the minimum ACC fuelling level will also effect the available turbine energy. The prediction of the ACC fuelling will be discussed later. The compressor pressure ratio is predicted to within an accuracy of +2.4% over the load and speed range, except at 1200 rpm/14.25 bar BMEP and 1800 rpm/11.39 bar BMEP (nominal) where the errors increase to +9.4% and +4.1% respectively. At all the test conditions the boost pressure is predicted higher than the test data (measured at the compressor outlet), only the error at the rated engine power reducing to -0.04%. Generally the trends with increasing load and speed are accurately reproduced, considering the assumptions that have had to be made about the compressor and turbine characteristics, and the underlying assumption of quasi-steady flow. The experimental and predicted operating points on the compressor map will be discussed in greater detail in section 5.4.

The prediction of the compressor pressure ratio will effect both the engine air flow and the behavior of the by-pass valve and the ACC, and the subsequent manifold pressures and the engine pumping work.

The errors in predicted engine A/F ratio are entirely due to inaccuracy in predicting the engine air flow rate, since the measured engine fuelling has been used at each operating condition, (assuming no error in the measured fuelling rate). The predicted variation in the engine A/F ratio with speed and load can be seen to follow the experimental trends well. At the lower speeds, 1200 rpm and 1800 rpm, the engine air flow rate is predicted higher than the test data, especially at 1200 rpm, where the error is as much as +7.2% at the lowest load. At 1800 rpm the errors are substantially less, being within +3%. The engine air flow is underpredicted at the highest engine speed, 2400 rpm, the magnitude of the error decreasing from -6.4% at the rated power to -3.8% at the minimum load, 5.70 bar BMEP (nominal). Errors in the predicted air flow rate through the engine can be caused by incorrectly predicting

the compressor and/or by-pass flow, poor inlet manifold pressure and/or temperature prediction, the effective flow areas of the inlet and exhaust valves or the exhaust manifold pressure (and hence the scavenge air flow during the valve overlap). However, the test values of engine A/F ratio and air flow, presented in Figs. 5.1, 5.2 and 5.3 are estimated using a procedure similar to that described in section 4.7.4 (i.e. from the inlet manifold conditions and engine speed by assuming a volumetric efficiency of 100%), and so are subject to some doubt. A comparison of the experimental and predicted exhaust manifold gas temperatures will also give an indication of the accuracy of the engine A/F ratio.

The computed exhaust temperatures shown in Figs. 5.1, 5.2 and 5.3 are compared with the measured exhaust manifold and turbine inlet temperatures. The experimental exhaust gas temperatures were measured using a simple thermocouple and thus represent the static temperatures in the manifolds (no compensation for radiation effects were considered), while the predicted values are the time averaged mean stagnation temperatures, and so are not directly comparable. Borman (23) has indicated that the measured exhaust temperature should lie between the time averaged and mass averaged temperatures, although the thermocouple should read a temperature closer to the mass averaged value, because of the variation in heat transfer coefficient with velocity. However, due to the large exhaust system volumes (a single "constant pressure" manifold being used) the difference between the time and mass averaged temperatures was predicted to be insignificant, (less than 3°C) and the flow out of the exhaust manifold and through the turbine is essentially "steady".

Comparing the experimental and predicted exhaust manifold gas temperatures, T_5, shows that the simulation predicts the effect of changing load and speed correctly, but the magnitude of the temperature errors varies from +2.6% at 1200 rpm/5.70 bar BMEP to -4.3% at the rated engine power. Generally the manifold temperature is predicted to be up to 5% lower than the measured values. The turbine inlet temperatures, T_3, are predicted to be between 1.6% and 9.2% below the measured values depending upon the operating conditions. The highest errors in turbine inlet temperatures occur while the burner is operating, at 1200 rpm/5.70 bar BMEP and 1800 rpm/3.80 bar BMEP (nominal) where the errors are -9.2% and -8.0% respectively. At the other test conditions the predicted gas temperatures are within -5% of the measured values.

The turbocharger speed is predicted extremely well, considering the assumptions that have been made in order to produce the compressor and turbine maps. The turbocharger speed is predicted to within 2% of the measured values, and is within +1% at the highest speed, 2400 rpm. Only at 1200 rpm/14.25 bar BMEP (nominal) is the error significant, +5.9%. The experimental and predicted compressor operating points are discussed further in section 5.4.

Having predicted the compressor speed and pressure ratio to an acceptable degree of accuracy, the compressor mass flow rate and efficiency predicted will depend upon the compressor map. The compressor flow rate is underpredicted at the highest engine speed, 2400 rpm, by between -2.6% at the rated power and -5.1% at 5.70 bar BMEP. At the other test conditions it is within 3%, except at 1200 rpm/14.25 bar BMEP where the error is +7.9%, and the speed and pressure ratio errors were the largest.

The overall A/F ratio and total BSFC will depend on how well the ACC model predicts the burner fuelling. This in turn will depend upon how well the boost pressure (which is the main burner control parameter) is predicted. At the lowest load conditions at 1200 rpm and 1800 rpm, the burner is required to increase the exhaust energy to maintain the minimum boost pressure level. At 1200 rpm/5.70 bar BMEP the ACC fuelling is underpredicted by -18.1% while the boost pressure, p_2, is overpredicted by +1.6%, and at 1800 rpm/3.80 bar BMEP the ACC fuelling is underpredicted by -14.1% and the boost pressure is +2.4% too high. The measured boost pressures (at the compressor outlet) are 178.5 kN/m^2 and 179.8 kN/m^2 at 1200 and 1800 rpm respectively, and the corresponding predicted values are 181.3 kN/m^2 and 184.1 kN/m^2. Increasing the boost pressure will lead to a reduction in the ACC fuelling, and so the higher boost levels predicted result in the lower burner fuelling rates. The simulation program therefore tends to predict a higher overall turbocharger efficiency than the measured data shows. There could be a number of reasons for this. For example, higher compressor and/or turbine efficiencies may be predicted either because of errors in the performance maps used for these components, or errors in the predicted operating points. However, the minimum boost level that is obtained using the Hyperbar system is predicted with acceptable accuracy. At the other operating conditions the boost is sufficiently high so that the burner is held in the minimum fuelling position. Any error in the ACC fuelling is therefore caused by the minimum fuelling threshold used in the fuelling characteristics, see section 4.8.6. There was some scatter in the original data, which was curve fitted, and also some

scatter in the ACC fuellings measured in the experimental tests, see Fig. 4.46. This causes errors in the predicted ACC fuelling rate of between -0.6%, at 1800 rpm/11.39 bar BMEP (nominal), and +10.9%, at the rated engine power. However, the importance of errors in the minimum fuelling rate will depend upon the proportion of the ACC fuelling to the total engine fuel flow rate, i.e. upon load and speed. For example, at the rated power the measured ACC fuelling is 5.7% of the total fuel supplied to the engine, and an error of +10.9% in the burner fuelling rate will increase this to 6.3% of the total fuelling.

The total BSFC shown in Figs. 5.1, 5.2 and 5.3 therefore reflects the errors in BMEP (also seen in the comparison of the engine BSFC) and the burner fuellings. Similarly the total A/F ratio reflects errors in the compressor flow and the ACC fuelling rate.

The by-pass valve is used to control the pressure difference between the compressor outlet and the exhaust system, according to eqn. (4.157). It does this by varying the valve position and hence the air flow rate that goes through the by-pass system. There is an additional parallel flow path between the compressor outlet and the exhaust system for the ACC air flow, which is not directly dependent on the valve position (but is dependent upon the inlet to exhaust pressure ratio).

Figs. 5.1, 5.2 and 5.3 show how well the by-pass valve can maintain the desired pressure drop across the engine. According to eqn. (4.157) under steady state conditions the parameter $(p_2-p_3)/(p_2-p_1)$ should be equal to the valve area ratio, A_2/A_1, which is 0.09 (in fact the ACC/diluting chamber pressure, p_6, is used in place of the turbine inlet pressure, p_3, in the following comparisons, because this is the parameter that is actually controlled by the by-pass valve). The simulation program does predict the correct pressure drop across the engine, by varying the valve position according to the boost pressure and engine speed. However, the measured pressure ratio shows that this cannot be achieved in practice. At the lowest engine speed, 1200 rpm, the pressure drop ratio across the valve is too high (up to 0.11), which implies that there is not enough flow through the by-pass system, while at 2400 rpm the opposite is true (the pressure drop ratio falling to 0.065 at the rated power). The valve does maintain the pressure ratio fairly closely at the intermediate speed of 1800 rpm however. No allowances for these variations from the ideal valve performance (which could be caused by the valve sticking, the positioning of the pressure transducer/manometer or a number of other reasons), have been allowed for

in the model.

The experimental and predicted boost and exhaust pressures are also shown, these being measured at the compressor outlet and turbine inlet. The predicted values are time averaged pressures which were found to vary from the mass averaged values by less than 1 kN/m^2 over the speed and load range, because of the steady nature of the compressor and turbine flows. It should be remembered that the measured and computed values do not represent the same quantity, measurements made under pulsating flow conditions using a normal U-tube manometer may not necessarily give the correct mean pressure.

The charge cooler outlet temperature has been held constant for the test data at 344 K (71°C) ± 3°C by varying the cooling water flow rate, and the predicted charge cooler outlet temperature has also been held constant at 344 K. The pressure drop across the cooler is predicted using eqn. (4.31) and the computed values agree with the test data to within ± 1 kN/m^2.

5.3 Description of the Steady State Performance Prediction.

Figs. 5.4, 5.5 and 5.6 show examples of the predicted engine performance with changes in load and speed. Fig. 5.4 is at 1200 rpm/5.70 bar BMEP (nominal), Fig. 5.5 at 2400 rpm/5.70 bar BMEP (nominal) showing the effect of varying the engine speed at constant load, and Fig. 5.6 is at 2400 rpm/17.09 bar BMEP (nominal), the rated power output, showing the effect of changing the load at constant speed.

Figs. 5.4a, 5.5a and 5.6a show crank angle histories of cylinder pressure, mean cylinder gas temperature and the heat transfer rate from the gas to the cylinder walls, mass flow rates through the exhaust and inlet valves, fuel burning rate and cylinder gas equivalence ratio, manifold pressures (inlet, exhaust, ACC/diluting chamber and mixer) and instantaneous cylinder torque. Also shown are the compressor and engine operating lines plotted on the compressor map. The turbine operating characteristics are plotted in Figs. 5.4b, 5.5b and 5.6b showing the available and actual turbine power, the velocity ratio U/C, the efficiency, the mass flow rate and the turbine inlet pressure and temperature. Figs. 5.4b, 5.5b and 5.6b also show the operating characterisics of the Hyperbar by-pass valve and ACC, including the instantaneous by-

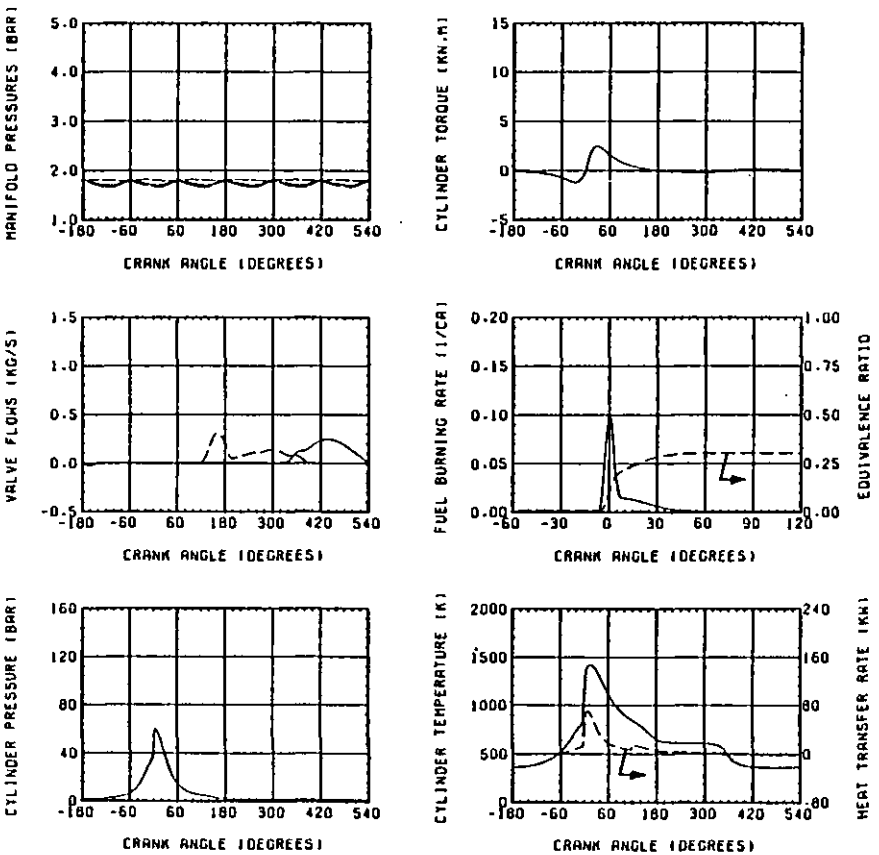

Engine

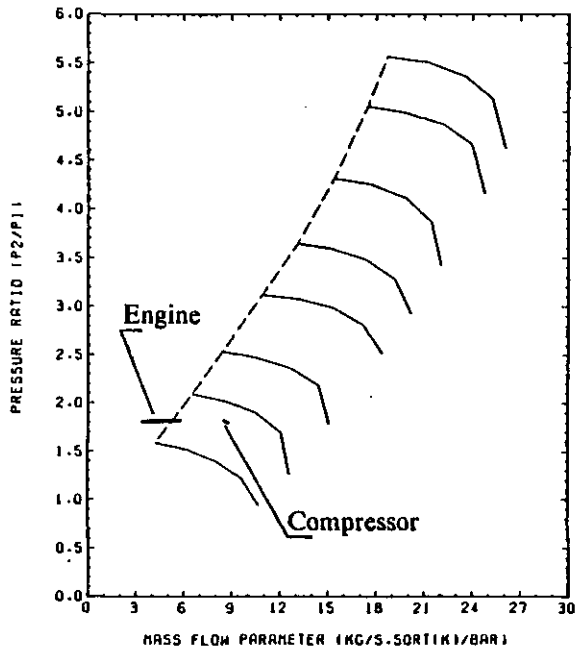

Compressor

Fig. 5.4a Predicted Engine Performance at 1200 rpm/5.70 bar BMEP (Nominal).

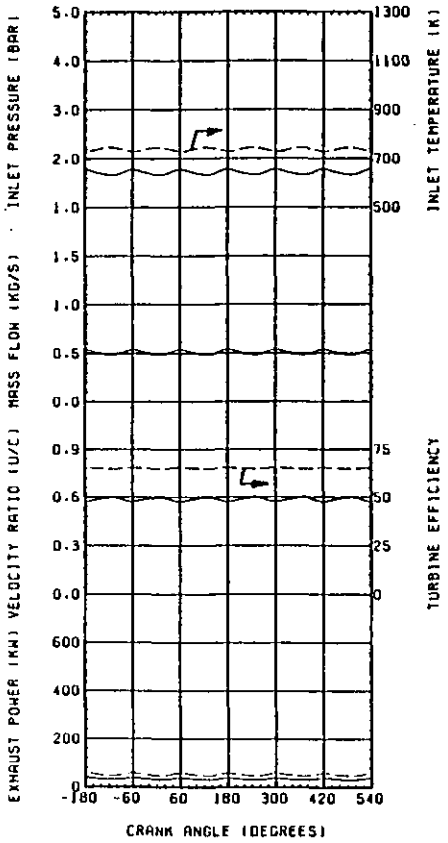

Turbine

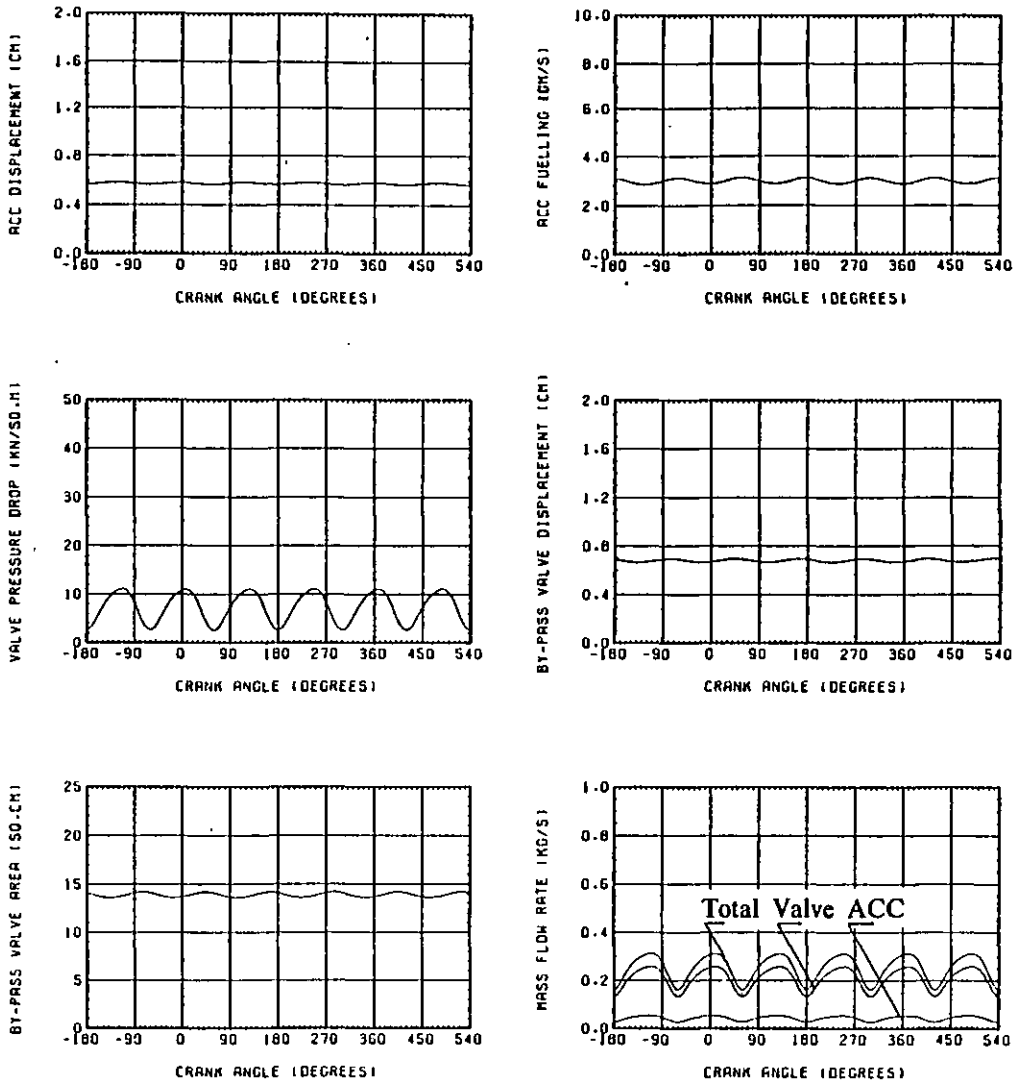

By-Pass System

Fig. 5.4b Predicted Engine Performance at 1200 rpm/5.70 bar BMEP (Nominal).

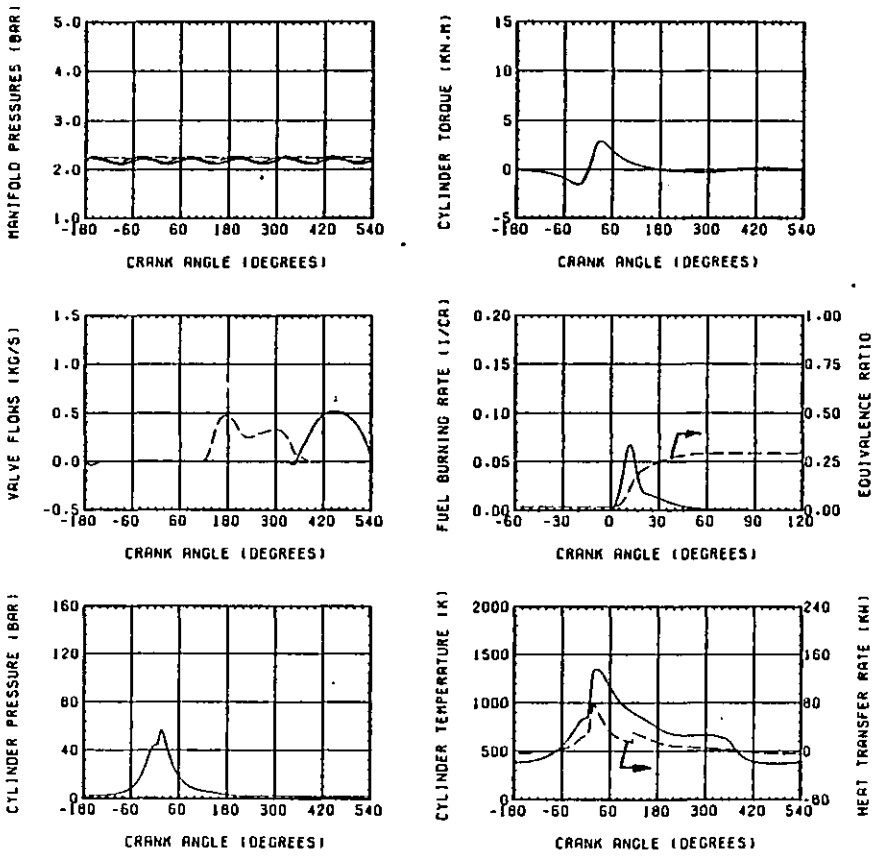

Engine

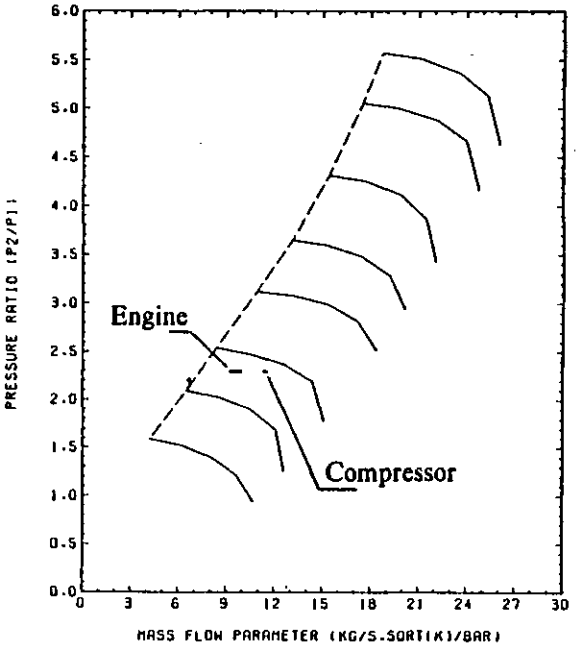

Compressor

Fig. 5.5a Predicted Engine Performance at 2400 rpm/5.70 bar BMEP (Nominal).

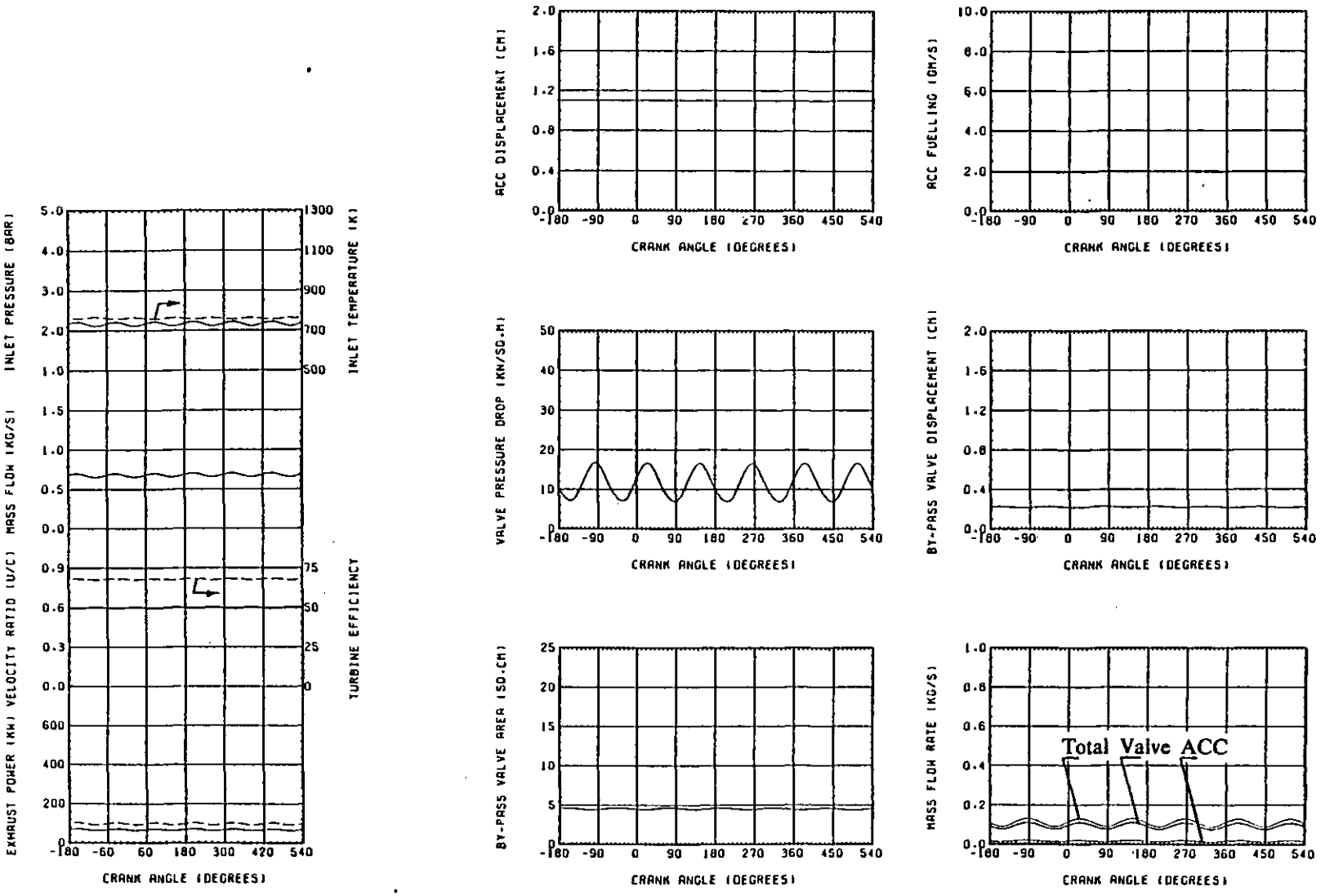

Fig. 5.5b Predicted Engine Performance at 2400 rpm/5.70 bar BMEP (Nominal).

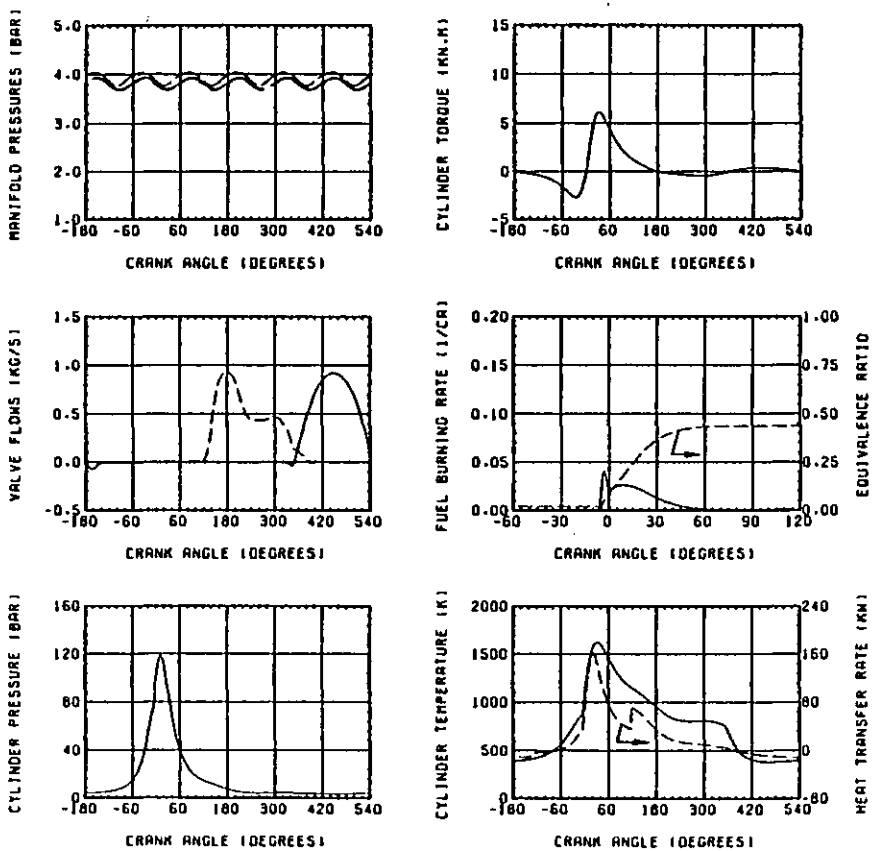

Engine

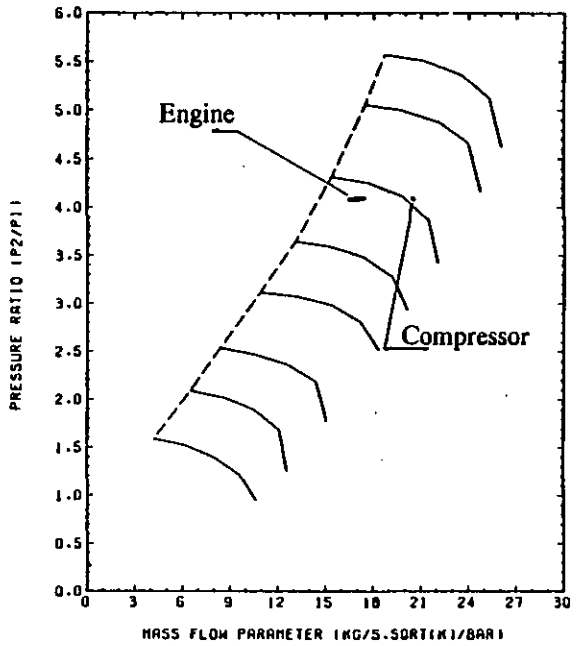

Compressor

Fig. 5.6a Predicted Engine Performance at 2400 rpm/17.09 bar BMEP (Nominal).

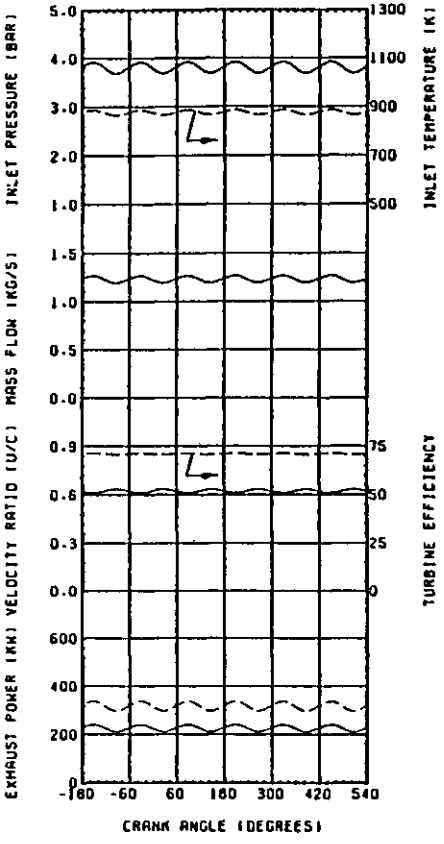

Turbine

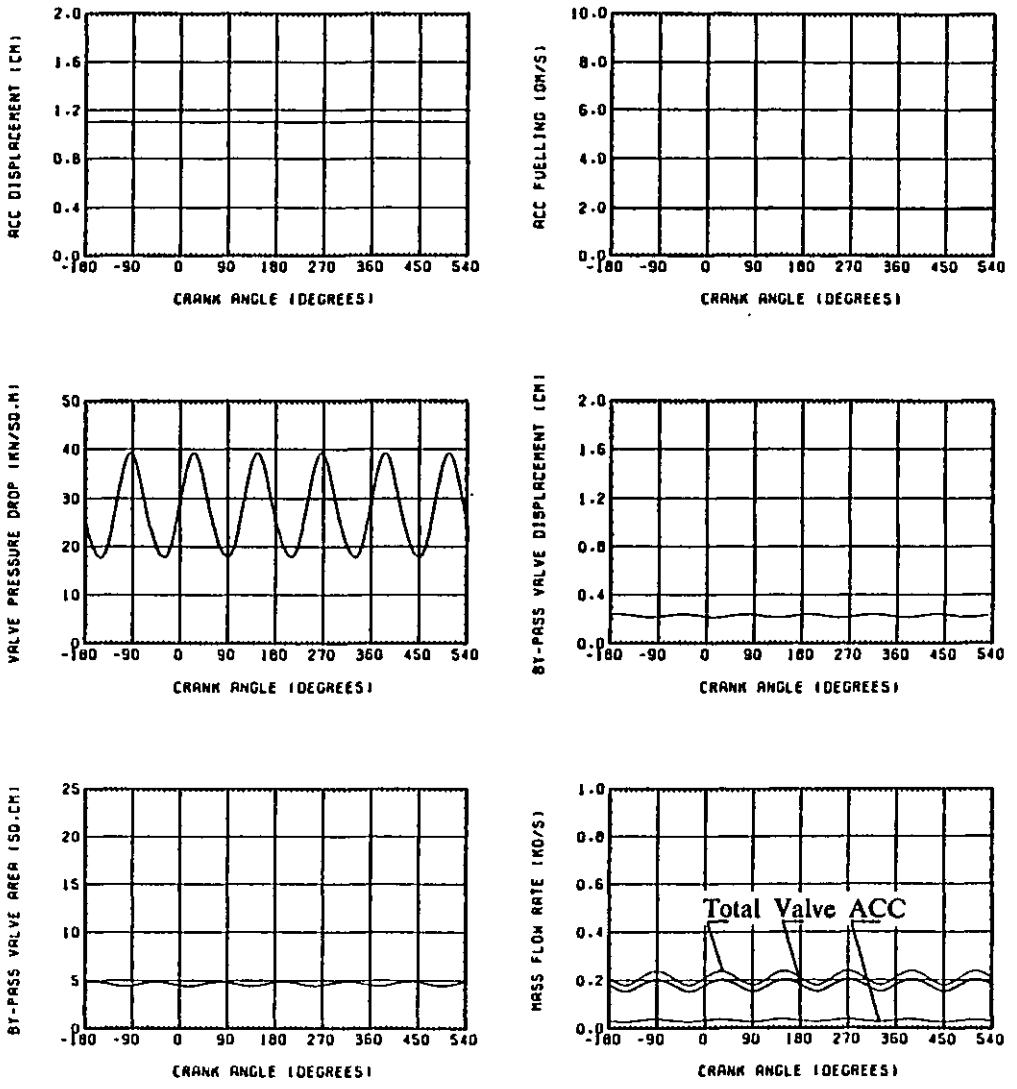

By-Pass System

Fig. 5.6b Predicted Engine Performance at 2400 rpm/17.09 bar BMEP (Nominal).

pass valve area and displacement, the air mass flow rate through the valve, the ACC ports and the total by-pass flow, the instantaneous pressure drop across the by-pass valve and the ACC displacement and fuelling.

At the lowest engine speed and load, Fig. 5.4a, the fuel burning rate diagram shows a large initial "premixed" burning spike, followed by a smaller "diffusion" burning portion. The predicted ignition delay is relatively long at this test condition, 1.60 ms (11.5°CA) due to the relatively low boost pressure (the boost temperature being held constant over the load and speed range). This results in a large proportion of the total fuel being injected during the delay period ($\beta=0.55$ in eqn. (4.67)). The peak cylinder pressure occurs at 6°CA ATDC.

The flow through the exhaust valve exhibits an initially high peak (blowdown), because of the high cylinder pressure when the exhaust valve opens, followed by a duration of steady flow, as the piston expels the gases from the cylinder on the exhaust stroke. Due to the characteristics of the by-pass system, the inlet manifold pressure is higher than the exhaust manifold pressure at the end of the exhaust stroke, and this positive pressure drop across the cylinder helps to scavenge the residual products from the combustion chamber during the valve overlap. The inward flow of air through the inlet valve, produces the initial pulse caused by the positive manifold to cylinder pressure drop during valve overlap, followed by a gradual acceleration and deceleration of the charge during the inlet stroke. There is a small period of reverse flow from the cylinder to the manifold immediately before the inlet valve closes, which causes some heating and/or pollution of the charge air in the manifold, and a slight reduction in trapped mass.

During the induction stroke the cylinder wall temperatures are higher than that of the incoming air, this results in heat transfer to the air (shown as negative heat transfer from the air) which reduces the volumetric efficiency of the engine. This effect becomes more pronounced as the wall temperatures increase (with speed and load) since the charge cooler air outlet temperature is held constant. The heat transfer rate from the cylinder gases shows a sharp rise following the increase in gas velocity at EVO, see section 4.4.2.3, the decrease in heat transfer coefficient at IVC being less noticable (see Fig. 5.4a).

It is unlikely that such a sharp discontinuity in the heat transfer coefficient, and heat

transfer rate, in the cylinder will occur in practice. A more realistic approach would be to gradually increase the heat transfer coefficient as the exhaust valve opens and the gas velocity increases. Similarly the heat transfer coefficient could be gradually reduced towards IVC. However, the errors introduced by this model are very small.

The boost pressure in the inlet manifold is relatively steady, while the exhaust manifold pressure shows six equal pulses from each cylinder in turn. The large "filling and emptying" type "constant pressure" manifold does not take into account the variations in exhaust pressure pulses due to the different cylinder positions.

As the engine speed is increased at (nominally) constant load, the position of the peak cylinder pressure can be seen to retard from 6°CA ATDC to 16°CA ATDC. Comparing Figs. 5.4a and 5.5a, the boost pressure increases slightly and the peak cylinder pressure falls (in both the experimental and computed results). The trapped A/F (or equivalence) ratio remains relatively constant over the speed range at constant load, while the computed ignition delay reduces from 1.60 ms to 0.99 ms due to the increased cylinder pressure and temperature (the heat transfer rate from the gas increases with engine speed, or gas velocity, but the cycle time reduces). The ignition point, however, is retarded as the speed increases because the dynamic timing is retarded with engine speed according to eqn. (4.36) and the ignition delay increases from 11.5°CA to 14.2°CA at 2400 rpm/5.70 bar BMEP. This combination of a shorter ignition delay (in time) and an almost constant trapped equivalence ratio results in a reduction in the proportion of the total fuel that is burnt in the "premixed" mode (β=0.42). The initial "premixed" peak can therefore be seen to reduce with increasing engine speed in Figs. 5.4a and 5.5a.

The initial exhaust blowdown pulse increases as the engine speed increases and Fig. 5.5a shows that there is some flow from the cylinder into the inlet manifold shortly after IVO due to the higher cylinder gas pressure at this speed.

The effect of increasing the engine load at constant speed, 2400 rpm, can be seen by comparing Figs. 5.5 and 5.6, which show the effect of changing the load from 5.70 bar BMEP to 17.09 bar BMEP (nominal).

The boost pressure has increased substantially, which results in higher cylinder pressures on the compression stroke and consequently a shorter ignition delay. At

17.09 bar BMEP the delay has reduced to 0.51 ms (7.4°CA), while the trapped equivalence ratio increases as the fuelling is increased. The result is a very small proportion of the fuel injected is burnt in the "premixed" mode (β=0.10) and the AFBR diagram shows that the combustion process is predominantly "diffusion" controlled.

The mass flow rates through the valves increases with load (or boost pressure) and the initial exhaust blowdown pulse increases with cylinder pressure at EVO. At the rated power there is a significant amount of reverse flow through the inlet valves into the manifold just before IVC.

The by-pass valve controls the exhaust system pressures and, at all speeds, the exhaust manifold pressure exceeds the inlet pressure for only short periods in the cycle (corresponding to the blowdown from each cylinder).

Figs. 5.4a, 5.5a and 5.6a also show the distribution of cylinder torque with changes in speed and load.

Comparing the compressor operating cycles with changes in speed, Figs. 5.4 and 5.5, and with load, Figs. 5.5 and 5.6, shows that the compressor operating line is fundamentally insensitive to variations in either speed or load, see section 5.4.

The mass flow rate through the by-pass valve will vary throughout the engine cycle, because of the pulsating exhaust pressure, while the compressor flow remains steady. Therefore, the flow into the inlet manifold, (the engine air flow) which is the difference between the compressor and by-pass flows, will vary throughout the cycle. This fluctuation in the engine operating point, plotted on the compressor map, can be seen in Figs. 5.4a, 5.5a and 5.6a. The magnitude in the fluctuations in the engine air flow rate will depend upon the boost pressure level (and hence p_2/p_3) and the engine speed (i.e. the cycle time).

A comparison of the turbine operating characteristics with variations in speed and load can be seen in Figs. 5.4b, 5.5b and 5.6b. The relatively steady turbine inlet pressure produces steady flow through the turbine, the flow increasing with both speed and load. The steady turbine flow ensures that the turbine velocity ratio, U/C, and hence the efficiency, does not vary greatly throughout the engine cycle. This can be

compared to the pulse type manifolds which display large variations in U/C and hence turbine efficiency, especially at low speeds and loads where the flow rate varies substantially (89). The high turbine efficiency, essential for the Hyperbar system operation, shows that the turbine efficiency characteristics assumed in section 4.2.2 are well matched for this particular engine, the operating U/C range being 0.5-0.7, and peak efficiency occuring at U/C=0.6, see Fig. 4.4.

The turbine inlet temperature can be seen to increase as the overall A/F ratio reduces with increasing load, see Figs. 5.5b and 5.6b.

Figs. 5.4b, 5.5b and 5.6b show the computed by-pass valve and ACC performance with varying speed and load. At 1200 rpm/5.70 bar BMEP the by-pass valve displacement and effective flow area are large, and so the air flow through the valve is high enough to compensate for the low engine air flow rate. The pulsations in the pressure drop across the valve, caused by the exhaust pulses from each of the 6 cylinders, can be clearly seen in Fig. 5.4b, which results in the variation in valve displacement and mass flow rate. The amplitude and mean value of these pulses increase with speed and load (i.e. primarily with boost pressure), but the frequency of the pulses is such that the valve has little chance to respond to the pressure pulses, see Fig. 5.6b.

The majority of the flow through the by-pass system goes through the valve, the by-pass valve flow area representing 82.8% of the total by-pass area at 1200 rpm/5.70 bar BMEP, 84.6% at 2400 rpm/5.70 bar BMEP and 85.0% at 2400 rpm/17.09 bar BMEP (nominal).

At the lowest speed, the ACC is displaced from the minimum fuelling position, Fig. 5.4b, and the fluctuations in ACC gas pressure can be seen to effect the burner fuelling rate, the pressure fluctuations causing disproportionately large fluctuations in fuelling because of the burner fuelling characteristics, see Fig. 4.46. At the higher speed, Fig. 5.5b and 5.6b, the ACC is held in the minimum fuelling position by the higher exhaust/ACC pressure.

5.4 Comparison of the Experimental and Predicted Compressor Operation.

Fig. 5.7 shows the experimental and predicted compressor operating lines at each of the three engine speeds, 1200, 1800 and 2400 rpm, discussed in the previous sections.

The experimental data shows that the compressor flow is not a unique function of pressure ratio (see section 3.3.4) but tends to reduce slightly as the engine speed falls, moving the compressor operating line closer to the surge line. The experimental test data plotted in Fig. 5.1 shows that the pressure drop across the by-pass system is too high at the lowest speed, 1200 rpm, because the by-pass flow is lower than the design value. Conversely at 2400 rpm the pressure drop is too low, Fig. 5.3, implying that the by-pass flow is too high. At 1800 rpm the by-pass system is working according to the design specification, Fig. 5.2. This variation in by-pass flow from the ideal, results in the total compressor flow being too low at 1200 rpm and too high at 2400 rpm.

The pressure drop across the by-pass system is due to:-

(1) The pressure drop across the by-pass valve, which is largely determined by the valve area ratio, A_2/A_1.

(2) The pressure drop across the diluting chamber and ACC ports.

(3) The pressure drop across the exhaust mixing device.

The pressure losses across items (2) and (3) are not directly controllable and therefore, for given components, will vary according to the mass flow rates passing through them.

The predicted compressor operating lines at these three engine speeds are also shown in Fig. 5.7 and display a similar trend, with the operating line moving closer to surge as the engine speed reduces. However, the movement of the operating line with changes in engine speed is less than that measured experimentally, primarily because the by-pass valve control over the pressure drop is more accurately maintained. There are a number of possible reasons for errors in the model, and these will be discussed

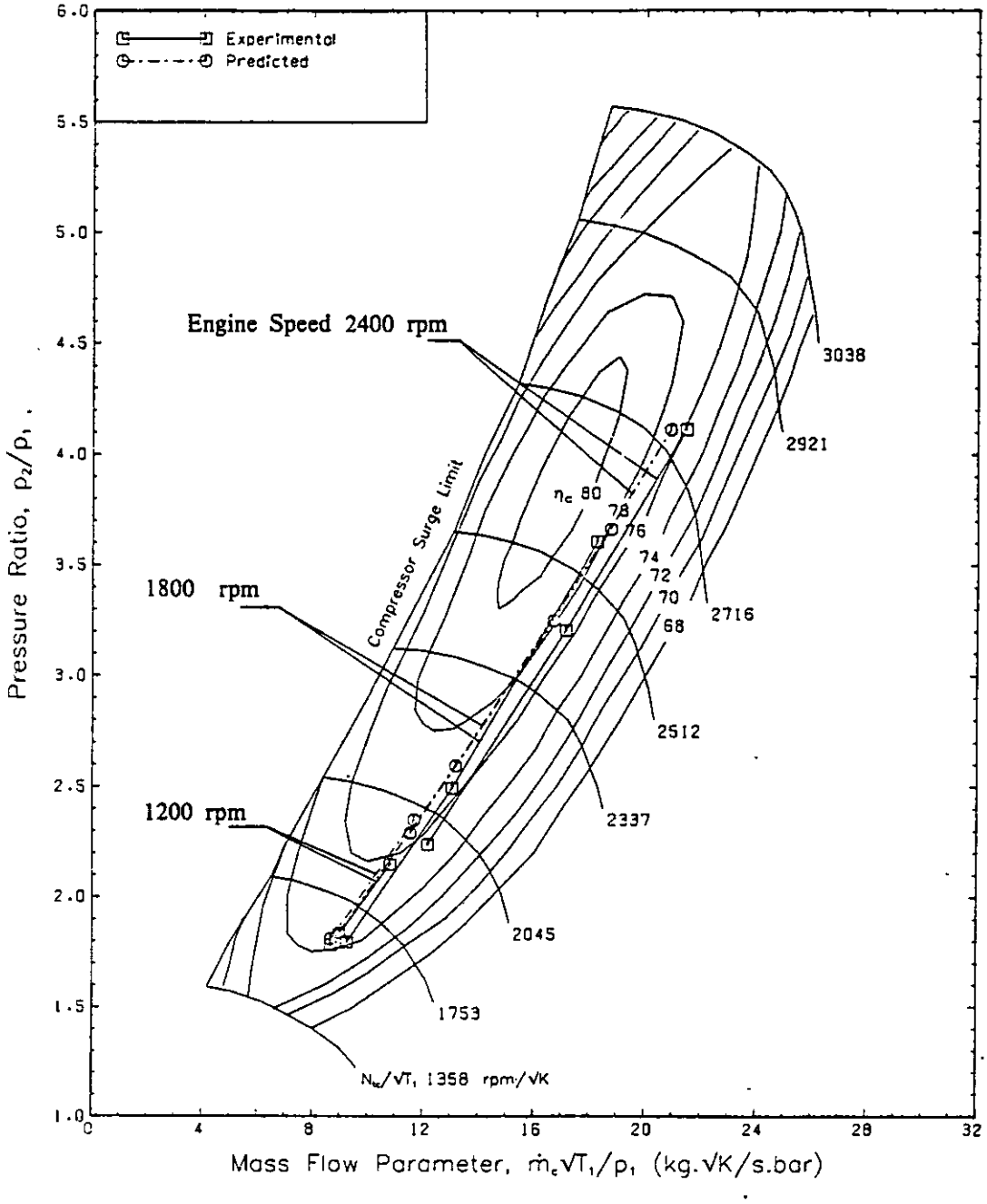

Fig. 5.7 Comparison of Experimental and Predicted Compressor Operating Lines.

in detail in Chapter 6. Generally the compressor operating characteristics are predicted very well by the model, over the range of engine speeds and loads tested. It can be seen that the compressor operating line is matched well away from the surge line, but is to the right (at higher mass flow rates) of the optimum compressor efficiency line.

Fig. 5.8 shows the predicted mean engine and compressor operating lines at 1200, 1800 and 2400 rpm. No accurate measurements of the engine flow have been made for comparison. The diagram shows the relative magnitude of the engine and by-pass flows and gives an indication of the possible speed range of the engine. When the engine speed increases the by-pass flow reduces to maintain the total compressor flow constant (for a given compressor pressure ratio). Eventually a speed will be reached where the engine and compressor flows are equal and the by-pass system can no longer control the engine pressure drop, which effectively limits the engine maximum speed for a given valve design.

In practice, the by-pass flow is a combination of the flows through the by-pass valve and the ACC ports. To ensure combustion in the burner, a certain minimum ACC air flow is required. Therefore the actual maximum engine speed is further limited.

Fig. 5.8 shows that while the total by-pass flow is generous at all speeds at high loads (high p_2/p_1), as the load falls the by-pass flow reduces and at 2400 rpm a point may eventually be reached where the total by-pass flow is required by the burner (i.e. the valve is closed) as the ACC fuelling increases to maintain the minimum boost level. The predicted ACC air mass flow rate can also be seen in Fig. 5.8, which shows the increase in ACC air flow required at low loads, 1200 and 1800 rpm, and the natural characteristic of the ACC, that increases the air flow through the fixed port areas (with the ACC idling) as the compressor pressure ratio (load) increases.

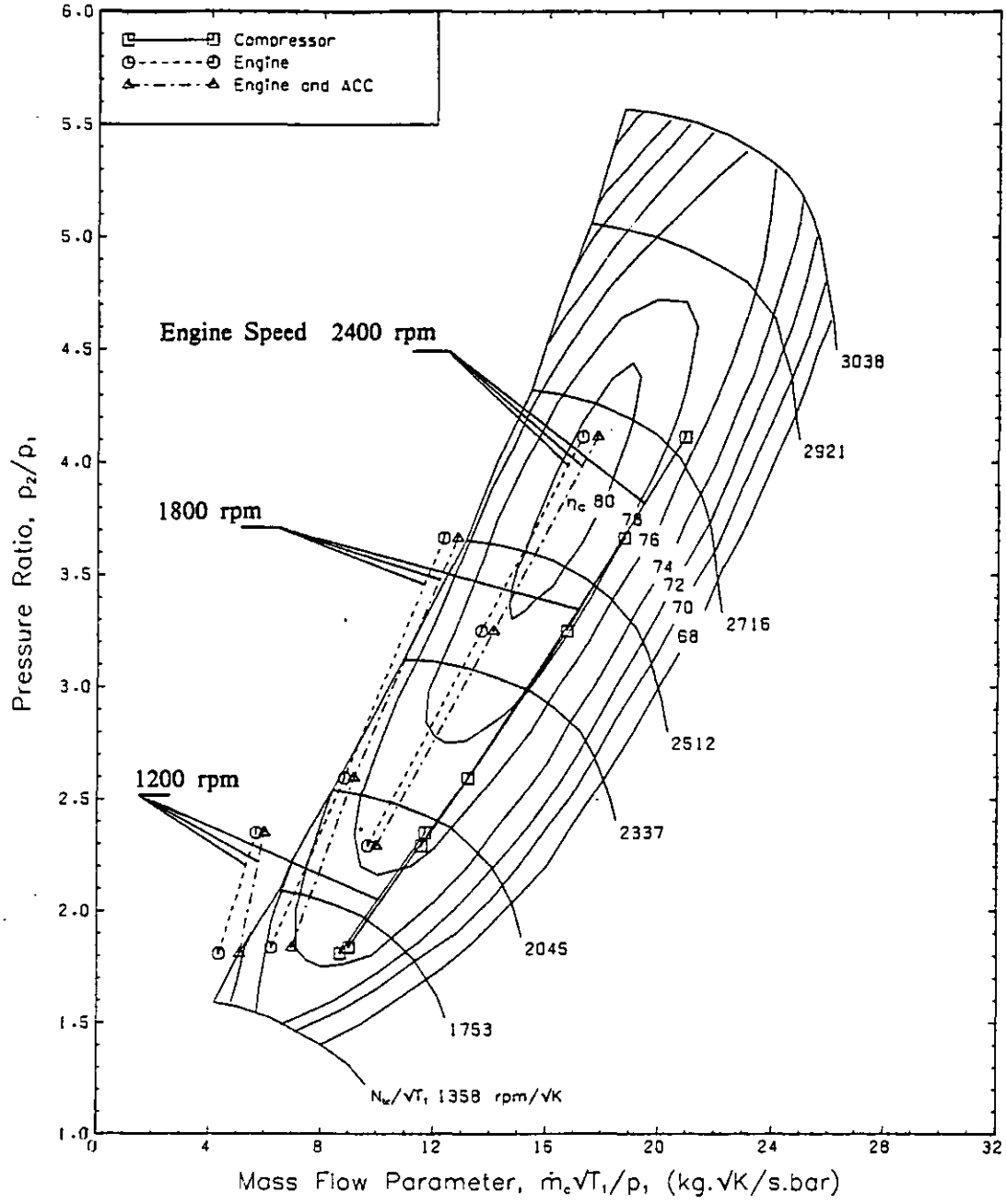

Fig. 5.8 Predicted Compressor, Engine and By-Pass Compressor Operating Lines.

CHAPTER 6

PARAMETRIC STUDY

6.1 Introduction.

The detailed mathematical simulation model has been shown in Chapter 5 to be capable of predicting the steady state engine performance to within an acceptable degree of accuracy (typically within 2-3%). Due to various problems encountered during the experimental testing of the 6 cylinder Hyperbar turbocharged diesel engine, very little actual test data has been recorded.

The simulation model has therefore been used to investigate the influence of various engine and Hyperbar design parameters on the steady state performance of the entire system. This parametric study is intended to show the sensitivity of the system to changes in the key engine design parameters, such as compression ratio and injection timing, and to optimise the Hyperbar system components, such as the by-pass valve area ratio, the ACC fuelling characteristics, the minimum boost pressure level, etc.

The principal objectives of studying the effects of varying the Hyperbar and engine system geometry were to:-

(1) Increase the engine low speed torque.

(2) Minimise the overall BSFC.

(3) Reduce the complexity of the system, if possible.

(4) Improve our understanding of the interaction between the various components in the system.

In addition, methods of improving the transient response of the engine have also been investigated. These are discussed in detail in Chapter 7. However, there is often a conflict between the system design that will give the optimum steady state

performance, and that which will give the best transient response, and this will be discussed in Chapter 7.

6.2 Effect of the Exhaust System Pressure Losses.

6.2.1 Introduction.

It was shown in section 5.4 that the by-pass system pressure losses will affect the position of the steady state compressor operating point. A comparison of the experimental and predicted engine performance for this engine suggests that the model underestimates the pressure drop through the by-pass ducting at low speeds, and so overestimates the surge margin, and underestimates the movement of the compressor operating line towards surge as the engine speed reduces.

Fig. 4.58 shows diagramatically the layout of the Hyperbar system model. A number of orifices have been used to connect the various components of the engine and by-pass system. The orifice areas will affect the flow through each path of the system and represent:-

(1) The by-pass valve, connecting the compressor outlet to the ACC/diluting chamber, with a variable orifice area, A_{01}.

(2) The ACC port area, A_{02}, which allows flow from the compressor outlet into the burner. This area is also variable.

(3) The inlet manifold orifice area, A_{03}, connecting the compressor outlet to the charge cooler, (in fact, the flow into the inlet manifold is taken to be the difference between the instantaneous compressor and by-pass flows).

(4) The exhaust manifold orifice area, A_{04}, connecting the exhaust manifold to the mixer.

(5) The flow area connecting the ACC/diluting chamber to the exhaust mixer, A_{05}.

(6) The turbine flow area, A_{06}, which is, in fact, the swallowing capacity characteristic of the turbine.

The by-pass flow is controlled by the by-pass valve and ACC ports, A_{01} and A_{02} respectively, and the ACC/diluting chamber to mixer area, A_{05}. Changing any of these areas will alter the flow resistance of the by-pass system, and therefore the ratio of the by-pass flow to the turbine flow (i.e. the by-pass flow ratio).

The engine flow is controlled by the compressor and by-pass flows and the orifice area, A_{04}, as well as the actual engine flow resistance. The exhaust manifold orifice area, A_{04}, will control the engine back pressure, and therefore the pumping work and scavenging efficiency.

The pressure drop across the orifices A_{04} and A_{05} will depend upon the mass flow rates through them. The by-pass valve and ACC orifices, A_{01} and A_{02}, do not behave in the same way, because these flow areas will vary according the the relative upstream and downstream pressures.

The pressure losses in the exhaust system were therefore varied by changing the flow areas of the fixed geometry orifices, A_{04} and A_{05}, which are determined in practice by the design of the exhaust mixer, see section 4.8.12.

6.2.2 Effect of Reducing the ACC/Diluting Chamber-Mixer Flow Area.

The effect of halving the flow area of the orifice connecting the ACC/diluting chamber to the exhaust mixer, A_{05}, has been investigated at 1200 rpm/19.71 bar BMEP, this being the nominal BMEP with the standard orifice areas, (the engine fuelling being held constant). This operating condition was chosen because at low speeds a high proportion of the total flow passes through the by-pass system, and at high loads the compressor pressure ratio is high, and so the pressure losses are relatively large.

Halving the flow area of the orifice, A_{05}, results in an increase in the pressure drop across it, from 3.8 kN/m^2 to 12.7 kN/m^2. The mixer pressure reduces from 271.6 kN/m^2 to 264.9 kN/m^2, and the pressure drop across the exhaust manifold orifice,

A_{04}, increases slightly from 3.3 kN/m^2 to 3.4 kN/m^2, due to the increase in engine flow rate caused by restricting the by-pass system. The total air flow through the system reduces by 3.8%, and so the compressor operating point moves closer to surge, (the change in compressor pressure ratio is small, increasing from 2.93 to 2.95). The proportion of the total flow that goes through the by-pass system reduces from 51.1% to 47.9%. As the ACC fuelling remains at the idling setting (because of the high engine load) the ACC gas temperature rises by 18 K, which increases the turbine inlet temperature slightly, by 9 K, because the exhaust manifold gas temperature reduces by 15 K (the engine A/F ratio increases from 28.0 to 28.7).

The effect on the by-pass system operation of halving A_{05} can be seen in Fig. 6.1. The by-pass valve effective flow area reduces by 12.9%, because the reduced ACC/diluting chamber outlet area causes an increase in pressure in this control volume. This tends to close the by-pass valve and restrict the flow rate into the ACC/diluting chamber until a new equilibrium position is reached. The ACC A/F ratio does not change significantly (increasing from 11.2 to 11.5) because the flow area remains constant, with the burner on minimum fuelling, and the pressure ratio across the ACC ports and upstream density increase slightly.

The reduction in exhaust manifold pressure causes an increase in positive pumping work, and therefore an increase in engine BMEP, and reduction in BSFC, of 0.7%. The movement of the compressor operating point closer to the surge line results in a reduction in turbocharger speed of approximately 100 rpm, and an increase in compressor efficiency from 77.5% to 78.0%, see Fig. 6.2.

6.2.3 Effect of Reducing the Exhaust Manifold-Mixer Flow Area.

The effect of halving the orifice area connecting the exhaust manifold to the mixer, A_{04}, while maintaining the ACC/diluting chamber-mixer flow area at the standard value, has also been predicted. The effect on the by-pass system performance can be seen in Fig. 6.1.

The overall effect on the by-pass system is small, the by-pass valve effective flow area increasing by only 0.8%. There is a small increase in the proportion of the by-pass to total flow from 51.1% to 52.1%, due to the increased flow resistance through the

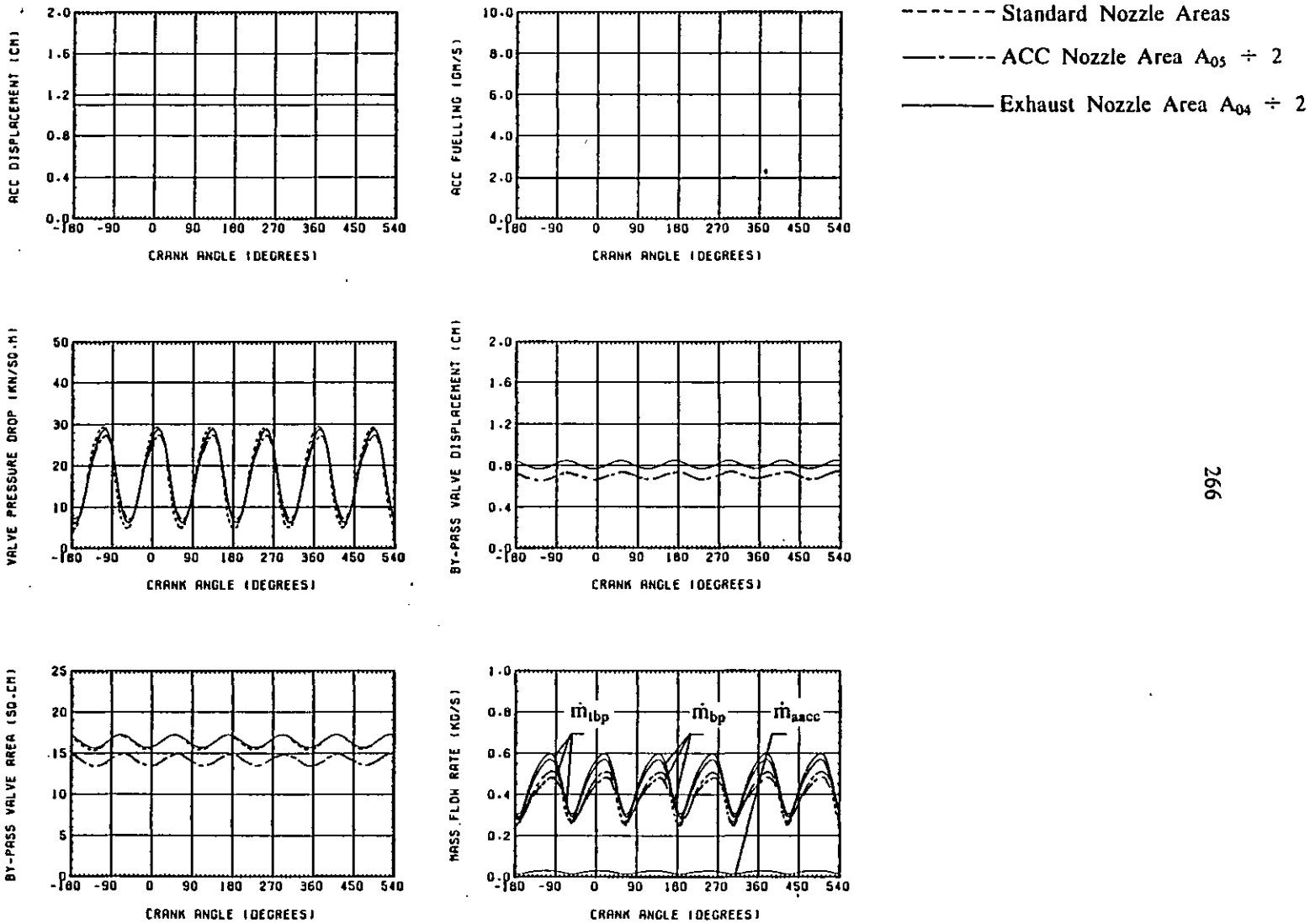

Fig. 6.1 Effect of the Exhaust System Nozzle Areas on the Hyperbar System Performance at 1200 rpm/19.71 bar BMEP (Nominal).

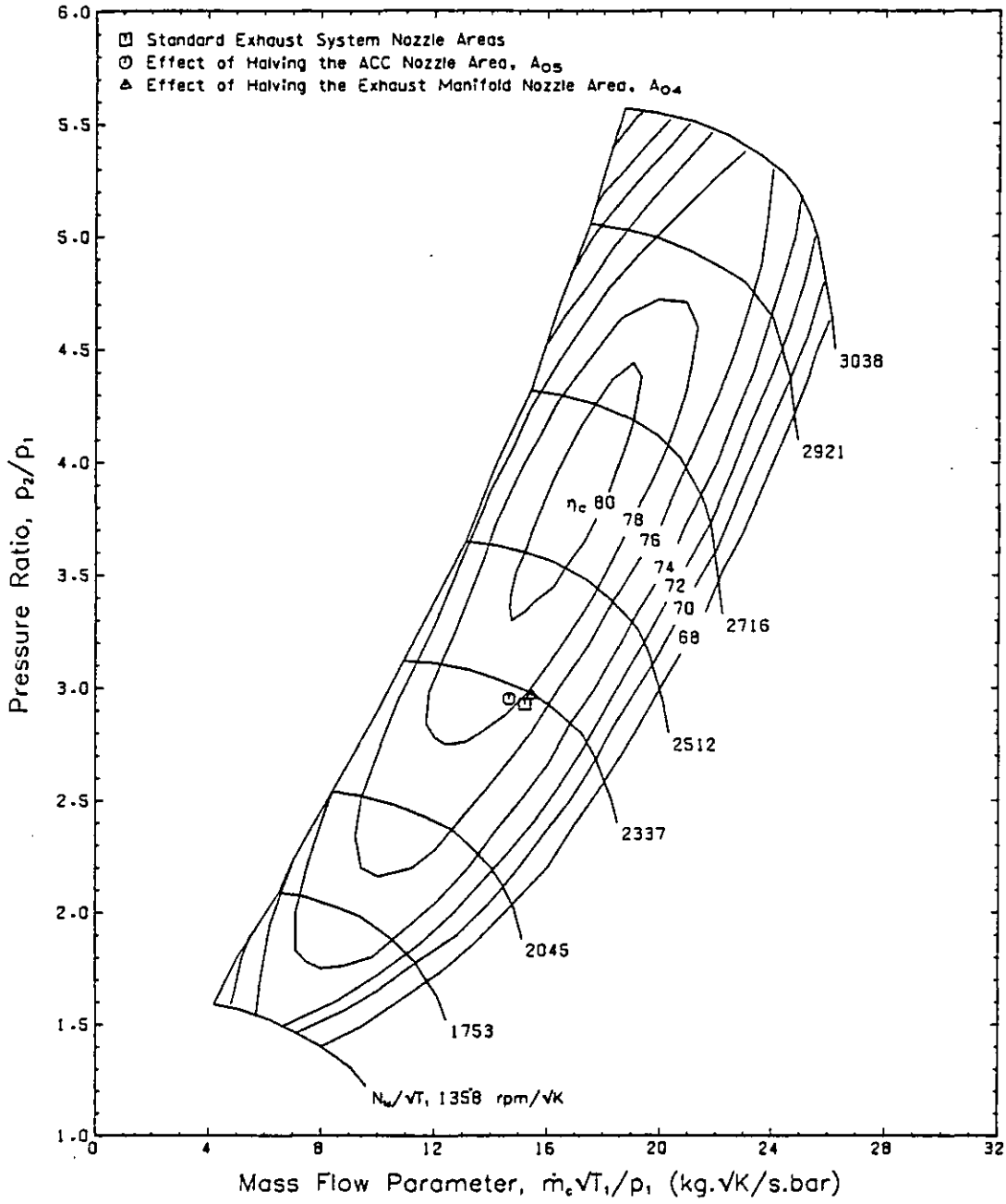

Fig. 6.2 Effect of the Exhaust System Nozzle Areas on the Compressor Operation at 1200 rpm/19.71 bar BMEP (Nominal).

engine. The engine pumping work increases to maintain the air flow, and so the BMEP falls, and the BSFC increases, by 0.4%. The exhaust manifold pressure increases from 274.9 kN/m^2 to 287.7 kN/m^2, and the pressure drop across the exhaust orifice, A_{04}, increases from 3.3 kN/m^2 to 12.8 kN/m^2.

The compressor mass flow rate increases by 1.6%, and the pressure ratio and turbocharger speed both increase, by 1.3% and 0.8% respectively. This moves the compressor operating point slightly closer to the 78% efficiency loop, the actual efficiency increasing only marginally. The compressor operating point is also shown in Fig. 6.2.

6.2.4 Discussion.

The errors in predicting the compressor operating lines, for constant engine speeds, discussed in section 5.4, can be explained by errors in the flow resistances of the by-pass and exhaust system ducting. The restriction caused by the by-pass valve/diluting chamber flow area (see section 4.8.1) has been ignored in the simulation model, while the orifice areas A_{04} and A_{05}, have been calculated and the coefficients of discharge estimated. Only flow tests for the actual by-pass system will enable a more accurate estimate of the by-pass system flow resistances, or effective flow areas, to be calculated.

It has been shown in the previous sections that the compressor operation is more sensitive to changes in the flow resistance of the by-pass system than to changes in the exhaust system. It was therefore decided to leave the areas, A_{04} and A_{05}, at their original values and accept that there may be some errors in the calculation of the by-pass system mass flow rates. Without additional data, a better estimate of the flow areas can only be obtained by trial and error, i.e. comparing the engine performance predicted over the load and speed range with the test data, using different values of A_{04} and A_{05}. The flow areas could then have been adjusted to achieve the best possible correlation between the experimental and predicted pressures in the various control volumes. However, because of the pulsating nature of the pressures (particularly in the exhaust manifold) the accuracy of such a procedure would be subject to some doubt. In addition, it was not possible to measure the by-pass, or engine, mass flow rates to verify the accuracy of the model.

6.3 Effect of the By-Pass Valve Area Ratio.

6.3.1 Introduction.

The steady state pressure drop across the by-pass valve depends upon the guage boost pressure and the valve area ratio, for a fixed valve inclination, eqn. (4.157). For a given valve pressure ratio and upstream conditions, the mass flow rate across the by-pass valve is proportional to the valve area, eqn. (4.162). The by-pass valve area ratio therefore controls both the flow rate through the by-pass system and the engine scavenge pressure drop.

The effect of the valve area ratio, A_2/A_1, on the engine performance has been investigated. The valve area ratio has been reduced from the standard value of 0.09 by increasing the head diameter, D_1, and by reducing the stem diameter, D_2, see Fig. 4.33. The valve mass, m, and damping coefficient, λ, have been held constant at the values established in section 4.7, and the valve is assumed to be mounted with its axis horizontal, so that the effects of gravity are neglected.

The influence of the damping chamber jet size could possibly be simulated by varying the value of the damping coefficient, λ. This has not been investigated, because insufficient experimental data was available to establish a reliable correlation between the jet size and the damping coefficient.

The valve position, x, will obviously be influenced by the choice of head diameter, D_1, and coefficient of discharge, c_d. Increasing the value of c_d for a given geometry will tend to make the valve close (i.e. x will reduce) to maintain the same effective flow area. Similarly increasing D_1 will also make the valve close for a given A_2/A_1. Therefore, unless the valve is fully open, changing the coefficient of discharge will only result in a change in the valve position, x, and consequently c_d has been held constant. In practice, c_d will vary with the valve displacement, x, and the pressure ratio, p_3/p_2, but insufficient test data was available to establish a reliable correlation between these parameters, see section 4.7.

6.3.2 Effect of Reducing the By-Pass Valve Area Ratio.

The effect of varying the by-pass valve area ratio, A_2/A_1, and consequently the by-pass valve characteristics and engine pressure drop, was investigated at the rated engine power, 2400 rpm/17.09 bar BMEP (nominal). This operating condition has a high compressor pressure ratio and flow, and a low by-pass flow ratio.

The by-pass valve area ratio, see Fig. 4.33, can be reduced in the following ways, by:-

(1) increasing the valve head diameter, D_1,

(2) reducing the valve stem diameter, D_2,

(3) a combination of (1) and (2).

Providing that the valve is operating correctly, there should be no difference to the engine performance whichever of these options is chosen, for a given valve area ratio.

The by-pass valve area ratio has been reduced from the standard value of 0.09, to 0.06 and 0.03. For the case of $A_2/A_1=0.06$ the valve area ratio was changed by:-

(1) increasing the head diameter and area, D_1 and A_1, and

(2) reducing the valve stem diameter and area, D_2 and A_2,

and for the case of $A_2/A_1=0.03$, the stem diameter and area were reduced only.

The effect of reducing the by-pass valve area ratio on the overall engine performance can be seen in Fig. 6.3. As A_2/A_1 is reduced, by reducing the valve stem diameter and area, the following observations can be made:-

(1) The engine BMEP reduces by 1.8% when A_2/A_1 is reduced from 0.09 to 0.03, due mainly to the increase in pumping work caused by the reduction in the pressure drop across the engine. There is also some effect on the

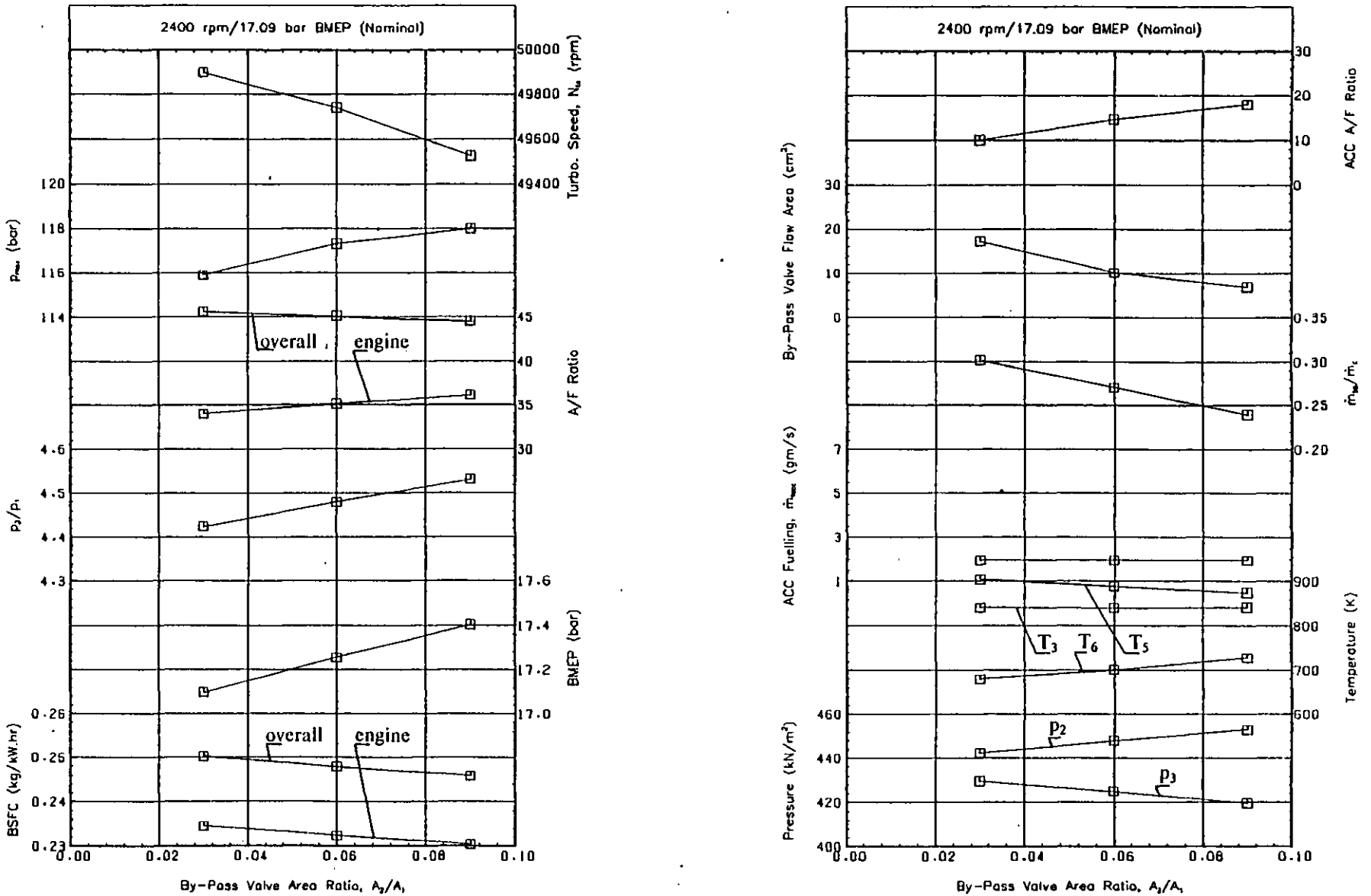

Fig. 6.3 Effect of the By-Pass Valve Area Ratio on the Overall Engine Performance at 2400 rpm/17.09 bar BMEP (Nominal).

engine combustion, due to the lower boost pressure level, and consequently longer ignition delay and increased premixed burning.

(2) The engine fuelling has been held constant for these tests, and the ACC burner is held in the idle position by the high boost pressure. Consequently both the engine and total BSFC are inversely proportional to the BMEP, and increase by 1.8% as the by-pass valve area ratio reduces to 0.03.

(3) The by-pass air flow must increase as the valve area ratio reduces, to reduce the pressure drop across the by-pass system. With $A_2/A_1=0.09$, 23.9% of the total compressor flow goes through the by-pass system, while with $A_2/A_1=0.03$ this has increased to 30.2%.

(4) The engine air flow rate reduces by 5.9% as A_2/A_1 is reduced from 0.09 to 0.03 due to the reduction in compressor delivery pressure, and consequently the engine A/F ratio reduces and the exhaust manifold gas temperature, T_5, increases by 30 K.

(5) The total compressor flow increases by 2.5% despite the drop in the compressor pressure ratio, p_2/p_1. Therefore the operating point on the compressor map moves to the right, away from the surge line, see Fig. 6.4. The increase in compressor flow results in an increase in the overall A/F ratio, but the turbine inlet temperature, T_3, does not change significantly.

(6) The compressor pressure ratio falls from 4.53 to 4.43 resulting in a reduction in the inlet manifold pressure and consequently in the maximum cylinder pressure (of 2.9 bar). The exhaust system pressure increases due to the action of the by-pass valve. Because of the increase in turbine inlet pressure of 10.0 kN/m^2, and the relatively small change in the mixer temperature, the turbine avaliable energy increases, this results in an increase in the turbocharger speed of 0.7%, but a reduction in the compressor pressure ratio. The compressor operating point moves to a less efficient point on the map as it moves away from the surge line, the efficiency falling from 75.4% to 72.8%.

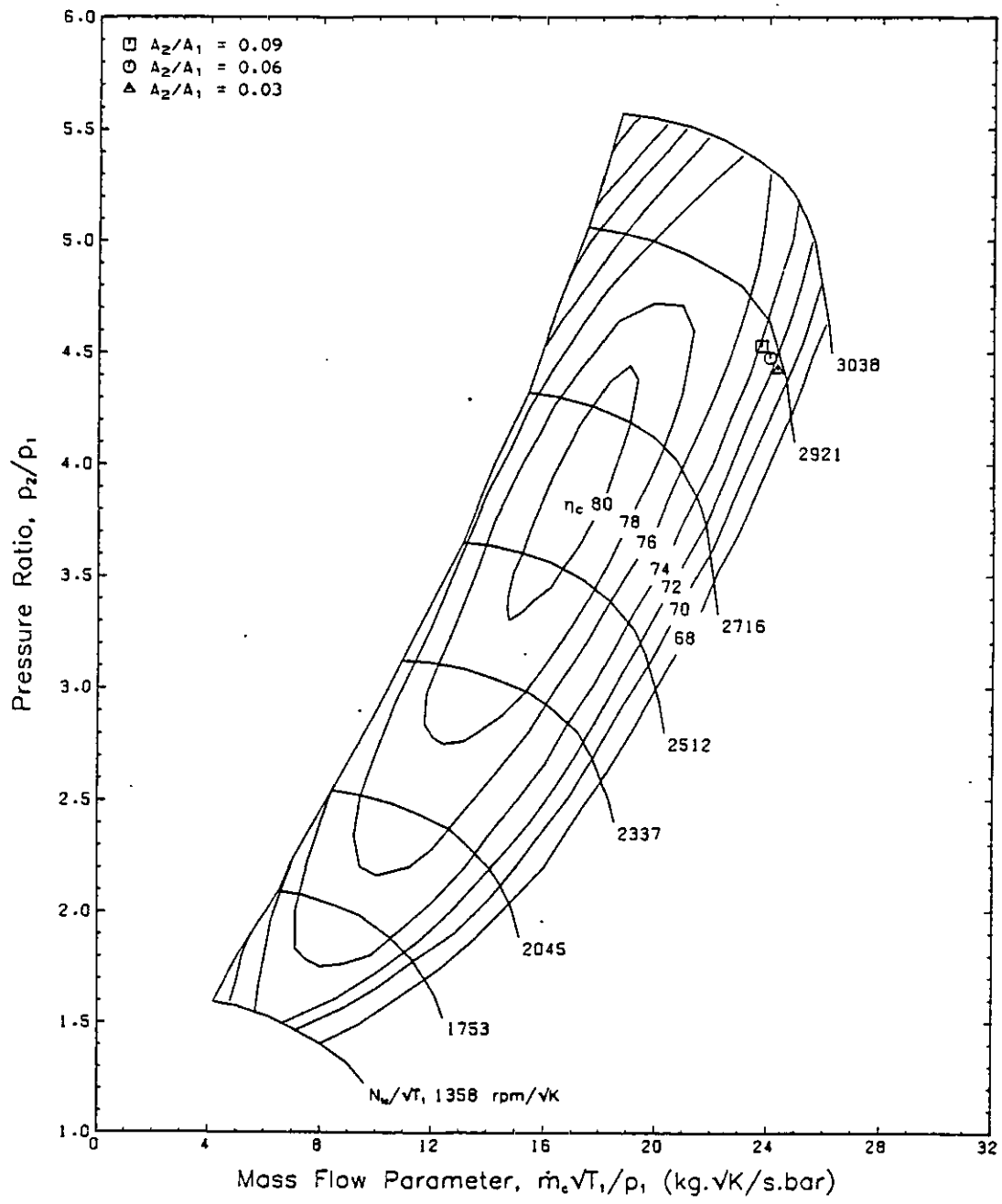

Fig. 6.4 Effect of the By-Pass Valve Area Ratio on the Compressor Operation at 2400 rpm/17.09 bar BMEP (Nominal).

(7) The by-pass valve controls the pressure drop between the compressor delivery and the ACC/diluting chamber. Extrapolating the pressures in Fig. 6.3 to the case where $A_2/A_1=0$ (i.e. the valve is fully open causing no restriction) shows that the ACC/diluting chamber pressure will be equal to the compressor delivery pressure. The exhaust manifold pressure is higher than the ACC pressure, and at a by-pass valve area ratio of approximately 0.05 becomes equal to the inlet manifold pressure. Further reduction in valve area ratio causes the engine to be counter scavenged, because of the negative pressure drop. With a by-pass valve area ratio of 0.03, the mean exhaust manifold pressure is 6.3 kN/m^2 above the inlet pressure.

(8) As the by-pass flow increases, the overall by-pass A/F ratio increases (because the fuelling rate is constant). Consequently the ACC gas temperature, T_6, reduces by 47 K for a change in A_2/A_1 from 0.09 to 0.03, and there is a greater proportion of lower temperature gas from the by-pass entering the mixer. This is compensated for somewhat by a smaller proportion of higher temperature gas (by 30 K) from the engine exhaust manifold.

(9) The by-pass valve opens to increase the flow area, and consequently reduce the pressure drop, the effective area increasing by 148.5%. The reduced pressure drop across the ACC ports, together with the lower density upstream (compressor delivery) conditions, result in less air flow through the ACC ports, and a consequent reduction in the actual ACC A/F ratio from 17.97 to 9.96. However, the greater air flow through the by-pass valve into the ACC/diluting chamber more than compensates for this, see item (8), the overall by-pass A/F ratio increasing from 169.7 to 219.2.

Fig. 6.5 shows the predicted by-pass system performance for A_2/A_1 values of 0.09, 0.06 and 0.03 respectively, and clearly shows the changes in the valve pressure drop, valve displacement and effective flow area, mass flow rate through the ACC and by-pass valve, and the ACC displacement and fuelling (which do not change because the boost pressure is high enough to maintain the ACC at idle).

The effect of reducing the by-pass valve area ratio, A_2/A_1, by increasing the head diameter, D_1, and area, A_1, to give an area ratio of 0.06 was also investigated. The

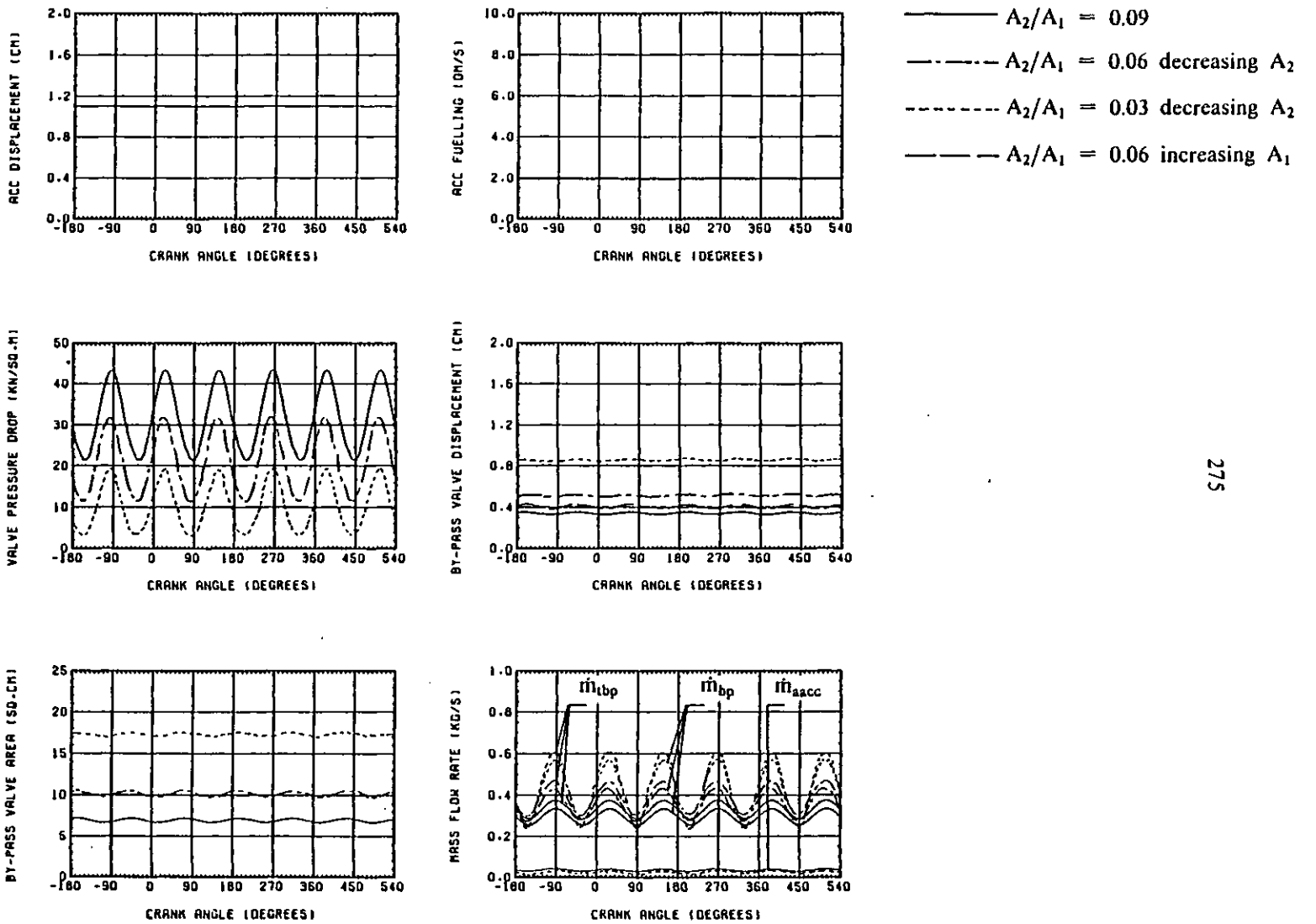

Fig. 6.5 Effect of the By-Pass Valve Area Ratio on the Hyperbar System Performance at 2400 rpm/17.09 bar BMEP (Nominal).

overall performance results were identical to the case described above, where the area ratio was reduced by reducing the stem diameter and area. However, the valve displacement was smaller, with the larger valve head diameter, giving the same effective flow area. Fig. 6.5 also shows the by-pass characteristics for the case where A_1 and D_1 were increased.

6.3.3 Discussion.

As the by-pass valve area ratio is reduced, there are two important effects on the engine and turbocharger performance:-

(1) The scavenge pressure drop across the engine reduces, increasing the engine pumping work.

(2) The total compressor flow increases, despite the reduction in pressure ratio.

At high loads and speeds the engine benefits from having a larger by-pass valve area ratio, which gives better scavenging, a higher engine A/F ratio, greater positive pumping work and consequently lower engine and total BSFC. The compressor operates closer to surge and, depending on the match, in a higher efficiency region of the compressor map.

Conversely at the low speeds and loads a large by-pass valve pressure drop (area ratio) cannot be sustained without burning extra fuel in the ACC to supply the required turbine energy. The extra ACC fuelling will increase the total BSFC by a far greater amount than any reduction due to increased positive pumping work, with a larger A_2/A_1, and consequently the thermal efficiency of the engine will reduce.

At low boost pressures, p_2, the scavenge pressure drop, (p_2-p_3), including the pressure drop across the charge cooler (which will be small at low engine air flow rates), will not benefit greatly by increasing A_2/A_1. The engine scavenging is not so important because the engine A/F ratio is relatively high at idling conditions, so a low value of valve area ratio is desirable. The choice of the valve area ratio will therefore be a compromise, for the fixed geometry system described.

The by-pass valve area ratio will also dictate the shape, and positioning of the operating line on the compressor map, which further constrains the range of values of A_2/A_1 that can be used. Increasing the by-pass valve area ratio, reduces the by-pass flow and so moves the compressor operating line closer to the engine operating line (and also closer to the surge line). This restricts the maximum speed that the engine can run at without ACC burner assistance to maintain the required pressure drop. As it is undesirable to use the burner at high speeds, except at very low loads, or possibly to increase the engine A/F ratio, the speed limit of the engine together with the compressor and turbine match must also be taken into account.

The by-pass valve area ratio, A_2/A_1, of 0.09, used on this engine, appears to work well, except at high engine speeds where the engine and compressor flows are nearly equal, and the by-pass valve can no longer control the engine pressure drop. Some deviation of the actual by-pass valve operation from the ideal must also be taken into consideration, see section 5.2, and allowances must be made for wear, etc. when selecting a suitable valve arrangement.

It has been shown in section 3.3.4 that the effective valve area ratio can be altered while the engine is running by the use of a suitable control system. So for a fixed geometry by-pass valve the scavenge pressure drop can be controlled by varying the control pressure, p_0. However, some method of regulating p_0 is required to give the desired scavenge pressure drop characteristics and best overall fuel consumption. This is discussed in the following sections.

6.4 Changing the By-Pass Valve Geometry by Varying the Control Pressure.

6.4.1 Introduction.

It has been shown that the compressor operating line can be positioned on the map by varying the geometry and/or inclination of the by-pass valve. However, once the geometry of the by-pass system is decided upon, the compressor operating line is fixed. Obviously the operating line should be positioned on the compressor map so that the compressor is working at the highest possible efficiency over the load and speed range of the engine.

In most cases, for a given geometry, the compressor operating line will not coincide exactly with the peak efficiency line on the compressor map. This can be seen in Fig. 5.7. It is, however, possible to modify the shape of the compressor operating line to optimise the compressor efficiency, by varying the by-pass valve control pressure.

6.4.2 Effect of Varying the By-Pass Valve Control Pressure.

The geometry of the by-pass valve is shown diagramatically in Fig. 4.33. Assuming that it is mounted horizontally, the steady state form of the equation of motion for the valve can be written, from eqn. (4.152), as:-

$$(p_2 - p_3).A_1 - (p_2 - p_1).A_2 + (p_0 - p_1).A_3 = 0 \qquad (6.1)$$

In order to simplify the analysis the damping piston will not be considered, so that:-

$$A_3 = A_2 \qquad (6.2)$$

eqn. (6.1) then becomes:-

$$\frac{(p_2 - p_3)}{(p_2 - p_0)} = \frac{A_2}{A_1} \qquad (6.3)$$

where,

p_0 = by-pass valve control pressure (kN/m^2)

Fig. 6.6 shows the effect of the control pressure, p_0, on the by-pass system pressure drop, (p_2-p_3), for various different compressor delivery pressures, p_2, and a fixed geometry by-pass valve ($A_2/A_1=0.09$). The way in which the control pressure can be changed to give a variable geometry effect to the by-pass system is shown in Fig. 6.7. If the control pressure is greater than the ambient pressure, p_1, then the by-pass valve will open further, which will increase the by-pass system flow (and therefore the compressor flow) and reduce the pressure drop across the by-pass system. Reducing the control pressure below ambient has the opposite effect, causing an increase in the effective valve area ratio and by-pass system pressure drop, and a corresponding reduction in the by-pass system air flow. Obviously the air flow rate through the ACC

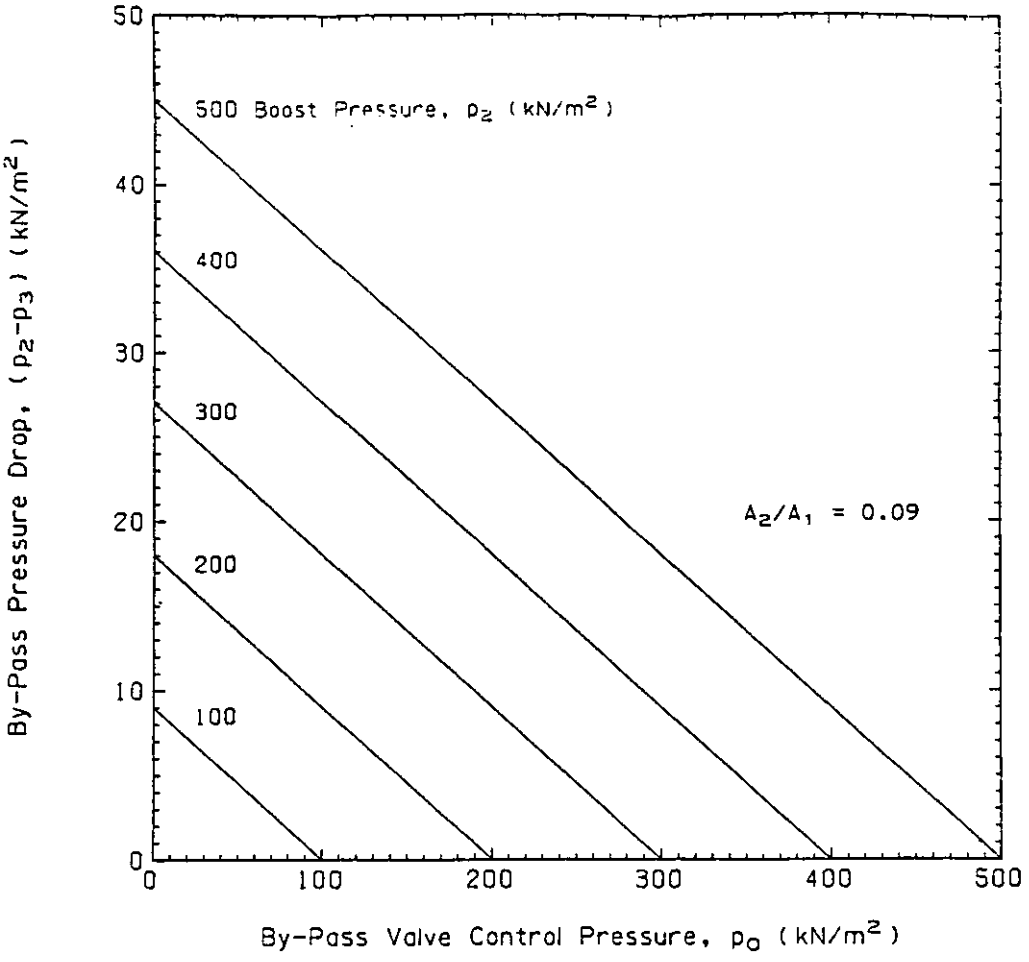

Fig. 6.6 Effect of the By-Pass Valve Control Pressure p_0 on the By-Pass Pressure Drop.

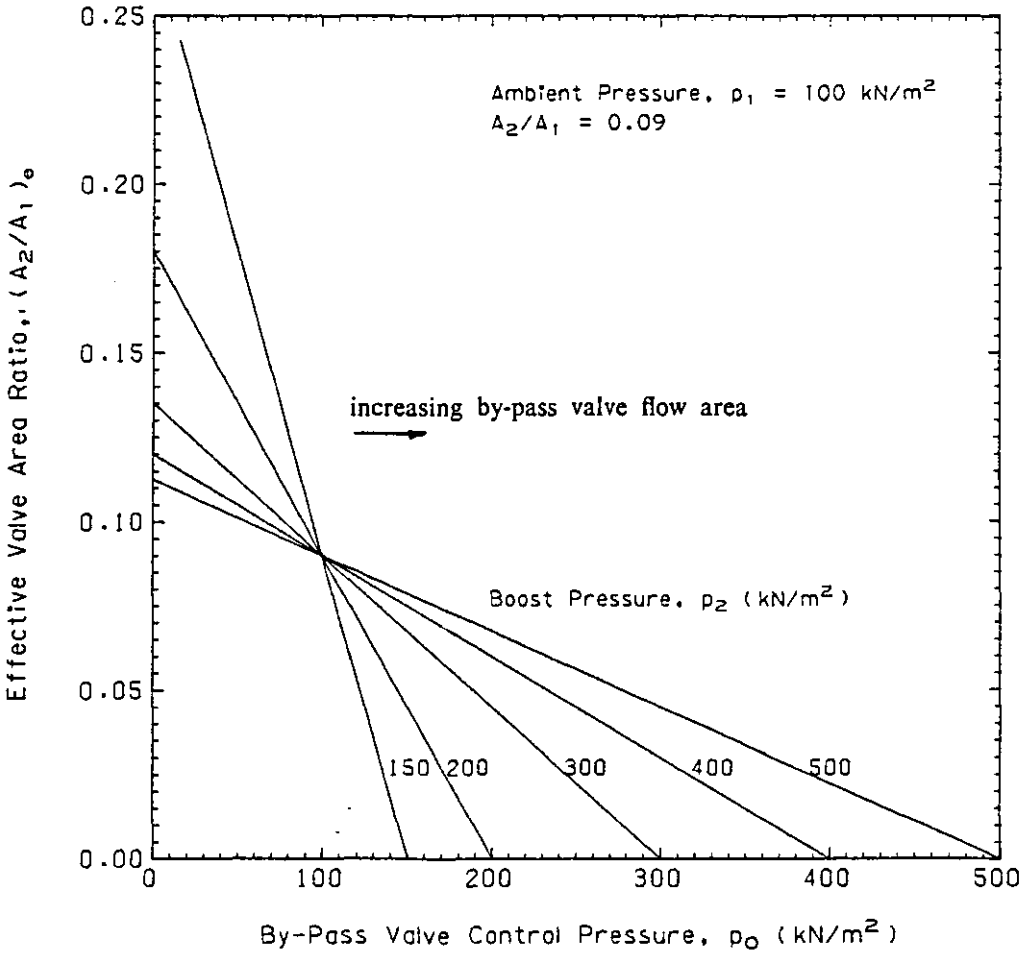

Fig. 6.7 Effect of the By-Pass Valve Control Pressure p_0 on the Effective Valve Area Ratio.

ports will be affected by changes in the pressure drop across the by-pass system, and this will effectively limit the changes that can be made to the geometry of the by-pass system.

6.4.3 Effect of the By-Pass Valve Control Pressure on the Engine Performance.

Fig. 6.8 shows the predicted compressor operating point at 2000 rpm/18.97 bar BMEP (nominal) with the control pressure set to ambient, $p_0 = 100$ kN/m^2. Comparing this operating point with the line of best compressor efficiency, shows that the mass flow rate is too high for this compressor, and there is a corresponding drop in compressor efficiency from the optimum value of 80.5% (at this pressure ratio) to 76.6%.

In order to improve the compressor efficiency the by-pass flow must be reduced. In this particular example, the total compressor flow is 16.5% higher than the optimum flow at a pressure ratio of 3.90. At this condition 8.3% of the total by-pass flow passes through the ACC ports and 91.7% through the valve. The by-pass system flow represents 30.4% of the total compressor flow.

If the compressor operating point is to be optimised to give the peak compressor efficiency at this pressure ratio, the by-pass valve effective area must be reduced from 9.0 cm^2 to approximately 4.4 cm^2. Closing the by-pass valve will result in an increase in the pressure drop across the ACC ports, and a consequent increase in the ACC air flow, but this is a relatively small percentage of the total by-pass flow. Fig. 6.9 shows the effect on the engine and turbocharging system performance of reducing the control pressure from 100 kN/m^2 to 0 kN/m^2 (a vacuum). The effect on the compressor operating point is shown in Fig. 6.8. The results are similar to those described in the previous section for changes in the by-pass valve area ratio.

Reducing the control pressure, p_0, causes the by-pass valve to close, which increases the pressure drop across the by-pass system and reduces the air flow rate through it. The effective valve area ratio increases from 0.090 with $p_0 = 100$ kN/m^2 (ambient) to 0.105 with p_0 reduced to 50 kN/m^2 and 0.120 with $p_0 = 0$ kN/m^2. The increased pressure drop across the engine causes a small improvement in the pumping work, and hence a rise in the BMEP, with a corresponding reduction in both the engine and overall BSFC of 0.7%, over the range of control pressures tested.

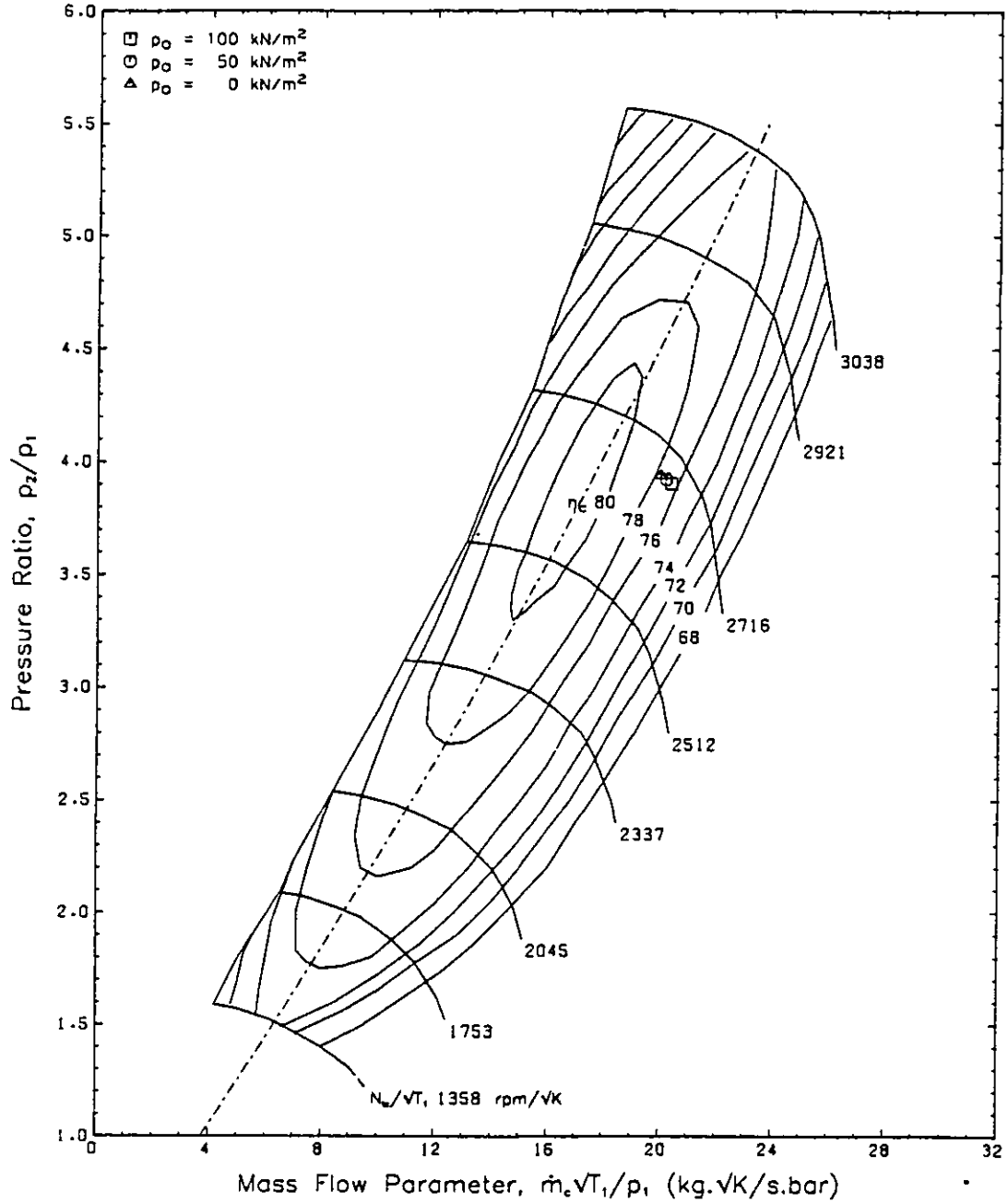

Fig. 6.8 Effect of the By-Pass Valve Control Pressure on the Compressor Operation at 2000 rpm/18.97 bar BMEP (Nominal).

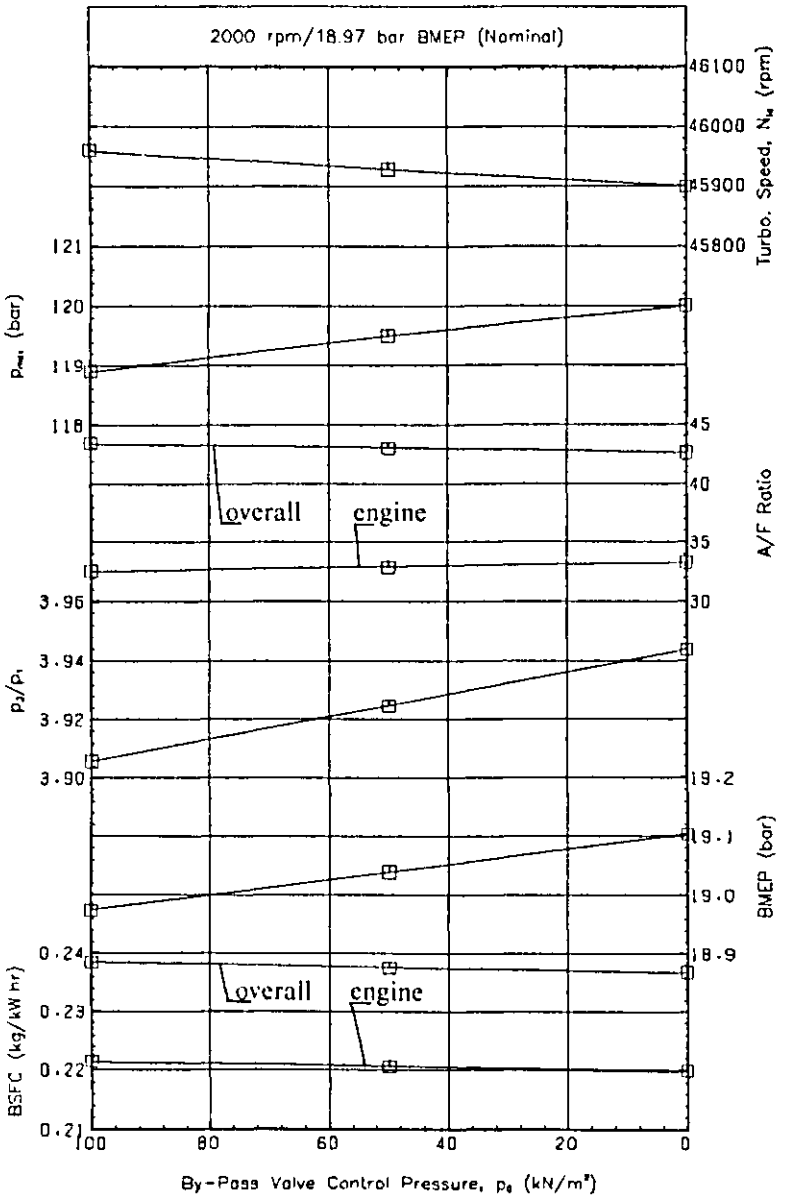

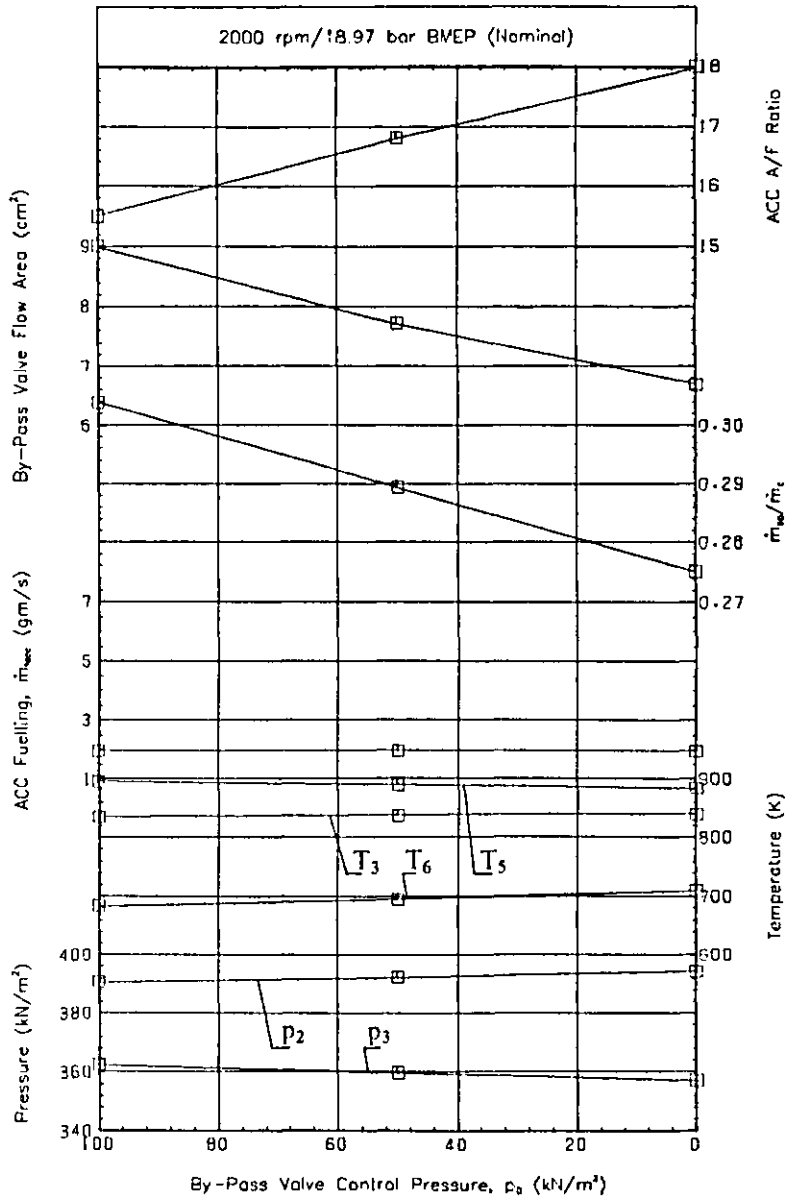

Fig. 6.9 Effect of the By-Pass Valve Control Pressure on the Overall Engine Performance at 2000 rpm/18.97 bar BMEP (Nominal).

The compressor flow reduces by only 1.9% with the minimum control pressure, partly because of the increase in compressor pressure ratio and engine air flow. The engine A/F ratio increases by 2.2%, which reduces the exhaust manifold gas temperature by 11 K. The overall A/F ratio reduces from 43.4 to 42.6 because of the drop in compressor flow and the constant engine and ACC fuelling rates.

The maximum cylinder pressure increases with the increase in boost pressure, caused by the reduction in the control pressure, and the turbocharger speed reduces slightly.

The increase in the pressure drop across the ACC ports results in an increase in the ACC A/F ratio from 15.5, with $p_0=100$ kN/m^2, to 18.0 with $p_0=0$ kN/m^2, (the upstream pressure is also higher), but the overall by-pass system flow reduces, because of the smaller valve area, and so the overall by-pass A/F ratio reduces from 185.2 to 164.5. This results in an increase in the ACC gas temperature of 25 K. The by-pass flow ratio reduces from 30.4% to 27.5%.

The turbine efficiency does not change significantly, despite the drop in the inlet pressure.

6.4.4 Discussion.

The tests described in the previous section show that the by-pass valve control pressure can be used to modify the compressor operating line, but that the effect is very small. In this example, because the operating point was to the right of the optimum operating point (at a higher mass flow rate), it was necessary to reduce the control pressure below ambient. Even using a perfect vacuum on the control side of the by-pass valve will not reduce the compressor flow enough to achieve the optimum compressor efficiency. It is also undesirable to have pressures below ambient on the control side for purely practical reasons.

A better solution would be to rematch the compressor so that the optimum compressor efficiency line is always slightly to the right of the actual operating line (with the control pressure at ambient). In this case the compressor flow must be increased, and this can be achieved by opening the by-pass valve, i.e. by increasing the control

pressure above ambient, see Fig. 6.7. A simple pressure regulating device could then be used to vary the control pressure, p_0. However, this solution also poses some problems. In this case, the compressor is normally operating very close to surge (i.e. to the left of the highest efficiency line) and the control pressure is raised to increase the compressor air flow rate. A failure in the control system may cause the compressor to surge (particularly if the surge margin is very small), which is totally unacceptable.

If the complete by-pass valve system, shown in Fig. 4.33, is considered, then the damping piston can be used to amplify the influence of the control pressure, p_0. The steady state form of eqn. (4.152) can be written as:-

$$(p_2 - p_3) = (p_2 - p_1).\frac{A_2}{A_1} - (p_0 - p_1).\frac{A_3}{A_1} \qquad (6.4)$$

where,

A_3/A_1 = damping piston area ratio.

Fig. 6.10 shows the influence of the damping piston area ratio, A_3/A_1, the compressor delivery pressure, p_2, and the by-pass valve control pressure, p_0, on the by-pass system pressure drop, (p_2-p_3).

For a given control pressure, p_0, (above the ambient pressure, p_1) and boost pressure, p_2, increasing the damping piston area ratio, A_3/A_1, causes a considerable reduction in the valve pressure drop, and an increase in the by-pass and compressor flow rates. Therefore, the damping piston can be used to achieve the desired change in compressor flow without having to resort to very high or low control pressures, p_0. This system has the additional advantage that the control pressure can be applied to either side of the damping piston, depending upon the compressor match. It may also be possible to improve the compressor operating efficiency by simply rematching the compressor (in this case increasing the size of the compressor build). But the by-pass characteristics may still require some modification to match the compressor operating line to the peak efficiency line.

In all the examples discussed so far the by-pass valve position and effective flow area are regulated pneumatically. An alternative solution is to vary the valve position

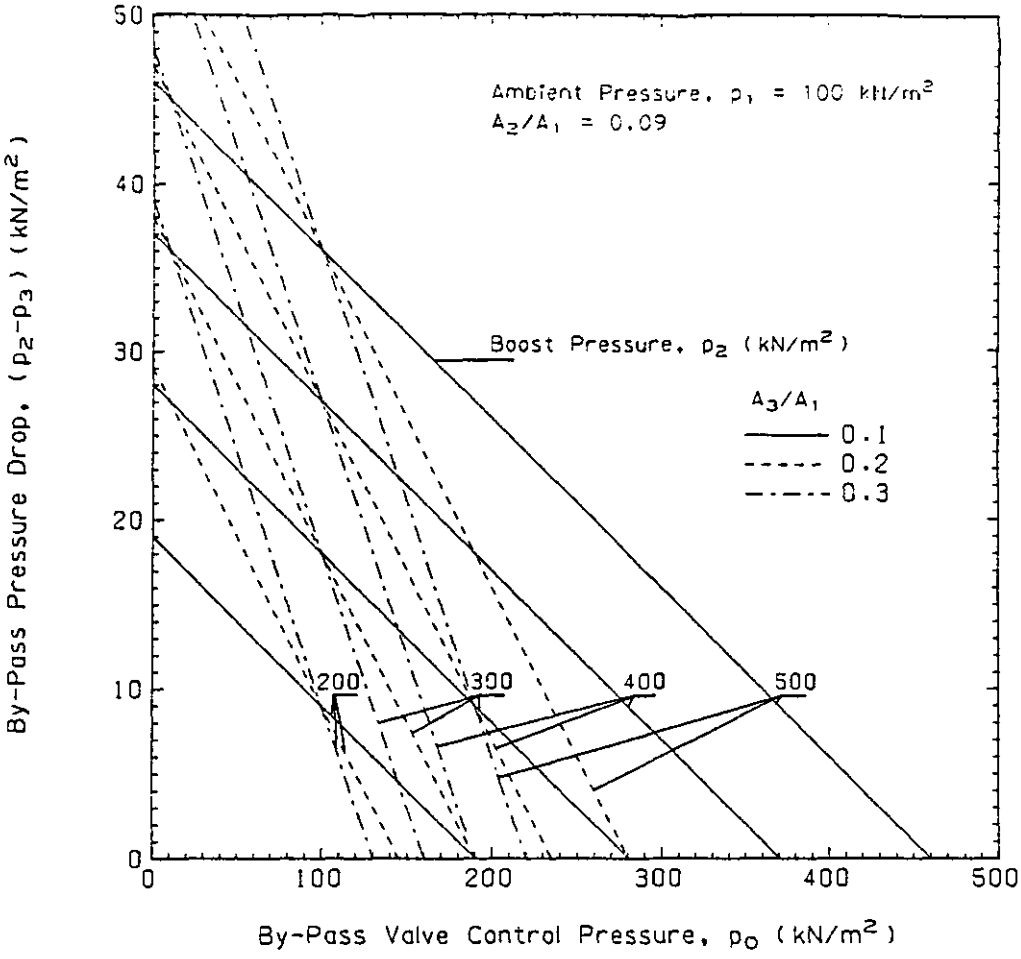

Fig. 6.10 Effect of the By-Pass Control Pressure p_0 and the Damping Piston Area Ratio A_3/A_1 on the By-Pass Pressure Drop.

mechanically, and to use pressure, temperature and flow sensors to supply signals to an actuator, which controls the valve position. This alternative will be discussed in Chapter 8.

6.5 The Auxiliary Combustion Chamber.

6.5.1 Introduction.

Fig. 4.45 shows the various forces acting on the ACC controlling its position, and therefore the air and fuel flows. Assuming that the geometry of the ACC is fixed then its position. is controlled by:-

(1) The initial spring preload, F_o.

(2) The spring rate, k.

(3) The fuel control pressure, p_f.

(4) The air control pressure, p_c.

(5) The ACC chamber pressure, p_{acc}.

Of these parameters it is only possible to vary items (1) to (4) directly, while the ACC chamber pressure, item (5), is largely determined by the boost pressure and the by-pass valve area ratio, the steady state position of the ACC being given by eqn. (4.172).

It is obvious that p_f, p_c and F_o all have a similar influence on the ACC position, so for instance, increasing p_f by an amount, Δ, will have the same effect as increasing p_c by $(\Delta.A_4/A_5)$, or increasing F_o by $(\Delta.A_4)$. It was therefore decided that only the fuel control pressure, p_f, should be varied to control the ACC, and that p_c and F_o should be held constant.

The spring rate, k, controls the range of boost pressures over which the ACC operates between maximum and minimum fuelling. The higher the value of k, the larger the

range of boost pressure over which the ACC will operate, see Fig. 4.54. For these tests the spring rate has been maintained constant, at the measured value.

The relationship between the ACC displacement, x, and the effective flow area is given in section 4.8.7.3, however the ACC flow geometry can easily be varied, if required, to change the proportion of the by-pass flow that goes through the ACC ports. This can result in less control over the pressure drop by the by-pass valve in some circumstances.

The possible variations in ACC fuelling rate with boost pressure are shown diagramatically in Fig. 6.11. This characteristic can be varied by simply altering the input fuelling versus displacement data and/or the relevant control parameters. The following variations from the standard data have been considered:-

(1) Reducing the minimum fuelling level.

(2) Increasing the maximum fuelling level.

(3) Changing the fuel control pressure, p_f.

(4) Changing the spring rate, k.

(5) Holding the ACC at maximum fuelling regardless of the boost pressure.

Of these parameters, the effect of items (1) and (3) are discussed in the following sections. The effect of holding the ACC on maximum fuelling during a transient, item (5), is discussed in section 7.3.3. Under normal conditions, the maximum fuelling supplied by the burner, item (2), is sufficient for this engine, and an increase in this level would only be required to achieve very high BMEP's (in excess of 30 bar) at low engine speeds (provided that the thermal and mechanical loading limits of the system are not exceeded). The spring rate, k, item (4), only regulates the control over the minimum boost pressure level, and this is discussed in section 6.8.2.

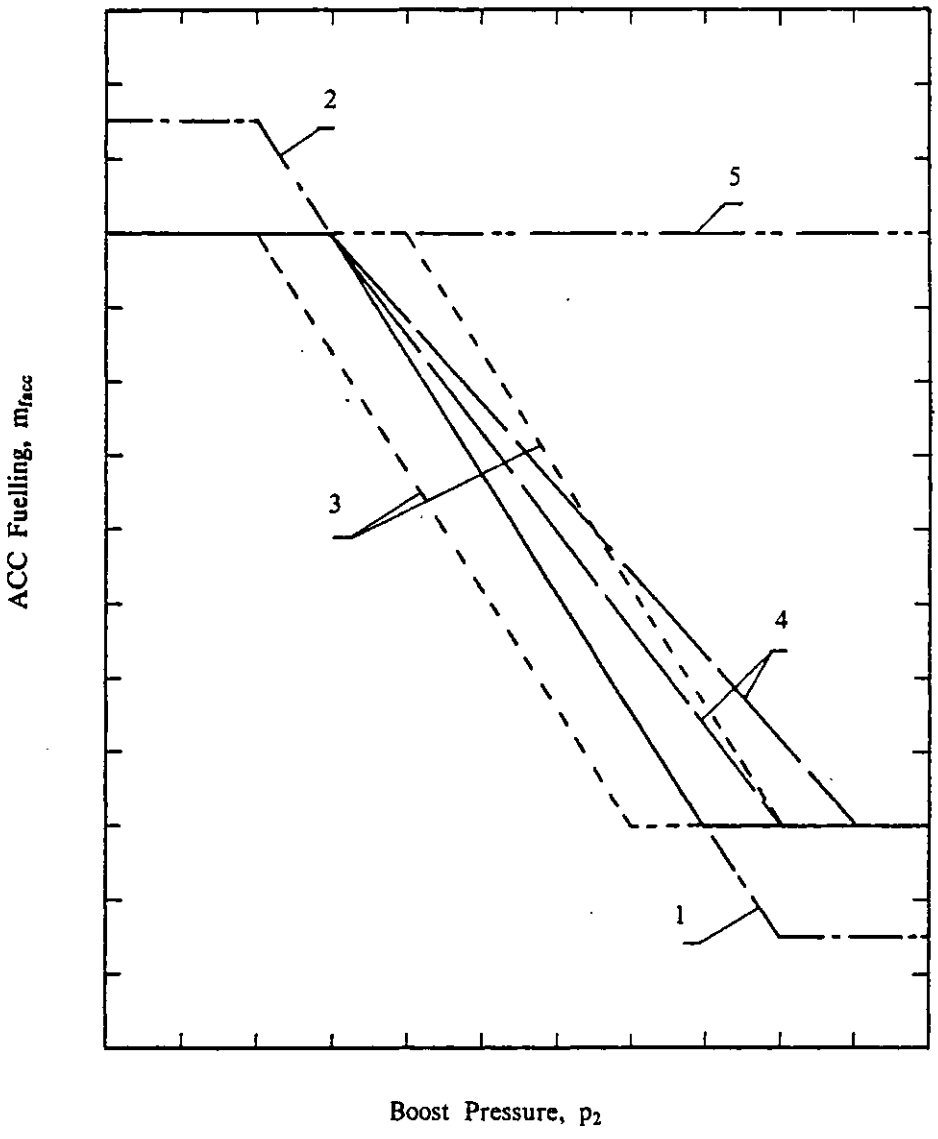

Fig. 6.11 Possible Variations in the ACC Fuelling Characteristics.

6.5.2 Effect of Reducing the Auxiliary Combustion Chamber Minimum Fuelling.

The effect of reducing the ACC minimum fuelling rate on the overall engine performance was investigated at 2400 rpm/17.09 bar BMEP (nominal). At this operating condition the boost pressure is sufficiently high to maintain the ACC at its maximum displacement, and therefore the burner is idling. The ACC fuelling versus displacement characteristics are given in Fig. 4.47. The minimum fuelling was reduced in two steps, from the standard rate of 1.953 gm/s, to 1.0 gm/s and finally 0 gm/s (i.e. if the boost is sufficiently high the burner fuelling is cut off completely).

The effect of these reductions in ACC minimum fuelling on the engine and turbocharging system performance can be seen in Fig. 6.12. As the ACC fuelling is reduced the turbine energy reduces and the compressor pressure ratio falls from 4.53 to 4.18 (with zero ACC fuelling). This results in a reduction in the total air flow through the system of 6.6%, when the ACC fuelling is reduced from 1.953 gm/s to 0 gm/s. The reduction in boost pressure causes a reduction in engine A/F ratio (because the engine fuelling remains constant) of 6.4%, and a corresponding increase in the exhaust gas temperature of 23 K. The peak cylinder pressure falls by 5.7 bar as the boost pressure reduces with lower ACC fuelling rates, but the effect on the BMEP is small, -0.5%. Because the engine BMEP remains substantially constant, the engine BSFC remains constant, but the total BSFC reduces in proportion to the reduction in the ACC fuelling, causing an improvement in total BSFC of 5.8%, with zero ACC fuelling.

As the ACC fuelling reduces, the gas temperature in the burner falls, becoming approximately equal to the compressor delivery temperature when the fuelling is cut off completely, (there is some heat transfer from the ACC and reverse flow from the mixer). This reduction in by-pass gas temperature more than compensates for the increase in exhaust manifold gas temperature (even at this high speed, where the by-pass flow ratio is low) and consequently the turbine inlet (mixer) temperature falls by 35 K. This effect would be more pronounced at lower engine speeds, where the by-pass to compressor flow ratio is higher. The pressures in the ACC, exhaust manifold and mixer reduce as the boost pressure falls, due to the action of the by-pass valve.

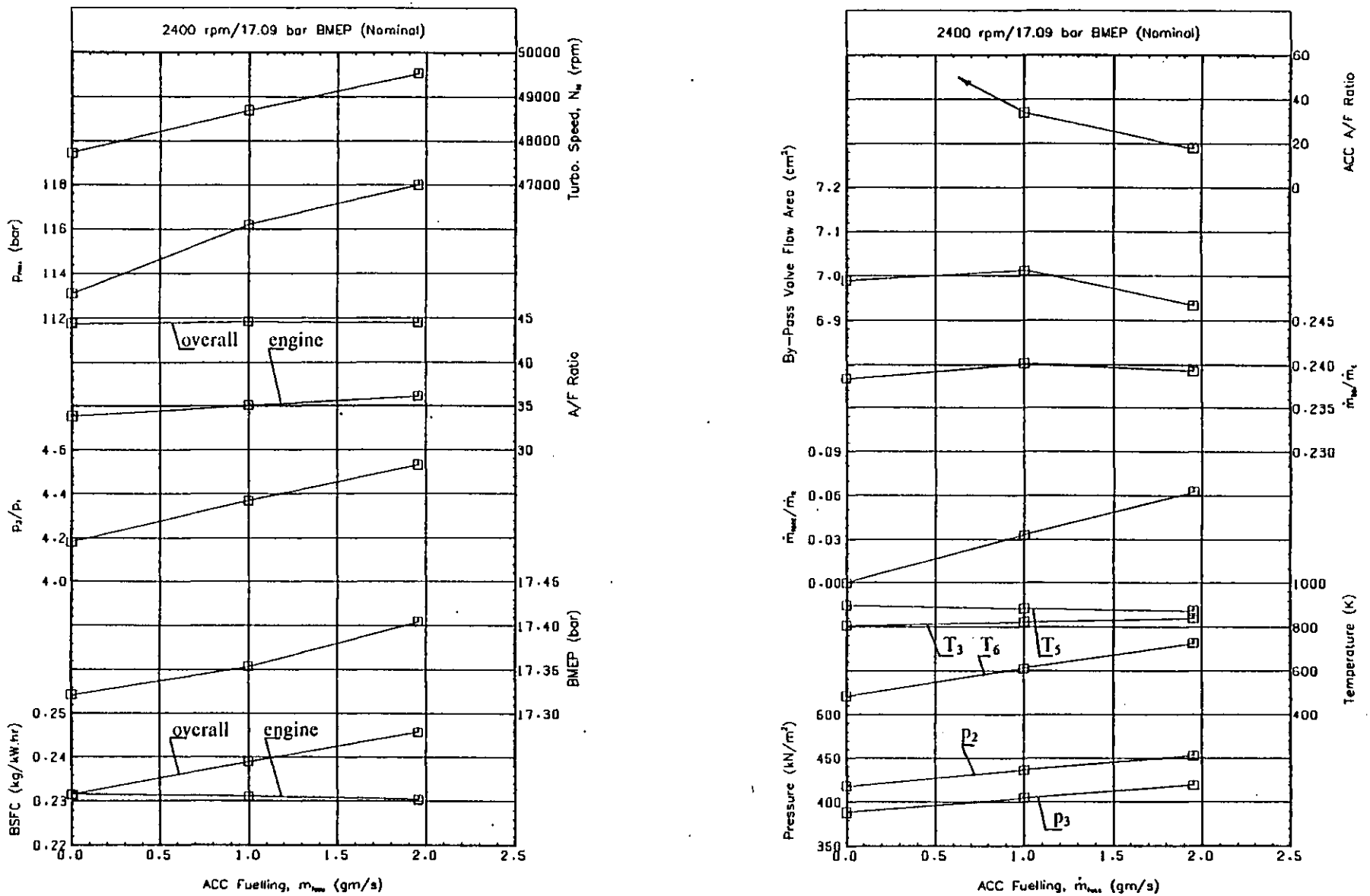

Fig. 6.12 Effect of the Minimum ACC Fuelling Level on the Overall Engine Performance at 2400 rpm/17.09 bar BMEP (Nominal).

Fig. 6.13 shows the effect of reducing the ACC minimum fuelling rate on the performance of the by-pass valve and ACC. The by-pass valve opens slightly as the ACC fuelling reduces, the effective flow area increasing by 0.8% as the fuelling reduces to zero. The by-pass valve characteristic is such that, as the boost pressure falls so the pressure drop across the by-pass system also reduces, eqn. (4.157), and so the valve flow area must increase to reduce the flow resistance across the by-pass system. The proportion of the total flow that goes through the by-pass system stays almost constant at 24%, but the proportion of the by-pass flow that actually goes into the combustion chamber, through the ACC ports, reduces from 10.6% to 10.5% as the by-pass valve flow area increases. The ACC A/F ratio increases from 18.0, with the standard fuelling, to 33.9 with 1.0 gm/s, and infinity with zero ACC fuelling.

Fig. 6.14 shows the effect of reducing the ACC minimum fuelling rate on the compressor operating point at 2400 rpm/17.09 bar BMEP (nominal). The reduction in boost pressure, turbocharger speed and air flow rate can clearly be seen. The change in the predicted compressor efficiency is negligible (approximately +0.1%).

6.5.3 Effect of the Auxiliary Combustion Chamber Fuel Control Pressure.

By varying the fuel control pressure, p_f, the relationship between the ACC displacement, x, and the boost pressure, p_2, can be modified, eqn. (4.172). Lowering the fuel control pressure increases the ACC displacement, x, for a given boost pressure, and therefore reduces the ACC fuelling, within the limits of the ACC travel.

The effect of lowering the ACC fuel control pressure from 1100 kN/m^2 to 866 kN/m^2 and 632 kN/m^2 has been investigated. The engine operating conditions chosen for this test was 800 rpm/1.24 bar BMEP (nominal). At this condition the engine exhaust energy is low and therefore the burner must be used to ensure that the boost pressure does not fall below the minimum design value.

Fig. 6.15 shows the fuelling versus boost pressure relationships for the three fuel control pressures investigated. As the fuel control pressure is reduced, it can be seen that a lower boost pressure is reached before the burner starts to increase the ACC fuelling, and the exhaust gas energy level. The minimum boost pressure level will therefore fall. All these tests have been performed with the standard by-pass valve and

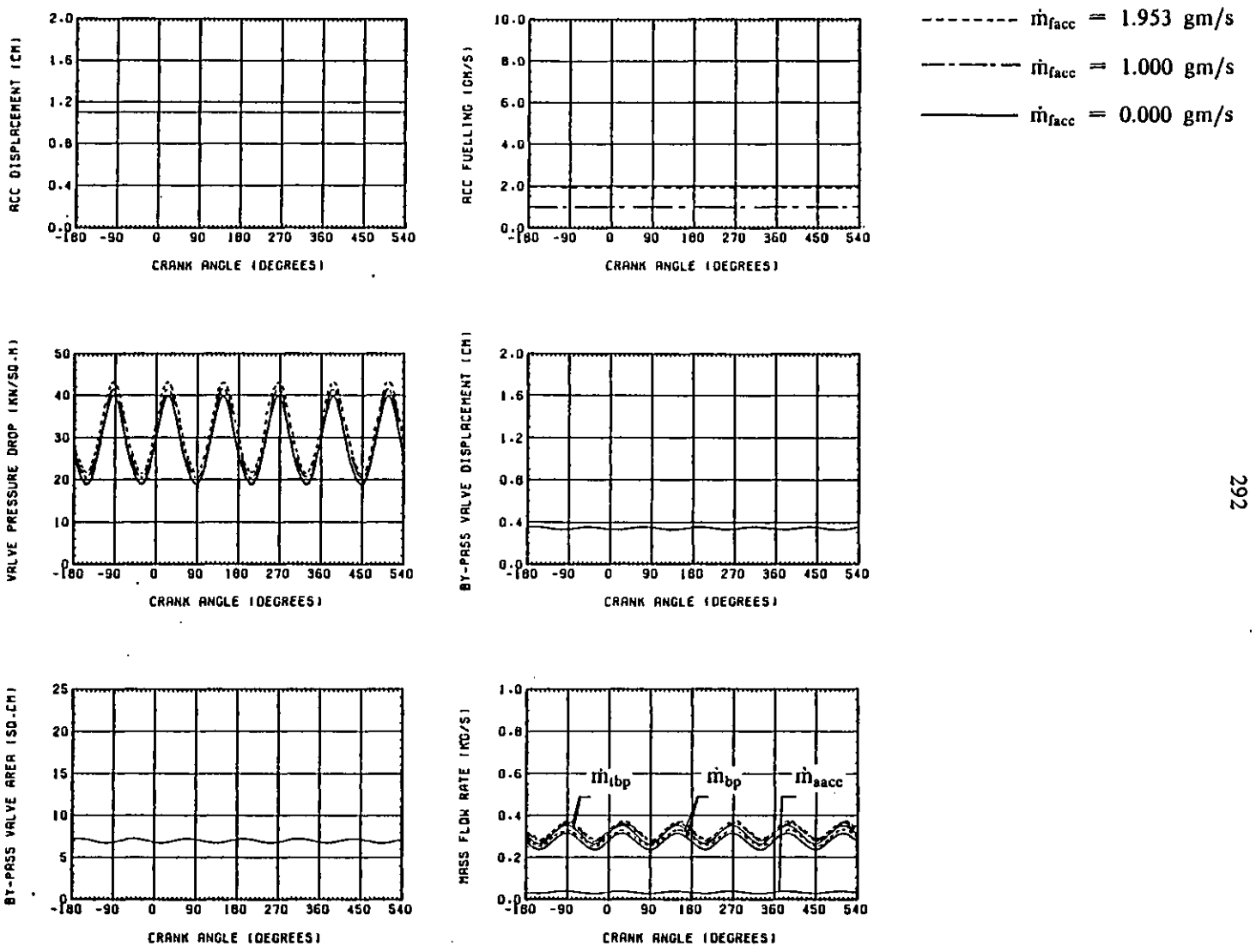

Fig. 6.13 Effect of the Minimum ACC Fuelling Level on the Hyperbar System Performance at 2400 rpm/17.09 bar BMEP (Nominal).

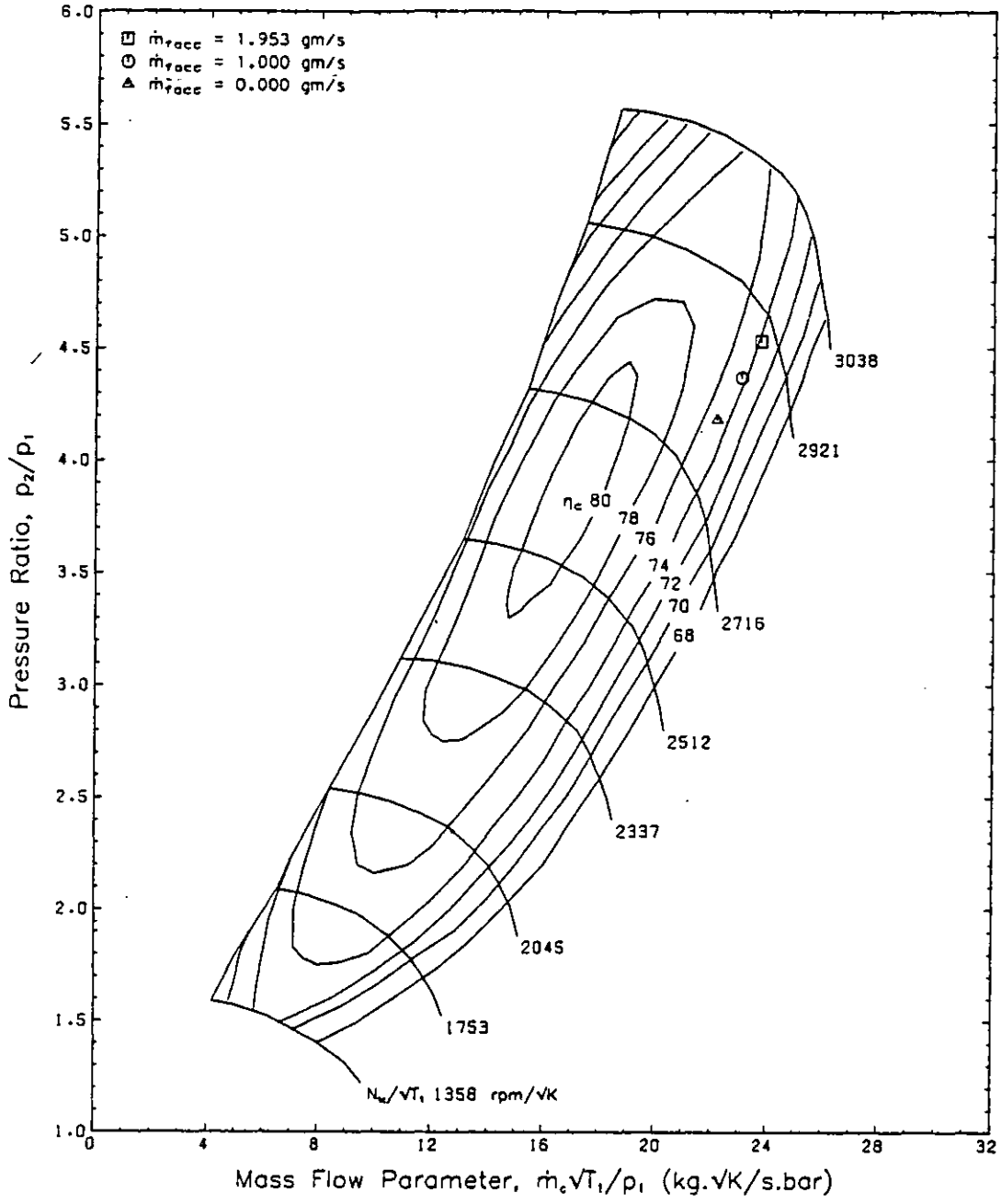

Fig. 6.14 Effect of the Minimum ACC Fuelling Level on the Compressor Operation at 2400 rpm/17.09 bar BMEP (Nominal).

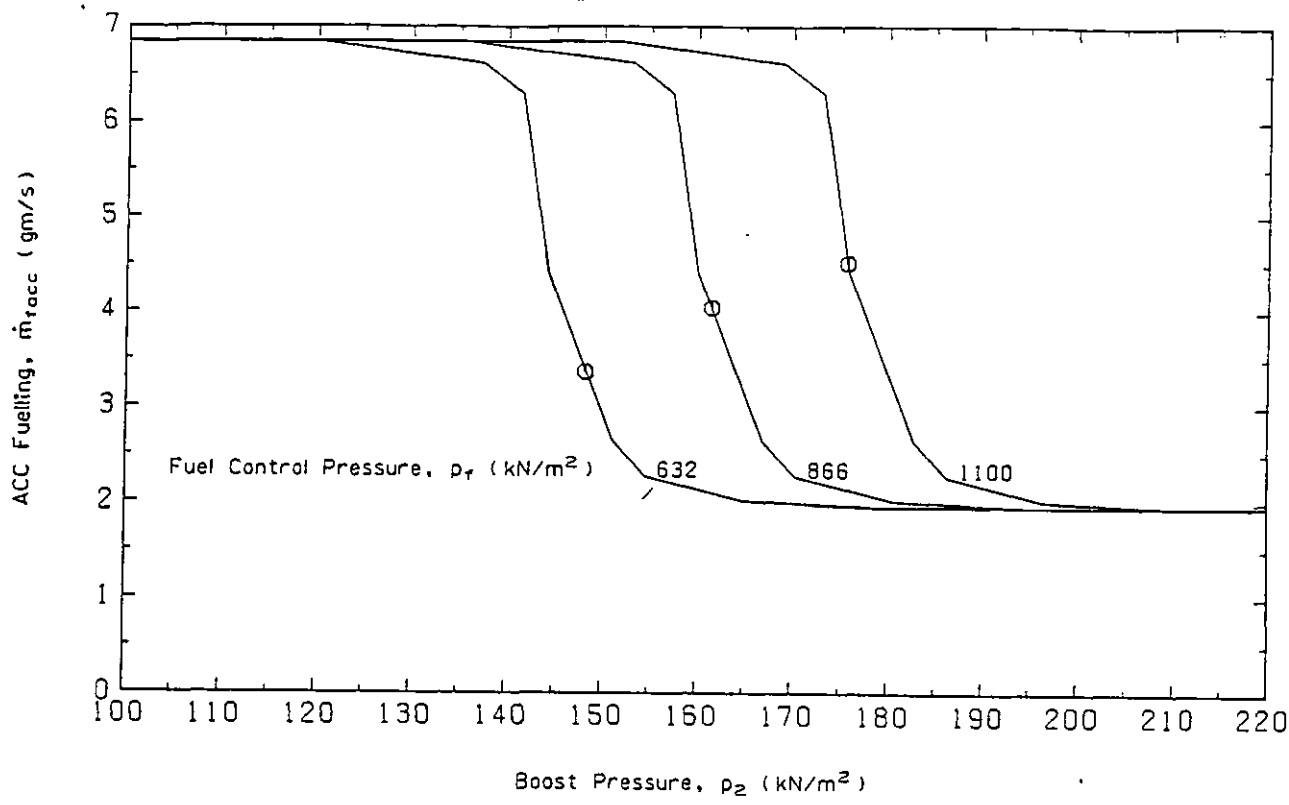

Fig. 6.15 Effect of the ACC Fuel Control Pressure.

ACC geometry, only the fuel control pressure has been varied.

Fig. 6.16 shows the effect of reducing the ACC fuel control pressure on the predicted engine and turbocharging system performance. The boost pressure drops almost linearly with the reduction in p_f, the compressor pressure ratio reducing from 1.76 to 1.48 when p_f was reduced from 1100 kN/m^2 to 632 kN/m^2. This causes a reduction in the inlet manifold pressure, and therefore the engine A/F ratio of 16.8% (the engine fuelling being held constant). The exhaust manifold gas temperature increases by 13 K as the engine A/F ratio reduces, (at this low load condition the engine A/F ratio is very high, and so the change in exhaust gas temperature is relatively small). The engine BMEP increases by 3.5% as p_f is reduced to 632 kN/m^2 and consequently the engine BSFC reduces in proportion. As the boost pressure falls, so the engine pumping work reduces, because of the action of the by-pass valve reducing the scavenge pressure drop, but this is offset by the effect of the changes in engine A/F ratio and increasing ignition delay on combustion. The ignition delay increases from 11.1°CA to 13.2°CA as the boost pressure falls. The maximum cylinder pressure reduces from 44.0 bar to 36.2 bar, causing a reduction in the FMEP of 3.8%, and retards from 4°CA ATDC to 9°CA ATDC. The operating points on the compressor map can be seen in Fig. 6.17. This shows the reduction in boost pressure, turbocharger speed, air flow rate and compressor efficiency as the operating point moves away from the high efficiency region of the map.

Fig. 6.18 shows the effect of the fuel control pressure on the performance of the by-pass valve and ACC burner. At this speed and load, the ACC will move according to the fluctuations in the ACC gas pressure, which are in turn affected by the exhaust pressure pulses. Fig. 6.18 clearly shows how small fluctuations in the ACC displacement can cause significant pulsations in the ACC fuelling. The ACC fuelling can be seen to fall as the displacement increases, with reduced fuel control pressure. This fall in ACC fuelling results in a reduction in the total engine fuelling, and an improvement in the total BSFC, in addition to that caused by the increase in BMEP. This amounts to a reduction in total BSFC of 23.6% when p_f is reduced from 1100 kN/m^2 to 632 kN/m^2. This effect is comparatively large because at this low load condition the ACC fuelling is a large proportion of the total fuelling (81.9% for p_f=1100 kN/m^2). The effect of the drop in ACC fuelling and reducing total air flow on the overall A/F ratio is small, falling from 86.4 to 85.5. The turbine inlet (mixer) temperature reduces slightly, by 25 K, as the ACC fuelling is reduced, as does the

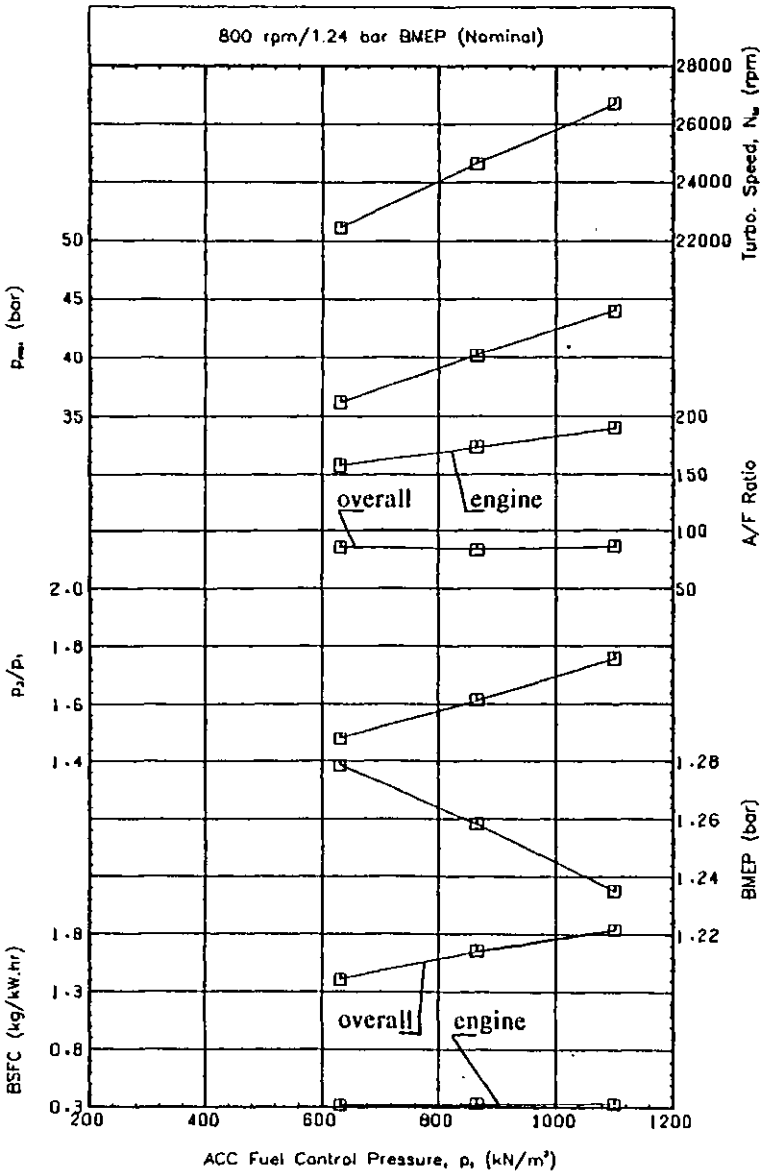

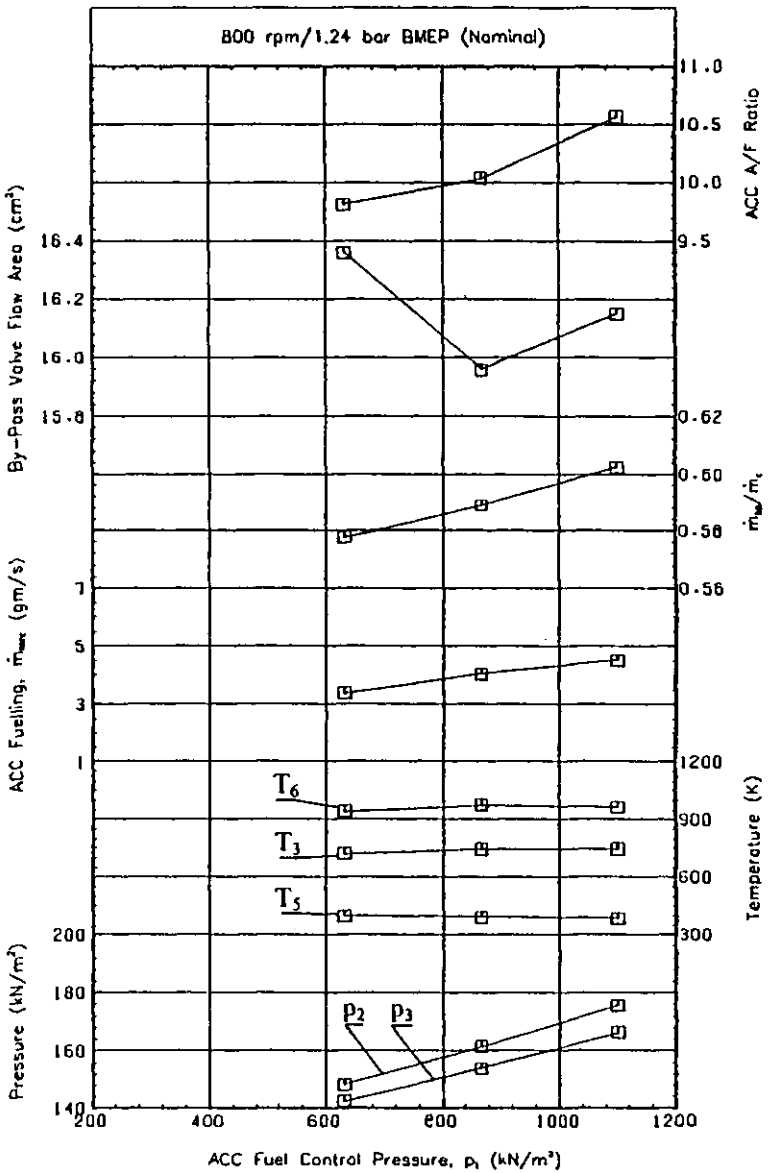

Fig. 6.16 Effect of the ACC Fuel Control Pressure on the Overall Engine Performance at 800 rpm/1.24 bar BMEP (Nominal).

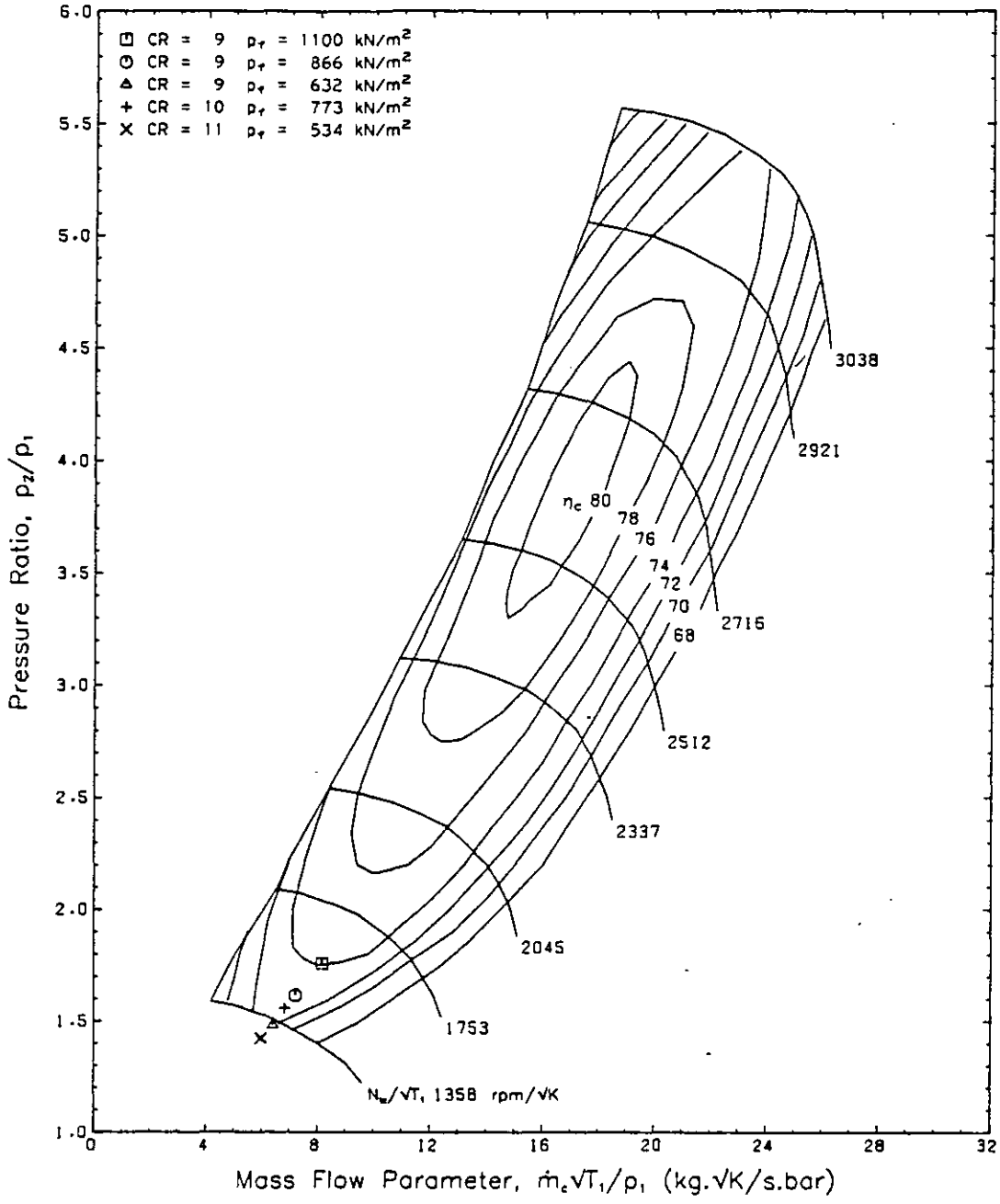

Fig. 6.17 Effect of the ACC Fuel Control Pressure on the Compressor Operation at 800 rpm/1.24 bar BMEP (Nominal).

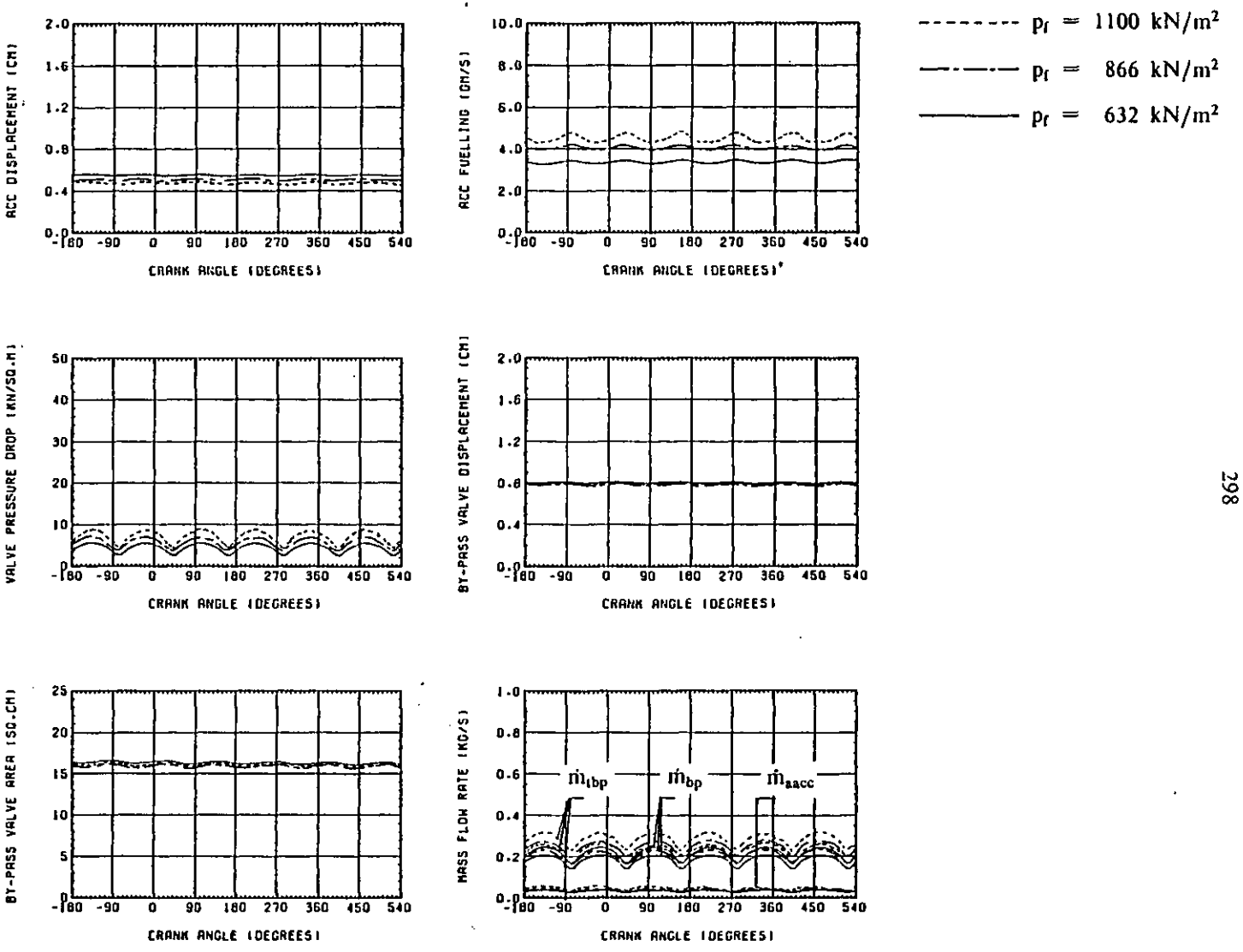

Fig. 6.18 Effect of the ACC Fuel Control Pressure on the Hyperbar System Performance at 800 rpm/1.24 bar BMEP (Nominal).

gas temperature in the ACC, by 24 K. The mean ACC fuelling versus boost pressure points for the three fuel control pressures investigated are also shown in Fig. 6.15.

The by-pass valve effective flow area does not vary significantly to maintain the scavenge pressure ratio at 0.09, because the by-pass flow reduces as the boost pressure falls. The proportion of by-pass flow to total compressor flow reduces from 60.2% to 57.8%, with p_f=632 kN/m^2, and the ACC A/F ratio actually falls from 10.6 to 9.8 as the fuel control pressure reduces. When the fuel control pressure is reduced, the ACC displacement increases, and the fuelling and ACC port areas reduce. The pressure ratio across the ACC ports reduces, as does the upstream air density, as p_f is reduced, and because of the ACC port area and fuel flow characteristics, the air flow reduces faster than the fuel flow, and so the A/F ratio falls.

6.5.4 Discussion.

The main purpose of the ACC burner at high engine loads is to ensure that the boost pressure and air flow rates are high enough to maintain a realistic engine A/F ratio (and therefore reasonable exhaust gas temperatures) at high engine fuellings. If the boost pressure is sufficiently high (greater than approximately 2 bar, for the standard system) then the ACC operates with the burner idling, unless very large loads are required.

With the burner idling, the contribution of the fuel burnt in the exhaust system to the turbine energy is usually small. This contribution reduces as the engine speed reduces (because the overall by-pass air flow increases and hence the temperature rise created by the ACC fuelling diminishes), while the proportion of the total fuelling used by the burner increases as the engine load reduces.

Therefore, if it is physically possible, some gain in overall engine BSFC will result if the burner idling fuelling rate can be reduced to zero. The main problem appears to be maintaining a stable flame in the ACC with a large range of fuel flow rates. If the burner fuelling is reduced to zero, then it must ignite reliably when required. If the boost pressure is low enough to be on the border between the fuelling being "on" or "off", then engine operating changes may result in the burner switching "on" and "off" at high frequency, but this will depend upon the design of the control system

employed.

Any reduction in the ACC minimum fuelling rate will, however, result in a proportional reduction in the total BSFC, and is worth pursuing if the engine is operating for long periods at low speeds and medium loads, where the ratio of the idling burner fuelling to total fuelling is highest.

At very low loads the ACC fuelling increases to maintain the desired boost level necessary to ensure that ignition occurs in the engine cylinders with the low geometric compression ratio. The ACC fuelling is therefore a large proportion of the total engine fuelling (in this example as much as 80%). Any reduction in the ACC fuelling will therefore cause a proportional benefit in total BSFC. However, a low engine compression ratio is required in order to limit the engine mechanical loading at high engine speeds and loads, and ignition problems may occur at low loads if a minimum boost pressure level is not maintained. Any reduction in the fuel control pressure, must therefore be accompanied by an increase in the air pressure and/or temperature in the cylinder when the fuel is injected, to ensure that ignition will occur reliably. The cylinder pressure (and temperature) can be raised by increasing the compression ratio, while the temperature can be increased by by-passing the charge cooler and/or heating the charge air, either by recirculating some of the exhaust gas into the inlet manifold, or burning extra fuel in the induction system.

Burning extra fuel in the inlet manifold to raise the charge temperature at low loads is practical, but requires a control system to operate the burner and the igniter which must respond to changes in charge temperature. The effect on engine BSFC is obvious, and the deterioration will be more significant in the case of the Hyperbar system which normally runs at high engine A/F ratio's.

There are also problems with recirculating exhaust gas into the inlet manifold to raise the charge temperature, due to the operation of the by-pass valve. The valve maintains the boost pressure higher than the exhaust pressure to give a constant scavenge pressure drop ratio. Taking into account the pressure loss through the charge cooler, any recirculation of exhaust gas is only possible when the exhaust system pressure is higher than the inlet manifold pressure. Such a system has been designed and built for this engine, the recirculation valve being controlled by the inlet manifold temperature using exhaust gas taken from the turbine inlet, however no test results

were available at the time of writing.

The charge cooler can also be by-passed at low speeds and loads, which gives a direct, though limited, increase in the inlet air temperature, and also a small increase in the inlet pressure, because the pressure loss through the charge cooler is no longer present. For example, at this test condition, 800 rpm/1.24 bar BMEP, with the fuel control pressure at 1100 kN/m^2, an increase in the charge temperature of 52 K could be achieved using a charge cooler by-pass. The volume of the induction system is also effectively reduced (by 48.8% for this engine), but such a system requires two control valves. During a transient the charge cooler could be continuously by-passed which will result in a more rapid build up in the inlet manifold pressure, and hence the engine air flow (depending upon the increase in boost temperature, i.e. the compressor efficiency).

The benefits of reducing the minimum boost pressure, by reducing the ACC fuelling (via a reduction in the ACC fuel control pressure), while maintaining the same ignition delay (by either increasing the engine compression ratio, increasing the charge temperature, or some combination of the two) are therefore worth investigating, because of the benefits in total BSFC that can be achieved at low loads and speeds. The reduction in the scavenge pressure drop with a lower boost pressure (because of the by-pass valve action) is not considered to be important at low loads, because the engine A/F ratio is high enough for scavenging and component temperatures to be acceptable.

While section 6.5.3 has been limited to a discussion of the effect of the fuel control pressure, p_f, a consideration of eqn. (4.172) shows that the same effects can be achieved by varying the initial spring force, F_o, the air control pressure, p_c, the various control areas in the ACC, A_4, A_5 and A_6, and the by-pass valve area ratio, A_2/A_1, because each influence the relationship between the boost pressure, p_2, and the ACC displacement, x. The fuel control pressure, p_f, has been used to illustrate the effects on the engine performance, because it is the parameter in eqn. (4.172) that is most easily varied in practice, (by using a simple pressure relief valve on the fuel control pressure outlet from the ACC). Other parameters require either design changes (such as A_4, A_5 and A_6) or extensive modifications to the system (e.g. to allow variations in F_o), or will effect other parts of the system (e.g. the valve area ratio, A_2/A_1). The relationship between the boost pressure and the ACC fuelling is also

influenced by the spring rate, k, which has been assumed to be constant, and of a fixed value. There is no reason why a variable rate spring (e.g. one wound from a tapered steel rod), could not be used.

6.6 Effect of Reducing the Minimum Boost Level and Increasing the Compression Ratio.

6.6.1 Introduction.

Section 6.5 clearly shows the improvement in total BSFC that can be achieved at low loads and speeds, by reducing the minimum boost pressure level. However, if the ACC fuelling characteristic is modified to maintain a lower minimum boost level, by reducing the ACC fuel control pressure, then some action must be taken to ensure that the appropriate conditions are maintained in the engine cylinders for ignition to occur. Of the alternatives discussed in section 6.5.4, the most promising is to increase the engine geometric compression ratio. This option has the additional advantage of increasing the thermodynamic efficiency of the cycle, by increasing the expansion ratio, without significantly reducing the engine air flow rate (but the exhaust pressure and temperature, and therefore the energy level, will reduce for a given A/F ratio). However, increasing the engine compression ratio will result in higher peak cylinder pressures, and hence mechanical loading, at high speeds and loads, unless some action is taken. This will be discussed further in section 6.7.

The effect of reducing the minimum boost level and increasing the engine compression ratio was investigated at the same low load condition used in section 6.5, i.e. 800 rpm/1.24 bar BMEP (nominal). As the engine compression ratio was raised from 9:1 to 10:1 and 11:1 the boost level was reduced accordingly to keep the ignition delay (and therefore the ignition point) as near as possible to that predicted with the standard ACC characteristics (i.e. 11.1°CA).

The duration of the predicted ignition delay is governed by the mean gas pressure and temperature in the cylinder during the delay, eqn. (4.41). The mean pressure, p_m, can be controlled by varying the boost pressure level and the engine compression ratio, but control of the mean temperature, T_m, is more difficult, this being a function of the compressor pressure ratio and efficiency, the charge cooler effectiveness and coolant

inlet temperature, the ambient temperature, the compression ratio, the scavenging efficiency, the heat transfer during the compression stroke (wall temperatures, mean piston velocity, gas pressure and temperature), etc. Therefore in order to estimate the amount that the boost pressure can be lowered, for a given increase in compression ratio, an attempt was made to match the mean pressure, p_m, during the ignition delay to that predicted with the standard geometry. The procedure, assuming isentropic compression up to the ignition point, is discussed in detail in Appendix A.

Having estimated the required inlet manifold pressure, $p_{2'}$, this was then related to the fuel control pressure, p_f. Fig. 6.19 shows a correlation between the compressor pressure ratio, p_2/p_1, and the fuel control pressure, p_f, obtained from the predictions discussed in section 6.5.3, at this engine speed and load. This correlation was used as a guide to estimate the appropriate value of p_f for a given engine compression ratio.

The best correlation between the fuel control pressure and the compressor pressure ratio at this test condition is given by:-

$$\frac{p_2}{p_1} = 1.11 + 5.88.10^{-4}.p_f \qquad (6.5)$$

where,

p_f = fuel control pressure (kN/m^2)

p_2/p_1 = compressor pressure ratio.

6.6.2 Effect of Increasing the Engine Compression Ratio.

The compression ratio was increased in two steps from the standard value of 9:1, to 10:1 and 11:1. Using the method described in Appendix A and eqn. (6.5) the ACC fuel control pressure was estimated to be 773 kN/m^2 with CR=10:1, and 534 kN/m^2 with CR=11:1, giving estimated compressor pressure ratio's, p_2/p_1, of 1.56 and 1.42 respectively, from eqn. (6.5). Fig. 6.20 shows the effect of increasing the compression ratio and reducing the minimum boost pressure level on the overall engine and turbocharging system performance.

With an increase in compression ratio to 10:1 and a reduction in p_f to 773 kN/m^2,

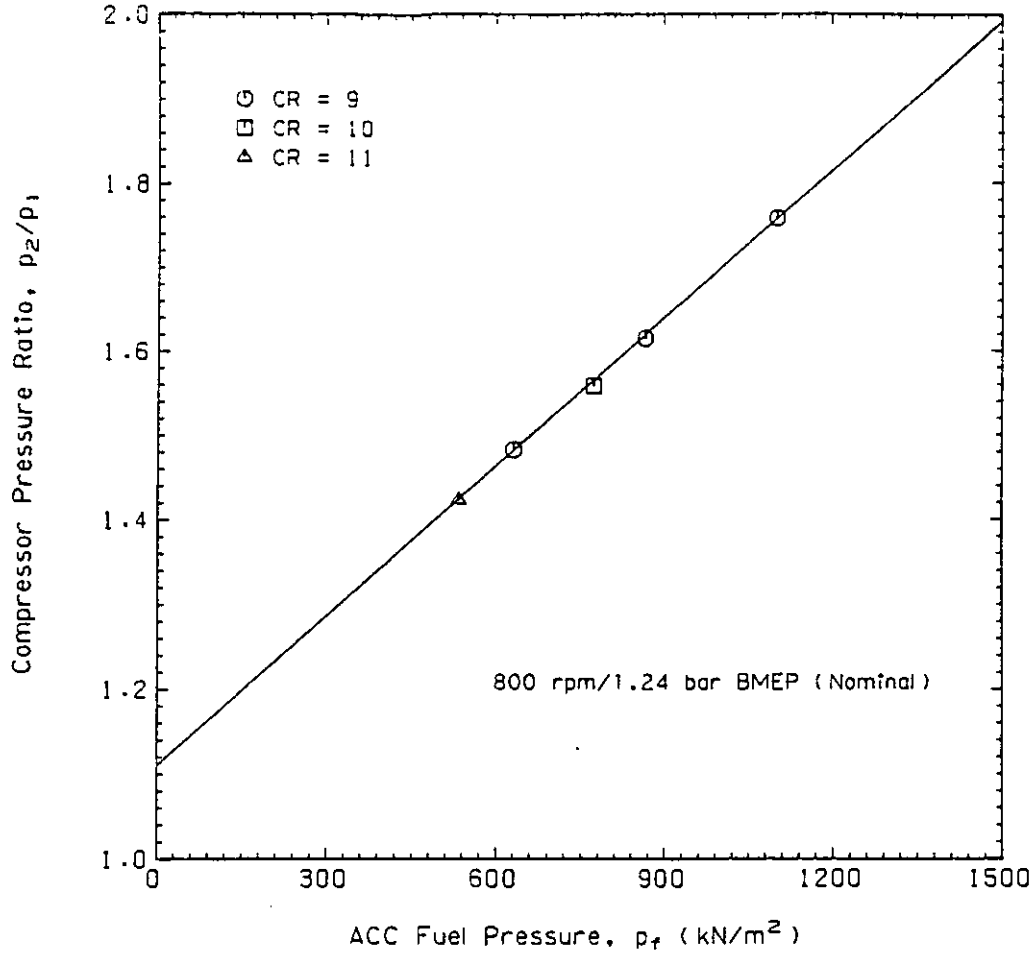

Fig. 6.19 Variation of Compressor Pressure Ratio with ACC Fuel Control Pressure.

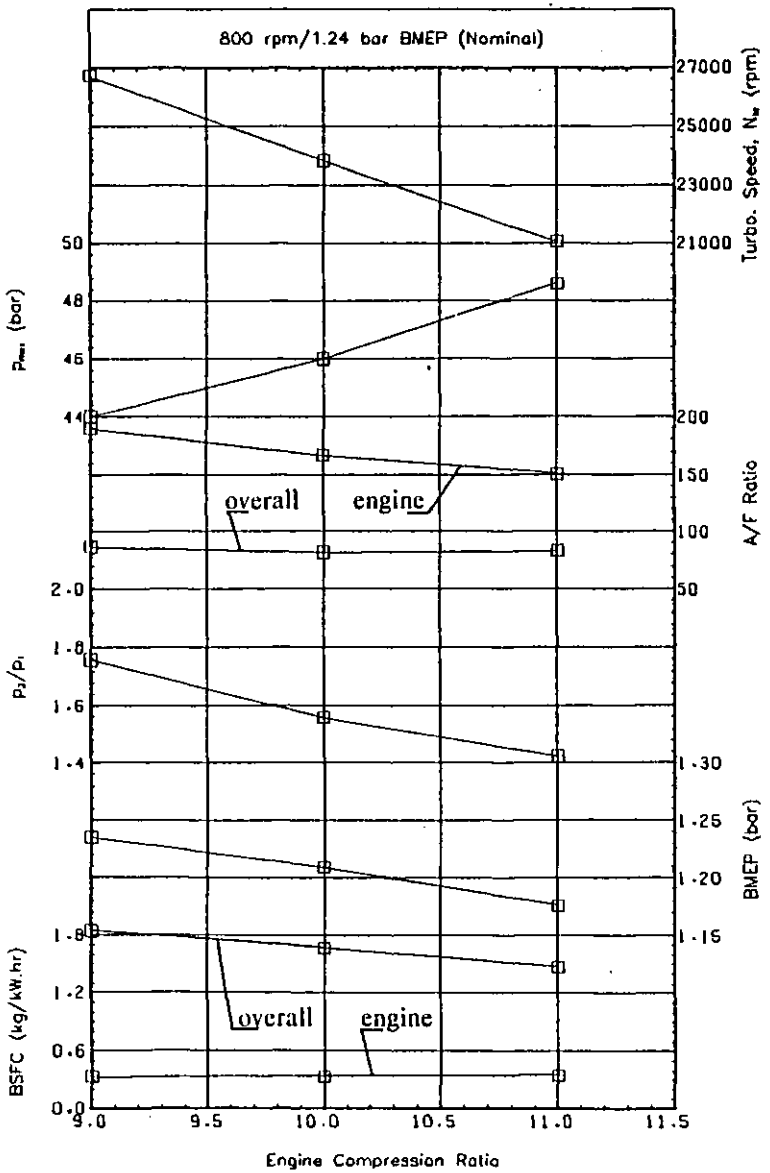

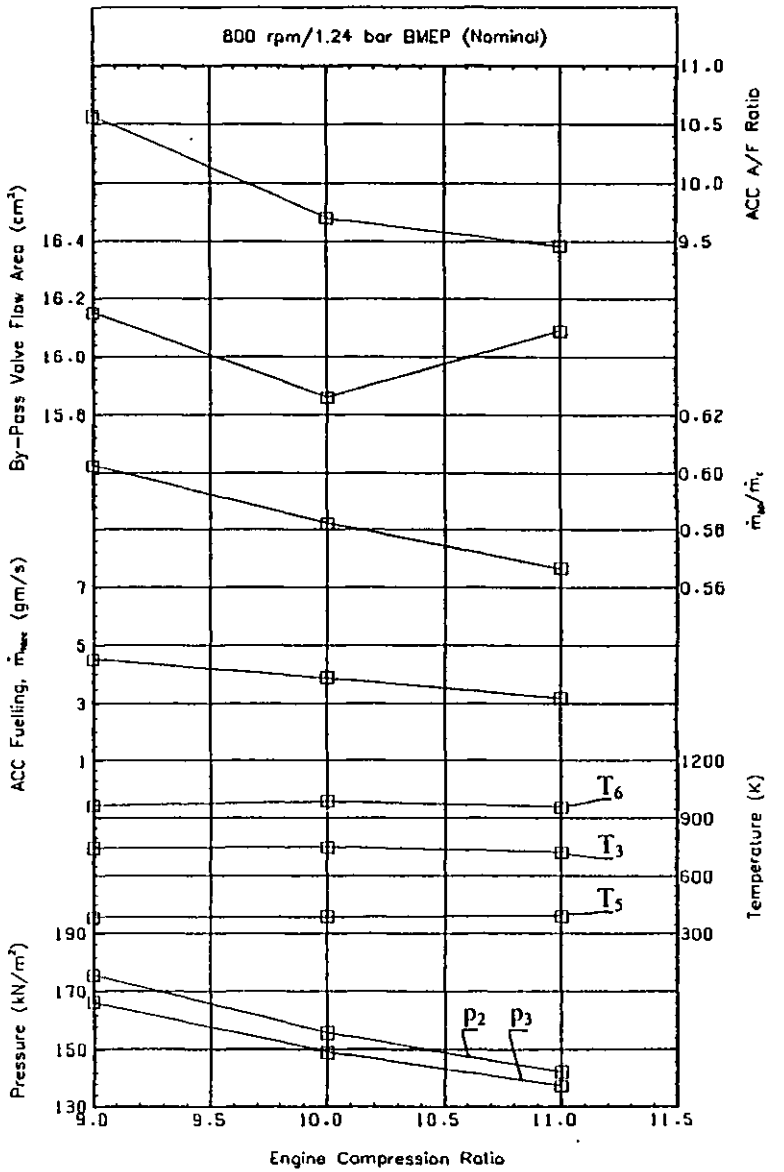

Fig. 6.20 Effect of the Compression Ratio and the ACC Fuel Control Pressure on the Overall Engine Performance at 800 rpm/1.24 bar BMEP (Nominal).

the compressor pressure ratio reduces to 1.56, and with CR=11:1, p_2/p_1 is 1.42. These values are also plotted on Fig. 6.19 and show a very good agreement with the correlation developed. Unfortunately due to the simplifying assumptions made in Appendix A, and the lack of control over the mean gas temperature during the ignition delay, it was not possible to keep the ignition delay exactly constant at 11.1°CA. The actual ignition point advancing from 6.0°CA BTDC with CR=9:1 to 6.8°CA BTDC with CR=10:1 and 7.6°CA BTDC with CR=11:1. This reduction in ignition delay as the compression ratio is increased, suggests that the boost pressure level should be lowered even further at both test conditions to retard the start of combustion. However, the procedure described in Appendix A does give a good initial estimate of the boost pressure level required.

As the compression ratio is increased the engine BMEP falls (by 4.8% for the 11:1 compression ratio) despite the increase in thermodynamic efficiency resulting from the increased expansion ratio. There are three main reasons for this:-

(1) As the boost pressure level falls, the action of the by-pass valve reduces the scavenge pressure drop across the engine, and therefore reduces the positive pumping work.

(2) As the boost pressure level falls the trapped equivalence ratio increases (for constant engine fuelling) which effects the AFBR. Also the lack of control over the ignition delay will affect the start of combustion and the subsequent AFBR.

(3) The peak cylinder pressure rises as the compression ratio increases, which increases the frictional losses, according to eqn. (4.130), by up to 2.2%.

This reduction in BMEP results in a proportional increase in the engine BSFC of 4.8%, with a compression ratio of 11:1. The engine A/F ratio reduces by 20.5% as the boost pressure level falls, causing an increase in the exhaust manifold gas temperature of 7 K, despite the increased engine expansion ratio, but the effects are small because of the high engine A/F ratio at low loads (as much as 189.6 with the standard compression ratio and fuel control pressure). Similarly scavenging and metal temperatures are largely unaffected by the reduction in scavenge pressure ratio, (the liner and piston wall temperatures increasing by 2 K and the cylinder head gas side

metal temperature by 6 K).

As the ACC fuel control pressure is reduced and the boost pressure falls the ACC fuelling also reduces, and because this represents the major proportion of the total fuelling (81.9% for the standard geometry), there is a significant benefit in the overall BSFC. A reduction in ACC fuelling rate of 29.2% from the standard case is predicted for a compression ratio of 11:1, which results in a reduction in total BSFC of 20.1%. The operation of the Hyperbar by-pass valve and burner can be seen in Fig. 6.21. Further benefits can be achieved by reducing the ACC fuel control pressure, p_f, at compression ratio's of 10:1 and 11:1 until the ignition delay is 11.1°CA.

The overall A/F ratio does not change significantly, reducing from 86.4 to 82.8 with the 11:1 compression ratio, due to the reduction in compressor pressure ratio and ACC fuelling rate, which govern the overall air and fuel flows at this operating condition. As the ACC fuel control pressure reduces, the burner fuelling and port areas reduce, but due to the effect of the reducing upstream air density and pressure ratio across the ports, the air flow reduces more than the fuel flow, and so the ACC A/F ratio reduces from 10.6 to 9.5.

The by-pass valve area does not change significantly to control the scavenge pressure ratio, but the proportion of the by-pass flow to total air flow reduces from 60.2% with CR=9:1, to 56.7% with CR=11:1, as the boost pressure falls. The overall effect is little change in either the ACC gas temperature, -7 K, or the mixer temperature, -22 K, due to the relatively high overall A/F ratio's involved.

The mean compressor operating points with these three compression ratio's are also shown in Fig. 6.17. The compressor mass flow rate, pressure ratio and speed all fall as the ACC fuel control pressure is reduced, and the efficiency drops as the operating point moves to a less efficient region of the map. The turbine efficiency also reduces, by 4.0%, as the expansion ratio and turbocharger speed reduce, although the blade/speed ratio remains almost constant at U/C=0.6, which is close to the peak efficiency, see Fig. 4.4

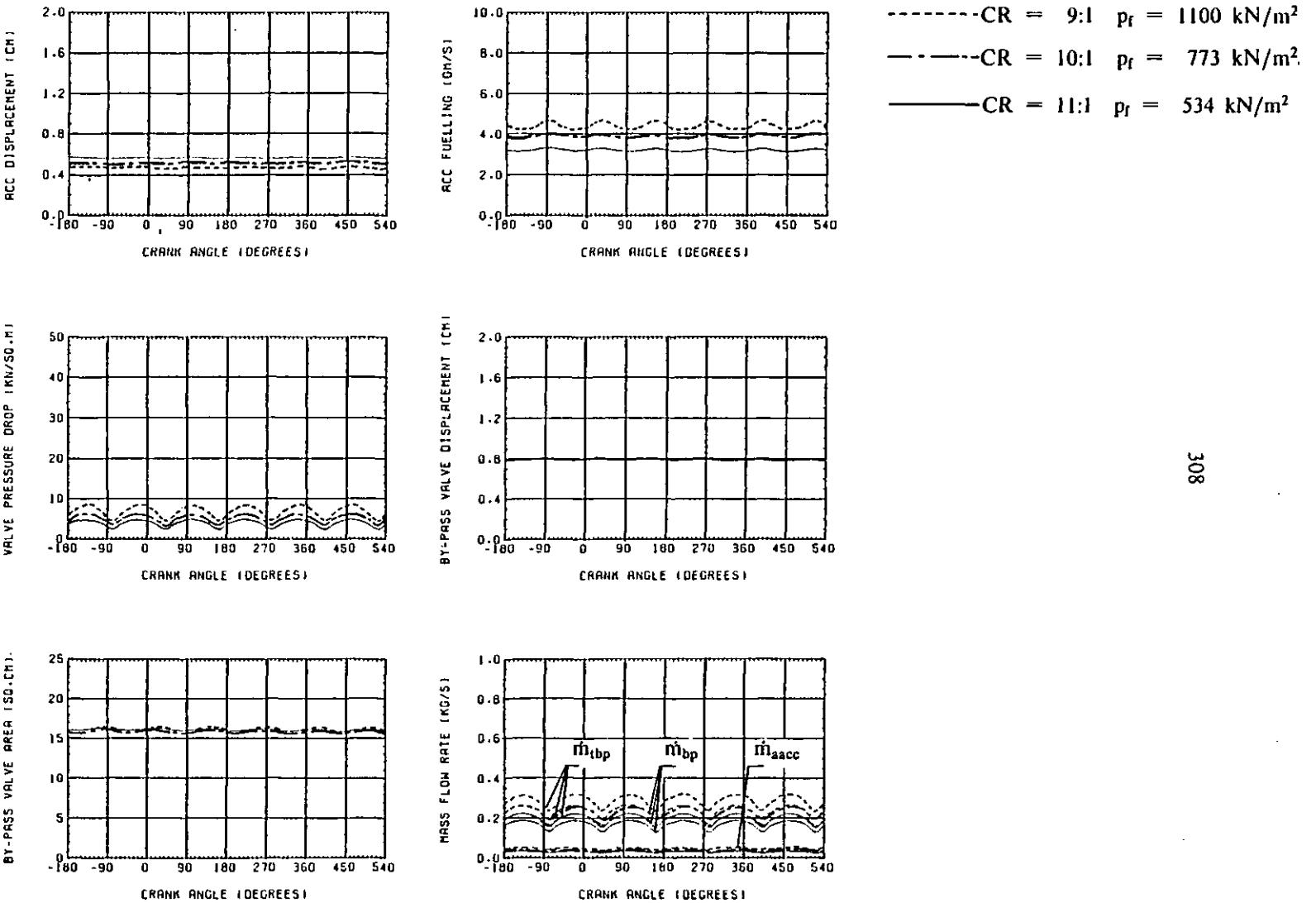

Fig. 6.21 Effect of the Compression Ratio and the ACC Fuel Control Pressure on the Hyperbar System Performance at 800 rpm/1.24 bar BMEP (Nominal).

6.6.3 Discussion.

It is difficult to predict exactly how much the boost pressure level can be reduced when the compression ratio is increased, to achieve the same ignition delay, due mainly to the lack of control over the gas temperature, which has a significant effect on the delay. However, the procedure outlined in Appendix A does give a good approximation to the change in fuel control pressure that is required.

The boost pressure has been matched to give, as closely as possible, the same ignition point, irrespective of the engine compression ratio, to ensure that the engine performance will not deteriorate at low loads due to poor combustion. The optimum engine performance may be achieved by allowing the delay to shorten or lengthen by controlling the boost pressure. This has not been investigated.

This study has shown the considerable reduction in BSFC that can be achieved by reducing the ACC fuelling requirement at low loads and speeds, where the burner fuelling is the major proportion of the total. If the engine is to operate for long periods at idle and low loads, then a reduction in the minimum boost level, coupled with a method of controlling the ignition timing (such as a change in compression ratio) is essential. In the limit the Hyperbar engine reverts to the design of a conventionally turbocharged high BMEP engine, with the minimum boost pressure being ambient, and zero ACC fuelling.

However the Hyperbar system is not designed primarily to operate at low loads. The low geometric compression ratio is necessary to allow high boost pressures at any engine speed without exceeding the mechanical loading limits. If the decision is taken to raise the compression ratio from 9:1 to, say 10:1, to take advantage of the reduced BSFC at low loads, then some action must be taken to avoid excessively high peak cylinder pressures at high loads and speeds.

Assuming that variable compression ratio is not a practical alternative, at its current stage of development, the main parameter that can be used to control the peak cylinder pressure is the injection timing. Retarding the injection at high loads will reduce the peak cylinder pressure, which then occurs later in the cycle. This results in

a reduction in IMEP, and consequently an increase in BSFC (depending upon the reduction in FMEP with the lower peak cylinder pressure). The thermal efficiency of the cycle will therefore reduce at high loads.

The injection timing can be retarded until the peak cylinder pressure occurs just before TDC, due to the compression process alone, but the resulting fall in BMEP may prohibit this. Retarding injection timing at high loads and increasing the compression ratio may therefore require the engine rating to be lowered.

Reducing the minimum boost pressure level in the way described in section 6.6.2 can also result in a deterioration in the transient performance of the engine. Starting from a low load and speed, the engine A/F ratio is reduced and the compressor and turbine are operating at less efficient points on their respective maps. This may become significant if, for example, the engine is accelerated from a low initial speed and load, with the load increasing with the engine speed (e.g. a vehicle or propeller law type loading), or if a large load is suddenly applied at a low engine speed. The effect of the boost pressure level and compression ratio on the transient response of the engine is discussed in Chapter 7.

The choice of the minimum boost pressure level, and the engine compression ratio is therefore a matter of compromise, depending upon the rating and application of the engine.

6.7 Effect of Retarding the Static Injection Timing.

If the engine compression ratio is increased, and the minimum boost level reduced, to improve the part load fuel consumption, then at high loads and speeds the maximum cylinder pressure limit will probably determine the maximum engine power output. The simplest way of controlling the peak cylinder pressure is via the injection timing.

Fig. 6.22 shows the effect of retarding the static injection timing from the standard value of 20°CA BTDC. The engine speed is 2400 rpm and the load is 21.56 bar BMEP with the normal injection timing. For these tests the ACC burner is idling, and the standard compression ratio of 9:1 was used.

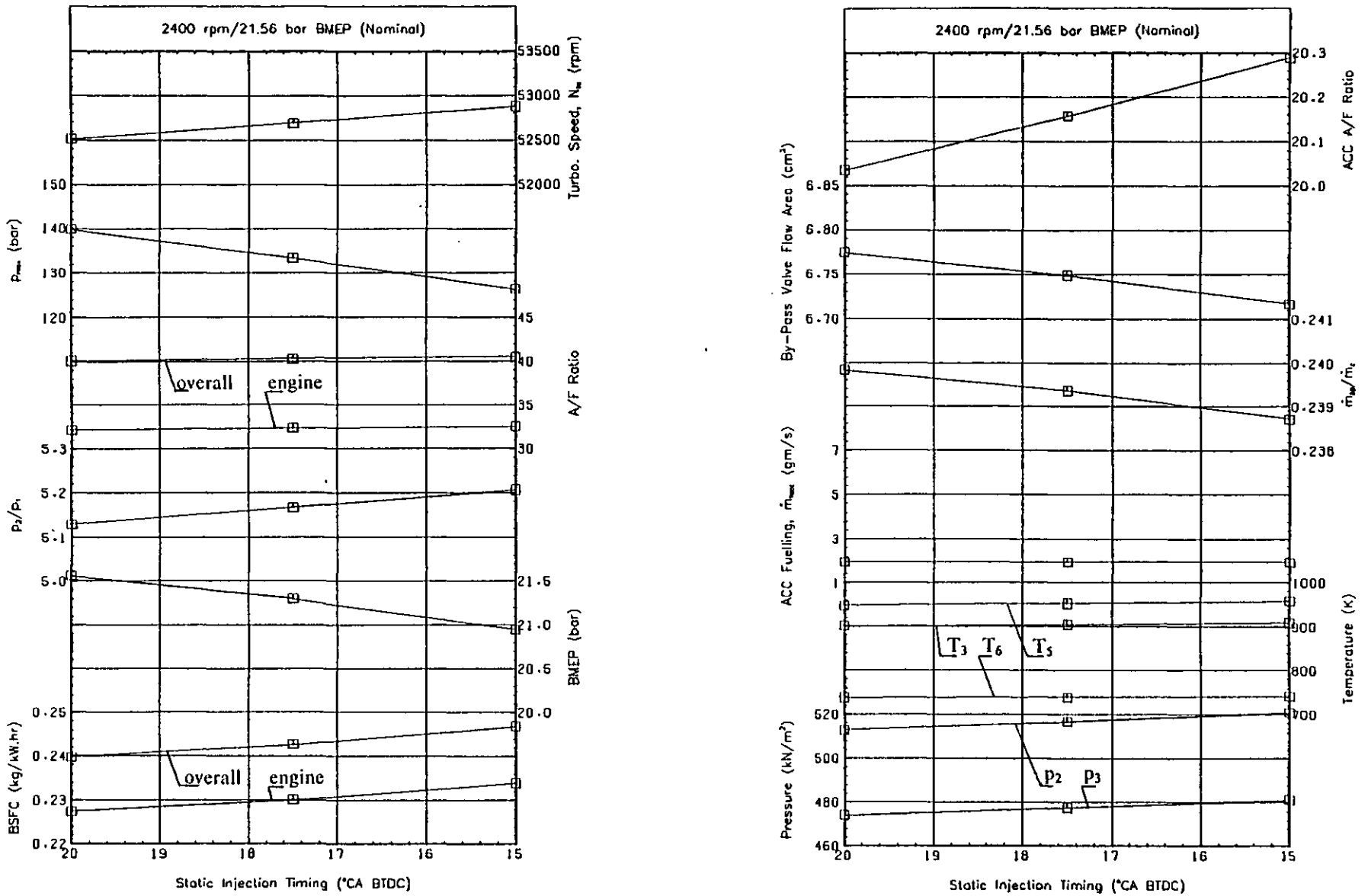

Fig. 6.22 Effect of the Static Injection Timing on the Overall Engine Performance at 2400 rpm/21.56 bar BMEP (Nominal).

Retarding the static injection timing by 5°CA causes a drop in BMEP of 2.8%, with constant engine fuelling, and a corresponding increase in both the engine and total BSFC (the ACC fuelling remaining constant). The maximum cylinder pressure falls from 139.8 bar to 126.4 bar (9.6%), while the compressor pressure ratio increases by 1.5%, because of the increased exhaust gas energy caused by the combustion occuring later in the cycle. Maximum cylinder pressure occurs at 15°CA ATDC with the injection timing retarded, compared to 13°CA ATDC originally. The ignition delay reduces from 4.8°CA to 4.3°CA with the later injection, but at this high speed and load there is effectively no "premixed" combustion ($\beta=0$).

The compressor flow increases by 1.0%, as the boost pressure and turbocharger speed increase with the injection timing retarded 5°CA, and so the overall and engine A/F ratio's increase by a similar amount. The exhaust, ACC and turbine inlet temperatures all rise slightly, despite the increase in both the engine and overall A/F ratio, mainly because of the higher exhaust manifold gas temperature, 10 K, resulting from the later combustion in the engine cylinders.

As the boost pressure rises, with the injection timing retarded, the by-pass valve area reduces by 0.8%, to maintain the valve pressure drop ratio at 0.09, reducing the proportion of the total by-pass flow that passes through the valve, (the ACC flow area remaining constant) and also reducing the proportion of the total flow through the by-pass system, from 24.0% with the standard injection timing to 23.9% with 5°CA retard. The ACC A/F ratio increases from 20.0 to 20.3 as the timing is retarded, because of the increase in air flow through the ports, caused by the higher boost pressure and port pressure ratio.

6.7.1 Discussion.

If the option of increasing the engine compression ratio and reducing the minimum boost pressure level is adopted, retarding the static injection timing at high speeds and loads is probably the most effective method of controlling the peak cylinder pressure. For an increase in BSFC of 2.8%, the peak cylinder pressure can be reduced by 9.6%, at the maximum engine speed.

A system for retarding injection timing according to the load (i.e. boost pressure or

rack position), and engine speed can be adopted relatively easily. However, any reduction in the minimum boost level and injection timing will also effect the transient response of the engine, see section 6.6.3. Whether or not the engine can accept large load changes without producing excessive smoke will depend in part, on the minimum boost level, as this determines the amount of air in the cylinders at the start of the load change.

If a great deal of time is spent idling, the benefits of reducing the ACC fuelling and using a higher compression ratio will be large enough to compensate for the increase in BSFC at full load, when the injection timing must be retarded.

6.8 Part Load Performance at 1200 rpm.

6.8.1 Introduction.

A comparison between the experimental and predicted engine performance at 1200 rpm, 1800 rpm and 2400 rpm was described in Chapter 5. Unfortunately only a limited amount of test data was available at each engine speed, and so it was not possible to confirm that the system behavior was being predicted accurately at extremely high and low loads.

As the engine load reduces the engine exhaust energy decreases, and so the system relies on the burner to provide the energy required to maintain the minimum boost pressure level, necessary for good combustion in the engine cylinders.

At high loads, as the engine fuelling is increased, the engine A/F ratio reduces, because engine air flow does not increase at the same rate as the fuelling. Eventually a point is reached when either the engine exhaust gas temperature reaches a practical limit, the smoke becomes excessive or the thermal loading of the engine components becomes prohibitive. The ACC can then be used to provide extra exhaust energy and so increase the engine air flow, which enables the engine load to be increased even further.

The predicted low load engine performance at 1200 rpm will be discussed in section 6.8.2, and the engine performance at high loads in section 6.8.3. After the part load

performance of the engine has been discussed, possible control strategies for the ACC burner will be developed in the following sections.

6.8.2 Low Load Performance.

The engine and turbocharger system performance at three relatively low load levels, 6.04 bar, 2.76 bar and 0.90 bar BMEP, at 1200 rpm was investigated. The overall engine and turbocharger performance is shown in Fig. 6.23.

As the engine fuelling reduces the FMEP reduces, but becomes an increasingly large proportion of the total IMEP (19.0%, 32.8% and 59.3% at 6.04 bar, 2.76 bar and 0.90 bar BMEP respectively). Consequently the engine BSFC increases as the load reduces and a larger proportion of the fuel is used to overcome the frictional losses.

The ACC burner controls the minimum boost pressure level by supplying extra energy for the turbine as the load reduces. The burner fuelling increases from 3.03 gm/s at 6.04 bar BMEP, to 4.28 gm/s at 0.90 bar BMEP, while the compressor pressure ratio falls only slightly, from 1.81 to 1.76. It is obvious from the ACC fuelling characteristic, Fig. 6.24, that the boost pressure must fall slightly as the load reduces in order to cause an increase in the ACC fuelling. The ACC port areas increase as the burner fuelling increases, but the steep gradient of fuelling versus boost pressure means that the ACC A/F ratio reduces as the load falls, from 14.4 to 11.1.

The increase in ACC fuelling at lower loads causes a sharp increase in the total BSFC, in addition to that caused by the rising engine BSFC. At 0.90 bar BMEP the ACC fuelling is 74.1% of the total, compared to 37.8% at 6.04 bar BMEP.

Because the compressor pressure ratio is maintained at the minimum level by the burner, the compressor flow does not change greatly as the load reduces (the engine flow reduces by only 3.7% between 6.04 bar and 0.90 bar BMEP, because of the slight reduction in boost pressure). Therefore as the engine fuelling reduces the engine A/F ratio increases from 55.8 to 178.3 at 0.90 bar BMEP. This causes the drastic reduction in the exhaust manifold gas temperature from 598 K to 402 K, seen in Fig. 6.23, and the corresponding reduction in turbine energy supplied by the engine. The overall A/F ratio is influenced, in general, by the rate at which the burner fuelling

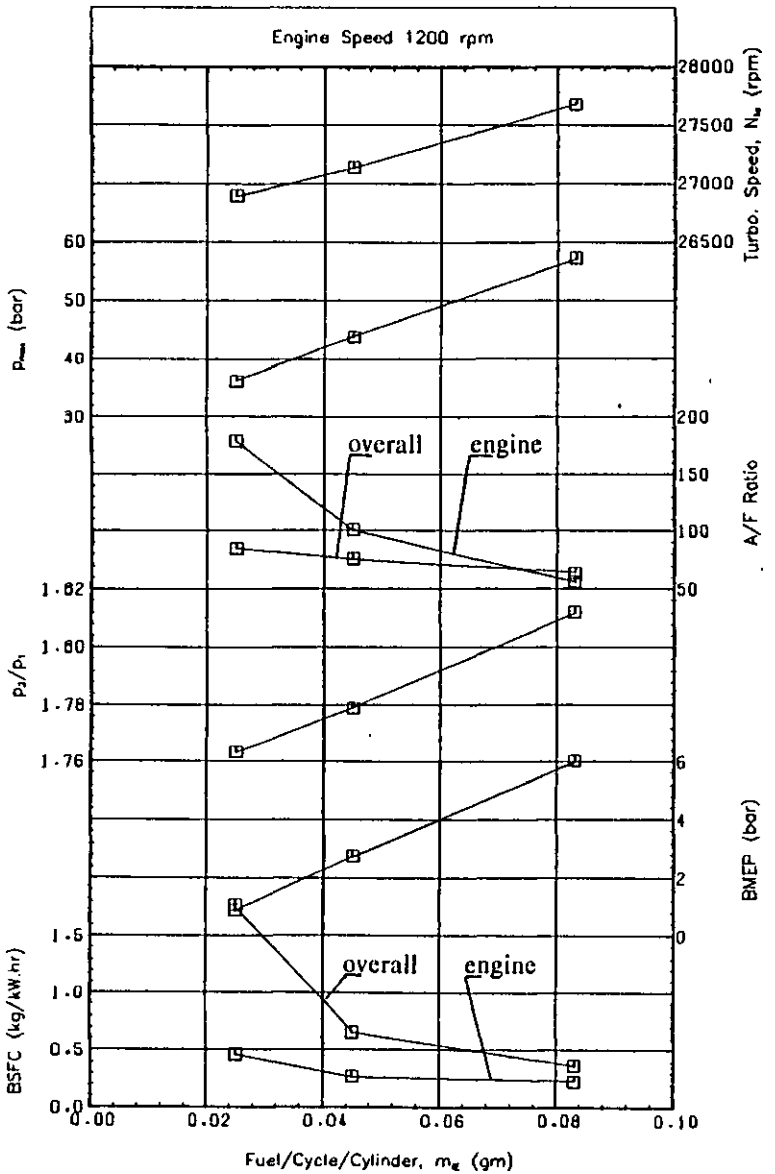

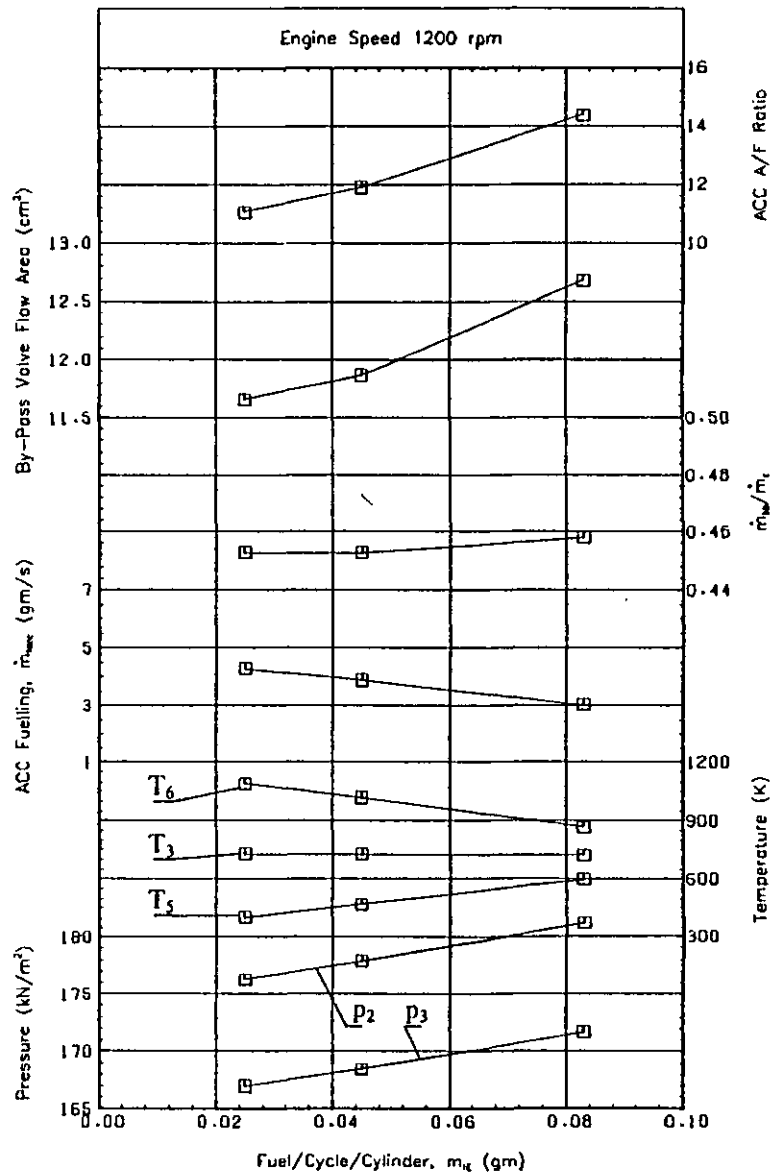

Fig. 6.23 Effect of the Load on the Overall Engine Performance at 1200 rpm.

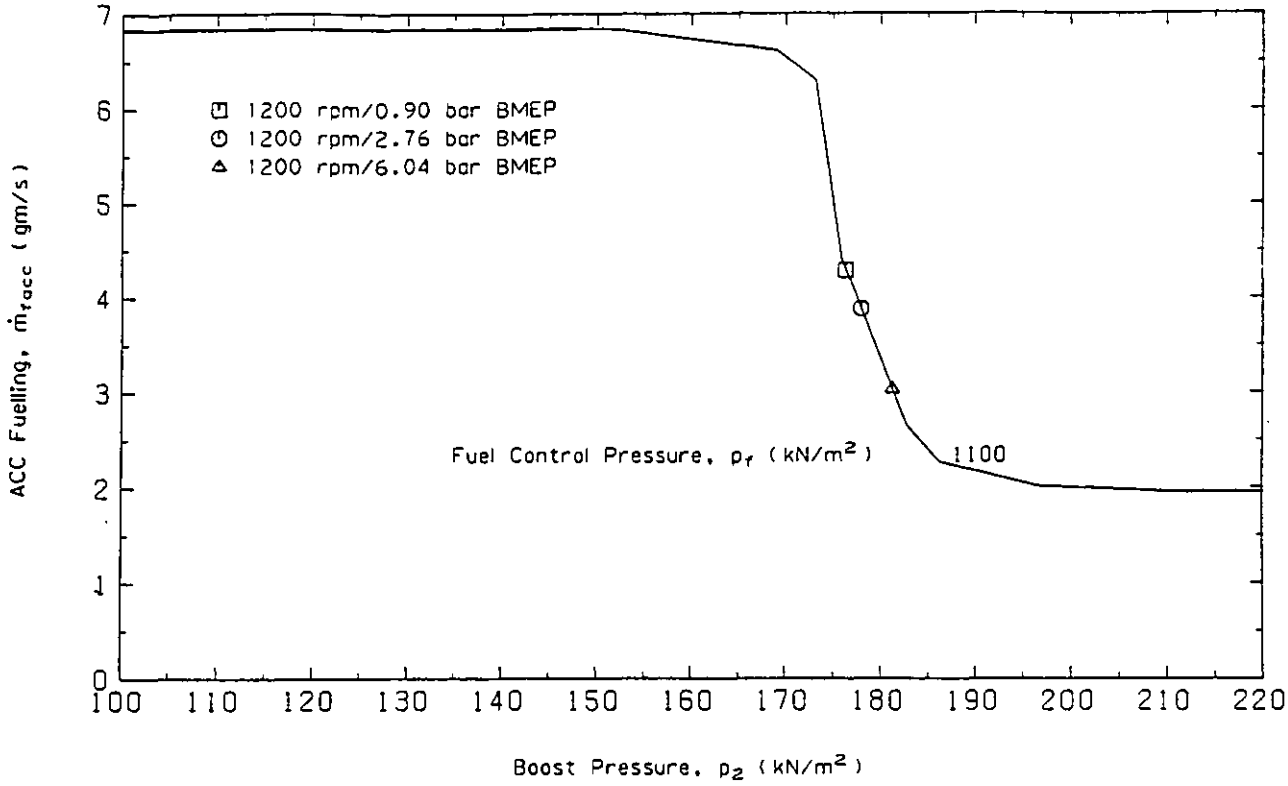

Fig. 6.24 Effect of the Engine Load on the ACC Fuelling Rate.

increases compared to the rate at which the load reduces (the compressor flow rate reducing by only 4.6% between 6.04 bar and 0.90 bar BMEP). For these tests there was an increase in the overall A/F ratio from 64.0 to 84.5 as the load reduced.

The movement of the operating point on the compressor map can be seen in Fig. 6.25, which shows the reduction in pressure ratio, speed, mass flow rate and efficiency as the load reduces.

The peak cylinder pressure is affected by the slight reduction in boost pressure, which also lengthens the ignition delay from 13.3°CA at 6.04 bar BMEP, to 14.8°CA at 0.90 bar BMEP, causing combustion to occur later in the cycle, with a greater proportion of premixed burning. At the lowest load, the peak cylinder pressure (of 36.2 bar) is barely above the compression pressure, and occurs at 14°CA ATDC.

The by-pass valve effective flow area reduces slightly as the load falls (by 8.0% from 6.04 bar to 0.90 bar BMEP) in order to maintain the correct scavenge pressure drop ratio of 0.09. As the ACC port areas increase, with reducing load, so the proportion of the total by-pass flow that goes through the valve reduces from 81.5% at 6.04 bar to 78.6% at 0.90 bar BMEP. Fig. 6.26 shows the by-pass valve and ACC operation predicted. The effect of slight pulsations in the ACC position on the ACC fuelling rate is noticable at all three loads.

In the ideal case, the compressor pressure ratio should remain constant at the minimum level, irrespective of the engine load, and the turbine inlet temperature should also remain constant (for a fixed scavenge pressure ratio and constant compressor and turbine efficiencies), see Fig. 3.5. The mixer temperature is predicted to be almost constant at the loads tested, increasing by only 5 K as the load reduces, despite the large decrease in exhaust manifold gas temperature of 196 K with load. Fig. 6.23 shows how the ACC gas temperature increases by 221 K to balance the reduction in exhaust gas temperature, (approximately 45% of the total flow goes through the by-pass at this speed).

For comparison, Figs. 6.27 and 6.28 show experimental part load performance at 1500 rpm, 2000 rpm and 2500 rpm for the Poyaud 6L 520 engine, from Melchior and Andre-Talamon (97). This is a 6 cylinder, four stroke engine (bore 0.135 m, stroke 0.122 m, compression ratio 9.2:1) rated at 73.5 kW (100 metric h.p.) per cylinder,

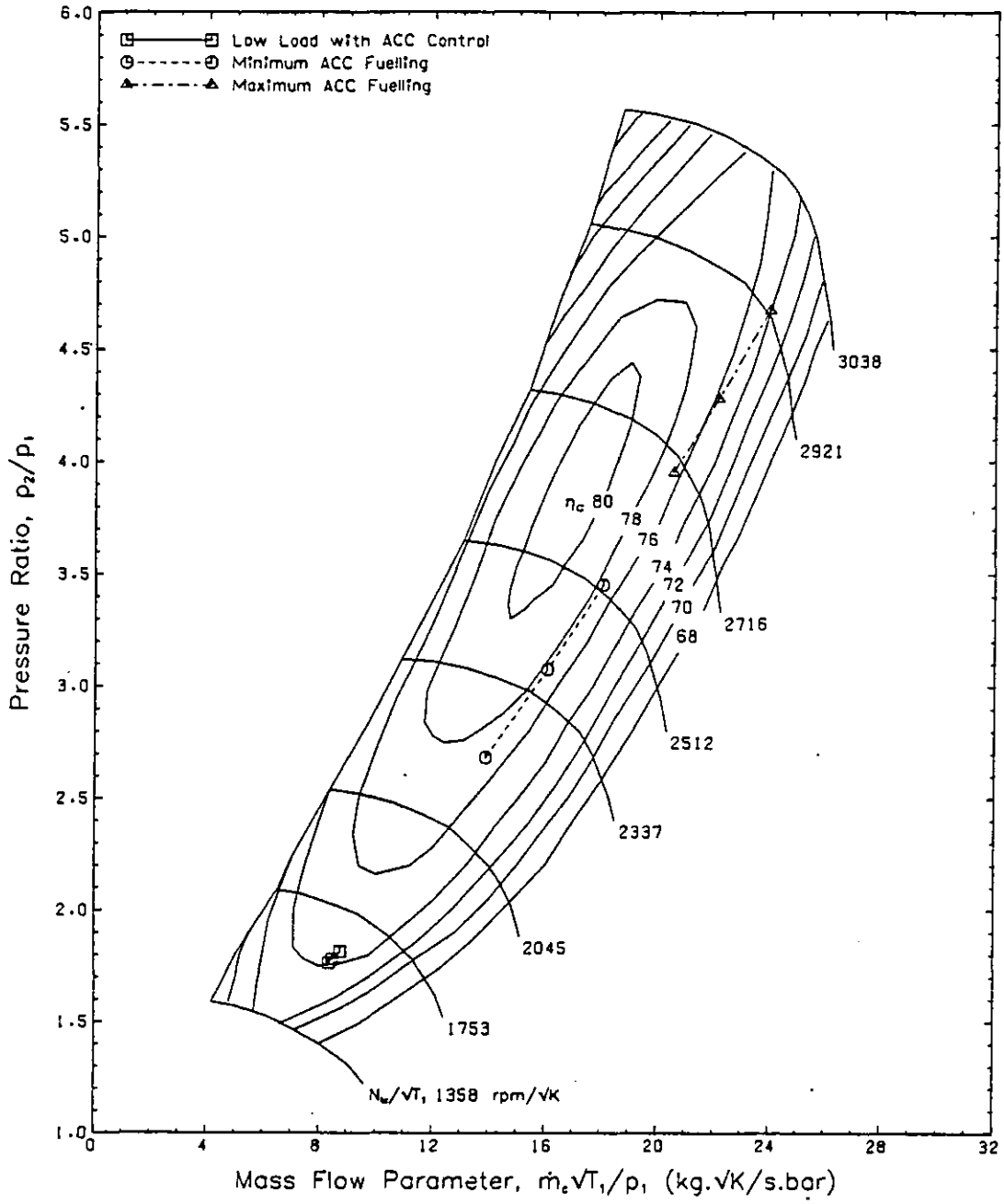

Fig. 6.25 Effect of the Load on the Compressor Operation at 1200 rpm.

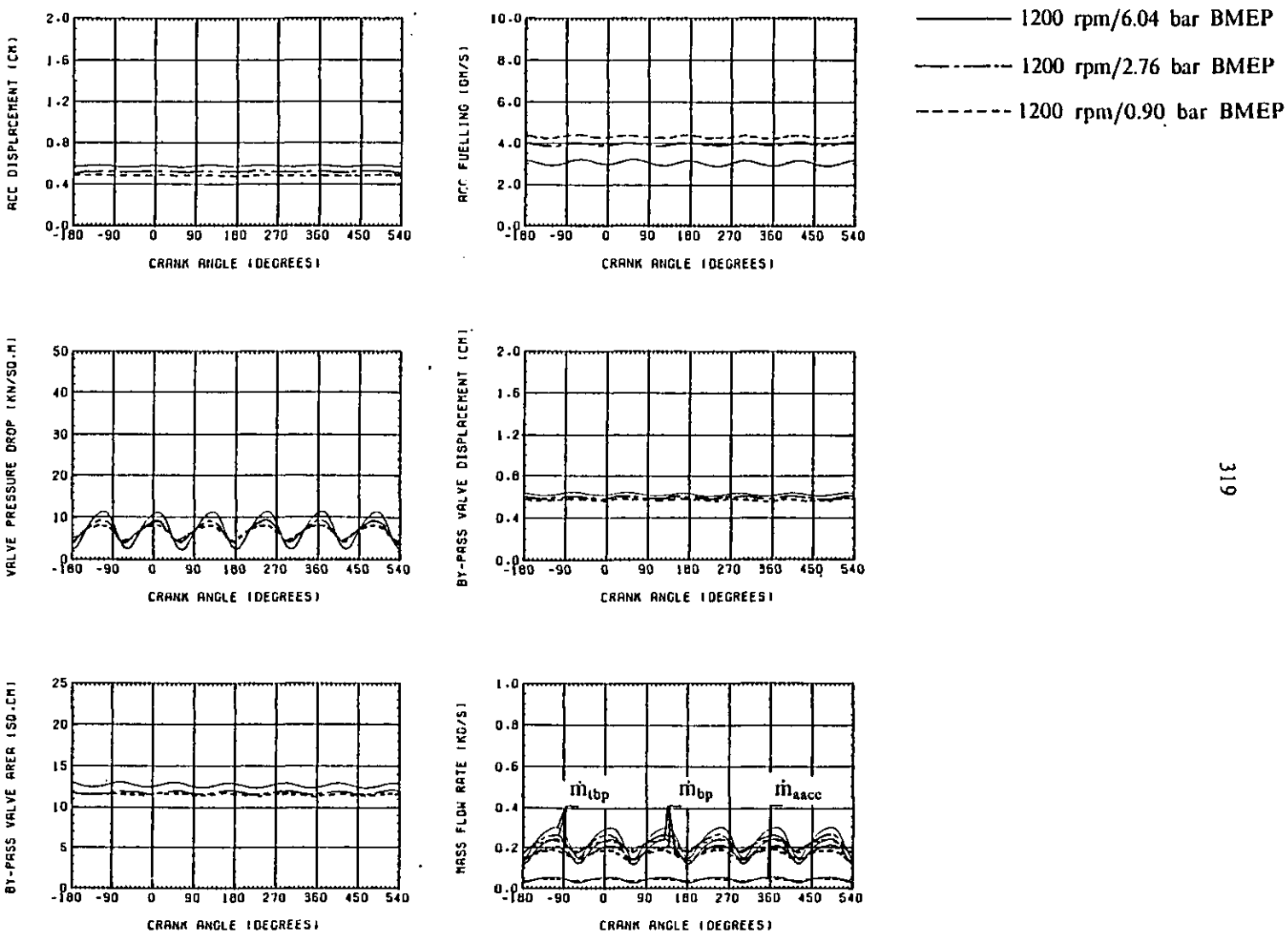

Fig. 6.26 Effect of the Load on the Hyperbar System Performance at 1200 rpm.

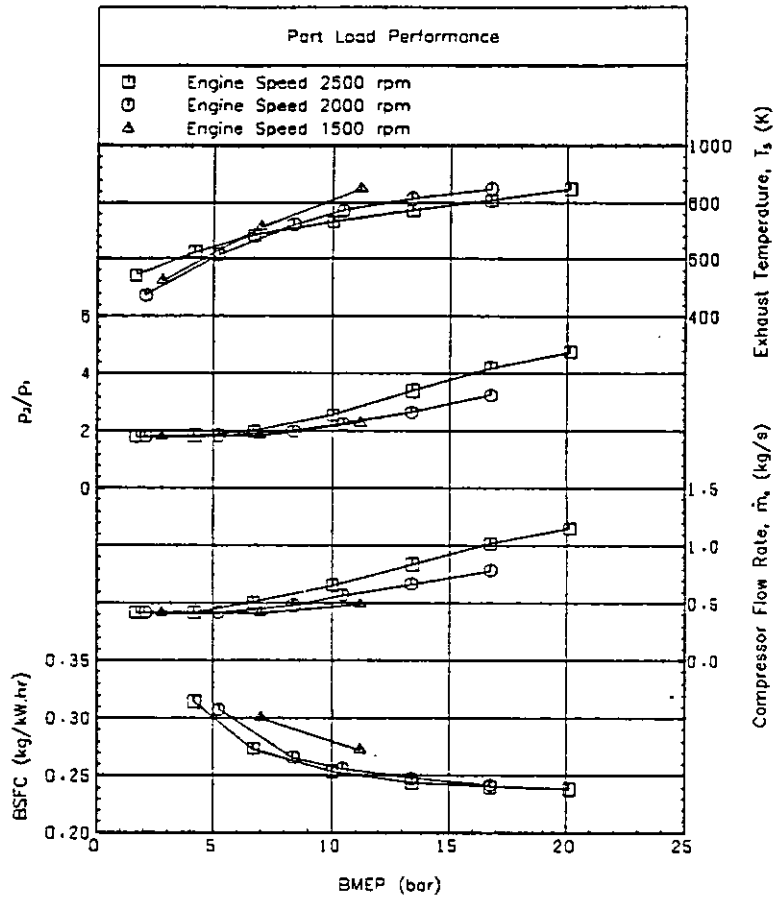

Fig. 6.27 Experimental Performance for the Poyaud 520 Hyperbar Engine, from (97).

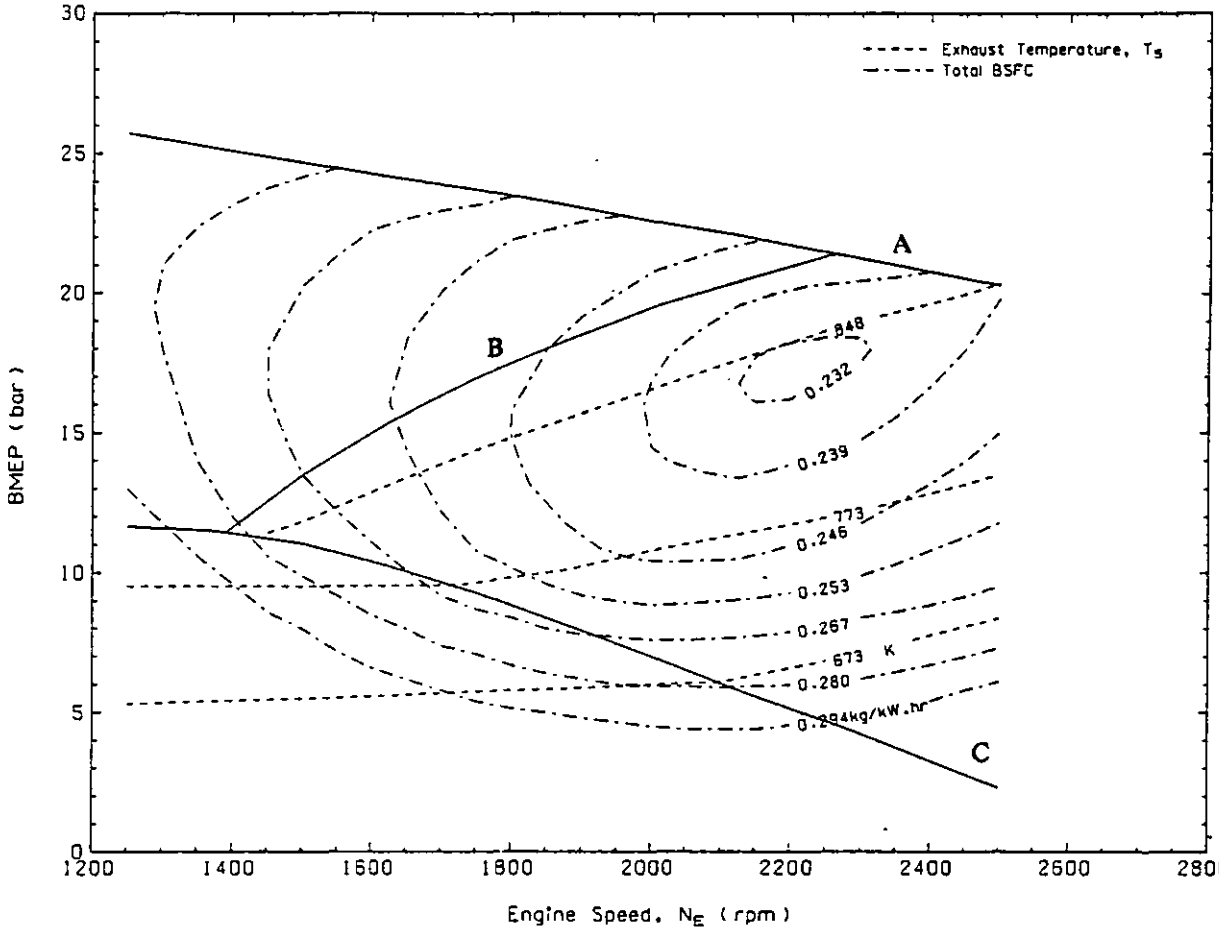

Line A represents the BMEP that can be achieved with a constant maximum cylinder pressure of 140 bar.

Line B represents the BMEP above which the ACC must be used to hold the exhaust manifold gas temperature constant

Line C represents the BMEP below which the ACC must be used to maintain the minimum boost pressure level

Fig. 6.28 Operating Regimes for the Poyaud 520 Hyperbar Engine, from (97).

and fitted with a Brown Boveri RR 150 turbocharger, capable of pressure ratio's of up to 5. While little data was available at very low loads, Fig. 6.28 indicates that at low speeds (below 1375 rpm) the burner has to be used continuously, at low loads to maintain the boost pressure at the minimum level, and at higher loads to control the exhaust manifold gas temperature.

6.8.3 High Load Performance.

The ACC burner can also be used to increase the exhaust energy, and therefore the compressor pressure ratio and air flow, to enable very high BMEP's to be achieved at any engine speed. Extra engine air flow is required at high loads when either the exhaust gas temperature limit, or the smoke limit, or some other parameter dependent on the engine A/F ratio (such as the piston, cylinder head or exhaust valve temperature) is reached. The ACC fuelling then has to be increased by some action, such as increasing the burner fuel control pressure. A suitable control system, linked to the engine operating conditions, is therefore required to modify the normal burner characteristics.

The effect of increasing the burner fuelling from the idle rate (1.953 gm/s) to the maximum rate (6.842 gm/s) was investigated at 1200 rpm. The engine load was increased, by increasing the engine fuelling, to give an increase in BMEP from 17.17 bar to 24.63 bar BMEP, with the burner in the idle position. The burner was then held in the maximum fuelling position, by increasing the fuel control pressure, p_f, from 1100 kN/m^2 to 6000 kN/m^2 and the tests repeated at the same engine fuellings. The effect on the overall engine and turbocharger performance is shown in Fig. 6.29.

As the engine load increases with the burner idling, the engine A/F ratio falls, resulting in an increase in exhaust manifold gas temperature. The boost pressure increases as the load increases, and the compressor and engine flows both increase. The by-pass air flow rate also increases, but stays at approximately the same proportion of the total compressor flow (increasing from 50.6% at 17.17 bar BMEP to 52.4% at 24.63 bar BMEP). As the. boost pressure increases so the maximum cylinder pressure increases. The ignition delay reduces and the trapped equivalence ratio increases, which influences the combustion process. The positive pumping work

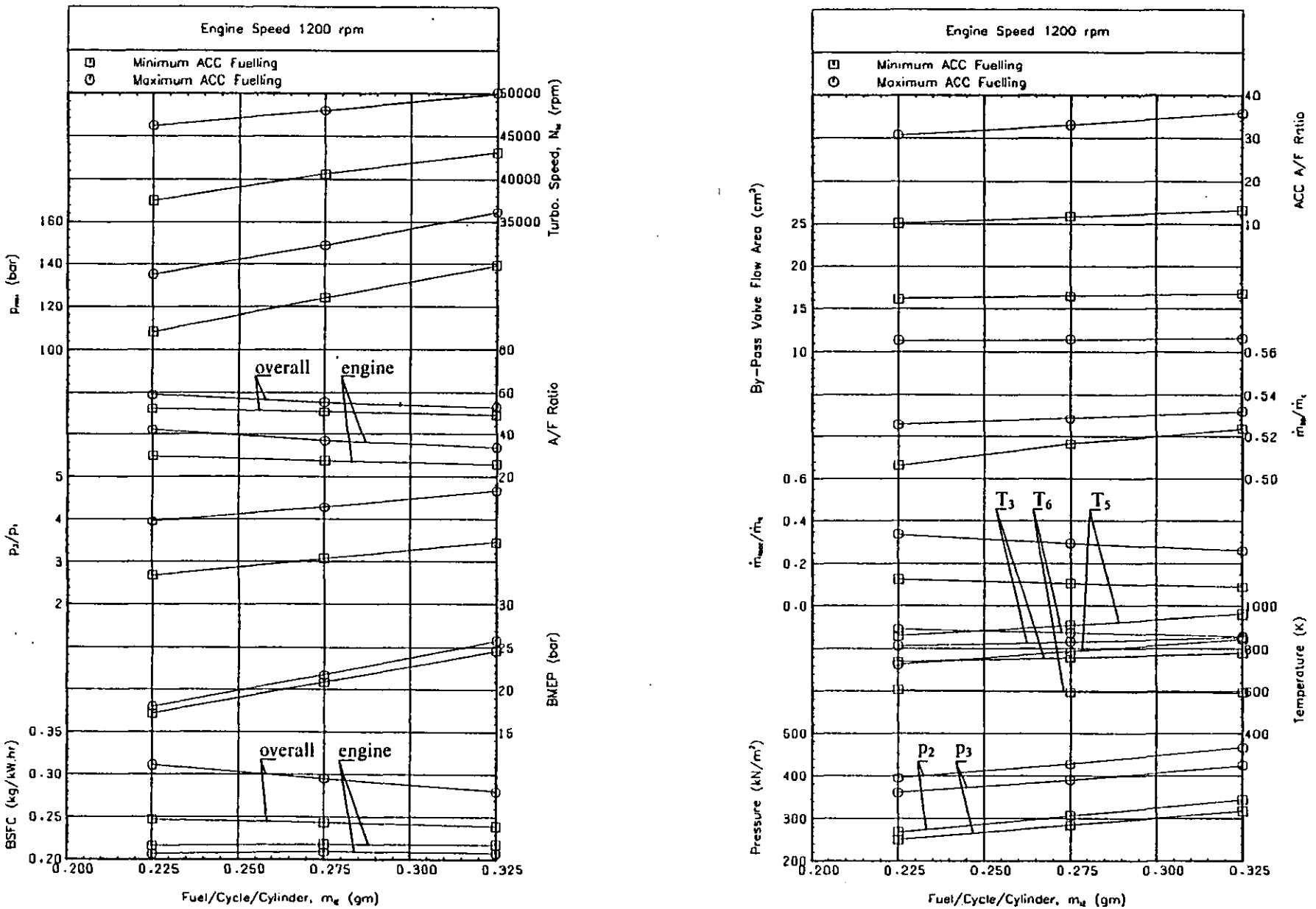

Fig. 6.29 Effect of the Load and ACC Fuelling on the Overall Engine Performance at 1200 rpm.

increases as the boost pressure rises, because the action of the by-pass valve increases the scavenge pressure drop.

The engine BSFC is not greatly affected by the load over the range of engine fuellings investigated, increasing by 0.7% between 17.17 bar and 24.63 bar BMEP. The FMEP increases as the peak cylinder pressure rises, by 9.2%, but becomes a smaller proportion of the IMEP, reducing from 8.9% at 17.17 bar to 6.9% at 24.63 bar BMEP.

The maximum cylinder pressure increases by 28.5%, for an increase in BMEP of 43.4% with the ACC idling, and at the highest load, 24.63 bar BMEP, has reached the manufacturers recommended peak cylinder pressure limit of 140 bar.

The failure of the compressor pressure ratio and the mass flow rate to increase in direct proportion to the increase in engine fuelling, means that the total A/F ratio reduces with increasing load from 52.5 to 49.2. This results in an increase in the turbine inlet temperature of 43 K.

The turbine inlet (mixer) temperature is almost mid way between the exhaust manifold gas temperature and the by-pass gas temperature, because approximately 50% of the total flow goes through the by-pass at this engine speed. The exhaust gas temperature rises rapidly with increasing load, by 102 K, while the ACC gas temperature reduces by 13 K as the boost pressure increases (at constant ACC fuelling), because of the increase in pressure ratio across the ACC ports and the increase in upstream (compressor outlet) gas density. The by-pass valve area increases by 3.5% as the load increases to maintain the correct scavenge pressure drop ratio of 0.09. The effect of increasing the engine load on the performance of the by-pass valve and ACC can be seen in Fig. 6.30.

Fig. 6.25 shows the compressor operating line as the load increases with the ACC burner idling. The compressor pressure ratio, speed and mass flow rate all increase as the load increases, and the compressor efficiency increases by 0.2% as the operating point moves to a higher efficiency part of the map. The turbine efficiency also increases by 1.2% as the load increases.

With the ACC held in the maximum fuelling position, similar trends to those

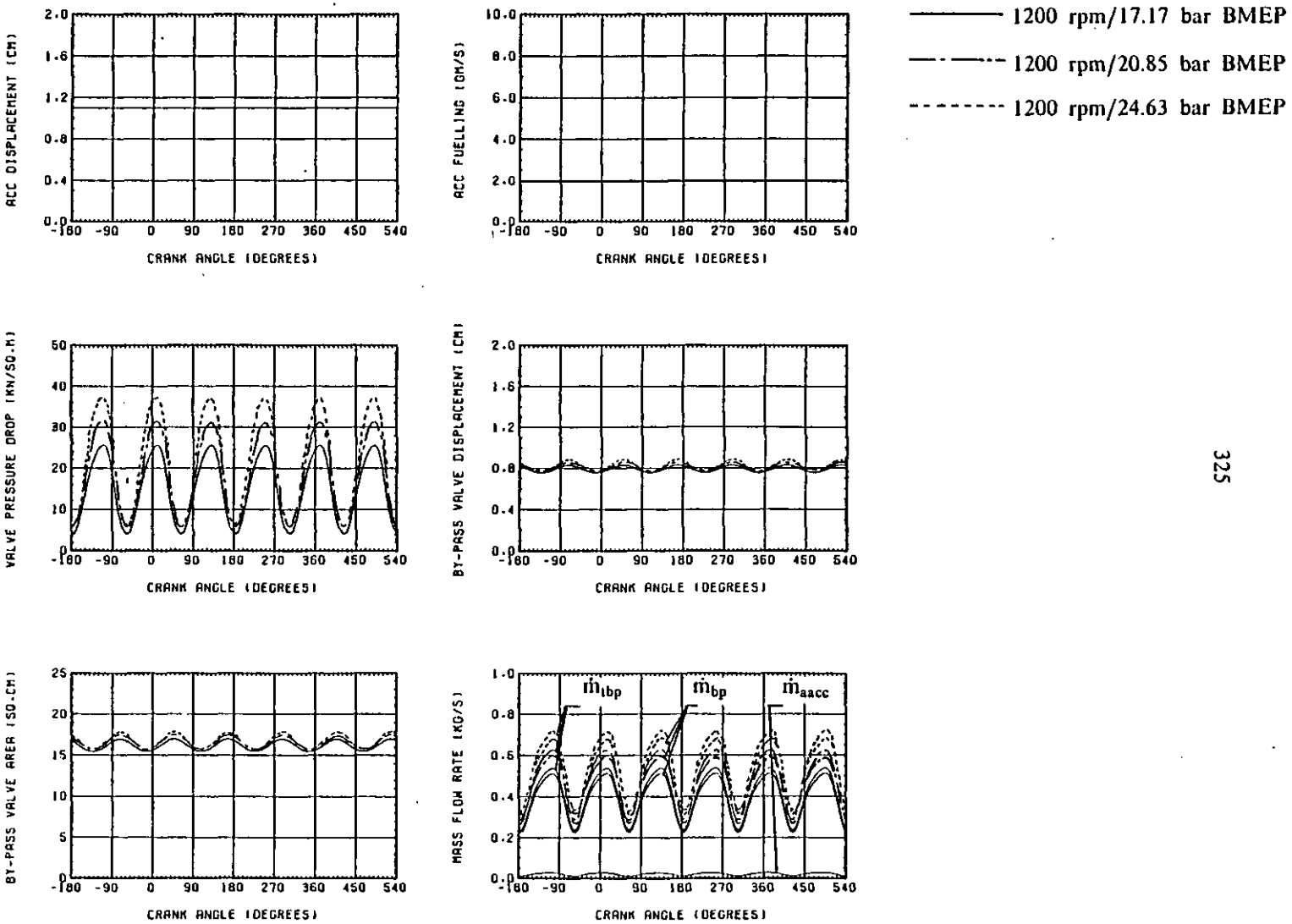

Fig. 6.30 Effect of the Load on the Hyperbar System Performance at 1200 rpm with the Minimum ACC Fuelling Level.

described above can be seen in Fig. 6.29, at the same engine fuellings. However because of the extra energy provided by the ACC burner, the compressor pressure ratio and mass flow rate are greatly increased. The increase in pumping work with boost pressure, offsets the increase in FMEP with maximum cylinder pressure, and the overall engine BMEP increases (by 4.7% at the lowest fuelling level and by 4.9% at the highest fuelling), resulting in a corresponding reduction in engine BSFC. The increased ACC fuelling, however, means that the total BSFC increases by a large amount over the load range investigated (by 25.8% at the lowest load and by 17.1% at the highest engine fuelling).

The peak cylinder pressure rises less steeply with increasing load (21.8% for an increase in load of 43.7%) with the ACC held in the maximum fuelling position, but the manufacturers maximum cylinder pressure limit of 140 bar is reached at a much lower load, 19.28 bar BMEP, due to the effect of the higher boost pressure.

Because of the increase in engine A/F ratio, resulting from the increase in boost pressure, the engine exhaust manifold gas temperature falls with the increased ACC fuelling. The ACC port areas are relatively large, and so a large proportion of the total by-pass flow goes through them, increasing from 4.7% to 32.6% at the highest engine fuelling as the ACC position is moved to maximum fuelling. The by-pass valve therefore closes slightly to control the scavenge pressure ratio, and the ACC A/F ratio increases. But the overall by-pass A/F ratio reduces (from 210.3 to 92.1 at the lowest load, and from 282.9 to 108.9 at the highest load) resulting in a much greater temperature rise across the by-pass system with the ACC at maximum fuelling, ranging from 421 K to 358 K as the load increases. The reduction in the exhaust manifold gas temperature and increase in by-pass gas temperature causes an increase in the turbine inlet gas temperature, ranging from 76 K at the lowest load to 70 K.

Fig. 6.31 shows the effect of increasing the ACC fuelling at these three loads on the by-pass system performance. Fig. 6.25 also shows the compressor operating line with the ACC at maximum fuelling. The compressor operating efficiency reduces as the load increases, by 0.8%, in contrast to the turbine efficiency, which increases by 0.4%. The resulting overall turbocharger efficiency falls with increasing load.

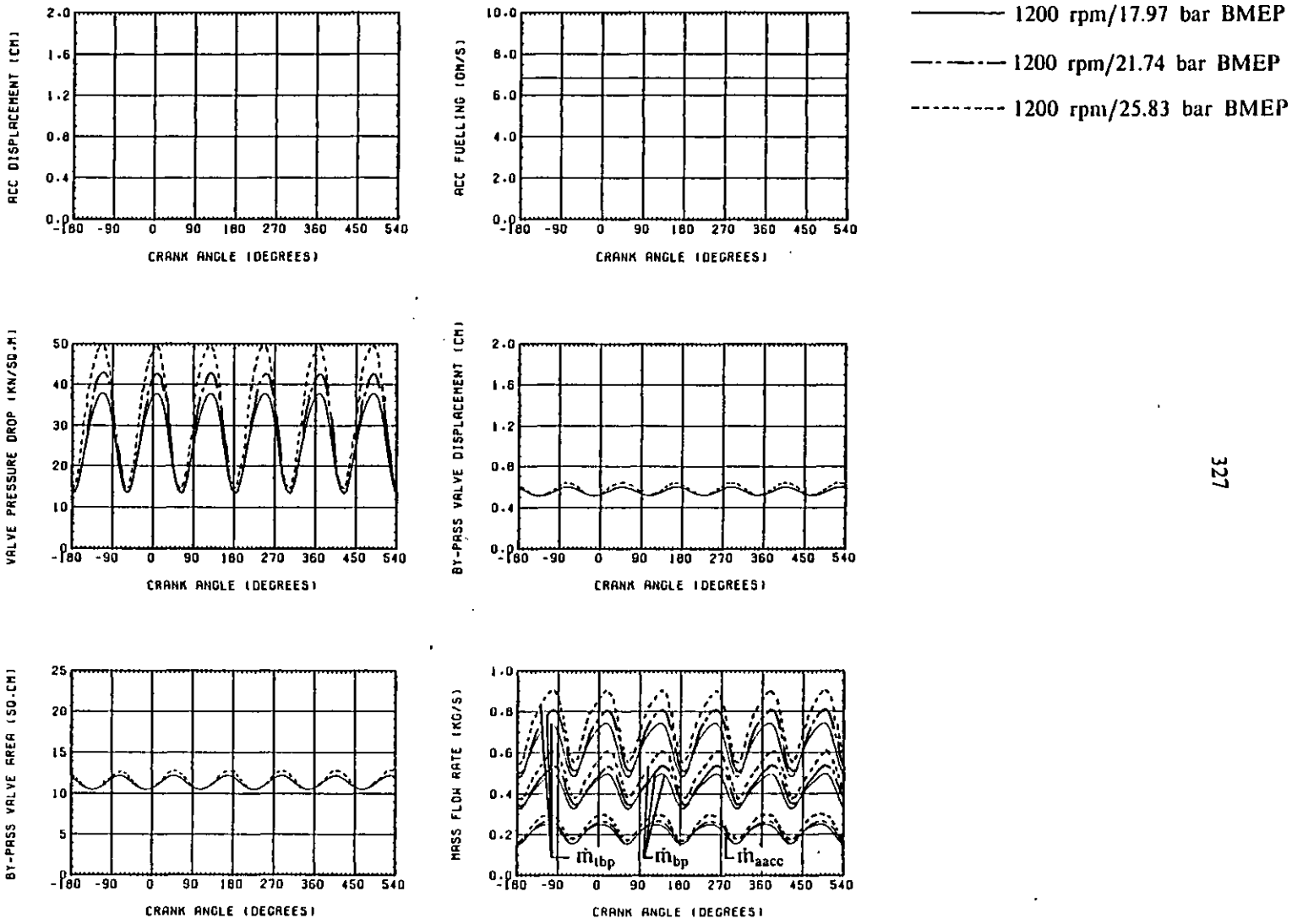

Fig. 6.31 Effect of the Load on the Hyperbar System Performance at 1200 rpm with the Maximum ACC Fuelling Level.

6.8.4 Discussion.

In the previous section it has been shown how the engine A/F ratio can be increased by increasing the ACC burner fuelling. This allows the exhaust gas temperature and engine thermal loading (in particular the temperature of the exhaust valves) to be controlled by varying the ACC fuel control pressure. However there is also a significant increase in the total BSFC. It is therefore necessary to control the ACC fuelling so the minimum ACC fuel flow rate is used, for a given engine load and speed, while the engine A/F ratio is kept high enough to maintain the exhaust temperature, smoke, etc. below their limiting values.

The turbine inlet temperature has not yet been discussed in detail, because the temperature level was significantly lower than the exhaust manifold gas temperature. This parameter, however, has an important influence on the turbocharger performance limits. It can be seen from Fig. 6.29 that as the ACC fuelling is increased a point will be reached where this temperature level may become a limiting parameter. If this is the case, then any increase in the ACC fuelling will reduce the exhaust manifold gas temperature, but increase the by-pass gas temperature, which may increase the turbine thermal loading.

The effect on the mixer temperature will depend upon the relative temperatures and the engine speed (i.e. the proportion of the total flow that goes through the by-pass system). Eventually a point is reached where the engine load cannot be increased any further. The limiting BMEP may not be due to thermal loading, but to mechanical loading of the cylinder (i.e. the peak cylinder pressure) or turbocharger overspeed (or choke) at high pressure ratio's. Fig. 6.29 clearly shows how the increase in boost pressure affects the peak cylinder pressure and turbocharger speed.

A control system of some kind must therefore be developed to find the optimum ACC fuelling for a given engine speed and load. This is discussed in section 6.10. Assuming that the ACC burner fuelling is controlled by means of the fuel control pressure, p_f, Fig. 6.32 shows the relationship between the boost pressure, p_2, the fuel control pressure, p_f, and the ACC displacement, x. The relationship between the ACC displacement and fuelling can be seen from Fig. 4.47.

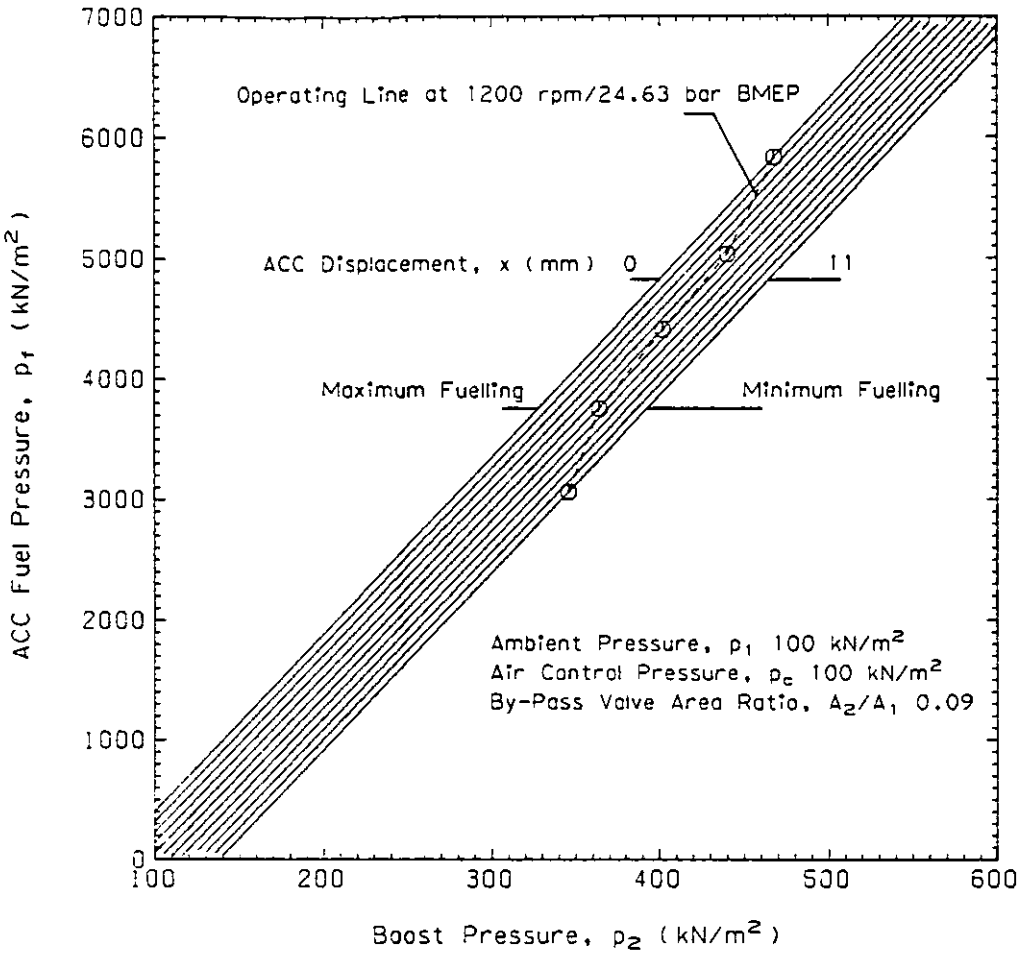

Fig. 6.32 Effect of Varying the ACC Fuel Control Pressure on the Boost Pressure and the ACC Displacement.

Also plotted on Fig. 6.32 is the operating line between maximum and minimum ACC fuelling at 1200 rpm with constant engine fuelling, (the BMEP varying from 24.63 bar with minimum ACC fuelling to 25.83 with maximum ACC fuelling). It can be seen that varying the fuel control pressure, p_f, between 3064 kN/m^2 and 5834 kN/m^2 will cause the ACC to move from minimum to maximum fuelling at this load and speed. The increase in ACC fuelling with displacement is non-linear (see Fig. 6.24), and therefore the increase in fuel control pressure required to achieve a given increase in ACC fuelling will also be non-linear.

Fig. 6.33 shows the effect of increasing the fuel control pressure so that the ACC displacement goes from 11 mm (minimum fuelling) to 0 mm (maximum fuelling) on the engine and turbocharger system performance at 1200 rpm. The main effect on the engine performance occurs between displacements of 4 mm and 7 mm, where the fuelling characteristic is steepest, see Fig. 6.24. With the fuel control pressure below 3064 kN/m^2 there will be no effect on the engine performance by changing the fuel control pressure, because the ACC will be in the idle position.

As the burner fuelling is increased, the exhaust gas temperature reduces, due to the increase in compressor pressure ratio and engine A/F ratio. The by-pass gas temperature increases, and the result is an increase in the turbine inlet temperature. The engine BMEP increases with the boost pressure as does the maximum cylinder pressure, which rapidly exceeds the manufacturers limit of 140 bar. The small reduction in engine BSFC, and the large increase in total BSFC, with the increase in ACC fuelling can be seen in Fig. 6.33. The shape of the ACC A/F ratio versus fuel control pressure curve will be governed by the way in which the port areas and ACC fuelling increase with ACC displacement, as well as by the boost pressure and scavenge pressure drop ratio characteristics.

So for a given engine speed, the maximum load that can be obtained will depend upon the various restrictions placed on the engine performance, for example:-

(1) smoke limit,

(2) maximum cylinder pressure limit,

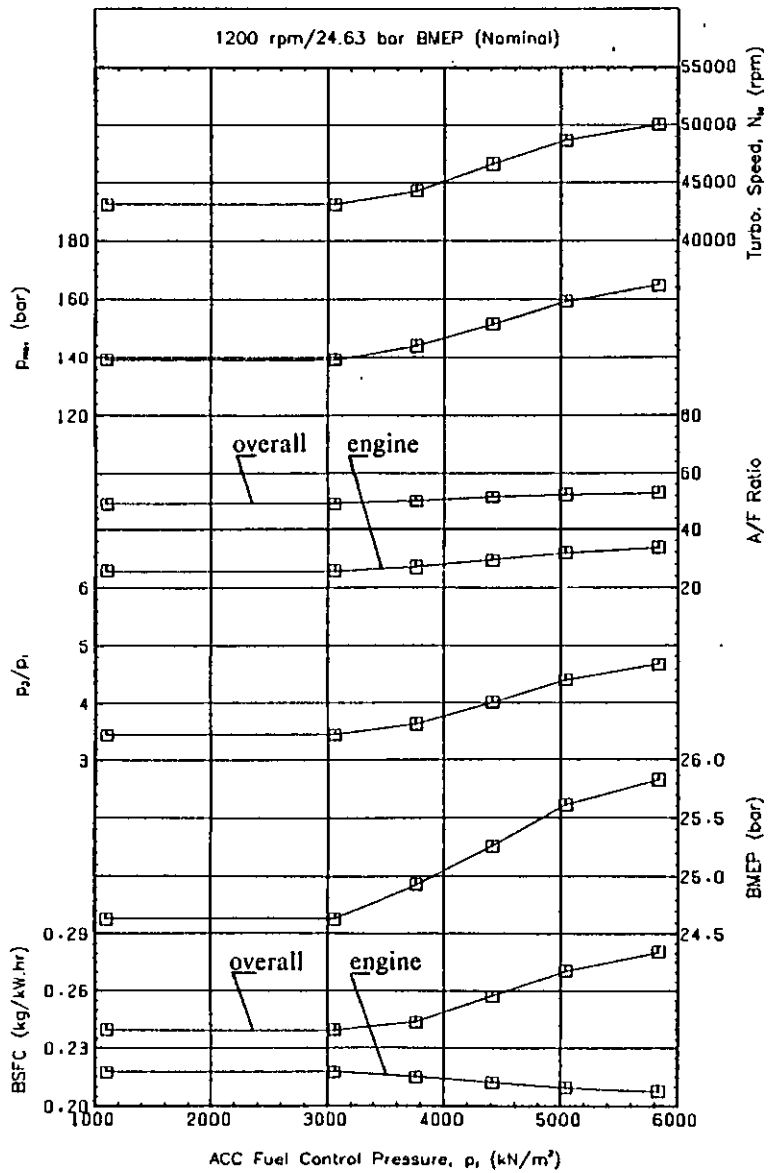

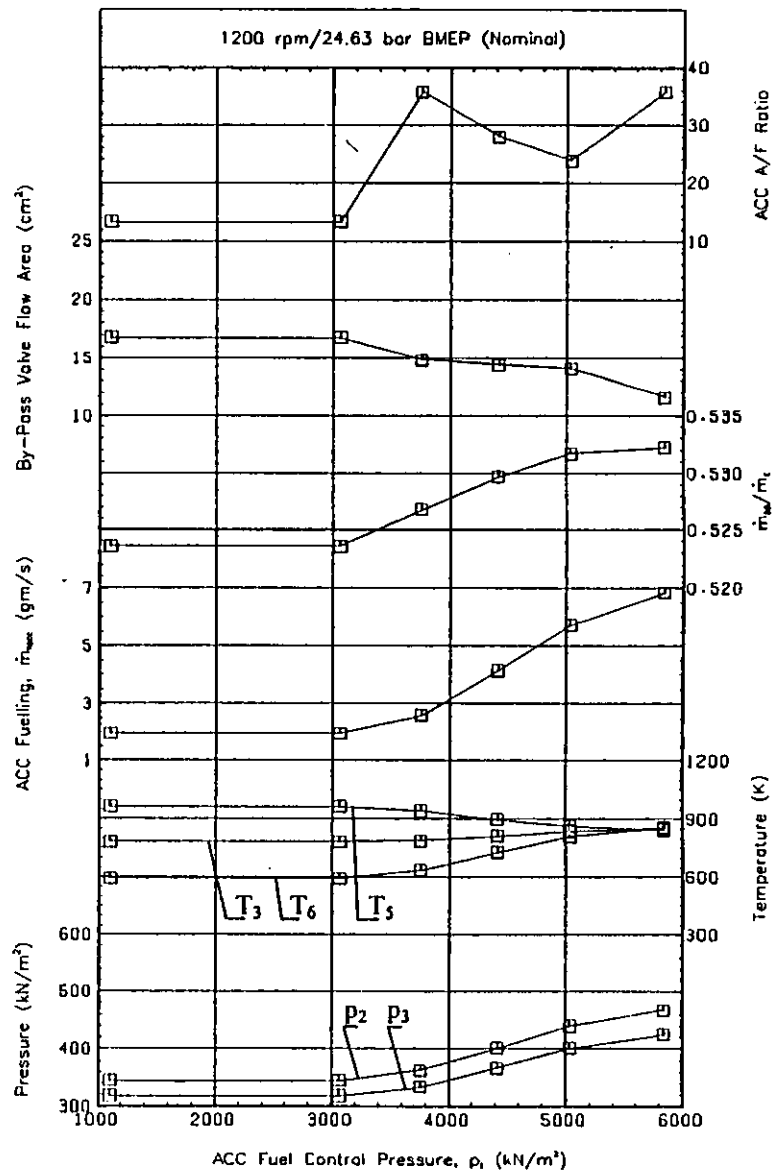

Fig. 6.33 Effect of the ACC Fuel Control Pressure on the Overall Engine Performance at 1200 rpm/24.63 bar BMEP (Nominal).

(3) exhaust manifold gas temperature limit,

(4) turbine inlet temperature limit,

(5) compressor operating limits (e.g. maximum speed, surge, choke),

(6) engine component temperature limits (e.g. piston, exhaust valve(s)).

The ACC fuelling must therefore be minimised, while these limits are adhered to.

6.9 Maximum Torque Curve.

6.9.1.Introduction.

Five engine speeds, 800, 1200, 1600, 2000 and 2400 rpm, have been used to predict the standard maximum engine torque curve. The engine fuellings at each speed were taken from the curve fits of the fuel pump characteristics for this engine, at the maximum rack limit (see section 4.6.6). No boost controlled rack limiting device (aneroid) was considered to be necessary at this rating, the maximum engine output being 17.09 bar BMEP (nominal) at 2400 rpm.

6.9.2 Maximum Torque Curve with the Minimum Burner Fuelling.

Fig. 6.34 shows the maximum engine performance over the speed range with the fuel pump set to the maximum rack limit, and the ACC idling. Maximum BMEP occurs at 1500 rpm with a torque rise of 14.5% from the maximum engine speed (2400 rpm). The difference between the engine and total BSFC becomes more significant as the engine speed reduces, because the ACC fuelling rate is constant, and the engine fuelling rate reduces with engine speed, consequently the ACC fuelling becomes a larger proportion of the total. For example, at 800 rpm, the total BSFC is 19.5% higher than the engine BSFC, while the difference is only 6.7% at 2400 rpm.

The engine A/F ratio increases as the boost pressure rises, with increasing engine speed. At low speeds the smoke limit will probably be reached, the engine A/F ratio

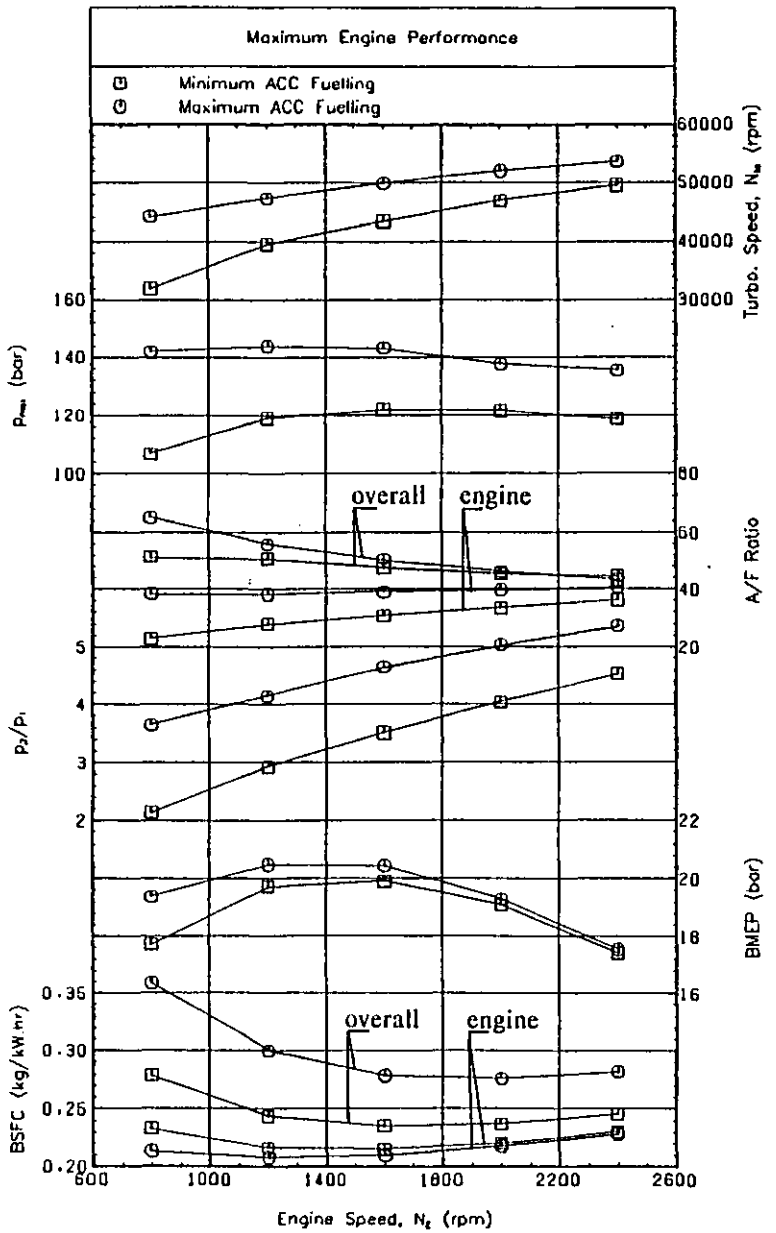

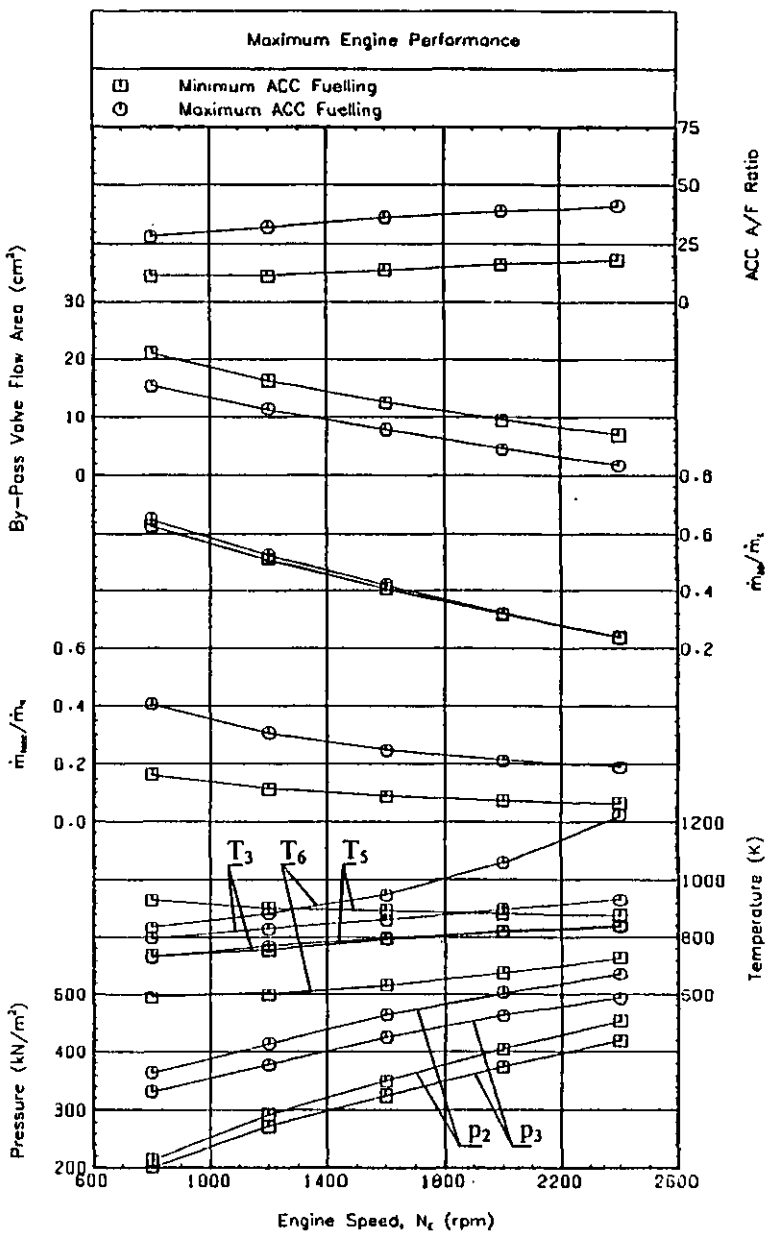

Fig. 6.34 Effect of the ACC Fuelling Level on the Overall Engine Performance at the Maximum Fuel Pump Rack Position.

being only 23.0 at 800 rpm (the total A/F ratio is 51.5 at this speed). As the engine A/F ratio increases, the exhaust manifold gas temperature reduces from 930 K at 800 rpm to 875 K at 2400 rpm, and so the burner will be required first at low engine speeds, for a predefined exhaust gas temperature limit.

As the speed increases the proportion of the total compressor flow that goes through the by-pass system reduces, from 62.7% at 800 rpm to 23.9% at 2400 rpm. The by-pass valve closes as the engine speed rises to maintain the correct scavenge pressure drop ratio (0.09). Thus at higher boost pressures the pressure drop across the by-pass system will be greater.

The total A/F ratio reduces as the engine speed increases from 800 rpm, because the air supply cannot increase at the same rate as the fuel flow rate (engine speed). At higher engine speeds, however, the fuelling/cycle/cylinder starts to reduce, because of the volumetric efficiency characteristics of the fuel pump, and this produces the characteristic torque curve seen in Fig. 6.34. This results in a continuously increasing turbine inlet (mixer) temperature, between 800 and 2400 rpm, rising from 735 K to 842 K. The ACC gas temperature increases by 137 K over this speed range, partly because of the increase in boost temperature, T_2, (from 384 K to 496 K). The overall by-pass A/F ratio increases between 800 and 1200 rpm (from 198.0 to 232.4) but reduces thereafter to 169.7 at 2400 rpm, due to the effects of changing engine speed and boost pressure on the by-pass air flow.

The peak cylinder pressure rises as the boost pressure increases, but the constant static injection timing and injection delay (in terms of time) retards the dynamic injection timing as the speed increases (from 17.1°CA BTDC at 800 rpm to 11.3°CA BTDC at 2400 rpm). This effect tends to limit the peak cylinder pressure which, at this rating, peaks at 121.9 bar at 1600 rpm.

As the exhaust gas temperature is relatively high, and the minimum ACC fuelling is used, the reducing ACC gas temperature as the engine speed falls tends to dominate the final turbine inlet temperature, because the proportion of the by-pass flow to total flow increases as the speed reduces. This results in the low turbine inlet temperatures at low engine speeds, and therefore lower boost pressures. The ACC will therefore be required to control the minimum boost pressure level first at low engine speeds, for a given load.

Throughout the speed range the majority of the total by-pass flow goes through the by-pass valve, the ACC port flow increasing as the boost pressure, and pressure drop across the ports, increase with engine speed. The proportion of ACC flow to total by-pass flow increases from 6.2% to 10.6% as the speed increases. The by-pass valve and ACC performance can be seen in Fig. 6.35. The mean pressure drop across the valve increases with boost pressure but the magnitude of the oscillations in pressure across the valve does not vary significantly (being typically 20-25 kN/m^2). These pulses cause the valve to oscillate more at lower engine speeds, due to the greater amount of time available for the valve to accelerate from one position to another. The oscillations have almost completely died out at 2400 rpm. The fact that the by-pass valve area is not constant, nor in phase with the exhaust pulses, (due to the valve inertia and damping) causes the by-pass valve flow to be slightly out of phase with the flow pulsations through the constant area ACC ports.

The compressor operating line over the speed range is shown in Fig. 6.36. This can be seen to be to the right of the peak efficiency area of the map. Rematching with a slightly larger compressor should, therefore, give some improvement in the steady state compressor efficiency (although the transient response of the turbocharger may suffer if the inertia is increased).

6.9.3 Maximum Torque Curve with the Maximum Burner Fuelling.

Increasing the ACC fuelling at a given engine speed allows the BMEP to be increased provided that the other engine and turbocharger limits are not exceeded. The increase in torque possible over the speed range therefore depends upon the particular limits that are applied to the engine performance.

Fig. 6.34 also shows the maximum torque curve over the engine speed range with the burner in the maximum fuelling position. The engine fuellings are identical to those used in section 6.9.2. for this comparison (i.e. the pump is not rematched).

With the burner delivering the maximum fuelling a substantial increase in boost pressure can be achieved over the speed range, the effect being more prominent at lower engine speeds. The resulting increase in the engine A/F ratio causes a reduction

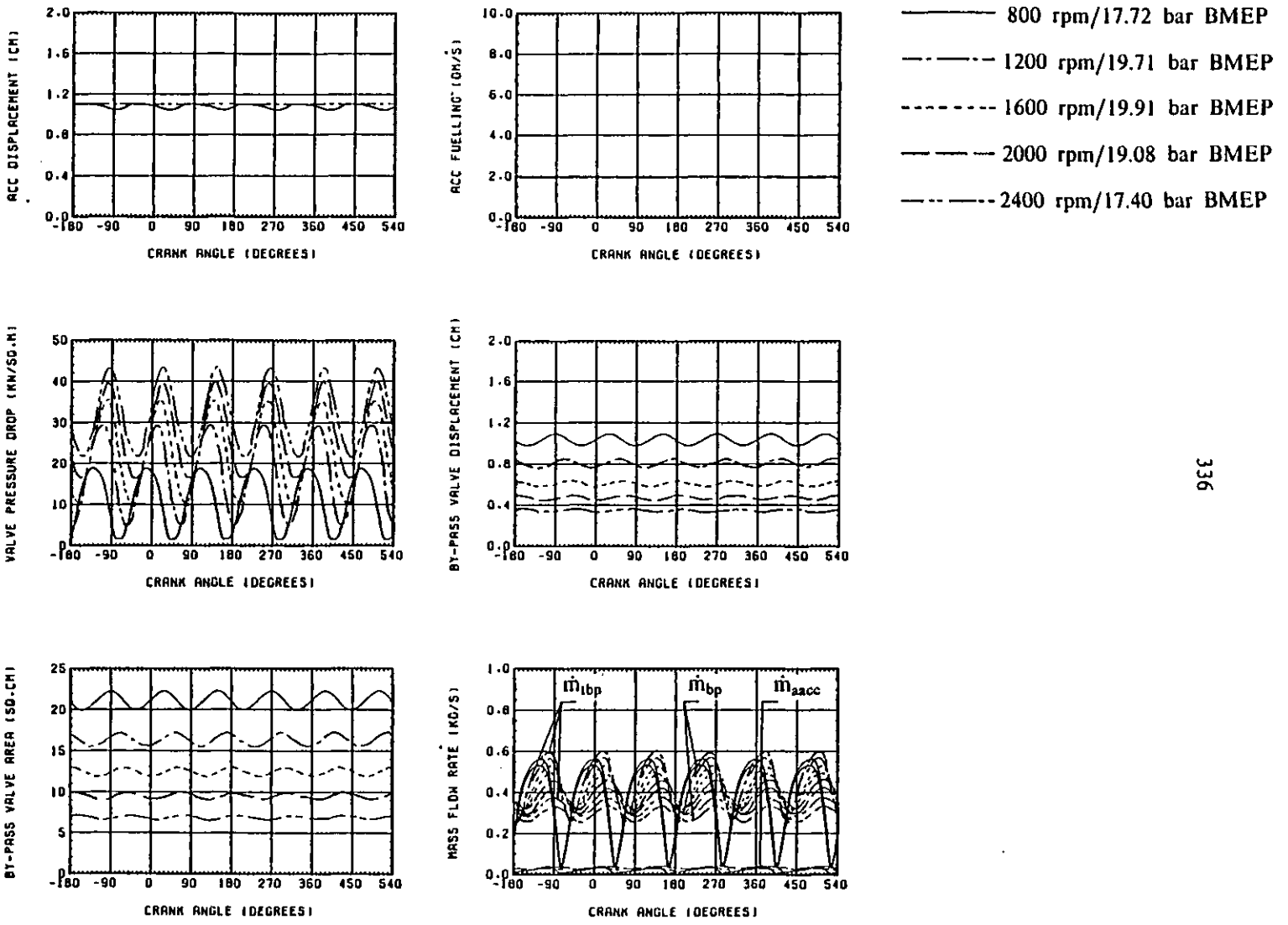

Fig. 6.35 Effect of the Engine Speed on the Hyperbar System Performance with the Minimum ACC Fuelling Level.

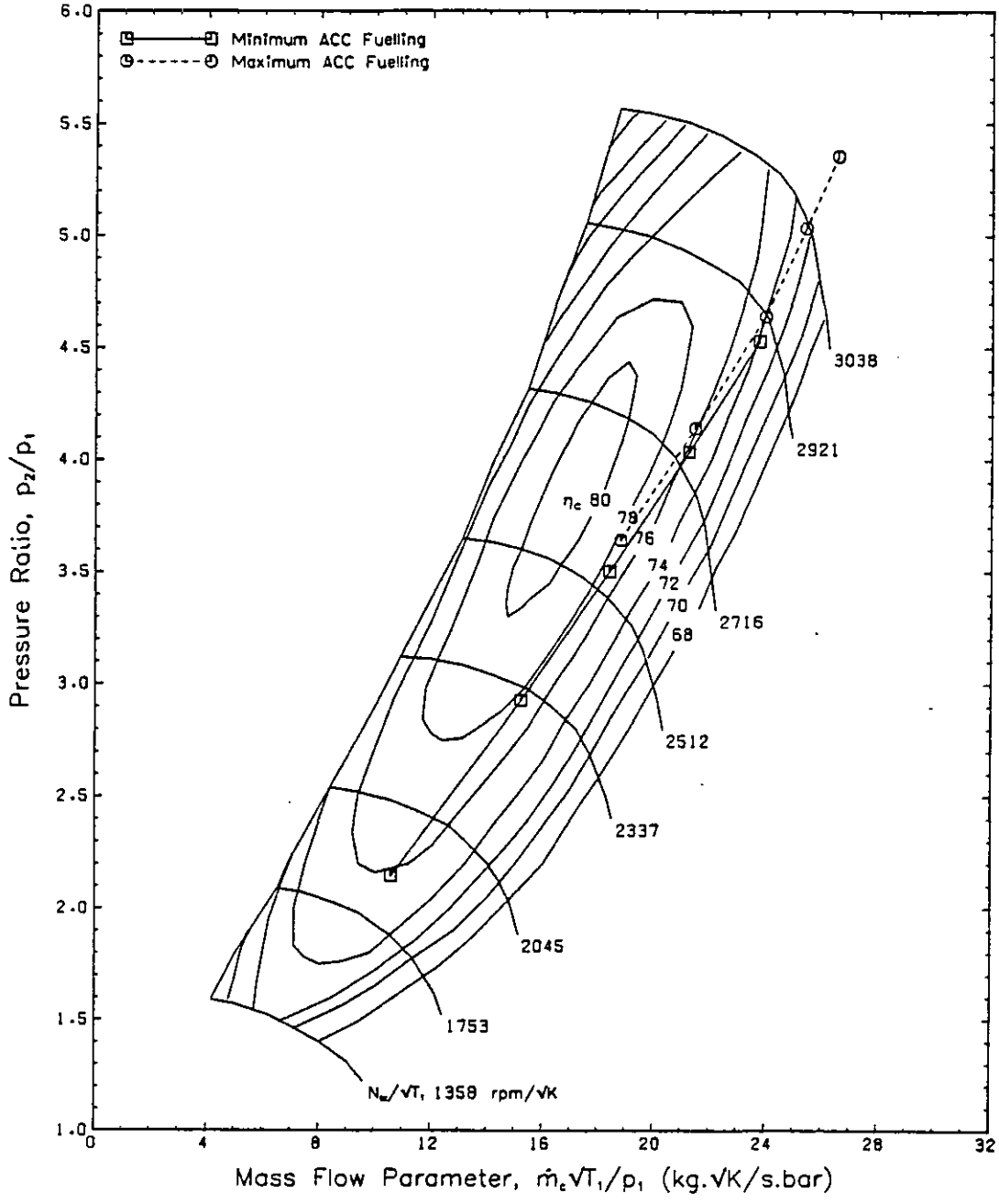

Fig. 6.36 Effect of the Engine Speed and the ACC Fuelling Level on the Compressor Operation at the Maximum Fuel Pump Rack Position.

in the exhaust manifold gas temperature and smoke, especially at low engine speeds.

The increase in scavenge pressure drop with boost pressure (because of the by-pass valve action) causes an increase in the positive pumping work. Also the higher boost pressure and temperature reduces the ignition delay and advances the start of combustion. This results in higher peak cylinder pressures, and an increase in the engine BMEP by as much as 9.3% at 800 rpm, the increase falling to only 0.7% at 2400 rpm. The FMEP increases somewhat due to the effect of higher peak cylinder pressures on the frictional losses, (the largest increase being 13.2% at 800 rpm).

The compressor mass flow rate increases with the increase in boost pressure, but it can be seen from the compressor map, Fig. 6.36, that the compressor efficiency falls off rapidly at high engine (and compressor) speeds with the ACC held at maximum fuelling, reducing by as much as 4.1% at 2400 rpm. This will tend to limit the overall turbocharger efficiency.

There is a large increase in the ACC gas temperature with increases in fuelling, and this becomes more significant as the engine speed increases, and the by-pass air flow reduces. However, at the high engine speeds the by-pass flow is a small proportion of the total flow, 23.5% at 2400 rpm, the turbine inlet temperature therefore, increases by approximately 33 K for each speed increase of 400 rpm, between 800 and 2400 rpm.

The proportion of by-pass flow to compressor flow is very close to that predicted for the case where the ACC was in the minimum fuelling position, over the entire speed range. The by-pass valve area will be smaller with the ACC at maximum fuelling because a larger proportion of the total by-pass flow goes through the ACC ports. At 2400 rpm the valve is almost closed, with 76.6% of the total by-pass flow going through the ACC ports. Any further increase in speed would result in the valve closing completely, and it would then be unable to control the scavenge pressure drop ratio and the compressor operating line. The pressure drop across the ACC ports would then be dependent on the mass flow rate through them.

The maximum engine BMEP of 20.55 bar occurs at a lower engine speed, 1400 rpm, with increased ACC fuelling due to the larger increase in boost pressure at the lower speeds, and the maximum torque is 17.2% greater than that at maximum power,

compared to 14.5% with the burner idling.

Fig. 6.37 shows the performance of the Hyperbar system over the speed range with the ACC held in the maximum fuelling position and can be compared with Fig. 6.35, with the minimum ACC fuelling at the same speeds. The reduced by-pass valve displacement, effective flow area and air flow rate with the ACC held at maximum fuelling is particularly apparent. As the engine speed increases, the proportion of the total by-pass flow that goes through the valve decreases from 73.2% at 800 rpm, to 66.9% at 1200 rpm and 58.2% at 1600 rpm. At 2000 rpm a greater proportion of the by-pass flow goes through the ACC ports, with only 44.5% going through the valve. At 2400 rpm only 23.4% of the total by-pass flow goes through the valve and its pulsation amplitude, effective flow area and displacement are very small.

In practice the ACC fuelling will reduce with increasing engine speed, see section 6.10, and such high ACC flow rates will not normally be encountered. It should be noted that the relative ACC and by-pass valve flows depend upon their coefficients of discharge, which have both been assumed to be constant (i.e. independent of displacement and pressure ratio) and equal to 0.65 for this analysis.

6.9.4 Using the Burner to Increase the Engine Low Speed Torque.

The ACC burner can be used to allow an increase in the engine fuelling and hence torque over the entire speed range. However, the extent to which the BMEP can be increased at any speed will depend upon the particular limits imposed by the engine thermal and mechanical stresses.

The following limitations were used to predict the maximum engine performance for the case with the burner idling, and with the burner fuelling varied until one, or more, of the following limiting conditions were reached:-

(1) Maximum cylinder pressure, 140 bar.

(2) Maximum turbine inlet temperature, 973 K (700°C).

(3) Minimum engine A/F ratio, 23.5.

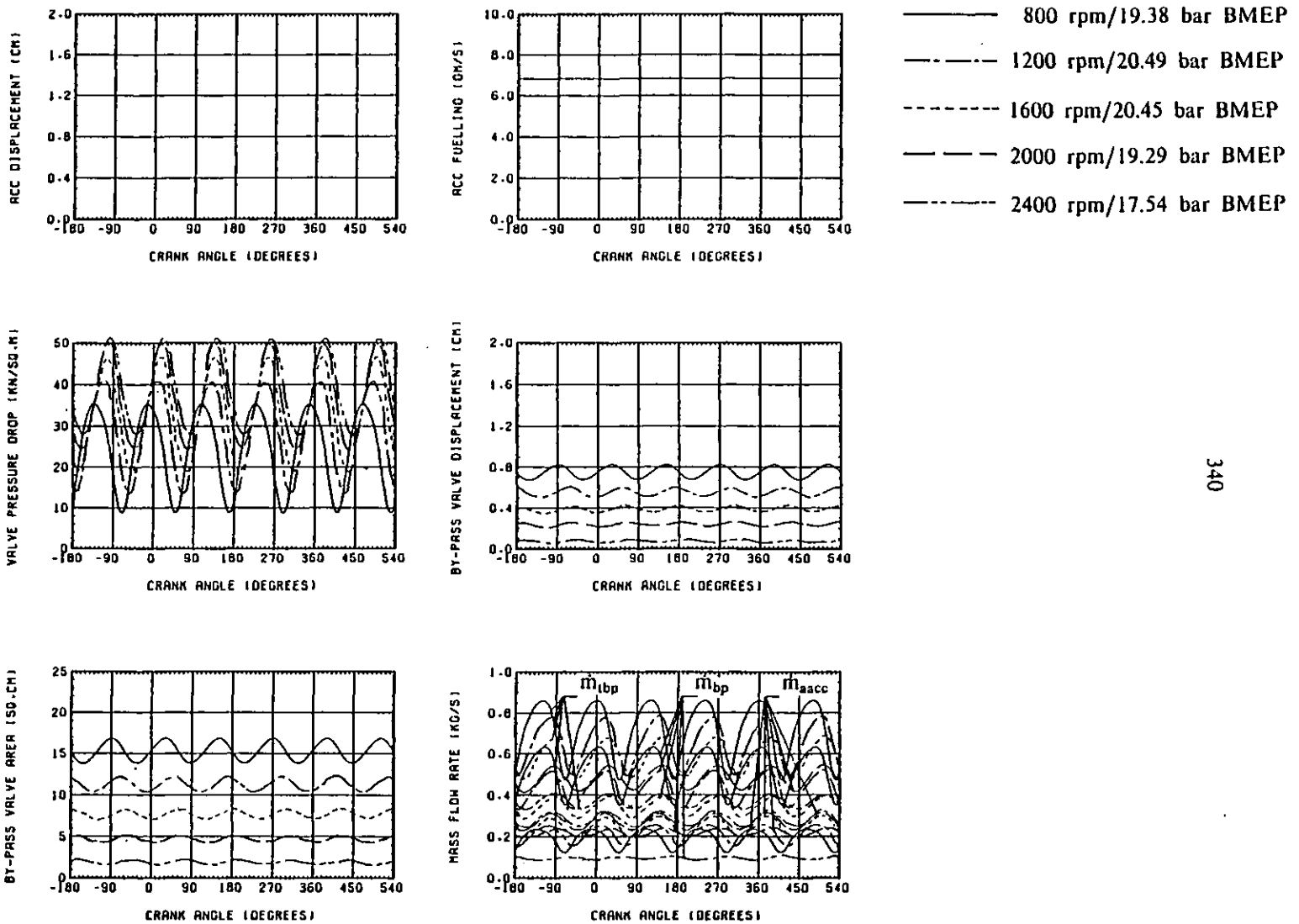

Fig. 6.37 Effect of the Engine Speed on the Hyperbar System Performance with the Maximum ACC Fuelling Level.

(4) Maximum exhaust manifold gas temperature, 973 K (700°C).

The maximum cylinder pressure can be used as a measure of the mechanical loading of the engine, while the exhaust manifold gas temperature gives an indication of the thermal loading of the piston and exhaust valves, which are the most difficult components to cool in practice. Similarly the inlet temperature limit indicates the thermal loading of the turbine, and the engine A/F ratio limit can be regarded as a measure of the smoke produced by the engine.

The engine fuelling was increased at each speed until one or more of these limits was reached, with the burner idling, then the burner fuelling was increased to allow a further increase in engine load, if this was practical. For example, if the maximum cylinder pressure limit is reached first, increasing the burner fuelling will only make the situation worse, and so no improvement in performance can be achieved. The option of retarding the injection timing to reduce the maximum cylinder pressure was not considered at this stage.

There is a conflict between the action that must be taken by the control system, to maintain the engine operation within the particular limits specified. The burner fuelling must be increased to increase the engine A/F ratio and reduce the exhaust manifold gas temperature, while it must be reduced to decrease the peak cylinder pressure and turbine inlet temperature, for a given engine fuelling. Fig. 6.38 shows diagramatically the effect of the engine and ACC fuelling on the engine performance parameters listed above, for a given engine speed. The limits to the ACC fuelling rate are determined by the design of the burner, and were considered as fixed throughout this analysis. The position and gradients of the various engine performance limiting parameters will vary with engine speed, and so Fig. 6.38 should not be considered as general. In this particular example (at a low engine speed, 800 rpm), with the ACC burner idling, the limit to the amount that the engine fuelling can be increased is determined when the minimum engine A/F ratio is reached, point (a). No further increase in engine power can be achieved at this speed without exceeding this predefined performance limit.

If the ACC burner fuelling is increased, then the boost pressure and engine air flow will increase and so the engine A/F ratio will rise. This allows a further increase in

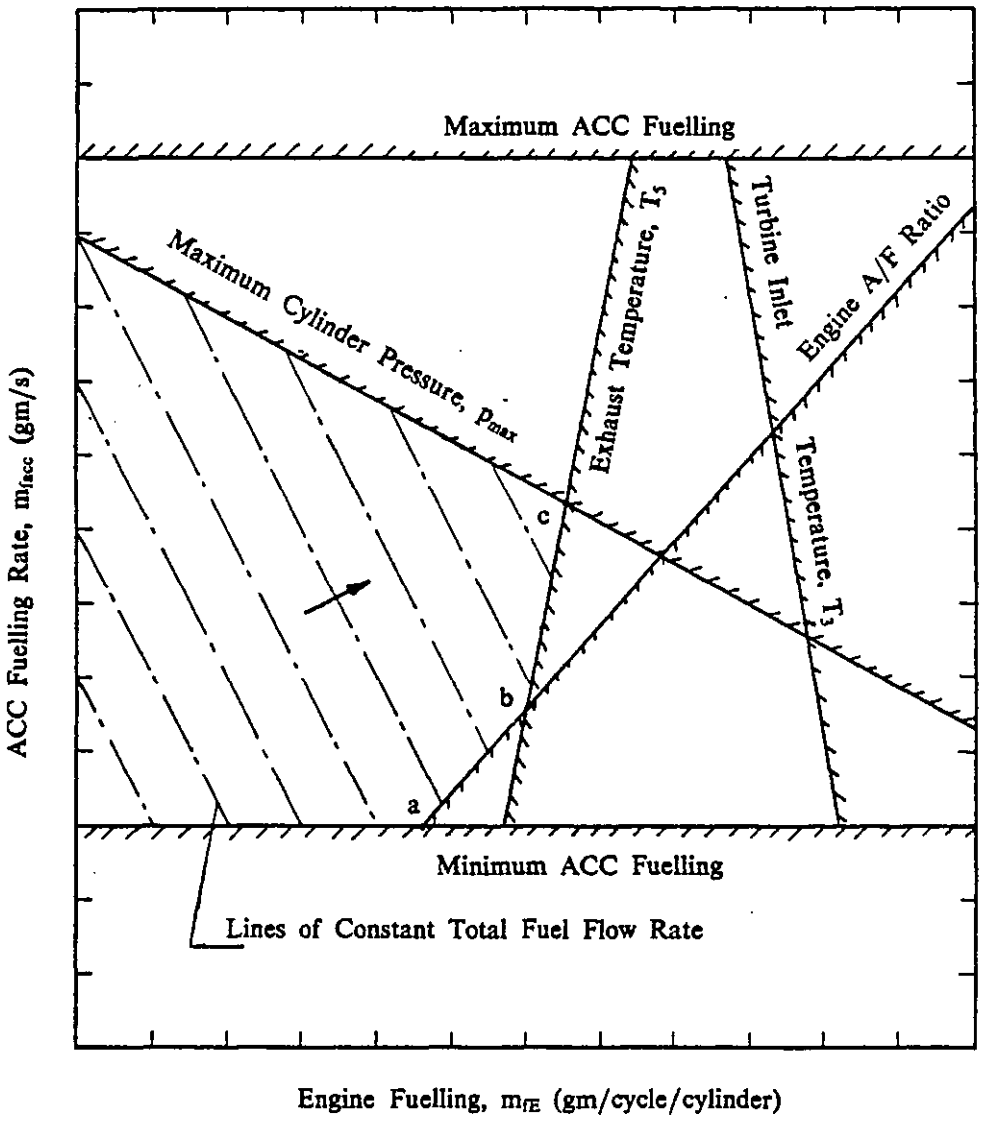

Fig. 6.38 Engine Performance Limitations at 800 rpm.

the engine output, by gradually increasing the engine and burner fuelling together, along line (a-b) until the exhaust manifold gas temperature limit is reached, point (b). In order to maintain the exhaust temperature at the limiting value, the ACC fuelling must now be increased substantially as the engine fuelling is increased, line (b-c). Finally the peak cylinder pressure limit is reached, point (c). Any further increase in the engine or ACC fuelling will result in either the exhaust manifold gas temperature or the peak cylinder pressure limits being exceeded (or both) and so no further increase in engine output is possible. Point (c) therefore gives the maximum engine fuelling that can be used, and the corresponding ACC fuelling.

Also shown on Fig. 6.38 are lines of constant total fuelling for the engine and burner. The rate of increase in total fuelling with increase in engine fuelling/cycle/cylinder will be proportional to the engine speed. If the engine is to be optimised to give the best total BSFC at maximum power, for a given engine speed, then the optimum point might not be point (c). In this example the increase in engine fuelling and BMEP, between points (b) and (c) is small, while the increase in total fuelling is quite large, due to the increase in ACC fuelling required to maintain the limiting exhaust gas temperature. Point (b) may therefore provide a much lower total fuel consumption, for a small reduction in engine power output. The final optimum point will depend to a large extent on the engine speed, because the burner fuelling becomes an increasing proportion of the total as the speed reduces.

6.9.5 Engine Performance with Optimum ACC Fuelling.

Fig. 6.39 shows the overall engine performance possible within the limitations discussed in section 6.9.4, with the ACC burner idling. At the low speed end of the operating range the engine output is limited by the engine A/F ratio. As the speed increases, the maximum cylinder pressure becomes the limiting parameter. Fig. 6.39 shows that the maximum torque occurs at 1200 rpm (half the rated engine speed) and is 15.4% higher than the torque at maximum engine power (21.56 bar BMEP). The BMEP at 1200 rpm (24.89 bar) is high by conventional engine standards, but is not excessive for a Hyperbar design. There is, therefore, some scope for increasing the engine performance (at very low speeds where the engine A/F ratio is the limiting parameter), by increasing the burner fuelling. At higher engine speeds (above 1200 rpm) the peak cylinder pressure limit is reached first, and increasing the burner

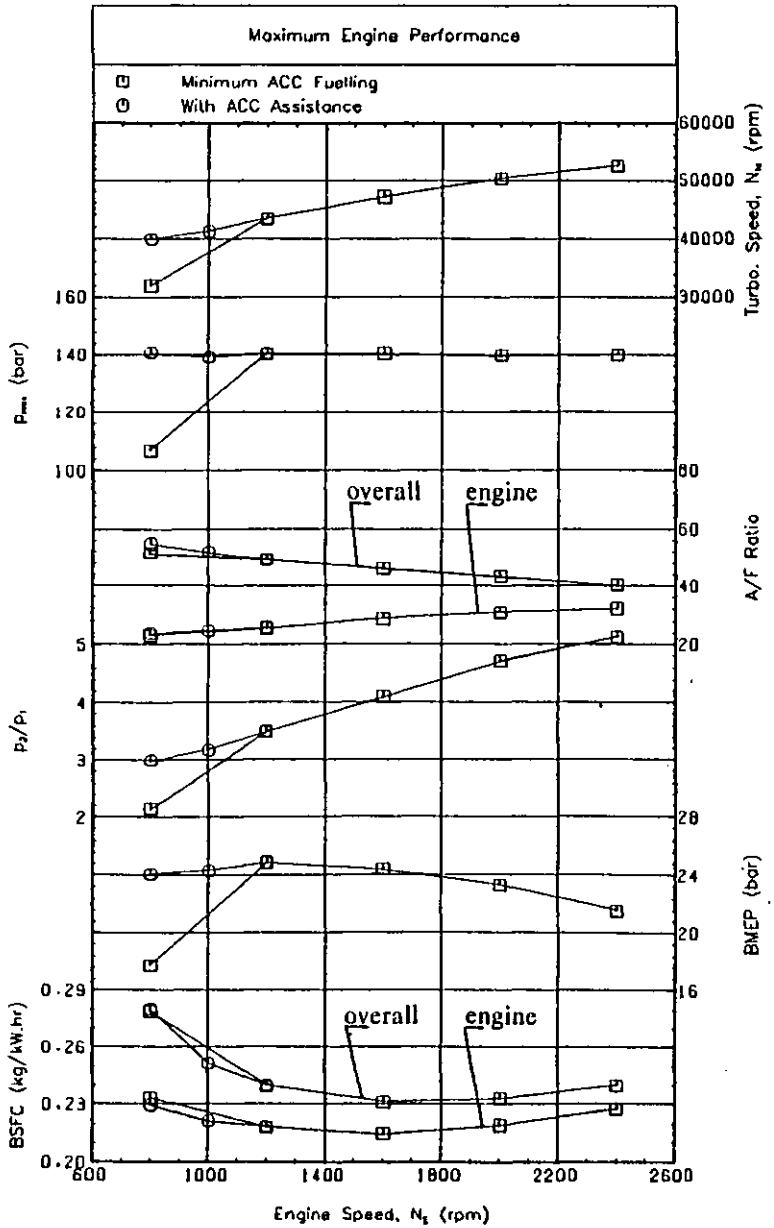

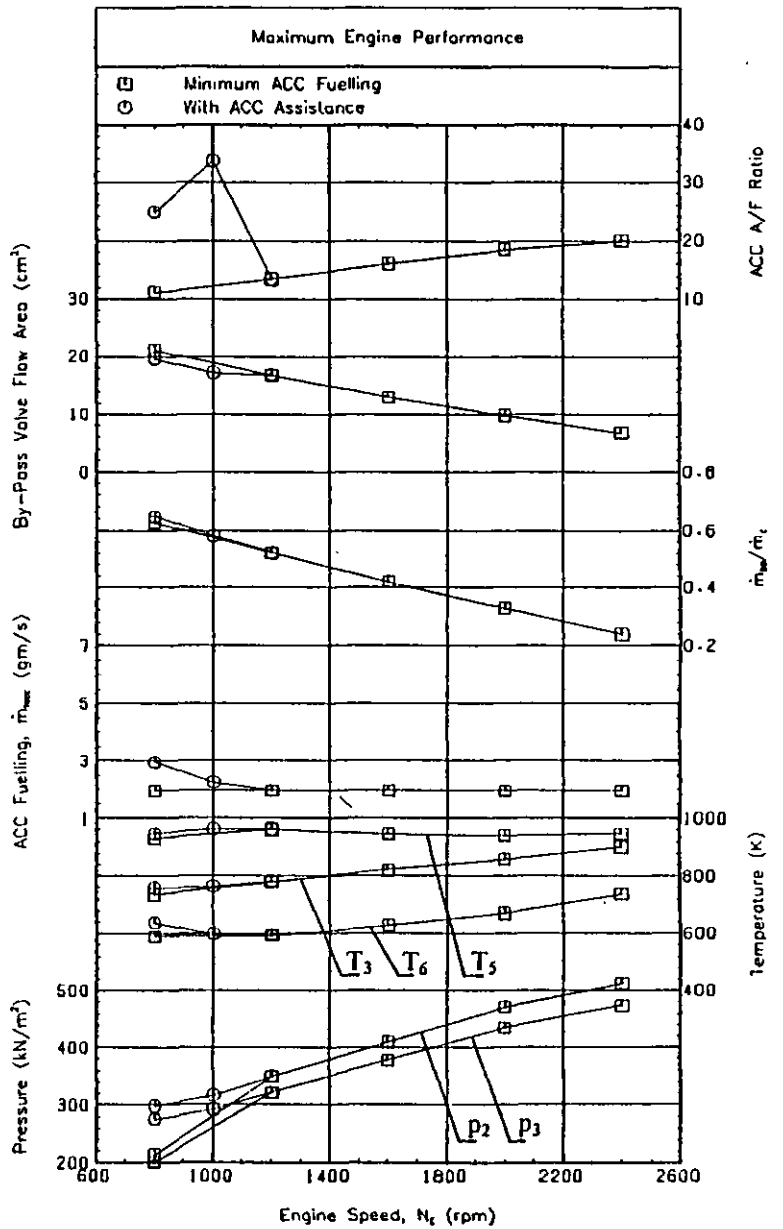

Fig. 6.39 The Limiting Engine Overall Performance with and without the ACC Assistance.

fuelling will only result in an increase in this parameter. Therefore, the engine performance shown in Fig. 6.39 is the maximum that can be obtained, above 1200 rpm, within the limits imposed. Retarding the static injection timing from the standard value used throughout this work (20°CA BTDC), will reduce the peak cylinder pressure and so allow the engine output to be further increased, at the expense of an increase in BSFC. The maximum engine power output predicted, with the burner idling, therefore corresponds to 21.56 bar BMEP at 2400 rpm.

Increasing the engine and burner fuelling at engine speeds below 1200 rpm enables the low speed torque to be increased, for the same limiting engine performance parameters. The increase in engine output possible at 800 rpm and 1000 rpm is shown in Fig. 6.39. At 800 rpm the engine BMEP can be increased from 17.72 bar to 24.09 bar (35.9%) before the engine A/F ratio and maximum cylinder pressure limits are reached. Similarly at 1000 rpm the BMEP can be increased to 24.32 bar when the exhaust manifold gas temperature and peak cylinder pressure limits are reached.

Because of the particular limits chosen for this exercise, no further increase in engine output can be obtained over the speed range. The ACC fuelling used at low engine speeds reduces as the engine speed increases, from 2.954 gm/s at 800 rpm to 2.237 gm/s at 1000 rpm, while the ACC fuel control pressure has to be increased from 2822 kN/m^2 to 3004 kN/m^2.

It should be emphasized, however, that the results obtained in these tests depend upon the particular limitations imposed on the engine performance.

6.10 Optimisation of the ACC Burner Fuelling.

6.10.1 Introduction.

The simulation program can be used to optimise the Hyperbar ACC fuelling at high engine loads, by adjusting the fuel control pressure, and therefore the ACC displacement. The control strategy used to regulate the burner fuelling will depend upon the particular parameters that limit the engine performance.

Obviously the minimum burner fuelling, for a given engine output is required,

provided that the various parameters discussed in section 6.9.4 are not exceeded. Therefore at a given engine speed and fuelling, there will be a minimum value of ACC fuelling that will give the best total BSFC. Similarly at a given engine speed, the maximum power output that can be achieved will depend upon the burner fuelling and the particular limitations imposed.

Various simple strategies for controlling the ACC (and engine) fuelling have been investigated, and are discussed in the following sections.

6.10.2 A Simple Control Routine to Limit the Exhaust Manifold Gas Temperature.

At a given speed and load, the exhaust manifold gas temperature is primarily a function of the engine A/F ratio (assuming that the engine fuelling, injection timing, valve timing, etc. are held constant). Increasing the ACC fuelling level will increase the boost pressure and engine A/F ratio, and so reduce the exhaust gas temperature. Therefore a simple system for increasing (or decreasing) the ACC fuelling according to the exhaust gas temperature by varying the ACC fuel control pressure, p_f, has been developed.

An exhaust temperature limit of 900 K (627°C) was arbitrarily set at 1200 rpm/24.64 bar BMEP (the nominal output with the ACC idling), and the engine fuelling fixed. At this operating condition the steady state exhaust gas temperature was 956 K (683°C), the turbine inlet temperature was 778 K (505°C), the engine A/F ratio was 25.9 and the maximum cylinder pressure was 139.6 bar. With the ACC idling the fuel control pressure was set to the datum value of 1100 kN/m^2, and the ACC fuelling rate was 1.953 gm/s.

The control system calculates the error between the exhaust gas temperature (time averaged) and the limiting temperature at the end of each engine cycle. It then adjusts the fuel control pressure, p_f, according to the error, to either increase or decrease the ACC fuelling for the next engine cycle. In this case the ACC fuelling must be increased to reduce the exhaust gas temperature. As the ACC fuelling increases so the boost pressure and engine A/F ratio increase, as does the maximum cylinder pressure, but the exhaust manifold temperature reduces. Increasing the boost pressure also increases the exhaust system pressure and, in particular, the ACC gas

pressure (because of the by-pass valve action and the extra ACC fuelling) which tends to reduce the ACC fuelling due to the dynamics of the ACC, see section 4.8.3. This means that the increase in ACC fuel control pressure usually needs to be larger than that calculated by simply considering the temperature error. A flow chart for this simple control system is shown in Fig. 6.40.

Fig. 6.41 shows the results obtained using this simple control routine. After the three engine cycles required to achieve steady initial conditions, the control routine increases the fuel control pressure, and hence the ACC fuelling, to reduce the exhaust gas temperature. The values of the parameters plotted in Fig. 6.41 are the values for the particular cycle number, and therefore the ACC fuel pressure for cycle number 8, for example, is based on the temperature error at the end of the previous cycle (cycle number 7).

Unfortunately the ACC fuelling does not increase linearly with fuel control pressure, because of the ACC fuelling characteristics, and a more sophisticated routine is required to take account of this, see section 6.10.3. As the temperature error is reduced, less action is taken by the control routine, reducing the temperature asymptotically to the pre-defined limit.

It takes 13 engine cycles to reduce the exhaust manifold gas temperature from 956 K to 900 K, during which time the ACC fuel control pressure has been increased to 4380 kN/m^2, and the fuelling increased from 1.953 gm/s to 3.992 gm/s (i.e. by 104.4%). The engine A/F ratio has increased from 25.9 to 29.3, and the turbine inlet temperature raised from 778 K to 811 K to provide the increase in compressor pressure ratio from 3.47 to 3.99. The increase in boost pressure causes an increase in engine pumping work and so the BMEP increases from 24.64 to 25.26 bar (by 2.5%), but the additional ACC fuelling required means that the total BSFC increases from 0.239 kg/kW.hr to 0.256 kg/kW.hr (7.1%). The maximum cylinder pressure increases with the boost pressure, from 139.6 bar to 151.0 bar when the engine performance has stabilized.

From Fig. 6.41 it is easy to envisage a control system that takes the appropriate action to control the engine A/F ratio, or one that reduces the ACC fuelling to limit the maximum cylinder pressure, or turbine inlet temperature. Conversely if the exhaust gas temperature were below the limit, the engine fuelling could be increased or the

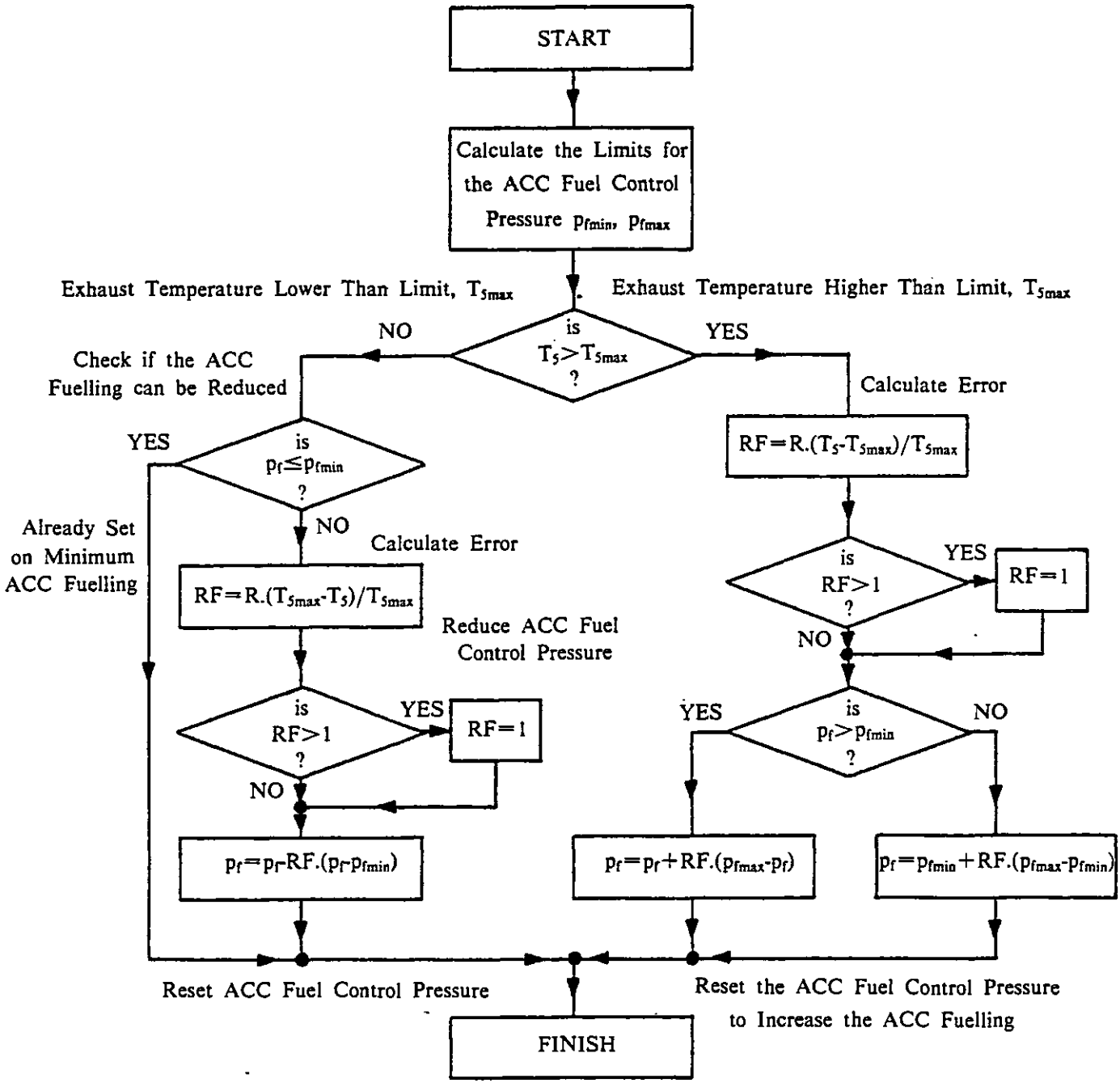

Fig. 6.40 Flow Diagram for a Simple Control System to Limit the Exhaust Manifold Gas Temperature, T_5, to a Predefined Value, T_{5max}, by Varying the ACC Fuelling.

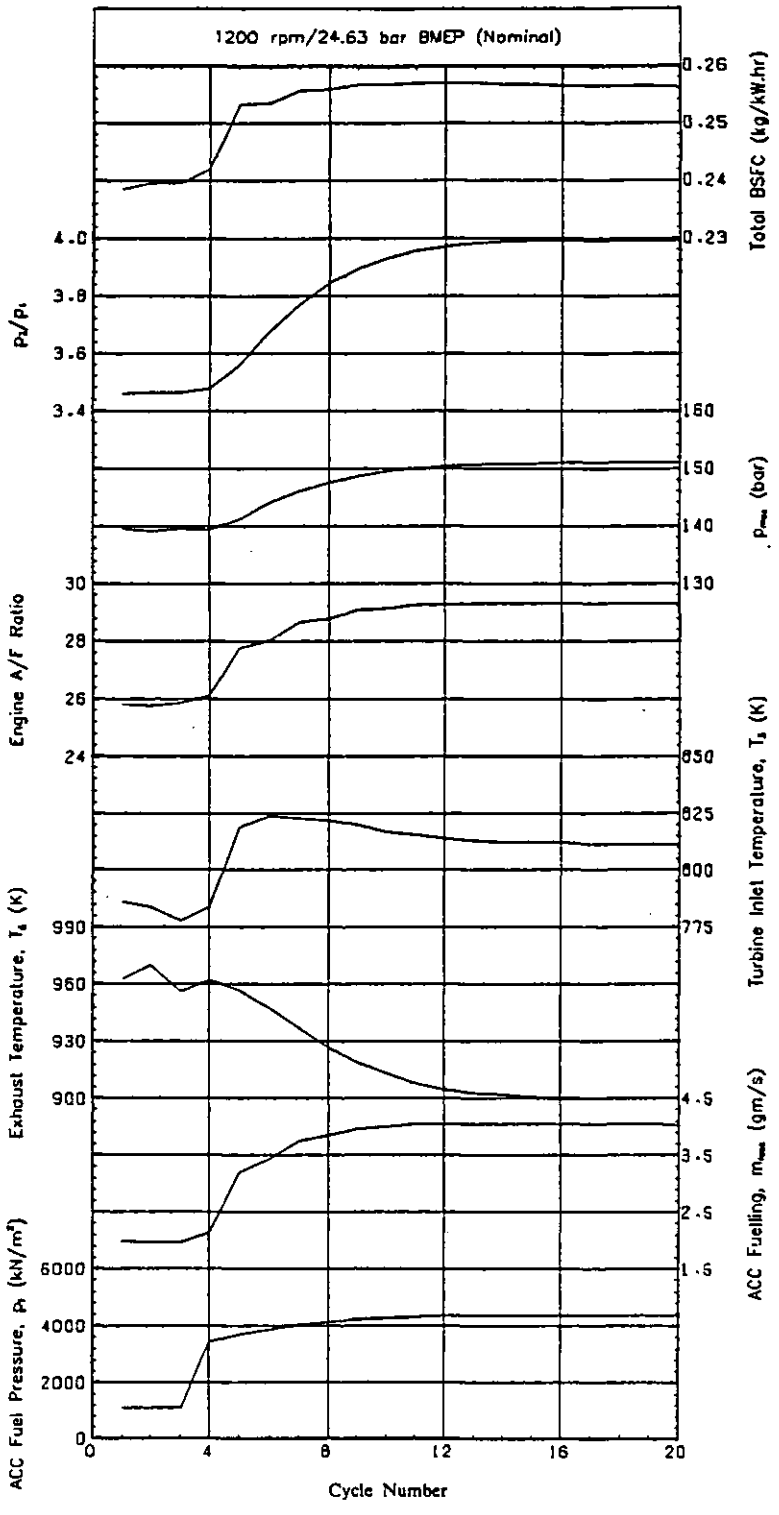

Fig. 6.41. Engine Performance using a Simple Control Routine to Limit the Exhaust Manifold Gas Temperature, T_5, to 900 K.

ACC fuelling reduced.

Assuming that the ACC fuelling is initially set at the minimum level, the engine load could be increased until the exhaust gas temperature limit was reached. Then the engine and ACC fuelling could be increased together to maintain the exhaust temperature on the limit, while increasing the engine power output. This process could continue until:-

(1) a predetermined power output is reached,

(2) the maximum ACC fuelling level is reached, or

(3) some other limiting parameter (e.g. maximum cylinder pressure) is reached.

A more sophisticated control routine is discussed in section 6.10.3 which takes other parameters apart from the exhaust manifold gas temperature into account, and also varies the engine fuelling.

6.10.3 A Control Routine to Maximise Engine Power Output.

Based on the experience gained with the simple exhaust gas temperature control routine, described in section 6.10.2, a more sophisticated control routine has been developed. This routine works within certain predefined limits for various engine performance parameters. The engine limitations used in the following example are given in section 6.9.4.

The engine speed was fixed, and the control routine was designed to maximise the engine fuelling (for maximum BMEP) and minimise the ACC fuelling (for best overall BSFC). As explained in section 6.9.4 the final operating point found by this method may not be the most economical (i.e. it will find point (c) and not point (b) in Fig. 6.38).

A flowchart showing the control strategy for this "second generation" ACC control routine is shown in Fig. 6.42. The simulation program was first run for a number of cycles steady state with an initial estimate of the engine fuelling, selected to give

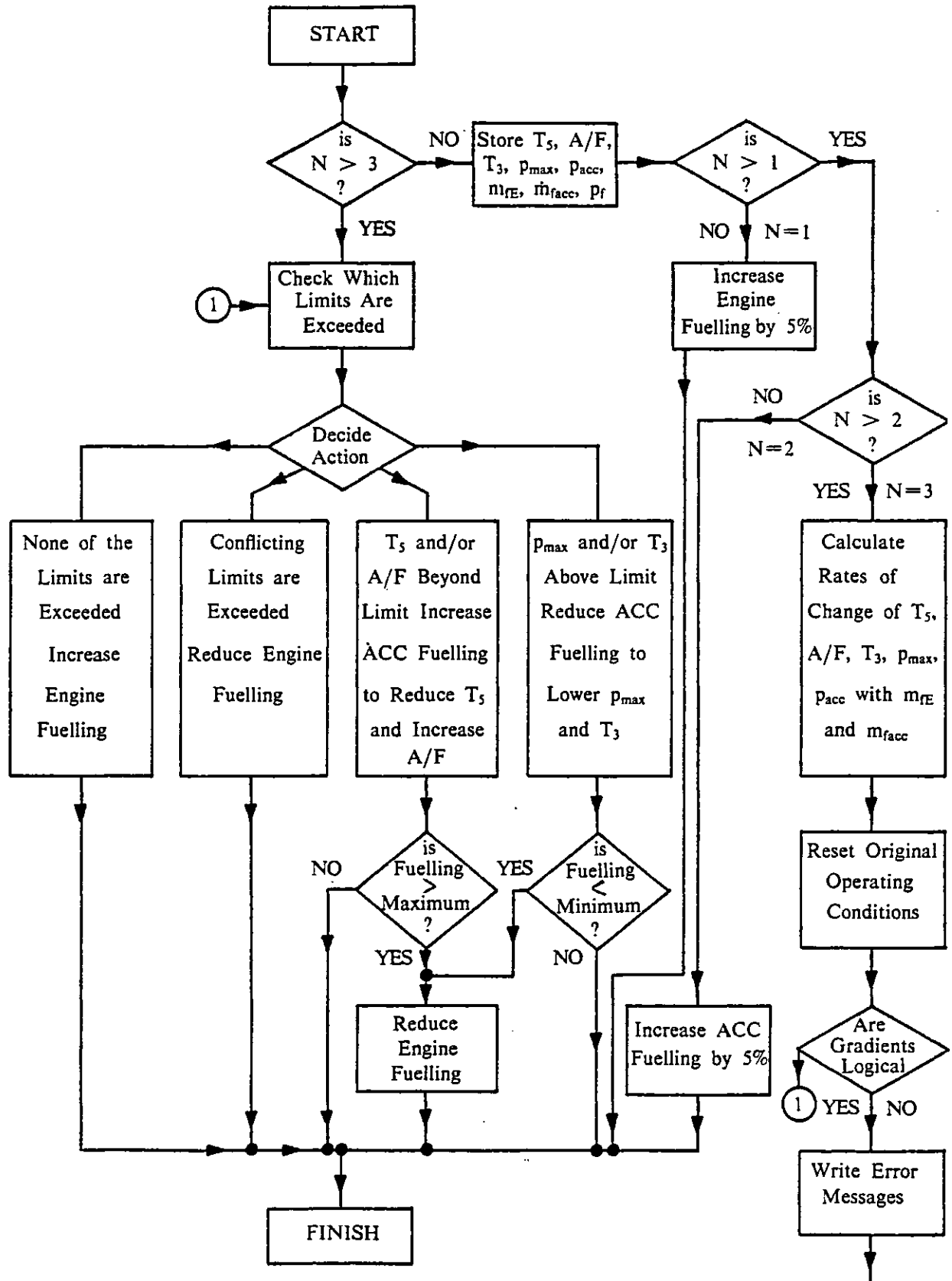

N = Call Number for Control Subroutine

Fig. 6.42 Flow Diagram for the "Second Generation" Control System to Limit the Exhaust Gas Temperature, T_5, the Engine A/F Ratio, A/F, the Turbine Inlet Temperature, T_3, and the Maximum Cylinder Pressure, p_{max}, by Varying the ACC and Engine Fuellings.

approximately the desired power, and with the ACC idling (i.e. with the datum ACC fuel control pressure of 1100 kN/m^2) to obtain the starting conditions. The engine fuelling was then increased, typically by 5%, and the rates of change of the parameters to be controlled (i.e. the exhaust gas temperature, the engine A/F ratio, the turbine inlet temperature and the maximum cylinder pressure) were then calculated. In addition, the rate of change of the ACC gas pressure with engine fuelling was also calculated, because any increase in the exhaust pressure will result in a reduction in the ACC fuelling, in the operating range of the burner. This parameter was also used to speed up the convergence of the control routine, when changes to the engine and ACC fuellings were made. The engine fuelling was then fixed, and the ACC fuelling was increased, by increasing the ACC fuel control pressure, by approximately 5%. The rates of change of the limiting parameters, and the ACC gas pressure, with ACC fuelling were then calculated.

Having obtained the rates of change of the engine performance parameters with engine and ACC fuelling, it was then assumed that the gradients would not change significantly over the range of engine and ACC fuelling changes encountered during the optimisation at a given engine speed. This assumption will not affect the final operating point that is found, but will affect the speed of convergence of the routine. The values of the various limiting parameters were then compared with their preset limits. The following action was then taken by the control routine:-

(1) If either the engine exhaust gas temperature exceeded its limit, or the engine A/F ratio was lower than its limiting value, the ACC fuelling was increased, by increasing the ACC fuel control pressure, p_f, so that the exhaust temperature was reduced below the limit (by a preset amount) and/or the engine A/F ratio was increased above its limit (again, by a preset amount, typically 1%). If the burner was already on maximum fuelling (i.e. there was no further control possible with the burner) then the engine fuelling was reduced until the offending parameter(s) fell within their preset limits.

(2) If either the turbine inlet temperature or the maximum cylinder pressure exceeded their respective limits, the ACC fuelling was reduced (by reducing the ACC fuel control pressure until the offending parameter(s) fell below the limit, again by 1%). If the ACC was already in the minimum fuelling

position, the engine fuelling was reduced to decrease the turbine inlet temperature and/or the peak cylinder pressure.

(3) If one or more of the parameters from (1) and one or more from (2) both exceed their respective limits (for example, the engine A/F ratio and the peak cylinder pressure), then there is a conflict in the action that must be taken by the burner. One wants to increase the burner fuelling and the other to reduce it. Therefore, the only alternative is to reduce the engine fuelling, while holding the fuel control pressure constant. The engine fuelling was reduced until all the offending parameters were within their preset limits. Note that holding the fuel control pressure constant, with reducing engine fuelling, will probably increase the burner fuelling, in the operating range of the burner.

(4) If none of the parameters exceeded their preset limits, the engine fuelling (and hence the BMEP) could be increased. The ACC fuel control pressure was held constant, which meant a reduction in the ACC fuelling (because of the increase in the ACC gas pressure with load), unless the burner was already in the idle (minimum fuelling) position.

Fig. 6.43 shows a typical result of this type of optimisation technique. The engine speed was 1000 rpm and the load was initially 18.51 bar BMEP, with the ACC burner idling. At this condition the exhaust manifold gas temperature was 923 K (compared to the limit of 973 K), the engine A/F ratio was 25.6 (23.5), the turbine inlet temperature was 751 K (973 K) and the maximum cylinder pressure was 110.9 bar (140 bar), on cycle number 10.

The control routine then increased the engine fuelling by 5% from cycle number 11, and stored the new values of the performance parameters on cycle number 14. The exhaust manifold gas temperature had increased by 16 K, the turbine inlet temperature by 5 K, the maximum cylinder pressure by 4.3 bar, but the engine A/F ratio had reduced from 25.6 to 25.2. From cycle number 15, the ACC fuel control pressure was increased from 1100 kN/m^2 to 2049 kN/m^2 and the engine fuelling was held constant (5% higher than the original fuelling). The ACC fuelling increased by 3.3% by cycle number 18 (this was less than expected because the increase in the ACC gas pressure reduces the burner fuelling slightly) and the exhaust manifold gas

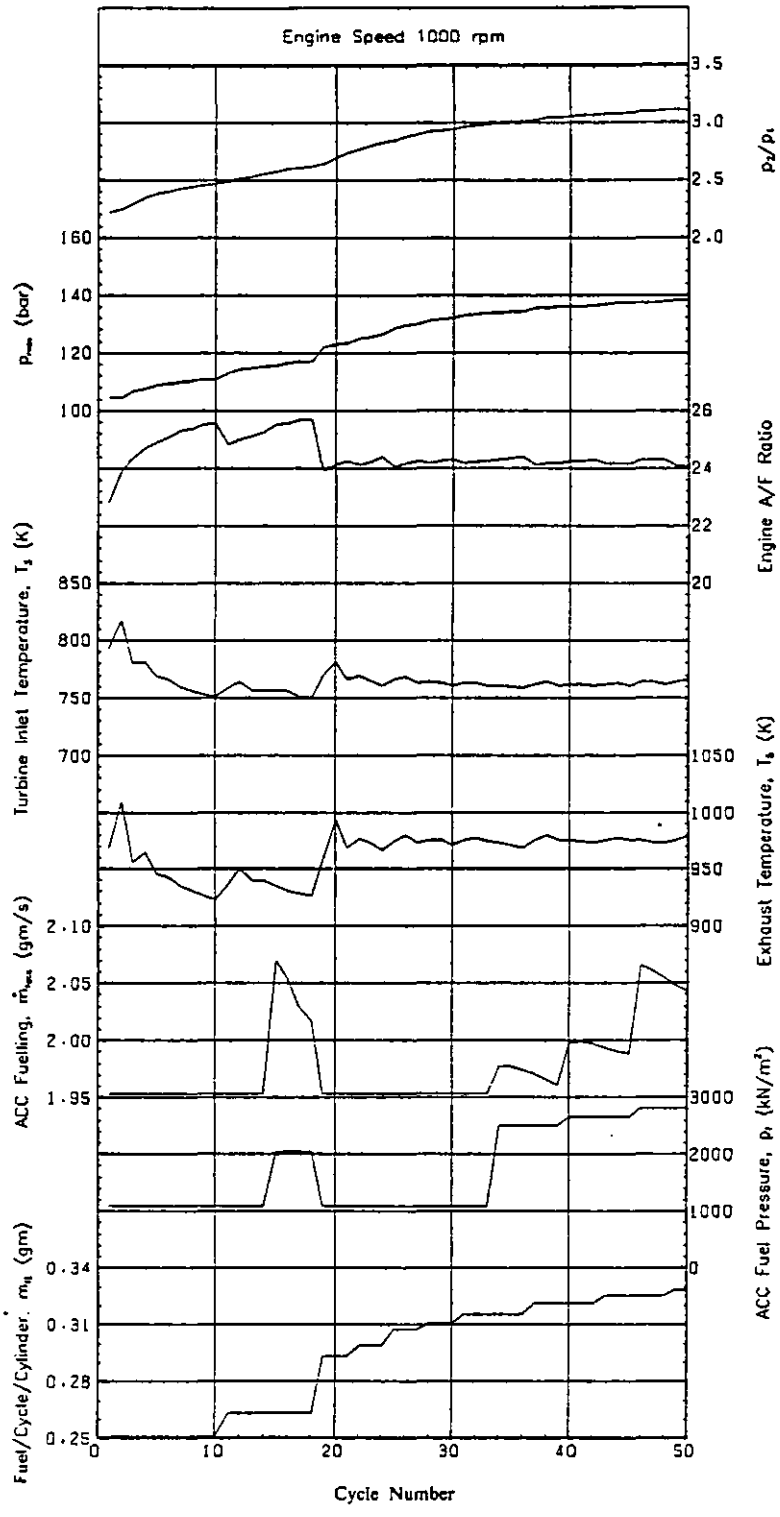

Fig. 6.43 Engine Performance using a Control Routine to Maximise the Engine Fuelling and Minimise the ACC Fuelling Level.

temperature reduces by 13 K and the turbine inlet temperature by 6 K (because of the increase in boost pressure). The maximum cylinder pressure increased by 1.8 bar and the engine A/F ratio increases from 25.2 to 25.7. The rates of change of these performance parameters (including the ACC gas pressure) with engine and ACC fuelling were then calculated and checked.

Based on the engine performance at the end of cycle number 10 (the starting conditions) the control routine estimated that the engine fuelling could be increased by 17.0%, with the minimum ACC fuelling level. This was done on cycle number 19, and by the end of cycle number 21, all the performance parameters were still below their respective limits, and so the engine fuelling was increased by a further 2.4% of the original fuelling. This process continued with the performance parameters being checked every 3 engine cycles (24, 27, 30, 33, etc.) and the engine fuelling increased when all the parameters were within their limits. On cycle number 31 the engine fuelling had been increased by 25.9% of the original fuelling, but the exhaust manifold gas temperature limit was exceeded on cycle number 33. All the other parameters were within their respective limits, and so the ACC fuel control pressure was increased from 1100 kN/m^2 to 2510 kN/m^2 on cycle number 34. This lowered the exhaust manifold gas temperature and allowed the engine fuelling to be further increased (to 28.3% higher than the original value) on cycle number 37. This again caused the exhaust gas temperature to rise above its limit on cycle number 39, and so the ACC fuel pressure was increased to 2661 kN/m^2 on cycle number 40. This allowed a further increase in the engine fuelling on cycle number 43, which was compensated for by an increase in the ACC fuel control pressure to 2800 kN/m^2 on cycle number 46. There is a final increase in the engine fuelling on cycle number 49, to a value 31.0% higher than the original fuelling. A further increase in ACC fuelling will be required on cycle number 52, to reduce the exhaust gas temperature, but the limit of the engine performance has almost been reached, the maximum cylinder pressure having risen from 110.9 bar on cycle number 10, to 138.2 bar on cycle number 50 (the limit being 140 bar).

Using this procedure, by cycle number 48 (the last cycle calculated with all the parameters within their respective limits), the engine fuelling has been increased by 29.6% and the BMEP by 30.8%, (this value coinciding with the predicted engine performance at 1000 rpm described in section 6.9.5). The ACC fuel control pressure was increased from 1100 kN/m^2 to 2800 kN/m^2, and the ACC fuelling increased by

5.2%. This results in a reduction in the total BSFC of 3.4%, due mainly to the reduction in the FMEP, expressed as a percentage of the IMEP, from 7.6% on cycle number 10, to 6.4% on cycle number 48. The compressor pressure ratio has increased from 2.47 to 3.10 and the overall A/F ratio from 50.3 to 51.4. The by-pass valve closes slightly as the load increases (the effective flow area reducing by 6.6%), but the ACC port area increases by 219.8% as the fuelling increases, and the overall by-pass A/F ratio increases from 209.1 to 265.9. The ACC A/F ratio also increases considerably from 9.0 to 35.5 as the port areas increase with the fuel control pressure. At this engine speed, the exhaust manifold gas temperature and the maximum cylinder pressure will be the limiting parameters, the turbine inlet temperature and engine A/F ratio remaining well within their predefined limits.

In this example changes to the engine and ACC fuelling were made every three engine cycles, to give the program sufficient time to respond, and only one control variable (the engine or ACC fuelling) was varied at a time. More sophisticated control systems can, of course, be developed.

6.10.4 Discussion.

A method for optimising the engine power output and ACC fuelling has been discussed in section 6.10.3. There are obviously many different limiting parameters that could be taken into account in such a study, such as exhaust smoke, metal temperatures, etc., and there are other control parameters that could have been used, for example, the injection timing could have been retarded if the peak cylinder pressure limit was reached, as an alternative to lowering the engine and/or ACC fuelling.

The control routine described in section 6.10.3 attempts to show the potential of this type of optimisation technique, and gives a good indication of the optimum engine and ACC fuellings required for the highest engine power output at a given engine speed. The system becomes a good deal more complicated if other parameters, and other control influences, are taken into account. Probably the best use can be made of such an optimisation technique to find the highest BMEP that can be obtained at a given speed, with the best BSFC, i.e. point (b) in Fig. 6.38.

6.11 Engine Performance Characteristics.

The simulation program has been used to predict the BSFC of the Hyperbar engine over the entire operational load and speed range. Fig. 6.44 shows the total BSFC as a function of engine speed and BMEP, for an engine rating of 21.38 bar BMEP at 2400 rpm. The minimum total BSFC of 0.233 kg/kW.hr occurs at 1600 rpm/24.0 bar BMEP, which is very close to the maximum torque point. This coincides with the minimum BSFC of the Poyaud engine, shown in Fig. 6.28, which occurs at 2200 rpm/17.0 bar BMEP (0.232 kg/kW.hr). The best brake thermal efficiency that can be achieved using the Hyperbar system is therefore of the order of 36.4% (assuming that the lower calorific value of the fuel, C_v, is 42450 kJ/kg). This compares with a value slightly in excess of 34% predicted by Wallace and Winkler (161), see Fig. 2.6.

Also shown on Fig. 6.44 is line C, representing the BMEP below which the burner fuelling must be increased to maintain the minimum boost pressure level. Line C therefore represents a compressor delivery pressure, p_2, of approximately 212 kN/m^2 (it is actually the ACC gas pressure that controls the movement of the ACC, and not p_2). Comparing Figs. 6.28 and 6.44 shows that at maximum engine speed, the burner need only be used below 2.3 bar BMEP, but that this threshold increases as the speed reduces, to around 10 bar BMEP at 1250 rpm. For operating points below line C, the BSFC increases very rapidly with reducing load. At 1200 rpm/2.0 bar BMEP for example, the BSFC is 0.90 kg/kW.hr, which represents a brake thermal efficiency of only 9.4%.

In general, the predicted engine BSFC agrees very well with the test data presented in (97), for the Poyaud 520 engine. The maximum BMEP, line D, shown in Fig. 6.44 represents the maximum torque curve for the engine with a conventional fuel pump. Also shown is line A, which is the BMEP that can be achieved with a fixed maximum cylinder pressure limit of 140 bar, and corresponds to line A in Fig. 6.28. Provided that none of the other engine performance parameters exceed their limits, a maximum BMEP of approximately 26 bar should be possible at the lowest engine speed, for this engine build. Predicted BMEP's in excess of 24 bar at engine speeds below 1200 rpm can be achieved by increasing the ACC burner fuelling, if the exhaust temperature limit is exceeded, see section 6.9.5.

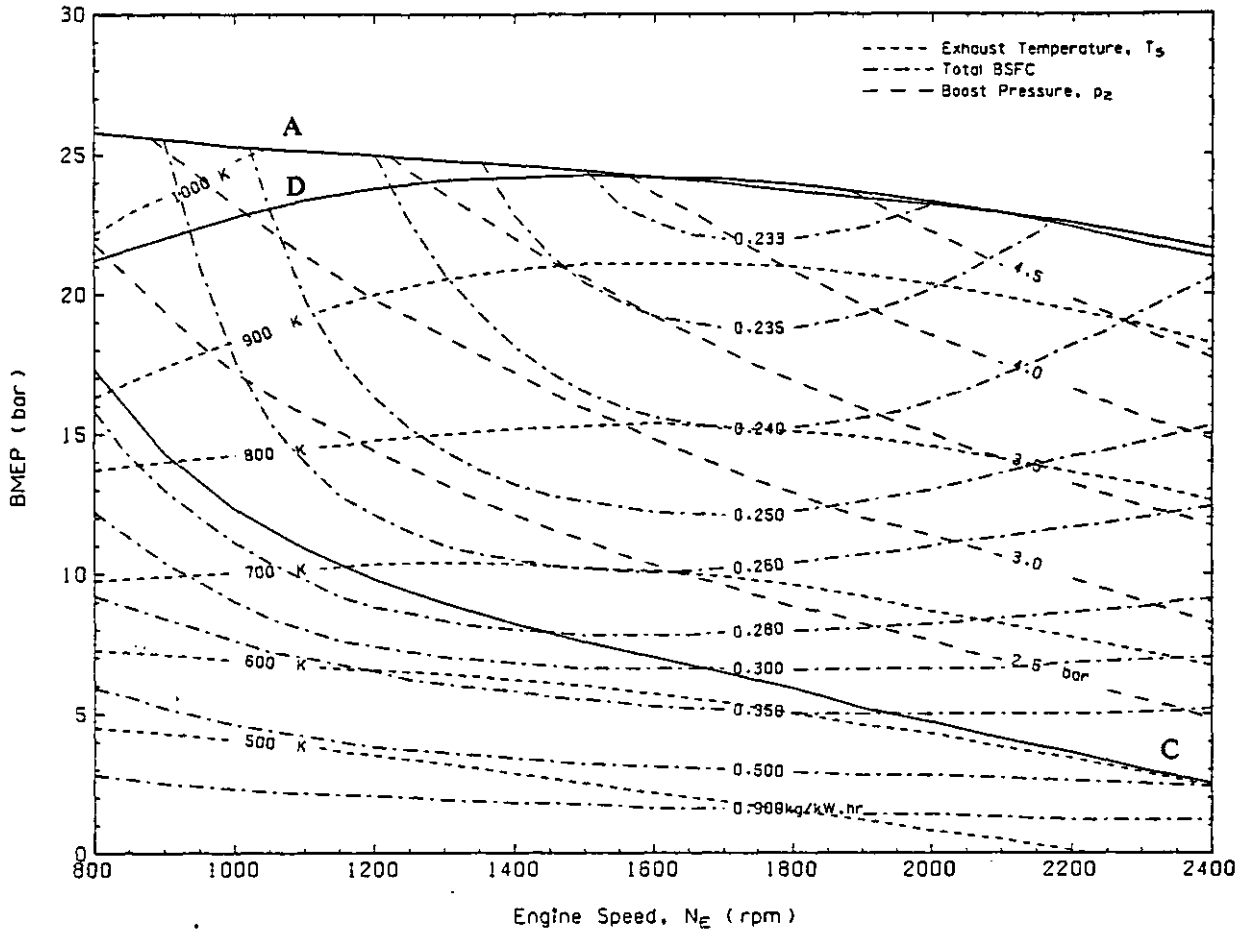

Line A represents the BMEP that can be achieved with a constant maximum cylinder pressure of 140 bar.

Line C represents the BMEP below which the ACC must be used to maintain the minimum boost pressure level

Line D represents the maximum torque curve using a conventional fuel injection pump

Fig. 6.44 Predicted Engine Performance Map for the Hyperbar Engine.

The threshold at which the burner fuelling must be increased, to control the exhaust manifold gas temperature (or the engine A/F ratio), line B in Fig. 6.28, has not been shown in Fig. 6.44. The shape and position of this line will depend upon the particular limits imposed. It is this increase in ACC fuelling at low speeds that causes the total BSFC to increase, rather than decrease, as the load increases, see Fig. 6.28. Lines of constant exhaust manifold gas temperature ranging from 500 K to 1000 K are shown in Fig. 6.44. The increasing exhaust gas temperature as the speed reduces, for a given BMEP, means that the burner will be required first at low speeds, to increase the engine A/F ratio, see Fig. 6.28.

Lines of constant compressor pressure ratio ranging from 2.5 to 4.5 are also shown in Fig. 6.44. This demonstrates the increase in boost pressure, and consequently the engine air flow rate, that can be achieved with increasing engine speed and load.

Fig. 6.44 clearly shows the most efficient operating regions for this Hyperbar turbocharged engine, and the performance limits that can be expected. The increase in specific fuel consumption at low speeds and loads is particularly apparent, and the engine performance limitations, such as peak cylinder pressure and exhaust manifold gas temperature (in addition to the smoke, the engine A/F ratio, the turbine inlet gas temperature and the cylinder component temperatures), must also be considered when deciding the most suitable design and application for this engine.

CHAPTER 7

TRANSIENT RESPONSE

7.1 Introduction.

The "filling and emptying" simulation model described in Chapter 4 was originally developed to predict both the steady state and transient performance of turbocharged diesel engines (89). The additions to the model that enable the Hyperbar system to be simulated, have also been written to allow the transient response of the engine and turbocharging system to be predicted.

Unfortunately no transient experimental test data for the Hyperbar version of the engine, described in Chapter 5, was available to verify the predicted engine response. However, experimental transient test data for a two stage turbocharged version of the same engine, at a similar rating, has been used to test many of the component models described in Chapter 4.

In this chapter the predicted engine response to a given load/demand speed schedule is compared with experimental test data for a two stage turbocharged version of this engine. Similar models are then used to predict the response of the Hyperbar engine to acceleration and load application tests. The effects of varying some of the important engine design parameters, such as turbocharger inertia, ACC fuelling and engine compression ratio are described. These tests are intended to show the sensitivity of the models to changes in engine design parameters, and to indicate the optimum Hyperbar system design to achieve good transient response.

In order to compare the Hyperbar system with a conventionally turbocharged engine, the response tests were repeated for the two stage turbocharged engine at the same ratings.

7.2 Comparison of Experimental and Predicted Two Stage Turbocharged Engine Response.

7.2.1 Description of the Two Stage Turbocharged Engine.

Experimental transient response tests on a two stage turbocharged, aftercoled version of the Hyperbar engine have been performed by the engine manufacturer. The important engine dimensions (bore, valve timing and camshaft profiles, etc.) were identical to that of the Hyperbar engine. There were, however, detailed changes to the engine design (for example, the stroke was 99.74%, and the connecting rod length was 99.52% of the Hyperbar dimensions). The engine was rated at the same power output at the maximum engine speed, 2400 rpm, as the Hyperbar version, and this meant that the rated BMEP was increased to 17.14 bar (compared to 17.09 bar) because of the slightly smaller swept volume of the two stage turbocharged engine. The compression ratio was increased from 9.0:1 to 10.5:1 because at low speeds and loads the boost pressure is very low, and a higher engine compression ratio is required to ensure good combustion. At high speeds and loads the boost pressure for this engine was lower than that of the Hyperbar version, (at 2400 rpm/17.14 bar BMEP the HP inlet manifold pressure is 346 kN/m^2 (absolute), compared to 400 kN/m^2 for the Hyperbar engine at the same rating) and so the same static injection timing (20°CA BTDC) could be used without excessive peak cylinder pressures.

A poppet valve wastegate was fitted in parallel to the LP turbine to limit the maximum boost pressure level. The wastegate was controlled by the LP compressor outlet pressure, and opened when this reached approximately 185 kN/m^2 (absolute). Little data was available about the wastegate, and its characteristics were therefore estimated, based on a comparison of experimental and predicted steady state engine performance data. A boost controlled rack limiter (aneroid) was used to restrict the engine fuelling at low boost pressures. The aneroid used the HP inlet manifold pressure as its control signal, and allowed the maximum rack limit to be reached only after the boost pressure reached 240 kN/m^2 (absolute). Aneroid D had a linear, single slope, boost versus rack position characteristic, see Fig.7.13. The compressor and turbine matches were selected by the engine manufacturer, and the rotating inertia of

the system (engine, carden shaft and dynamometer) was measured.

Despite the changes in combustion chamber geometry, compression ratio (the original correlation was developed for a single stage turbocharged version of this engine with a compression ratio of 12:1) and fuel injection equipment, the same models have been used for the ignition delay and the AFBR as for the Hyperbar engine (see section 4.3). The fuel pump characteristics have been scaled, where necessary, to ensure that the two stage turbocharged engine had the same power output as that measured by the manufacturer. The characteristics of the electronic two speed governor were identical to those described in section 4.6.4.

7.2.2 Description of the Engine Test.

The engine was tested on a Froude FO 351 dynamometer. The dynamometer controller was set initially to 800 rpm/1.69 bar BMEP, (although the measured starting speed and load was 857 rpm/0.96 bar BMEP for this particular test) and a speed ramp of 370 rpm/s was applied, the load increasing up to the rated output of 17.14 bar BMEP at 2400 rpm. The instantaneous torque, speed and throttle position were recorded from the Froude dynamometer controller and the instantaneous rack position and boost pressure were recorded from the electronic governor.

The measured engine load (BMEP) during the transient was used as input to the simulation program, and the predicted engine speed response was then compared with the measured data. However, this can lead to problems in predicting the engine performance. The measured load BMEP is, in fact, a function of the measured engine acceleration, which may not correspond exactly to the predicted acceleration. Therefore, in the predicted case, the controller may not be taking the correct action to hold the engine acceleration constant at 370 rpm/s. The results, therefore, compare the experimental and predicted engine response to a given load versus time schedule. Alternatively, a mathematical model of the controller could have been used to reproduce the measured engine response exactly, and the resulting load torque compared to the measured experimental data. The throttle setting was increased linearly from its initial value (corresponding to a steady state speed of 857 rpm and load of 0.96 bar BMEP) to the maximum throttle position in 0.4 seconds.

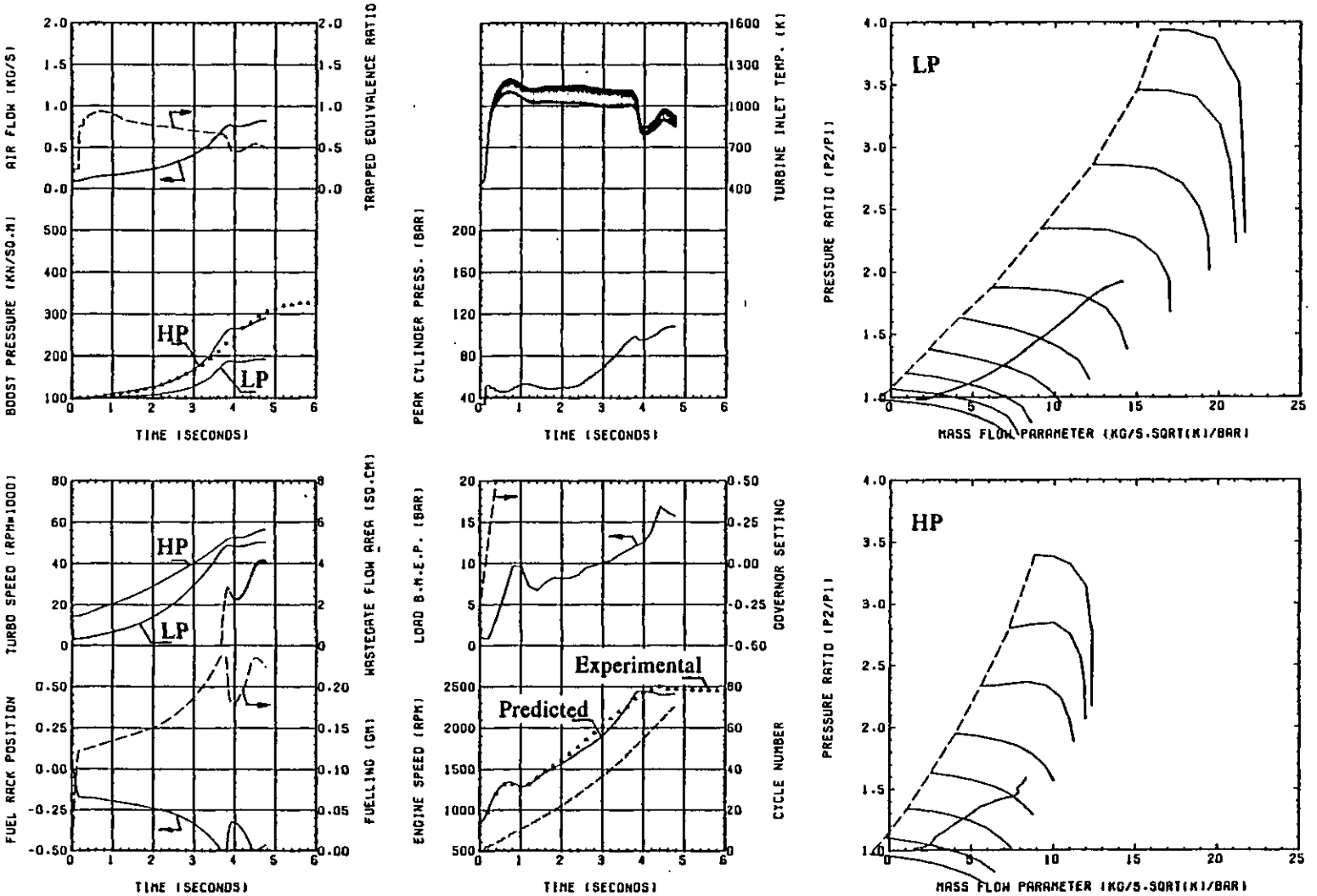

Fig. 7.1 Comparison of Experimental and Predicted Transient Response for the Two Stage Turbocharged Aftercooled Engine.

The experimental and predicted engine response is shown in Fig. 7.1. It can be seen that the measured and predicted engine speeds agree very well during the first two seconds of the test. In this period the HP boost pressure is very low (less than 126 kN/m^2), because of the low initial speed and load, and the low initial turbocharger acceleration. The simulation program predicts that the aneroid will control the engine fuelling for the first 3.7 seconds and this prevents the trapped equivalence ratio from exceeding unity. After two seconds the predicted engine speed drops below the measured values until 3.6 seconds has elapsed. During this period the load BMEP will be too high because the predicted engine acceleration is lower than that measured. If a dynamometer model were used for the predicted response, it would reduce the load BMEP to increase the engine acceleration slightly during this period. The engine then accelerates up to 2400 rpm, taking 3.8 seconds in the simulation, compared to 3.9 seconds measured experimentally. At this point the governor controls the engine fuelling to hold the maximum engine speed, while the load increases.

The predicted HP boost pressure shows a very good agreement with the measured data over the first three seconds of the response, but then increases more rapidly than the test data shows. A possible reason for this is the late opening of the wastegate, which controls the HP and LP turbine expansion ratio's. The simulation predicts that the wastegate starts to open after 3.6 seconds when the LP boost pressure reaches 185 kN/m^2, and then attempts to hold it at this level. The effect of the wastegate operation on the HP and LP turbocharger speeds, the boost pressures, the engine air flow rate and compressor operating lines can quite clearly be seen in Fig. 7.1. The results show that the simulation program can predict the transient response of a conventional two stage turbocharged version of this engine to a given load/demand speed schedule with acceptable accuracy.

The Hyperbar engine is, of course, a good deal more complicated than the two stage turbocharged version, and the response characteristics of the by-pass valve and ACC burner were not known. A comparison of the Hyperbar engine response with that of the two stage turbocharged engine, however, gives a good indication of the merits and demerits of the Hyperbar system, when dealing with load and speed changes. This will be considered in the following sections.

7.3 Hyperbar Engine Transient Response.

7.3.1 Description of the Propeller Law Loading Test.

Two completely different types of transient test have been investigated. The first was a propeller law loading, where the engine power increases as the cube of the engine speed. For this test the engine and load inertia was measured by the manufacturer for the 6 cylinder engine mounted on a dynamometer with a small flywheel and a carden shaft. The two speed electronic governor described in section 4.6.4, has been used, without an aneroid. The engine was accelerated, at maximum demand speed (throttle setting), from the low initial load at 800 rpm. The brake load being given by:-

$$P = K.N_E^3 \tag{7.1}$$

where,

N_E = engine speed (rpm)

P = power absorbed by the load (kW)

K = constant ($kW.min^3$)

Equation (7.1) can be written to give the load BMEP as a function of the engine speed:-

$$LBMEP = \frac{120.K.N_E^2}{V_{sw}} \tag{7.2}$$

where,

LBMEP = Load Brake Mean Effective Pressure (kN/m^2)

V_{sw} = swept volume (m^3)

or

$$LBMEP = K_1.N_E^2 \tag{7.3}$$

where,

$$K_1 = \frac{120.K}{V_{sw}} \tag{7.4}$$

The constant, K_1, in eqn. (7.3) was chosen so that the rated engine BMEP (1709 kN/m^2) was absorbed at the maximum engine speed (2400 rpm). Eqn. (7.3) therefore gives:-

$$K_1 = 2.967.10^{-4} \qquad kN.m^{-2}.min^2 \tag{7.5}$$

The initial engine speed was 800 rpm, and the corresponding load, from eqns. (7.3) and (7.5) was 190 kN/m^2.

The engine response to this loading schedule is shown in Fig. 7.2. The demand speed (throttle setting) was increased linearly from the initial value, (required to maintain 800 rpm/190 kN/m^2 BMEP), to the maximum demand speed in 0.3 seconds. The response of the fuel pump rack can be seen to be almost directly proportional to the change in demand speed, as expected for a two speed governor. After the fuel pump rack reaches its maximum travel limit the engine fuelling reduces slightly as the engine speed increases, because of the shape of the fuel pump delivery characteristics, see Fig. 4.32.

The engine can be seen to accelerate quite rapidly, reaching 2400 rpm after 2.37 seconds, after which the governor controls the maximum engine speed. Also shown are the turbocharger speed, the boost (inlet manifold) pressure, the maximum cylinder pressure and the trapped equivalence ratio (for cylinder no. 1), the compressor and engine air flow rates and the turbine inlet and exhaust manifold gas temperatures. It is important to note that the compressor mass flow rate is relatively steady during an engine cycle, while the engine and by-pass flow rates fluctuate with time, see Fig. 6.35, and so plotting the engine mass flow rate only gives an indication of the values occuring at specific points in the cycle (in this case every 120°CA).

The Hyperbar engine normally operates with a relatively high engine A/F ratio. The turbine inlet gas temperature is initially much higher than the exhaust manifold gas temperature, because of the high engine A/F ratio and the burner assistance, (required

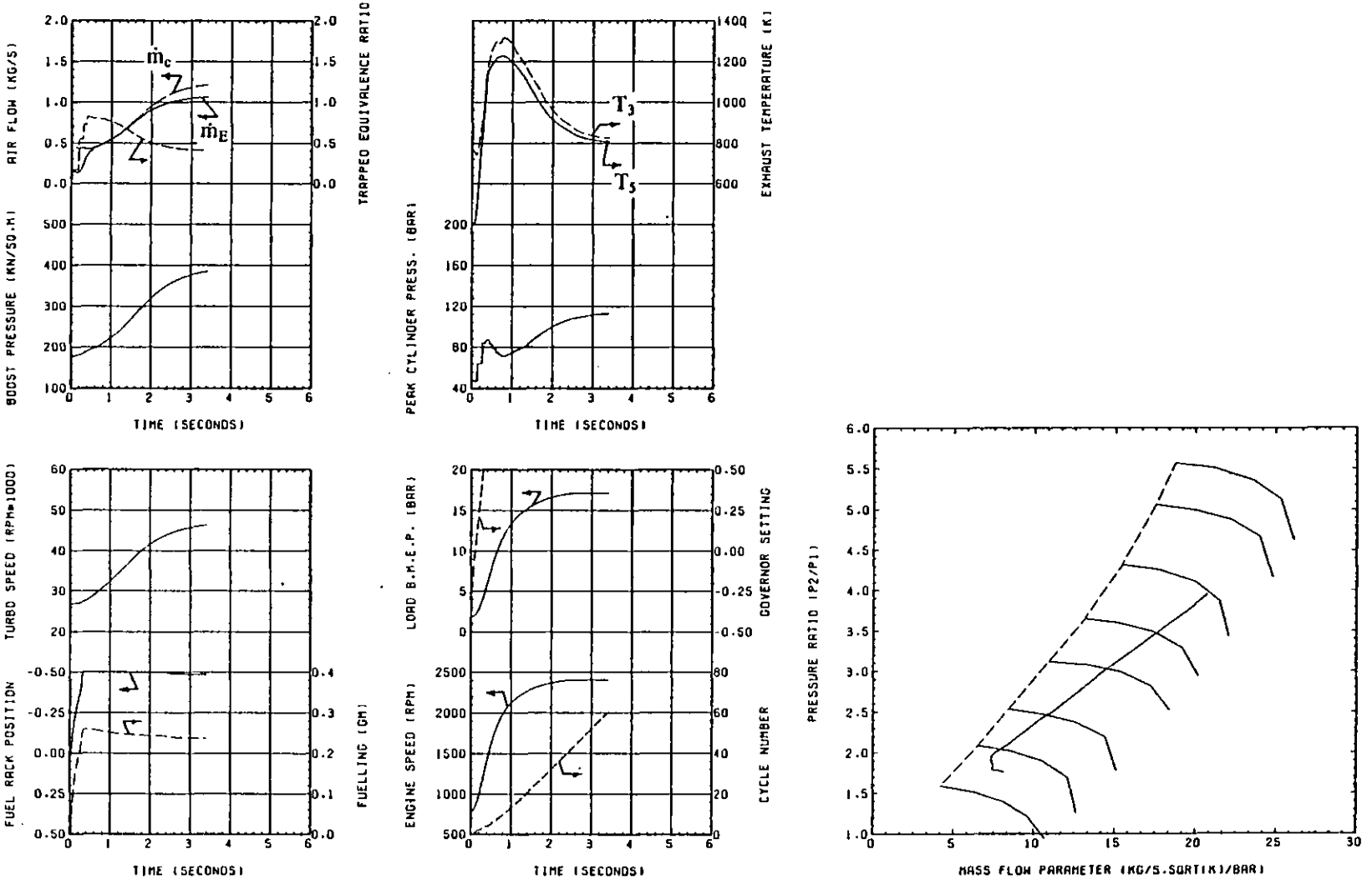

Fig. 7.2a Response of the Hyperbar Engine to a Propeller Law Loading Schedule.

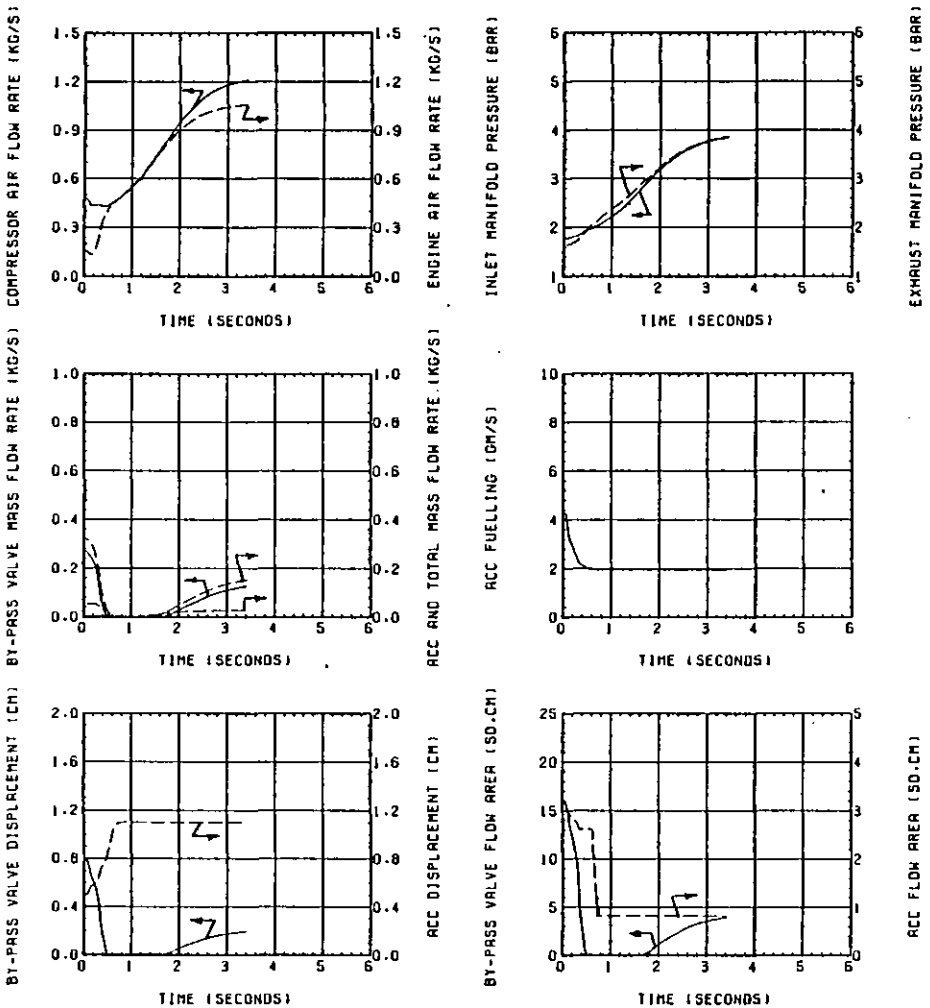

Fig. 7.2b Response of the Hyperbar Engine to a Propeller Law Loading Schedule.

to maintain the minimum boost pressure level). These temperatures converge towards the end of the test as the engine A/F ratio reduces and the ACC moves to the idling position.

At this rating the ratio of the full load to initial fuelling (which is 7.8:1 at 800 rpm) and the relatively high initial boost pressure for the load, means that the smoke emission during the critical early stages of the transient should not cause the problems that it does with conventional single or two stage turbocharged engines.

Also shown in Fig. 7.2 is the movement of the compressor operating line during the transient. In the early stages of the test the operating line moves towards the surge line. During transients the Hyperbar by-pass system will not behave in the same way as it does during steady state operation, due to the response of the turbocharger, by-pass valve, ACC, etc. and the capacitance effects of the various manifolds in the system.

Fig. 7.2b shows the response of the Hyperbar system components during the acceleration. The by-pass valve is initially at a relatively large opening, because of the low engine speed. As the engine speed and fuelling increase the exhaust pressure builds up faster than the boost pressure, due to the inertia of the turbocharger and the compressibility of the working gases. Consequently the by-pass valve closes during the early part of the acceleration. The ACC air flow also reduces to zero, despite the fact that the effective flow area has reached its minimum value, because of the adverse pressure gradient across the ACC ports (no reverse flow being permitted in the model). The compressor and engine air flows are therefore equal. This explains the movement of the compressor operating line towards the surge line. As the turbocharger accelerates and the boost pressure rises, the by-pass valve opens again and the ACC port pressure drop becomes positive.

The ACC initially supplies a high fuelling rate, because of the very low starting load at 800 rpm. Therefore a significant proportion of the total turbine energy, required to maintain the minimum boost level, is provided by the burner. As the exhaust pressure builds up, the ACC fuelling is reduced to the minimum level, but there is a substantial period of time during the transient (approximately 1.0 seconds) where no air is flowing through the by-pass system. The by-pass A/F ratio therefore becomes very rich during this period, the ACC equivalence ratio reaching 1.47 after 1.19

seconds, and much of the fuel injected will be wasted, this will also result in an increase in exhaust smoke. Clearly it would be preferable to reduce the ACC fuelling to zero in these circumstances (the Hyperbar system design described in (98) has a fuel cut off, see section 4.8).

Alternatively some method of increasing the boost pressure, during the transient, without increasing the exhaust pressure, must be found.

7.3.2 Effect of Turbocharger Inertia.

A conventionally turbocharged diesel engine response is very sensitive to the turbocharger inertia, which influences the engine air supply, and hence the torque that can be developed with an acceptable smoke limit. Because of the high pressure ratio's required from a single stage radial turbocharger, the diameter and consequently the rotating inertia (which is approximately proportional to the fifth power of the diameter) of the Hyperbar turbocharger is considerably higher than that of conventional automotive turbochargers. Reducing the inertia of the turbocharger should therefore improve the response of the boost pressure to changes in speed and/or load. The transient test described in section 7.3.1 has also been repeated with the turbocharger inertia reduced to 67% and 33% of its original value. The results are shown in Fig. 7.3.

It can be seen that the Hyperbar system is far less sensitive to turbocharger inertia than conventionally turbocharged engines. The engine response improves as the turbocharger inertia is reduced, but the differences are small. The main reason for this is that the engine normally runs with a high A/F ratio, and as the load is applied, and the engine fuelling increases, the trapped equivalence ratio does not become excessively rich (which results in a reduction in engine power). There is no need for an aneroid rack limiter to restrict the engine fuelling during the early part of the transient, (when the boost is relatively low) and so in each of these tests the rack moves to maximum fuelling as the demand speed increases.

The lower turbocharger inertia does improve the turbocharger response significantly and results in a more rapid build up of boost pressure and air flow rate. This in turn reduces the trapped equivalence ratio, smoke and exhaust temperatures. Comparing the

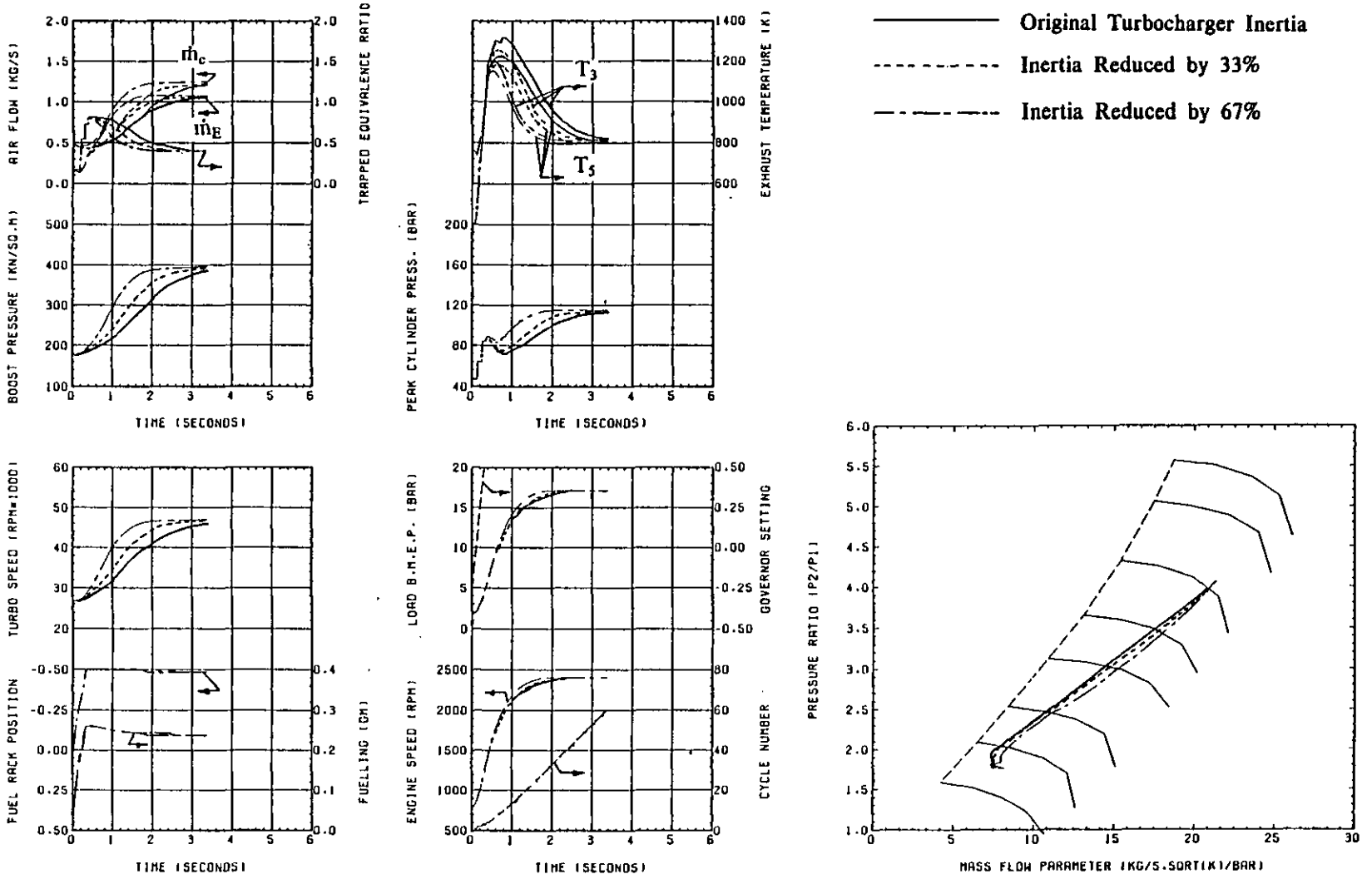

Fig. 7.3a Effect of the Turbocharger Inertia on the Engine Response to a Propeller Law Loading Schedule.

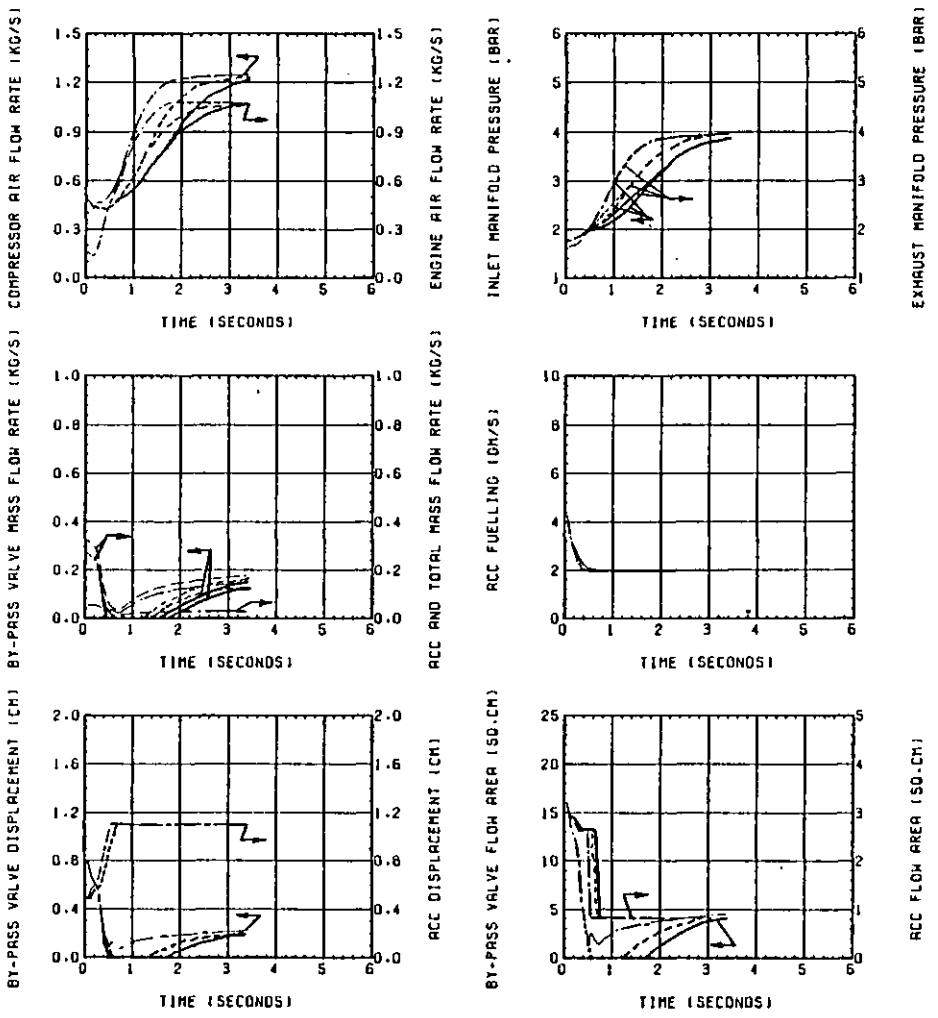

Fig. 7.3b Effect of the Turbocharger Inertia on the Engine Response to a Propeller Law Loading Schedule.

compressor operating lines, reducing the inertia limits the movement of the compressor operating line towards the surge line. Therefore a low turbocharger inertia is desirable if the surge margin is small.

The faster rise in boost pressure with reduced turbocharger inertia means that the by-pass valve does not close completely when the inertia is reduced to 33% of its original value, Fig. 7.3b. The transient by-pass A/F ratio is therefore much more favourable, the peak ACC equivalence ratio reducing from 1.47 with the standard inertia to 1.37 (after 0.90 seconds) and 0.60 (after 0.72 seconds) with the inertia reduced to 67% and 33% respectively, increasing the efficiency of the ACC burner. The scavenge pressure drop across the engine is also improved with the lower turbocharger inertia.

7.3.3. Effect of Holding the ACC at Maximum Fuelling.

The acceleration from 800 rpm to 2400 rpm described in section 7.3.1 was repeated using the original turbocharger inertia value, with the ACC held in the maximum fuelling position for the duration of the test, by increasing the burner fuel control pressure. The results are shown in Fig. 7.4.

Initially the boost pressure is much higher due to the increase in turbine energy provided by the burner. The boost pressure remains higher throughout the test and the turbocharger accelerates slightly faster. The increase in compressor and engine air flow rates result in lower trapped equivalence ratio's and exhaust temperatures throughout the test. The engine response is significantly quicker during the early stages, but later on the very high load is the dominant factor. The final boost pressure, turbocharger speed, air flow rate, maximum cylinder pressure and turbine inlet temperature are considerably higher than for the case where the ACC is idling. The exhaust manifold gas temperature is lower due to the increase in engine A/F ratio.

With the ACC held in the maximum fuelling position, the ACC port areas are relatively large. Consequently the by-pass valve cannot adequately control the engine pressure drop throughout the test, the valve remaining closed for the majority of the time, with all the by-pass flow passing through the ACC ports. The peak ACC equivalence ratio reduces from 1.47, with the standard ACC fuelling, to 0.89 (after 0.71 seconds) with the ACC held in the maximum fuelling position. Only after

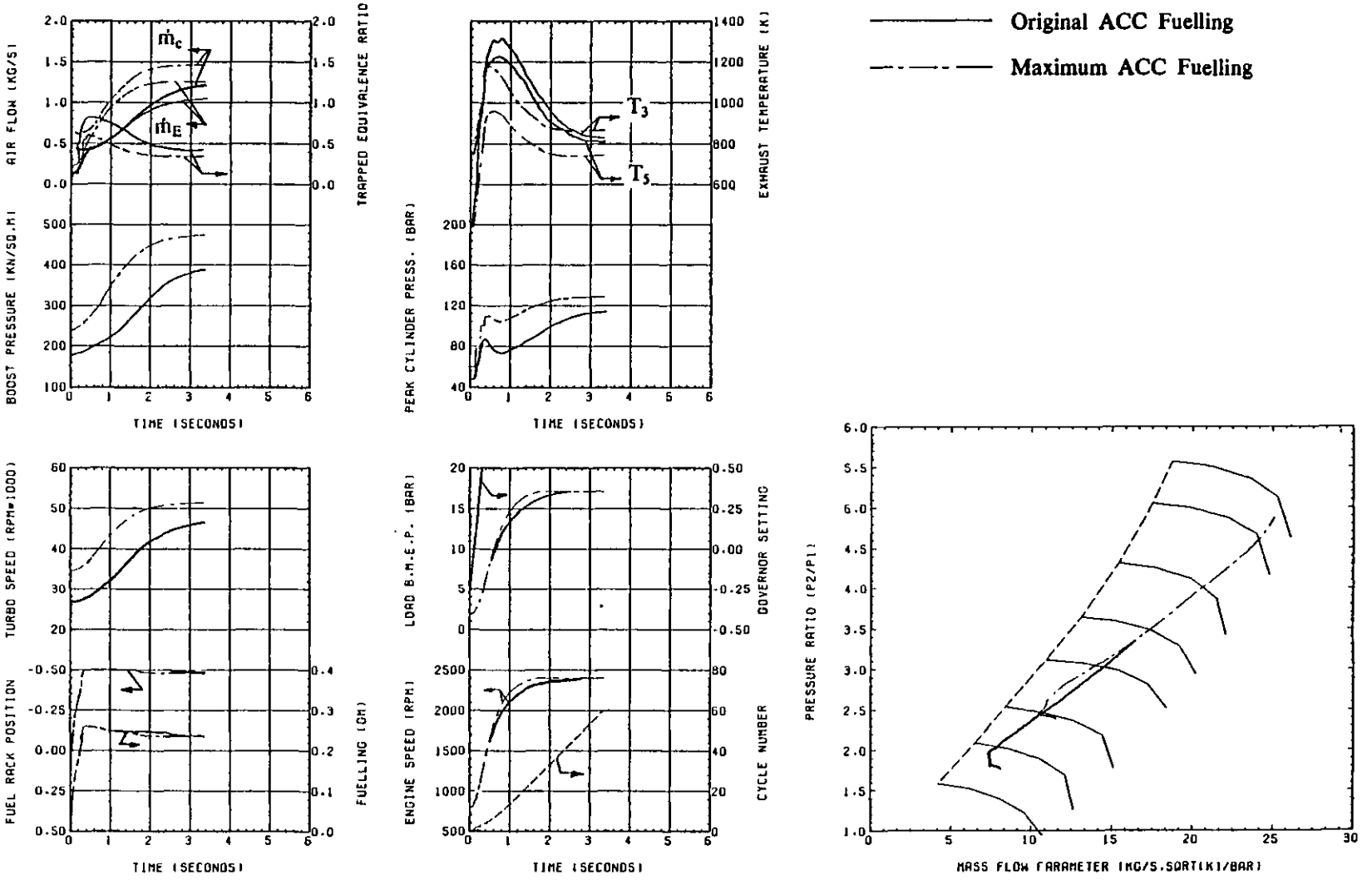

Fig. 7.4a Effect of Holding the ACC at Maximum Fuelling on the Engine Response to a Propeller Law Loading Schedule.

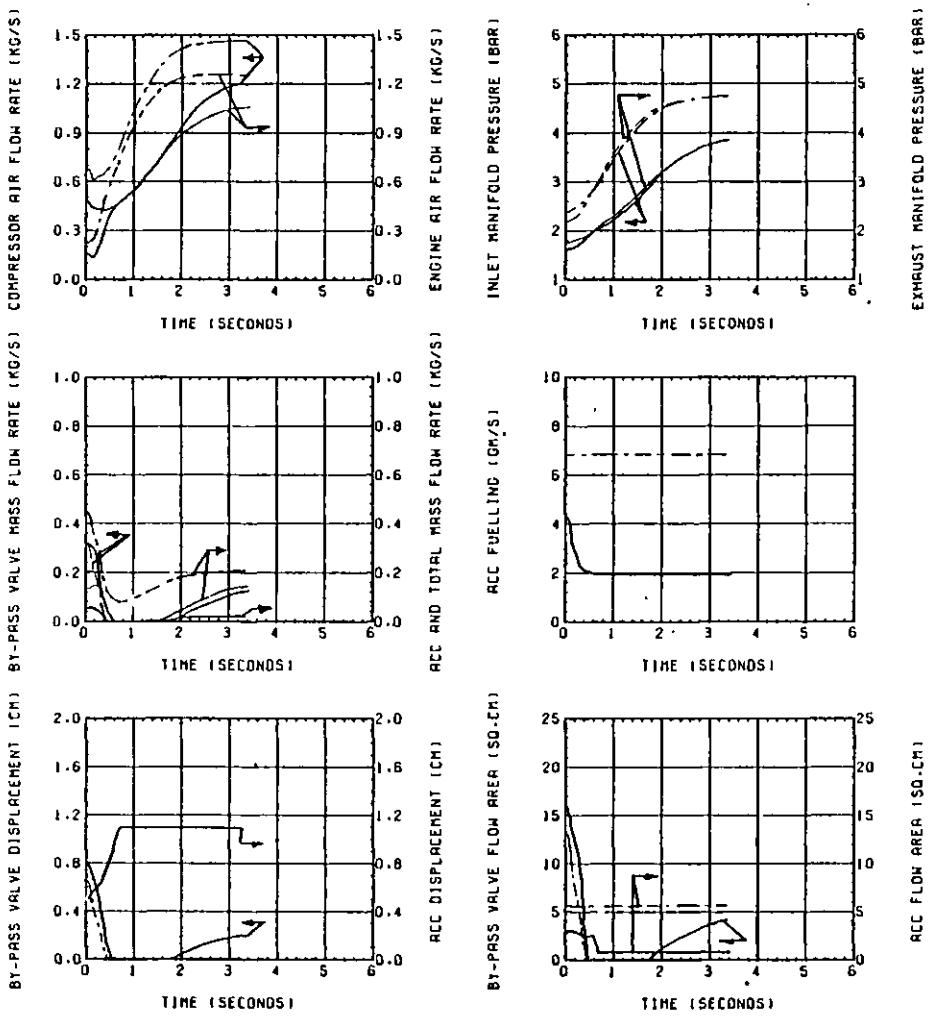

Original ACC Fuelling

Maximum ACC Fuelling

Fig. 7.4b Effect of Holding the ACC at Maximum Fuelling on the Engine Response to a Propeller Law Loading Schedule.

considerably more time than the duration of this test will the boost pressure converge to the final, steady state, level with the by-pass valve slightly open.

Generally, there is an improvement in the engine response but at the expense of the excess fuelling required by the burner. To operate in this fashion in practice will, however, require advance knowledge that the transient is going to occur, or is likely to occur, so that the ACC fuel control pressure can be increased beforehand.

7.3.4 Effect of Increasing the Engine Compression Ratio.

In section 6.6 the effect of increasing the engine compression ratio from 9.0:1 to 11:1, and reducing the fuel control pressure from 1100 kN/m^2 to 534 kN/m^2, on the steady state engine performance was discussed. The effect of these changes on the engine response to the propeller law loading, described in section 7.3.1, has also been investigated.

The engine rating has been maintained at 17.09 bar BMEP, and the initial speed and load are the same as described in setion 7.3.1. The engine response is shown in Fig. 7.5, and is compared with the response of the standard engine, from Fig. 7.2.

Reducing the ACC fuel control pressure has little effect on the engine response. The minimum boost pressure level is reduced from 180 kN/m^2 to 140 kN/m^2 and the initial turbocharger speed and air flow rate are lower. Throughout the acceleration the engine and total air flow are therefore lower with the higher engine compression ratio. The fuel pump rack position and engine fuelling are comparable for both tests and consequently, with the lower boost pressure level the trapped equivalence ratio is much richer and the exhaust smoke will be correspondingly higher. Both the engine exhaust and the turbine inlet temperatures are higher with the 11:1 compression ratio. The peak cylinder pressure is higher with the increased engine compression ratio, despite the lower boost pressure level, the static injection timing being maintained at 20°CA BTDC.

The ACC fuelling is significantly less with the lower boost pressure level, because the initial ACC fuelling required to maintain the minimum boost pressure level at 140 kN/m^2 is lower. Fig. 7.5b shows that the by-pass valve stays closed for a longer

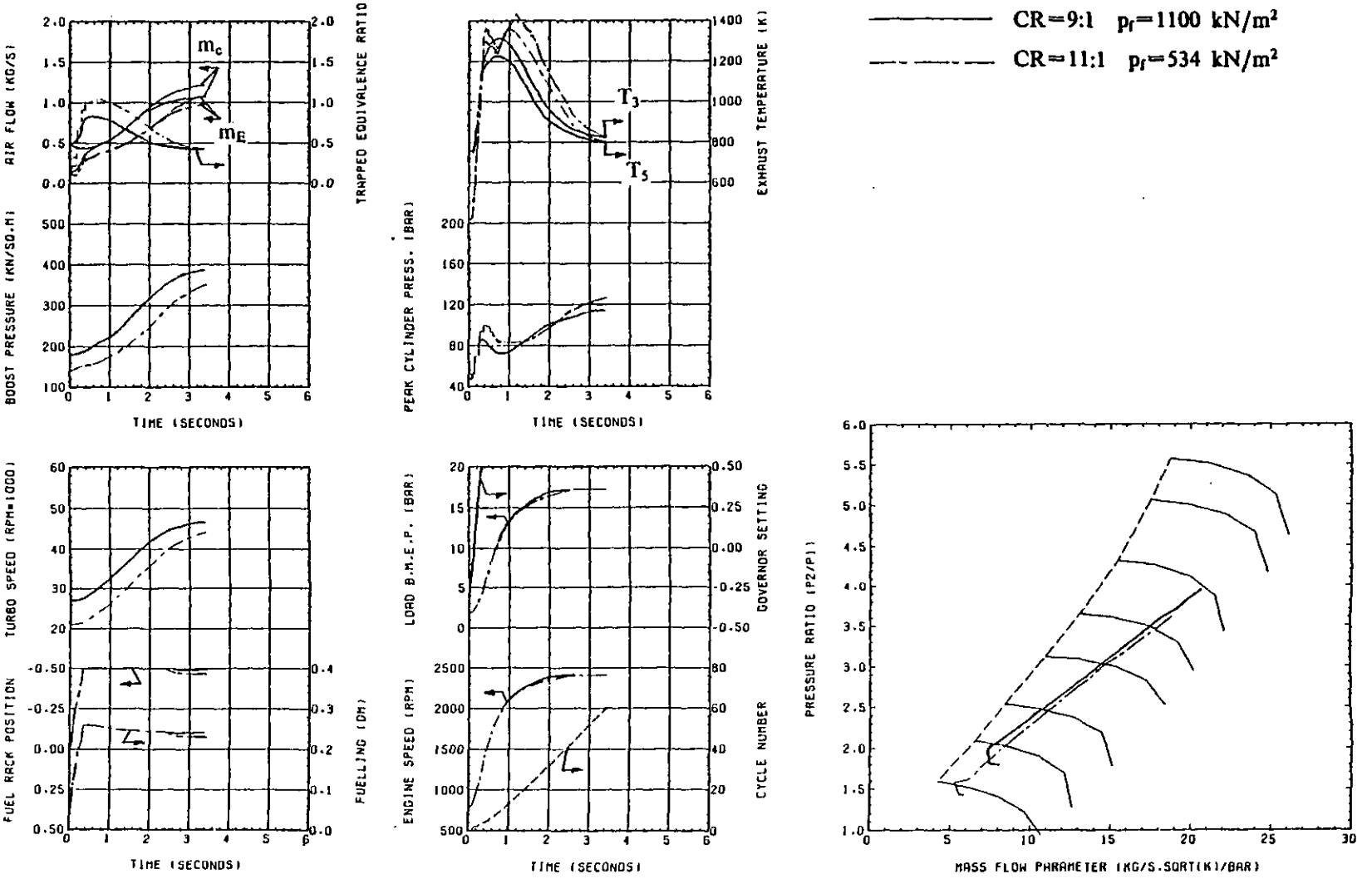

Fig. 7.5a Effect of Compression Ratio and Minimum Boost Pressure Level on the Engine Response to a Propeller Law Loading Schedule.

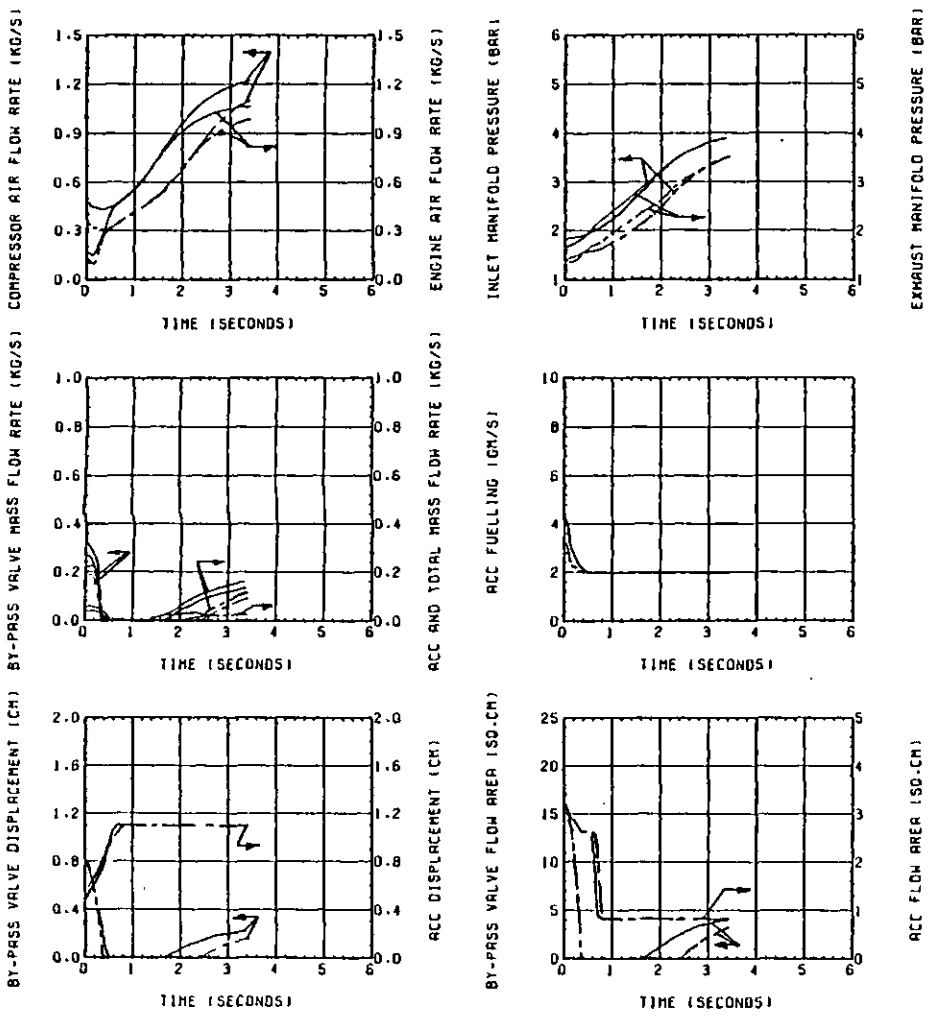

CR=9:1 p_f=1100 kN/m²

CR=11:1 p_f=534 kN/m²

Fig. 7.5b Effect of Compression Ratio and Minimum Boost Pressure Level on the Engine Response to a Propeller Law Loading Schedule.

duration (approximately 2 seconds) with the higher engine compression ratio because the exhaust pressure is considerably higher than the boost pressure. The by-pass flow is reduced which lowers the compressor flow and moves the operating line closer to surge. The peak ACC equivalence ratio reaches 1.78 after 1.08 seconds which is a considerable increase on that with the standard geometry (1.47), due to the lower minimum boost pressure level (and is beyond the limits of the gas property curve fits).

Overall there is no advantage in using the lower boost pressure level in terms of engine response, but the smoke output will be significantly worse. An aneroid rack limiter may be required to control the trapped engine A/F ratio, and an ACC cut off will also be needed. There will be, however, a significant reduction in both the steady state and transient fuel consumption.

7.3.5 Generator Type Loading Tests.

A number of transient response tests have been performed for the Hyperbar engine to simulate a sudden load application, similar to that encountered in power generation applications.

In order that relatively large loads could be applied to the engine, the rating was increased from 17.09 bar BMEP to 21.36 bar BMEP at the maximum engine speed of 2400 rpm, by increasing the engine fuel pump output.

The governor characteristics used to simulate the electronic two speed governor are not suitable for power generating applications, because the governor has no control over the engine speed in the mid speed range, this will result in a large speed droop which will cause severe fluctuations in the electrical frequency. Consequently the characteristics of a mechanical all speed governor have been used.

The governor characteristics used for these tests are shown diagramatically in Fig. 7.6, and are discussed in detail in section 4.6.2. The speed droop from no load to the rated load at 1500 rpm (24.19 bar BMEP) is defined as 4% of the rated speed (1500 rpm). Therefore the no load engine speed is 1560 rpm. A linear governor control spring has been used to simplify the analysis.

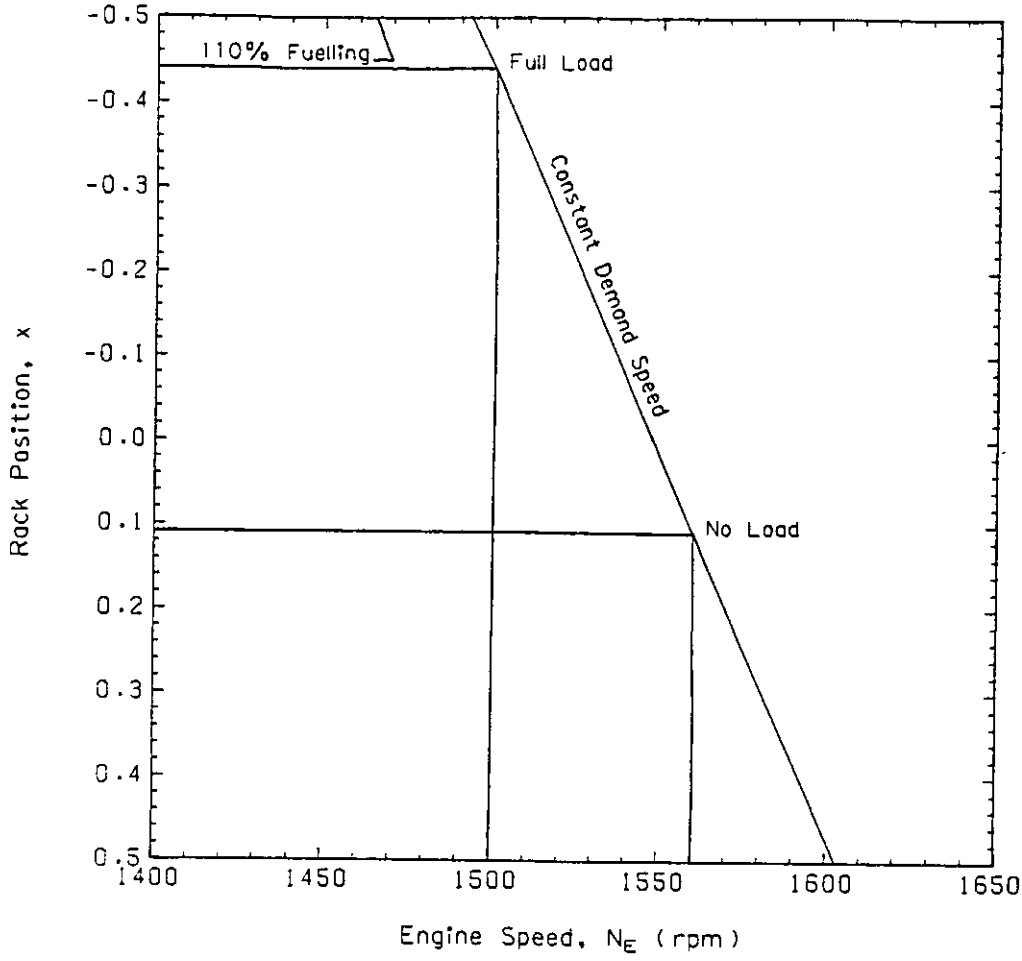

Fig. 7.6 Ideal Governor Characteristic for Electricity Generating Applications.

The fuel pump output has been increased to allow 10% overfuelling from the maximum rated fuel pump delivery, which should enable the engine to recover from load applications of up to 100%.

The combined rotating inertia of the engine and load has been chosen to simulate the high inertia of a typical generator set, and is approximately 6.7 times that of the engine and dynamometer, used in the previous propeller law loading tests.

7.3.6 Effect of the Applied Load on Engine Response.

Fig. 7.7 shows a 50% load application, corresponding to 12.10 bar BMEP, from an initial speed of 1560 rpm and load of 0 bar BMEP. The load was increased linearly from no load to 50% load in 0.3 seconds. Fig. 7.8 shows the effect of increasing the applied load to 70% (16.93 bar BMEP) in the same time interval and Fig. 7.9 shows a 100% load application (24.19 bar BMEP).

As the applied load increases the engine speed droop increases, the final steady state speeds being 1532 rpm with a 50% load application, 1520 rpm with a 70% load application and 1502 rpm with a 100% load application. In each case the speed droop is within 4% of the rated speed (i.e. less than 60 rpm). The predicted minimum engine speeds during the transient were 1529 rpm, 1514 rpm and 1475 rpm with 50%, 70% and 100% load applications respectively. In each case the engine speed recovers to its final steady state value within 4 seconds (in 2.27, 2.68 and 3.29 seconds respectively).

The ACC burner ensures that the initial boost pressure and turbocharger speed are relatively high, and so the trapped equivalence ratio does not become excessively rich, even when the maximum load is applied, and this ensures good engine response. As the applied load increases so does the initial engine speed drop, and so the fuel pump rack travel and engine fuelling both increase. This results in a faster turbocharger acceleration and more rapid build up in boost pressure, although the higher trapped equivalence ratio's result in higher exhaust temperatures and increased smoke.

The initial movement of the compressor operating line towards the surge line increases with an increase in the applied load, and this could cause surging problems when very

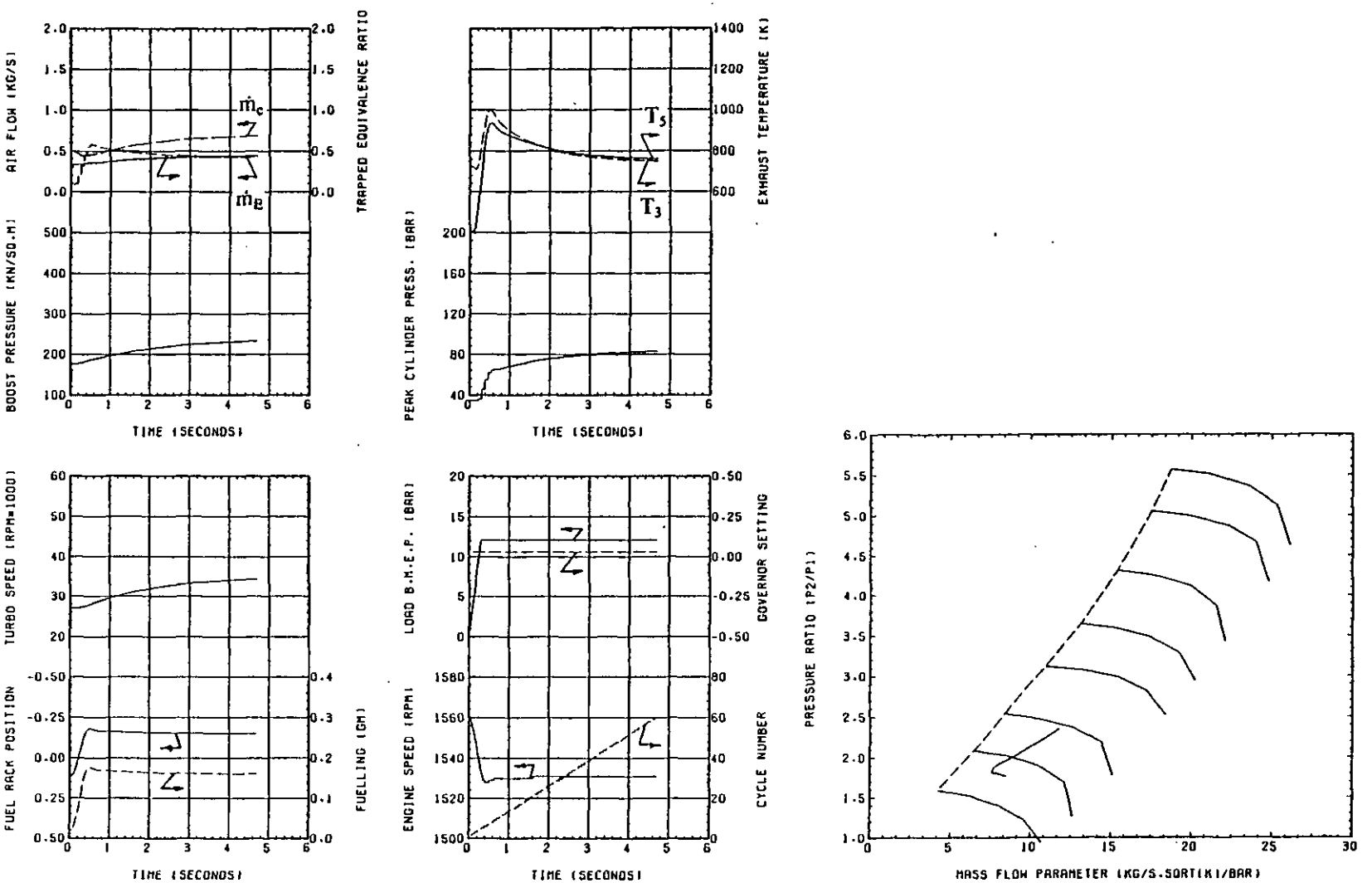

Fig. 7.7a Engine Response to a 50% Load Application from 1560 rpm/0 bar BMEP.

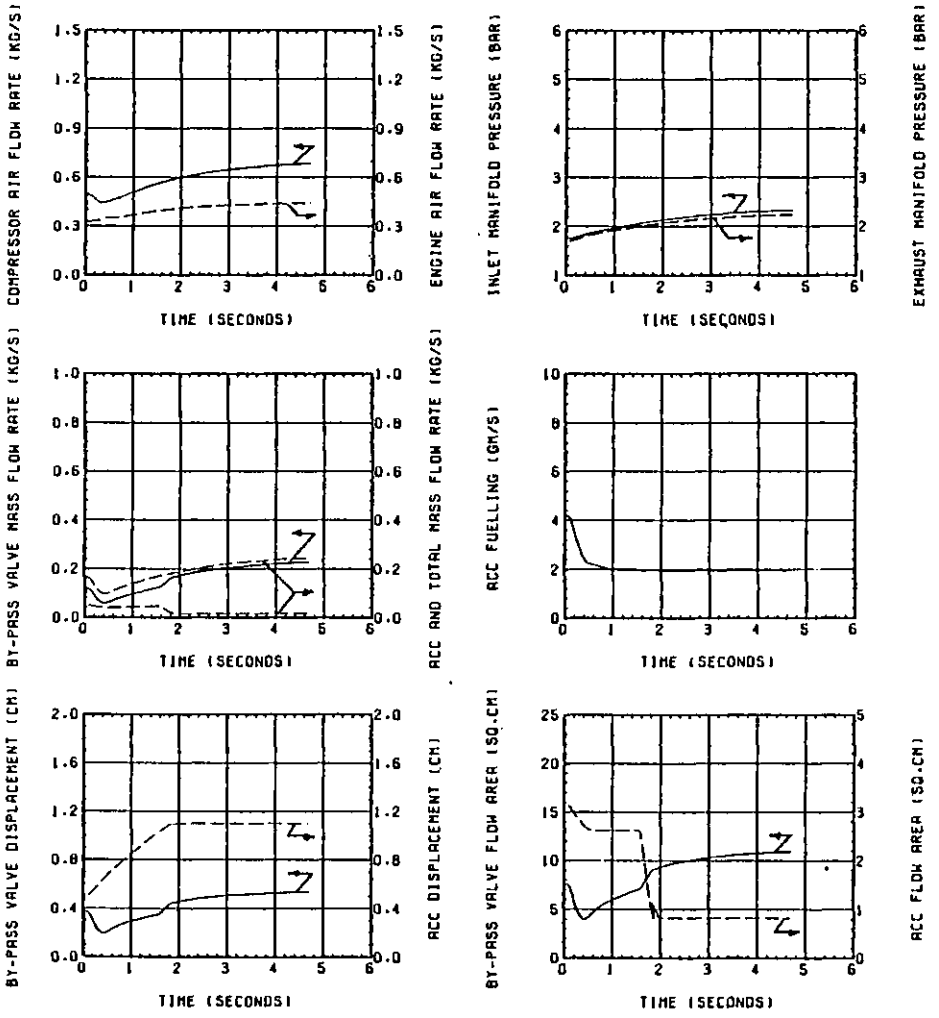

Fig. 7.7b Engine Response to a 50% Load Application from 1560 rpm/0 bar BMEP.

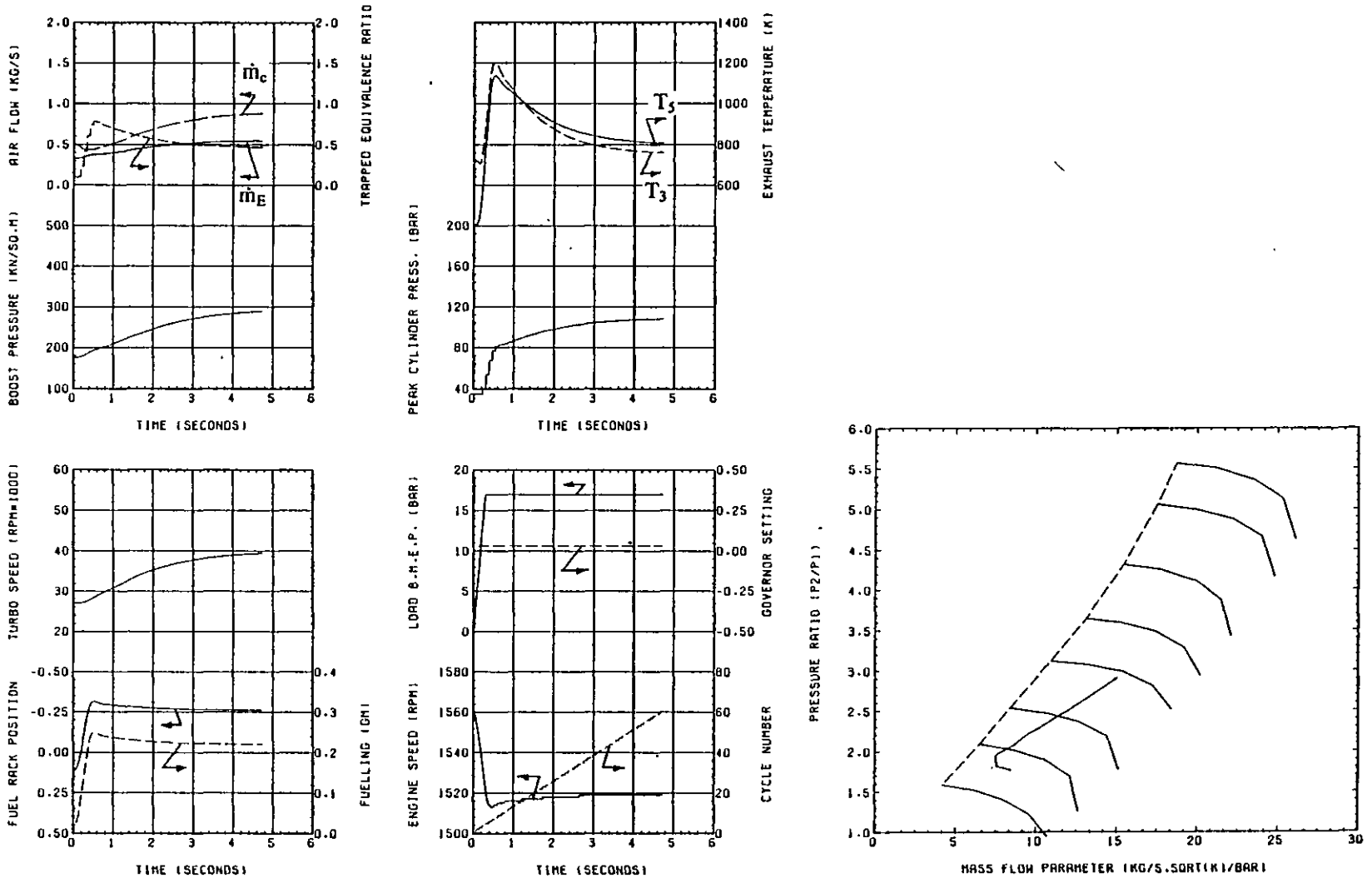

Fig. 7.8a Engine Response to a 70% Load Application from 1560 rpm/0 bar BMEP.

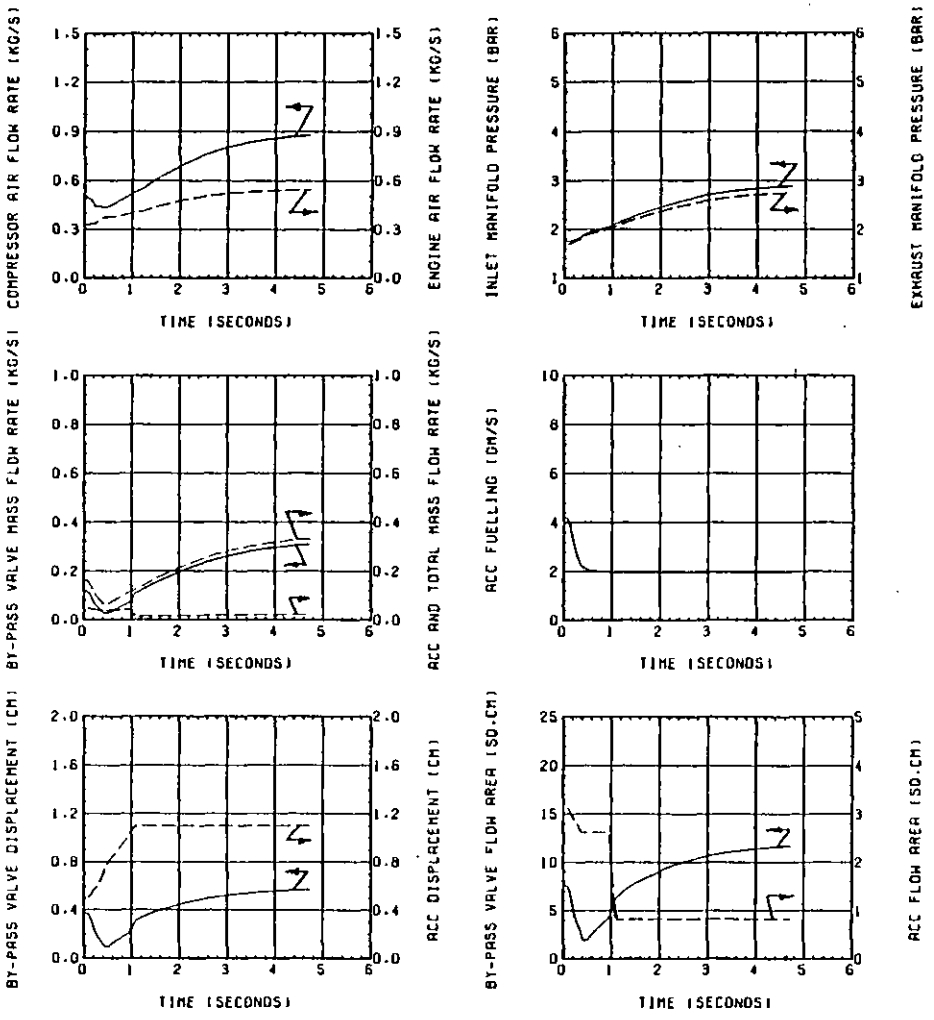

Fig. 7.8b Engine Response to a 70% Load Application from 1560 rpm/0 bar BMEP.

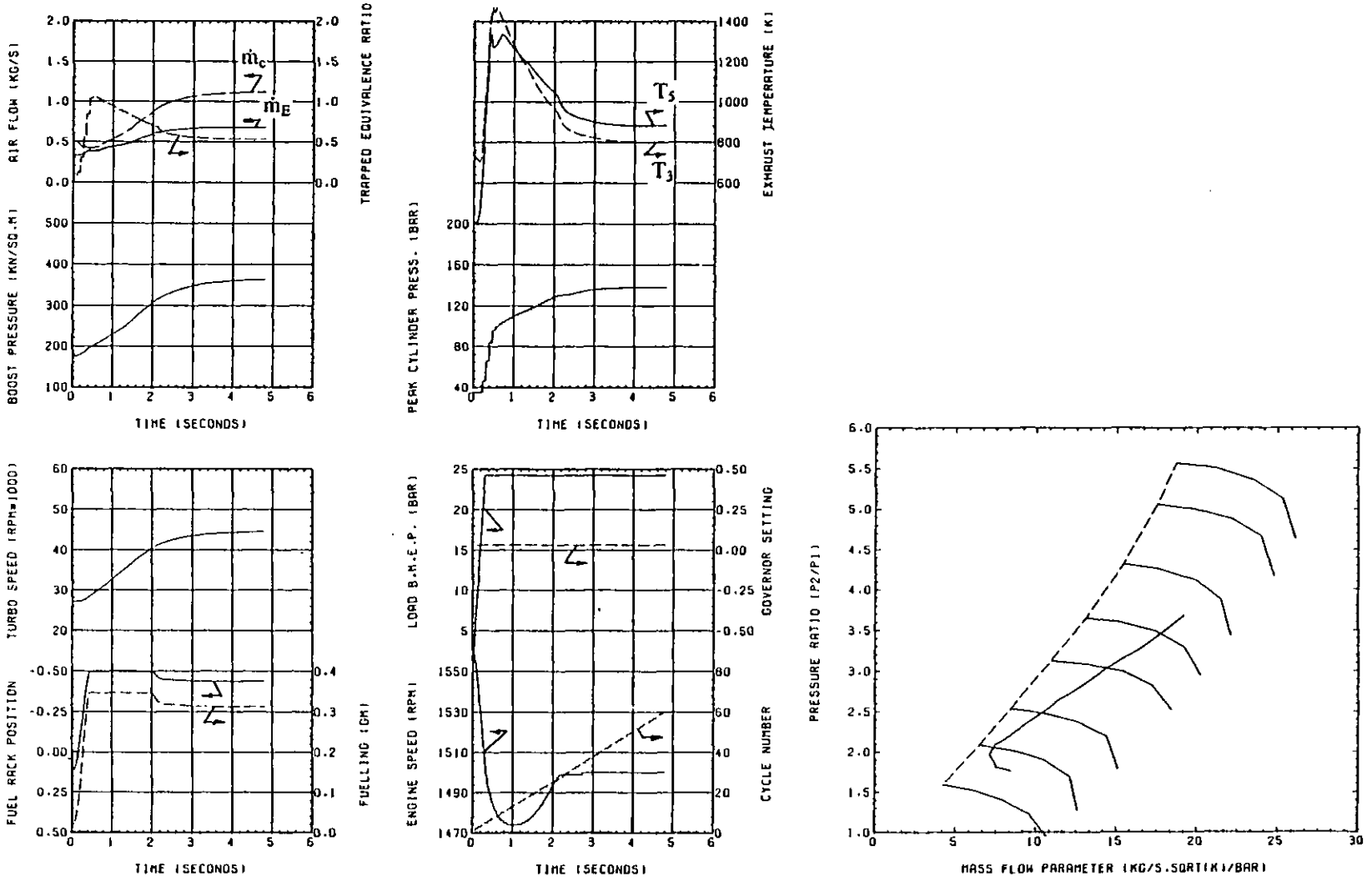

Fig. 7.9a Engine Response to a 100% Load Application from 1560 rpm/0 bar BMEP.

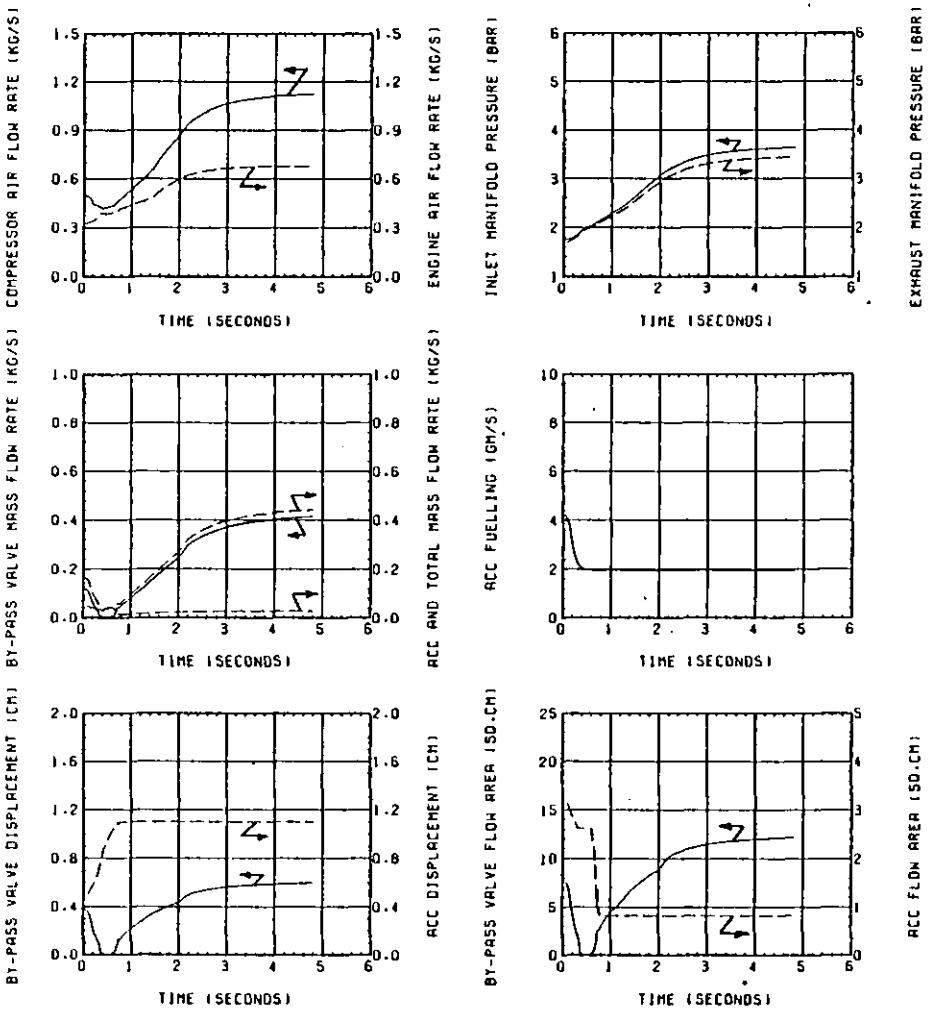

Fig. 7.9b Engine Response to a 100% Load Application from 1560 rpm/0 bar BMEP.

high loads are applied, see Fig. 7.9.

The by-pass valve closes for a short time during the highest load application but remains open for the 50% and 70% tests, see Figs. 7.7b, 7.8b and 7.9b. This reduces the drop in total compressor flow as the load reduces and so controls the movement of the operating line on the compressor map. The greater time taken for the exhaust pressure to build up during the lower load applications means that the ACC fuelling remains higher for longer, assisting the turbocharger response. The peak ACC equivalence ratio increases from 0.39 (after 0.23 seconds) for a 50% load application, to 0.48 (after 0.47 seconds) with a 70% load application and 0.75 (after 0.47 seconds) with a 100% load application.

The response of the Hyperbar engine is compared with that of the two stage turbocharged version to the same load application tests in section 7.4.

7.3.7 Effect of Increasing the ACC Damping.

The initial speed (1560 rpm) and load (0 bar BMEP) used for the load application tests, described in section 7.3.5, mean that the ACC burner fuelling is high at the start of the transient. This ensures that the boost level is adequate for good combustion in the engine cylinders. It can be seen from Fig. 7.9b that as the load increases the engine boost and exhaust pressures increase, and the ACC moves to reduce the combustion chamber fuelling and port areas to their minimum values. The reduction in ACC fuelling with time depends upon the various control pressures, the geometry of the burner and the build up of exhaust gas pressure in the ACC. The burner motion is also influenced by its inertia and damping. If the damping coefficient is arbitrarily increased, from the value established in section 4.8.5, then the ACC should move more slowly from its initial position to the minimum fuelling position as the boost and exhaust pressures build up. This should result in an increase in the exhaust energy earlier in the transient (provided that sufficient air is available to burn the extra fuel), and consequently faster turbocharger response and a more rapid build up in the boost pressure and the engine air flow.

The ACC damping coefficient was arbitrarily increased by a factor of 10 and the 100% load application test was repeated. The results are shown in Fig. 7.10.

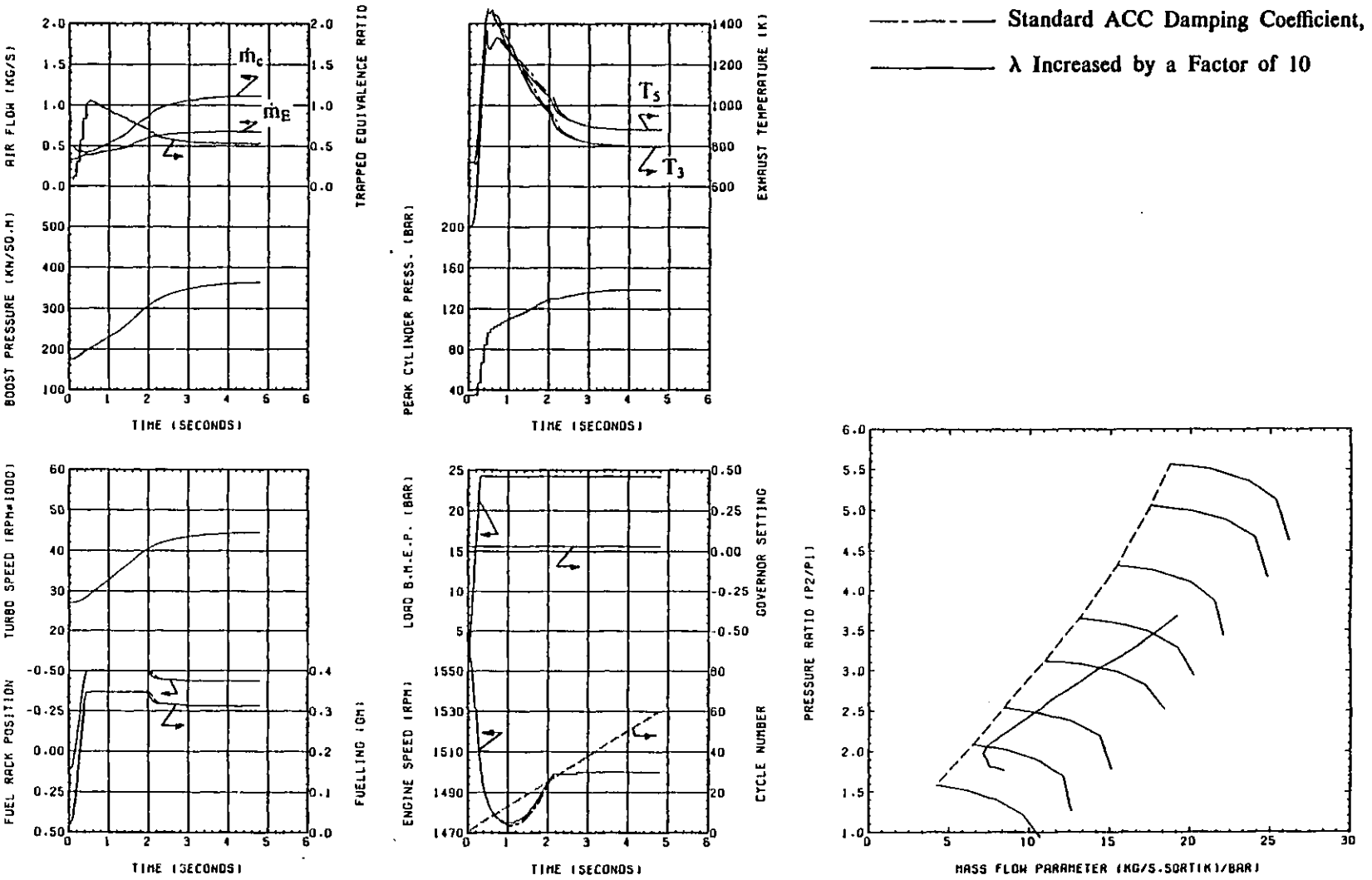

Fig. 7.10a Effect of the ACC Damping Coefficient on the Engine Response to a 100% Load Application from 1560 rpm/0 bar BMEP.

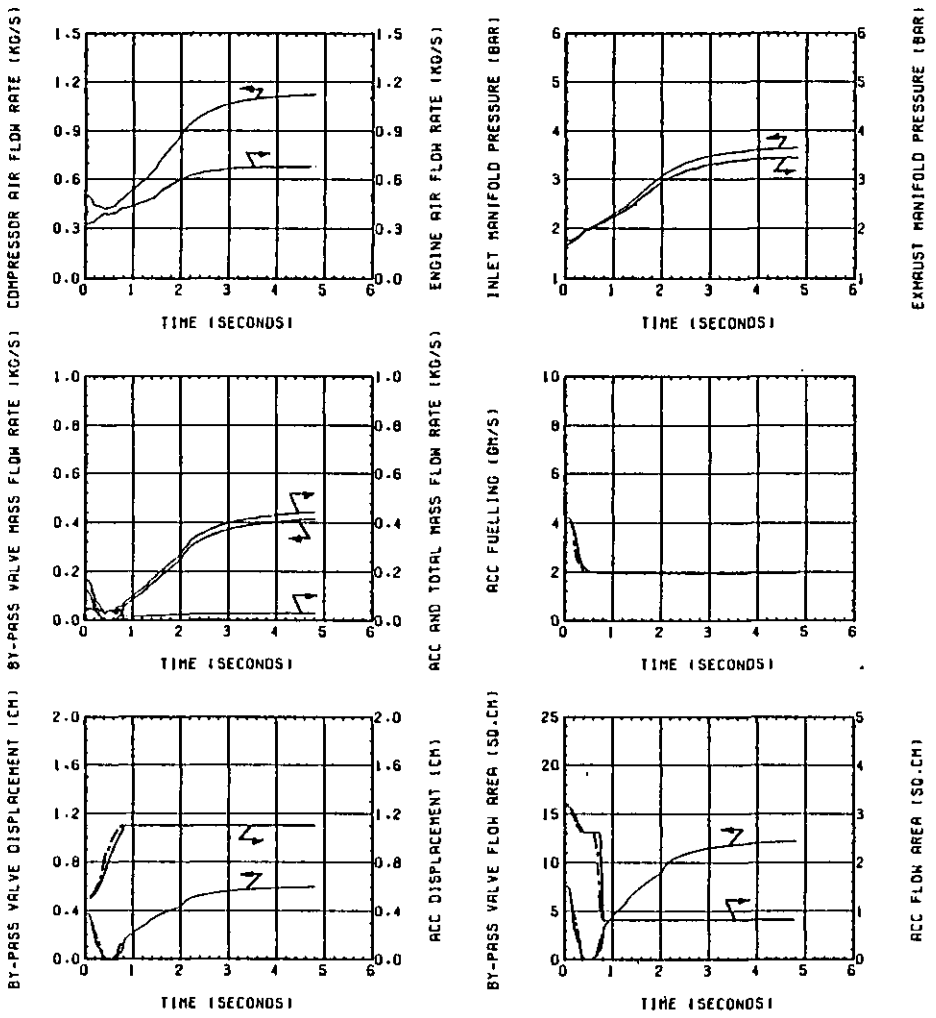

Standard ACC Damping Coefficient, λ

λ Increased by a Factor of 10

Fig. 7.10b Effect of the ACC Damping Coefficient on the Engine Response to a 100% Load Application from 1560 rpm/0 bar BMEP.

Increasing the ACC damping does result in a slower movement in the ACC to the minimum fuelling position and an increase in the initial ACC fuelling, but the effects are small. The effect on the turbocharger speed response and hence the boost pressure and air flow rate are negligible and so the overall effect on the response to a 100% load application is very small, and the differences cannot easily be seen in Fig. 7.10. Unfortunately the fuelling is increased in the period where the by-pass air flow is very low. Any increase in the ACC fuelling will result in an increase in the exhaust gas pressure which will, in turn, reduce the ACC fuelling, and so the effect is limited. The peak ACC equivalence ratio increases from 0.75 to 0.78 (after 0.47 seconds) by increasing the ACC damping by a factor of 10.

There is no noticable reduction in the motion of the compressor operating line towards the surge line during the early part of the test, and the overall effect of increasing the ACC damping to improve this type of transient is small. A better way of increasing the ACC fuelling would be to increase the ACC fuel control pressure, as demonstrated in Fig. 7.4. The results do indicate, however, that a large error in the estimation of the ACC damping coefficient (which was not known) will not drastically effect the accuracy of the predicted engine response.

It is also conceivable that stiction, (which has not been taken into account in the mathematical simulation model, see section 4.8.3) will considerably influence the motion of the ACC during rapid changes in engine load and/or speed.

7.3.8 Effect of Increasing the Engine Compression Ratio on Load Acceptance.

The generator type engine configuration described in section 7.3.5 has been modified by increasing the compression ratio to 11:1 and reducing the minimum boost pressure level to 140 kN/m^2 (by lowering the fuel control pressure to 534 kN/m^2, as described in section 7.3.4). For this test the engine output was maintained at 24.19 bar BMEP at 1500 rpm. However, with the increased compression ratio the peak cylinder pressure exceeded the manufacturers limit of 140 bar, and consequently the static injection timing was retarded from 20°CA BTDC to 12°CA BTDC. The engine fuelling at 1500 rpm/24.19 bar BMEP had to be reduced by 2.1% to achieve the desired power output, the effect of increasing the compression (expansion) ratio being

greater than that of retarding the injection timing. Consequently the fuel pump and governor were modified slightly to maintain the same speed droop characteristic.

A 100% load application of 24.19 bar BMEP was applied in 0.3 seconds from an initial speed of 1560 rpm and load of 0 bar BMEP. The resulting engine speed response is shown in Fig. 7.11, and is compared with the response of the standard engine shown in Fig. 7.9.

With the lower ACC fuel control pressure the initial boost pressure level is reduced and the turbocharger has to accelerate through a larger speed range during the transient. But the ACC fuelling, and consequently the turbine energy level, is lower with this engine configuration. The engine A/F ratio becomes excessively rich during the early part of the transient due to the rapid change in rack position and the reduced engine air flow. This results in excessive exhaust smoke and a deterioration in the engine response, which can be seen in Fig. 7.11. The initial engine speed drops from 1560 rpm to 1360 rpm, compared to a drop of only 85 rpm with the standard configuration. The engine does not recover to its final steady state speed of 1500 rpm within the duration of the test (5 seconds), but takes only 3.29 seconds to recover with the higher minimum boost pressure level.

Retarding the static injection timing throughout the test is not strictly necessary and results in some deterioration of the engine performance, (but an increase in the exhaust gas energy). However, it does effectively control the peak cylinder pressure to within the limits achieved with the standard engine geometry. A mechanism that retards the injection timing only when a predetermined maximum cylinder pressure level is reached would improve the engine response.

The compressor surge margin is acceptable for both engine configurations, and the peak exhaust and turbine inlet temperatures are similar in both cases, occuring when the trapped equivalence ratio approaches unity.

The transient ACC fuelling is reduced with the lower minimum boost level but the by-pass valve closes for a slightly longer duration, see Fig. 7.11b. The peak ACC equivalence ratio increases from 0.75 (after 0.47 seconds) to 1.21 (after 0.39 seconds) by reducing the minimum boost pressure level, and so a fuel cut off will be required.

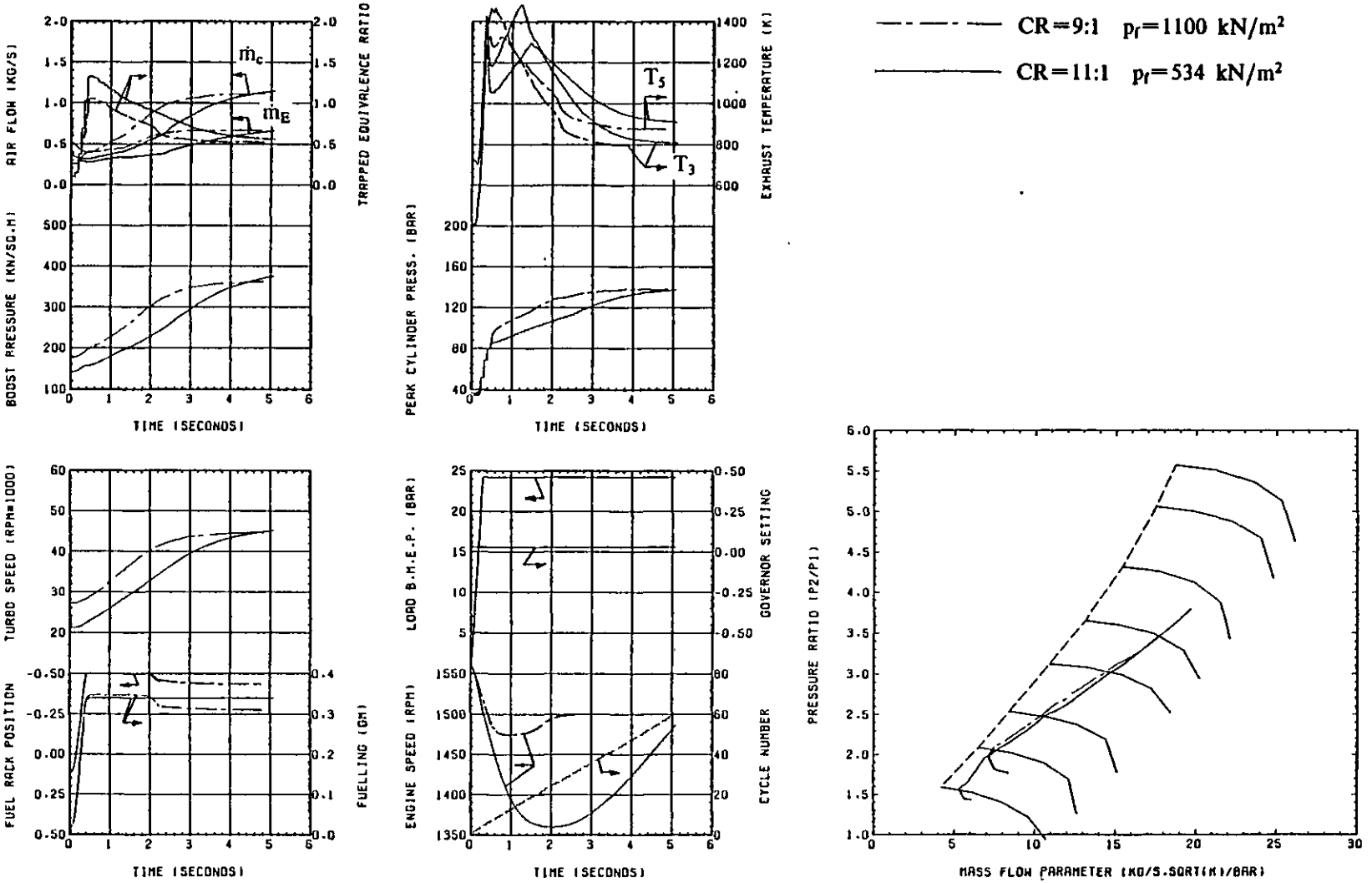

Fig. 7.11a Effect of Compression Ratio and Minimum Boost Pressure Level on the Engine Response to a 100% Load Application from 1560 rpm/0 bar BMEP.

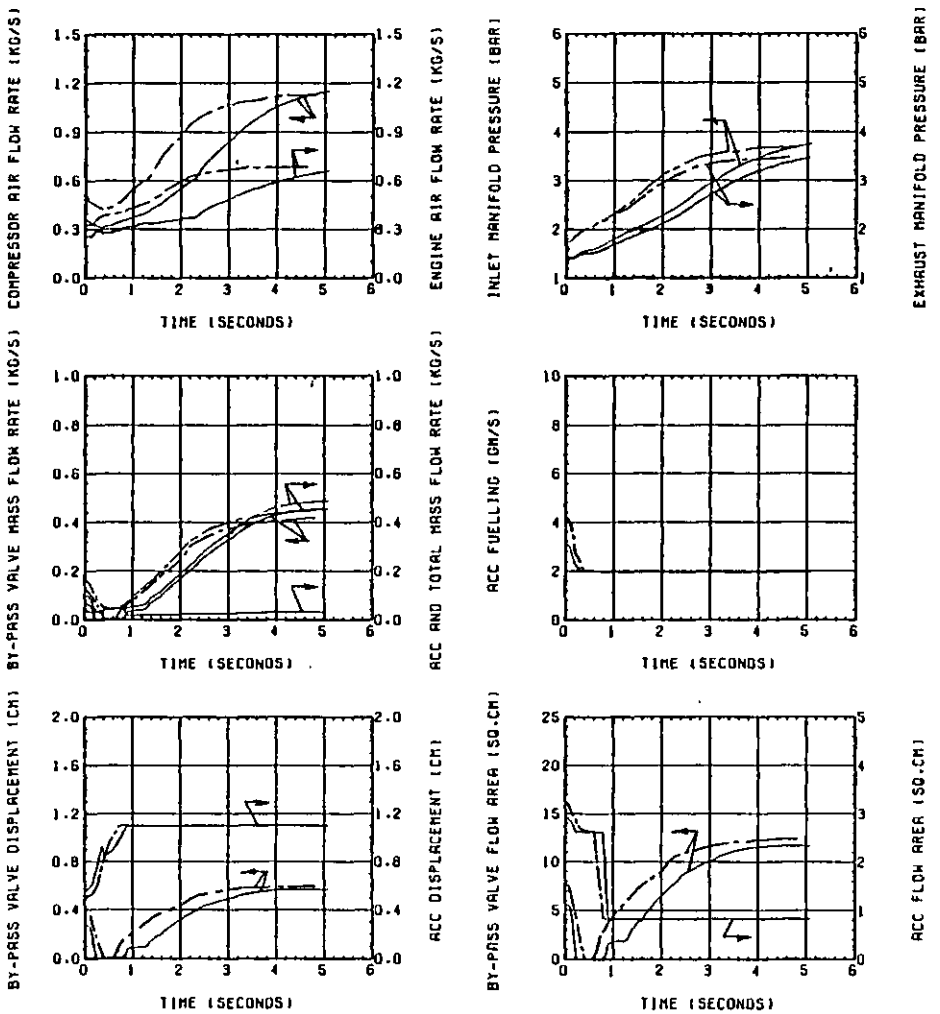

CR=9:1 p_f=1100 kN/m²

CR=11:1 p_f=534 kN/m²

Fig. 7.11b Effect of Compression Ratio and Minimum Boost Pressure Level on the Engine Response to a 100% Load Application from 1560 rpm/0 bar BMEP.

The Hyperbar engine has shown itself to be very good at accepting large sudden load applications, due mainly to the high engine A/F ratio at the start of the load application (maintained by the ACC burner). By reducing the minimum boost pressure level, the initial A/F ratio is reduced, and so is the engines ability to accept rapid changes in fuelling without producing excessive smoke. However, the penalty that must be paid for this excellent transient performance is the high part load fuel consumption. The minimum boost level, and consequently the engine compression ratio and the ACC fuelling characteristics are therefore a compromise, that depend upon the application of the engine.

In the following sections the response of a conventional two stage turbocharged engine to the same acceleration and load application tests will be considered. This engine represents the extreme case of a high BMEP engine with the minimum boost pressure level reduced to atmospheric (or even lower), and no burner assistance. The advantages and disadvantages of this system and the Hyperbar system will then be contrasted.

7.4 Comparison of the Hyperbar System and Two Stage Turbocharging.

7.4.1 Introduction.

The two stage turbocharged, aftercooled version of this engine is described in section 7.2.1. This engine, rated at the same output as the Hyperbar engine, has been subjected to the same transient response tests as described in the preceding sections. This enabled a direct comparison of the two turbocharging systems to be made.

7.4.2 Propeller Law Loading Tests.

The propeller law loading for the engine rated at 17.14 bar BMEP at 2400 rpm (the slight increase in BMEP compared to the Hyperbar engine is explained in section 7.2.1), is defined in the same way as for the Hyperbar engine, see section 7.3.1. The same governor characteristics have been used but the fuel pump characteristics have been scaled, because the two stage engine requires only 97% of the engine fuelling at the maximum engine speed to achieve the same power output. The response of the two stage engine to the propeller law loading is shown in Fig. 7.12, which also shows

the Hyperbar engine response for comparison.

Because of the low initial engine speed and load (800 rpm/190 kN/m^2) the boost pressure was initially very low (both compressors operating at pressure ratio's of less than unity). The aneroid, type E shown in Fig. 7.13, was a modified version of aneroid D, described in section 7.2.1, and restricts the engine fuelling initially, by holding the rack position constant until the HP boost pressure exceeds 114 kN/m^2. The engine appears to be overfuelled during the early stages and this can be seen from the high trapped equivalence ratio (greater than unity). The resulting reduction in exhaust temperature and engine power, which is accompanied by excessive smoke is evident in Fig. 7.12.

The low engine fuelling dictated by the low boost pressure, via the aneroid, means that the engine acceleration is much slower than that of the Hyperbar engine. This can be seen by comparing the engine fuellings. The aneroid actually controls the engine fuelling for the first 3.49 seconds of the acceleration, (while the HP boost pressure is below 240 kN/m^2) which limits the engine BMEP that can be achieved, and hence the engine acceleration.

The boost pressure builds up very slowly. The wastegate starts to open after 3.45 seconds and opens rapidly as the LP boost pressure increases, which limits the LP turbocharger speed and the LP boost pressure quite effectively. Controlling the LP exhaust manifold pressure, via the wastegate, increases the energy available in the HP turbine and causes the HP turbocharger speed to increase, although the overall engine air flow is effectively controlled by the wastegate. The operating lines on the HP and LP compressor maps are also shown in Fig. 7.12, which demonstrates the influence of the wastegate, and the low boost pressure and poor compressor efficiency at the start of the test.

The main reason for the superior response of the Hyperbar engine is that the engine air flow rate is much higher initially, as is the boost pressure, because of the ACC burner action. Consequently the fuel pump rack can can go to maximum fuelling as fast as the governor will allow it (for a two speed governor in the mid speed range the rack position is directly proportional to the demand speed). The generous air supply means that the maximum fuelling can be used without causing excessively rich trapped equivalence ratio's, with the resulting smoke and deterioration in engine

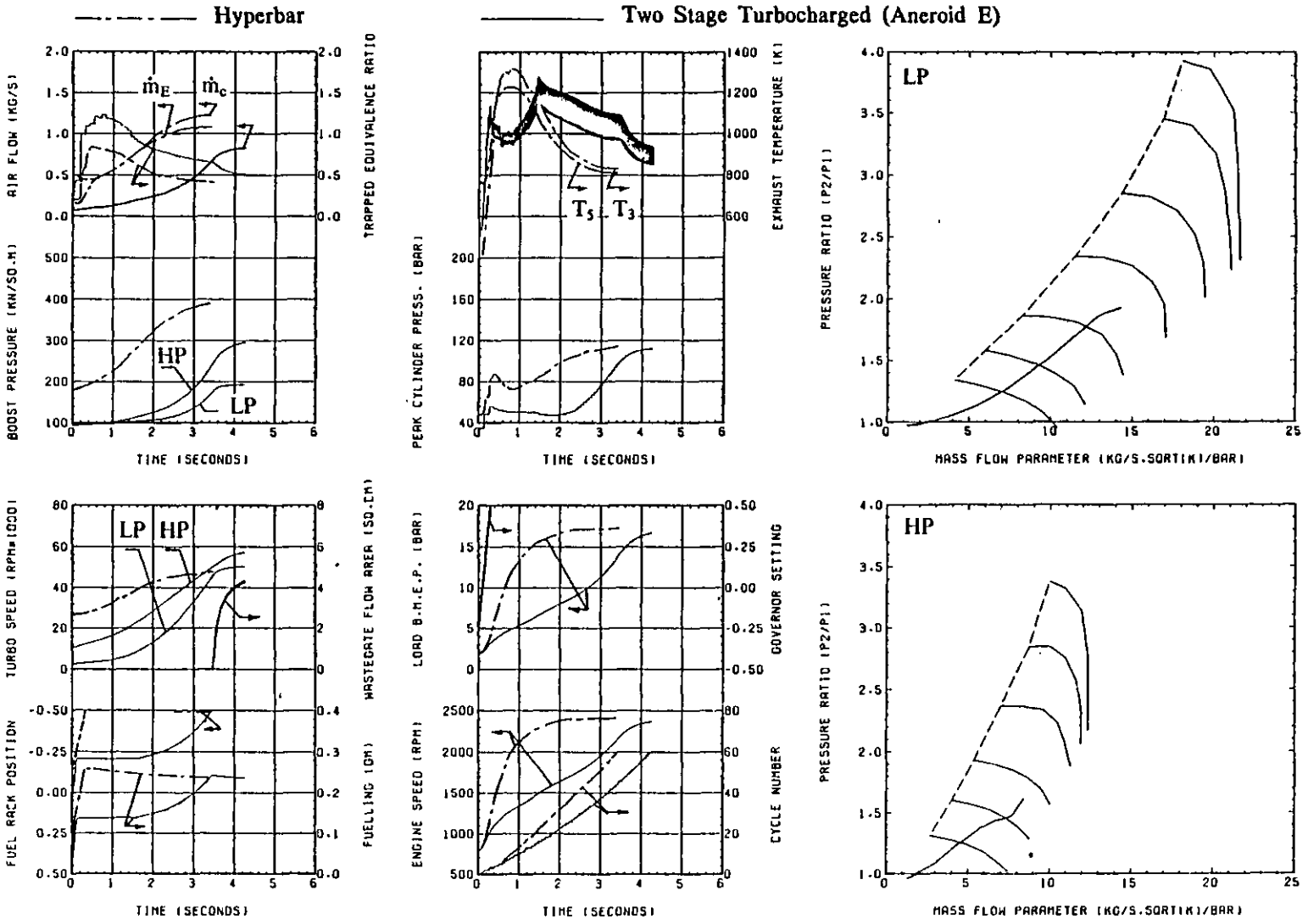

Fig. 7.12 Comparison of Hyperbar and Two Stage Turbocharged Engine Response to a Propeller Law Loading Schedule.

response. For Hyperbar engines of higher ratings an aneroid rack limiter, or some other type of fuel pump controller, may be required, because of the increase in the ratio of the no load to the full load fuelling, (alternatively the minimum boost pressure level could be raised).

The higher inertia of the Hyperbar turbocharger does not appear to hinder the response for this test. The turbocharger only has to accelerate through a relatively small speed range, compared to both the HP and LP turbochargers of the two stage turbocharged engine.

The main problem for the two stage turbocharged engine in that the initial boost pressure is very low and so the air supply and fuel supply (because of the aneroid) are low. The turbocharger acceleration is also poor because of the low energy level in the exhaust system.

7.4.3 Load Application Tests.

Because of the poor response of the two stage turbocharged engine to the propeller law loading, the aneroid characteristic was first optimised, before the load application tests, described in section 7.3.6 for the Hyperbar engine, were repeated.

The engine was rated at the same power output at 1500 rpm (24.25 bar BMEP) as the Hyperbar engine, and so did not produce the same power as the Hyperbar engine at the maximum engine speed (2400 rpm), due to the fuel pump characteristics used.

The fuel pump characteristics for the two stage turbocharged engine were scaled, because this engine required only 95% of the Hyperbar engine fuelling, to produce the same power output at 1500 rpm. As in the case of the Hyperbar tests the fuel pump output was designed to give 10% overfuelling during transient operation. Consequently the governor characteristics were also modified slightly, although the differences were small (the slopes of the rack position versus speed lines, for constant demand speed, were reduced by 1.3%).

For these tests the wastegate was held closed throughout the transient to ensure the maximum possible boost pressure and engine air flow were achieved. However, as the

wastegate was designed to open when the LP boost pressure reaches 185 kN/m^2, see section 7.2.1, holding it shut will only effect the later stages of the response test. There was no danger of the engine being over boosted during the short duration of this test, because of the poor response of the turbocharging system (relative to that of the Hyperbar system). The wastegate could be allowed to open when the final steady state engine speed was reached, if required.

7.4.4 Comparison of Boost Controlled Rack Limiters.

A comparison of three different aneroids was carried out for a load application of 70% of the maximum engine BMEP at 1500 rpm (i.e. 16.98 bar), from an initial speed of 1560 rpm and load of 0 bar BMEP (as described in section 7.3.6). The load was applied linearly in 0.3 seconds at constant demand speed (throttle setting).

The engine response using aneroid A, see Fig. 7.13, is shown in Fig. 7.14. The engine speed finally settles at 1520 rpm and first reaches this speed after 2.75 seconds. The speed drop as a percentage of the initial and rated engine speeds is 11.9% and 8.4% respectively, the minimum speed being 1374 rpm after 1.49 seconds. The engine can be seen to recover to its final steady state speed in 2.8 seconds.

However the smoke produced, as indicated by the trapped equivalence ratio, is totally unacceptable due to a poor aneroid match. In addition the severe engine overfuelling during the early stages of the load application results in a deterioration in the engine response, due to a reduction in the engine power and exhaust gas temperature, and hence the available turbine energy and turbocharger response.

The aneroid match is very important in this application, since the engine starts off at no load with a very low initial boost pressure (the HP inlet manifold pressure at 1560 rpm/0 bar BMEP is only 6 kN/m^2 above atmospheric). Aneroid A allows the rack to travel to x=-0.276, while the boost pressure is below 114 kN/m^2 which corresponds to 65.5% of the maximum possible engine fuelling at 1500 rpm (this is 110% of the rated fuelling). Fig. 7.14 shows how the aneroid gradually allows the fuelling to increase as the boost pressure rises until the maximum rack limit is reached after 2.35 seconds. Soon after this the engine speed recovers to its final steady state value, and the governor adjusts the fuelling to maintain this speed.

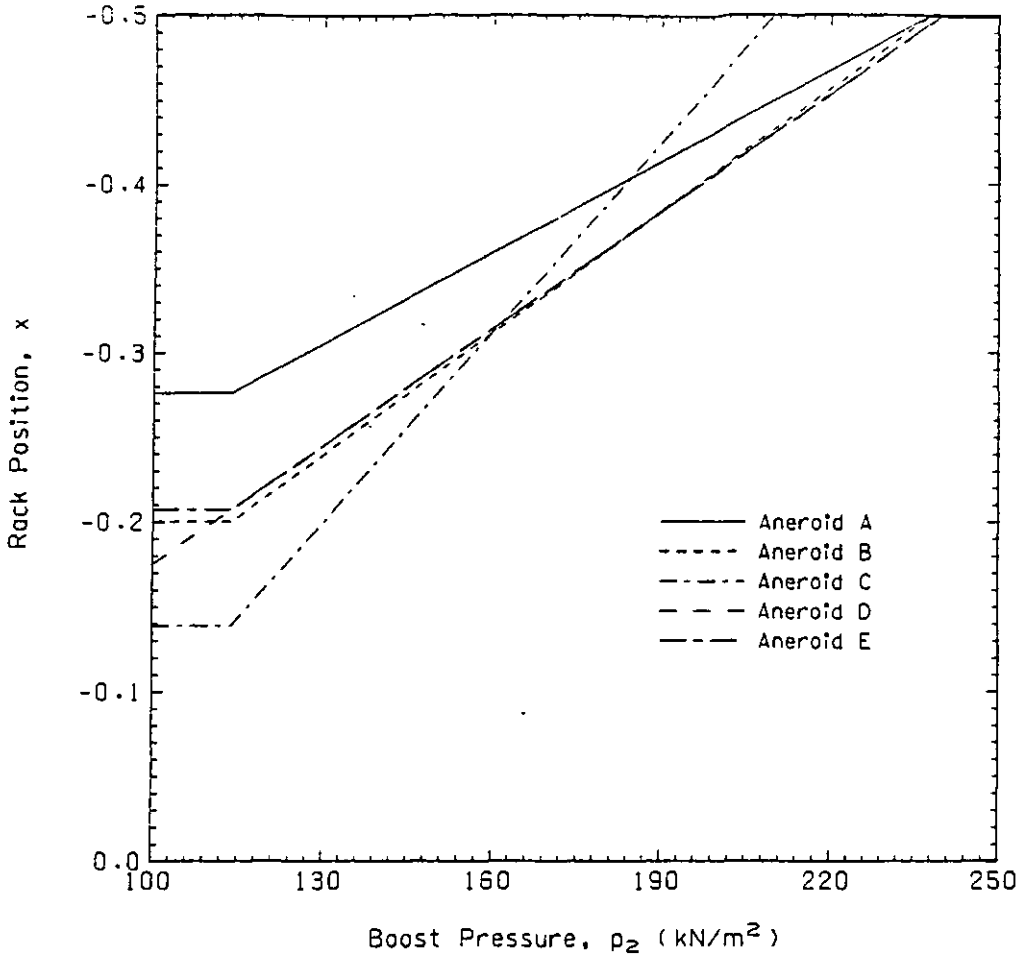

Fig. 7.13 Aneroid Characteristics.

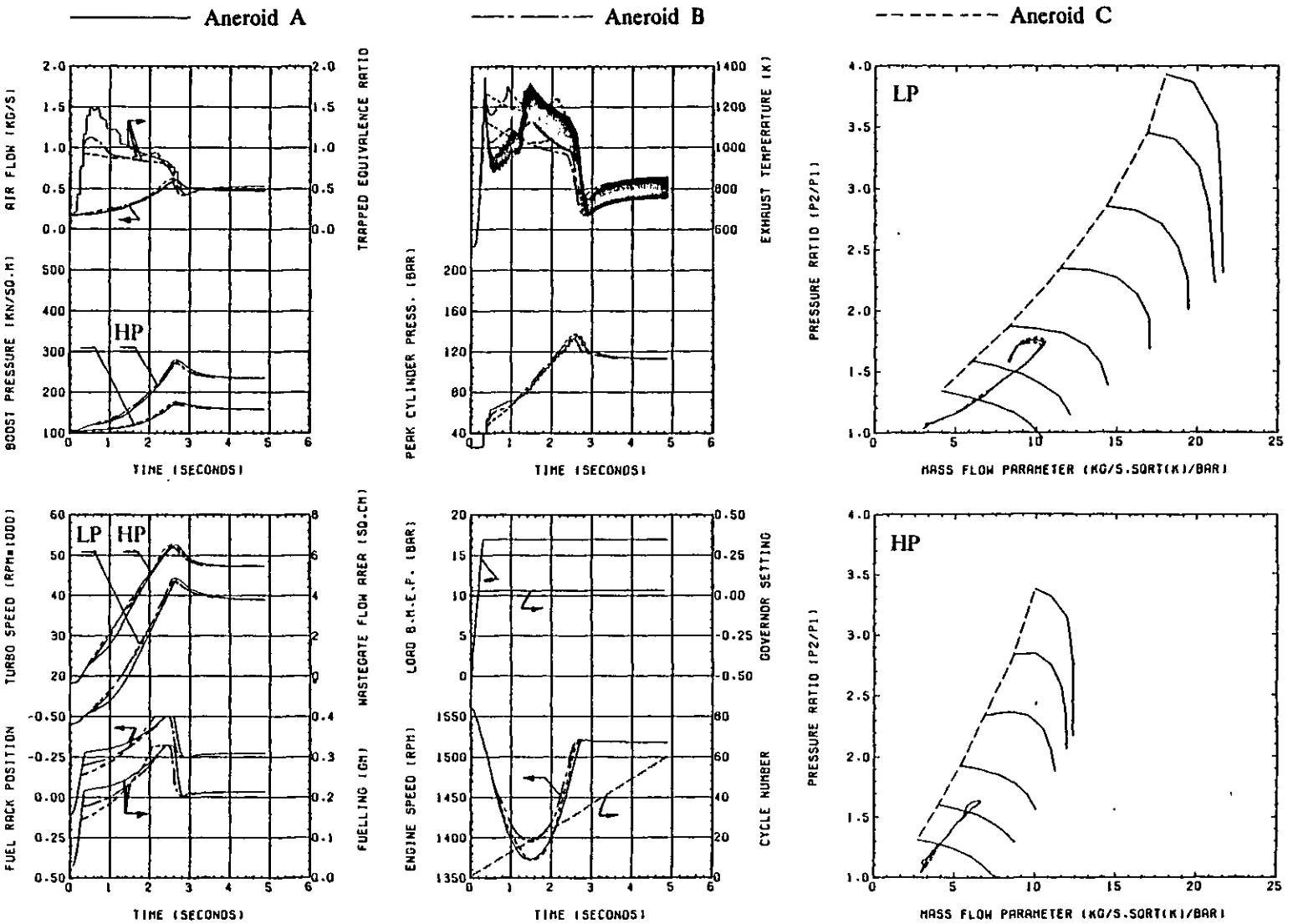

Fig. 7.14 Comparison of Two Stage Turbocharged Engine Response to a 70% Load Application from 1560 rpm/0 bar BMEP with Different Aneroid Designs.

7.4.4.1 Revised Rack Limiter - Aneroid B.

The aneroid characteristics were revised in an attempt to reduce the initial overfuelling caused by aneroid A. Aneroid B is also shown in Fig. 7.13. The result of using this aneroid on exactly the same 70% load application test is also shown in Fig. 7.14. Aneroid B works over the same boost pressure range as A (up to 238 kN/m^2), and has a single slope characteristic. However the initial rack travel allowed up to a boost pressure of 114 kN/m^2 is reduced from x=-0.276 to x=-0.200, (x=-0.5 corresponds to the maximum fuelling) and consequently the gradient of rack travel versus boost pressure is steeper. Less fuel is therefore allowed over the entire operating range of the controller using aneroid B.

Fig. 7.14 shows that aneroid B reduces the amount and duration that the trapped equivalence ratio exceeds unity, and so reduces the engine smoke, in addition the exhaust temperature reduction due to overfuelling is smaller. The effect on engine response is that the minimum engine speed increases from 1374 rpm after 1.49 seconds (aneroid A) to 1396 rpm after 1.48 seconds. Therefore the percentage speed drop, based on the initial and rated engine speeds, reduces to 10.5% (compared to 11.9% for aneroid A) and 6.9% (8.4%) respectively. The engine first recovers to its steady state speed of 1520 rpm after 2.65 seconds (compared to 2.75 seconds for aneroid A) and so there is some improvement in the engine performance as well as a reduction in engine smoke.

While the smoke has been reduced by using aneroid B and the engine performance improved, the trapped equivalence ratio is still excessively rich during the early stages of the test.

7.4.4.2 Revised Rack Limiter - Aneroid C.

A third boost controlled rack limiter, aneroid C, see Fig. 7.13, was used to try and overcome the shortcommings of aneroid B. This aneroid also had a single slope characteristic, similar to A and B, but allowed less fuel at the lower boost pressures (to reduce the initial high trapped equivalence ratio's). The gradient of the rack position versus boost pressure for aneroid C was increased so that the maximum rack limit was reached when the HP boost pressure reached 210 kN/m^2. This meant that aneroid C permits higher fuelling than aneroid B above boost pressures of 159 kN/m^2, and higher than aneroid A above 183 kN/m^2. This allows greater engine power when the boost pressure and air flow have increased from their initial values.

The result of using aneroid C for the 70% load application test is also shown in Fig. 7.14. The trapped equivalence ratio never exceeds unity, and the fuelling level is maintained close to stoichiometric over the range of aneroid operation. The engine speed drops from its initial value of 1560 rpm to 1373 rpm after 1.58 seconds, and the engine speed drop based on the initial and rated engine speeds is 12.0% and 8.5% respectively. The final engine speed of 1520 rpm was first reached after 2.67 seconds, after which the governor reduces the engine fuelling to control the engine speed.

Comparing the results of these three aneroids shows that:-

(1) Aneroid C tends to underfuel the engine initially while aneroids A and B overfuel it.

(2) Aneroid B has the smallest engine speed drop, to 1396 rpm, compared to 1374 rpm for aneroid A and 1373 rpm for aneroid C.

(3) The minimum engine speed occurs after 1.48 seconds with aneroid B, compared to 1.49 seconds for aneroid A and 1.58 seconds for aneroid C.

(4) Aneroid B takes the least time to recover to 1520 rpm (2.65 seconds) but is only marginally better than aneroid C (2.67 seconds) which produces the least smoke. Aneroid A is the worst in this respect, taking 2.75 seconds to

recover. Note that the minimum engine speed occurs latest for aneroid C which has one of the fastest recovery times.

7.4.5 Other Load Application Tests.

Aneroid C gives the best overall engine performance with regard to engine recovery, speed drop and smoke emission, and was used for all the subsequent tests. Fig. 7.15 and 7.16 show the result of a 50% load application (12.12 bar BMEP) and a 100% load application (24.25 bar BMEP) respectively. As before the initial speed and load was 1560 rpm/0 bar BMEP, and the load was applied linearly in 0.3 seconds.

7.4.5.1 50% Load Application.

For this load application, Fig. 7.15, the final steady state engine speed of 1532 rpm was reached after 1.66 seconds. The minimum engine speed, 1501 rpm, occured after 0.95 seconds, which corresponds to a speed drop of 3.8% of the initial speed, and 0% of the rated speed (1500 rpm).

The trapped equivalence ratio is controlled very effectively and the engine fuelling is limited by aneroid C for the majority of the test. When the final steady state speed is first reached, after 1.58 seconds, the governor reduces the engine fuelling to stabilize the engine speed.

Due to the relatively low load applied, and the aneroid control, the turbocharger speeds do not overshoot their final steady values (as was seen in the 70% load application tests) and consequently the operating lines, when plotted on the compressor maps appear to have a different form to that shown in the earlier tests.

When compared to the Hyperbar engine speed response for the same rating and applied load, the two stage turbocharged engine shows a greater initial speed drop (59 rpm compared to 31 rpm) but the recovery times are very similar.

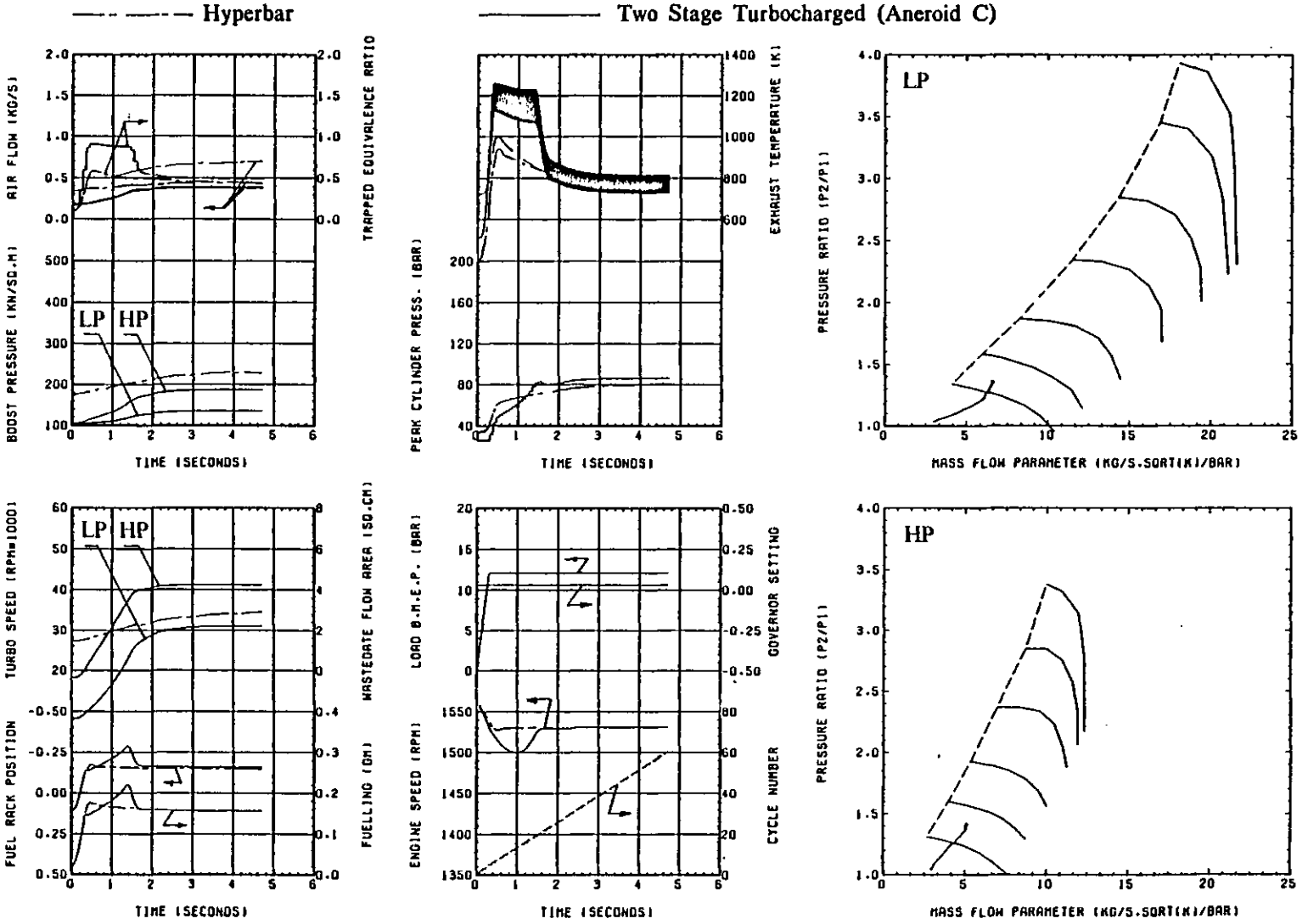

Fig. 7.15 Comparison of Hyperbar and Two Stage Turbocharged Engine Response to a 50% Load Application from 1560 rpm/0 bar BMEP.

7.4.5.2 100% Load Application.

The Hyperbar engine has been shown to be capable of recovering from a 100% load, applied in 0.3 seconds, and so the two stage turbocharged engine was tested under the same conditions for comparison. Fig. 7.16 shows the results.

The fuelling required by the engine to give the steady state engine power corresponding to the applied load (24.25 bar BMEP at 1500 rpm) will not be reached until the HP boost pressure reaches 194 kN/m^2 (at 1500 rpm) using aneroid C, and this does not occur until 3.09 seconds after the start of the test, see Fig. 7.16. This means that the engine is not capable of producing the full load torque until 2.79 seconds after the full load has been applied. By this time the engine speed has dropped to 908 rpm. Maximum fuelling (110%) was not reached until 4.19 seconds after the start of the transient by which time the engine speed had dropped to 859 rpm. Fig. 7.16 shows that as the engine speed keeps falling the boost pressure falls and the aneroid actually starts to reduce the engine fuelling. The load is either too large or has been applied too rapidly for the engine ever to recover.

The effect of the reducing engine speed is that both compressors will eventually surge as the air flow reduces. The HP compressor surges first in this particular test because the pressure ratio is higher as more work is done in the HP stage at low overall boost levels, and due to the actual turbocharger matches chosen. The simulation program can take no account of compressor surge and in this particular case the compressor map to the left of the surge line, (indicated by the dashed lines on the compressor maps) is treated in a similar way to the rest of the map to avoid numerical problems. The predicted response after one or other of the compressors starts to surge is therefore purely hypothetical.

The effect of the aneroid is particularly interesting in this test, the trapped equivalence ratio can be seen to be maintained close to stoichiometric throughout, indicating that the actual engine output is close to the optimum (slightly more fuelling could have been allowed by the aneroid, but would not effect the overall response greatly). Fig. 7.16 also shows the Hyperbar engine response for comparison, from Fig. 7.9.

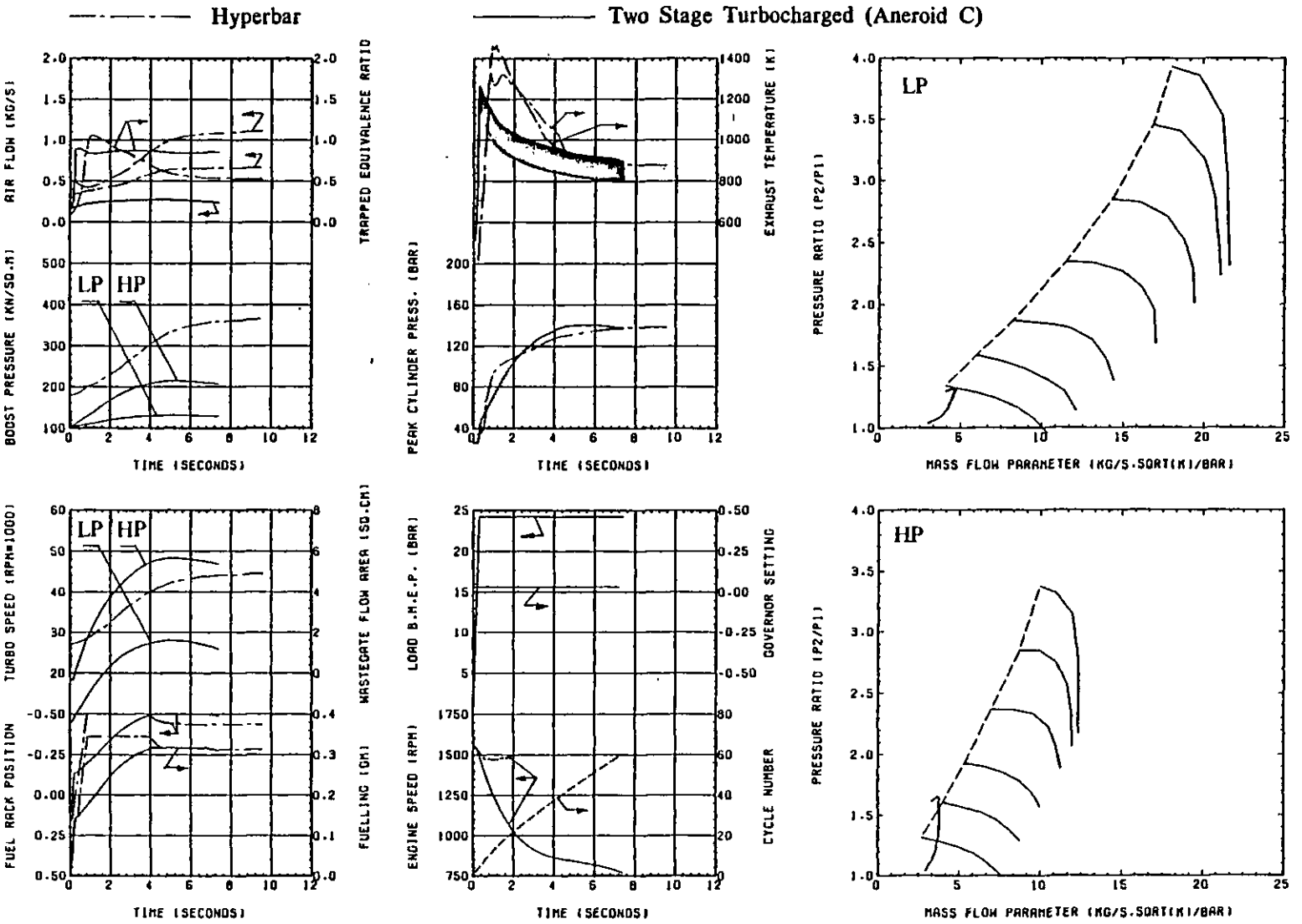

Fig. 7.16 Comparison of Hyperbar and Two Stage Turbocharged Engine Response to a 100% Load Application from 1560 rpm/0 bar BMEP.

7.5 Discussion.

The British Standard Specification for engine speed governing (25) states that, "... the maximum possible amount of a sudden increase in load from zero is ... for turbocharged 4 stroke engines: a function of the Brake Mean Effective Pressure at the declared power". The relationship between the declared power and the applied load is shown in Fig. 7.17. In the tests carried out on the two stage turbocharged and Hyperbar engines, the declared rating was 24.25 bar BMEP and 24.19 bar BMEP respectively (approximately 24.2 kPa) at 1500 rpm. Therefore from Fig. 7.17 the engine only has to be capable of accepting 32% of this load (i.e. 7.75 bar BMEP) in a sudden load application from no load.

The British Standard does not, however, define "a sudden increase in load". For all the tests described the load has been increased linearly from 0 bar BMEP up to the maximum load BMEP in 0.3 seconds. Both the Hyperbar and the two stage turbocharged versions of this engine can deal quite easily with a 50% load application, as demonstrated in sections 7.3.6 and 7.4.5, and are therefore well within the limits imposed by the British Standard Specification. However, whether or not the two stage turbocharged engine can accept a 100% load application will depend upon the rate at which the load is applied. The definition of "a sudden increase in load" is therefore very important.

The recommended maximum engine speed drop according to (25) is defined as:-

$$\left(\frac{N_{min} - N_i}{N_r}\right).100 \leq 10\% \qquad (7.6)$$

for class A_1 governing.

where,

N_{min} = minimum engine speed (rpm)

N_i = idling engine speed (rpm)

N_r = declared engine speed (rpm)

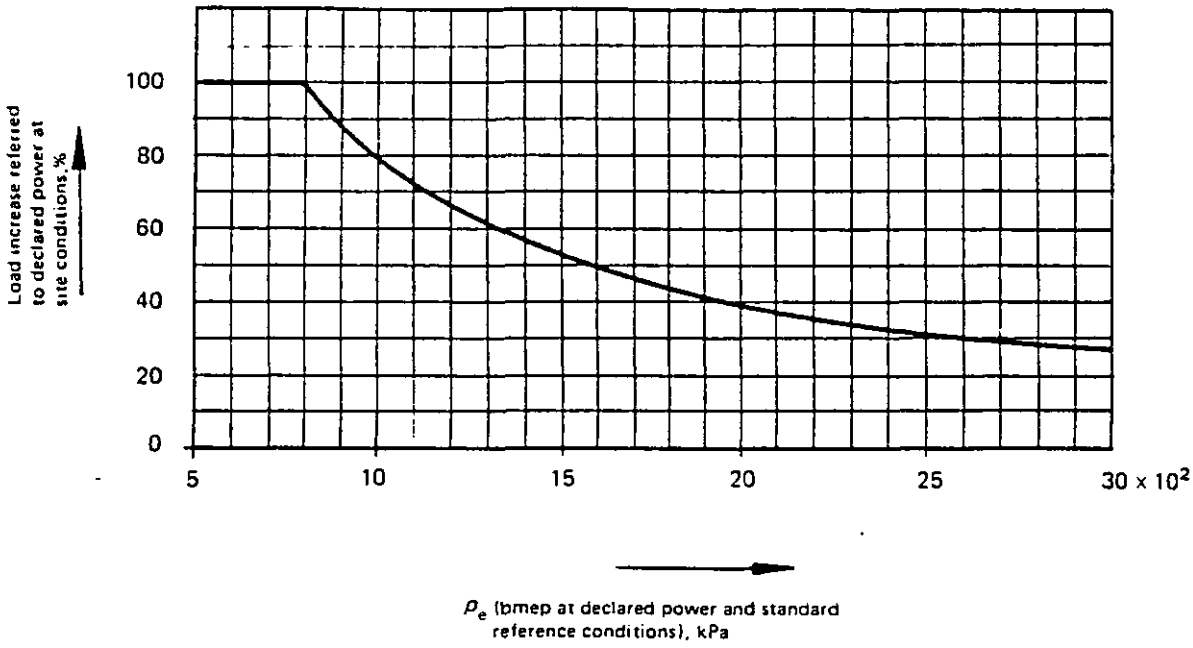

Fig. 7.17 The Maximum Possible Sudden Load Increase from Zero of Turbocharged 4 Stroke Engines as a Function of the BMEP at the Declared Power, from (25).

For a 50% load application the speed drop as defined by equation (7.6) is -3.9% for the two stage turbocharged engine and -2.1% for the Hyperbar engine. With a 70% load application this increases to -12.5% and -3.1% respectively. Only the Hyperbar engine can accept a 100% load application and in this case the percentage speed drop is -5.7%. Aneroid C has been used for all these comparisons.

For a class A_1 type governor the speed droop is defined as:-

$$\left(\frac{N_i - N_r}{N_r}\right).100 \leq 5\% \qquad (7.7)$$

All these tests have been performed with an idling speed of 1560 rpm and a rated speed of 1500 rpm, which gives a speed droop of 4% according to equation (7.7).

Both engines are therefore capable of giving very accurate (class A_1) speed governing, and are well within the limits imposed by BS 5514:Part4:1979. The Hyperbar version, however, is capable of accepting much higher (or more rapid) load applications without stalling, and has a smaller speed drop (corresponding to a change in the generating frequency) after the load has been applied. The penalty for this improvement in response is an increase in fuel consumption which may become prohibitive, especially at idling conditions.

The response of a conventionally turbocharged two stage engine at the same rating has been compared to the Hyperbar engine. The performance of the two stage turbocharged engine has been shown to be very dependent on the aneroid characteristics, because of its inability to produce high boost pressures (and air flow rates) at low loads and speeds. Optimising the aneroid for a given application can lead to significant improvements in the engine response and smoke. However the optimum aneroid characteristics will depend upon the application, and a control system developed to limit the engine fuelling during load applications (where the speed is decreasing and the fuel pump output is increasing at a fixed rack position) will be significantly different to one optimised for a vehicle type acceleration, against a fixed or varying load, where the engine speed increases and the fuel pump output will usually decrease at a fixed rack position, see Fig. 4.32. Whether or not the Hyperbar engine requires an aneroid depends upon a number of factors, such as the engine rating (the ratio of the full load to no load fuelling), the minimum boost pressure

level, the turbocharger inertia, the compressor and turbine match and the effectiveness of the by-pass control systems.

CHAPTER 8

FUTURE DEVELOPMENTS

8.1 Introduction.

The "filling and emptying" simulation model has been described and its ability to predict the steady state and transient performance of the Hyperbar system have been demonstrated. In section 8.2 suggestions are made as to how the mathematical model can be improved, and the experimental test data required to verify possible changes is described.

A general description of the current Hyperbar system control strategy is given in section 8.3, which also outlines some of the advantages and disadvantages of this design.

Based on the results obtained using the simulation model, a number of improvements that can be made to the system are described in section 8.4. These improvements represent a possible design philosophy for the next generation of Hyperbar turbocharged engines.

8.2 Development of the Simulation Model.

The "filling and emptying" simulation model has been shown to be capable of predicting the steady state performance of a high BMEP Hyperbar turbocharged engine to within an acceptable degree of accuracy. Numerous assumptions have been made in the development of the model, to ensure that the core required to load and run the program, and the CPU time used, are within reasonable limits, especially when running transient response predictions. This has resulted in the need for extensive experimental test data to verify the simplifying assumptions made, and to develop empirical correlations for some of the major components. The correlations developed have been based on a fundamental understanding of the operation of the particular system(s) involved. These have been used in cases where the actual system is too

complex to model accurately (e.g. the combustion process), and/or a significant reduction in computer time can be made (e.g. the ACC burner dynamics and fuel regulating system).

Future development of the simulation program should concentrate on improving the "Apparent Fuel Burning Rate" combustion model in this low compression ratio, high BMEP, engine. This requires extensive accurate experimental test data. The correlation derived in this work does, however, give a good indication of the effects of combustion, and the influence of design changes to the engine and turbocharging system, on the combustion process. Other parameters, such as injection pressure and rate and air swirl and turbulence may also be considered in the correlation, if the data is available. Similarly, a very simple model is used for combustion in the ACC burner. The model takes no account of local conditions in the ACC, the injected spray pattern, air velocity or the swirl port position. However, it is not appropriate to use a very complex model for combustion in the ACC, when a relatively simple model has been used for combustion in the engine cylinders, unless a detailed design study of the ACC is required. In this case, the simulation program may be used to calculate the boundary conditions for a more detailed model. Steady state data for gas turbine combustion chambers may provide useful information for developing the ACC combustion model.

No attempt has been made to model the ACC fuel control system because the complexity of such a model is not justified. The simplified model should, however, be capable of simulating the overall effects of the ACC burner accurately. In particular the transient performance of the burner, during both steady state and transient engine operating conditions should be studied. The burner damping coefficient has been estimated in order to ensure stable operation, but the actual value is not known. Flow tests on the burner and by-pass valve will give a better indication of the losses in the by-pass system and the actual by-pass flow. Alternative air supply systems for the ACC could also be investigated, for example, air could be taken from downstream of the charge cooler rather than the compressor outlet, or an electrical air pump could be used to allow the burner to operate when the exhaust pressure would normally be higher than the boost pressure, e.g. during transients, and the ACC fuelling could be shut off or reduced when the ACC air flow rate reduces. Additions to the simulation model to study the effects of a regenerator type by-pass heat exchanger could be included (see section 3.3.5), and the feasibility of such a scheme investigated.

The simple Hyperbar control routine, demonstrated in section 6.10, could be developed and used as a design tool for optimising the performance of a microprocessor based control system. Such a system could optimise the engine steady state and transient performance, while ensuring the best overall fuel consumption, within predefined engine parameter limits. An example of a suitable engine management system is given in section 8.4.

This investigation has concentrated on optimising the design of the Hyperbar engine system to improve the engine performance, (i.e. to increase the engine BMEP and reduce the overall BSFC). No account has been taken of the emissions characteristics of the engine, compared to that of conventional single or two stage turbocharged diesel engines at the same rating. The model is not, at present, capable of predicting the important emissions, such as NO_x, CO and smoke. Further work on a suitable emissions model will be useful, for optimising the engine design.

8.3 Description of the Current Hyperbar System Control Strategy.

The Hyperbar turbocharging system described in this work represents the current development of this system. The design has the following features:-

(1) The by-pass valve is pnuematically driven, by the boost and exhaust gases to maintain a fixed pressure drop ratio, eqn. (4.157), over the operating range of the engine. There is no direct control over the valve position, and it is difficult to modify the pressure drop ratio, except via an external pneumatic control pressure applied to the damping piston (section 6.4). The instantaneous position of the by-pass valve is not controlled and any errors in its operation cannot easily be detected (e.g. seizure of the valve). Correct operation of the valve is essential to prevent the compressor from surging, to ensure sufficient air is available to the ACC, and to maintain the compressor operating in the high efficiency region of the map. These requirements are often contradictory. This design has the important advantage of being very simple.

(2) The Auxiliary Combustion Chamber is pneumatically and hydraulically driven, in this case by the ACC gas pressure (and perhaps an air control pressure) and the fuel control pressure. The fuel is atomised mechanically at high fuel flow rates, and pneumatically (using high velocity air jets) at low fuel flow rates. Extra air enters the ACC via variable area ports, which are controlled by the chamber position. This air, from the compressor outlet, is used to ensure adequate mixing and good combustion in the burner. The burner is ignited initially using a high energy igniter plug.

The fuel flow range of the burner is limited (the ratio of the maximum to minimum fuelling rate being 3.5:1) and is regulated, primarily, by the burner position. The burner operates to maintain the minimum, preset, boost pressure level and, when required, the fuel control pressure can be raised to ensure that sufficient air is available to the engine so that high torque can be achieved at any speed.

(3) The start up procedure for the engine is considerably complicated by its low geometric compression ratio. The turbocharger must first be started mechanically using an electric starter motor. Once air is available in the ACC, the burner can be ignited and the turbocharger is operated as a gas turbine until stable operation is achieved, when the starter motor is declutched. The engine is then started, and is supplied with a combination of boost air from the compressor and exhaust gas from the ACC. This ensures a high enough charge pressure and temperature for ignition in the engine cylinders. The exhaust gas recirculation system is mechanically operated. Once the engine is running stably, and the minumum boost level is achieved, the exhaust gas recirculation can be shut off and the engine operated normally.

The current system has the advantage of being relatively simple and therefore reliable. It is based on sound mechanical and thermodynamic principles, but has the disadvantage of being relatively inflexible and unsophisticated. A greater degree of control over the by-pass valve and the ACC burner is required. Linking the by-pass valve and the ACC motion to the engine operating conditions, such as speed and load, should enable the efficiency of the system to be improved considerably. It is the poor part load BSFC that really detracts from the Hyperbar system. Future developments

should, therefore, be aimed at a greater degree of control over the engine and ACC burner fuel systems.

8.4 A Microprocessor Based Engine Management System.

8.4.1 Introduction.

In order to improve the operating efficiency of the Hyperbar system, a greater degree of control over the individual components in the system is required. Information regarding the operation of the ACC and by-pass valve must be related to the operating demands on the engine, i.e. the load and speed. Some form of "intelligent" control system is required that can decide the engine fuelling, ACC fuelling, by-pass valve air flow, compressor pressure ratio, etc., to optimise the important parameters such as BSFC, smoke, exhaust temperatures, metal temperatures, maximum cylinder pressure, etc.

Microprocessor based on-board engine management systems (EMS) are being developed by many of the major engine manufacturers, and have already been applied in production systems, particularly on spark ignition engines (162). At present the EMS have been designed primarily to meet emission legislation in the USA, Europe and Japan. The systems have been used to control the engine A/F ratio, which must be maintained close to stoichiometric, to ensure efficient operation of the three way catalyst systems which control the exhaust emissions (48,52,144,145). However more sophisticated systems have been developed for turbocharged petrol engines to control the boost pressure and spark timing in order to aviod knock, and to improve the response of the vehicle and its sensitivity to different grades of fuel (120,162).

Future engine management systems will be based on adaptive control systems (20,47,121,144) rather than the simpler "look up table" systems most commonly used at the present time (17,59,60,120). Adaptive control systems can take account of deterioration in the engine throughout its life, can react to changes in external conditions (such as the fuel quality or ambient conditions) and will be capable of "learning" in order to optimise the engine fuel consumption, while maintaining other important parameters, such as emissions, within predefined limits.

The development of a suitable microprocessor based EMS for the Hyperbar engine requires the following items:-

(1) A microprocessor, together with the appropriate software, memory and power supply.

(2) Sensors to detect the parameters that have to be controlled, such as exhaust gas temperature, and the controlling parameters, such as the fuel pump rack position.

(3) Actuators to allow changes to the controlling parameters to be made, e.g. to vary the fuel pump rack position to increase the engine fuelling.

(4) Safety variable monitoring that will shut down the system, or give the appropriate warnings, if there are any problems with either the engine or the control system.

For automotive applications, a logical development is to combine the engine and transmission control systems, to ensure the maximum efficiency for the entire vehicle system. Such a device has already been developed by Lucas/CAV (85), based on an analogue control system. Simpler systems based on engine speed (and possibly load) control have also been reported (133).

8.4.2 Requirements for an Engine Management System.

The effectiveness of the EMS will be strongly dependent on the reliability of the actuators and sensors used. It is therefore essential that the minimum number of sensors are used to supply the information required to control the engine.

The choice of sensors and actuators for an EMS will depend upon the following considerations:-

(1) Cost.

(2) Performance (i.e. accuracy, linearity, resolution, stability, response,

natural frequency, etc.).

(3) Reliability.

(4) Size and weight.

(5) Power requirements.

(6) Input and output signals.

Fig. 8.1 shows typical parameters that are required to be measured and/or controlled for the Hyperbar EMS. These parameters are defined in Table 8.1.

It is evident that the large number of sensors required will result in a high initial cost, and potentially poor reliability. It is therefore necessary to reduce the number of sensors to an absolute minimum, and use approximate theory to relate the signals obtained from a few reliable sensors to the control information required. In addition the sensors must be selected so that they interfere as little as possible with the parameters that they are trying to measure and should, preferably, have digital outputs to avoid the need for separate analogue to digital converters (ADC's).

In comparison with the sensors and actuators, the cost of the microprocessor and its associated hardware is very low. However, the cost of developing, and testing, suitable software may be considerable. The microprocessor electronics should be very reliable, and the low cost of such components encourages the development of suitable dual circuit, or back up systems.

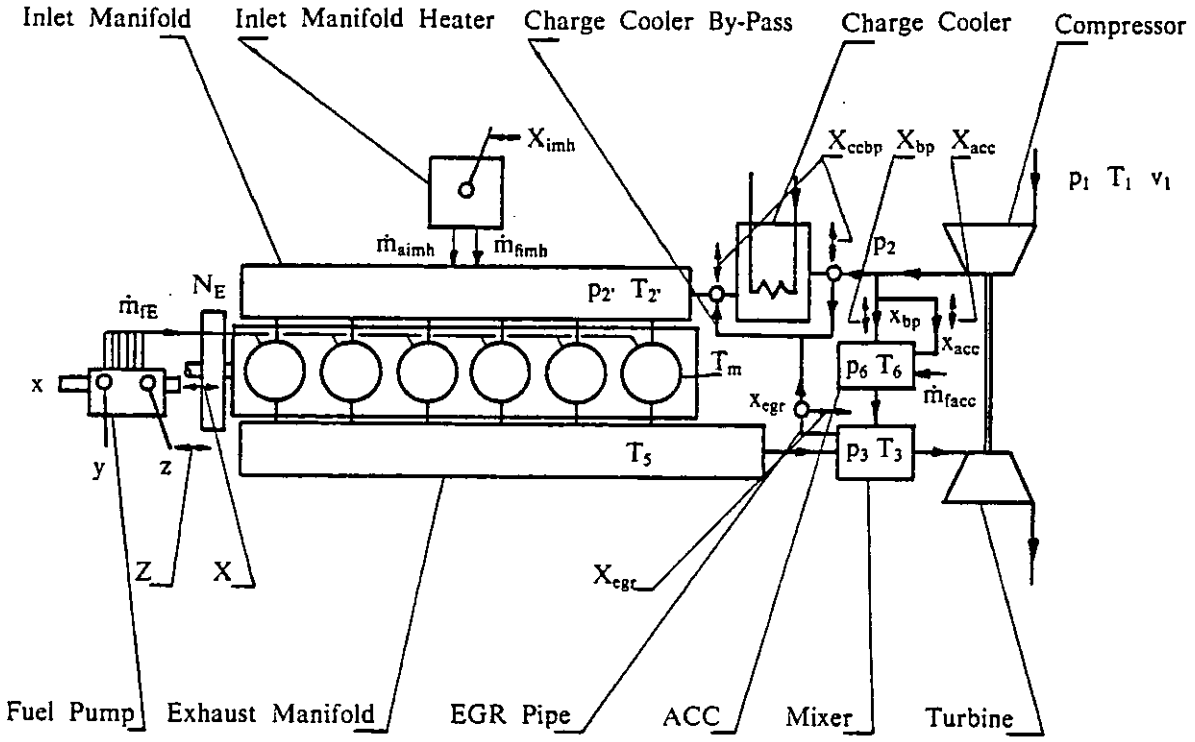

Fig. 8.1 Sensors and Actuators Required for the Engine Management System.

Table 8.1 Sensors and Actuators for the Hyperbar System EMS.

Sensors

Pressures.

** (1) Ambient (or compressor inlet) pressure, p_1.
** (2) Compressor outlet pressure, p_2.
* (3) Inlet manifold pressure, $p_{2'}$.
* (4) ACC gas pressure, p_6.
** (5) Turbine inlet pressure, p_3.
(6) Maximum cylinder pressure, p_{max}.

Temperatures.

** (1) Ambient (or compressor inlet) temperature, T_1.
(2) Compressor outlet temperature, T_2.
** (3) Inlet manifold temperature, $T_{2'}$.
* (4) Exhaust manifold gas temperature, T_5.
* (5) ACC gas temperature, T_6.
** (6) Turbine inlet gas temperature, T_3.
* (7) Metal temperatures, T_m.

Mass Flow Rates.

** (1) Compressor air flow rate (or velocity and density), $\dot{m}_c$.
(2) Engine air flow rate, $\dot{m}_E$.
(3) By-pass air flow rate, $\dot{m}_{bp}$.
(4) ACC air flow rate, $\dot{m}_{aacc}$.
(5) Inlet manifold heater air flow rate, $\dot{m}_{aimh}$.
(6) Engine fuel flow rate, $\dot{m}_{fE}$.
(7) ACC fuel flow rate, $\dot{m}_{facc}$.

(8) Inlet manifold heater fuel flow rate, $\dot{m}_{fimh}$.

(9) Inlet manifold heater air flow rate, $\dot{m}_{aimh}$.

(10) Exhaust gas recirculation flow rate, $\dot{m}_{egr}$.

Emissions.

(1) Smoke density, s_d.

(2) Hydrocarbons, HC.

(3) Oxides of Nitrogen, NO_x.

Speeds.

** (1) Engine speed, N_E.

(2) Turbocharger speed, N_{tc}.

Positions.

** (1) Demand speed (throttle position), y.

** (2) Fuel pump rack position, x.

* (3) Injection timing, z.

* (4) By-pass valve position, x_{bp}.

* (5) ACC position, x_{acc}.

* (6) Exhaust gas recirculation valve position, x_{egr}.

Torques.

(1) Engine load torque, τ_L.

* are referred to in the text.

Actuators

(1) Fuel pump rack position, X.

(2) Injection timing, Z.

(3) By-pass valve position, X_{bp}.

(4) ACC position, X_{acc}.

(5) EGR valve position, X_{egr}.

(6) Charge cooler by-pass valve position, X_{ccbp}.

(7) Inlet manifold heater controller position, X_{imh}.

8.4.3 Microprocessors for Engine Management Systems.

There are many microprocessors currently available that are suitable for an on-board engine control system, for example, processors are manufactured by Fairchild, Intel, Motorola, National, NEC, Texas, Zilog, etc. The specification of these processors vary considerably, and so the choice of a suitable microprocessor will largely depend upon the application. The processors can be classified according to their:-

(1) Word length (4,8 or 16-bit)

(2) Program execution time, this gives a better representation of the capability/processing speed of a processor than the cycle time or execution time (176).

(3) LSI technology (e.g. PMOS, NMOS, CMOS, etc.).

(4) Instruction set, this influences the efficiency with which real time processes can be carried out.

The power of a microprocessor can best be demonstrated by describing the specification of an advanced single chip microcomputer, the NEC μPD7811G. How the processor can be configured to perform the necessary control functions for an automotive EMS is demonstrated by the UEL general purpose microcomputer.

A single chip microcomputer, the NEC μPD7811G, will perform all the functions necessary for simple SI engine control (60), Fig. 8.2. This has a central processor unit (CPU), a 4 k-byte program read only memory (ROM), 256 byte data random access memory (RAM) with the stand-by function in the 32 byte area of on chip 256 byte RAM, 44 input/output (I/O) lines, 8-bit ADC, multi-functional 16-bit timer/event counter, two 8-bit timers, serial communication interface, multiple source interrupt system and on-chip clock generator. The μPD7811G also has a system expansion capability bus-compatible with the Intel 8085A, which can cover a wide range of applications from stand alone control systems to relatively large control systems.

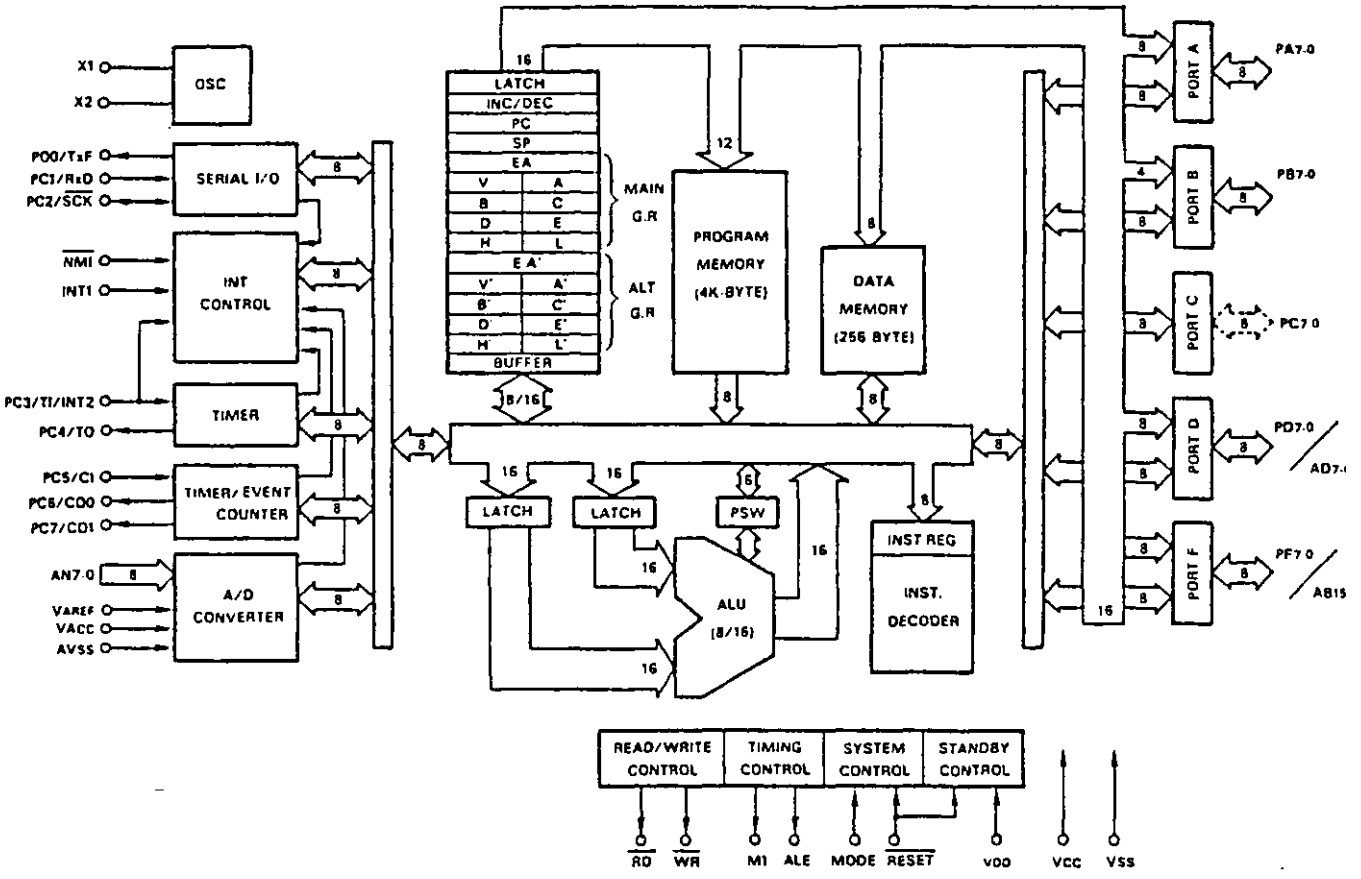

Fig. 8.2a Block Diagram of the μPD7811G Microcomputer, from (60).

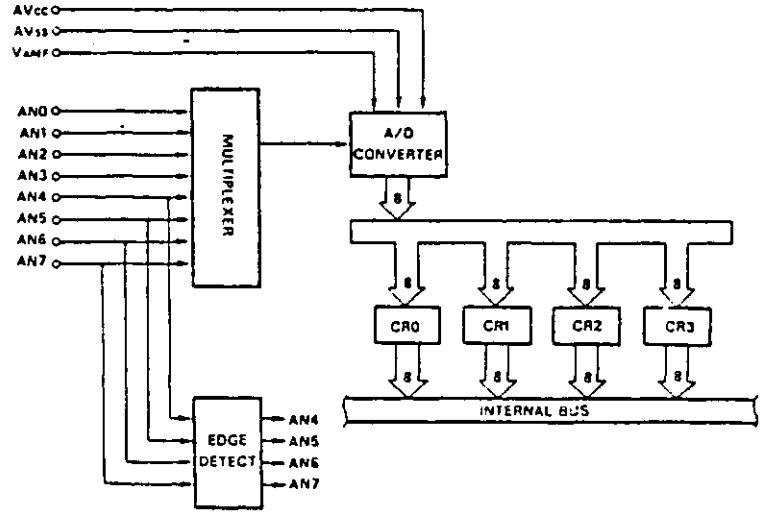

Fig. 8.2b Block Diagram of the μPD7811G Analogue to Digital Converter, from (60).

The μPD7811G contains seventeen 8-bit registers and four 16-bit registers. There is a program counter (16-bit), stack pointer (16-bit), and two sets of accumulator, vector register, six 8-bit general purpose register and extended accumulator (16-bit).

The arithmetic logic unit (ALU) performs such data processing as 8-bit arithmetic logic operation, shift and rotation, 16-bit arithmetic logic operation and shift, and 8-bit multiplication with double precision (16-bit) and 16-bit ÷ 8-bit division. The μPD7811G is capable of addressing a memory of up to 64 k-bytes. With the exception of the on-chip ROM area (0 to 4096), both the program and data memory areas can be used without distinction. A reset/stand-by release start address and call table are provided in the on-chip ROM area, and twelve methods for addressing source operands are possible.

The 8-bit ADC, also shown in Fig. 8.2, has eight time multiplexed analogue inputs (AN0-AN7) and four conversion result registers (CR0-CR3) for holding the results of the conversions. The serial communication interface is useful for serial linking peripheral devices as well as multiple μPD7811G's through universal asynchronous protocols with high speed, full duplex and double buffering type. The serial communication interface also has other modes of operation, namely synchronous mode and I/O expansion mode. Full details of this microprocessor, and an example of its application to a SI engine system, are given by Idogawa et. al. (60).

A microprocessor controlled EMS comprises of three main elements:-

(1) The microprocessor with its associated logic.

(2) The memory complex.

(3) The interface units.

A microprocessor control system, developed by Ultra Electronic Controls (UEL), is used in the Swedish S-tank to operate the combined gas turbine and diesel power plant (74). A similar analogue controller has been developed by UEL for the Crysler Aspen gas turbine car (44). The UEL digitally programmed analogue computer, the PAC-500 has also been used by Reams et. al. (116) to control the amount of fuel injected and the amount of EGR in an IDI diesel engine.

A general purpose digital microcomputer has also been developed by UEL suitable for a wide range of different power units (44), Fig. 8.3. The 16-bit microcomputer has a clock rate of 10 MHz and an average cycle time of 3.5 μs. Its associated logic functions include a power-up initial reset, direct memory access, three level interrupt and hardware multiply/divide. There is also a "watchdog" unit, the function of which is to monitor the microprocessor to check whether it is working correctly.

There are two memory sections, the executive block (3kx16) held on UV erasable programmable memory (EPROM), and up to 2x(3kx16) memory blocks that are user programmable. Each of the latter can be either a RAM or an EPROM. The function of the executive block is to provide links, subroutines, etc. for the user program, and to handle interrupts and safety routines. Access to the RAM is through a serial communication link to the system support hardware, and there is a standby electrical supply to ensure that the volatile data store is retained when the power is switched off.

Forming the interface are I/O data handling and universal asynchronous receiver transmitter (UART) systems. Analogue data for both input and output are handled by 12-bit $\pm$ 10V bipolar converters multiplexed to the individual I/O conditioning circuits. The switch data in this application are latched to/from the microprocessor data bus through transistor-transistor logic (TTL), compatibility with which is ensured by means of input and output conditioning circuits.

RS 422 standard protocol is used in the serial communication link between the external peripheral equipment and the UART system. Its function is to transmit, in series along a single line, digital data for subsequent reassembly into parallel form. Without it, such data would have to be transmitted simultaneously along a number of parallel lines.

Conversion of the analogue and switch input signals to a form suited to the interface, and amplification of the outputs as necessary, are performed by the I/O conditioning circuits. The switch input signals are filtered and levelled to suit the interface. Switch outputs from the interface latches are amplified to the current and voltage levels required. The basic system is designed on the assumption that external switch loads are returned through the supply negative circuit.

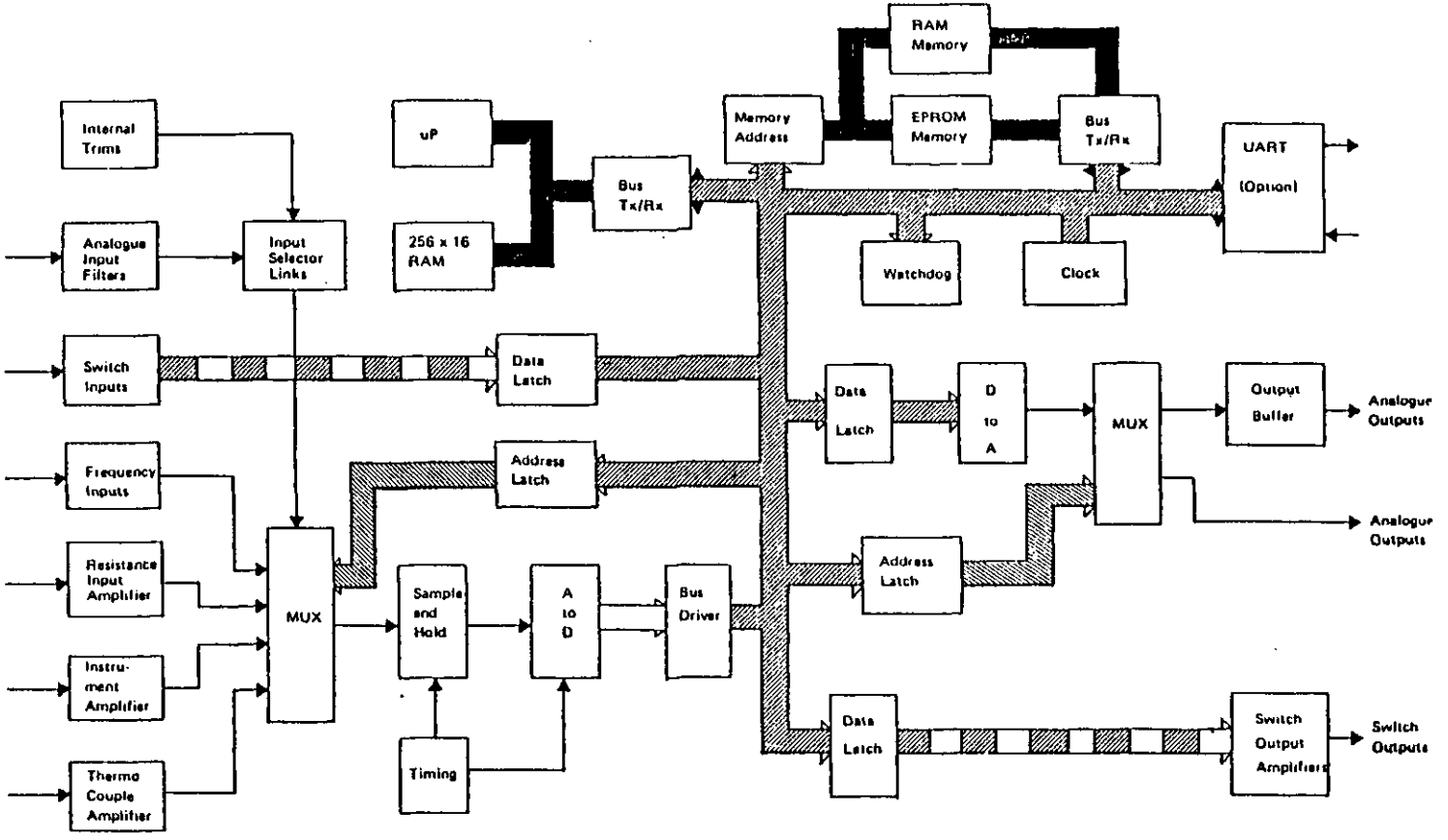

Fig. 8.3 Schematic Illustration of the Internal Organisation of the UEL Digital Microprocessor, from (44).

Thermocouple signals are cold-junction compensated at the common negative terminal, to suit K type thermocouples or the instrumentation wire. Chopper amplifiers are used for each channel with a common bridge reference. Transformer coupling of each amplifier prior to demodulation allows thermocouple circuits to be electrically isolated from the main power supply. Consequently, earth leakage can exist without performance loss.

Frequency signals, for example from magnetic pulse probes (normally in the range 2-10 kHz), are converted to DC voltages proportional to frequency. Other circuits are available for amplifying low level signals (e.g. from a strain guage bridge) and there is circuitry for internal trims and filtering for external potentiometric or voltage source signals.

The 500 mA proportional drives are employed to supply output currents proportional to input voltages for actuator control. Other output currents proportional to input voltages are provided by 1 mA proportional drive amplifiers. Voltage drive circuits serve instrumentation and external amplifiers. Since these are voltage followers, their input and output voltages are equal.

The complete package, weighing 7.5 kg, is 320 mm long, 222 mm wide and 103 mm high. Its operating temperature range is -40°C to +85°C. The casing is splash-proof and the unit can withstand accelerations of 50 m/s^2 at frequencies of 10 to 500 Hz. Shock load accelerations of 1000 m/s^2 can also be tolerated.

8.4.4 Selection of Sensors and Actuators.

There are a number of pressure sensors either commercially available or under serious development (109,132,178). The requirements for pressure transducers in automotive applications are outlined in section 8.4.2. Temperature measurement can be made using conventional thermocouples which are relatively inexpensive and reliable. The response of the thermocouple will depend upon its size, materials and construction, and usually a compromise between reliability and good response has to be reached. Position measurements can be made using potentiometers or linear variable displacement transducers (LVDT's), depending on the velocity of the component and the resolution

required. While transducers are available for measuring instantaneous air flow rates (23,178), these are mostly in the prototype stage or else are unsuitable for vehicle applications. Measurement of air velocity using hot wires has been developed for automotive applications (88), but the long term reliability of such a system has yet to be proved. In order to obtain the air mass flow rate, the air density is also required with this system.

Engine speed can be measured using a magnetic pick up on the flywheel or fuel pump camshaft, or an optical shaft encoder, however, the former system is usually preferred because of its lower initial cost. Turbocharger speed can be measured using a magnetic pick up, but this is considered to be unnecessary (see section 8.4.6). Maximum cylinder pressure can be measured using strain guage washers around the cylinder head or injector bolts, but a correlation between boost pressure, injection timing, speed and fuelling may eliminate the need for this sensor. Metal temperatures can be measured using thermistors. Smoke cannot conveniently be measured, but may be related to the engine A/F ratio. Other emissions, such as NO_x, have not been considered at this time.

The majority of the commercially available transducers give an analogue signal output. A microprocessor based EMS will therefore require analogue to digital processing circuits (ADC's) which may significantly increase the cost of the electronic hardware. In addition the time required for the analogue to digital conversion will determine the frequency at which the signal, can be sampled. The accuracy of the ADC (i.e. the number of bits used) will depend upon the resolution required from the output signal, and the microprocessor word length.

Probably the most critical component in the introduction of electronic engine control is the actuator (38). Actuators, or servo mechanisms, are required to control a number of components in the system. Whether the actuator applies an analogue or digital change in position, velocity, etc., depends upon the particular device being controlled. The adjusting power can be generated by electro-motors, electro-pneumatic devices as well as by electro-hydraulic means. It is important to consider all aspects of the servo components before choosing a device for a particular application (51). For example, the analogue actuator used to control the fuel pump rack position should ideally produce a force that is independent of the rack position, but constraints such as cost, weight, drive current and the influence of inertia on response time will dictate the

final design to a large extent (85).

Actuators are required to control the fuel pump rack position, the injection timing, the by-pass valve position, the ACC position, the EGR and charge cooler by-pass valves and the inlet manifold heater fuel and air pumps in the design described in the following sections.

8.4.5 Control Functions of the Engine Management System.

The EMS must perform the following functions:-

(1) Control the engine fuelling, $\dot{m}_{fE}$, by considering the demand speed, y, the engine speed, N_E, and the load torque, τ_L, according to a predefined governor strategy (i.e. the EMS must act like an automotive, all speed, isochronous, etc., governor as required). It must also allow overfuelling for starting and/or during transients.

(2) Control the injection timing, z, to minimise the engine BSFC (and emissions) while ensuring that the peak cylinder pressure is below a predefined limit.

(3) Control the ACC fuelling, $\dot{m}_{facc}$, so that the minimum boost level is maintained, the engine A/F ratio is high enough so that excessive smoke and/or metal temperatures are not produced, and the exhaust manifold gas temperature is below a predefined limit. The ACC gas temperature, turbine inlet gas temperature, maximum cylinder pressure and turbocharger speed must all be kept below their respective limiting values.

(4) Control the by-pass valve displacement, x_{bp}, so that the compressor is operating in the best efficiency area of the map, the ACC A/F ratio is sufficient for good combustion, the ACC and turbine inlet temperatures are below their respective limiting values, and the scavenge pressure drop across the engine is acceptable.

(5) Control the charge cooler by-pass valve position, X_{ccbp}, and the exhaust gas recirculation valve position, x_{egr}, to maintain the inlet manifold temperature

above a predefined level in order to ensure good combustion in the engine. If the inlet pressure, $p_{2'}$, is higher than the exhaust pressure, p_3, then the inlet manifold heater may be required to raise the temperature of the inlet air in some circumstances.

8.4.6 Simplifying Assumptions to Reduce the Number of Sensors.

The following simplifying assumptions can be made in order to reduce the number of sensors required to operate the EMS:-

(1) The engine air mass flow rate is dependent on the engine speed and inlet manifold conditions only, i.e.

$$\dot{m}_E = \left(\frac{p_{2'}}{R_{2'}.T_{2'}}\right)\frac{V_{sw}.\eta_v.N_E}{120} \tag{8.1}$$

It is assumed that the gas constant for air, $R_{2'}$, the swept volume, V_{sw}, and the volumetric efficiency, η_v, are all constant. Providing that the valve overlap is not too large (this is usually true for automotive type engines), the scavenge flow can be neglected, or else incorporated in the volumetric efficiency term. Equation (8.1) can therefore be written as:-

$$\dot{m}_E = \frac{k_1.p_{2'}.N_E}{T_{2'}} \tag{8.2}$$

where,

$$k_1 = \frac{V_{sw}.\eta_v}{120.R_{2'}} \tag{8.3}$$

(2) The engine fuel flow rate, $\dot{m}_{fE}$, is a function of the engine speed (or fuel pump speed), N_E, and the rack position, x, only (the effect of injection timing, z, on fuelling being neglected), thus:-

$$\dot{m}_{fE} = f_1 (N_E , x) \tag{8.4}$$

The relationship defined by eqn. (8.4) can be found from the steady state characteristics of the fuel pump (see section 4.6.6).

(3) The total instantaneous by-pass mass flow rate, $\dot{m}_{tbp}$, is the difference between the compressor mass flow rate, $\dot{m}_c$, and the engine mass flow rate, (from eqns. (8.2) and (8.3)), thus:-

$$\dot{m}_{tbp} = \dot{m}_c - \dot{m}_E \tag{8.5}$$

and $\dot{m}_{tbp}$ can be divided into the flow through the valve, $\dot{m}_{bp}$, and the ACC ports, $\dot{m}_{aacc}$, by assuming that the pressure drop across the by-pass valve and ACC ports and the upstream conditions are equal at any instant in time.

The flow through each path will then be dependent upon the effective flow area of each device, A_e, thus:-

$$\dot{m}_{bp} = \frac{m_{tbp}.A_{ebp}}{(A_{ebp}+A_{eacc})} \tag{8.6}$$

and,

$$\dot{m}_{aacc} = \frac{m_{tbp}.A_{eacc}}{(A_{ebp}+A_{eacc})} \tag{8.7}$$

where,

$$A_{ebp} = f_2 (x_{bp}) \tag{8.8}$$

and,

$$A_{eacc} = f_3 (x_{acc}) \tag{8.9}$$

Therefore, knowing the position of the by-pass valve, x_{bp}, and the ACC, x_{acc}, and their flow characteristics, eqns. (8.8) and (8.9), it is possible to estimate the flow through the different parts of the by-pass system.

(4) The ACC fuelling, $\dot{m}_{facc}$, is a function of the ACC fuel control valve position only, x_{acc}, thus:-

$$\dot{m}_{facc} = f_4 (x_{acc}) \tag{8.10}$$

Note: this implies that the ACC fuelling cannot be increased independently of the ACC air flow except by varying the pressure drop across the ports and/or the upstream density, see section 4.8.

(5) The maximum cylinder pressure, p_{max}, is a function of the engine speed, N_E, the boost pressure, $p_{2'}$, the engine fuelling, $\dot{m}_{fE}$, and the injection timing, z, only:-

$$p_{max} = f_5 (N_E , p_{2'} , \dot{m}_{fE} , z) \qquad (8.11)$$

(6) The maximum turbocharger speed limit, $(N_{tc})_{max}$, can be expressed as a maximum compressor pressure ratio limit, $(p_2/p_1)_{max}$, because the operating region on the compressor map should always reduce to a unique line, thus:-

$$(N_{tc})_{max} = f_6 ((p_2/p_1)_{max}) \qquad (8.12)$$

(7) The exhaust manifold gas temperature, T_5, the metal temperatures, T_m, and the smoke density, s_d, can all be controlled by varying the engine A/F ratio.

(8) The amount of exhaust gas that is recirculated is a function of the EGR valve position, x_{egr}, the exhaust temperature, T_3, the pressure ratio across the EGR valve, $p_3/p_{2'}$, and the upstream pressure, p_3:-

$$\dot{m}_{egr} = f_7 (x_{egr} , T_3 , p_3 , p_{2'}) \qquad (8.13)$$

Recirculation can only occur when p_3 is greater than $p_{2'}$. When the EGR valve is open the charge cooler is automatically by-passed by varying the cooler by-pass valve position, X_{ccbp}.

(9) Additional air and fuel are only burnt in the inlet manifold if the air temperature, $T_{2'}$, is below a predefined limit, and the inlet pressure, $p_{2'}$, is greater than the exhaust pressure, p_3, so that no EGR can be used.

The fuel and air flows delivered by the inlet manifold heater are a function of the engine speed, N_E, and the inlet temperature, $T_{2'}$, only:-

$$\dot{m}_{fimh} = f_8 (N_E , T_{2'}) \quad (8.14)$$

$$\dot{m}_{aimh} = f_9 (N_E , T_{2'}) \quad (8.15)$$

(10) During transient operation the difference between the engine and load torques can be expressed in terms of the system inertia, I_t, and the rate of change of engine speed, dN_E/dt, thus:-

$$\tau = (\tau_I - \tau_L - \tau_F) = I_t \frac{dN_E}{dt} \quad (8.16)$$

where τ indicates torques (N.m) and the subscripts I, L and F represent indicated, load and friction values respectively.

Ideally a torque sensor should be used in the governor control (with a signal filter to eliminate cyclic fluctions in the measured torque), because the speed change signal used in eqn. (8.16) is the response of the system to a change in torque, and will give zero output during steady state conditions ($dN_E/dt=0$). This signal will therefore always lag any change in the actual torque. A governor with load sensing has been shown to significantly reduce the transient speed errors caused by rapid load changes (170). This is especially important in electricity generating applications, when the frequency must be maintained during rapid load changes. Under steady state conditions the rack position can be used as an indication of the engine load.

Using these simplifying assumptions, the list of sensors required in Table 8.1 can be reduced from 35 to 19 (indicated by an *). With the possible exception of the compressor air mass flow rate sensor, these are the most reliable and cost effective of the sensors currently available.

8.4.7 Engine Management System Logic.

In order to simplify the explanation of the logic of the proposed EMS for the Hyperbar engine, the system has been divided into four groups, showing the sensors required and the calculation procedure to control each of the actuators in turn:-

(1) The fuel pump rack position, X, and injection timing, Z.

(2) The by-pass valve position, X_{bp}.

(3) The ACC position, X_{acc}.

(4) The EGR and charge cooler by-pass valve positions, X_{egr} and X_{ccbp}, (including the inlet manifold heater controller position, X_{imh}).

These control systems will, of course, interact, and this is indicated in the following diagrams, in addition some parts of the system are repeated for clarity. A brief explanation of the logic for each system follows.

8.4.7.1 Fuel Pump Rack Position and Injection Timing Control Logic.

The control of the fuel pump rack position effectively performs the function of the governor. The control strategy used is similar to that described in section 4.6.4 for the CAV electronic governor (85). The fuelling logic can be programmed to produce any type of governor characteristic, for example, an automotive two-speed governor, an all-speed governor, an isochronous governor for electrical power generation, etc.

The fuel pump rack position and injection timing control logic is shown in Fig. 8.4. For a two speed governor the rack position demand is determined by the signal from the demand speed, y, and the engine speed, N_E, on a "lowest wins" basis, unless the speed falls into the idle region, in which case the throttle signal is modified to give the correct idling characteristic.

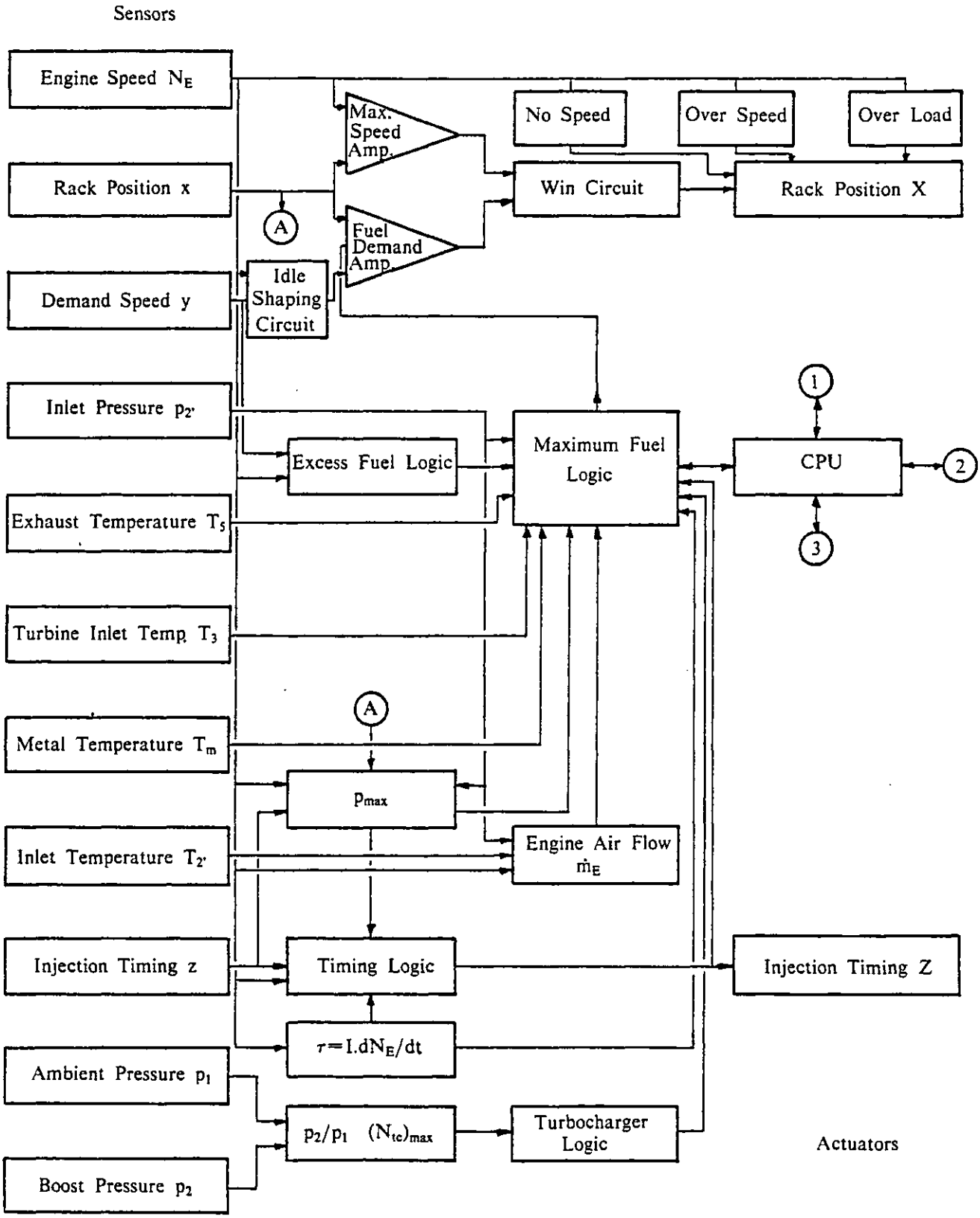

Fig. 8.4 Fuel Pump Rack Position and Injection Timing Control Logic.

A number of important engine parameters are used to modify the maximum demand engine speed signal, y, such as the boost pressure, $p_{2'}$, the exhaust and turbine inlet gas temperatures, T_5 and T_3 respectively, the metal temperatures, T_m, the maximum cylinder pressure, p_{max}, the maximum turbocharger speed, $(N_{tc})_{max}$, the smoke density, s_d, the engine A/F ratio, (the later acting as an aneroid rack limiter). The maximum torque curve can be determined by specifying the rack limit as a function of the engine speed. In addition the reaction of the system to a failure of any of the sensor signals must be carefully considered, e.g. no speed, over speed and over load.

The control logic differs from that described by Leonard (85) in three fundamental aspects:-

(1) The governor control is digital rather than analogue in nature, using microprocessor control.

(2) Load sensing is included in the control of the rack position and injection timing.

(3) The injection timing can be advanced/retarded to increase the engine torque or reduce the peak cylinder pressure.

8.4.7.2 Inlet Manifold Air Heater Control Logic.

The inlet manifold heater system is of particular importance for this engine because of its low compression ratio. Fig. 8.5 shows the control logic for the inlet manifold heater and exhaust gas recirculation valve.

Fuel is normally only burnt in the inlet manifold in cases where the inlet pressure, $p_{2'}$, is higher than the turbine inlet pressure, p_3, and no EGR can be used. The air mass flow rate into the engine is considered to be proportional to the engine speed, N_E, and the inlet manifold air density, (i.e. $p_{2'}$ and $T_{2'}$). Therefore, the amount of heating required is determined by the engine air flow rate and the temperature error signal $(T_{ref}-T_{2'})$.

The relatively small quantity of fuel burnt in the inlet manifold is atomised and

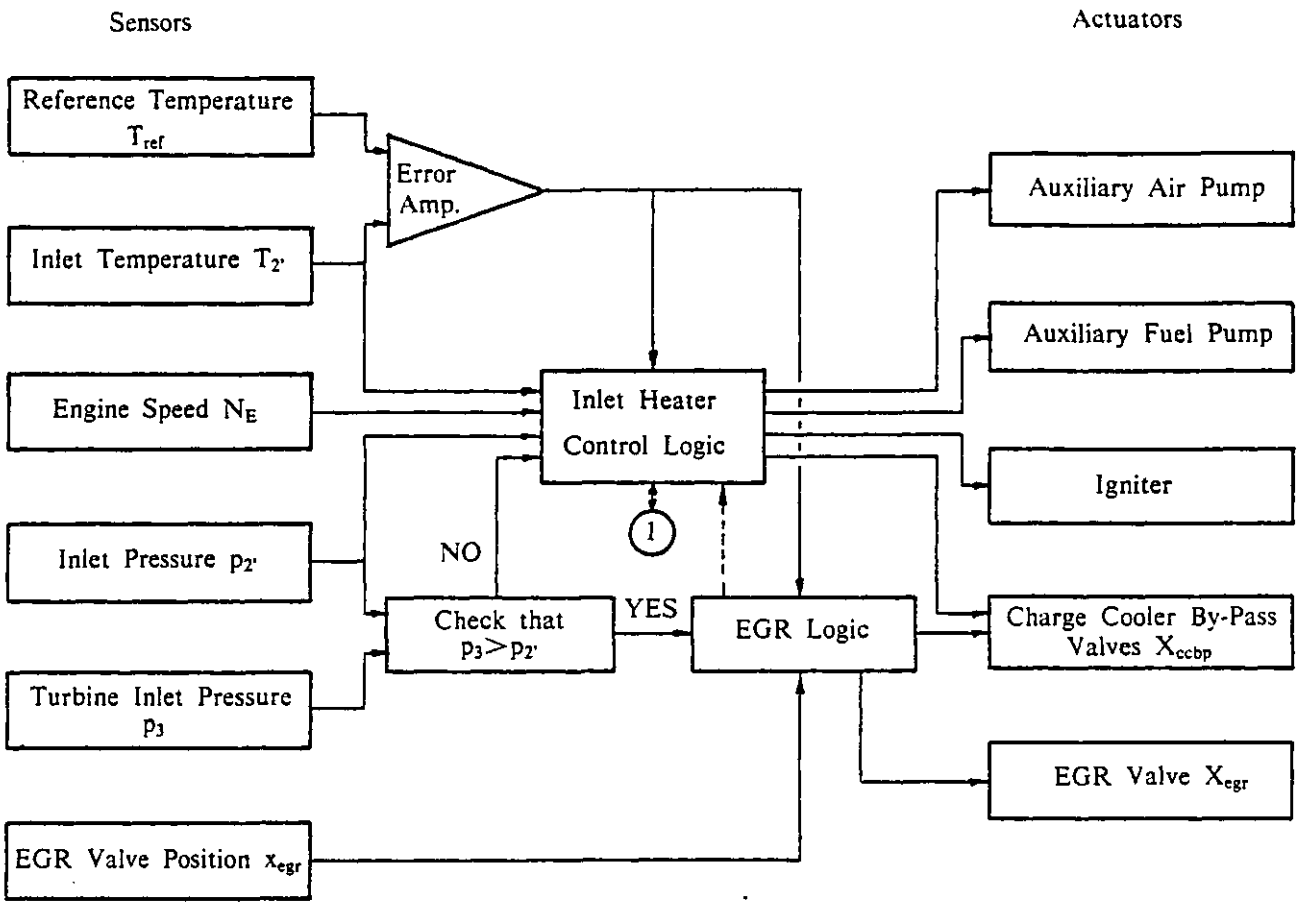

Fig. 8.5 Inlet Manifold Air Heater Control Logic.

distributed by swirling air jets, and ignited by a high energy ignition system. The fuel delivery is a function of the pump speed which can be controlled in either open loop (Fig. 8.5) or closed loop mode.

The heater system can be designed to respond to low metal and/or exhaust temperatures, T_m and T_5 respectively, if required (not shown), and correct operation of the burner is indicated by the change in the inlet temperature signal, $T_{2'}$.

Recirculation of the exhaust gas from the turbine inlet, at pressure p_3 and temperature T_3, is preferred to operation of the inlet manifold heater, because no extra fuel is required, and the energy necessary to drive the fuel and air pumps and the igniter is saved. However EGR is only possible if p_3 is higher than the inlet pressure, $p_{2'}$. The EGR valve is controlled in closed loop mode in Fig. 8.5.

If either (or both) systems are used to increase the inlet temperature, control valves are closed on both the inlet and exit of the charge cooler, and the engine air flow by-passes the cooler. These valves can also be closed to reduce the inlet system volume during transients, which enables the inlet manifold pressure, $p_{2'}$, to build up more rapidly.

Numerous safety circuits are required for the operation of the inlet heater system and these are described in more detail by Leonard (85).

8.4.7.3 By-Pass Valve Position Control Logic.

The by-pass valve position is determined by a mechanical closed loop control system in contrast to the pneumatic system described in section 8.3. While this is certainly more expensive and complicated (and therefore potentially less reliable) it does allow various alternative control functions apart from the regulation of the engine pressure drop ratio, $(p_2-p_3)/(p_2-p_1)$, to be taken into account. For example, the by-pass valve can be controlled to optimise the compressor efficiency, provided that all the other limiting criteria are satisfied.

The control logic for the by-pass valve is shown in Fig. 8.6. The function of the by-pass valve control system is primarily to regulate the pressure drop ratio. The

Sensors

Actuators

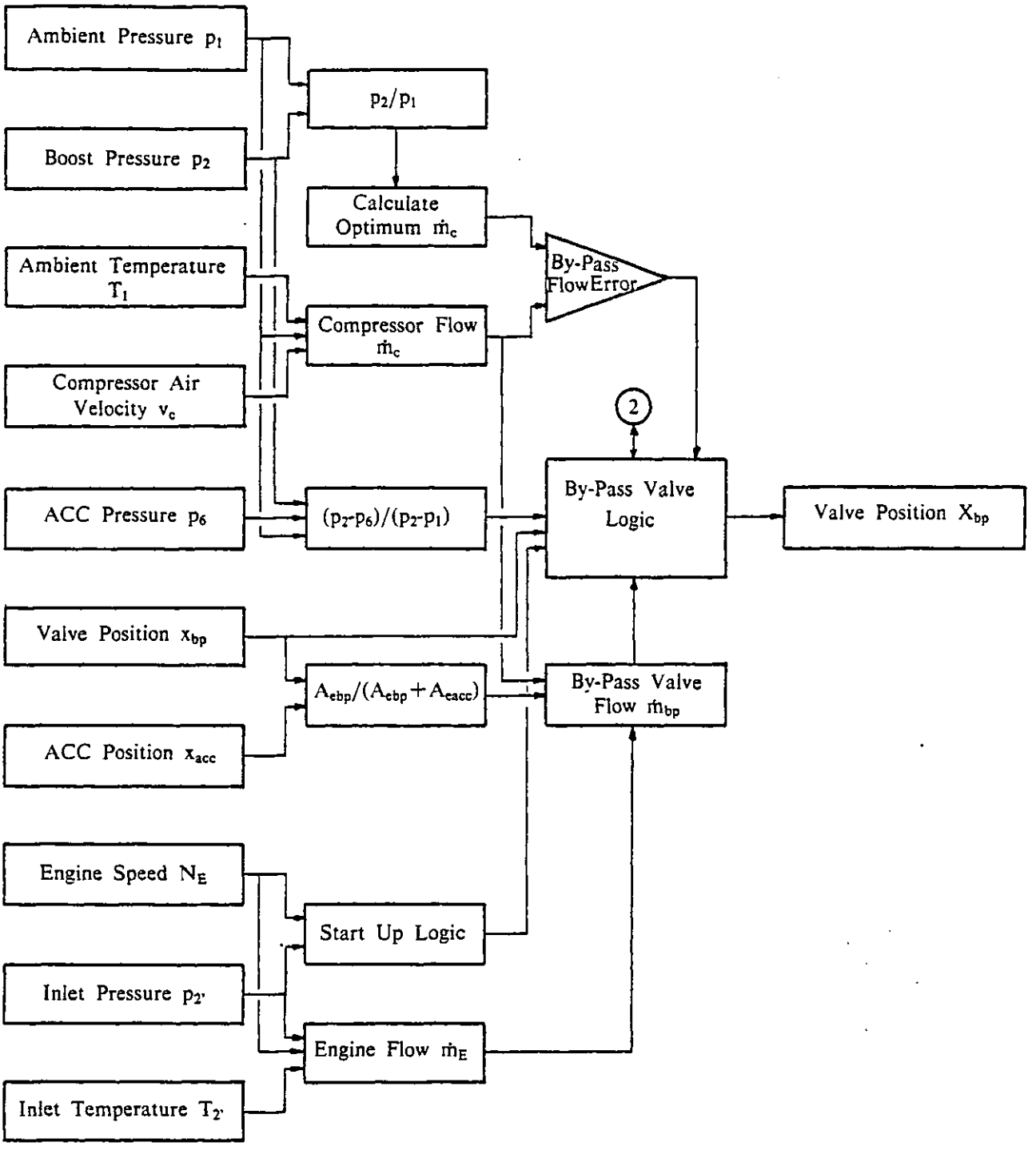

Fig. 8.6 By-Pass Valve Position Control Logic.

secondary function of the by-pass valve logic is to compare the compressor flow rate, $\dot{m}_c$, with the optimum compressor flow for the best efficiency (which is a function of the pressure ratio, p_2/p_1, only) and adjust the compressor flow by increasing or decreasing the by-pass valve flow area accordingly. Obviously changes in the by-pass valve flow will affect the pressure drop ratio, and these two criteria may, in some cases, be incompatible. The by-pass valve logic is supplied with the estimated valve flow, $\dot{m}_{bp}$, calculated from the engine flow, using eqn. (8.2), the compressor flow, $\dot{m}_c$, and the effective area ratio between the by-pass valve and the total by-pass system, eqn. (8.6).

During starting, when the engine is not rotating the speed signal is zero. The by-pass valve is then opened fully, and this allows all the air from the compressor to circulate through the by-pass system. When a predetermined boost level, p_2, is reached the engine can be started and the by-pass valve reverts to its normal operating mode.

8.4.7.4 Auxiliary Combustion Chamber Position Control Logic.

The logic for the ACC position control is shown in Fig. 8.7. The purpose of the ACC logic is to minimise the ACC fuelling under all operating conditions, while maintaining the important engine parameters within predefined limits. Checks are made of the engine A/F ratio, the exhaust manifold gas temperature, T_5, the minimum boost level, p_2, and the torque required, τ. If any of these parameters are outside their operating range then the ACC fuelling must be increased. Similarly checks are made of the turbine inlet temperature, T_3, the maximum cylinder pressure, p_{max}, and the boost pressure, p_2, (which can be used to detect turbocharger overspeed, eqn. (8.12)). If any of these limits are exceeded then the engine or ACC fuelling must be reduced.

Other safety checks, such as the ACC A/F ratio can be made to ensure that the fuel is burning in the combustion chamber (not shown in Fig. 8.7). If the A/F ratio is too rich, then the ACC gas temperature, T_6, will increase if the equivalence ratio is less than unity or decrease for rich mixtures, and this can also be detected.

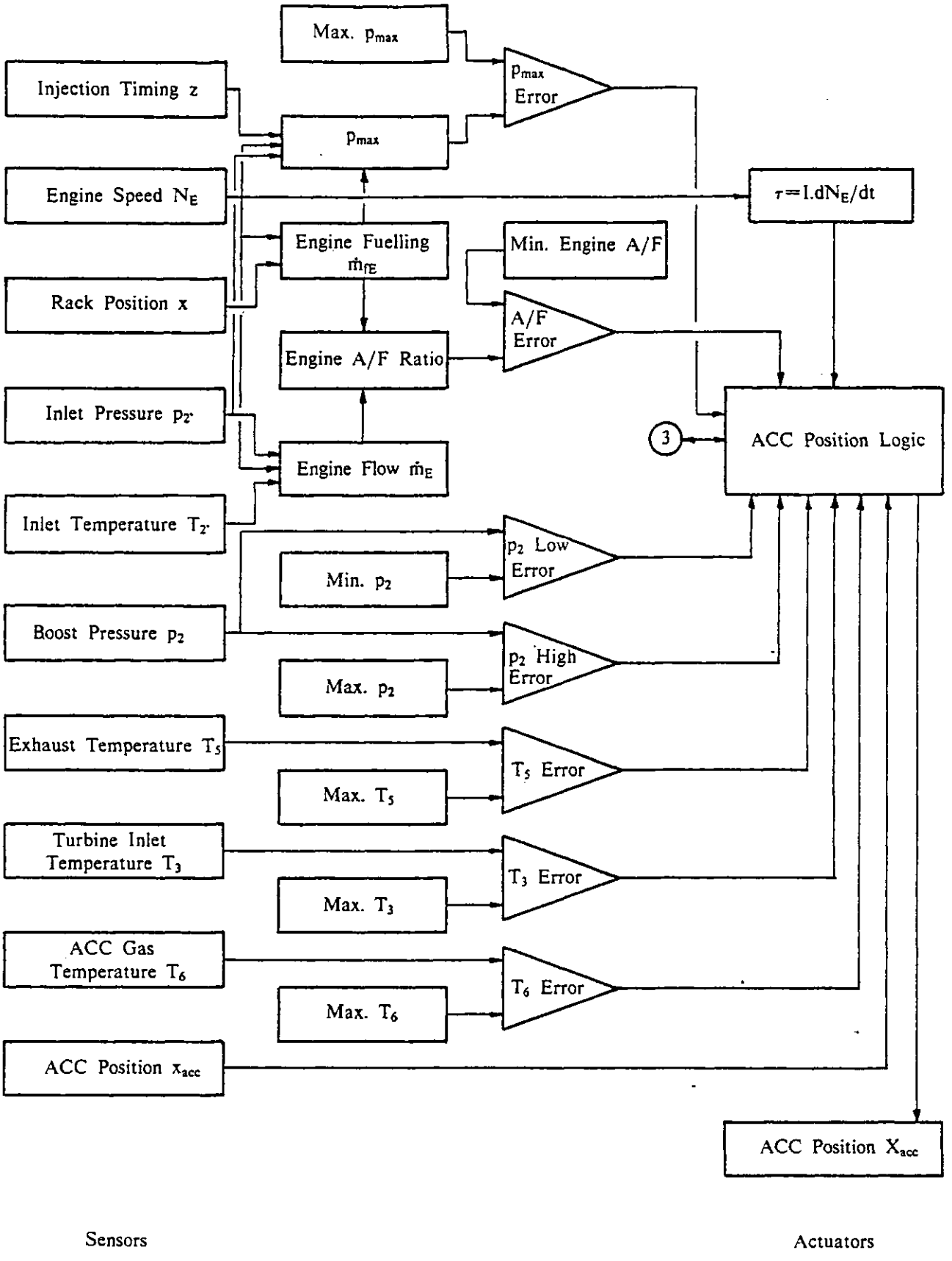

Fig. 8.7 Auxiliary Combustion Chamber Position Control Logic.

8.4.8 A Simpler Engine Management System.

Despite the simplifying assumptions outlined in section 8.4.6, the EMS described in section 8.4.7 still requires a total of 19 sensors to operate. The number of sensors required can be reduced still further, without a drastic reduction in the engine control, by making the following additional assumptions:-

(1) The inlet manifold pressure, $p_{2'}$, can be related to the compressor delivery pressure, p_2, and the engine mass flow rate, $\dot{m}_E$, given by eqn. (8.2). This implies that the pressure drop across the charge cooler can be related, approximately, to the mass flow rate through it, i.e.:-

$$p_{2'} = f_{10} (p_2 , \dot{m}_E) \qquad (8.17)$$

When the charge cooler is by-passed then the inlet manifold pressure, $p_{2'}$, will be approximately the same as the compressor delivery pressure, p_2, if the pressure losses in the valves and ducting can be neglected.

(2) The ACC gas pressure, p_6, is approximately equal to the turbine inlet pressure, p_3. The pressure difference will actually depend upon the by-pass flow rate (i.e. the engine speed and load):-

$$p_6 = p_3 \quad . \qquad (8.18)$$

(3) The exhaust manifold gas temperature, T_5, and the ACC gas temperature, T_6, can be controlled by regulating the engine and by-pass A/F ratio's respectively. This assumes that the other sensors are working correctly, and that the turbine inlet temperature, T_3, is the most critical in the exhaust system. Thus:-

$$T_5 = f_{11} (A/F_E , T_{2'}) \qquad (8.19)$$

$$T_6 = f_{12} (A/F_{oacc} , p_2/p_1 , T_1) \qquad (8.20)$$

eqn. (8.20) can be derived from eqn. (4.179) by assuming a compressor efficiency.

(4) Providing that the engine A/F ratio is controlled correctly, then high metal temperatures, T_m, will only occur if there is a major engine failure, e.g. a loss of coolant, which can be detected by other means, such as the coolant or oil temperature guage.

(5) Only the demand speed, y, and the fuel pump rack position, x, are measured. This means that the injection timing, the by-pass valve and the ACC control systems will operate as open loop systems.

(6) There is no EGR. If the inlet manifold temperature, $T_{2'}$, is below the reference value, then the inlet air is heated by the inlet manifold heater only. The charge cooler is not by-passed and so the inlet heating system will be less economical.

This reduces the number of sensors from 19 to 10. Of these 3 are required to measure the compressor air flow rate (the ambient pressure, p_1, temperature, T_1, and the compressor flow velocity, v_c). The engine demand speed, y, and actual engine speed, N_E, are required for the governor operation. The rack position, x, is controlled in closed loop mode to ensure accurate engine speed control, and is used to calculate the engine fuelling (with N_E). The compressor delivery pressure, p_2, is required to regulate the by-pass system, engine pressure drop and the compressor operating line. The inlet manifold temperature, $T_{2'}$, is required to ensure that the engine combustion does not deteriorate at low loads, and is also used to calculate the engine air flow rate. The turbine inlet pressure, p_3, gives the pressure drop across the by-pass system (with p_2) and is regulated to ensure that the engine scavenge pressure drop is always positive. The turbine inlet temperature, T_3, is regarded as a major safety variable, because in high BMEP applications (and particularly in this case where there is a burner in the exhaust system) excessive turbine inlet temperatures can rapidly lead to turbocharger failure (17).

These transducers therefore represent the minimum required to operate the EMS and are indicated by an ** in Table 8.1. The number of actuators can be reduced from 7 to 5 if the EGR and charge cooler by-pass systems are not required.

8.4.9 General Comments on the Engine Management System.

The system described in the preceding sections gives details of a "first generation" EMS. Obviously the number of sensors and actuators used in the system depends upon the degree of control required. The system becomes inherently less reliable as the number of sensors increases. Some fail-safe operating procedure must therefore be defined, in the event of a failure of one, or more, of the sensors, (this is particularly important in automotive applications).

The system described in section 8.4.7 requires 19 sensors and 7 actuators, and may not be cost effective for an automotive type power unit. However, the cost of the control system becomes relatively less significant if used on very large diesel generating sets, for example. A simpler and more economical system, requiring only 10 sensors and 5 actuators has been described in section 8.4.8.

Another important advantage of a microprocessor based EMS is its ability to detect, and to a certain extent diagnose problems, in both the engine and the EMS itself, and to signal the operator accordingly. External diagnostic and testing equipment can be used to check the engine using the EMS sensors, instead of requiring separate sensors to be fitted for the purpose. The benefits include the potential for rectification of faults before they occur and a reduction in the time required to diagnose a problem, which should lead to lower operating costs.

CHAPTER 9

CONCLUSIONS

The mathematical simulation model, originally developed by Marzouk (89) for a conventional turbocharged diesel engine, has been extended to enable the performance of an experimental high BMEP Hyperbar turbocharged engine to be predicted. Models have been developed for the by-pass. valve and Auxiliary Combustion Chamber, essential to the operation of the Hyperbar system. In addition, a simplified heat release calculation procedure (used to simulate the combustion process) has been developed for use with poor quality cylinder pressure data, in contrast to the very accurate data usually required for such an analysis.

Extensive steady state test data, measured by the engine manufacturer, has been used to develop the detailed models of individual components in the system. The geometry and dynamics of both the by-pass valve and the ACC are taken into account in the model, which allows specific design changes (such as variations in the by-pass valve area ratio or the ACC port areas) to be considered. The steady state engine performance can therefore be predicted from a knowledge of the engine geometry, the turbocharger characteristics, the Hyperbar system geometry and the running conditions (i.e. the engine speed and fuelling). The model can also be used to predict the transient performance of the engine and turbocharging systems, but requires additional data for the fuel pump and governor characteristics, and engine dynamics. This allows the effect of design changes on both the steady state and transient performance of the engine to be assessed.

The by-pass valve model was derived from a consideration of the geometry of the system. A comparison of the experimental and predicted valve dynamics at a fixed steady engine speed and load was used to find the dynamic parameters in the system (the inertia and damping terms). As no flow data was available for the by-pass valve, a coefficient of discharge was assumed. Any error in this value will not significantly affect the engine or turbocharging system performance (provided that the valve is not fully open), but will cause an error in the predicted valve position.

Because of the complicated fuel system used for the ACC, the fuel supplied by the burner was assumed to be a function of the ACC position only. Experimental evidence was used to support this simplification. The instantaneous position of the ACC, and hence the fuelling and air flow areas were calculated by considering the dynamics of the ACC system, together with the various controlling forces (such as the air pressure, the fuel pressure and the exhaust gas pressure) that act upon it. The inertia of the ACC was calculated by considering the masses of all the moving parts, but the damping ratio has had to be estimated.

A number of experimental cylinder pressure diagrams, photographed from oscilloscope traces, were used to develop a correlation for the "Apparent Fuel Burning Rate" in this engine. The procedure can be used in cases where accurate cylinder pressure data is not available, and allows the effects of combustion to be predicted at loads and speeds other than those measured.

A comparison of the experimental and predicted engine performance over the operating range of the engine has shown that the model can predict the effects of load and speed changes very well. The overall engine performance parameters can all be predicted to within an acceptable accuracy. Compressor flow, engine flow, and consequently by-pass flow, are predicted to within 2-3% of the measured values, despite the fact that very little information about the turbocharger characteristics was known. The relative pressures and temperatures in the inlet and exhaust systems are predicted very well, but the model cannot accurately reproduce some of the anomalies in the by-pass system performance, since the actual valve cannot adequately control the pressure drop across the engine at some operating conditions, particularly at very low and high engine speeds.

Other pressure losses in the by-pass system were estimated by considering the various flow paths involved. Errors in these flow losses could account for the small error in predicting the movement of the compressor operating line towards surge, as the engine speed reduces.

The operation of the ACC burner to maintain the minimum boost pressure level at low loads is predicted very well, although the burner fuelling rate at low loads is actually higher than predicted. This could be due, in part, to experimental measurement errors, but is probably influenced by the assumptions made for the

combustion process in the ACC, and errors in the compressor and turbine operating points.

The A/F ratio predicted for the burner (based on the fuel input and air flow through the ports and cooling channels), increases with engine load, at constant speed, once the burner has reached the minimum fuelling position, because of the increase in boost pressure and the pressure drop across the ACC ports. Typical values range from A/F ratio's of 8.6, at 1200 rpm/14.25 bar BMEP, to 16.1, at 2400 rpm/17.09 bar BMEP. As the boost pressure reduces, the ACC fuelling and port areas increase and the A/F ratio increases to 14.4 at 1200 rpm/5.70 bar BMEP and 17.0 at 1800 rpm/3.80 bar BMEP.

Errors in the prediction of peak cylinder pressures are mainly due to the fact that the AFBR correlation was developed using test data for a conventional single stage turbocharged version of this engine. Consequently the compression ratio, combustion chamber geometry and fuel injection system changes will introduce errors.

Engine frictional losses appear to be overpredicted by the Chen and Flynn (29) correlation (which was never intended for this type of engine) but the changes in FMEP with load and speed are adequately represented.

No attempt has been made to model the inlet manifold air heater, which uses exhaust gas to raise the charge temperature when required. For the steady state experimental tests the inlet air temperature was held constant by varying the charge cooler water flow rate. Experimental data for a charge cooler similar to that used on this engine was used to develop correlations for use in later tests.

A parametric study of the effects of the important variables in the Hyperbar turbocharging system on the engine performance has been carried out.

The by-pass valve area ratio, A_2/A_1, controls the relative pressures in the inlet and exhaust systems, and the proportion of the total compressor flow that passes through the engine. The choice of area ratio will also determine the operating line on the compressor map, and therefore the compressor efficiency. The valve is designed to ensure that the compressor operating line is independent of engine speed.

The choice of area ratio will depend, to a large extent, on the compressor match. At high loads and speeds the engine will benefit from a large value of A_2/A_1, which leads to better scavenging, higher engine A/F ratio's, lower cylinder wall temperatures, greater positive pumping work and hence lower BSFC. The compressor operates closer to the surge line with a larger valve area ratio, where the efficiency is generally higher. Conversely at low speeds and loads a large by-pass valve pressure drop (area ratio) cannot be sustained without burning extra fuel in the ACC, because of the low turbine energy availability. This results in a severe deterioration in total BSFC because the benefits of increased positive pumping work decrease as the boost pressure falls. With the Hyperbar system, at low loads the engine A/F ratio is high, relative to conventionally turbocharged engines, and so extra scavenge air flow is not usually required.

The effective area ratio of a pneumatically controlled by-pass valve can be modified by varying the control pressure acting on the damping piston. The degree of control achieved will depend upon the damping piston area ratio, A_3/A_1 and the range of the control pressure. However a control system is required which will also vary the control pressure according to the error between the actual and optimum compressor flow rates to achieve the maximum compressor efficiency. Some variation in the effective valve area ratio can be achieved by inclining the by-pass valve axis. However, the valve inclination will usually be fixed, for a given design, and so the degree of control that can be achieved using this method is limited.

The Hyperbar system is designed so that as the boost pressure falls the ACC fuelling increases to maintain a predetermined minimum boost level, necessary to ensure good combustion with a low engine compression ratio. The burner is never completely extinguished in the design considered, due to the problems associated with reigniting it reliably on demand. The idling fuelling level is therefore maintained irrespective of the engine speed and load. This minimum fuelling level can be reduced to zero (i.e. the burner can be extinguished) without any significant deterioration in the engine performance once a critical load level (which is speed dependent) is reached. This results in a corresponding improvement in the total BSFC, which is particularly important if the engine is operating for long periods at low speeds and medium loads, where the ratio of idling burner fuelling to total fuelling is the highest.

This is really a design problem. The burner must be made to operate with a stable

flame at very low fuelling rates (i.e. the turn down must be increased from 3.5:1 used in this design), or else a reliable ignition system must be developed that will enable the ACC fuelling to be reduced to zero when required, and ignited instantaneously on demand.

One way of reducing the total engine fuel consumption is to reduce the minimum boost pressure level required by the engine, and therefore the ACC fuelling required to maintain it. This is particularly important if the engine has to operate for long periods at low speeds and loads, where the engine exhaust energy is low.

The minimum boost pressure level can be lowered by reducing the ACC fuel control pressure. However, because of the low engine compression ratio (necessary to enable high speeds and loads without excessive cylinder mechanical loading), reducing the boost pressure level alone is not feasible, as this will lead to a deterioration in the combustion at low loads and even misfiring. Reducing the minimum boost level will also limit the transient response of the engine, because of the reduced engine A/F ratio at low loads.

A method of maintaining good ignition conditions in the engine with a lower minimum boost pressure level needs to be found. The effect of increasing the engine compression ratio and lowering the minimum boost level has been investigated. This results in benefits to the BSFC, due to the reduced ACC fuelling required and to an increase in the thermal efficiency of the engine with the higher compression (expansion) ratio. Unfortunately a higher geometric compression ratio limits the engine output at high speeds because of the increase in mechanical loading. Retarding the injection timing at high speeds and loads to limit the peak cylinder pressure has also been investigated, but this also leads to a loss in thermal efficiency and a corresponding increase in BSFC.

The choice of compression ratio, minimum boost pressure level and injection timing is therefore a compromise, and will depend upon the duty cycle of the engine and the maximum power required.

If the overall engine performance is limited by certain predefined engine parameters, for example, engine exhaust and turbine inlet temperatures, maximum cylinder pressure, minimum engine A/F ratio, smoke, etc., then it is possible that the engine

load can be increased, at a given speed, by increasing the ACC burner fuelling. Whether or not the burner can be used in this way will depend upon the particular limitations imposed.

The most useful way of improving the engine performance using the ACC burner occurs at low engine speeds where the engine A/F ratio and exhaust gas temperature (a measure of the thermal loading of the engine) are close to their limits, and these determine the amount of power that the engine can produce. Increasing the ACC fuelling results in an increase in the engine A/F ratio (because of the increase in boost pressure), which should reduce the exhaust gas temperature, metal temperatures and smoke. This allows the engine fuelling to be increased, which allows a large increase in the low speed torque to be achieved.

As the burner fuelling is increased the maximum cylinder pressure increases, because of the increase in boost pressure, and the turbine inlet temperature also rises. Once either of these parameters reaches its limiting value, no further increase in engine torque is possible by varying the ACC fuelling. Obviously the minimum possible burner fuelling for a given speed and load is required, provided that all the engine performance parameters are within their preset limits.

The maximum engine torque curve that can be achieved within the following constraints has been predicted:-

(1) Engine exhaust gas temperature, 973 K.

(2) Engine A/F ratio, 23.5.

(3) Turbine inlet gas temperature, 973 K.

(4) Maximum cylinder pressure, 140 bar.

With the ACC in the minimum fuelling position the engine torque is limited by the maximum cylinder pressure at speeds above 1200 rpm, and by the engine A/F ratio and exhaust gas temperature at lower engine speeds. Therefore it was only possible to increase the torque below 1200 rpm by increasing the engine and ACC fuellings. A 35.9% increase in BMEP was possible at 800 rpm (from 17.72 to 24.09 bar BMEP)

using the burner. The corresponding increase in total BSFC was relatively small (0.5%), because the mechanical efficiency of the engine increases with load, at constant speed.

A relatively flat torque curve can be achieved in this way, with a BMEP of 21.56 bar at the maximum engine speed (2400 rpm), and peak torque occuring at 1200 rpm (24.89 bar BMEP). This represents a 15.4% torque rise at 50% engine speed.

The way in which the burner is operated to improve the engine performance will depend upon the particular limits imposed on the engine performance parameters. A control routine has been developed which will optimise the engine and ACC fuellings to give the maximum possible engine power at a given engine speed within certain predefined limits (such as those described above). The control routine monitors the important engine parameters, such as A/F ratio, and regulates the engine and ACC fuelling accordingly. Other controlling influences, such as injection timing, can easily be incorporated into the system as required. Alternatively the control routine could be modified to find the best BSFC operating point for a given engine power, but this would involve varying the engine speed and load, and would therefore require a continuously variable transmission if the output shaft speed is to be held constant.

The minimum total BSFC that can be achieved for this engine is approximately 0.233 kg/kW.hr which corresponds to a maximum brake thermal efficiency of 36.4%. This compares with thermal efficiencies of around 42.9% (0.198 kg/kW.hr) that can be achieved by current two stage turbocharged engines at the same rating.

No experimental transient response data was available for the Hyperbar engine, and therefore a comparison with the predicted response of the same engine in two stage turbocharged form has been carried out. Two different types of response tests have been investigated:-

(1) A propeller law loading from 800 rpm to 2400 rpm/17.09 bar BMEP, using an automotive two-speed governor.

(2) Rapid load applications of 50%, 70% and 100% of the rated BMEP at 1500 rpm (24.19 bar), using an isochronous governor similar to that used for electricity generation.

Some experimental data was available for a transient response test on the two stage turbocharged engine, and a comparison with predicted performance showed reasonable agreement.

The effect of varying some ot the key design parameters in the Hyperbar system on its response to an acceleration against a propeller law loading was investigated. Reducing the turbocharger inertia was found to have little effect on the engine response, although the turbocharger accelerates faster and the boost pressure and air flow increase more rapidly with a lower inertia. This is because the minimum boost level maintained by the burner system ensures that sufficient air is available at low loads to allow maximum fuelling to be applied very rapidly without causing excessively rich engine A/F ratio's, which result in a deterioration in the engine performance and excessive smoke. No boost controlled rack limiter (aneroid) was found to be required at this rating.

As the engine accelerates, the compressor operating line deviates from the steady state position, and tends to move towards the surge line. This effect is reduced by lowering the turbocharger inertia, and is caused by the response of the components of the turbocharging system. The by-pass valve closes completely during engine acceleration (because the boost pressure cannot respond as rapidly as the exhaust pressure) and so, to some extent, the Hyperbar system loses normal control during rapid transients. In addition a device to cut off the ACC fuelling when the boost pressure falls below the exhaust pressure is essential.

If the ACC is forced into the maximum fuelling position at the start of the transient and held there throughout, then the turbocharger speed, boost pressure and engine air flow rate will initially be much higher than in normal engine operation. This allows an even greater increase in engine fuelling, for a given engine A/F ratio limit, when the load and/or demand speed changes, and so should improve the engine response. However, it was found that this procedure was unnecessary unless the engine rating is very high, as sufficient air is available at the start of the test provided that the minimum boost pressure level is maintained.

Holding the ACC in the maximum fuelling position means that the ACC port areas are large and so the majority of the by-pass flow goes through the ACC. The by-pass

valve therefore has difficulty in controlling the engine pressure drop and remains closed until the final steady state conditions are approached. However, to operate the engine in this fashion requires a previous knowledge of the load and/or speed change, because it is not economical to hold the ACC in the maximum fuelling position indefinitely.

Increasing the engine compression ratio from 9:1 to 11:1 and reducing the minimum boost pressure level from 180 kN/m^2 to 140 kN/m^2 has been shown to improve the steady state fuel consumption considerably. However, if the engine is subjected to rapid increases in fuelling, such as occur during the acceleration or load application tests, the transient engine A/F ratio decreases, because of the lower initial boost pressure. This results in higher transient exhaust gas temperatures and smoke. During the propeller law acceleration tests, it was found that the maximum cylinder pressure was higher, and the by-pass valve was closed for longer, which moved the compressor operating line closer to surge. This caused little disadvantage at this rating (17.09 bar BMEP), and provided that the smoke increase is not excessive, the improvement in BSFC is worthwhile. An aneroid may be required if the smoke increases significantly, which will result in a noticable deterioration in the engine response.

Load changes of 50%, 70% and 100% of the rated load at 1500 rpm (24.19 bar BMEP) have been applied in 0.3 seconds, from no load at 1560 rpm. These tests are very severe, the British Standard Specification for turbocharged engines only requires that the engine is capable of accepting a 32% load application at this rating. The engine and load inertia were increased to represent a typical value for a generating set, and the fuel pump capacity was increased to allow 10% overfuelling, in order that the engine could recover from a 100% load application.

The Hyperbar engine was capable of accepting all these load applications without difficulty. The recovery time and initial speed drop increase with the applied load, but in all cases the final steady engine speed was reached within 4 seconds. The trapped A/F ratio during the early part of the transient decreases as the applied load increases, and a rack limiter will be required for the 100% load application if excessive smoke is to be avoided. It was also found that the initial movement of the compressor operating line towards surge is greater as the applied load increases and the initial engine speed drop increases.

Increasing the damping in the ACC will slow down its movement from its initial position, which maintains a relatively high fuelling level to control the minimum boost level. The ACC fuelling should therefore be higher during the early part of the load application, where good turbocharger response is required. However, it was found that the engine response to a 100% load application was relatively insensitive to the ACC damping, because the pressure drop across the ACC ports limits the burner air flow. There was no noticable increase in the surge margin during the transient. Holding the ACC in the maximum fuelling position during the load application is therefore a preferable alternative.

If the compression ratio is increased to 11:1 and the minimum boost level reduced to 140 kN/m^2, at the rating of the generator type engine (24.19 bar BMEP) it was found to be necessary to retard the injection timing by 8°CA, so that the manufacturers maximum cylinder pressure limit was not exceeded. The deterioration in BSFC caused by the retarded injection timing offsets, to some extent, the gains made by reducing the ACC fuelling rate. The lower initial ACC fuelling means that the turbocharger has to accelerate through a larger speed range than in the standard configuration, with lower available turbine energy. Consequently for a 100% load application the engine A/F ratio becomes excessively rich during the early stages of the transient, which causes a reduction in the engine torque and unacceptable exhaust smoke. The initial engine speed drop increases from 85 rpm to 200 rpm with the higher compression ratio build, and the engine takes longer than 5 seconds to recover to its final steady speed, compared to 2.1 seconds for the standard build.

These tests show that the minimum boost pressure level must be determined as a function of the engine rating if good transient response is to be achieved. Setting the engine compression ratio and minimum boost level to achieve good combustion during steady state operation is not sufficient.

The various response tests for the Hyperbar engine were repeated for a two stage turbocharged version of the same engine. In each case the engine rating was the same for both engines, although it was necessary to modify the governor characteristics slightly for the load application tests because of the higher thermal efficiency of the two stage version.

A comparison between the two engines showed that the two stage turbocharged version

produces no boost pressure at low loads, and it was therefore necessary to limit the amount of fuel injected, using an aneroid. This causes a large reduction in the torque that the engine can produce at low boost pressures, and a drastic deterioration in the transient response. The two stage engine was unable to match the performance of the Hyperbar version in either the acceleration or load application tests. For example, in the propeller law loading acceleration, the two stage engine takes 4.21 seconds to reach 2370 rpm, compared to 1.98 seconds for the Hyperbar version.

The response of the two stage engine to the load application tests was found to be very sensitive to the aneroid characteristics. This engine was incapable of recovering from a 100% load application, however, it should be reiterated that a conventionally turbocharged engine at this rating would not normally be expected to be subjected to such a severe load change. The fact that the Hyperbar turbocharged version has such good load acceptance characteristics implies that it would be ideal for generating applications, where rapid load changes are common. In this situation, the poor part load fuel consumption might be acceptable.

In the current Hyperbar systems both the by-pass valve and the ACC are controlled pneumatically (with additional hydraulic control in the case of the ACC). Such a control strategy has the advantages of being inexpensive, relatively easy to manufacture and therefore inherently reliable. However, the degree of control that can be exercised over the operation of the system is limited, and this is one of the main reasons why the total fuel consumption of the Hyperbar turbocharged engine is very high, compared to a conventional two stage turbocharged engine of the same rating. Other reasons for the high total BSFC are inherent to the system, such as poor engine thermal efficiency with reduced compression ratio.

A microprocessor controlled Engine Management System has been proposed (but not built) which replaces the governor, inlet air heating system and the by-pass valve and ACC control systems with closed loop control over the important operating parameters, such as rack position, injection timing, by-pass valve position, ACC position, etc.

The EMS, described in Chapter 8, requires 19 sensors to monitor pressures, temperatures, air flow rates and positions. This number of sensors is considered to be excessive and will result in a reduction in the potential reliability of the system. Simplified functional relationships have been used to to estimate other operating

parameters, such as maximum cylinder pressure, and so eliminate the need for even more sensors. With the exception of the compressor air flow measuring system, all the sensors used are relatively inexpensive, reliable and well established for automotive engine control. A total of 7 actuators are required to control the engine operation. The number of sensors and actuators can be reduced to 10 and 5 respectively by using additional simplifying relationships, and not having an EGR system. Future developments should lead to improved sensor design, with possible reductions in cost, as the automotive industry relies more heavily on electronic control systems for engine optimisation.

The Hyperbar system has a number of important advantages over conventional two stage turbocharging systems at very high ratings (20-30 bar BMEP), in particular the improved transient response and high torque at low engine speeds. The EMS should improve the operating efficiency of the engine considerably which will, in turn, lead to a wider acceptance of this system.

In conclusion, the Hyperbar turbocharging system is relatively complex, when compared to conventionally turbocharged diesel engine systems, but is at an early stage of its development. The control of the ACC burner is extremely important, as it is the poor part load fuel consumption that detracts from the overall efficiency of the system. The burner should be capable of idling at zero fuelling and ignite instantaneously and reliably on demand. An external control system to regulate the burner fuelling and by-pass valve position will allow very high torques to be achieved at any engine speed. The control system must also monitor and respond to certain important engine parameters such as exhaust temperatures and peak cylinder pressure. Injection timing control will enable the engine power output to be further increased. The by-pass valve should be controlled mechanically, rather than pneumatically, and will then be capable of varying the by-pass system pressure drop to maintain the compressor operating at the peak efficiency for a given pressure ratio. A microprocessor based system could provide the degree of control required for the next generation of Hyperbar turbocharged engines.

APPENDIX A

Calculation of the Required Boost Level for a Given Engine Compression Ratio to Maintain the Ignition Delay Constant.

Simplifying the compression process, by assuming it to be isentropic, we have, for a perfect gas:-

$$p_4 = p_3 \cdot \left(\frac{V_3}{V_4}\right)^{\gamma} \qquad (A.1)$$

where,

p_3 = cylinder pressure at BDC (kN/m^2)

p_4 = mean cylinder gas pressure during the ignition delay (kN/m^2)

V_3/V_4 = "effective compression ratio"

γ = specific heats ratio (assumed to be 1.4 for air)

The gas temperature at the end of the "effective" compression stroke is given by:-

$$T_4 = T_3 \cdot \left(\frac{V_3}{V_4}\right)^{\gamma-1} \qquad (A.2)$$

where,

T_3 = cylinder temperature at BDC (K)

T_4 = mean cylinder gas temperature during the ignition delay (K)

In order to simplify the analysis we can assume that p_3 and T_3 are the mean conditions in the induction manifold, since it is these conditions that will ultimately be controlled. Using the standard engine geometric compression ratio of 9:1, the simulation program predicts the following values:-

$p_3 = 175\ kN/m^2$ $\quad T_3 = 307\ K$

$p_4 = 2980\ kN/m^2$ $\quad T_4 = 684\ K$

From eqns. (A.1) and (A.2) the "effective compression ratio" can be estimated as:-

$$\frac{V_3}{V_4} = \left(\frac{2980}{175}\right)^{1/1.4} = 7.57$$

$$\frac{V_3}{V_4} = \left(\frac{684}{307}\right)^{1/0.4} = 7.41$$

The discrepancy between these values is due to the simplifying assumptions that have been made. Therefore a reasonable "effective compression ratio" for the standard engine build can be taken as 7.5.

Now at BDC the cylinder volume, V_{cyl}, is given by:-

$$V_{cyl} = \frac{\pi}{4}.B^2.S + V_{cl} = V_3 \qquad (A.3)$$

$$V_{cl} = \frac{\pi}{4}.B^2.S.\left(\frac{1}{CR-1}\right) \qquad (A.4)$$

where,

B = bore (m)
CR = geometric compression ratio
S = stroke (m)
V_{cl} = clearance volume at TDC (m^3)
V_{cyl} = cylinder volume at BDC (m^3)

The clearance volume using the standard compression ratio of 9:1 can be calculated from eqn. (A.4), and the cylinder volume at BDC from eqn. (A.3). Using the "effective compression ratio" of 7.5, the cylinder volume at the end of the effective compression stroke can be calculated:-

$$V_4 = \frac{V_3}{7.5} = V_i + V_{cl} \qquad (A.5)$$

where,

V_i = cylinder volume at the end of compression (m^3).

So the inlet manifold pressure, p_3, required for a given compression ratio can be calculated from eqn. (A.1), where V_3 and V_4 are given by eqns. (A.3) and (A.5), V_{cl} is given by eqn. (A.4) and p_4 is taken as 2980 kN/m^2 (from the simulation program

prediction for the standard geometry).

The charge cooler pressure drop is a function of the dynamic head at the compressor outlet (charge cooler inlet), and can be estimated from the previously predicted pressure losses at this operating condition, or by using the compressor pressure ratio, p_2/p_1, and the compressor efficiency, η_c, to obtain the compressor outlet temperature, T_2, and eqns. (4.29) and (4.30).

REFERENCES

1 ANDRE-TALAMON T.
Suralimentation Parallèle et Suralimentation Série.
Entropie, No. 74, March-April, 1977, pp. 39-44.

2 ANDRE-TALAMON T.
New Aspects of Turbocharger Utilisation with the Hyperbar Parallel Supercharging.
Turbocharging and Turbochargers Conference, Inst. Mech. Engrs., C66/78, 1978.

3 ANNAND W.J.D.
Heat Transfer in the Cylinders of Reciprocating Internal Combustion Engines.
Proc. Inst. Mech. Engrs., Vol. 177, No. 36, 1963.

4 ANNAND W.J.D.
Choice of a Computing Proceedure for Digital Computer Synthesis of Reciprocating Engine Cycles.
Journal of Mechanical Engineering Science, Vol. 10, No. 3, 1968, pp. 289-290.

5 ANNAND W.J.D. and ROE G.E.
Gas Flow in the Internal Combustion Engine.
G. T. Foulis, 1974.

6 ANSDALE R.F.
A Reconnaissance of Supercharging Technology 1902-1980.
SAE 810003, 1981.

7 AUSTEN A.E.W. and LYN W.T.
Relation Between Fuel Injection and Heat Release in a Direct-Injection Engine and the Nature of the Combustion Processes.
Proc. Inst. Mech. Engrs., No. 1, 1960-1.

8 BAAZAARI Z.
Transient Response of High Output Turbocharged Diesel Engines.
Ph.D Thesis, University of London, 1979.

9 BASILETTI J.C. and BLACKBURNE E.F.
Recent Developments in Variable Compression Ratio Engines.
SAE 660344, 1966.

10 BENSON R.S.
Experiments on a Piston Controlled Port.
The Engineer, Vol. 210, Nov. 25, 1960, pp. 875-880.

11 BENSON R.S.
A Comparative Study of the Cyclic Operating Conditions in the Compressor Delivery in Single and Two-Stage Turbochargers Under High Boost Conditions.
Turbocharging and Turbochargers Conference, Inst. Mech. Engrs., C75/78, 1978.

12 BENSON R.S. and BARUAH P.C.
Some Further Tests on a Computer Program to Simulate Internal Combustion Engines.
SAE 730667, 1973.

13 BENSON R.S. and SCRIMSHAW K.H.
An Experimental Investigation of Non-Steady Flow in a Radial Gas Turbine.
Proc. Inst. Mech. Engrs., Vol. 180, Pt. 3J, 1965-6.

14 BENSON R.S. and WHITEHOUSE N.D.
Internal Combustion Engines, Volumes 1 and 2.
Pergamon Press, 1979.

15 BENSON R.S. and WHITFIELD A.
An Experimental Investigation of the Non-Steady Flow Characteristics of a Centrifugal Compressor.
Proc. Inst. Mech. Engrs., Vol. 180, Pt. 1, No. 27, 1965-6.

16 BENSON R.S. and WHITFIELD A.
A Quasi-Steady Flow Representation of Centrifugal Compressor Performance Characteristics in Non-Steady Flow Systems.
Proc. Inst. Mech. Engrs., Vol. 182, Pt. 3H, 1967-8.

17 BENSTEIN E.H. and WOOD H.J.
Applications and Performance Levels of Radial Inflow Turbines.
SAE Paper 653D, 1963.

18 BERCHTOLD M. and GULL H.P.
Road Performance of a Comprex Supercharged Diesel Truck.
SAE Trans., Vol. 68, 1960, pp. 367-379.

19 BERENYI S.G. and RAFFA C.J.
Variable Area Turbocharger for High Output Diesel Engines.
SAE 790064, 1979.

20 BHOT S.R. and QUAYLE R.S.
The Control of Ignition Timing to Achieve Maximum Fuel Economy.
Automotive Electronics Conference, Inst. Mech. Engrs., C174/81, 1981.

21 BISHOP I.N.
Effect of Design Variables on Friction and Economy.
SAE Paper 812A, 1964.

22 BORMAN G.L.
Mathematical Simulation of Internal Combustion Engine Processes and Performance Including Comparison with Experiment.
Ph.D Thesis, University of Wisconsin, 1964.

23 BOWLER L.L.
Electronic Fuel Management-Fundamentals.
SAE 800539, 1980.

24 BRANDS M.C.
Helmholtz Tuned Induction System for Turbocharged Diesel Engine.
SAE 790069, 1979.

25 BRITISH STANDARDS INSTITUTION.
Specification for Reciprocating Internal Combustion Engines: Performance.
Part 4, Speed Governing.
B.S.I., No. BS 5514:Part 4:1979.

26 BROWN W.L.
The Caterpillar IMEP Meter and Engine Friction.
SAE 730150, 1973.

27 BUSH J.E. and LONDON A.L.
Design Data for "Cocktail Shaker" Cooled Pistons and Valves.
SAE 650727, 1965.

28 CARNAHAN B., LUTHER H.A. and WILKES J.O.
Applied Numerical Methods.
Wiley and Sons, 1969.

29 CHEN S.K. and FLYNN P.
Development of a Single Cylinder Compression Ignition Research Engine.
SAE 650733, 1965.

30 CHIU W.S., SHAHED S.M. and LYN W.T.
A Transient Spray Mixing Model for Diesel Combustion.
SAE 760128, 1976.

31 CHOLVIN R.L.
Turbocharger Controls.
SAE Paper 546A, 1962.

32 CROSS R.K., LAKRA P. and O'NEILL C.G.
Electronic Fuel Injection Equipment for Controlled Combustion in Diesel Engines.
SAE 810258, 1981.

33 CSER G.
Some Results of Combined Charging Application.
Turbocharging and Turbochargers Conference, Inst. Mech. Engrs., C64/78, 1978.

34 DOERFLER P.K.
Comprex Supercharging of Vehicle Diesel Engines.
SAE 750335, 1975.

35 DUFLOT F.
Experimentation Realisee Par La S.N.C.F. Avec Un Moteur Diesel A Tres Haute Suralimentation (Hyperbar).
CIMAC D81, Session B4, 13th International Congress, Vienna, 1979.

36 EICHELBERG G.
Investigations on Internal Combustion Engines.
Engineering, Vol. 148, Oct. 27 p. 463, Nov. 17 p. 547, Dec. 1 p. 603 and Dec. 22 p. 682, 1939.

37 EISELE E., HIERETH H. and POLZ H.
Experience with Comprex Pressure Wave Supercharger on the High-Speed Passenger Car Diesel Engine.
SAE 750334, 1975.

38 EISELE H.
Electronic Control of Diesel Passenger Cars.
SAE 800167, 1980.

39 ELLOR J.E.
The Development of the Merlin Engine.
SAE Trans., Vol. 52, No. 8, 1944.

40 FLAXINGTON D. and SZCZUPAK D.T.
Variable Area Radial-Inflow Turbines.
Turbocharging and Turbochargers Conference, Inst. Mech. Engrs., C36/82, 1982.

41 FREESE R.G. and NIGHTINGALE D.R.
A Practical and Theoretical Investigation Into the Application of Mechanical Superchargers to Diesel Cars.
Turbocharging and Turbochargers Conference, Inst. Mech. Engrs., C53/82, 1982.

42 FRENCH C.C.J.
Problems Arising from the Water Cooling of Engine Components.
Proc. Inst. Mech. Engrs., Vol. 184, Pt. 1, No. 29, 1969-70.

43 FRENCH C.C.J.
Taking the Heat Off the Highly Boosted Diesel.
SAE 690463, 1969.

44 GARRETT K.
Microprocessor Control for Diesel Engines.
Automotive Engineer, August-Sept., 1980, pp. 21-25.

45 GENERAL ELECTRIC COMPANY.
Properties of Combustion Gases/System: C_nH_{2n}-Air. Volumes 1 and 2.
G.E.C. Aircraft Gas Turbine Development Department, Ohio, USA, 1955.

46 GHADRI-ZAREH M.S. and WALLACE F.J.
Variable Geometry vs. Two Stage Turbocharging of High Output Diesel Engines.
Turbocharging and Turbochargers Conference, Inst. Mech. Engrs., C63/78, 1978.

47 GORILLE I.
Digital Engine Control for European Cars.
SAE 800165, 1980.

48 GRIMM R.A., BREMER R.J. and STONESTREET S.P.
GM Micro-Computer Engine Control System.
SAE 800053, 1980.

49 GROENEWOLD G.M., WELLIVER D.R. and KAMO R.
Performance and Sociability of Comprex Supercharged Diesel Engine.
ASME, 77-DGP-4, 1977.

50 GRUNDY J.R., KILEY L.R. and BREVICK E.A.
AVCR 1360-2 High Specific Output-Variable Compression Ratio Diesel Engine.
SAE 760051, 1976.

51 GRUNER R.
Actuators for Electronic Systems in Automotive Vehicles.
Automotive Electronics Conference, Inst. Mech. Engrs., C171/81, 1981.

52 HAMBURG D.R. and SHULMAN M.A.
A Closed-Loop A/F Control Model for Internal Combustion Engines.
SAE 800826, 1980.

53 HARDENBERG H. and FRAENKLE G.
The Effect of Charge Air Cooling on Exhaust Emissions and Power Output of Turbocharged Diesel Engines.
Turbocharging and Turbochargers Conference, Inst. Mech. Engrs., C71/78, 1978.

54 HARDENBERG H.O. and HASE F.W.
An Empirical Formula for Computing the Pressure Rise Delay of a Fuel from its Cetane Number and from the Relevant Parameters of Direct-Injection Diesel Engines.
SAE 790493, 1979.

55 HARP J.L. and OATWAY T.P.
Centrifugal Compressor Development for a Variable Area Turbocharger.
SAE 790066, 1979.

56 HIROYASU H. and ARAI M.
Development and Use of a Spray Combustion Modeling to Predict Diesel Engine Efficiency and Pollutant Emissions.
5th International Automotive Propulsion Systems Symposium, 1980.

57 HIROYASU H. and KADOTA T.
Models for Combustion and Formation of Nitric Oxide and Soot in Direct Injection Diesel Engines.
SAE 760129, 1976.

58 HOLZHAUSEN G.H. and ALFANO D.L.
Power Transfer to Improve Transient Response of a Turbocharged Diesel Engine.
Turbocharging and Turbochargers Conference, Inst. Mech. Engrs., C41/82, 1982.

59 HONIG G., DECKER H. and ROHDE S.
Electronic Spark Control Systems.
Part I: Microcomputer-Controlled Ignition System.
Part II: Bosch Knock Control.
SAE 810059, 1981.

60 IDOGAWA Y., MATSUDA M. and MAEHASHI Y.
A New Microcomputer Application for Engine Control System.
Automotive Electronics Conference, Inst. Mech. Engrs., C189/81, 1981.

61 ILMARI E.J.
The Spray Impingement Theory of Ignition Delay in Small Swirl Chamber Diesel Engines.
Thesis for Degree of Doctor of Technology, Inst. of Tech., Helsinki, 1965.

62 IVES A.P. and TRENNE M.U.
Closed Loop Electronic Control of Diesel Fuel Injection.
Automotive Electronics Conference, Inst. Mech. Engrs., C201/81, 1981.

63 JAKOB M. and HAWKINS G.A.
Elements of Heat Transfer.
Wiley International Edition, 1957.

64 JANOTA M.S.
Quasi-Steady Analysis Applied to Turbo-Charged Engine Performance.
Ph.D Thesis, University of London, 1969.

65 JANOTA M.S., HALLAM A.J., BROCK E.K. and DEXTER S.G.
The Prediction of Diesel Engine Performance and Combustion Chamber Component Temperatures Using Digital Computers.
Proc. Inst. Mech. Engrs., Vol. 182, Pt. 3L, 1967-8.

66 JAPIKSE D.
Turbocharger Turbine Design and Development.
Turbocharging the Internal Combustion Engine, Imperial College, Sept., 1979.

67 JENNY E.
Non-Stationary Phenomena in Radial Compressors, Especially in Supercharging Sets of I.C. Engines.
Schweizerische Bauzeitung, 79, 182, 1961. (B.S.R.A. Translation No. 1395).

68 KAMO R.
Higher BMEP Prospect for Vehicular Diesels.
Turbocharging and Turbochargers Conference, Inst. Mech. Engrs., C62/78, 1978.

69 KAMO R. and BRYZIK W.
Adiabatic Turbocompound Engine Performance Prediction.
SAE 780068, 1978.

70 KELLETT E., BETTERIDGE J.F. and MISTOVSKI M.
Investigation of Diesel Engine and Turbocharger Interaction.
Proc. Inst. Mech. Engrs., Vol. 182, Pt. 1, No. 15, 1967-8.

71 KNIGHT B.E.
Fuel Injection System Calculations.
Proc. Inst. Mech. Engrs., No. 1, 1960-1.

72 KOLLBRUNNER T.A.
Comprex Supercharging for Passenger Diesel Car Engines.
SAE 800884, 1980.

73 KRIEGER R.B. and BORMAN G.L.
The Computation of Apparent Heat Release for Internal Combustion Engines.
ASME, 66-WA/DGP-4, 1966.

74 KRONOGARD S.O.
The Volvo Dual Powerplant for Military Vehicles.
SAE 660017, 1966.

75 KUNBERGER K.
Hyperbar Turbocharging System for Low Compression Ratio Engines.
Diesel and Gas Turbine Progress Worldwide, July-August, 1974, pp. 10-12.

76 KYRTATOS N. and WATSON N.
An Aerodynamic Method for Control and Range Improvement of Rotary Compressors.
ASME, 80-GT-31, 1980.

77 LANCASTER D.R., KRIEGER R.B. and LIENESCH J.H.
Measurement and Analysis of Engine Pressure Data.
SAE 750026, 1975.

78 LAWTON B.
The Turbocharged Diesel Wankel Engine.
Turbocharging and Turbochargers Conference, Inst. Mech. Engrs., C68/78, 1978.

79 LEDGER J.D., BENSON R.S. and FURUKAWA H.
Improvement in Transient Performance of a Turbocharged Diesel Engine by Air Injection into the Compressor.
SAE 730665, 1973.

80 LEDGER J.D., BENSON R.S. and FURUKAWA H.
Performance Characteristics of a Centrifugal Compressor with Air Injection.
Proc. Inst. Mech. Engrs., Vol. 187, 35/73, 1973.

81 LeFEUVRE T., MYERS P.S. and UYEHARA O.A.
Experimental Instantaneous Heat Fluxes in a Diesel Engine and Their Correlation.
SAE 690464, 1969.

82 LEISING C.J., PUROHIT G.P., DeGREY S.P. and FINEGOLD J.G.
Waste Heat Recovery in Truck Engines.
SAE 780686, 1978.

83 LeMERER M.R.
Moteurs Diesel à Très Haut Rapport de Suralimentation.
Sté Budi, France.

84 LeMERER M.R. and TORD J.F.
Moteurs Diesel de Hautes Performances de Moins de 1.8 kg au Cheval.
CIMAC, Barcelona, 1975.

85 LEONARD G.H.
Power Train Control for a Heavy Vehicle- A Production System.
Automotive Electronics Conference, IEE, No. 181, 1979.

86 LYN W.T.
Calculations of the Effect of Rate of Heat Release on the Shape of the Cylinder-Pressure Diagram and Cycle Efficiency.
Proc. Inst. Mech. Engrs., No. 1, 1960-1.

87 LYN W.T.
Study of Burning Rate and Nature of Combustion in Diesel Engines.
Ninth Symposium on Combustion, Acedemic Press, 1963.

88 MANGER H.
LH-Jetronic- a New Gasoline Injection Injection System with a Hot Wire Air Mass Meter and a Microprocessor Controlled ECU.
Automotive Electronics Conference, Inst. Mech. Engrs., C180/81, 1980.

89 MARZOUK M.
Transient Response of Turbocharged Diesel Engines.
Ph.D Thesis, University of London, 1976.

90 MARZOUK M. and WATSON N.
Some Problems in Diesel Engine Research With Special Reference to Computer Control and Data Acquisition.
Proc. Inst. Mech. Engrs., Vol. 190, No. 23/76, 1976.

91 McAULAY K.J., WU T., CHEN S.K., BORMAN G.L., MYERS P.S. and UYEHARA O.A.
Development and Evaluation of the Simulation of the Compression-Ignition Engine. Parts 1 and 2.
SAE 650451, 1965.

92 MEGUERDICHIAN M. and WATSON N.
Prediction of Mixture Formation and Heat Release in Diesel Engines.
SAE 780225, 1978.

93 MEIER E.
Two Stage Turbocharging.
Brown Boveri Review, Vol. 52, No. 3, 1965.

94 MELCHIOR J.
Suralimentation des Moteurs Diesel par le Procédé Hyperbar.
Entropie, No. 48, Nov.-Dec., 1972, pp. 5-12.

95 MELCHIOR J.
Brevet, France, No. 2087095.

96 MELCHIOR J.
Brevet, France, No. 2179310.

97 MELCHIOR J. and ANDRE-TALAMON T.
Hyperbar System of High Supercharging.
SAE 740723, 1974.

98 MELCHIOR J. and ANDRE-TALAMON T.
A Combustion Chamber for use in a Supercharging System for an Internal Combustion Engine.
Patent Specification, London, No. 1458754, 15th Dec., 1976.

99 MELCHIOR J. and ANDRE-TALAMON T.
Brevet, France, No. 2265979.

100 MELCHIOR J. and ANDRE-TALAMON T.
Brevet, France, No. 2284766.

101 MELCHIOR J. and ANDRE-TALAMON T.
Brevet, France, No. 2308792.

102 MEYER A.
The Free-Piston Engine.
Mechanical Engineer, April, 1947.

103 MILLINGTON B.W.
The Supercharging of High-Speed Diesel Engines by Mechanically Driven Compressors.
Proc. Inst. Mech. Engrs., Auto. Div., 1956-7, pp.229-239.

104 MILLINGTON B.W. and HARTLES E.R.
Frictional Losses in Diesel Engines.
SAE 680590, 1968.

105 MITCHELL J.E.
An Evaluation of Aftercooling in Turbocharged Diesel Engine Performance.
SAE Trans., Vol. 67, 1959.

106 NAGAO F., IKEGAMI M. and OSHIMA K.
An Analysis of Combustion Knock in a Diesel Engine.
Bulletin JSME, 10, No. 39, 1967, pp. 532-42.

107 NETTEL F.
Control System for Turbocharged Compression Ignition, Internal Combustion Engines.
US-Patent 2608051, August 26th 1952. (Anm. August 24th, 1947).

108 NEWHALL H.K. and STARKMAN E.S.
Thermodynamic Properties of Octane and Air for Engine Performance Calculations.
SAE Progress in Technology, Vol. 7, "Digital Calculations of Engine Cycles", SAE, 1963.

109 OAKES J.A.
A Pressure Sensor for Automotive Application.
Automotive Electronics Conference, Inst. Mech. Engrs., C181/81, 1981.

110 OBERT E.F.
Internal Combustion Engines and Air Pollution.
Intext Educational Publishers, 1973.

111 PACHERNEGG S.J.
Heat Flow in Engine Pistons.
SAE 670928, 1967.

112 PENNY N.
The Development of the Glass Ceramic Regenerator for the Rover 2S/150R Engine.
SAE 660361, 1966.

113 POWELL H.N.
Applications of an Enthalpy-Fuel/Air Ratio Diagram to "First Law" Combustion Problems.
ASME, 56-SA-68, 1956.

114 POWELL M.J.D.
A Fortran Subroutine for Solving Systems of Non-Linear Algebraic Equations.
Harwell Report, AERE-R5947, 1968.

115 RAUTENBERG M., MOBARAK A. and MALOBABIC M.
The Charging of Diesel Engines for Passenger Cars Using Turbochargers with Adjustable Turbine Guide Vanes.
ASME, 82-GT-41, 1982.

116 REAMS L.A., WIEMERO T.A., LEVIN M.B. and WADE W.R.
Capabilities of Diesel Electronic Fuel Control.
SAE 820449, 1982.

117 RICARDO H.R.
The Supercharging of Internal-Combustion Engines.
Proc. Inst. Mech. Engrs., Vol.162, 1950, pp. 421-428.

118 RICARDO H.R. and HEMPSON J.G.G.
The High-Speed Internal-Combustion Engine.
Blackie and Sons Limited, 1972.

119 ROBINSON R.R. and MITCHELL J.E.
Development of a 300 psi (21.1 kp/cm^2) BMEP Continuous-Duty Diesel Engine.
ASME, 66-DGEP-9, 1966.

120 RYDQVIST J.E., SANDBERG L. and WALLIN R.
A Turbocharged Engine with Microprocessor Controlled Boost Pressure.
SAE 810060, 1981.

121 SAWADA D. and SHIGEMATSU T.
Improvement of Spark Ignition Knock Detector Performance by Learning Control.
SAE 810057, 1981.

122 SCHMIDT F.A.F.
Theoretische Untersuchung und Versuche über Zundverzug und Klopfvorgang.
VDI-Forschungsheft, 392, 1938, pp. 1-14.

123 SCHWARZBAUER G.E.
Turbocharging of Tractor Engines with Exhaust Gas Turbochargers and the BBC-Comprex.
Turbocharging and Turbochargers Conference, Inst. Mech. Engrs., C69/78, 1978.

124 SCHWEITZER P.H.
The Tangent Method of Analysis for Indicator Cards of Internal Combustion Engines.
Bulletin No. 35, Penn. State Eng. Exp. Sta., Sept., 1926.

125 SHAHED S.M., CHIU W.S. and LYN W.T.
A Mathematical Model of Diesel Combustion.
Proc. Inst. Mech. Engrs., C94/75, 1975.

126 SHAHED S.M., CHIU W.S. and YUMLU V.S.
A Preliminary Model for the Formation of Nitric Oxide in Direct Injection Diesel Engines and its Application in Parametric Studies.
SAE 730083, 1973.

127 SHIPINSKI J.H., MYERS P.S. and UYEHARA O.A.
A Spray-Droplet Model for Diesel Combustion.
Proc. Inst. Mech. Engrs., Vol. 184, Pt. 3J, 1970.

128 SHIPINSKI J.H., UYEHARA O.A. and MYERS P.S.
Experimental Correlation Between Rate-of-Injection and Rate-of-Heat-Release in a Diesel Engine.
ASME, 68-DGP-11, 1968.

129 SITKEI G.
Heat Transfer and Thermal Loading in Internal Combustion Engines.
Akademiai Kiado, Budapest, 1974.

130 SITKEI G.
Uber den Dieselmotorischen Zundverzug.
MTZ, 24, 6th June, 1963, pp. 190-4.

131 SITKEI G. and RAMANAIAH G.V.
A Rational Approach for Calculation of Heat Transfer in Diesel Engines.
SAE 720027, 1972.

132 SKINNER W.
Capacitive Pressure Transducer.
Automotive Electronics Conference, Inst. Mech. Engrs., C191/81, 1981.

133 SMITH C.
Electronic Speed Governing.
Diesel Engineering, Spring, 1979, pp. 19-20.

134 SMITH J.M.
A Fixed-Head Concept Diesel Engine.
Proc. Inst. Mech. Engrs., Vol. 186, 16/72, 1972.

135 SOCIETE RATEAU.
Dispositif de Suralimentation d'un Moteur Thermique.
Brevet d'invention Francais, No. 864443, 17th Jan., 1941.

136 STREIT E.E.
Mathematical Simulation of a Large Pulse-Turbocharged Two-Stroke Engine.
Ph.D Thesis, University of Wisconsin, 1970.

137 STREIT E.E. and BORMAN G.L.
Mathematical Simulation of a Large Turbocharged Two-Stroke Engine.
SAE 710176, 1971.

138 SUMMERAUER I., SPINNLER F., MAYER A. and HAFNER A.
A Comparative Study of the Acceleration Performance of a Truck Diesel Engine with Exhaust-Gas Turbocharger and with Pressure-Wave Supercharger Comprex.
Turbocharging and Turbochargers Conference, Inst. Mech. Engrs., C70/78, 1978.

139 TANASAWA Y.
On the Combustion Rate of a Group of Fuel Particles.
Technology Reports of Tohoku University, 18, No. 1, 1953, pp. 61-74.

140 TAYLOR C.F.
The Internal Combustion Engine in Theory and Practice, Volumes 1 and 2.
The M.I.T. Press, 1978.

141 TAYLOR D.H.C., WHATTAM M. and JANOTA M.S.
Comparison of Single and Two-Stage Turbocharging on a Medium-Speed Four-Stroke Diesel Engine at High B.M.E.P.'s.
CIMAC, A19, 1971.

142 TIMONEY S.G.
A New Concept in Traction Power Plants.
Proc. Inst. Mech. Engrs., Vol. 180, Pt. 2A, No. 3, 1965-6.

143 TOYODA T., INOUE T., MITSUDA T., AOKI K. and YAEGASHI T.
Some of the New Control Strategies for Electronic Engine Control System.
Automotive Electronics Conference, Inst. Mech, Engrs., C170/81, 1981.

144 TOYODA T., INOUE T., YAEGASHI T. and AOKI K.
Electronic Engine Control Systems for the Smaller Passenger Car.
SAE 800894, 1980.

145 TOYODA T., YAMAKAWA Y., INOUE T., OISHI K. and HATTORI K.
Development of Closed Loop Secondary Air Control Three-Way Catalyst System.
SAE 800399, 1980.

146 TRENNE M.U. and NOWAK V.J.
An Overview of Electronic Controls for Passenger Car Diesel Engines.
IEEE, Convergence, 1980.

147 TSAO K.C., MYERS P.S. and UYEHARA O.A.
Gas Temperature During Compression in Motored and Fired Diesel Engines.
SAE Trans., Vol. 70, 1962.

148 VINCENT E.T. and HENEIN N.A.
Thermal Loading and Wall Temperature as Functions of Performance of Turbocharged Compression-Ignition Engines.
SAE Trans., Vol. 67, 1959.

149 WALLACE F.J.
The Differential Compound Engine.
SAE 670110, 1967.

150 WALLACE F.J.
Differential Compound Engine.
Proc. Inst. Mech. Engrs., Vol. 187, 48/73, 1973.

151 WALLACE F.J., ADGEY J.M. and BLAIR G.P.
Performance of Inward Radial Flow Turbines Under Non-Steady Flow Conditions.
Proc. Inst. Mech. Engrs., Vol. 184, Pt. 1, No. 10, 1969-70.

152 WALLACE F.J. and ALDIS C.A.
Comprex Supercharging Versus Turbocharging of a Large Truck Diesel Engine.
Turbocharging and Turbochargers Conference, Inst. Mech. Engrs., C39/82, 1982.

153 WALLACE F.J., BAGHERY A. and ZIARATI M.R.
Variable Geometry Turbocharging for Transport Engines.
Turbocharging and Turbochargers Conference, Inst. Mech. Engrs., C38/82, 1982.

154 WALLACE F.J. and BLAIR G.P.
The Pulsating-Flow Performance of Inward Radial Flow Turbines.
ASME, 65-GTP-21, 1965.

155 WALLACE F.J., FEW P.C. and CAVE P.R.
The Differential Compound Engine: Interim Test Results and Assessment of Future Development.
Proc. Inst. Mech. Engrs., Vol. 183, Pt. 3B, 1968-9.

156 WALLACE F.J., FEW P.C. and CAVE P.R.
The Differential Compound Engine - Further Development.
SAE 710085, 1971.

157 WALLACE F.J., HARGREAVES M.R.O., BOWNS D.E. and CAVE P.R.
The Differential Compound Engine- Part 2: Transient Response of the Differential Compound Engine (DCE) Compared with Conventional Turbocharged Engines.
SAE 740722, 1974.

158 WALLACE F.J. and MILES J.
Performance of Inward Radial Flow Turbines Under Unsteady Flow Conditions with Full and Partial Admission.
Proc. Inst. Mech. Engrs., Vol. 185, 77/71, 1970-1.

159 WALLACE F.J. and SIVAKUMARAN K.
The Differential Compound Engine- Part 1: Steady State and Emission Characteristics.
SAE 740721, 1974.

160 WALLACE F.J., WHITFIELD A. and ATKEY R.C.
Experimental and Theoretical Performance of a Radial Flow Turbocharger Compressor with Inlet Prewhirl.
Proc. Inst. Mech. Engrs., Vol. 189, 43/75, 1975.

161 WALLACE F.J. and WINKLER G.
Very High Output Diesel Engines- A Critical Comparison of Two Stage Turbocharged, Hyperbar, and Differential Compound Engines.
SAE 770756, 1977.

162 WALLACE T.F.
BUICK'S Turbocharged V6 Powertrain for 1978.
SAE 780413, 1978.

163 WALLACE W.A. and LUX F.B.
A Variable Compression Ratio Engine Development.
SAE Trans., Vol. 72, 1964.

164 WATSON N.
Turbochargers for the 1980's- Current Trends and Future Prospects.
SAE 790063, 1979.

165 WATSON N.
Resonant Intake and Variable Geometry Turbocharging Systems for a V8 Diesel Engine.
Turbocharging and Turbochargers Conference, Inst. Mech. Engrs., C40/82, 1982.

166 WATSON N. and MARZOUK M.
A Non-Linear Digital Simulation of Turbocharged Diesel Engines Under Transient Conditions.
SAE 770123, 1977.

167 WATSON N., MARZOUK M. and BAAZAARI Z.
Turbocharger System Options for Vehicle Engines.
Turbocharging and Turbochargers Conference, Inst. Mech. Engrs., C61/78, 1978.

168 WATSON N., MARZOUK M. and BAAZAARI Z.
An Evaluation of Two Stage Turbocharging for Efficient High-Output Diesel Engines.
ASME, 78-DGP-2, 1978.

169 WATSON N., PILLEY A.D. and MARZOUK M.
A Combustion Correlation for Diesel Engine Simulation.
SAE 800029, 1980.

170 WEBB C.R. and JANOTA M.S.
Governors with Load Sensing.
Proc. Inst Mech. Engrs., Vol. 184, Pt. 1, No. 9, 1969-70.

171 WELBOURN D.B., ROBERTS D.K. and FULLER R.A.
Governing of Compression-Ignition Oil Engines.
Proc. Inst. Mech. Engrs., Vol. 173, No. 22, 1959.

172 WERTZ J.L. and HEITMAN P.W.
Predicting the Reliability of Ceramic Turbine Components.
SAE 800194, 1980.

173 WHITEHOUSE N.D., STOTTER A., GOUDIE G.O. and PRENTICE B.W.
Method of Predicting Some Aspects of Performance of a Diesel Engine using a Digital Computer.
Proc. Inst. Mech, Engrs., Vol. 176, No. 9, 1962.

174 WHITEHOUSE N.D. and WAY R.J.B.
Rate of Heat Release in Diesel Engines and its Correlation with Fuel Injection Data.
Proc. Inst. Mech. Engrs., Vol. 184, Pt. 3J, 1969-70.

175 WIEBE I.I.
Habempirische Formel für die Verbrennungsgeschrwindigkeite.
Verlag der Akademie der Wissenschaften der VdSSR, Moscow, 1956.

176 WIJEYAKUMAR S.
Microcomputer Control System for Diesel Engines.
Ph.D Thesis, University of London, 1981.

177 WINKLER G. and WALLACE F.J.
Thermodynamic-Mechanical Modelling of the Turbocharged Diesel Engine.
Int. Conf. on Applied Numerical Modelling, Paper 6.2, July, 1977.

178 WOLBER W.G.
Automotive Engine Control Sensors '80.
SAE 800121, 1980.

179 WOLFER H.H.
Der Zündverzug im Dieselmotor.
VDI-Forschungsheft, 392, 1938, pp. 15-24.

180 WOSCHNI G.
A Universally Applicable Equation for the Instantaneous Heat Transfer Coefficient in the Internal Combustion Engine.
SAE 670931, 1967.

181 WOSCHNI G. and ANISITS F.
Experimental Investigation and Mathematical Presentation of Rate of Heat Release in Diesel Engines Dependent Upon Engine Operating Conditions.
SAE 740086, 1974.

182 WOSCHNI G., BEINEKE E. and FLENKER H.
Calculation of the Performance of One- and Two-Stage Turbocharged Medium Speed Diesel-Engines.
Turbocharging and Turbochargers Conference, Inst. Mech. Engrs., C53/78, 1978.

183 WU H.L.
Prediction of Wall Temperatures Inside Diesel Engines by Digital Computer.
The Engineer, Nov. 25th, 1966, pp. 789-794.

184 YANO T.
Performance of Centrifugal Blower Under Pulsating Flow.
Bulletin of JSME, Vol. 6, No. 23, 1963.

185 ZAPF H.

Beitrag zur Untersuchung des Wärmeübergangs Während des Ladungswechsels im Viertakt-Dieselmotor.

MTZ, 30, 12, 1969, pp. 461-5.

186 ZEHNDER G. and MEIER E.

Exhaust-Gas Turbochargers and Systems for High-Pressure Charging.

Brown Boveri Review, Vol. 64, No. 4, 1977.

187 ZIMMERMAN K.D.

Uber dem Zundverzug bei der Dieselmotorischen Verbrennung.

Diss. Karlsruhe, 1962, p. 138.

188 ZINNER K.

Verfahren zum Betrieb einer Brennkraftmaschine mit Abgasturboaufladung und Einrichtung zur Durchführung Dieses Verfahrens.

Deutsche Offenlegungsschrift 1451910, 10th July, 1969.

ANONYMOUS PUBLICATIONS

189 Poyaud 520 Series Engines.
Gas and Oil Power, Winter, 1972, pp. 196-8.

190 5 to 1 Ratio Turbocharger.
Gas and Oil Power, Spring, 1974, p. 38.

191 HYPERBAR Turbocharged Engines.
Gas and Oil Power, Spring, 1975, p. 16.

192 Hyperbar Today.
Diesel Engineering, Summer, 1979, pp. 72-8.

193 Forty-Cylinder Hyperbar-Charged Engine.
Diesel Engineering, Spring, 1979, pp. 37-40.

194 Turbomeca High Pressure-Ratio Turbocharger.
Diesel Engineering, Spring, 1979, p. 53.